

2001 USNC/URSI National Radio Science Meeting



100 Years of Communications 1901-2001
Transatlantic to Geosynchronous

URSI Digest

Boston, Massachusetts
The Sheraton Boston Hotel
July 8-13, 2001



$\frac{2}{3}$

174
79
174 Re

224

459
458
410

USNC/URSI
National Radio Science Meeting



2001 Digest

July 8-13, 2001
Boston, Massachusetts

Held in conjunction with:
IEEE Antennas & Propagation Society
International Symposium

U.S. Student Travel for Student Paper Competition sponsored by
National Science Foundation

CHAIRMAN'S WELCOME

Welcome to Boston, where it all began ...

On behalf of the steering committee I would like to welcome all of you to Boston for the 2001 IEEE International Antennas and Propagation Symposium and USNC/URSI National Radio Science Meeting. The meeting will be held during the week of July 8-13, 2001. We have prepared a full technical program with several special sessions, a variety of short courses and workshops, and a comprehensive array of exhibitors.

The conference will be held at the newly remodeled Sheraton Boston Hotel, located in downtown Boston, convenient to numerous attractions such as Old Ironsides (the oldest commissioned warship in the world); Boston Common and Public Garden, with its Make Way For Ducklings statues; Fenway Park, home of the ever-interesting Red Sox; The Prudential Mall Complex; and world-famous Symphony Hall. The hotel is located 5 miles from Logan International Airport.

Boston is an exciting city, and we have drawn on its many resources to put together an appealing social program with activities for all ages, individuals, families, groups, and tastes. In addition to the Sunday evening Social and the traditional Wednesday Awards Banquet, we have planned Monday evening at the Boston Museum of Fine Arts and a Tuesday evening Boston Harbor Cruise, with a lobster dinner. We are offering daytime bus tours to historic Lexington and Concord, birthplace of our nation; to Salem, Mass, for a visit to the House of Seven Gables, the Salem Witch Museum, and historic Pickering Wharf; and a picnic cruise to George's Island, one of the secret treasures of Boston Harbor. We also provide information on several of the many 'do-it-yourself' tours available, such as the Duck Tour, where you cruise the streets and waterways of Boston in an authentic World War II amphibious vehicle.

I hope your plans for July 2001 include attending the APS/URSI Conference. We have an excellent experience planned for you!

Robert V. McGahan, General Chair
Sensors Directorate
Air Force Research Laboratory
Hanscom Air Force Base Massachusetts 01731-2909

STEERING COMMITTEE

General Chairman

Robert V. McGahan
Air Force Research Laboratory
781-377-2526
mcgahan@ieee.org

Vice Chairman

Jeffrey Herd
MIT Lincoln Laboratory
781-377-4214
herd@ll.mit.edu

Vice Chairman / Student Competition

Robert J. Mailloux
Air Force Research Laboratory
781-377-3710
robert.mailloux@hanscom.af.mil

Technical Program Committee Co-Chairs

Ronald Fante
MITRE Corporation
781-271-5503
rfante@mitre.org

Allen Fenn

MIT Lincoln Laboratory
781-981-7630
ajf@ll.mit.edu

Local Arrangements

Michael Fiddy
University of Massachusetts Lowell
978-934-3306
michael_fiddy@uml.edu

Exhibits / Industrial Liaison

Jonathan Williams
Spike Broadband Systems
781-271-6916
jhwill@ieee.org

Special Sessions

Keith Trott
Raytheon Corporation
978-440-3506
ktrott@ieee.org

Workshops/Short Courses

Hans Steyskal
Air Force Research Laboratory
781-377-2052
hans.steyskal@hanscom.af.mil

Finance Committee

Livio Poles
Air Force Research Laboratory
781-377-4087
livio.poles@hanscom.af.mil

Digest/Publications

Robert V. McGahan
Air Force Research Laboratory
Douglas Drew
Channing Bete Company
Kathleen Ballos
Ballos Associates

Database

Kathleen Ballos
Ballos Associates

URSI Liaison

B. Rama Rao
MITRE Corporation
781-271-6415
br Rao@mitre.org

Call for Papers

Sean Duffy
Pamela Haddad
MIT Lincoln Laboratory

APS AND URSI REVIEWERS

Robert Adams	Robert Mailloux, Student papers
Edward Altshuler	Krys Michalski
Robert Atkins	A. Michelson
Herb Aumann	David Mooradd
S. Balasubramanian	Robert Nevels
Frank Barnes	Eugene Ngai
Gary Brown	David Pozar
Blair Carlson	B. Rama Rao
Richard Davis	Carey Rappaport
Sean Duffy	Dan Schaubert
S. ElGhazaly	Jay Schindler
Ronald Fante, Chair	J. Schoenberg
Alan Fenn, Co-Chair	Mike Shields
John Foster	Gary Somers
Om Gandhi	Hugh Southall
Mark Gouker	Hans Steyskal
Susan Hagness	Ross Stone
Hsui Han	Steve Targonski
Jeff Herd	Lucien Teig
Lisa Hubbard	Keith Trott, Special Sessions
David Jones	P. L. Uslenghi
Peter Kao	E. Westwater
Kris Kim	Frank Willwerth
David Lamensdorf	Jonathan Williams
Min-Chang Lee	Amir Zaghloul
Robert McGahan	

AWARDS

IEEE 2001 Awards

2001 IEEE Electromagnetics Award

Fawwaz Ulaby

Antennas and Propagation Society 2001 Awards

2001 Distinguished Achievement Award

Peter Clarricoats

2001 Chen-To Tai Distinguished Educator Award

Professor Emeritus Ronold W. P. King

2001 S. A. Schelkunoff Transactions Prize Paper Award

Jun-Sheng Zhao and Weng Cho Chew

for their paper "Integral Equation Solution of Maxwell's Equations from Zero Frequency to Microwave Frequencies," October 2000

Honorable Mention for the Schelkunoff Award

Akira Ishimaru, John D. Rockaway, Yasuo Koga, and Seong-Woo Lee

for their paper "Sommerfeld and Zenneck Wave Propagation for a Finitely Conducting One-Dimensional Rough Surface," September 2000

H. A. Wheeler Applications Prize Paper Award

Christophe Granet, Trevor S. Bird, and Graeme L. James

for their paper "Compact Multimode Horn with Low Sidelobes for Global Earth Coverage," July 2000

Honorable Mention for the H. A. Wheeler Award

Wei-Chun Chang, Gregory J. Wunsch, and Daniel H. Schaubert

for their paper "Back to Back Measurement for Characterization of Phased Array Antennas," July 2000

R. W. P. King Award

Filippo Capolino

for the paper "Time Domain Green's Function for an Infinite Sequentially Excited Periodic Line Array of Dipoles," co-authored with Leopold Felsen, June 2000

Honorable Mention for the R. W. P. King Award

Sean M. Duffy

for the paper "An Enhanced Bandwidth Design Technique for Electromagnetically Coupled Microstrip Antennas," February 2000

2001 AP-S/URSI B Awards

Raj Mittra Travel Grant Recipients

Igor V. Ivanchenko , National Academy of Sciences of Ukraine
Ugur Oguz , Bilkent University, Turkey
Yair Shifman , Technion - Israel Institute of Technology

2001 IEEE Fellows

Thomas Giles Campbell

For achievements in theoretical electromagnetics and measurement techniques.

Lawrence Carin

For the development of short pulse scattering techniques to detect objects in clutter that have lead to practical methods for detection of buried land mines.

Daniel De Zutter

For the application of Maxwell's equations and for the development of numerical solution methods in electromagnetic scattering, antennas, and microwave circuits.

Peter S. Hall

For contributions to the development and application of microstrip antennas and active integrated antenna arrays.

Ehud Heyman

For contributions to theory of time domain electromagnetics and of pulsed beam radiation, propagation, and scattering.

Jian-Ming Jin

For contributions to computational electromagnetics and its applications to antennas, radar scattering, microwave circuits, and biomedical technology.

Krzysztof A. Michalski

For the development of numerical solution methods in electromagnetic scattering, antennas, and microwave circuits.

Jaganmohan B.L. Rao

For contributions to array antennas and wide-angle scanning antennas.

Roberto G. Rojas

For contributions to the understanding of high frequency electromagnetic radiation and scattering.

Robert Avery Shore

For contributions to high-frequency scattering theory.

Tadashi Takano

For development of antennas for radio communications and space activities.

Edgeworth Rupert Westwater

For theoretical and experimental contributions to the development of radiometers for atmospheric water vapor and temperature profiling.

EXHIBITORS

Ansoft Corporation	Fractal Antenna Systems, Inc.
Artech House Publishers	GIL Technologies
BAE Systems	IEE/INSPEC
BlueTest AB	L3 ESSCO
ComLab Communications	Nearfield Systems
Comsol	Newnes
CST of America, Inc.	TICRA Fond
EM Software and Systems	John Wiley & Sons, Inc.
EMAG Systems	Zeland Software
Flomerics Incorporated	

CORPORATE SPONSOR

L3 ESSCO
Tuesday Afternoon Break

SHORT COURSES

Genetic Algorithms in Engineering Electromagnetics: Concept, Implementation and Applications, Prof. Yahya Rahmat-Samii, University of California, Los Angeles.

Frequency Selective Surfaces: Theory and Design, Prof. Ben A. Munk, The Ohio State University.

Practical Consideration in the Design of Antennas for Wireless Communication, Dr. Tuli Herscovici, Spike Technologies, Inc.

Wireless Propagation and Smart Antennas, Professor R. Janaswamy, Naval Postgraduate School, Monterey, CA.

EMI/EMC Computational Modeling for Real-World Engineering Problems, Dr. Omar M. Ramahi, University of Maryland, Dr. Bruce Archambeault, IBM.

Engineering Applications of the Fast-MoM and Green's-Function-Based Wavelets, Dr. Ali R. Baghai-Wadji, Vienna University of Technology, Austria.

Fractal Antennas, Prof. Douglas Werner, The Pennsylvania State University.

Smart Antennas and Space-Time Adaptive Processing (STAP), Prof. Tapan K. Sarkar, Syracuse University.

RF MEMS for Antenna Applications, Dr. James R. Reid, Capt. USAF, AF Research Laboratory.

Photonics for Phased Array Systems, Dr. Charles Cox, Dr. Ed Ackerman, Photonic Systems, Burlington, Mass.

Radar Reflectivity of Land and Sea: 1975 to 2000, Dr. Maurice W. Long, Private Consultant.

Microstrip Antennas, Dr. Rod Waterhouse, Royal Melbourne Institute of Technology, Australia.

TABLE OF CONTENTS

Monday Morning

SESSION		TITLE	PAGE
1	APS/URSI B (S)	Historical Overview of Wireless	1
2	APS/URSI B	FDTD Theory I	5
6	APS/URSI B (S)	Future Research Directions in FEM	7
7	URSI B	High Frequency Techniques	13
10	URSI A	Measurements for Material and Field Characterization	25
12	URSI A/B	Dielectric and Lens Antennas	37
13	APS/URSI A/B	Elements and Electronics	49
14	APS/URSI K (S)	RF Coil Design and Simulation for High Field MRI	53

Monday Afternoon

SESSION		TITLE	PAGE
17	URSI B	Numerical Benchmarking	57
18	URSI B	Wideband Antennas	69
19	URSI B	Array Analysis and Design	81
20	URSI B	Scattering	93
21	URSI G (S)	Space Weather: System Effects	105
22	URSI B	Electromagnetic Theory	117
23	APS/URSI B	Propagation Theory	129
24	APS/URSI B	Microstrip Antenna Analysis	131
25	URSI B	Methods for Layered and Stratified Media	133
26	URSI B	Antenna Design Optimization	143
30	APS/URSI B	Antenna Measurements and Calibration	149

Tuesday Morning

SESSION		TITLE	PAGE
32	APS/URSI B (S)	Grand Challenges in CEM	155
34	APS/URSI B	Array Design including Mutual Coupling	165
38	URSI A	Calibration Techniques and Package Structure	177
39	URSI A	Transient and Ultrawideband Measurements	185
41	URSI B	Application of Numerical Methods	191
42	APS/URSI B	Reflector and Feed Designs	203

Tuesday Afternoon

SESSION		TITLE	PAGE
45	APS/URSI (S)	Tribute to Professor R.W.P. King	205
46	URSI A	Wireless Antenna and Base Station Design	213
49	URSI F	Propagation Effects: Satellite and Urban Environment	225
57	URSI B	Rough Surfaces and Random Media	237

Wednesday Morning

SESSION		TITLE	PAGE
58	APS/URSI B	FDTD and Multi-Resolution Methods	249
59	APS/URSI B	Fast Numerical Techniques for Integral Equations	261
64	URSI B	Guiding Structures and Circuits I	265
66	URSI B (S)	Rough Surface Scattering I	277
70	APS/URSI B	Inverse Scattering	285

Wednesday Afternoon

SESSION		TITLE	PAGE
79	APS/URSI B (S)	Fractal Antennas	297
80	APS/URSI B (S)	RF MEMS for Antenna Applications	299
82	URSI H	Space-Based Sounding	303
83	URSI H	Waves in the Ionosphere	309
84	APS/URSI B (S)	Rough Surface Scattering II	313
87	URSI B	Multigrid and Fast Multipole Applications	325
89	URSI B	Novel Time Domain Methods	333
90	URSI D	Distributed and Filter Structures	339

Thursday Morning

SESSION		TITLE	PAGE
91	APS/URSI B	Adaptive Arrays in Communications	347
92	APS/URSI (S)	History of Phased Arrays	349
93	URSI B	Efficient and Higher Order Methods	355
99	URSI B	Guiding Structures and Circuits II	367
103	URSI F	Propagation Modeling	373

Thursday Afternoon

SESSION		TITLE	PAGE
108	APS/URSI B	Complex Media	381
112	APS/URSI B	Frequency and Polarization Diversity	391
113	URSI F	Calibration and Remote Sensing	393
114	URSI B	Frequency and Polarization Diversity	403
118	URSI K	Biology and Medicine	415

Historical Overview of Development of Wireless

Chairs: R. Mailloux, USA and T. Sarkar, USA

	Page
8:00 A Chronology of Developments of Wireless Communication and Electronics from 1831-1920, <i>T. Sarkar*, Syracuse University, M. Salazar-Palma, Universidad Politecnica de Madrid, D. Sengupta, University of Detroit at Mercy</i>	APS
8:20 A Chronology of Developments of Wireless Communication and Electronics from 1921-1940, <i>M. Salazar-Palma*, Universidad Politecnica de Madrid, T. Sarkar, Syracuse University, D. Sengupta, University of Detroit at Mercy</i>	APS
8:40 Early Proposals of Wireless Telegraphy in Spain: Franceso Salva Campillo (1751-1828), <i>J. Romeu*, A. Elias, Universitat Politecnica de Catalunya (UPC)</i>	APS
9:00 Wireless Before Marconi, <i>I. Lindell*, Helsinki University of Technology</i>	2
9:20 Maxwell, Hertz, The Maxwellians and The Early History of Electromagnetic Waves, <i>D. Sengupta*, University of Michigan, T. Sarkar, Syracuse University</i>	APS
9:40 Marconi and the First Microwave Links, <i>O. Ricci, G. Pelosi, S. Selleri*, University of Florence</i>	APS
10:00 A Radioscientist's Reaction to Marconi's First Transatlantic Wireless Experiment – Revisited, <i>J. Belrose*, Communications Resource Centre Canada</i>	APS
10:20 The Authenticity of the "Newman" Notebook and Its Reference to the "Yagi Antenna", <i>S. Usami*, Komazawa Women's University, G. Sato, Antenna Giken Co., Ltd.</i>	APS
10:40 Radar At Fort Monmouth 1940 Through 2010, <i>A. Tarbell*, US Army, W. Kenneally, Mitre Corporation</i>	3
11:00 Antenna Developments of the 1950s to the 1980s, <i>A. C. Schell*</i>	APS

URSA National Radio Society Meeting (Boston), July 2001

Wireless before Marconi

I.V. Lindell

Helsinki University of Technology

P.O. Box 3000, Espoo 02015HUT, Finland

Tel: +358-9-451-2266, e-mail: ismo.lindell@hut.fi

The idea of the telegraph without wires was floating around long before Marconi's basic experiments in 1896, which is generally considered as the year of birth for wireless. In the present paper different ideas and tested possibilities for the resistive, inductive and electromagnetic wireless telegraph are reviewed.

Campillo 1795 resistive telegraphy uses two electrodes in water

The resistive telegraph was suggested in 1838 by Karl Steinheil in Göttingen. He studied the possibility of using railroad tracks to replace the telegraph wires and found that the ground is a good conductor of electricity. The idea was first tested with electrodes submerged in water by Samuel Morse in 1842, and thereafter a number of other scientists, in hopes to find a workable means of communication between ships and stations on the shore under foggy weather conditions.

The inductive telegraph was first seen as a possibility to link a moving train to the telegraph network and a wholly workable system was constructed by Thomas A. Edison in 1885. Successful attempts to connect islands to mainland stations by inductive means were made in the 1890's in Great Britain.

The first experiments leading to the electromagnetic telegraph were made by Joseph Henry in 1842 by observing the current induced to a wire loop by the discharge of a Leyden jar in another wire loop. By simple means he found that the discharge current was actually oscillatory. After Maxwell's theory in 1864 many scientist were attempting to produce 'electromagnetic light', but problems in generation and detection kept the pace slow. Its application to wireless telegraphy became a hot topic only after an article by Sir William Crookes was published in 1892 pointing out the practical significance of electromagnetic waves.

T.L. invented 1729 Stephen Gray in London

*1866 Konis aerial telegraphy - Balise saw charged
by electrodes in air and then discharged*

1880 Polbear electrodeless telephore

1842 Henry first om wave telegraph

*1875 Edison wireless telegraphy "extends
distance"*

URSI National Radio Science Meeting
(Boston), July 2001.

**"RADAR AT FORT MONMOUTH
1940 THROUGH 2010"**

Allan B. Tarbell
US Army,
Communications-
Electronics Command

William J. Kenneally
Mitre Corporation

Since the earliest days of radar, the Fort Monmouth research and development community has been at the forefront of technology, invention, operational system development and deployment. From the SCR-270 [Signal Corps Radar] fielded in Hawaii which provided early warning – albeit unheeded – of the Japanese attack on Pearl Harbor in December 1941 to today's small, but high performance, SAR/MTI systems designed for unmanned aircraft, the stream of technology has resulted in better systems and opened pathways to new capabilities.

This presentation will briefly discuss some of these systems and the technology that made them possible. The key to advances in radar has been both evolutionary and revolutionary through the discovery and development of new components and completely new technologies. This remains true today as component improvements, signal processor hardware, and signal processing algorithms and techniques have dramatically increased radar performance in the past few years.

This success of developing radar systems over the past decades, however, cannot be extrapolated into the future on a 1:1 basis. Along with improved, more capable systems have come, in many cases, prohibitively increased costs. World threats have changed. The US Army is rewriting its "master plan" for future combat systems and the way it fights. This presentation will provide insight into where the Army is likely to go in future radar developments and how cost is limiting the ability to apply the latest technologies to get there.

Secret Radar Lab near Ft. Monmouth
SCR-268 used to assist IR sensor to
do accurate tracking 105 MHz
SCR-270 aircraft detection radar

SCR means Signal Corps Radar, not radar. To be
secret



FDTD Theory I

Chairs: A. Taflove, USA and S. Hagness, USA

	Page
8:00 A Multilevel Subgridding Scheme for Two-Dimensional Finite-Difference Time-Domain Method, <i>C. Chang*</i> , <i>S. Jeng</i> , <i>National Taiwan University</i>	APS
8:20 Modeling of Near-Field Sources in the Finite-Difference Time-Domain (FDTD), <i>M. Potter*</i> , <i>M. Stuchly</i> , <i>University of Victoria</i> , <i>M. Okoniewski</i> , <i>University of Calgary</i>	APS
8:40 Modeling Chiral Media Using a New Dispersive FDTD Technique, <i>A. Akyurtlu*</i> , <i>D.H. Werner</i> , <i>Pennsylvania State University</i>	APS
9:00 FDTD Computation of Dispersive Effects for a Body of Revolution, <i>J. Grando*</i> , <i>ONERA</i>	APS
9:20 FDTD Formulation for Bi-Anisotropic Medium, <i>X. Bao</i> , <i>W. Zhang*</i> , <i>Southeast University</i> , <i>L. Li</i> , <i>The National University of Singapore</i>	APS
9:40 Accuracy Improvement Technique Applied to Non-Uniform FDTD Cells Using High-Order Implicit Scheme, <i>T. Namiki</i> , <i>Fujitsu Limited</i> , <i>K. Ito*</i> , <i>Chiba University</i>	APS
10:00 Efficient Non-Uniform Orthogonal Mesh Generation Algorithm for Cylindrical FDTD Applications, <i>G. Zhou*</i> , <i>Hefei University of Technology</i> , <i>Y. Chen</i> , <i>University of South Carolina</i> , <i>G. Shen</i> , <i>Hong Kong Polytechnic Institute</i>	APS
10:20 A Linear Bicharacteristic FDTD Method, <i>J. Beggs*</i> , <i>NASA/Langley Research Center</i>	APS
10:40 An Implicit LU/AF FDTD Method, <i>J. Beggs*</i> , <i>W. Briley</i> , <i>NASA/Langley Research Center</i>	APS
11:00 A Comparison of the Dispersion Error of Higher-Order Finite-Difference Time-Domain Schemes with Daubechies' Multi-Resolution Time-Domain, <i>K. Shlager*</i> , <i>Space Systems Loral</i> , <i>J. Schneider</i> , <i>Washington State University</i>	APS
11:20 On the Convergence of Simple FDTD Feed Models for Antennas, <i>T.W. Hertel*</i> , <i>G. Smith</i> , <i>Georgia Institute of Technology</i>	APS
11:40 FDTD Analysis of Leaky-Wave Vertical-Cavity Surface-Emitting Lasers, <i>T. W. Lee*</i> , <i>S. Hagness</i> , <i>D. Zhou</i> , <i>L. Mawst</i> , <i>University of Wisconsin-Madison</i>	6

FDTD Analysis of Leaky-Wave Vertical-Cavity Surface-Emitting Lasers

Tae-Woo Lee, Susan C. Hagness, Delai Zhou, and Luke Mawst

Department of Electrical and Computer Engineering
University of Wisconsin, Madison, WI 53706-1691
tae-woo@cae.wisc.edu, hagness@engr.wisc.edu

For many optical communications and signal processing applications, high-power single-transverse-mode operation is desired in vertical-cavity surface-emitting lasers (VCSELs). This remains an unresolved issue in VCSEL design. The lateral dimensions of the VCSEL cavity have been defined by a variety of methods, including the air-post technique, proton implantation, and oxidation to form current apertures. Small-diameter VCSELs provide single-mode operation, but limit the output power to a few milliwatts. Larger diameter VCSELs provide higher coherent output powers, but suffer from multi-mode operation.

A number of theoretical analyses have been conducted in an effort to understand transverse-mode competition. The scalar beam-propagation method and the effective index method have been used effectively for simplified VCSEL structures. Full-vector electromagnetics models, such as cylindrical-coordinate FDTD schemes, are needed to fully understand the complex nature of transverse-mode competition and polarization effects in VCSELs. For this purpose, we have developed an axially symmetric FDTD solver with uniaxial perfectly-matched-layer (UPML) boundary conditions and FFT-Pade linear extrapolation routines.

In this paper, we present an FDTD analysis of a novel antiguiding VCSEL structure designed for achieving single-mode operation. The negative-effective-index guiding structure in the radial direction, referred to as a simplified antiresonant reflecting optical waveguide (S-ARROW), introduces higher lateral radiation losses for the higher-order transverse modes. As a result, these leaky-wave VCSELs may remain single mode at output powers greater than 10 mW (continuous wave).

We have conducted a comprehensive parametric study using FDTD simulations to understand the effects of each design parameter on the modal behavior of the S-ARROW VCSEL. Pulse excitations are used to obtain the frequency response of the cold cavity. This permits the identification of resonant frequencies and quality factors. Sinusoidal excitations are used to identify the mode profile at a given resonant frequency. By analyzing the radiation loss as a function of key structural dimensions, we are able to identify those design parameters which cause the first-order mode to have substantially higher radiation losses than the fundamental mode. Those specific design parameters represent the optimum design for achieving single-mode operation with high output powers.

Future Research Directions in Finite Element Methods

Chairs: J. Volakis, USA and J. Lee, USA

	Page
8:00 A Hierarchical Design Environmental for Coupled Electromagnetic, Thermal, Circuit and System Simulation, <i>Z. Cendes*</i> , <i>Ansoft Corp</i>	8
8:20 Orthogonal Tangential Vector Bases for Rapid Convergence with Multilevel Preconditioned Solvers, <i>D. K. Sun*</i> , <i>Ansoft Corp</i> , <i>J. F. Lee</i> , <i>The Ohio State University</i> , <i>Z. Cendes</i> , <i>Ansoft Corp</i>	9
8:40 Hybridization of Finite Methods with Other Techniques to Solve Complex Problems, <i>R. Lee*</i> , <i>J.F. Lee</i> , <i>P. Pathak</i> , <i>The Ohio State University</i>	APS
9:00 Antenna Design Using Rigorous Hybrid Finite Element Computational Toolsets, <i>J. Volakis*</i> , <i>Z. Li</i> , <i>Y.Erdemli</i> , <i>G. Kiziltas</i> , <i>University of Michigan</i>	APS
9:20 Multigrid Finite Element Methods for Electrodynamc Problems: A Critical Look at their Advantages and Shortcomings, <i>Y. Zhu*</i> , <i>A. Cangellaris</i> , <i>University of Illinois at Urbana-Champaign</i>	10
9:40 Wavelet Based Finite Element Method, <i>G. Pan*</i> , <i>K. Wang</i> , <i>Z. Zhang</i> , <i>B. Techtent</i> , <i>B. Gilbert</i> , <i>Arizona State University</i>	11
10:00 Adaptive Mesh Refinement for Vector Finite Element Methods, <i>J. F. Lee*</i> , <i>R. Lee</i> , <i>The Ohio State University</i>	12

A Hierarchical Design Environment for Coupled Electromagnetic, Thermal, Circuit and System Simulation

Zoltan J. Cendes
Ansoft Corporation
Pittsburgh, PA 15219
zcendes@ansoft.com

Wireless, the internet, pagers, cell phones- the demand for more and better advanced communication systems is constantly increasing. To design these complex high performance systems in a timely manner, new types of simulation tools are required. Since signals at high frequency are primarily electromagnetic in nature, a basic requirement is to model electromagnetic behavior. However, it is insufficient to model electromagnetics in isolation: to understand system operation it is necessary to know how the electromagnetic behavior affects thermal, circuit and system level performance. Thus, a key requirement for new simulation tools is the seamless integration of electromagnetic simulation techniques within the wider context of thermal, circuit and system level simulation. This paper presents a complete hierarchical design environment for the coupled electromagnetic, thermal, circuit and system simulation of communications systems. We begin with a software "desktop" where projects are defined and design goals are identified. System level schematics are produced using system level models, and the components on the system level are refined hierarchically by means of circuit and electromagnetic field simulation. The primary electromagnetic computational engines employed in this environment are the three-dimensional finite element simulation tool Ansoft HFSS and the planar method of moments tool Ensemble®. A new technology called Full-Wave Spice™ is employed to provide efficient, analytical transformations between the electromagnetic and circuit levels. FullWave Spice uses reduced-order models of the dominant poles and zeros of the electromagnetic system to provide broadband fast frequency sweeps and rapid, detailed transient waveforms at the circuit level. Further, the losses computed in the electromagnetic simulation are imported into a three-dimensional thermal simulation program to determine the heating effects and resulting temperature distribution in various system components. The seamless integration of electromagnetic, thermal, circuit and system level simulation provides a complete hierarchical design environment for communication systems.

Orthogonal Tangential Vector Bases for Rapid Convergence with Multilevel Preconditioned Solvers

Din-Kow Sun¹, *Member, IEEE*, Jin-Fa Lee², *Member, IEEE*, Zoltan Cendes¹, *Member, IEEE*

¹Ansoft Corporation
4 Station Square
Pittsburgh, PA 15219

²ECE Department
Ohio State University
Columbus, OH 43212

In 1980, Nedelec defined a set of vector finite element basis functions having the property that their tangential components are continuous across the element boundaries. However, this tangential vector basis set is not unique and can be defined in many ways. This paper suggests that the best choice - indeed the optimal choice - is that basis set which results in the fastest convergence when the resulting matrix is solved by using the conjugate gradient algorithm. The goal of constructing tangential vector bases should therefore be to allow efficient preconditioning, and thus not only reduce the condition number of the system matrix, but eliminate or at least weaken the indefiniteness of the system matrix. We first derive an admissible set of vectors of order p , and decompose this set into two subspaces—rotational and irrotational (gradient). We then reduce the number of vectors by making them orthogonal to all previously constructed lower order bases. The remaining vectors are made mutually orthogonal in both the vector space and the range space of the curl operator. The resulting vector basis functions provide maximum orthogonality while maintaining tangential continuity of the field. The zero order space is further decomposed using a tree-cotree formulation to eliminate convergent problems at extremely low frequencies. This successive orthogonalization is performed on a regular tetrahedron, and is therefore not strictly valid on tetrahedra of arbitrary shape. Empirical results, however, demonstrate that the orthogonality is largely preserved with meshes of arbitrary shape and the resulting global finite element matrix is therefore well suited for solution with the multilevel preconditioned conjugate gradient method (MPCG). Numerical experiments show that number of iterations needed for solution by MPCG is basically a constant, regardless of the order of the basis or of the matrix size. Computational speed is improved by several orders of magnitude due to the fast matrix solution of MPCG and to the high accuracy of the higher order bases.

Multigrid Finite Element Methods for Electrodynamical Problems: A Critical Look at their Advantages and Shortcomings

Yu Zhu and Andreas C. Cangellaris

ECE Department, University of Illinois at Urbana-Champaign
1406 West Green Street, Urbana, IL 61801, U.S.A.

Tel: 217-333-6037; Fax: 217-333-5962; E-mail: (yuzhu, cangella)@uiuc.edu

Finite element methods (FEM) are the methods of choice for electromagnetic analysis of structures exhibiting significant geometric and material complexity. Geometric complexity often leads to FEM matrices of very large dimensions even for structures of moderate electrical size. Thus, iterative methods are utilized for the numerical solution of the FEM system. However, even with the use of some of the most common preconditioners (Y. Saad, *Iterative Methods for Sparse Linear Systems*, PWS, 1996), the convergence of iterative solvers is often unpredictable and deteriorates as the dimension of the FEM matrix increases. This presentation examines the suitability of multigrid methods for improving the convergence of the iterative solution of FEM approximations of time-harmonic electromagnetic problems.

The success of multigrid methods in the efficient solution of finite difference and FEM approximations of elliptic partial differential equations is well documented in the literature. One of the most attractive attributes of multigrid methods is their superior convergence rate irrespective of grid size. However, their application to the FEM modeling of time-harmonic electromagnetic problems has been rather limited (e.g. K. Brackenridge, *Copper Mountain Conf. On Multigrid Methods*, 1993; P. E. Atlamazoglou et al, *IEEE Trans. Antennas Propagat.*, 47, 1071-1079, 1999). The primary reason for this is the less-spectacular-than-anticipated performance of multigrid methods, attributed to the wave nature of the solutions that are approximated. Recent studies have shed light into the various factors that impact the performance of multigrid methods when applied to wave problems, and several approaches are currently under investigation for improved convergence and robustness. It will be shown in this presentation that, once the reasons that have prevented multigrid methods perform effectively in the iterative FEM solution of wave problems are well understood, robust multigrid algorithms can be developed that can be used as effective preconditioners in the iterative solution of large FEM approximations of both scalar and vector electromagnetic boundary value problems. In addition to the detailed presentation of the mathematical formulation and the fundamental steps in the development of an effective multigrid preconditioner, several numerical studies will be presented from their application to the electromagnetic analysis of both two- and three-dimensional scattering and radiation problems. These studies will be used to illustrate the superior convergence attained through the use of the multigrid preconditioners. Furthermore, they will help identify some of the limits of their applicability and motivate the discussion on new ideas and potential research topics toward the further enhancement of the convergence of iterative FEM solvers for time-harmonic electromagnetics.

Wavelet Based Finite Element Method

G. Pan*, K. Wang, Z. Zhang, B. Techentin and B. Gilbert

Abstract

The Finite Element Method (FEM) is one of the most general-purpose numerical methods and has been applied extensively in electromagnetic modeling and simulation. Nevertheless, the basis function in the FEM are essentially Lagrange based interpolation functions. While higher order basis functions improve the numerical accuracy and speed up the convergence, they increased the complexity of the algorithm and bandwidth of the system matrix dramatically, especially the cubic or higher orders are used. Lagrange based interpolation matches only the function at the node (or edge) by linear, quadratic, cubic, etc. polynomials depending on the interpolation order. However, the slope (derivative) and curvature (2^{nd} derivative) have never been matched, no matter how high the order is. Attempts were made to address the slop and curvature by using the splines because of the short support and nice features of splines. Unfortunately, simultaneous system equations in terms of function and derivative values must be solved before the splines can be employed to the FEM. This complicity has rendered too sophisticated, if not impossible to incorporated into the FEM.

Recently advance in wavelets has opened an opportunity to reconsider the problem. We employ the multiwavelets, which have a support of 2, the same as that of 2^{nd} order Lagrange interpolant. In the multiwavelets, the functions, 1^{st} derivative, 2^{nd} derivative are completely uncoupled, resulting in simple and efficient Galerkin based algorithms. As a result, the corresponding system bandwidth is slightly larger than the linear FEM, and is smaller than the cubic ones. Yet, it can matches the function and slope, if the multiplicity is selected to be 2; or match the function, slop and the curvature if the multiplicity is selected 3. Numerical examples demonstrated high efficiency and accuracy. Comparison to previous publications are provided.

Adaptive Mesh Refinement for Vector Finite Element Methods

Jin-Fa Lee* and Robert Lee

The Ohio State University, Department of Electrical Engineering
ElectroScience Laboratory, 1320 Kinnear Road
Columbus, Ohio 43212

E-mail: jinlee@ee.eng.ohio-state.edu Phone: (614)292-7270

When a finite element analyst designs a finite dimensional discretization (the mesh, the order of basis functions for each element), the process usually involves a mixture of experience, intuition, and guesswork. If the results of the finite element approximation appear reasonable then these are accepted; if not, then the discretization is redesigned. The drawbacks of this procedure are obvious. Without an a-posteriori error estimate there is no reliable way to judge the acceptability of the numerical solution. If the analyst's intuition fails when designing the discretization, it is also liable to fail when evaluating the worthiness of the results. Furthermore, if the initial solution is rejected then an entirely new set of data, representing the new mesh, the order of basis functions for the new mesh, must be prepared by the analyst. This is very costly and wasteful procedure without any guarantee that the new discretization is sufficiently accurate. Consequently, the adaptive approach and a-posteriori estimates of the accuracy of the numerical solutions are of great interest recently. However, despite some recent publications on the

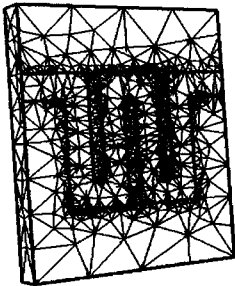


Figure 1: A sample mesh generated using an h-version adaptive mesh refinement.

adaptive mesh refinement in application of vector finite element methods to electromagnetic problems, the basic notions, aims and goals, principles for comparisons etc. are not yet well established.

In this talk, we will review the developments and advancements in the h-, p- and hp-adaptive mesh refinement in the finite element methods. Numerical results using a novel error functional approach, which estimates the reaction of

the error field, will be discussed. At the end, we will also describe our view of what are the major challenges still remain and suggestions for further research.

High-Frequency Techniques

Chairs: R. Burkholder, USA and R. Tiberio, Italy

	Page
8:00 Radiation of a Line Source Located at the Focal Line on the Convex Side of A Hyperbolic Cylinder, <i>P.L.E. Uslenghi*, University of Illinois at Chicago</i>	14
8:20 Formal and Computational Aspects of the Creeping-Ray Problem On a Singly Coated Doubly Curved Convex Surface, <i>P. Hussar*, E. Smith-Rowland, IIT Research Institute</i>	15
8:40 Physical Optics Scattering from a Plane Plate Illuminated by a Gaussian Beam in Terms of a Contour Integral, <i>P. Bolli, E. Martini, G. Pelosi, S. Selleri*, University of Florence</i>	16
9:00 An Efficient Hybrid Technique for Analyzing Scattering from Large Open-Ended Cavities with Complex Cylindrically Periodic Terminations, <i>T. W. Ang*, T. T. Chia, DSO National Laboratories, R. Burkholder, The Ohio State University</i>	17
9:20 Calculation of the RCS from the Double Reflection Between Plane Facets and Curved Surfaces, <i>F. Saez de Adana*, S. Nieves, E. Garcia, I. Gonzalez, O. Gutierrez, M.F. Catedra, Universidad de Alcala</i>	18
9:40 Evaluation of Surface Fields Within the Paraxial Region of a Source Excited Circular Cylinder with an Impedance Boundary Condition, <i>C. Tokgoz*, R. Marhefka, P. Pathak, The Ohio State University</i>	19
10:00 Heuristic Incremental Diffraction Coefficients for Dielectric Screens, <i>A. Toccafondi*, A.Polemi, R.Tiberio, University of Siena</i>	20
10:20 UAPO Diffraction Coefficients for an Anisotropic Dielectric Half-Plane: Oblique Incidence, <i>C. Gennarelli, University of Salerno, G. Pelosi, C. Pochini, University of Florence, G. Riccio*, University of Salerno</i>	21
10:40 A Numerical Comparison of UTD and MoM Solutions for the Scattering by an Object Buried in a Lossy Medium, <i>F. Bertoncini*, University of Pisa, R.G. Kouyoumjian, The Ohio State University, G. Manara, P. Nepa, University of Pisa</i>	22
11:00 Fast Physical Optics (FPO) Algorithms for Multiple Bounce Scattering, <i>A. Boag*, Tel Aviv University, E. Michielssen, University of Illinois at Urbana-Champaign</i>	23
11:20 Cylindrical Luneburg Lens Geometry and Edge Illumination Analysis, <i>A. Boriskin*, A.I. Nosich, The A. Usikov Institute of Radio-Physics and Electronics</i>	24

RADIATION OF A LINE SOURCE LOCATED AT THE FOCAL LINE
ON THE CONVEX SIDE OF A HYPERBOLIC CYLINDER

P. L. E. Uslenghi

Department of Electrical and Computer Engineering
University of Illinois at Chicago

851 South Morgan Street, Chicago, Illinois 60607-7053, USA
Phone: 312 996 6059; Fax: 312 996 8664; Email: uslenghi@uic.edu

It is well known that geometrical optics provides the exact solution for the field scattered by a paraboloid of revolution under axial incidence of the primary plane wave. This remarkable result is valid for a perfectly conducting paraboloid (C. E. Schensted, *J. Appl. Phys.*, 1955) as well as for a penetrable isorefractive paraboloid (S. Roy and P. L. E. Uslenghi, *IEEE Trans. Antennas Propagat.*, 1997). The question arises as to whether a similar result may be established for a two-dimensional problem. Since a paraboloid may be considered as a limiting case of a hyperboloid with one of the foci removed to infinity, the corresponding two-dimensional problem that this work addresses is the radiation of a line source located at the focal line on the convex side of a hyperbolic cylinder.

Very few results are available for boundary-value problems involving hyperbolic cylinders. The only exact result appears to be the field of an arbitrarily located line source on the convex side of a hard cylinder, that was determined by Bloom (1964) as a complicated series of certain special functions (see Bowman et al., *Electromagnetic and Acoustic Scattering by Simple Shapes*, chapter 5. New York: Hemisphere, 1987).

In the present work, the electric or magnetic uniform line source is located at the focal line on the convex side of an infinitely long hyperbolic cylinder. The cylinder is made of either a perfect conductor or a penetrable isorefractive material. The geometrical optics incident, reflected and (if present) transmitted fields are expressed in hyperbolic cylinder coordinates. A determination is made of the accuracy of these fields in representing the exact solution to the boundary-value problem, by substitution of the fields into Maxwell's equations.

**Formal and Computational Aspects of the Creeping-Ray Problem
On a Singly Coated Doubly Curved Convex Surface**

Paul Hussar* and Edward Smith-Rowland
IIT Research Institute
185 Admiral Cochrane Drive
Annapolis, MD 21401

Phussar@iitri.org 410-573-7703 fax: 410-573-7364

Recently it has been demonstrated (P. Hussar and E. Smith-Rowland, 1999 North American Radio Science Meeting, July 11-16, 1999) that an order $k^{-2/3}$ solution for Maxwell's Equations in the vicinity of a convex doubly-curved impedance surface can be obtained by modifying the canonical cylinder solution via an *ansatz* involving pervasive application of a geometrical substitution due to Pathak and Wang (P. H. Pathak and N. N. Wang, *IEEE Trans. Antennas Propag.*, AP-29, pp. 911-922, 1981). The similarity in problem formulation between the case of an impedance surface and the case of a thinly coated surface raises the possibility of the existence of a companion solution for coated surfaces. In this paper we will describe both the formal extension of the earlier result to the singly-coated-surface case, and the computational aspect of the general coated-surface creeping-ray problem, which is the identification and tracking of pole locations that vary with the surface geometry along the creeping-ray geodesic

Construction of an order $k^{-2/3}$ solution for the case of a singly coated surface requires construction of order $k^{-2/3}$ solutions external to and internal to the coating, as well as matching of tangential fields at the outer coating boundary. The external solution is similar in form to the solution for the impedance case, except that the normalized surface impedance and its inverse are replaced by functions of a form adapted from the cylindrical case via our method. The construction of both our external and internal solutions relies on the assumption that the coating thickness is of order k^1 .

Our representation of creeping-ray fields is in the usual form of a series of modes attenuated by exponential factors that involve integrals occurring over the length of the creeping-ray geodesic. Computation of these integrals requires identification of pole locations that apply at each integration point along the geodesic. The pole locations are obtained as roots of an equation that occurs in the canonical cylinder problem, except that the cylinder radius and the geodesic direction with respect to the cylinder axis are replaced by effective values determined from the general convex-surface geometry according to our substitution method. Existing techniques for determining these roots, namely the contour-integral method (B. K. Singaraju, D. V. Giri, and C. E. Baum, *Math. Note 42, Air Force Weapons Lab.*, 1976) and Davidenko's method (K. Naishadham and L. B. Felsen, *IEEE Trans. Antennas Propag.*, 41, pp. 304-313, 1993), are inconvenient in that *a priori* estimation of the root loci is required. We will describe novel strategies by which the roots can be computed both automatically and with a high degree of computational efficiency. These strategies include an intelligent initial contour-integral search and a tracking algorithm that is based on Davidenko's method and follows pole locations under variation of cylinder-radius and geodesic-direction parameters.

Physical Optics Scattering from a Plane Plate Illuminated by a Gaussian Beam in Terms of a Contour Integral

P. Bolli, E. Martini, G. Pelosi, S. Selleri*
Department of Electronics and Telecommunications
University of Florence
Via C. Lombroso 6/17, 50134 Firenze - Italy

Gaussian beams are extremely useful wave objects for modelling directive sources as feeding horns or reflector antennas, since a field expansion in a Gaussian beam series needs much less terms for a given accuracy than, for example, a plane wave expansion. Hence the Physical Optics (PO) analysis of a reflector antenna can be made more efficient by using the former expansion rather than the latter. Scattered field computation requires the evaluation of a surface integral over the PO currents induced all over the object by the incident field.

For perfectly conducting plane scatterers and plane wave illumination the surface integral can be reduced to a line integral over the contour of the plate, which is much faster to compute. This can be done also if the source is an electric Hertzian dipole at a finite distance rather than a plane wave (P.M. Johansen *et al.*, "An Exact Line Integral Representation of the Physical Optics Scattered Field...", *IEEE Trans. Antennas Propagat.*, Vol. 43, No. 7, pp. 689-696, 1995).

On the other hand Gaussian beams can be seen as generated by an isotropic, linear or dipolar source placed in a position identified by complex co-ordinates (A.C. Green *et al.*, "Properties of the Shadow Cast by a Half-Screen when Illuminated by a Gaussian Beam," *J. Opt. Soc. Amer.*, Vol. 69, No. 11, pp. 1503-1508, 1979). The real part of the co-ordinates actually determines position in the real space, while the imaginary part determines width and focusing direction of the beam.

In this contribution the line integral technique, valid for dipole sources in the real space is extended to dipole sources in the complex space, so as to allow for the fast line-integral computation of the PO scattered field also for the Gaussian beam illumination case.

This way both the very efficient Gaussian beam series expansion and the very fast line integral technique are used, resulting in a net reduction of computing cost for the evaluation of the PO scattered field.

An Efficient Hybrid Technique for Analyzing Scattering from Large Open-Ended Cavities with Complex Cylindrically Periodic Terminations

T. W. Ang[†] and T. T. Chia
Centre for Electromagnetics
DSO National Laboratories
20 Science Park Drive, S118230, Singapore

R. J. Burkholder
Department of Electrical Engineering
Ohio State University
ElectroScience Laboratory
1320 Kinnear Road, Columbus, Ohio 43212, USA

Scattering from the interior of a complex jet engines inlet is important as it contributes significantly to the overall radar cross section (RCS) of a modern jet aircraft. Numerical computation of electromagnetic scattering by jet engine inlet is often considered a grand challenge because the geometry of the inlet is both complicated and electrically large. High frequency asymptotic techniques have shown to be accurate and computationally efficient for evaluating the RCS of electrically large cavity that has simple interior geometry. For cavity with complex interior geometry, numerical techniques will be more appropriate as the assumptions used in high frequency method are often no longer valid. However, the computational costs (memory and CPU time) associated with numerical methods to model a large cavity can exceed even the most powerful supercomputer.

In this paper, we will present a hybrid technique based on the iterative physical optics (IPO) method and the integral equation method for analyzing scattering from large open-ended cavities with complex cylindrically periodic termination. The principle of this technique is to split the geometry of the engine inlet into two sub-domains – air intake (front section) and engine termination section, separated by a fictitious surface. As the front section is almost always electrically large with simple interior geometry, a IPO technique employing the forward-backward iterative algorithm with fast far-field approximation for accelerating the surface integration will be used to compute the scattering from this section. For the termination section, an integral equation based on the dyadic Green's function technique for cylindrically periodic terminations is employed. Two forms of periodic Green's function were derived: "completely absorbing" and "completely reflecting". Using this periodic formulation, we need only to model a segment of the engine termination section – which is often electrically large and periodic in geometry. To further reduce the computational costs, a 3-D wavelet transform technique was also applied to obtain sparse impedance matrices that can be efficiently solved by sparse solvers. Finally, a connection scheme employing waveguide modes as expansion function on the fictitious surface is used to obtain the complete scattering from the jet engine inlet. Numerical results generated by the hybrid technique will be presented for realistically large cavities with complex terminations.

**CALCULATION OF THE RCS FROM THE DOUBLE REFLECTION
BETWEEN PLANE FACETS AND CURVED SURFACES.**

F. Saez de Adana , S. Nieves, E. García, I. González,
O. Gutiérrez, M.F. Cátedra
*Dept. Teoría de la Señal y Comunicaciones
Escuela Politécnica, Universidad de Alcalá
28806 Alcalá de Henares. Madrid. Spain
Fax: +34 91 885 6699. E-mail: felipe.catedra@uah.es*

This communication presents a method to obtain the contribution to the monostatic Radar Cross Section (RCS) of the double reflection between plane facets and curved surfaces. This method is applied to arbitrary targets composed by any dielectric and/or magnetic material. The bodies are modeled by using NURBS surfaces.

Although the scattering mechanisms that contribute to RCS of a body are very diverse, the reflection determines in general its shape. However, the scattering mechanisms of higher order like double iterations between different parts of the target, even when they are not so outstanding from a global point of view as the simple reflection, they are not less important because in certain angular margins they can represent a substantial contribution in the RCS of the body. In the past, the double reflection between plane facets has been profusely treated, to analyze dihedral reflectors, whose contribution to the RCS is very important in certain structures. However, the scattered field due to the iteration between a flat facet and a curved surface can also be so considerable as the RCS contribution between two flat facets in other targets. This work allows to evaluate the contribution of these kind of structures.

The method developed is a combination of the Geometrical Optics (GO) and the Stationary Phase Method (SPM). The GO-SPM approach makes possible to obtain the double reflection between a plane facet and a curved surface with arbitrary geometry and position in an efficient way. The reflection in the plane facet is treated using GO applying the Image Theory. In that way, the image currents can be obtained from the induced currents in the curved surface and can be integrated by using the SPM. The curved surfaces are classified in singly and doubly curved. The contribution of stationary phase and boundary segments is considered in the first case and the stationary phase, boundary and vertex points are taken into account in the second one.

Evaluation of Surface Fields within the Paraxial Region of a Source Excited Circular Cylinder with an Impedance Boundary Condition

Çağatay Tokgöz*, Ronald J. Marhefka and Prabhakar H. Pathak

The Ohio State Univ., Dept. of Electrical Eng., ElectroScience Lab.
1320 Kinnear Rd., Columbus, OH, 43212-1191, U.S.A.

It is well-known that the evaluation of the high frequency surface fields by the conventional Uniform Theory of Diffraction (UTD) usually becomes less accurate within the paraxial region of a circular cylinder. In the case of a perfectly conducting (PEC) circular cylinder, the UTD solution for the surface fields was improved to yield better accuracy by including some correction terms (J. Boersma and S. W. Lee, Electromagnetics Lab., Univ. of Illinois, Rep. 78-17, 1978). These correction terms were derived by a method in which a two-term Debye expansion was used to asymptotically represent the Hankel functions in the spectral integral formulation of the relevant surface Green's function for a source excited PEC circular cylinder, and then the spectral integral was evaluated analytically in an exact fashion. In another work pertaining to a more complex situation, an initial and useful attempt was made to describe the high frequency surface fields on a circular cylinder with an impedance boundary condition (IBC) (R. J. Pogorzelski, *Radio Sci.*, 389-399, 1996); these fields were expressed in terms of Fock type integrals which were then evaluated by a numerical scheme. However, more needs to be done to obtain an efficient and sufficiently accurate results within the paraxial region of an IBC circular cylinder, which is the subject of the present work. In this work, a spectral integral formulation for the surface Green's function pertaining to an IBC circular cylinder is expressed in an approximate form by employing a two-term Debye expansion for Hankel functions within the integral. Then, the Green's function is decomposed into two parts; one pertaining to the planar IBC case and the other associated with the correction due to curvature by assuming that the radius of the circular cylinder is sufficiently large. Unlike the treatment for the PEC circular cylinder, the spectral integrals involved in the Green's function are evaluated asymptotically, since an exact analytical evaluation does not appear to be possible because the integrals are substantially more complicated for the case of IBC than is for the PEC case. The solution obtained in this work will be described and some numerical results will be shown for calculating the mutual coupling between conformal antennas on an IBC circular cylinder.

HEURISTIC INCREMENTAL DIFFRACTION COEFFICIENTS FOR DIELECTRIC SCREENS

A. Toccafondi, A. Polemi, and R. Tiberio

*Department of Information Engineering, University of Siena,
Via Roma 56, 53100 Siena Italy,
E-mail: alberto.toccafondi@ing.unisi.it*

High frequency methods have been providing useful tools for treating a variety applications involving antennas operating in the presence of environmental structures. Several practical applications involve large complex dielectric structures; in these cases the assumption of perfect electrical conductor (p.e.c.) boundary conditions (b.c) results in a lack of accuracy in predicting the actual electromagnetic field. Significant examples are found in describing the electromagnetic propagation in urban and indoor environments for mobile and wireless communications.

Within this framework, a thin dielectric half-plane is an important local canonical problem. Simple heuristic high-frequency expressions of a UTD dyadic diffraction coefficient for thin dielectric screens have recently been presented by the authors, which provide a significant improvement with respect to those originally introduced by Burnside (W. D. Burnside, K. W. Burgener, *IEEE Trans. Ant. Prop.*, **31**, 1, 1983). Most noticeably these expressions, that of course provide a uniform description of the field across the shadow boundaries, explicitly satisfy reciprocity and exhibit dominant contributions that at the first order satisfy the b.c. at the faces of the screen.

As occurs in any standard ray method, there are serious difficulties in predicting the field close to and at caustics of diffracted rays. In order to overcome these difficulties it is useful to define local, incremental field contributions to be distributed and then integrated along specific lines on the actual object. In this paper a simple approximate incremental diffraction coefficients for a thin dielectric screen are presented. As was done for extending the UTD, these coefficients, that are now derived in the framework of ITD (R. Tiberio and S. Maci, *IEEE Trans. Ant. Prop.*, **42**, 5, 1996), are obtained by heuristically modifying the formulation, for defining incremental field contributions at the edge of a p.e.c. half-plane. The final incremental dyadic expression exhibits reciprocity, and recovers the known ITD dyadic expression for both p.e.c and p.m.c b.c.. This formulation is applicable at any incidence and observation aspect, and naturally leads to the heuristic UTD ray field representation, when it is applicable. Numerical results will be presented and discussed during the oral presentation.

UAPO DIFFRACTION COEFFICIENTS FOR AN ANISOTROPIC DIELECTRIC HALF-PLANE: OBLIQUE INCIDENCE

C. Gennarelli (1), G. Pelosi (2), C. Pochini (2), G. Riccio* (1)

(1) D.I.I.E. – University of Salerno, via Ponte Don Melillo, 84084 Fisciano (SA), Italy.

(2) D.E.T. – University of Florence, via C. Lombroso, 50134 Florence, Italy.

Abstract.

The high frequency analysis of the scattering by dielectric structures has great importance in electromagnetic theory as well as in many application areas, because of the massive use of these materials in the current technology. In this framework, the scattering of a normally incident plane wave by an anisotropic dielectric half-plane, which is homogeneous and isotropic with respect to the directions parallel and orthogonal to the layer, has been recently considered in (Yazici and Serbest, *IEEE Trans. Antennas Propagat.*, **47**, 1476-1484, 2000). In particular, by modelling the structure as an infinitesimally thin sheet and using the second-order boundary conditions introduced in (Idemen, *Electron. Lett.*, **24**, 663-665, 1988), reflected, transmitted and diffracted field terms are obtained via the classical Wiener-Hopf procedure. The same problem has been tackled in (Gennarelli, Pelosi, Riccio and Toso, *Day on Diffraction 2000*), where a uniform asymptotic Physical Optics (UAPO) solution for the diffraction coefficients has been proposed.

Aim of this work is to extend the aforementioned UAPO solution to the case of an arbitrarily polarized plane wave skewly incident with respect to the edge. According to the UAPO approach, the first step consists in the derivation of a PO approximation for the electric and magnetic surface currents induced in the considered anisotropic structure. This is accomplished by resorting to the second-order boundary conditions introduced by Idemen in order to relate the Geometrical Optics (GO) field to such currents. Then, a uniform asymptotic evaluation of the corresponding radiation integral provides the edge diffracted field, which obviously compensates the GO field discontinuities at the shadow and reflection boundaries.

It must be stressed that the obtained solution for the diffracted field, although approximated, is uniform, accurate, easy to handle and simple to implement in a computer code.

A Numerical Comparison of UTD and MoM Solutions for the Scattering by an Object Buried in a Lossy Medium

F. Bertoncini

Dept. of Electrical Systems and Automation, University of Pisa, Pisa, Italy

R.G. Kouyoumjian

ElectroScience Laboratory, The Ohio State University, Columbus, OH, USA

G. Manara, P. Nepa

Dept. of Information Engineering, University of Pisa, Pisa, Italy

The detection, location and description of buried objects is relevant to remote sensing and geological applications. The Uniform Geometrical Theory of Diffraction (UTD) has been extended and used to calculate the scattering from an object located in a lossy medium. When a plane wave is incident on a plane interface between air and a lossy medium, an inhomogeneous plane wave is excited in the lossy medium. Let this be incident on a polygonal cylinder, which may have a perfectly conducting or impedance surface. The field scattered by the cylinder is of interest for both TE and TM polarizations.

Using uniform edge diffraction coefficients, a UTD solution has been obtained for the field scattered by the polygonal cylinder in a lossy medium of infinite extent. The scattered field is composed of the reflected field and the singly-diffracted field together with the fields of rays doubly- and triply-diffracted from the edges. Calculations of the scattered field are found to be in excellent agreement with those obtained from a Moment Method (MoM) solution of this problem.

Next, the same scatterer located in a lossy half space was treated ray optically, and the presence of the interface was included in the solution (F. Bertoncini *et al.*, *IEEE Trans. Antennas and Propag.*, to appear). Within the lossy medium the total scattered field is the sum of the fields reflected and diffracted from the polygonal cylinder, the field reflected from the interface between the two media and a lateral wave field. In air, the scattered field was determined by a generalization of the physical optics method.

In this paper a MoM solution to the problem is obtained. A special Green's function for the half space occupied by a lossy medium is used to find the relevant integral equation for the currents on the polygonal cylinder. The analysis results in an impedance matrix with two terms. The first term is just the impedance matrix for the scatterer in an unbounded lossy medium. The elements of this matrix have been determined for the comparison mentioned earlier. The second term accounts for the presence of the interface. The currents on the cylinder together with the special Green's function are employed to calculate the scattered field in air and in the lossy medium. These calculations are compared with those obtained from the UTD solution to assess the accuracy of the UTD solution. The excitation of the lateral wave field and the interaction between the scatterer and the interface are of special interest.

Fast Physical Optics (FPO) Algorithms for Multiple Bounce Scattering

Amir Boag*

Department of Physical Electronics
Tel Aviv University
Tel Aviv 69978, Israel

Eric Michielssen

Electrical and Computer Engineering Dept.
University of Illinois at Urbana-Champaign
1406 W. Green, Urbana, IL 61801

High frequency scattering by arbitrary shaped bodies conventionally is analyzed using Physical Theory of Diffraction (PTD) augmented Physical Optics (PO) based schemes. For electrically large scatterers, the computation time is dominated by PO integrations. Analysis of multiple bounce scattering phenomena by conventional PO requires multiple surface integrations that become computationally exceedingly expensive. By necessity, often, all bounces except for the last one are modeled by ray tracing.

In this paper, we present a scheme that permits the numerically efficient evaluation of multiple PO integrals. We target the evaluation of the backscattered field for a contiguous range of aspect angles and frequencies. For simplicity, we analyze a two-dimensional scattering problem dominated by double bounce phenomena involving two surfaces of roughly the same size and separated by a distance comparable to their dimensions. The number of field sampling points on the surfaces is proportional to their electrical dimensions, i.e. of $O(N)$, where $N=kR$, k is the wavenumber, and R the radius of the smallest sphere circumscribing the scatterer. To sufficiently resolve the scattering pattern, the latter should be evaluated at a number of points proportional to the scatterer size. Similarly, the number of frequency points is also of $O(N)$. The proportionality factors implicit in the above estimates depend on the acceptable error level and the specific quadrature rule used, as well as on the desired level of oversampling of the scattering pattern. Thus, the computational cost of a straightforward double PO integration each using $O(N)$ field samples for $O(N)$ far-field directions and $O(N)$ frequencies requires $O(N^4)$ operations. Here, we propose a novel domain decomposition algorithm that aims to lower this cost. We decompose the scatterer surfaces into subdomains and compute the scattering patterns directly for each pair of them. The scattering patterns of the subdomains are evaluated at a smaller number of points and subsequently interpolated, thus providing computational savings. The phase common to all points in a given pair of subdomains is removed from the scattering pattern prior to interpolation. Later, we aggregate these patterns into the overall pattern of the scatterer. The aggregation step involves phase restoration and addition. The domain decomposition algorithm in effect reduces the computational cost of evaluating the double integrals from $O(N^4)$ to $O(N^3)$. A multilevel algorithm is obtained upon starting from pairs of small subdomains, for which the scattering patterns are computed directly, and repeating the aggregation step, while doubling the subdomain sizes. The multilevel algorithm attains an asymptotic complexity of $O(N^2 \log N)$. The proposed technique is directly applicable to the analysis of multi-bounce scattering phenomena.

CYLINDRICAL LUNEBURG LENS GEOMETRY AND EDGE ILLUMINATION ANALYSIS

Artem V. Boriskin* and Alexander I. Nosich

Institute of Radio-Physics and Electronics of the National Academy of Sciences of Ukraine

Kharkov 61085, Ukraine Email: a_boriskin@yahoo.com

The paper studies the effects accompanying the beam transmission through and scattering by a circularly-layered dielectric cylinder. The beam is simulated by the field of a Complex Source-Point (CSP) line current. We concentrate on the Discrete Luneburg Lens (DLL) focusing effect. Dielectric lenses find applications in wide frequency range. LL is a remarkable special case of lens shaped as inhomogeneous dielectric sphere (R. K. Luneburg, *The Mathematical Theory of Optics*, Brown Univ. Press, 1941) or circular cylinder. In the microwave range, lenses are candidate antennas for the wide-band multi-beam and mechanically scanning communication systems (C.A. Fernandes, *IEEE Antennas Propagat. Magazine*, 41, 141-151, 1999).

Analysis and design of LL and other lenses frequently involves a number of approximations that neglect either one or both of two finite parameters: size of the lens and beam width of the source. We use an approach that does not have such drawbacks. An efficient and accurate algorithm is based on the exact series solutions for the field in each layer, addition theorem for cylindrical functions, and recurrent formulas.

The family of curves in presented Figure enables one to optimize the DLL directivity in the case of the fixed geometry of the lens and fixed frequency, by changing only the edge illumination. Here a CSP feed illuminates a DLL in symmetric manner and is placed near to its surface. This is because in the Geometrical Optics approximation the focus is just on the LL surface. One can see that the minimum acceptable number of layers is two, although even a uniform cylinder displays focusing features; the optimal edge illumination is approximately -8 dB. Other results are concerned with the excitation of the Whispering Gallery Modes in DLL. Frequency scans of the directivity show that WGMs undermine the DLL performance but this effect can be smoothed by increasing the number of layers.

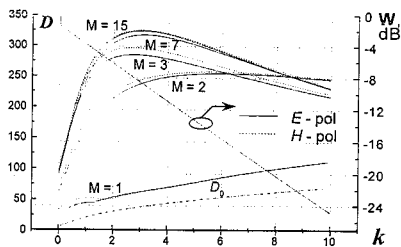


Fig.2 Directivity of LL and the lens edge illumination versus the beam-width parameter
 D_0 is the directivity of CSP in the free space

Measurements for Material and Field Characterization

Chairs: S. Riad, USA and W. Davis, USA

	Page
8:00 Investigation of Different Metallisation Alloys For Planar Antennas on Glass Substrate, <i>M. Bourry*, M. Drissi, National Institute of Applied Sciences, M. Sarret, University of Rennes</i>	26
8:20 Measurements of Thin Radar Absorbing Materials, <i>T. Williams*, M.A. Stuchly, University of Victoria, P. Saville, Defence Research Establishment Atlanta</i>	27
8:40 Fundamental Study of Wave Absorber Using Resistive-Film at 700GHz Band, <i>M. Hanazawa*, Aoyama Gakuin University, Y. Abe, National Defense Academy, O. Hashimoto, Aoyama Gakuin University, Y. Yasuoka, National Defense Academy, K. Wada, Aoyama Gakuin University</i>	28
9:00 Imbedded Antennas for Measurement of the Electrical Properties of Materials, <i>N. Madan*, C. Furse, Utah State University</i>	29
9:20 New Phase Shifter Designs Based on Multilayer Ferro-electric Materials Technology, <i>Z. Zhang*, Y. Muralidhar, M.F. Iskander, Z. Yun, University of Utah</i>	30
9:40 Optimized Resistive Dipoles for Field Strength Measurements, <i>J. Waldmann*, J. Kantz, F. Landstorfer, University of Stuttgart</i>	31
10:00 Test Zone Field Compensation Using Planar Data, <i>P. Rousseau*, The Aerospace Corporation</i>	32
10:20 Prediction of Shielding Degradation Arising from Variation in Contact Impedance of Inter-Metallic Junctions, <i>L. Li*, O. Ramahi, University of Maryland – James Clark School of Engineering</i>	33
10:40 Detection of Chafed Insulation in Aging Aircraft Wiring, <i>B. Waddoups*, C. Furse, Utah State University</i>	34
11:00 Passive Intermodulation on Large Reflector Antennas, <i>P. Bolli*, P. Pelacchi, G. Pelosi, S. Selleri, University of Florence</i>	35

INVESTIGATION OF DIFFERENT METALLISATION ALLOYS FOR PLANAR ANTENNAS ON GLASS SUBSTRATE

M. BOURRY*, M. DRISSI, M.SARRET(**)

Laboratoire de Composants et Systèmes de Télécommunications (LCST) of the
National Institute of Applied Sciences (I.N.S.A), Rennes, FRANCE

(**)Groupe de Microélectronique et Visualisation (G.M.V), from University of
Rennes, France

E-mail:mbourry@insa-rennes.fr

Recent technological advances in planar antennas are facilitating their integration in the environment. The performances of transparent conducting oxide alloys (TCO) on glass substrate have progressed to the point where they are seriously being considered for WLAN and teletoll applications. It offers the advantage of transparency and the size/weight of the antenna is not any more a problem.

The present paper treats different alloys made of Indium tin oxide (ITO) deposited by magnetron sputtering. This material is known as a binary TCO with a low absorption coefficient, a good conductivity in the TCO family and it has a lot of others advantages as good hardness and low toxicity.

The studied microstrip structures are made on a boro-silicate glass substrate used for the LCD display systems, the size of the substrate is 2 inches square and its thickness is 1.1 mm. Its relative permittivity is 5.74 and the loss tangent is around 0.0036.

The stability of the metallisation layer during the process for each condition of deposition and their interests in term of cost have been studied. It concerns the conductivity and the crystallographic structure of the different alloys versus conditions of deposition and any optical properties. The required designs are shaped by the photolithography of the resist. The metallisation layer is then etched under hydrogenated plasma (RIE).

The developed process is used to realise microstrip line resonators and planar antennas. The scattering parameters and the Q factor resonator have been measured and will be presented. The obtained intrinsic losses will be evaluated for several deposition conditions. Finally, the far field characteristics of the realised antenna with the different alloys will be discussed.

Measurements of Thin Radar Absorbing Materials

T. Williams¹, M. A. Stuchly¹ and P. Saville²

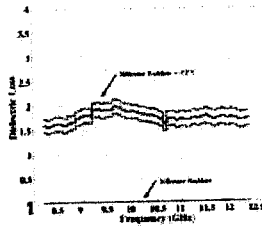
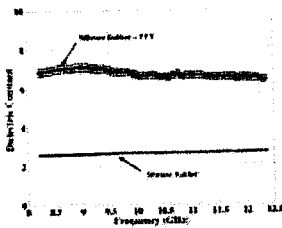
¹Department of Electrical and Computer Engineering, University of Victoria
P.O. Box # 3055, Stn. CSC, Victoria, BC, V8W 3P6, Canada
Email: william@ece.uvic.ca

²Defence Research Establishment Atlantic, Dockyard Laboratory (Pacific)
CFB Esquimalt, PO Box 17000 Stn Forces, Victoria, B. C. V9A 7N2

New organic polymer-based materials are being developed at the Department of National Defense in Canada to be used as radar absorber in tile configuration. Since these materials are thin, less than 1 mm, there is a need for new measurement techniques to facilitate accurate and easy determination of the electrical properties. Previously, many procedures have been used to measure the complex permittivity and permeability of materials in X-band waveguide. Traditional problems encountered with thin samples include difficulty with accurate initial sample positioning, and maintaining the sample in place. Typical measurements with Vector Network Analyzer (VNA) have large errors at the frequencies at which test sample length is a multiple of a half wavelength.

In this work, the method of measurement employs a two-layer structure within the waveguide: a thin unknown material to be measured is supported by a material of known properties. The unknown material thickness is not variable, but the thickness of the two-layer structure can be arbitrarily selected and thus the measurement accuracy can be increased. Sample placement is no longer an issue, as the two-layer structure has adequate thickness to remain immobile. Two measurement of the two-layer structure have been explored. One method incorporates the known sample into the measurements. The other method uses the calibration of the VNA to eliminate the known layer. Because both reflection and transmission data are collected, the one with the highest accuracy can be used solely when non-magnetic materials are measured.

To obtain the complex permittivity and permeability of the unknown sample, two differing optimization methods are used, namely a Gauss-Newton least squares routine (Jarvis, 1992) and genetic algorithms. The procedure converges to a low-order polynomial representation of a single/multi-term Debye model because of the limited frequency range of the X-band waveguide, and the relaxation of the material typically is outside the test frequency range. Proper configuration of constraints ensures the causality principle. Below the permittivity data and measurement uncertainty are shown for the template material and one new material.



Fundamental Study of Wave Absorber Using Resistive-Film at 700GHz Band

Masahiro Hanazawa † Yasuhiko Abe ‡ Osamu Hashimoto †
Yoshizumi Yasuoka ‡ Kouji Wada †

†Aoyama Gakuin University
6-16-1 Chitosedai, Setagayaku,
Tokyo, 157-8572 Japan
Tel. & Fax. : +81-3-5384-1121

‡National Defense Academy
1-10-20 Hashirimizu, Yokosuka,
Kanagawa, 239-8686 Japan
Tel. : +81-468-41-3810 Fax. : +81-468-44-5903

E-Mail : hana@ee.aoyama.ac.jp, yasube@cc.nda.ac.jp, hasimoto@ee.aoyama.ac.jp,
yasuoka@cc.nda.ac.jp, wada@ee.aoyama.ac.jp

Abstract

Many types of electromagnetic(EM) wave absorbers have already been realized. Furthermore, we have investigated variations $\lambda/4$ EM wave absorbers using resistive films at microwave and millimeter-wave bands[1]. The good performances such as high absorption, frequency flexibility and high transparency were obtained by proposed absorbers[2]. Recently, utilized frequency bands for EM wave applications are shifted to the high frequency region such as the sub-millimeter wave band. Some of applications for sub-millimeter wave band, i.e., antenna, filter, and active circuit have been presented for future use[3].

In the present paper, we propose a 700 GHz band wave absorber using Indium Tin Oxide(ITO) resistive-film. The wave absorber consists of spacer(Poliethilen Telephthalate:PET), absorption film (ITO) and reflection film(aluminum evaporation film). Figure 1 shows a schematic model of the proposed wave absorber. The absorber design is performed by using the transmission line model. We actually fabricated the wave absorber with ITO film using the designed values. The theoretical and measured results of absorption characteristics of the absorber are shown in Fig.2. It was confirmed that the peak absorption of about 15dB was obtained.

We plan in the near future to establish the improved designed procedure of the absorber including value of surface resistance, dielectric constant of PET at 700GHz.

References

1. O. Hashimoto, T. Abe, Y. Hashimoto, T. Tanaka, and K. Ishino, "Realization of Resistive-Sheet Type Wave Absorber in 60 GHz Frequency Band," Electronics letters, Vol.30, No.8, pp.657-658 (1994).
2. K. Takizawa and O. Hashimoto, "The Transparent Wave Absorber Using Resistive Tin Film at V-band Frequency," IEEE Trans. Microwave Theory and Techniques, Vol.47, No.7, pp.1137-1141(1999).
3. P.F. Golden et al, "Focal Plane Image System for Millimeter Wavelengths," IEEE Trans. Microwave Theory and Techniques. Vol.43, No.10 pp.1664-1675(1993).

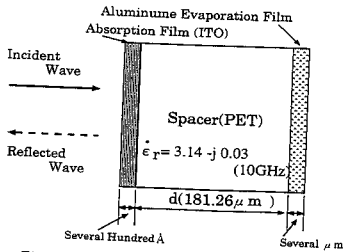


Fig.1. Schematic model of wave absorber

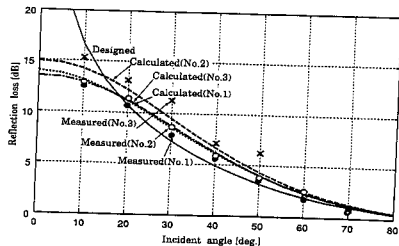


Fig.2. Absorption characteristics

Imbedded Antennas for Measurement of the Electrical Properties of Materials

Nitin Madan, Cynthia Furse

Department of Electrical and Computer Engineering
Utah State University
Logan, Utah 84322-4120
Phone: (435) 797-2870
FAX: (435) 797-3054
Furse@ece.usu.edu

Abstract

The electrical properties of materials (electrical permittivity and conductivity) are of great interest in a myriad of applications. These include measurement of moisture of soil, grain and wood, fat content of meat, dairy and food products, composition of the ionosphere, electrical properties of human tissues and phantoms used to simulate them, ripeness and quality of produce, geological mapping for geophysical prospecting, and numerous measurements of chemical composition.

This paper describes the response of five types of microstrip antennas to a lossy dielectric layer of corn kernels. The antennas are shaped as a spiral, a serpentine, a dipole, a rectangular patch, and a capacitive gap. The effect of size, feedpoint and ground pin location, substrate material and thickness, superstrate material and thickness, and other antenna parameters on the sensitivity of these antennas to varying electrical properties of the material above the antenna is given. The resonant frequency and complex antenna impedance are considered in order to determine antenna configurations that are most sensitive to variation in the changes in electrical properties.

The ground pin on the spiral and serpentine antennas roughly doubles their electrical length by acting as a pseudo ground plane. A layer of material placed on top of the serpentine, spiral, dipole, and patch antennas increases their electrical length (decreasing the resonant frequency), damps out the resonance (decreasing the real part of the impedance), and eventually (when the material is sufficiently high dielectric or conductivity) changes the antenna from a radiating structure to a simple capacitor or inductor (real part of the impedance very small). The antenna is effectively "shorted out" by the material above it. A patch antenna with a gap, on the other hand, is operated well below the resonant frequency. Its capacitance (measured as input impedance) is changed by the fringing fields across the gap as they pass through the material under test that is placed on top of the patch.

Specific relationships between the antennas and superstrate materials were found using numerical simulation methods. These relationships were verified by testing four prototype antennas with a variety of superstrate materials. The spiral and serpentine antennas were found to be the most sensitive to the superstrate materials. The dipole antenna was considered to be impractical because of its long length. The patch antenna

New Phase Shifter Designs Based on Multilayer Ferroelectric Materials Technology

Zhijun Zhang,* Muralidhar Y., Magdy F. Iskander, and Z. Yun
Electrical Engineering Department
University of Utah
Salt Lake City, UT 84112

Abstract

Filters, phase shifters, and phased antenna array designs that are based on MicroElectroMechanical (MEMS) devices have recently received considerable attention. The low cost, high performance, and successful operation at higher microwave and even millimeter-wave frequencies have certainly sparked a significant research activity in this area. Ongoing research activities continue to address remaining limitations of the MEMS technology including the required relatively high biasing voltage, stiction, dielectric breakdown, packaging, limited capacitance tunability, and lower Q inductors for filter designs. Ferroelectric materials, on the other hand, are characterized by change in permittivity with applied dc bias voltage. This change in permittivity can be used to change the electric length of a transmission line and hence in the design of low-cost phase shifters. Integrated use of Ferroelectric materials with other technologies such as the Continuous Transverse Stubs (CTS) technology may also result in the development of novel low-cost phased antenna arrays and filter designs.

A commonly used Ferroelectric material in this application is $\text{Ba}_x\text{Sr}_{1-x}\text{TiO}_3$ (BSTO) and recent advances in the development of these materials have resulted in lowering the dielectric constant (~ 100), decreasing the loss tangent ($\tan\delta < 0.0009$), and in a significant increase in tunability as well as reduction in sensitivity of the material to temperature variations. It is, however, generally felt that microwave device designs based on this technology still exhibit high insertion losses. Much of these losses are related to the conductor losses that result when the devices are loaded with these high dielectric constant Ferroelectric materials. Therefore, it is important that besides lowering the loss tangent in the Ferroelectric materials, say, by Mn doping, and in addition to reducing the sensitivity to temperature variation through baseline biasing, new phase shifting designs be developed to overcome the insertion loss limitations.

In this paper, we describe new phase shifter designs that are based on the use of the Ferroelectric materials technology. The novel aspect of the design procedure is related to the use of multilayer dielectric materials including a highly tunable Ferroelectric material. This method of using multilayer dielectric materials leads to the confinement of the electromagnetic energy predominantly in the high dielectric constant Ferroelectric material and away from the conductor, thus significantly reducing the conductor losses. In addition, the multilayer dielectric material structure is designed in such a way so as to increase the input impedance of the device and hence further contribute to the reduction in conductor losses. Results from simulation studies including parallel plate, coplanar, and microstrip transmission line geometries will be described and advantages and limitations of each of these designs will be discussed. The effectiveness of the proposed multilayer dielectric approach in reducing insertion losses will be evaluated in each geometry, and its impact on the achievable tunability will be quantified. For the parallel plate transmission line structure, it is shown that insertion losses may be reduced by a factor of one hundred when a multilayer arrangement is used (two layers of air, $\epsilon_r = 0$, are placed on both sides of the Ferroelectric material of $\epsilon_r = 416$). Specifically, the normalized value of the insertion loss (relative to the case of a fully loaded line with Ferroelectric material) varied from 0.11% for Ferroelectric materials with $\epsilon_r = 416$ to 18% when $\epsilon_r = 100$, respectively. In the simulated cases, the frequency was 30 GHz and the top and bottom layers of low dielectric materials considered were air of thickness 0.02mm. It is also shown that the coplanar design presents an advantage of higher input impedance even when loaded with the high ϵ_r material, and hence is easier to match and integrate with conventional microwave circuits. For a coplanar line, however, the proposed multilayer dielectric loading results in a significant loss in tunability. The multilayer design showed minimal effect (15%) on the tunability when applied to the parallel plate transmission lines. Other drawbacks of this design, however, include unacceptably low input impedance as compared to a coplanar waveguide, as well as difficulties in the feeding arrangement. In contrast to the coplanar and parallel plate transmission line phase shifters, designs based on microstrip lines present a middle ground and a compromise between the input impedance and the tunability values. These results, as well as results illustrating the impact of the biasing circuit on the insertion losses, will be described in the presentation.

Optimized Resistive Dipoles for Field Strength Measurements

Jan Waldmann, Julia Kantz, Friedrich Landstorfer

Institute for Radio Frequency Technology - University of Stuttgart
Pfaffenwaldring 47 - D-70550 Stuttgart - Germany

1. Principle of Measurement – Resistive Dipoles

Usually probes for the measurement of electric field strengths between 10 MHz and 10 GHz are designed for flat frequency response. In order to cover a large frequency band, lossy dipole structures are used which provide adequate damping of the inevitable dipole resonances. Fig. 1 shows the optimum resistance per unit length along such a dipole for a flat frequency response.

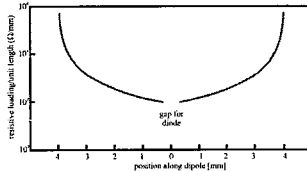


Fig.1: Typical resistive loading for flat frequency response probe

2. Safety Limits

Safety standard levels as issued e.g. by IRPA or FCC define a limit of the electrical field strength up to which the exposure of humans to these fields is considered safe. These field strength limits for various reasons (penetration depth, body resonances etc.) are frequency dependent. In order to be able to relate field strengths determined with a flat-response probe to the according safety limits, the frequency of the measured signal has to be identified. In case this information is not available, or the spectrum of the measured signal contains more than one frequency, the safety status cannot be determined with a single measurement.

3. Optimized Resistive Dipoles for On-Measurement Evaluation of Safety Status

Weighting the signal of the field strength probe with the inverse of the safety limit results in an output voltage which remains constant over frequency, if the field strength measured corresponds to a constant percentage of the frequency-dependent safety limit.

Thus the safety status can easily be checked with one measurement. The necessary "weighting" can approximately be achieved by an appropriate resistive loading of the probe dipoles. Using numerical computations based on the Method of Moments, the resistive loading according to Fig. 2 was varied and optimized. The detector circuitry has been considered in the computations

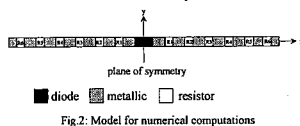


Fig.2: Model for numerical computations

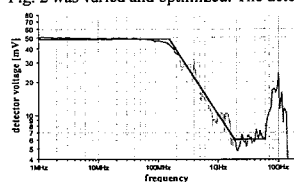


Fig.3: Measurement result of shaped dipole

only as far as the linear components are concerned while the non-linear diode was approximated by its junction capacitance of $C_j = 0.2$ pF, only. The result of the optimization process in terms of the frequency response of the probe is given in Fig. 3. The output voltage for constant field strength follows nicely the safety limits. On this basis a personal radiation hazard monitor can be designed whose output directly displays the measured field strength related to the safety limit.

Test Zone Field Compensation Using Planar Data

Paul Rousseau
The Aerospace Corporation
El Segundo, CA

When the patterns of an antenna are measured in real time in a test facility (such as a far-zone range, a tapered chamber, or a compact range), the quality of the test facility is often judged by how well the test zone field (TZF) matches that of an ideal plane wave. The ideal plane wave has a flat amplitude and phase response over a planar surface. Unfortunately, all test facilities have a TZF that is not a perfect plane wave because of various errors, such as room scattering, cable leakage, or imperfections in the source antenna. Over the years, various algorithms for processing the measured data to correct for the errors in the TZF have been proposed. One of the most general approaches, which takes advantage of existing spherical near-field computational algorithms, was developed by Donald Black and Ed Joy (D. N. Black and E. B. Joy, *IEEE Trans. Ants Prop.*, 362-368, April 1995). In their approach, they use a small rotationally symmetric probe to measure the TZF over a spherical surface. Then the TZF is expanded into a spherical mode expansion (SME). The antenna under test (AUT) is also measured in a spherical coordinate system. The measured response of the AUT may be written as a superposition of the product of the AUT SME coefficients and the TZF SME coefficients. Using this formulation, and given the SME coefficients of the TZF, it is possible to solve for the AUT SME coefficients and thereby obtain the AUT far-zone patterns. Black and Joy's method works well when the TZF is characterized on a spherical surface using the probe on a spherical positioner. However, it is more common for the TZF to be characterized by probing the field on a planar surface. This is done because it is much more direct to judge the quality of the TZF compared to a perfect plane wave when the TZF probe is scanned over a planar surface.

An algorithm is presented to compute the TZF SME when data is given from a probe that is scanned over a planar surface. This allows one to then utilize the method of TZF compensation developed by Black and Joy even when the TZF is characterized only over a planar surface. Several numerical examples are presented to validate the method, where the AUT is modeled as an array of elemental current sources. In the examples, the TZF is generated using a primary source plus interfering sources. For some test cases, the interfering source is cross polarized to demonstrate the ability to compensate for relatively high cross-polarization levels in the TZF.

Prediction of Shielding Degradation Arising from Variation in Contact Impedance of Inter-metallic Junctions

Lin Li and Omar M. Ramahi
Calce Electronic Products and Systems Center
Mechanical Engineering Department
James Clark School of Engineering
University of Maryland
College Park, MD 20742
oramahi@calce.umd.edu

A major task of EMI shields is to maintain shielding effectiveness through proper enclosure design. In most cases, separable connections are necessary in shielding enclosure design, and consequently, inter-metallic junctions are introduced as a result of the use of gaskets, connectors, internal compartments, and ventilation panels in an enclosure. When two dissimilar metals are brought in contact with each other, there is a risk of corrosion. Since the shielding effectiveness of an enclosure depends on good electrical conductance and low-impedance paths across the metallic junctions, corrosive residues at these junctions could change the impedance, and subsequently, degrade the shielding performance of enclosure. The surface current flowing along the enclosure surface could be diverted and forced to flow through a different and unintended path that may have a larger loop area. As a result, higher emissions can be produced. Any slots or seams located in this unintentional current path may also be excited and produce higher emissions. This phenomenon is called corrosion-induced electromagnetic interference (CI-EMI). Furthermore, the increased impedance at junctions due to the corrosive residue increases the voltage drop at these junctions resulting in higher external radiation.

Zinc-coated steel enclosures with fingerstock-type gaskets made of beryllium copper, phosphor bronze, or stainless steel are most widely used in system-level shielding. Previous studies on this type of EMI shielding enclosures reported the CI-EMI observations in products during EMI regulatory testing, showing inconsistency in the radiated emission measurements and shielding degradation for various computer platforms within a short period of time.

In this work, we present experimental results showing the change in gasket impedance when subjected to harsh environmental conditions. Using numerical simulation, we show that the shielding effectiveness is highly dependent not only on the impedance of the gasket but also on the frequency and polarization of the internal excitation. Finally, we develop a numerical model to correlate the change in contact impedance to fields radiated external to the enclosure.

Detection of Chafed Insulation in Aging Aircraft Wiring

Brent Waddoups, Cynthia Furse

Department of Electrical and Computer Engineering
Utah State University
Logan, Utah 84322-4120
Phone: (435) 797-2870
FAX: (435) 797-3054
Furse@ece.usu.edu

Abstract

The degradation of electrical cabling and wiring in modern aircraft and spacecraft is a growing problem in the aerospace industry. Several in flight aircraft failures have been directly linked to problems caused by faulty wiring. The faults in the wiring can take many forms from miniscule cracks in the wiring insulation to short or open circuit conditions due to exposed or broken wiring. The possible loss of life and equipment associated with these problems is driving the industry to seek ways to detect and repair cabling faults before a catastrophic failure occurs.

Utah State University has developed a miniaturized low cost frequency domain reflectometer (FDR) device that may be integrated into an electrical cable connector and is capable of detecting and analyzing open and short-circuited wires. The FDR uses a stepped frequency routine to determine cable lengths and then compares the calculated cable lengths with a known good baseline cable tree and determines where open or short circuits may be found in a cable tree. The frequency range that the FDR can utilize to obtain the cable lengths is largely arbitrary and it is thought that a frequency set may be found that could not only detect open and short circuits, but cable insulation degradation as well.

This paper investigates the use of a time domain reflectometer (TDR) for detecting cable insulation degradation. In order to test the efficiency of the TDR in detecting cable insulation degradation the following procedure was used. Two sets of test wiring were selected from aircraft wiring available to Utah State University from NAVAIR. The first set of wiring was a control set used to obtain TDR signatures of wires that have no faults in them. The second set of wires, identical in length and composition to the first, was used as test wires. The second set of wires, or test wires, had a variety of simulated cable insulation degradation faults imposed upon them. The degradation faults ranged from a single slice in the insulation to a 2 cm section of insulation being cut away. The faults were exposed to various environmental conditions and TDR signatures were obtained for each test condition.

The TDR responses for the test wires under various conditions were then compared to the TDR responses for the control wires to determine how the degradation faults affected the TDR responses of the test wires. The comparison of the control wires and test wires was done both by visually inspecting the TDR responses of each and mathematically evaluating the responses. The mathematical evaluation of the response involved performing a Fourier Transform on the time domain data obtained from the TDR unit. By taking the difference in the magnitudes of the control wires and test wires and plotting that difference against the frequency spectrum of the FFT it is possible to determine critical frequencies of operation for the FDR unit already constructed by Utah State University. Several other types of faults in real aircraft-type cables are presented, from tests made with the NASA cable test sets.

Passive Intermodulation on Large Reflector Antennas

P. Bolli*, P. Pelacchi, G. Pelosi, S. Selleri
Department of Electronics and Telecommunications
University of Florence
Via C. Lombroso 6/17, 50134 Firenze - Italy

In this contribution an Electromagnetic Compatibility (EMC) problem that may occur in large antenna reflector is analysed. This kind of antenna are usually made up by several curved plates joined together. In previous works it has been shown how junctions between different metals or between two plates of the same metal can exhibit non-linear behaviours (P. Bolli *et al.*, "A Time Domain Physical Optics Approach to Passive Intermodulation Scattering problems," *IEEE AP-S Symposium*, Orlando, 11-16 July 1999 pp. 2018-2021). This implies that, when such a junction is illuminated by an electromagnetic radiation, intermodulated frequencies may be present in the scattered field. This phenomenon is known as Passive Intermodulation (PIM) and may give rise to EMC issues. For example if the signal to be detected is very faint, as in radioastronomy, strong noise signals even if at different frequencies can generate PIM components which could significantly spoil the signal.

In the aforementioned paper an heuristic technique was presented to take into account such phenomenon. The method chosen to investigate the PIM is the recently presented Time-Domain Physical-Optics (TD-PO) (E.Y. Sun *et al.*, "Time-Domain Physical-Optics," *IEEE Trans. Antennas Propagat.*, 42, pp. 9-15, 1994); this choice is bound to the requirements to find an high frequency, current-based and time-domain method. The former requirement is due to the largeness of the reflector, the latter to the non-linear nature of the PIM problem. The approach was used to analyse a planar square plate with a straight soldering. This test case was also validated thanks to a comparison with measures provided by Alenia Spazio Co., Rome.

In the present contribution the canonical problem of a planar plate is extended to a three-dimensional reflector antenna structure; where multiple junctions in radial and azimuth direction are present. Furthermore the heuristic model is enhanced by introducing also an equivalent magnetic current in the neighbourhood of the junction, besides the physical electric current, both of which are obtained as a non-linear function of the incident fields. Both the antenna far-field and near-field can be computed.

Finally it will be shown the comparison between the same reflector antenna with and without junctions; it is possible to predict that the main issue of such junctions would be both the signal degradation due to off-band noise and the presence of the intermodulated cross-polarised signals.

Dielectric and Lens Antennas

Chairs: A. Neto, USA and S. Maci, Italy

	Page
8:00 Green's Function for EM Field in a Microstrip Environment with Imperfectly Conducting Walls Using a Hertzian-Potential Impedance Boundary Condition, <i>M. Havrilla*, D. Nyquist, Michigan State University</i>	38
8:20 Gain Enhancement of a Dielectric Resonator Antenna Using A Finite Size Superstrate, <i>A. Ittipiboon*, A. Petosa, R. Siushansian, Communications Research Centre</i>	39
8:40 Analytical Solution for Gap-Excited, Leaky Slot Antenna Printed at the Interface Between Two Semi-Infinite Dielectrics, <i>A. Neto*, California Institute of Technology/JPL, S. Maci, University of Siena</i>	40
9:00 A 3-Beam, MEMS-Actuated, Leaky Wave Antenna, <i>A. Zaman*, R. Lee, NASA Glenn Research Center</i>	41
9:20 Radiation from an Arbitrarily Oriented Hertzian Dipole Over Two-Layered Anisotropic Medium with a Tilted Optic Axis, <i>A. Eroglu*, J.K. Lee, Syracuse University</i>	42
9:40 An Approximate Green's Function for a Finite Grounded Dielectric Slab, <i>L. Alatan*, O. A. Civi, Middle East Technical University, G. Ogucu, University of Gaziantep</i>	43
10:00 Using Scattering Data to Estimate the Radiation Characteristics of Spherically Symmetrical Lenses, <i>A. Parfitt*, N. Nikolic, CSIRO Telecommunications & Industrial Physics</i>	44
10:20 An Improved Evaluation of Radiation Pattern for Dielectric Lens Antennas, <i>D. Pasqualini*, F. Capolino, A. Toccafondi, S. Maci, University of Siena</i>	45
10:40 The Dome-Like Fresnel-Zone Antennas, <i>H. Hristov*, R. Feick, Universidad Tecnica Federico Santa Maria</i>	46
11:00 Analysis of Performance of a Class of Broadband Geodesic Lens with Steering Capabilities, <i>L. Sampaio*, L. Costa da Silva, Catholic University of Rio de Janeiro</i>	47
11:20 2-D Model of an Arbitrary-Shaped Dielectric Rod Antenna, <i>A. Boriskin*, A.I. Nosich, The A. Usikov Institute of Radio-Physics and Electronics, A. Altintas, Bilkent University</i>	48

Green's Function for EM Field in a Microstrip Environment with Imperfectly Conducting Walls using a Hertzian-Potential Impedance Boundary Condition

Mike Havrilla* and Dennis Nyquist

Department of Electrical Engineering
Michigan State University
East Lansing, MI 48824

Transmission line structures having metallic boundaries can exhibit significant losses at high operational frequencies if the conductors are imperfect. A common example is the microstrip transmission line structure. The purpose of this paper is to develop the EM field Green's function for a general three-dimensional current immersed in a microstrip background environment having an imperfectly-conducting ground plane.

The above Green's function can be identified by investigating the solution of the Hertzian potential Helmholtz equation $\nabla^2 \vec{\pi} + k^2 \vec{\pi} = -\vec{J} / j\omega\epsilon$ subject to continuity of the tangential electric and magnetic fields at the air/dielectric interface and the impedance boundary condition $\vec{E}_{\text{tang}} = Z_m \hat{n} \times \vec{H}_{\text{tang}}$ at the imperfectly-conducting ground plane. The vector \hat{n} is the unit normal pointing out of the conductor and $Z_m = (1 + j)\sqrt{\omega\mu_0 / 2\sigma}$ is the surface impedance of the ground plane. Using $\vec{E} = k^2 \vec{\pi} + \nabla(\nabla \cdot \vec{\pi})$ and $\vec{H} = j\omega\epsilon \nabla \times \vec{\pi}$, it will be shown that the impedance boundary condition in terms of Hertzian potentials can be written as

$$\pi_x = \pm \frac{1}{\sigma Z_m} \frac{\partial \pi_x}{\partial y}, \quad \pi_z = \pm \frac{1}{\sigma Z_m} \frac{\partial \pi_z}{\partial y}, \quad \frac{\partial \pi_y}{\partial y} = \pm j\omega\epsilon Z_m \pi_y - \frac{\partial \pi_x}{\partial x} - \frac{\partial \pi_z}{\partial z}$$

where π_x and π_z are components tangential to the imperfectly conducting ground plane, π_y is the normal component and the \pm sign is used for $\hat{n} = \pm \hat{y}$. Enforcement of the above boundary conditions will result in a solution for $\vec{\pi}$ in terms of a Hertzian potential dyadic Green's function, that is

$$\vec{\pi}(\vec{r}) = \int_V \vec{G}(\vec{r}, \vec{r}') \cdot \frac{\vec{J}(\vec{r}')}{j\omega\epsilon} dV'$$

The dyadic Green's function for the electric and magnetic fields can then be determined through careful application of the above expressions for \vec{E} and \vec{H} . One can also find the Green's function by treating the problem as an asymmetric slab waveguide and examining the solution as the bottom layer approaches that of a good conductor.

The Hertzian-potential impedance boundary conditions at the surface of an imperfect conductor will be determined and the Hertzian-potential and electric-field dyadic Green's function for the microstrip background environment will be developed.

GAIN ENHANCEMENT OF A DIELECTRIC RESONATOR ANTENNA USING A FINITE SIZE SUPERSTRATE

A. Ittipiboon*, A. Petosa and R. Siushansian

Communications Research Centre
3701 Carling Avenue, P. O. Box 11490, Station H, Ottawa,
Ontario, Canada K2H 8S2

Antennas such as microstrip patches, printed dipoles and dielectric resonator antennas are low profile and compact; properties which are very desirable in many mobile/wireless applications. However, due to their low gain characteristic, a single element of these antennas cannot deliver a high gain requirement. Therefore, more elements are needed, forming an array, which increases antenna feed network complexities and losses. Alternatively, antennas such as horns, lenses or reflectors may be used at the expense of compactness.

Control of the radiation properties of printed circuit antennas using a substrate-superstrate configuration has been reported in the literature (D. R. Jackson and N. G. Alexopoulos, *IEEE Trans. Antennas Propagat.*, vol. AP-33, pp.976-987, Sept. 1985). It was found that a superstrate configuration with a proper thickness and dielectric constant significantly enhanced the antenna gain. This high-gain has been attributed to a leaky-wave characteristic (D. R. Jackson and A. A. Oliner, *IEEE Trans. Antennas Propagat.*, vol. AP-36, pp.905-910, July 1988). The rate of the leakage depends on the layer parameters, which in turn, will control the size of the antenna. Since a patch antenna has a narrow bandwidth, the gain bandwidth of a patch with superstrate is not wide and the higher the gain, the narrower the bandwidth. Recently the dielectric resonator antenna (DRA), having a wider operational bandwidth, has been proposed as an alternative radiator to the microstrip patch. In this presentation, the concept of combining a finite-size superstrate with the DRA is proposed to overcome the drawback of the narrow gain bandwidth of a patch with a superstrate. The proposed antenna should also be very attractive for millimeter-wave applications due to its low loss nature.

The proposed antenna configuration consists of a DRA operating in the dominant mode and a finite dimension superstrate. The spacing, dimensions and the relative permittivity of the superstrate are used to control the radiation characteristics. They will serve as design parameters for gain enhancement. Preliminary results demonstrate that the bandwidth of the DRA with superstrate is comparable to that of the DRA without the superstrate. The bandwidth is found to be better than 10%. The resonating frequency remains largely unaffected. A gain of 10 dBi was measured as compared to 6 dBi of the DRA alone. It is expected that with a better superstrate optimization, a higher gain can be achieved. Details of the study and a discussion will be presented at the conference.

Analytical Solution for Gap-Excited, Leaky Slot Antenna Printed at the Interface Between two Semi-Infinite Dielectrics

Andrea Neto¹, Stefano Maci²

¹Caltech-Jet Propulsion Laboratory, 4800 Oak Grove Dr., MS 168-314, Pasadena, Ca, 91101

²Dept. of Information Engineering, Univ. of Siena, Via Roma 56, 53100, Siena, Italy

A method for the analytical calculation of the magnetic current for a gap-excited leaky slot antenna is presented. The solution procedure assumes a separability between transverse and longitudinal space dependence of the field, which is commonly used for thin slots. This procedure, which is conceptually the same as that adopted by *Mesa et al.* (on IEEE Transactions on Microwave Theory and Techniques, pp.: 207 -215, Feb. 1999), is based on *i)* expanding via Fourier transform the impressed magnetic field in spectral superposition of longitudinal traveling waves with k_x wave-number; *ii)* solving by a MoM scheme the two dimensional CMFIE for each traveling wave; *iii)* integrating in k_x all the travelling wave responses. However, at difference with the work of *Mesa et al.*, in the present case we express in explicit analytical form the final representation of the spectrum, thanks to: *iv)* the assumption of a given (but respecting edge-singularity) transverse dependence of the electric field; *v)* a razor blade testing on the slot axis of the two dimensional integral equation. Despite the simplicity of the solution, the final results well agreed with those from a rigorous full-wave analysis over a wide frequency range. The analytical spectral expression allows simple determination of the complex value of the propagating leaky-mode wave-number giving a useful guideline for the design of leaky antennas. A k_x spectral Fourier integration is necessary to obtain the space domain expression of the magnetic currents on the slot line. This latter can be performed asymptotically by deforming the original contour into the steepest descent path and capturing the residue associated to the pole encountered in this deformation. The SDP integration can be interpreted as a source dependent field, while the residue contribution accounts for the intrinsic properties of the slot line. This representation also allows the definition of entire domain MoM basis functions which describe the current variation very close to or inside the gap excitations when the antenna to be investigated is of finite length and thus resonant rather than leaky.

A 3-Beam, MEMS-Actuated, Leaky Wave Antenna

Afroz Zaman* and Richard Q. Lee
MS 54-8
NASA Glenn Research Center
21000 Brookpark Road
Cleveland, OH 44135

A microstrip leaky wave antenna (LWA) is based on the leakage properties of a microstrip transmission line. The structure can be seen either as a long rectangular patch or as a large open circuited microstrip line. Such an antenna radiates when excited in its first higher order propagating mode and when its dominant transmission line mode is suppressed. It has been shown that it is possible to generate a narrow tilted fan beam in the H plane of a LWA through a single excitation (C.Luxey and J.Laheurte, IEE Proc. Microwave Ant. & Prop. vol. 144, No. 6, Dec. 1997). A simple LWA based array for a tilted pencil beam has been proposed for automotive transceiver application (C. Hu et al, IEEE Trans. Antennas Propagat. vol. 45, No. 11, Nov. 1997). LWAs as frequency scanned elements have been proposed as an alternative to achieving beam scanning without phase shifters. But the frequency dependence limits the scan performance if a narrow frequency bandwidth is available and a wide-angle coverage is required. By periodically loading the radiating edges of a LWA with capacitors, single beam steering at a fixed frequency by varying the capacitor DC bias was demonstrated (C.Luxey and J.Laheurte, Electron Lett. vol. 36, No. 15, July. 2000). A 2-beam, scanning LWA integrated with a varactor tuned voltage controlled oscillator was demonstrated where beam steering was achieved by tuning the oscillator frequency with DC bias voltage (C. Wang et al. IEEE Trans. Antennas Propagat. vol. 47, No. 8, Aug. 1999).

In this paper, a novel 3-beam, MEMS actuated Leaky Wave Antenna is proposed. The antenna consists of two leaky wave structures placed symmetrically on both sides of a probe-fed patch antenna. The broadside patch structure is modified into a leaky wave structure by turning on a pair of MEMS based flex circuit actuators through applied DC voltage. A tilted beam is obtained with either the left or the right actuator pairs on, and a broadside beam is obtained with the actuators off. This geometry also introduces a transverse slit in the leaky wave structure that inhibits propagation of the dominant surface wave mode and provides a clean, narrow tilted beam. The flex circuit actuators are based on designs developed at University of Colorado in collaboration with NASA Glenn Research Center. Preliminary results show the validity of the predicted performance. Details of the analytical and experimental results will be presented and discussed.

RADIATION FROM AN ARBITRARILY ORIENTED HERTZIAN DIPOLE OVER TWO-LAYERED ANISOTROPIC MEDIUM WITH A TILTED OPTIC AXIS

Abdullah Eroglu* and Jay Kyoong Lee
Department of Electrical Engineering and Computer Science
Syracuse University
Syracuse, New York 13244-1240 USA

Electromagnetic radiation from dipole antennas over stratified anisotropic medium has been a major research topic because of its applications in many areas such as geophysics, microwave integrated circuit, submarine communication, etc. As a result there is a growing interest in using anisotropic substrates in electromagnetic systems containing active device substrates, microstrip antennas and circuits, and absorptive materials.

Most of the previous work in this research area was limited to radiation of dipoles over stratified medium for isotropic case. Researchers most of the time used the technique introduced by L.Tsang et al. [*J.Geophys. Res.*, **79**, 2077-2080, 1974] and J.J.H.Wang [*IEE Proc.*, part H, **132(1)**, 58-62, 1985] extended the technique to evaluate the radiation fields. This technique was based on the evaluation of numerical integration of radiation fields using FFT. But there are two shortcomings of this method. Because of limited central memory and execution speed, computation is limited to field points having a radial coordinate of several to several hundred wavelengths, depending on the nature of the particular integrand involved. In addition, convergence deteriorates as the distance (in z coordinate) between the source and field point decreases.

The more general calculation of far field radiation of dipoles over stratified anisotropic medium for two layer case has been done by Tsalamengas and Uzunoglu [*IEEE Trans. Antennas Prop.*, **38(1)**, 9-16, 1990] using the matrix method with Fourier transform technique. However, this method involves a tedious work on matrix calculations and radiation field derivations. Because of this the method is not practical for radiation field calculations when there exist more than two layers.

In this paper we introduce a practical way of calculating radiation fields due to an arbitrarily oriented dipole in the case when dipole is placed over two-layered uniaxially anisotropic medium with a tilted optic axis. Solutions to the problem of radiation are studied analytically by using dyadic Green's function of the anisotropic medium. Stationary phase method is used to evaluate the integrals in the far field. The results are checked numerically with the existing results by Tsalamengas and Uzunoglu [1990]. It is shown that our method greatly facilitated the calculation of radiation fields in comparison to the existing method by avoiding tedious matrix derivations and mathematical calculations and gave a neat final result by showing the polarization of the radiation fields clearly in the far field. Also our method can easily be extended to the cases involving more than two layers once the dyadic Green's function of the multi-layer medium is calculated.

An Approximate Green's Function for a Finite Grounded Dielectric Slab

Lale Alatan*¹

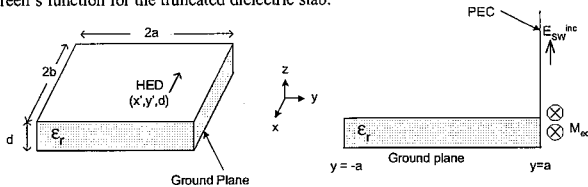
Özlem Aydın Civi¹

Gölgü Ögütcü²

¹Electrical & Electronics Eng. Dept.
Middle East Technical University
06531 Ankara, TURKEY

²Electrical & Electronics Eng. Dept.
University of Gaziantep
Gaziantep, TURKEY

Especially in applications like mobile communications, the dielectric substrate of microstrip antennas are restricted to small sizes due to the space limitations. In most studies which analyze microstrip patch antennas with finite grounded dielectric slabs, the current distribution on the patch surface and therefore the input impedance of the antenna are assumed not to be affected by the truncation of the ground plane and the dielectric slab. However both the experimental and the theoretical results presented in [1] implies that the input impedance of the antenna could vary up to 50% by changing the size of the grounded dielectric slab. In [1], the transmission line model is modified by including an edge admittance that models the scattering of surface waves from the edge formed by the truncation of the dielectric slab and the ground plane. However this method can be applied to only a certain class of patch antennas that could be analyzed by using transmission line model. In order to be able to analyze general microstrip antenna structures, we propose to modify the Green's function of an infinite grounded dielectric slab to take into account of the scattered surface waves from the edge of the truncated dielectric slab. The procedure used to obtain this modified Green's function can be summarized as follows: 1) Find the Green's function of a horizontal electric dipole on the infinite grounded dielectric slab, 2) by using the incident surface waves define equivalent magnetic currents at the dielectric-air interface ($y = a, z > 0$), 3) place a semi-infinite perfect electric conductor at the dielectric-air interface ($y = a, z > 0$), 4) by using the Green's function of a horizontal magnetic dipole placed on a conducting 90° wedge, find the total field due to the equivalent currents, 5) using the stationary formula given in [1], calculate the position dependent edge admittance, 6) using the edge admittance find the reflection coefficient of the surface waves, 7) repeat steps 3-6 for the other edge ($x = b$), 8) use these reflection coefficients to obtain an approximate Green's function for the truncated dielectric slab.



In [1], the edge admittance is obtained for the 2-dimensional problem; hence it does not include any information about the shape of the edge. However in our formulation 3-dimensional problem is considered and the edge admittance is obtained as a function of position along the edge. Therefore, by using this approximate Green's function, it will be possible to optimize the shape of the dielectric truncation to minimize the surface wave reflections. Numerical results will be demonstrated in the presentation.

[1] A. K. Bhattacharyya, "Effects of ground plane truncation on the impedance of a patch antenna", *IEEE Proceedings-H*, Vol.138, no. 6, pp. 560-564, December 1991.

USING SCATTERING DATA TO ESTIMATE THE RADIATION CHARACTERISTICS OF SPHERICALLY SYMMETRICAL LENSES

Andrew Parfitt and Nasiha Nikolic
CSIRO Telecommunications and Industrial Physics
PO Box 76, Epping NSW 1710, Australia

Abstract

There has been a recent increase in interest in lens antennas for wireless communications and other applications. Among these, the Luneburg lens has a multibeam capability that offers advantages for certain applications. A novel use of large Luneburg lenses has been proposed for the square kilometre array (SKA) radio telescope (Parfitt *et al.*, *URSI Radio Science Bulletin*, 293, June 2000). While an exact spherical-mode solution for a concentric spherical shell implementation is available, an arrangement of cubic blocks is more likely for larger lenses such as those that might be employed in the SKA. Finite difference time domain (FDTD) methods are suitable for modelling this assembly and offer the attraction of wideband computation. However, the long computation times involved in simulation are an impediment to the design and optimisation of integrated lens and feed systems.

In this paper we describe a method of estimating the radiation pattern from a lens and its feed using the results obtained from a single FDTD scattering computation applied to the lens alone. The scattered field is sampled at the locations of known equivalent or actual currents associated with the feed. Because the lens is spherically symmetrical, the sampling points can be rotated around the centre of the lens at a constant radius equal to the focal length of the lens in planes corresponding to those where the radiation pattern is required. Using reciprocity, the response in these planes can be plotted to give an estimate of the radiation pattern. An estimate of the gain of the lens and feed can be obtained by computing the response of the feed to the incident field and then normalising the radiation patterns accordingly.

Results for ideal dipole and aperture feeds are compared with those obtained using a spherical mode analysis.

The method is suitable for use in optimising the feed location for a given lens profile by minimising the amount of FDTD computation required when adjusting feed parameters for a given lens dielectric profile. Other spherically or cylindrically symmetrical problems, such as the radiation from antennas near to cylindrical masts, can also be solved using this method.

AN IMPROVED EVALUATION OF RADIATION PATTERN FOR DIELECTRIC LENS ANTENNAS

Davide Pasqualini, Filippo Capolino, Alberto Toccafondi and Stefano Maci
*Dept. of Information Engineering, University of Siena,
Via Roma, 56 - 53100 Siena, - Italy*

Dielectric lens antennas are often used in millimeter and sub-millimeter wave applications in order to obtain high directivity with integrated technology. Their shapes typically are elliptical, hemispherical or hyperhemispherical, and they are usually fed by slots, dipoles or patches. As can be inferred from the recent literature (D. Filipovic et al., *IEEE Trans. on Ant. and Prop.*, 45, 5, 1997), a rather standard method for evaluating the radiation pattern consists of integrating the Physical Optics (PO) equivalent currents on the lens surface. Although this method was found enough accurate even for predicting input impedance perturbations (A. Neto et al., *IEE Proc. Microwaves, Ant. and Prop.*, 146, 3, 1999), it does not provide a satisfactory estimate of the far field pattern far from boresight.

This fact may be attributed to neglecting the additional radiation mechanism produced by the lateral wave that is excited at the dielectric-air interface; this phenomenon occurs for those rays that impinge on the lens surface at its maximum waist where the incidence aspects are in the neighborhood of the critical angle. There, a PO approximation of the equivalent currents fails to account for the excitation of lateral waves that produces transition field. This diffraction effect may be accounted for by referring to the canonical problem of a dielectric half-space locally tangent at the actual lens surface. The solution of this canonical problem is either asymptotically evaluated for perpendicular polarization or numerically calculated for parallel polarization.

In a recent paper (D. Pasqualini et al., *Proc. of the 2000 IEEE Ant. and Prop. Soc. Int. Symposium*, Salt Lake City, July 2000) uniform high-frequency expressions for the equivalent electric and magnetic currents at the surface of an elliptical dielectric lens have been obtained, which provided a significant improvement to the PO currents. In this paper, the radiation integral of these currents is numerically performed; several examples have shown that the present formulation provides strong deviations from PO close to the maximum waist of the lens, where a transition field is required to match GO and the transition lateral wave. Calculations of radiation patterns will be shown during the oral presentation for several examples of elliptical and hyperhemispherical lens antennas fed by one or more elementary sources. It is noted that when the feeding element is not located at the lens focus, wide area on the lens surface occurs where standard GO fields are not adequate to provide an accurate evaluation of the radiation pattern.

THE DOME-LIKE FRESNEL-ZONE ANTENNAS
(OR HOW TO CONVERT A DOME INTO ANTENNA)

Hristo D. Hristov* and Rodolfo Feick
Department of Electronics Engineering
Universidad Técnica Federico Santa María
Av. España, Casilla 110-V, Valparaíso, Chile
chris@elo.utfsm.cl

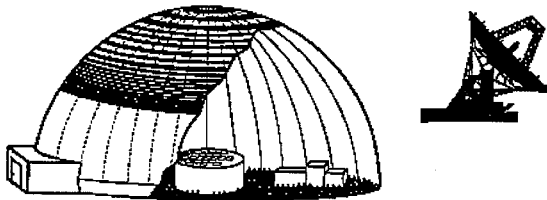
From the very beginning the main efforts in studying microwave/mm-wave Fresnel zone plates have been directed towards an increase of their focusing efficiency. This has been achieved by the following techniques: (a) use of reflector behind the zone plate, (b) division of each full-wave zone into a number of sub-zones filled up by phase-shifting compositions and (c) construction of three-dimensional plate lenses: spherical, parabolic, conical, etc. (*H. D. Hristov, Fresnel Zones, etc. Artech House, 2000*)

The microwave planar zone plate antenna has the advantage of being a flat construction that is cheap, light and easy to manufacture. With the purpose of maintaining the beauty of the urban environment, a flat antenna conformal to a building wall can be used instead of a classical parabolic one. But in order to increase the focusing, resolving and scanning properties, and to create different shaped radiation patterns the Fresnel zone plate (FZP) and antenna can be assembled conformable to a curvilinear natural or man-made formation. This is illustrated in the futuristic view of a dome-like ground to space communication /radio telescopic antenna, shown below.

The main disadvantage both of planar and curvilinear FZP antenna is that compared to the parabolic reflector antenna it is frequency sensitive and has lower radiation efficiency.

The microwave/millimeter-wave curvilinear FZ plates and antennas are still undeveloped and little known in practice, and it is no a wonder that there is no more than a score or so publications on the subject.

In the present paper we contrast the theoretical radiation characteristics of dome-like FZP lens antennas: spherical, parabolic, conical, etc. Also, a novel design of a spherical radio telescopic FZP antenna design is discussed.



Hybrid dome-like Fresnel zone lens antenna shown in contrast with classical large parabolic reflector antenna

Analysis of Performance of a Class of Broadband Geodesic Lens with Steering Capabilities

Luiz Eduardo Bittencourt Sampaio and Luiz Costa da Silva
Catholic University of Rio de Janeiro
Rua Marques de Sao Vicente 225, Gavea, RJ, Brazil

The geodesic lens under consideration is a guiding structure composed by two metallic revolution surfaces, with a common axis of revolution. Since the distance between the two surfaces is small, they can be described by their mean surface (locus of the midpoints of the common normals to the metallic surfaces). The generating curve of the mean surface is shown in Fig.1. It has a conical upper section (S1) and a lower section that has a given shape. It can be shown (K. S. Kunz, J. Appl. Phys., 25, 642-653, 1954) that, if the slant angle Ψ of the cone and the surface S2 are properly defined, a point source, located at the border line between S1 and S2, will generate an optical tube of rays with plane wave fronts, in the plane of development of the cone S1.

The performance of this kind of lens as broadband steerable antenna has the following impairments: a) Since the source is a point source, several sources are necessary for steering, and only one of them will be active for radiation at a given direction. b) The stand-by sources will produce interference on the active source.

Such problems can be overcome, building an antenna with only the conical section (S1), and applying the equivalence principle to determine the field distribution required for the excitation at the lower basis of the cone. It is verified that for an angle $\Psi=60^\circ$, the excitation has uniform amplitude and oscillating phase. For practical applications, this continuous source can be replaced by a set of discrete generators (For most applications, a maximum of 12 generators will be satisfactory). Since the amplitude of the excitation field is constant, all the generators will have the same power, and only phase control will be necessary for steering.

To analyze the radiation characteristics of such antenna, geometrical optics was applied to the determination of the antenna dimensions and excitation field distribution, and mode matching technique and optical physics to the determination of the fields at the aperture of the antenna and the radiation patterns. It was verified that it is possible to build antennas with half power beam width (in the horizontal plane) of the order of 8° , far out side lobes levels below -20dB , over more than 2 octaves. A typical radiation pattern for the main polarization, in the horizontal plane, at 3 and 12 GHz, is shown in Fig. 2

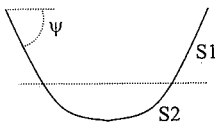


Fig. 1. Generating curve

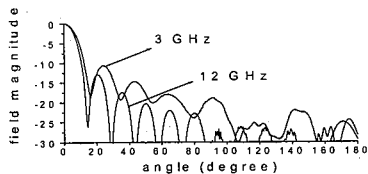


Fig. 2. Radiation patterns at 3 and 12 GHz

2-D MODEL OF AN ARBITRARY-SHAPED DIELECTRIC ROD ANTENNA

Artem V. Boriskin*, Alexander I. Nosich, and Ayhan Altintas¹

*Institute of Radio-Physics and Electronics
of the National Academy of Sciences of Ukraine, Kharkov 61085, Ukraine*

Fax: +380-572-441105, Email: a_boriskin@yahoo.com

¹*Bilkent University, Ankara 06533, Turkey*

In the microwave range, dielectric rods and lenses are candidate antennas for the wide-band multi-beam and mechanically scanning communication systems (C.A. Fernandes, *IEEE Antennas Propagat. Magazine*, 41, 141-151, 1999). The effect of the beam directivity improvement due to an arbitrary shaped dielectric cylinder as a 2-D model of a dielectric rod or lens antenna is studied. The beam is simulated by the field of a Complex Source-Point (CSP) line current. Efficient algorithm for the solution of 2D problem of wave scattering by smooth dielectric cylinders of arbitrary cross-sections is developed, based on the concept of analytical regularization (A.I. Nosich, *IEEE Antennas Propagat. Magazine*, 42, 34-49, 1999).

After presenting the fields as single-layer potentials over the scatterer contour, a set of singular integral equations (IEs) is obtained. Extraction and analytical inversion of the IEs singular parts corresponding to the circular-cylinder scattering is done by using a Galerkin scheme with angular exponents as global basis functions. This results in a Fredholm second-kind infinite-matrix equation having favorable features. Such a conversion guarantees point-wise convergence of numerical solution, i.e., a possibility to minimize the error down to machine precision by solving progressively greater matrices. In application to dielectric scatterers, this approach is also free from the heavy inaccuracies near to natural resonances that are intrinsic for conventional numerical approximations (G.L. Hower, *et al.*, *IEEE Trans. Antennas Propagat.*, AP-41, 982-986, 1993).

Basis properties of the algorithm are studied. Numerical results for the E- and H-wave scattering by cylinders characterized with a "super-elliptic" cross-section that simulates rectangle with rounded edges are obtained.

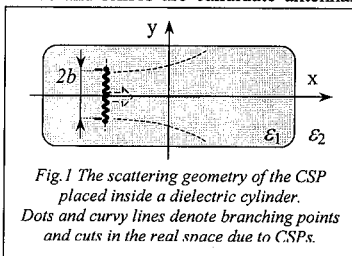


Fig.1 The scattering geometry of the CSP placed inside a dielectric cylinder. Dots and curvy lines denote branching points and cuts in the real space due to CSPs.

Elements and Electronics

Chairs: S. Targonski, USA and A. Kishk, USA

	Page
8:00 Numerical Analysis of Stacked Cylindrical Dielectric Resonator Antennas Excited by Coaxial Probes, <i>A. Kishk*, X. Zhang, A. Glisson, University of Mississippi</i>	APS
8:20 Analysis of a Hemispherical Dielectric Resonator Antenna with Very High Permittivity, <i>S. M. Jang, Syracuse University, B. Kolundzija*, University of Belgrade, T. Sarkar, Syracuse University</i>	APS
8:40 An Integrated Broadband Bowtie Antenna for THz Detection with a Double Quantum Well, <i>M. Khodier*, C. Christodoulou, University of New Mexico, J. Simmons, Sandia National Laboratories</i>	APS
9:00 Characterization of Multiple-Via Interconnections for Multilayer Chip and Module Designs, <i>C. W. P. Huang*, S. Hammadi, J. Lott, S. Al-Kuran, Anadigics Inc.</i>	APS
9:20 Radiation by Cavity-Backed Antennas on an Elliptic Cylinder, <i>C. W. Wu*, L. Kempel, E.J. Rothwell, Michigan State University</i>	APS
9:40 Dielectric Slab Based Leaky-Wave Antennas for Millimeter-Wave Applications, <i>T. Teshirogi*, Y. Kawahara, A. Yamamoto, Y. Sekine, N. Baba, M. Kobayashi, Anritsu Corporation</i>	APS
10:00 A RF Mass-Sensitive SAW Sensor with U-Groove Structure, <i>D. Zhu*, Zhejiang University, J. Zhu, Motorola Inc</i>	APS
10:20 A CMOS IC for RF Programmable Surface Acoustic Wave Filter, <i>D. Zhu*, Zhejiang University, J. Zhu, Motorola Inc</i>	APS
11:00 Optimisation of UHF Ferroelectric antenna Parameters by Means of Genetic Algorithm: A Broad Based Tutorial Paper, <i>C. Das Gupta, Indian Institute of Technology</i>	50
11:20 Experimental Study of Cassegrain antenna Unit of Fan-Beam Structure With Planar Metal-Dielectric Feeder, <i>C. Das Gupta, Indian Institute of Technology</i>	51

OPTIMISATION OF UHF FERROELECTRIC ANTENNA PARAMETERS BY MEANS OF GENETIC ALGORITHM: A BROAD BASED TUTORIAL PAPER

Chinmoy Das Gupta, Senior Member IEEE
Professor, Department of Electrical Engineering
Indian Institute of Technology, Kanpur, INDIA.

EXTENDED ABSTRACT

Systematic study of ferroelectrics for different applications by Vendik. O.G, one of the key persons of many space vehicle and defence projects of the ex-Soviet Union has been reported partially [1].

Successful realization of ferroelectrics as radiating element down upto UHF range had been reported independently by the author during 1988 APS Symposium at Syracuse [2]. It can be concluded that ferroelectric radiating elements can be considered as effective means of size reduction, which can be conveniently used in surveillance units. The unit had shown an axial mode virtually with no side lobe. The author did not have any computer-aided measurement set-up at that time to study the radiating characteristics of these reduced-size radiating elements.

In the present paper, systematic study of the ferroelectrics as radiating elements down to UHF range will be presented, with numerical study of the radiating characteristics of these elements. As reported earlier [3] for dielectric aerials experimental results are more optimistic than the theoretically predicted one having better directivity and lower side-lobes. Though the earlier theory [3] is quite satisfactory to start with, but better agreement can be expected by FDTD method.

Optimum parameter study first verified for conventional grounded monopole radiator and subsequently for these reduced size radiators by means of SIMPLEX MATLAB package and GENETIC algorithm will be presented in the conference. In order to check the effectivity of the SIMPLEX MATLAB PACKAGE it is proposed to study the input impedance characteristics of chopped conical dipole which is worked out by MOM.

- [1] Vendik. O.G.: Dispersion characteristics of ferroelectrics at UHF range. (Invited paper) Third European Meeting on Ferroelectricity, Zurich Switzerland, 1975, Vol. 12, No. 1-4, pp. 85-95.
- [2] Chinmoy Das Gupta: Ferroelectric Antenna unit for UHF mobile communication system. Proceedings IEEE-URST International Symposium on Antenna and Propagation, Syracuse, 1988.
- [3] Kelly R: Dielectric Aerials, Mathuen's Monograph.

EXPERIMENTAL STUDY OF CASSEGARIAN ANTENNA UNIT OF FAN-BEAM STRUCTURE WITH PLANNAR METAL-DIELECTRIC FEEDER

Chinmoy Das Gupta, Senior Member IEEE
Professor, Department of Electrical Engineering
Indian Institute of Technology, Kanpur, INDIA.

EXTENDED ABSTRACT

Successful realization of planar metal-dielectric feeder at ku-band with multimode response and with side-lobe level much lower than 20 db, had been reported in APS Symposium of 1996.

In the proposed paper it is being used as a feeder in a Cassegrain Antenna Unit of Fan-Beam structure mainly using the mode at 16 Ghz. Though the realization of the parabolic reflector is much simpler, but the hyperbolic sub-reflector essentially needs the use of CNC milling machine for fabrication.

Intuitively the aspect ratio of X-Y dimension of the hyperbolic sub-reflector to that of the parabolic reflector has been selected for two values from which the optimum aspect ratio is yet to be found out. Design of hyperbolic sub reflector for the fan-beam structure has been done by using the same expressions as in the case of conventional Cassegrain antenna units.

In the present form of development of the unit it is showing quite narrow band response. From these experimental results the new aspect ratio which are not readily available in literature is to be worked out with standard available optimization tool. (Work is in progress.)

Experimental set-up for direct computer-aided measurement of the far-field having their own limitations has been set-up. The set-up consists of AD card operable only by 386 or 486 PC unit.

As the parts of the system are designed by semi-empirical method before taking the measurement of the far-field radiation pattern, the matched point has been found out by our wide-band network analyzer system working from UHF-20 Ghz.

In order to make proper impact on audience it is planned to make the presentation like Salesman's demonstration of the work with high powered Gunn-oscillator that can be carried conveniently from here along with the computer aided measurement system that has been built up.



RF Coil Design and Simulation for High Field Magnetic Resonance Imaging

Chairs: R. Lee, USA and O. Gandhi, USA

	Page
8:00 RF Coil Modeling and Analysis in High Field MRI: Lessons Learned, <i>R. Lee*, T. Ibrahim, The Ohio State University</i>	APS
8:20 A Numerical Study of the Field Dependence of Signal-to-Noise Ratio in High Field MRI, <i>M. Kowalski*, J. M. Jin, University of Illinois at Urbana-Champaign</i>	APS
8:40 Design of Radiofrequency Coils for Magnetic Resonance Imaging Applications at High Fields: Technological and Physical Feasibility Issues, <i>T. Ibrahim*, R. Lee, B. Baertlein, P.M. Robitaille, The Ohio State University</i>	APS
9:00 SAR and Induced Current Densities for RF and Gradient Magnetic Fields Used for MRI, <i>O.P. Gandhi*, The University of Utah</i>	54
9:20 Measuring RF Field Distributions in MR Coils with IR Sensors, <i>T. Ibrahim*, R. Gilbert, A. Abjuljalil, R. Lee, B. Baertlein, P. M. Robitaille, The Ohio State University</i>	APS
9:40 Volume Coils for Highest Field MRI, <i>T. Vaughan*, M. Garwood, K. Ugurbil, University of Minnesota</i>	APS
10:00 A Model for MR Image Shading in Multi-Mode Resonators, <i>J. Tropp*, GE Medical Systems</i>	55
10:20 Using Electromagnetic Field Calculations to Understand the Complexity of Magnetic Resonance Imaging (MRI) at High Magnetic Field Strength, <i>M. Smith*, C. Collins, Q. Yang, J. Wang, W. Liu, The Pennsylvania State University</i>	APS

SAR AND INDUCED CURRENT DENSITIES FOR RF AND GRADIENT MAGNETIC FIELDS USED FOR MRI

Om P. Gandhi

Department of Electrical Engineering, University of Utah, Salt Lake City, UT 84112, USA

A 6-mm resolution, 30-tissue anatomy-based model of the human body is used to calculate specific absorption rate (SAR) and the induced current density distributions for radiofrequency and switched gradient magnetic fields used for MRI, respectively [1]. For SAR distributions, the finite-difference time-domain (FDTD) method is used including modeling of 16-conductor birdcage coils and outer shields of dimensions that are typical of body and head coils and a new high-frequency head coil proposed for the 300-400 MHz band. SARs at 64, 128, and 170 MHz have been found to increase with frequency (f) as f^k where k is on the order of 1.1-1.2. The tables of the calculated maximum 1 kg and 100 g SAR may be used to calculate the maximum RF coil currents and/or free space axial RF magnetic fields that may be used in order not to exceed the safety guidelines. Because of the low frequencies associated with switched gradient magnetic fields, a quasi-static impedance method is used for calculation of induced current densities that are compared with the safety guidelines. This procedure has been used to calculate the maximum values of dB/dt that may be used without exceeding the IEC and FDA safety guidelines to avoid peripheral nerve stimulation.

- [1] O. P. Gandhi and X. B. Chen, "Specific Absorption Rates and Induced Current Densities for an Anatomy-Based Model of the Human for Exposure to Time-Varying Magnetic Fields of MRI," *Magnetic Resonance in Medicine*, Vol. 41, pp. 816-823, 1999.

A Model for MR Image Shading in Multi-mode Resonators
James Tropp

GE Medical Systems, 47697 Westinghouse Dr., Fremont CA 94539

The so-called bird-cage and TEM resonators (1,2), commonly used for RF transmission and reception in Magnetic Resonance Imaging (MRI), are multimode devices, excitation of whose principle, or fundamental, mode produces a spatially uniform radiofrequency **B** field in a volume to be imaged. The uniform RF **B** field produces in turn a uniform excitation of transverse magnetization in the specimen under test, giving rise, ideally, to an image which is free of shading artifacts. Deviations from the condition of uniformity produce correspondingly, a shaded image. Inasmuch as the normal modes of the resonator comprise mathematically a complete set, any excitation may be described as a superposition of modes, and in particular, a large class of deviations from uniform excitation may be attributed to the admixture of higher modes in the excitation.

Given the high rotational symmetry of the resonators in question, perturbation theory (3,4) shows that these mode mixtures arise from broken symmetry, such as accrues from the build-up of component tolerances, or asymmetric positioning of the specimen. Thus, the susceptibility of a given resonator to shading may be gauged by its sensitivity to mode mixing induced by asymmetry. The question further divides, depending whether the perturbation is reactive or resistive: here we consider only reactive perturbations.

We have studied two resonators – a TEM and a bird-cage – both designed for imaging the human head at 3.0 T, and operating at 127.6 MHz. Physically, the bird-cage constitutes a high-pass ladder, closed upon itself to form a cylinder (rungs parallel to axis); while the TEM is a comb-line of low pass pi circuits arrayed (axes parallel to axis) inside a cylindrical shield, which provides their common ground. Accurate RF circuit models and equations (5,6) allow realistic calculations of the mode mixtures induced by capacitive perturbations, which are then tested experimentally by adding capacitors to the actual resonators. The TEM was an end-capped, lumped element device (7) with shield radius 17.8 cm, and ribbon elements of width 2.3 cm on a bolt circle radius 14.3 cm; the overall element length of 19 cm. The bird-cage was a shielded device with end cap, of nominally identical dimensions, except that the width of the ribbon elements was slightly less: 1.9 cm. Both resonators employed conventional quadrature drive, with two, not four, drive points. The circuit model for the TEM was developed *a priori* (8); that for the bird-cage was obtained by measuring some of the coupling coefficients, (5), and also by back transforming the mode frequencies of the finished resonator (6).

The actual perturbations were applied by adding a large padding value ($\approx 40\%$) to the existing capacitor at one point on each resonator. For the TEM, having 18 pF and 20 pF capacitors at either end, 8.2 pF was added to a 20 pF cap. For the bird-cage, with 39 pF at either end, 15 pF was added to one cap. Figure 1 shows results of perturbation calculations: above for the bird-cage, below for the TEM: in each case the perturbed stick spectrum of calculated resonance positions, and a flux plot of the perturbed member of the principal mode pair. Note that the mode separation is much larger for the bird-cage, than for the TEM; and the derangement of the flux plot is correspondingly greater for the TEM than for the bird-cage. This accords with the expectations of quantum mechanical perturbation theory, whereby the strength of mixing varies inversely with the separation of the levels. Figure 2 is a comparison of theoretical and experimental image profiles, for a spherical phantom filled with silicon oil ($\epsilon \approx 1$). The experimental images (gradient recalled echo, TR = 50 ms, TE = 3.4 ms, flip 20 deg.) were obtained on a GE Signa scanner, at 3.0 T. The simulated images were calculated with the quadrature fields, using the approximation (valid for small flip angles), that the image intensity is proportional to squared magnitude of the RF field strength. In each case (experiment or simulation), the left-right meridian line of the image is displayed. The experimental and calculated images show, for the TEM, a dramatically larger sensitivity to perturbation, than for the bird-cage. However, the test in this case is extreme, and it is expected that the application of four point drive, rather than two point, would ameliorate the situation.

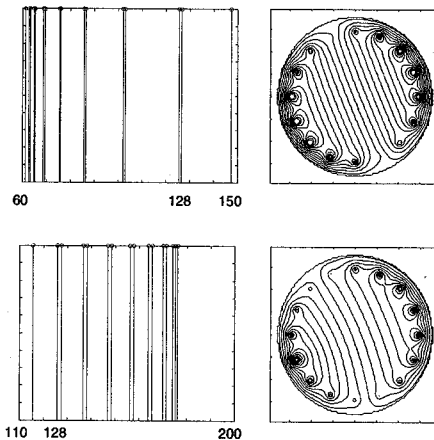


Figure 1: Perturbation calculations: bird cage (above) TEM (below); stick spectra (left), flux plots (right). Principal mode at 128 MHz, 90 MHz span. Note that mode order is opposite in the two resonators, also clear splitting of degenerate modes.

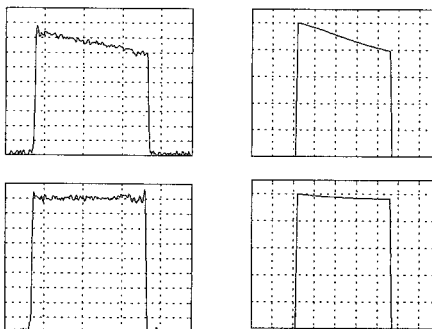


Figure 2: Observed (left) and calculated (right) image profiles of spherical oil phantom, for perturbed resonators: TEM (above) and bird-cage (below). The bird cage is relatively immune to the effects of added capacitance.

REFERENCES

1. J. T. Vaughan *et al.*, *Magn. Reson. Med.* **32**, 206, (1994).
2. C. Hayes *et al.*, *J. Magn. Reson.* **63**, 622, (1985).
3. P. Joseph and D.-F. Lu, *IEEE Med. Im.* **8**, 286 (1989).
4. J. Tropp *J. Magn. Reson.* **82**, 51, (1989).
5. J. Tropp *J. Magn. Reson.* **126**, 9, (1997).
6. M. Leifer *J. Magn. Reson.* **124**, 51, (1997).
7. J. Tropp *et al* Proc ISMRM. **7**, 2063(1999)
8. J. Tropp and J. T. Vaughan, Proc ISMRM. **7**, 421(1999)

Numerical Benchmarking, Strategies, and Applications

Chairs: G. Fikioris, Greece and J. Kotulski, USA

	Page
1:00 Electromagnetic Code Consortium Benchmark Development, <i>A. Greenwood*, Air Force Research Laboratory-Kirtland AFB</i>	58
1:20 What is Model Order Reduction?, <i>R. D. Stone*, J. F. Lee, R. Lee, The Ohio State University</i>	59
1:40 IS Semi-Inversion Always Advantageous?, <i>G. Fikioris*, National Technical University of Athens</i>	60
2:00 Strategy for Modeling Objects Obstructed by Foliage Above a Penetrable Ground: Spectral and Higher-Order Methods, <i>Q. H. Liu*, X. Xu, Z. Q. Zhang, G. Zhao, Duke University</i>	61
2:20 Comparison of Slot Modeling Techniques in the Frequency and Time Domain, <i>J. Kotulski*, W.A. Johnson, R.E. Jorgenson, L.K. Warne, D.J. Riley, Sandia National Laboratories</i>	62
2:40 A Hybrid Technique for the Simulations of the Field Scattered by a Finite Dielectric Shield Around a Phased Microstrip Antenna Array, <i>Q. Rao*, H. Hashiguchi, S. Fukao, Kyoto University</i>	63
3:00 The Application of SDA to Boxed Planar Structures with Complex Materials, <i>F. Mesa*, F. Medina, G. Plaza, Universidad de Sevilla</i>	64
3:20 Wave Scattering by Non Linear Ferromagnetic Materials, <i>P. Joly*, INRIA Rocquencourt, O. Vacus, Cea/CESTA BP2,</i>	65
3:40 TDIE-MoM Solutions for Scattering by Thin-Wire Antenna Using Spatio-Temporal Wavelet-Packet Expansions, <i>Y. Shifman*, Y. Leviatan, Technion - Israel Institute of Technology</i>	66
4:00 Modeling Frequency Selective Surfaces by the Finite Element Method, <i>I. Bardi*, R. Remski, D. Perry, Z. Cendes, Ansoft Corporation</i>	67
4:20 Quasi-Static Analysis of Fringe Capacitances for Horizontal and Vertical Annular Frills, <i>H. Y. Chao*, W. C. Chew, University of Illinois at Urbana-Champaign</i>	68

Electromagnetic Code Consortium Benchmark Development

Andrew D. Greenwood
Air Force Research Laboratory
Directed Energy Directorate
Kirtland AFB, NM
Andrew.Greenwood@kirtland.af.mil

The electromagnetic code consortium (EMCC) is a joint organization sponsored by the US Air Force, the US Army, the US Navy, and the National Aeronautics and Space Administration (NASA) whose purpose is to advance computational electromagnetic (CEM) code development. To this end, the consortium collects and distributes data for benchmark CEM problems. The description of an initial set of metallic benchmark problems consisting of the NASA almond, an ogive, a double ogive, a conesphere, and a conesphere with a gap appears in the "EM Programmer's Notebook" in the February, 1993 IEEE Antennas and Propagation Magazine. The problem descriptions include descriptions of the problem geometry as well as computed and measured radar cross section (RCS) data.

While the original benchmark problems exercise many features of an electromagnetic scattering code, the creation of additional benchmark cases allows more code features to be exercised, leading to better validation. Thus, a second generation of benchmarks is being developed. The second generation includes an antenna array on a finite ground plane, a trihedron, a cube, a pyramid, a prism, and a MUGU wedge. The antenna array includes three separate cases: (1) the ground plane is all metal, (2) the ground plane consists of two metal pieces with an air gap, and (3), the ground plane consists of two metal pieces with R-card in the gap. Measured radiation pattern data is available for each of these cases. The remaining cases are metallic objects with measured scattering data available.

One shortcoming of the new cases is the inclusion of only one antenna problem. The EMCC is actively seeking additional antenna cases, particularly cases in which near-field measurements are available. Anyone with a proposal for such a case is invited to contact the authors.

What is Model Order Reduction?

Rodney D. Slone, *Student Member, IEEE*, Jin-Fa Lee, *Member, IEEE*,
Robert Lee, *Member, IEEE*

ElectroScience Lab., Dept. of Electrical Engineering, Ohio State University
1320 Kinnear Road, Columbus, OH 43212 USA

Model Order Reduction (MORE) is a process in which the number of unknowns (order) of a mathematical representation (model) of a problem of interest is decreased. The mathematical representation of the system with the smaller number of unknowns is known as the reduced order model (ROM). Many reasons may motivate the application of a MORE procedure including macromodeling, domain decomposition, and fast sweep capability. All these reasons are ultimately related to obtaining a faster simulation time.

Once a reason for applying MORE is identified and the type of general approach is determined, it is necessary to choose some method to create the original mathematical model of the problem. Some of the popular modeling methods that have been used in conjunction with MORE are the method of moments (MoM), the finite difference time domain (FDTD), and the finite element method (FEM). After a modeling method has been chosen and applied to create the original, large order mathematical model, a MORE technique must be chosen and applied. A list of some MORE techniques follows.

In [Burke, et. al., *IEEE Trans. Magn.*, 25, 2807-2809, 1989] model based parameter estimation (MBPE) is used to create a fast frequency sweep ROM of a wire antenna modeled using MoM. In [Werner and Allard, *IEEE Trans. Antennas Propagat.*, 48, 383-392, 2000] MBPE is extended to create a simultaneous fast angle and frequency sweep ROM for a wire antenna.

A second MORE technique is the spectral Lanczos decomposition method (SLDM) which is presented in [Druskin and Knizhnerman, *Radio Sci.*, 29, 937-953, 1994] and used to solve 3D problems discretized using Yee's grid. In [Zunoubi, et. al., *IEEE Trans. Microw. Theory Tech.*, 46, 1141-1149, 1998] the FEM is used to model the problem domain.

The last types of MORE procedures are the Padé approximation via the Lanczos process (PVL) [Feldmann and Freund, *IEEE Trans. Comput.-Aided Des.*, 14, 639-649, 1995] and asymptotic waveform evaluation (AWE) [Pillage and Rohrer, *IEEE Trans. Comput.-Aided Des.*, 9, 352-366, 1990]. Initially they were applied in circuit analysis, but later they were used in computational electromagnetics.

In this talk, a tutorial on MORE will be presented in which the above mentioned techniques will be illustrated. The tutorial will be geared to spur the community's interest in this exciting topic.

IS SEMI-INVERSION ALWAYS ADVANTAGEOUS?

George Fikioris

Institute of Communication and Computer Systems
National Technical University
Department of Electrical and Computer Engineering
9 Iroon Polytechniou Street
GR 157-73 Zografou
Athens, Greece

Email: gfiki@cc.ece.ntua.gr

Many problems of electromagnetics are governed by Fredholm integral equations of the first kind. Often, it is possible to obtain a different equation describing the problem by analytically inverting *part* of the first-kind equation and obtaining an equation of the second kind. This procedure is called Semi-Inversion (or the Method of Analytical Regularization); the relevant operator is called the regularizer. It is a well-known rule that it is usually advantageous to apply a numerical method to the second-kind equation than to the original (first-kind) one. (In practice, a significant advantage is less matrix ill-conditioning.) The above are well-summarized in a recent article by Nosich (A. I. Nosich, "The method of analytical regularization," *IEEE Antennas Propagation Magazine*, **41**, 34—49, 1999). In particular, Nosich brings up a point that can be summarized as follows.

In a case where it is possible to find a set of orthogonal eigenfunctions of the regularizer, application of Galerkin's method to the original equation with these eigenfunctions as basis functions yields a regularized discretization scheme—meaning that for infinite matrix dimension, a second-kind infinite-matrix equation is obtained.

The above case is interesting and, perhaps, curious. The purpose of the present paper is to discuss it further, concentrating on finite matrix dimension. Specifically, when the regularizer satisfies certain conditions, we show that the Galerkin's method described above (applied to the first-kind equation) is *equivalent* to a particular numerical method applied to the second-kind equation. We specialize this general result to certain integral equations occurring in 2-D scattering problems.

Because of the aforementioned equivalence, the results in our paper appear to be an exception to the rule that second-kind equations are always preferable. We discuss this carefully from both the theoretical and practical points of view. In particular, the meaning of "equivalence" is clarified, and its interesting relation to matrix ill-conditioning is discussed.

Strategy for Modeling Objects Obstructed by Foliage Above A Penetrable Ground: Spectral and Higher-Order Methods¹

Q. H. Liu*, X. Xu, Z. Q. Zhang, G. Zhao
Department of Electrical and Computer Engineering
Duke University
130 Hudson Hall, Box 90291
Durham, NC 27708-0291

Detecting targets obstructed by foliage above a penetrable ground surface is an important problem in remote sensing, for example, using FOPEN (foliage-penetrating) radar. The complexity of modeling electromagnetic wave interaction with such objects is due to several factors: (1) the presence of many electrically large clutterers introduced by foliage, (2) the reflections from the ground surface and multiple scattering among objects, foliage clutter, and the rough ground surface, and (3) the electrically large objects of interest. These factors pose a formidable challenge in computational electromagnetics.

In this presentation we give an overview of our strategy to address this challenge in modeling foliage obstructed objects above a ground surface. We develop several spectral and higher-order methods for time- and frequency-domain simulation of electromagnetic wave propagation in such a complex environment.

In the frequency domain, we use a volume integral equation formulated using a multilayer Green's function to account for the ground surface and subsurface layers. The conventional method of moment is inefficient for the large problem encountered here. Therefore, we utilize a newly developed stabilized biconjugate-gradient method accelerated by the fast Fourier transform (FFT) algorithm. If the object is discretized into N unknowns, this new algorithm requires $O(N)$ computer memory and $O(N \log N)$ CPU time. In contrast, the conventional method of moment requires $O(N^2)$ memory and $O(N^3)$ CPU time. Our preliminary results show that we can solve a very large problem with 12.75 million unknowns on a SUN Workstation with 1.1 GBytes memory. Our results have been validated by Mie series for multilayer spheres and by other numerical results.

In the time domain, we utilize two newly developed pseudospectral time-domain (PSTD) methods, based on the FFT and Chebyshev polynomial approximation of spatial derivatives, respectively. The Fourier PSTD offers an entire-domain solution and is easy to implement; it is a spectral method for smoothly varying material properties, requiring only two points per minimum wavelength. However, the Fourier PSTD method suffers from the staircasing error for curved objects. On the other hand, the multidomain Chebyshev PSTD method divides the computational domain into object-conformal curved subdomains. Each subdomain is transformed into a cubic subdomain through curvilinear coordinate transformation, followed by expansion of fields in terms of Chebyshev polynomials. The patching conditions between subdomains are either the characteristic conditions or the physical boundary conditions, depending on whether the adjacent subdomains have the same or different materials. This Chebyshev PSTD method requires a coarse sampling of π points per wavelength, but allows a flexible representation of the geometry.

¹This work is supported in parts by the U.S. EPA under a PECASE grant CR-825-225-010, by the NSF under a CAREER grant ECS-9702195.

Comparison of Slot Modeling Techniques in the Frequency and Time Domain

J. D. Kotulski *, W. A. Johnson, R. E. Jorgenson,
L.K.Warne and D. J. Riley
Sandia National Laboratories, P. O. Box 5800,
Albuquerque, NM 87185-1152
jdkotul@sandia.gov

To analyze electromagnetic coupling into complex systems, techniques have to be developed to accurately predict coupling through slots present on the exterior surface on the geometry of interest. Although the small features inherent in a slot can be modeled by the mesh it is prohibitively expensive both in the frequency and time domain. The purpose of this paper is twofold. First the slot modeling implementation is described and explained in the context of the time (VOLMAX) and frequency domain(EIGER) electromagnetic codes used at Sandia National Laboratories. Once this is complete, the results obtained from these codes are compared for a number of test problems.

EIGER(Electromagnetic Interactions GenERalized) is an object oriented, frequency-domain method of moments code. An important capability in the code is how it deals with slots using sub-cell modeling techniques. There are a number of different algorithms that depend on the depth of the slot which are usually referred to as thick or thin slots. The different algorithms are described and compared to analytical models.

VOLMAX is a time domain code that uses a hybrid description of the volume of interest, which can include structured and unstructured grids. This solver can be used in either an explicit (direct time stepping) or an implicit (FEM time domain) algorithm. The focus on this paper will be on the slot models used in the implicit algorithm

Results from the two methods will be compared and conclusions will be drawn on their applicability to practical problems of interest.

Sandia is a multiprogram laboratory operated by Sandia Corporation, a Lockheed Martin Company for the United States Department of Energy under Contract No. DE-AC04-94A185000.

A Hybrid Technique for the Simulations of the Field Scattered by a Finite Dielectric Shield around a Phased Microstrip Antenna Array

**Qinjiang Rao, Hiroyuki Hashiguchi, Shoichiro Fukao
RASC, Kyoto University, Kyoto 611-0011, Japan**

The scattering of a finite dielectric shield around a phased microstrip antenna array is investigated by using a hybrid technique combining uniform physical theory of diffraction (PTD) and the moment method (MoM).

A theoretical investigation of the scattering of a perfectly conducting shield near a phased microstrip antennas array has been available. However, a shield is often made of metallic mesh with dielectric, the simulations of the field scattered by metallic shield with equivalent dielectric constant are needed in practical engineering. In present work, the scattering of electromagnetic wave by a dielectric shield around a microstrip phased array is studied by using a hybrid technique combining PTD and MoM.

In order to simulate the field scattered by a dielectric shield, the field radiated by a microstrip array, as an induced source on the shield, should be known at first. Microstrip elements, arranged in any planar configuration, are excited with linear phase distributions, distances between the elements are supposed to be changed according to the needed pattern. The impedance matrix can be used to calculate the current distribution on each element using the formula based on the assumption that the shield is in the far field of each array element, so the direct influence of the shield on the element electric current can be neglected, but the influence of element currents on other element voltages should be taken into account in the formula due to the coupling effects among elements. After the equation systems are solved, the complex amplitudes of the currents are known, and then, the calculation of the induced field on the dielectric shield can be conducted using the far-field formula. As a result, the field scattered by dielectric shield can be obtained finally.

This study can be extended to investigate further the influences of scattering on radiation pattern of any array. Therefore it can be useful for the analysis and design of clutter prevention fence for a general radar so as to reduce ground sidelobes of the radar.

The application of SDA to boxed planar structures with complex materials

Francisco Mesa[†], Francisco Medina^{††} and Gonzalo Plaza[†]

[†]Dept. Física Aplicada I, Facultad de Informática, Universidad de Sevilla, 41012 Sevilla (SPAIN). email: mesa@cica.es

^{††}Dept. Electrónica y Electromagnetismo. Facultad de Física. Universidad de Sevilla. Avda. Reina Mercedes s/n 41012-Sevilla (SPAIN)
Fax: +34 5 4239434; email: medina@cica.es

The recent technological advances in the research field of complex materials has stimulated the interest of a number of members of the electromagnetics and microwave communities in the analysis of planar transmission lines or devices having substrate layers with very general constitutive parameters. It is expected that the inclusion of complex materials in the design of such physical systems might lead to new microwave devices and/or enhance the performance of the currently existing ones. Thus, some of the methods commonly used to deal with the analysis of guidance or radiation in planar lines or antennas have been adapted to be able of accounting for the presence of layers made of anisotropic, gyrotropic, or even bi(an)isotropic materials. Among them, those methods based on using Fourier transform techniques (namely, SDA) have proved to be relatively simple and very efficient from the numerical perspective (D. Mirshekar-Syahkal, *Spectral Domain Method for Microwave Integrated Circuits*, Artech House, 1990). This method has been successfully extended to the analysis of *laterally open* structures with anisotropic and bi(an)isotropic substrates. Laterally *shielded* configurations having certain particular anisotropic media have also been properly treated in the literature. However, the application of SDA formulas, originally developed in the context of the analysis of open structures, to boxed configurations must be cautiously handled if nonisotropic materials are present. Thus, for instance, direct translation of spectral domain expressions used in the analysis of open longitudinally magnetized ferrite loaded guiding structures to the corresponding boxed case is not possible. Conceptual errors are involved in such step that could yield inaccurate numerical results. The presence of vertical (normal to the layered structure) electric or magnetic walls is not accounted for simply by means of the usual source mirroring procedure. Mirroring of the tensor constitutive parameters is also required. This is a question that has been implicitly addressed in the electromagnetics literature in various contexts, but it seems that some authors working on SDA are not completely aware of this fact. This could be due to the lack of a comprehensive discussion on this particular point in the frame of SDA. Our proposal here is to clarify the conditions under which SDA is suitable for the analysis of boxed planar lines including arbitrary complex linear media (anisotropic dielectrics, ferrites, magnetoplasmons, chiral media and so on) as substrates. It will be shown that whereas SDA can be always efficiently applied to study either laterally open or periodic structures, the simultaneous presence of lateral boundary conditions and nonisotropic materials requires further study. Thus, it will be reported the symmetry properties of the constitutive dyadics that makes it possible a rigorous application of SDA to that kind of structures.

Wave Scattering by non linear ferromagnetic materials

P. Joly
INRIA Rocquencourt
78 153 Le Chesnay Cedex, FRANCE

O. Vacus*
CEA/CESTA BP2
33 114 Le Barp, France

Magnetic materials are known to be absorbing; for this reason, they can be used as stealthy coating to decrease the RCS of a metallic target. But they are also non linear. Despite of that, modelisation of ferromagnetic materials is often done in the frequency domain, after linearization (Polder tensor). As far as scattering is concerned, the question is to know how long this approach is valid according to the power of the incident wave.

To this aim we have developed a FDTD method for approximating the non linear equations describing the electromagnetic field in a ferromagnetic material, namely the time Maxwell's equations coupled with the so-called Landau-Lifschitz-Gilbert law (LLG). All the internal contributions are taken into account (static field, anisotropy) but the exchange contribution. This FDTD method is based on a slight modification of the Yee's scheme and an original time discretization of the LLG equation (P. Joly, O. Vacus, *M2AN*, 33, 593-626, 1999). It leads to an implicit scheme which can be however explicitly solved: this ensures the efficiency of this kind of approach. Moreover the scheme preserves the basic properties of the continuous model as the conservation of the norm of the magnetization at any point, or the decay of the electromagnetic energy during the propagation within the material. Due to this energy decay, stability is proved under a classical CFL condition. This allows to perform long time experiments and to compute by fourier transform results on a broad range of frequencies.

But, above all, typical non linear effects can be observed. It is true for instance in the spectra of diffracted signals by a ferromagnetic layer: polarization of the electromagnetic wave is partly changed while new frequencies (harmonics) are created. We see that these effects can be significant as soon as the modulus of the incident magnetic field reaches the tenth of the modulus of the internal field computed at equilibrium.

TDIE-MoM Solutions for Scattering by Thin-Wire Antenna Using Spatio-Temporal Wavelet-Packet Expansions

Y. Shifman* and Y. Leviatan
Department of Electrical Engineering
Technion — Israel Institute of Technology
Haifa 32000, Israel
E-mail: shifman@ieee.org

To investigate the transient response of thin-wire antennas effective time-domain analysis techniques are always needful. In this case, a solution based on the time-domain integral equation (TDIE) is often preferable over FDTD since it requires a discretization of an unknown, which is confined to the antenna wires. To reduce the TDIE to matrix form, we use the method-of-moments together with standard pulse basis functions and in turn transform the resultant matrix equation into a spatio-temporal wavelet-packet basis. The idea is to exploit the sparsity of the solution in this spatio-temporal representation and thereby avoid a solution of the original large matrix. In this approach we iteratively construct and solve a reduced-rank (compressed) version of the transformed matrix equation until the desired degree of accuracy is attained. Results demonstrating the advantages of the suggested time-domain iterative matrix compression method over standard marching-on-in-time solutions will be presented.

Modeling Frequency Selective Surfaces by the Finite Element Method

I. Bardi, R. Remski, D. Perry and Z. Cendes
Ansoft Corporation, Four Station Square, Pittsburgh, PA 15219, USA

Frequency selective surfaces (FSS's) have garnered considerable attention in telecommunications, antenna design, and electromagnetic compatibility (EMC) in recent years. These surfaces provide uninhibited transmission in specific frequency bands but suppress transmission in other bands when an incident wave impinges their surface. Traditionally, FFS's involved producing a periodic lattice on the surface of a substrate. Recently, work has focused on fabricating these substrates using 3D photonic band gap (PBG) structures. Such structures are composed of unit cells containing implants periodically placed to form an artificial crystal lattice within the substrate. Modern PBG structures involve complex periodicities. The unit cell is often 3D, and the relationship of the field between the walls of the unit cell can be completely general. The shape of the unit cell can be arbitrary and the field across the cell can vary in a complex manner.

The aim of this paper is to describe special finite element procedures that can be used to analyze the reflection and transmission of incident waves from FSS's. The finite element method easily copes with the complicated shapes, anisotropic materials and arbitrary embeddings encountered with PML's. However, special procedures must be developed to include the description of periodic structures using unit cells and linked boundary conditions (LBC's) to replicate the infinite lattice, the use of the scattered field formulation for separating scattered and incident fields, and the application of perfectly matched layers (PML's) to absorb reflected waves but allow incident waves through. Since both the incident and the scattered field can be considered as guided waves, the commonly used Absorbing Boundary Conditions (ABC's) are not well suited to modeling such problems. The use of PML's together with the scattered field formulation, however, requires special measures to be employed. These special measures arise from the fact that the properties of PML materials depend on the propagation direction as determined by the incident angle, as well as the coupling with the incident field. PML's are not physical materials, so that sources due to incident waves in physical materials must be switched off. Another special measure is to modify the operator in the source terms, which would introduce an error in vacuum. This makes the scattered field more accurate in weak field regions. This is easily done, but provides an unorthodox technique.

The procedure will be described in this presentation and examples solved by the Ansoft High Frequency Structure Simulator (HFSS) will be used to demonstrate the effectiveness of the technique.

Quasi-static Analysis of Fringe Capacitances for Horizontal and Vertical Annular Frills

Hsueh-Yung Chao and Weng Cho Chew
Center for Computational Electromagnetics
Department of Electrical and Computer Engineering
University of Illinois at Urbana-Champaign
1406 West Green Street, Urbana, IL 61801

Fringe capacitance analysis is important for high-accuracy input impedance calculation of coaxial-fed structures, such as monopole antennas on ground planes and probes for non-destructive testing. As shown in our previous paper [Chao et al., IEEE AP-S, 1999], traditional impedance calculation by a delta-gap source model neglects two important factors: the contribution from fringe capacitances and the interaction of aperture fields with structures at the vicinity of an aperture. Our previous fringe capacitance calculation is based on the field calculation through a vector potential approach [Butler and Tsai, IEEE Trans., AP-21(1), 1973]. The resultant expression for the fringe capacitance of a horizontal frill is a triple integral in space domain [Misra, IEEE Trans., MTT-35(10), 1987]. By applying the Sommerfeld's identity and the addition theorem for Bessel functions, the capacitance can be expressed as a single integral in the spectral domain, which is equivalent to the lowest order approximation of capacitance in [Mahony, IEE Proc., 135(A)-7, 1988]. Instead of using the mode matching approach as Mahony, we propose a succinct method for deriving the quasi-static fringe capacitance and also discuss the evaluation of the semi-infinite integral in spectral domain. In order to further expedite the capacitance calculation, the dependence of the capacitance with respect to frill inner and outer radii is pre-calculated and fitted by a polynomial curve.

In addition, we will demonstrate that coaxial-driven feeds for dipole antennas can be modeled more accurately by a vertical frill source. By the equivalence principle, a voltage source at a wire gap can be replaced by a magnetic current ribbon with the gap sealed. In contrast to a delta-gap source, a magnetic frill source leads us to an input impedance that depends on both the wire radius and the gap distance. A succinct spectrum domain representation of the quasi-static fringe capacitance for a vertical frill will be presented. Numerical calculation of the input impedance of a dipole antenna will be compared with the results in [Junker et al., Microwave Opt. Tech. Lett., 12(3), 1996].

Wide Band Antennas

Chair: R. Haupt, USA

	Page
1:00 Wide Band Antenna Optimization CAD Tool, <i>Y. C. Chung*, R. Haupt Utah State University</i>	70
1:20 Two Novel, Ultra-Wide Bandwidth, Dual Linearly-Polarized Dielectric Antenna Designs, <i>P. Diez*, C.C. Chen, W.D. Burnside, The Ohio State University</i>	71
1:40 A New Microstrip Horn Antenna for Ultra-Wideband Applications, <i>C. Nguyen*, J.S. Lee, J.S. Park, Texas A&M University</i>	72
2:00 Wide-Band Patch Antennas with Asymmetric Microstrip Excitation, <i>A. Faraone*, Q. Balzano, Motorola Labs</i>	73
2:20 Bandwidth Enhancement Techniques for Printed Cloverleaf Antennas, <i>S. Silva*, H. Foltz, Virginia Polytechnic Institute and State University, C. Dietrich, R. Nealy, University of Texas - Pan American</i>	74
2:40 Broadband Application of High Impedance Ground Planes, <i>K.J. Golla*, P.J. Collins, S. Schneider, A.J. Terzuoli, Air Force Institute of Technology and Research</i>	75
3:00 A Wideband U-Slot Patch Antenna with Photonic Bandgap Structure, <i>R. Lee*, A. Zaman, NASA Glenn Research Center</i>	76
3:20 The Conical Spiral Antenna Probe for Underground Object Detection, <i>H. Raemer*, C. Rappaport, Northeastern University</i>	77
3:40 Gabor-Frame Phase-Space Beam Summation Formulation for Wideband Radiation from Apertures Sources, <i>A. Shlivinski*, E. Heyman, A. Boag, Tel Aviv University, D. Lugara, C. Letrou, I.N.T.</i>	78
4:00 Broadband Printed Quadrifilar Helical Antenna with Variable Wire Width, <i>J.C. Louvigne*, A. Sharaiha, D. Thouroude, Universite de Rennes</i>	79
4:20 Impedance Matching of Microstrip Antennas with a Parallel Resonant Circuit, <i>D.M. de Haaij*, J. Joubert, J. W. Odendaal, University of Pretoria</i>	80

Wide Band Antenna Optimization CAD Tool

You Chung Chung and Randy Haupt
Utah State University
Electrical and Computer Engineering
4120 Old Main Hill
Logan, UT 84322-4120
youchung@ieee.org
haupt@ieee.org

Abstract

Log period dipole array (LPDA) and helical antennas are commonly used broadband antennas. Number of elements wire thickness, element length, pitch angle, number of turns and element spacings are all parameters that impact the antenna performance. The parameters of both antennas are optimized with the user-friendly CAD tool using a hybrid genetic algorithm & local optimization method to have high gain, low voltage standing wave ratio (VSWR) of the antennas and low axial ratio of the helical antenna.

The element length, spacings and radii of LPDAs have been optimized for high gain and low VSWR over a specified bandwidth: (Y. C. Chung and R. L. Haupt, IEEE Aerospace Conference Digest, March, 2000). The paper showed that a hybrid GA & Nelder-Mead algorithm optimized the design of the log periodic dipole arrays worked better than using the Nelder-Mead down hill simplex or genetic algorithm alone.

In this paper we develop a CAD tool linked with NEC using a hybrid GA & local optimization method to design a broadband log period dipole array and helical antenna. The initial window allows the user to select a type of antenna (LPDA or Helical) and a frequency range. A user can change the number of elements, upper and lower limits of element length, radii and spacings, target gain and VSWR over the frequency range for the LPDA. For the helical antenna, a user can select the number of turn, radius, thickness of wire, pitch angle, and target parameters—gain, VSWR and axial ratio. In addition, a user can select the number of maximum evaluations, and the weighting factor of gain, VSWR, axial ratio of the helical and standard deviation of gain and VSWR in the evaluation function of algorithms. The pattern of the optimized antenna, and the antenna shape can be shown in the separated windows at the end of optimization. Finally, a user will have a log period dipole array or a helical antenna with high gain, good axial ratio and low VSWR over a specific bandwidth.

Two Novel, Ultra-Wide Bandwidth, Dual Linearly-Polarized Dielectric Antenna Designs

Pablo A. Diez, Chi-Chih Chen and Dennie Burnside
The Ohio State University ElectroScience Laboratory
1320 Kinnear Road, Columbus, Ohio 43212, USA
TEL: (614) 292-7981, FAX: (614) 292-7297

Two novel designs of an UWB, dual linearly-polarized dielectric horn antenna (DHA) and dielectric rod antenna (DRA) have been developed at OSU/ESL. A broad bandwidth launcher was used to launch fields into the dielectric body, where the fields are guided by the air-dielectric boundary conditions for the DHA design and by the fundamental hybrid mode for the DRA design. These dielectric antennas provide broad bandwidth and symmetric E-plane and H-plane radiation patterns.

The OSU/ESL developed UWB dual linearly-polarized dielectric antennas that provide broad beamwidth which are ideal for being used as a reflector illuminator or a probe antenna. The operational frequency range for the current DHA prototypes is from 3 to 18 GHz. The current DRA prototype is suitable for X-band near-field probing. Because of the reasonably constant patterns obtained through these frequency ranges, the use of dielectric materials is so desirable and advantageous. The value for the dielectric constant was selected to minimize the impedance mismatch both at the feed and at the radiation aperture, as well as to minimize the actual size of the antenna and therefore minimizing blockage. The operational characteristics of these antennas as well as measurement results obtained from the OSU/ESL compact range will be discussed. Figure 1 illustrates some of these results.

Frequency independent beam width and constant radiation patterns can be achieved. A good feeding structure not only will eliminate the possible excitation of higher order modes but also at the same time make the antenna broadband. Proper dielectric shaping and the proper use of absorbing material can control patterns variations due to edge diffraction and feed radiation leakage. Some design criteria as well as the study of the Radar Cross Section are of different DRA aperture shapes will also be discussed.

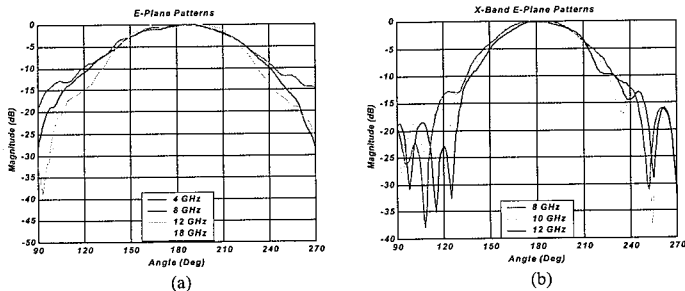


Figure 1 E-plane patterns at different frequencies for (a) DHA and (b) DRA

A NEW MICROSTRIP HORN ANTENNA FOR ULTRA- WIDEBAND APPLICATIONS

Cam Nguyen*, Jeong-Soo Lee, and Joong-Suk Park

Department of Electrical Engineering
Texas A&M University
College Station, TX 77843-3128

ABSTRACT

The development of wideband antennas has been an important subject for many decades. Recently, wideband antennas has received increasingly significant attention and interest for use in ultra-wideband (UWB) radar and communication systems for both military and civilian applications.

This paper reports on the development of a new UWB antenna. The antenna, based on microstrip transmission line, forms a horn and possesses an extremely wide bandwidth with small distortion and relatively high gain. It does not require a balun or transition at the input port and is inherently matched. Measured results show return loss of better than 10 dB from 0.2 to more than 20 GHz, gain from 7.5 dBi at 2.6 GHz to 17.6 dBi at 18 GHz, and good radiation patterns. Although not measured, the antenna should also perform well at much higher frequencies than 18 GHz. With proper size and shape, the antenna can achieve a relatively flat gain response over an extremely wide bandwidth. Measured transient responses of the antenna confirm its feasibility for use in UWB time-domain systems. Calculated and measured radiation patterns also agree reasonably well. The new antenna has many desirable characteristics and thus should be useful for many UWB applications.

Wide-Band Patch Antennas with Asymmetric Microstrip Excitation

Antonio Faraone* and Quirino Balzano
Motorola Labs, Corporate EME Research Lab
8000 W. Sunrise Blvd., Fort Lauderdale, FL 33322, USA

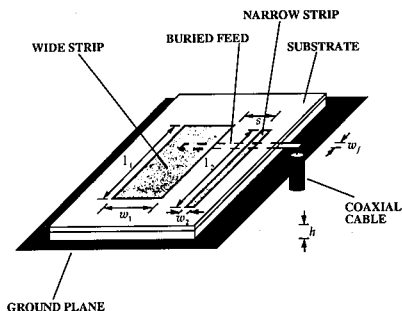
Introduction

Patch antennas offer the obvious advantage of low-profile geometry, low-cost realization, and reduced resonant length if loaded with high-permittivity substrates. They also feature desirable low mutual coupling in arrays. However, typically they are high-Q resonant structures, thus placing severe limitations on communication bandwidth (*Microstrip Antennas*, D. M. Pozar, and D. H. Schaubert Eds., IEEE Press, New York, 1995). In this report, a family of multi-element wide-band patch antennas is presented. A single buried microstrip line individually and collectively excites two- and three-element radiators. Electrically thin wide-band patch antennas have been realized using high dielectric permittivity substrate (alumina). The radiation pattern measurements indicate that the multi-resonant structures support modes that feature concurring or opposite currents on the different patches forming the radiator.

Results

We present results of an investigation on planar antennas featuring multiple patch elements that are excited by a buried 50-ohm microstrip line. Two different antenna configurations are described, one featuring two patch elements (in the figure), one wide and one narrow, the other featuring three of them, a wide one between two narrow ones. All elements are simultaneously excited by a buried microstrip crossing underneath them, so none of the antenna elements is parasitically coupled to a fed one, as in previous realizations. The mentioned designs have been granted US Patents 5,933,115 and 6,002,368.

Prototypes featuring impedance bandwidth (VSWR<2) greater than 5% on alumina substrate ($\epsilon_r = 10$) thinner than $\lambda_0/60$ were realized. Measurements demonstrate multi-resonant operation associated to the excitation of resonant modes that exhibit close resonance frequencies. Moreover, the radiation patterns exhibit a frequency-dependent behavior that can be associated with the excitation of concurrent or opposite currents on the antenna elements. A likely explanation of the observed behavior is that the asymmetric excitation (open-ended buried microstrip line) can excite both common and differential modes that exhibit different effective wavenumbers due to the dielectric substrate. Asymmetry in element width determines the ratio between the corresponding resonant wavelengths, which can be adjusted to obtain a wide, continuous impedance bandwidth. Design of quarter-wave and circularly polarized versions is also possible.



BANDWIDTH ENHANCEMENT TECHNIQUES FOR PRINTED CLOVERLEAF ANTENNAS

Saul Silva¹, Heinrich Foltz¹, Carl Dietrich², Randall Nealy²

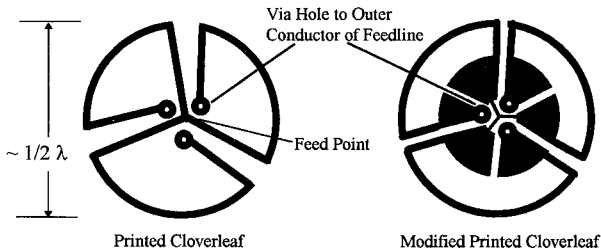
¹University of Texas - Pan American, Edinburg, TX

²Virginia Polytechnic Institute and State University, Blacksburg, VA

A large cloverleaf or "big wheel" antenna, consisting of three parallel connected horizontal loops, is useful as an azimuthally omnidirectional horizontally-polarized radiator. The loops are operated near series resonance, where each loop has a circumference of approximately one wavelength. The pattern shape is similar to that of a vertical dipole, and thus a possibility exists of using the cloverleaf in conjunction with a vertical dipole for omnidirectional polarization diversity.

In order to self-resonate the antenna and extend its operating bandwidth, a slotted disk structure as shown below can be added. The structure can be viewed as placing an open-ended slotline stub in parallel with the input to each loop. If the antenna is printed on a substrate which is thin compared to loop dimension but thicker than the slot width, the dielectric will have little effect on the resonant frequency of the loop radiators; however, the resonant frequency of the slots will be significantly changed. Through the selection of the slot length and the dielectric material, the slot can be made one-half-wavelength long (parallel resonant) in the same frequency range where the loop is series resonant. The parallel combination of the resonances creates a broadened, double tuned response.

Testing of prototypes shows that the patterns are uniform in azimuth to within ± 1 dB, and that stable patterns and impedance response can be obtained without a balun or choke sleeve on the feeding coax; however, cross-polarization performance may be impacted if a choke sleeve is not used. Initial unoptimized prototypes have shown a 2:1 SWR bandwidth of 17%, compared to 11% without the slotline structure; with further refinement it should be possible to at least double the bandwidth.



BROADBAND APPLICATION OF HIGH IMPEDANCE GROUND PLANES

K. J. Golla, P. J. Collins, S. Schneider, A. J. Terzuoli, Jr.
Air Force Institute of Technology and Research Laboratory, USA

Electrical conductors have long been the only materials available to antenna designers for reflecting structures. However, using the same conducting materials for both the antenna's radiating elements and the reflecting ground plane requires physical isolation between the two. Recently reported High Impedance Ground Plane (HIGP) structures offer a possible alternative. The HIGP exhibits high surface impedance to electromagnetic waves within a limited frequency stop-band. The high impedance surface creates image currents and reflections that are in-phase with a source rather than out-of-phase as it is with a conducting surface. Also, the high impedance surface suppresses surface waves while they propagate freely on a conducting surface. HIGP reflectors have been applied successfully to narrow band antennas such as wire monopoles and patches.

Broadband antenna applications are explored using a planar log-periodic zigzag antenna. Applying the log-periodic zigzag antenna to the surface of a homogeneous narrow band HIGP reveals that the high impedance ground plane alters the fundamental radiating modes of the antenna. While the antenna/ground-plane pair radiate within the expected band gap of the HIGP, the antenna no longer radiates from the expected log-periodic active region.

Broadband HIGP designs explore varying the scale of the ground plane elements to match the radiating elements of the applied log-periodic zigzag antenna. Small ground plane elements corresponding to the high frequency region of the antenna transition to larger elements scaled and positioned to match the low frequency regions of the antenna. However, measurements show the high frequency region of the ground plane shorts out all energy in frequencies below its active band gap. Low frequency energy cannot propagate over the high frequency region of the ground plane and never reaches the center feed region of the planar log-periodic antenna.

A Wideband U-Slot Patch Antenna with Photonic Bandgap Structure

Richard Q. Lee* and Afroz Zaman
MS 54-8
NASA Glenn Research Center
21000 Brookpark Road
Cleveland, OH 44135

Microstrip antennas inherently have very narrow bandwidths. Recently, many novel techniques, such as using parasitic elements, thick substrates, slots etc., have been introduced for bandwidth enhancement. In particular, U-slot patch antennas have been reported to have an impedance bandwidth of over 20%, about a ten-time increase over conventional patch antennas (K.F. Lee et al, IEE Proc. Microwave Ant. & Prop. Vol.144, No.5 Oct. 1997). The U-slot antennas reported in the literature generally have probe feed and air dielectrics of thickness of about 0.08λ . The use of U-slot compensates the large inductance associated with a long probe conductor while the air dielectric suppresses the surface wave in a thick dielectric, thus contributing to the overall excellent performance of the antenna. In practice, it is often desirable to fabricate the antenna on substrates with higher permittivity in order to reduce the size of the antenna (Y.P. Zhang et al, Microwave and Optical Technology Letters, Vol. 28, No. 2, Jan. 20, 2001). However, antennas fabricated on higher permittivity materials often have lower bandwidths since the bandwidth is inversely proportional to the effective dielectric constant. Furthermore, lower antenna efficiency and higher sidelobe levels could be resulted as a result of surface waves excited in thick substrates.

In this paper, a photonic bandgap (PBG) structure is proposed to enhance the efficiency and bandwidth of a U-slot antenna fabricated on a 62 mil Roger/Duroid 5880 substrate, which is approximately 0.08λ at the operating frequency of 11 GHz. By designing the stop-band of the PBG centered at the operating frequency of the patch antenna, the surface wave is suppressed and the energy radiated into the substrate is reflected back into free space. As a consequence, the radiation efficiency of the antenna could be significantly improved. In general, the stop-band center frequency f_c is a function of the period of the structure, which is approximately equal to one half of a guided waveguide at f_c , while the depth and bandwidth of the stop-band strongly depend on the circle radius and number of periods (D. Maytre, Pure Appl. Opt., Vol. 3, No. 6, Nov. 1994). In this work, two different PBG designs have been investigated. The first PBG design consists of an array of circular holes fabricated on the ground plane, and the second design replaces the holes with annular rings. The probe-fed U-slot antenna of dimensions (8 mm x 11.4 mm) is placed over a 2-D (7x8) PBG structure. Preliminary analytical results show good agreements with theory and predicted performance characteristics for both PBG designs. Details of analytical and experimental results will be presented and discussed.

ABSTRACT

THE CONICAL SPIRAL ANTENNA PROBE FOR UNDERGROUND OBJECT DETECTION

Harold Raemer and Carey Rappaport
Department of Electrical and Computer Engineering and
Center for Subsurface Sensing and Imaging Systems
Northeastern University, Boston, MA 02115

In underground object detection by ground penetrating radar, it is necessary to use an antenna with a bandwidth sufficiently large to accommodate wideband transmitted signals and wide receiver passbands. The high spatial resolution attainable with system bandwidths of the order of Gigahertz is limited by employment of antennas with insufficient bandwidths.

Recently the authors initiated an investigation of the use of a particular class of "frequency independent antenna", the conical spiral, in a GPR application. The antenna is used as a probe, thrust into the ground apex first at an angle of about 60 degrees from vertical and radiating primarily along the cone axis. This antenna offers promise of large bandwidth within the constraints of size and portability. The planned deployment method should provide significant enhancement of the information about nearby buried objects (e.g. mines) than the mechanical probes routinely used in mine detection work.

The basic reference sources are a series of papers published in the 1960's in AP Transactions by Rumsey, Dyson, Yeh, Mei and others, on the theory of frequency independent antennas in general and the conical spiral in particular, in free space. Our investigation extends this work to include the partial immersion of the antenna in a soil medium, the interactions between the antenna and the possibly rough air-ground interface and interactions between the antenna and the buried object that the radar is attempting to detect. The frequency range of interest is 500 MHz to 8GHz.

A MOM computation of the currents on a conical spiral antenna 52 cm. long and with a maximum diameter of 12 cm. immersed in dry sand, followed by evaluation of the near field pattern, was carried out by the authors and reported in a recent conference paper (SPIE Aerosence, Orlando, April, 2001). The present paper is a continuation of that work to include other soil media and to begin to address some of the effects of the air-soil interface and the buried object on the operation of the antenna.

Gabor-Frame Phase-Space Beam Summation Formulation for Wideband Radiation from Apertures Sources

Amir Shlivinski⁽¹⁾, Ehud Heyman⁽¹⁾, Amir Boag⁽¹⁾, Delphine Lugara⁽²⁾,
Christine Letrou⁽²⁾

⁽¹⁾Department of Physical Electronics, Tel Aviv University
Tel Aviv 69978, Israel, fax: +972-3-6423508, e-mail: heyman@eng.tau.ac.il

⁽²⁾I.N.T., 9 rue Charles Fourier, F-91011 EVRY Cedex, FRANCE
fax: 33 1 60 76 42 84 e-mail: Christine.Letrou@int-evry.fr

Phase-space formulations are an important tool for tracking high frequency wave fields since they provide systematic framework for ray-based spectrally uniform solutions in configurations of increasing complexity. Of particular interest are beam-based phase space formulations that make use of windowed configuration-spectrum transforms (e.g., the local Fourier transform in the frequency domain and the local-slant-stack-Radon transform in the time domain). The advantages of the beam formulations are: (a) The phase space data is a priori localized in the vicinity of the Lagrange manifold (the geometrical optics phase-space skeleton); (b) The beam propagators can be tracked in inhomogeneous media or through interactions with interfaces and, unlike the ray or plane-wave propagators, they are insensitive to transition zones.

An important advantage of the beam-based formulations is that they may be a priori discretized via the Gabor representation. Yet this formulation suffers from two fundamental difficulties: (a) The dual basis function that extracts the phase-space information from the data is distributed and quite irregular, giving rise to instabilities and non-local contributions; (b) The phase space lattice is constrained by the Gabor condition $XK = 2\pi$ (X and K being the spatial and spectral discretization step-sizes) whence the beam lattice (origins and directions) varies with frequency. This makes the conventional Gabor-based beam formulation inconvenient for wideband applications.

In this paper we present a wideband frame-based beam representation that accommodates the difficulties mentioned above. Using an overcomplete basis removes the Gabor constraint and adds another degree of freedom which makes it possible to use the same beam axes at all frequencies, thus leading to a wideband beam representation. The overcompleteness also smoothes out the dual (analysis) function thus yielding a localized regular representation. We also show that the set of iso-diffracting Gaussian-beam basis functions can be tuned to provide the most stable (i.e., "snuggest frame") representation for all frequencies. Furthermore, these basis functions can be transformed in a closed form into the time domain where they described the so-called iso-diffracting pulsed beam, leading to a new frame-phase space formulation for short-pulse fields directly in the time domain [REF]. A possible application is the derivation of a new Gabor-type discretized local Radon transform.

[REF] A. Shlivinski, E. Heyman, A. Boag, A. Flueraşu and C. Letrou, "A discretized-phase-space radon transform for time domain radiation from extended apertures," *This conference* .

Broadband printed quadrifilar helical antenna with variable wire width

J. C. Louvigné, A. Sharaiha and D. Thouroude
Lab. ART, Eq. Antennes et Technologie
Université de Rennes I, Campus de Beaulieu, Bât. 22
35042 Rennes Cedex, France
Email: jlouvign@univ-rennes1.fr

In the last years, the printed quadrifilar helical antenna (PQHA) has been widely proposed for use in various mobile communication systems due to its many advantages (light weight, low cost, circularly polarised and a very good axial ratio in the beamwidth). Such PQHA is obtained by printing the four arms on a thin dielectric substrate wrapped around a cylindrical support and can be analysed by using a method of moments formulation for arbitrary shaped wire antennas (B. Desplanches et al., *Microwave Opt. Tech. Lett.*, 6, 352-355, 1997). Dual band or wide band antennas are required for mobile communication systems. Nevertheless, the bandwidth of a conventional PQHA is typically of 5% which could be insufficient for such applications. A dual frequency band behaviour of this antenna can be obtained by using the mutual coupling effect between two PQHA fitted into each other giving a good impedance match in both the receive and the transmit bands (A. Sharaiha et al., *FR Patent N° 8914952*, November 1989). One of the major disadvantages of this antenna is their complex constructions.

This paper details the concept of a PQHA with variable wire width all along the antenna in order to increase its bandwidth. Experimental data indicate that a net increase is observed in the bandwidth (Bw) of the new PQHA built compared to the conventional one as can be seen in the figure below. In fact, we obtain in L Band a Bw of 14% instead of 7% (Bw is defined for $VSWR < 2$) and in S Band a Bw of 16% instead of 5%.

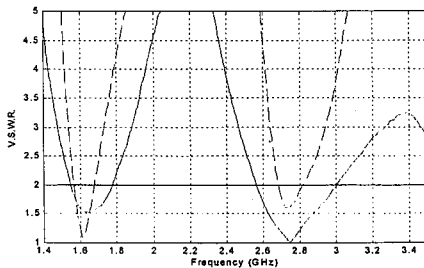


Figure: Measured V.S.W.R. of a conventional PQHA (dashed line) and a PQHA with variable wire width (solid line)

Impedance matching of microstrip antennas with a parallel resonant circuit

D.M. de Haaij*, J. Joubert, J.W. Odendaal
Centre for Electromagnetism
Department of Electrical, Electronic and Computer Engineering
University of Pretoria
Pretoria, 0002
South Africa
Tel: +2712 420-3604
E-mail: dehaaij@ieee.org

In the area of bandwidth enhancement of microstrip antennas various techniques have been investigated. Many of these techniques proved to be very effective in the enhancement of the bandwidth, but often the improvement is obtained with some trade-off in other antenna characteristics, such as radiation pattern, compactness and ease of fabrication. Impedance matching for microstrip patch antennas based on the real frequency technique was investigated by Pues *et al.* (H.F. Pues, A.R. van de Capelle, IEEE Trans. Antennas and Propagation, Nov. 1989, pp. 1345-1353). In this method a LC-ladder, normally consisting of a parallel-capacitor series-inductor combination, is utilised in the impedance matching circuit.

In this paper an alternative method of impedance matching for microstrip antennas is presented that exploits the RLC-resonant structure of the microstrip patch antenna. It is shown that by using a parallel-resonant LC-structure in the matching circuit the impedance bandwidth of a microstrip antenna can be improved by 50% or more. This technique utilises a combination of transmission line impedance and phase transformations with the required LC-resonant circuit to achieve a very simple and effective wideband match. The addition of impedance matching to the system ensures that a specified bandwidth is now obtainable with a lower substrate patch antenna. In a probe-fed antenna this will shorten the probe length resulting in lower cross-polarisation. A smaller ground plane will also suffice for the lower substrate height, effectively reducing the overall size of the antenna.

Examples are given to show the design process and the resulting improvement in bandwidth. The practical aspect of using matching circuits to improve the bandwidth of microstrip patch antennas is discussed, focusing on the physical limitations that exist on the capacitor and inductor values realizable with microstrip lines.

Array Analysis and Design

Chair: B.Rama Rao, USA

	Page
1:00 Sparse Array Realization of Collimated Short Pulse Beam Fields, A. Shlivinski*, E. Heyman, Tel Aviv University	82
1:20 Application of Two-Level Evolutionary Algorithms to Self-Structuring Antennas, C.M. Coleman*, E.J. Rothwell, Michigan State University, J.E. Ross, John Ross & Associates	83
1:40 Array Pattern Synthesis in the Presence of a Mounting Tower Using the Genetic Algorithm, T. Su*, K. Dandekar, H. Ling, The University of Texas at Austin	84
2:00 The Selection of Starting Points for Array Synthesis Using the Method of Generalised Projections, E. Botha*, University of Pretoria, D. McNamara, University of Ottawa	85
2:20 The Range Increase of Adaptive Versus Phased Arrays in Mobile Radio Systems: Interface Included, M. da Silveira*, J.W. Odendaal, J. Joubert, University of Pretoria	86
2:40 Ultra Broadband Antenna Array for Mobile/Wireless Communications, Square-Kilometer-Array Telescope and Other Applications, T.B. Vu*, City University of Hong Kong	87
3:00 Comparison of Beamforming Techniques for W-CDMA Communication System, H. J. Li*, T. Y. Liu, National Taiwan University	88
3:20 A Two Dimensional Coupled Oscillator Array with MMIC Frequency Multipliers, J. Shen*, L.W. Pearson, Clemson University	89
3:40 Precise Analysis of Commercial Log-Periodic Dipole Arrays Using Wire-Antenna Algorithms, A. Djordjevic*, A. Zajic, B. Kolundzija, University of Belgrade, T. Sarkar, Syracuse University	90
4:00 Ray Analysis of the Radiation from a Large Finite Phased Array of Antennas on a Grounded Material Slab, P. Janpugdee*, P. Pathak, The Ohio State University, P. Nepa, University of Pisa, O. A. Civi, Middle East Technical University, H.T. Chou, Yuan Ze University	91
4:20 Applications of Forward-Backward Method in the Fast Analysis of Two-Dimensional Array Structures, H. T. Chou*, H.K. Ho, Yuan Ze University	92

Sparse Array Realization of Collimated Short Pulse Beam Fields

Amir Shlivinski and Ehud Heyman

Department of Physical Electronics, Tel Aviv University
Tel Aviv 69978, Israel, fax: +972-3-6423508, e-mail: heyman@eng.tau.ac.il

In a recent paper [1] we have explored the kinematic properties of transient scanning arrays, i.e., arrays that are driven by pulsed waveforms and are controlled by the inter-element time shifts. The emphasis in there has been placed on the mechanisms and the conditions for the generation of various side lobe phenomena that characterize array sources. In particular it has been shown that the monochromatic grating lobes disappear in the ultra wide band limit, and are replaced by the *cross-pulse lobes* that depend on the pulse repetition rate. One may thus design sparse arrays whose inter-element spacing is much larger than the wavelength for all frequencies in the band, which basically does not suffer from severe side lobe problem.

The present paper is concerned with an array realization of source distributions for collimated short pulse beam fields. Several classes of analytic solutions for such fields have been introduced in the last two decades. These solutions are typically characterized by *non-uniform space-time source distribution*, whence each array-element in our discretized formulation must compensate for both the *amplitude* and the *waveform* variations of the idealized (i.e., continuous) distribution within the local cell. This sets a limit on the dimensions of each one of the cells in the array as a function of the local pulse-length and of the transverse variation of the source-waveform, for a given bound on the error of the far field transient radiation pattern. Another limit on the cell dimensions is set in order to avoid the *cross-pulse lobes* due to the pulse repetition rate. The final non-uniform array geometry (and thus the number of the array elements) is then determined by weighting the errors from the individual cells in order to meet the total error criterion within a given space-time window. It is shown that the cell dimensions (and thereby the array sparsity) are proportional to the error level allowed.

The general conditions derived are applied for an array realization of the so called complex source pulse beam (CSPB also termed iso-diffracting pulsed beam). The resulting non-uniform array is shown to be ultra-sparse (with inter-element spacing much larger than the wavelength for all frequencies in the band) when compared with a conventional monochromatic array design.

[1] A. Shlivinski and E. Heyman, "Analytical methods for antenna analysis and synthesis in the time domain," in *Proceedings of the Ultra-Wideband, Short-pulse Electromagnetics 5*, P.D Smith ed., June 2000, to be publish by Plenum Press, NY.

APPLICATION OF TWO-LEVEL EVOLUTIONARY ALGORITHMS TO SELF-STRUCTURING ANTENNAS

C. M. Coleman*, E. J. Rothwell
ECE Department
Michigan State University
East Lansing, MI 48824

J. E. Ross
John Ross & Associates
350 W 800 N, Suite 317
Salt Lake City, UT, 84103

A Self-structuring antenna (SSA) is capable of altering its electrical shape in response to changes in its electromagnetic environment. An SSA template is an arrangement of wires interconnected by controllable on or off switches and is the intended radiator or receiver of electromagnetic energy. The states of the switches determine the electrical characteristics of the SSA template. An embedded microprocessor is used to evaluate sensor feedback such as SWR or received signal strength to help make decisions on subsequent switch configurations. A binary search algorithm such as a genetic, simulated annealing, or Ant Colony Optimization (ACO) algorithm is used by the microprocessor to reduce the searching time required to find a switch configuration with desirable electrical characteristics. The SSA has been demonstrated in previous work both experimentally (C. M. Coleman, E. J. Rothwell, and J. E. Ross, *IEEE AP-S Int. Symp.*, Salt Lake City, Utah, 2000) and in simulation (J. E. Ross, E. J. Rothwell, C. M. Coleman, and L. L. Nagy, *URSI National Radio Science Meeting*, Salt Lake City, Utah, 2000). The SSA has recently been granted US patent 6178325.

One goal of this research is to synthesize non-intuitive template geometries with desirable capabilities. This is accomplished in part by incorporating a two-level evolutionary algorithm in the SSA simulation. The outer algorithm will generate varying template geometries (arrangements of wires and switch locations). The inner algorithm, performed for each template geometry, will evaluate the fitness of configurations (sets of template switch states) and search for optimal configurations. The NEC-4 program will be used as the EM solver to evaluate the fitness of template configurations by computing their electrical characteristics (pattern, impedance, received signal strength, etc.). The outer algorithm will generate subsequent template geometries based on information obtained from the inner algorithm.

An additional objective of this research is to use a two-level evolutionary algorithm to locate optimal search parameters for a given template geometry. An inner algorithm will search for optimal configurations. An outer algorithm will alter the parameters of the inner search algorithm to search for optimal algorithm parameters. For example, if an inner genetic algorithm is used, mutation rate, probability of crossover, fitness function, etc., will be varied. Use of these optimal parameters will reduce the time required to search for optimal configurations in experimental SSAs.

Array Pattern Synthesis in the Presence of a Mounting Tower Using the Genetic Algorithm

Tao Su*, Kapil Dandekar and Hao Ling

Department of Electrical and Computer Engineering
The University of Texas at Austin
Austin, TX 78712, USA

Smart antenna technology makes use of adaptive antenna arrays to increase system capacity and is an important component of 3rd generation wireless mobile systems. In the deployment of smart antennas, it is not always possible to mount the antenna on top of the basestation tower, since those positions are often already occupied by existing antenna systems. When the array is mounted at the mid-tower level, the pattern behavior of the array could be significantly degraded due to the presence of the tower. In this work, we explore array pattern synthesis in the presence of the mounting tower using the genetic algorithm (GA).

In our optimization process, the active element patterns of the array elements are first computed using the full-wave electromagnetic solver NEC. The element excitations are then optimized by the GA for each prescribed pattern. Two types of array patterns, the isotropic pattern for the access channel and the directive beam pattern for user channels are considered. For the isotropic pattern, the cost function is defined by the ratio between the minimum and maximum radiated field over the observation angle. For the beam pattern, the cost is penalized if the radiated field is below a desired level in the main beam or above the sidelobe level in the sidelobe range. Unlike conventional array synthesis in which the transition between the main beam and sidelobe is unconstrained, this region is also constrained here due to the strong tower effect.

Results are generated for a seven-element circular array of one wavelength diameter. The array operates at 1.9 GHz and is mounted next to a metal tower. The tower has a triangular cross section with 3 wavelengths on each side. The interaction is strong between the array and the tower, resulting in severe degradation in the array pattern if the element excitations for the free-standing array are used. Results of the GA synthesis for different prescribed beam patterns will be presented and the improvements discussed. The beamforming performance over different beam directions will also be compared and interpreted.

The Selection of Starting Points for Array Synthesis Using the Method of Generalised Projections

E.Botha[#], J.Joubert[#] & D.A.McNamara*

[#] University of Pretoria, Pretoria, South Africa 0002.

* University of Ottawa, 161 Louis Pasteur Street, Ottawa, Ontario K1N6N5, Canada.

The method of generalised projections has served as the basis for flexible approaches to the solution of problems in image processing, signal processing, pattern recognition, the synthesis of antenna arrays (eg. O.M.Bucci, G.D'Elia, G.Mazzarella & G.Panariello, *Proc.IEEE*, **82**, 358-371, 1994) and the synthesis of reflector antennas. Array synthesis procedures that use the method are attractive because of the quite natural way in which a wide variety of desirable constraints can be reliably implemented. Most numerical optimisation methods used for array synthesis require users to select an objective function whose minimisation they believe will lead to the best solution of the synthesis problem they have in mind. The process of selecting this objective function is thus unavoidably somewhat subjective, and altered solutions are obtained if the objective functions are changed. Achievement of a global optimum for a selected objective function does not necessarily imply that a global optimum has been reached for the actual synthesis problem. It is possible that the said objective function does not fully represent the array synthesis goals and constraints. The method of projections obviates the need to define such objective functions because of the intersection of sets approach inherent in its formulation.

The nemesis of the method is the occurrence of traps and tunnels (H.Stark & Y.Yang, *Vector Space Projections*, Wiley 1998). Traps prevent a solution from proceeding. Tunnels are those situations in which the solution is approached so slowly that for all practical purposes the algorithm has ceased functioning. The choice of a starting point (that is, the set of initial vector complex array element excitations, \hat{A}_0 say) is crucial to the success of the method. A properly selected \hat{A}_0 will be one that is sufficiently close to the solution to prevent the algorithm from experiencing a trap. In the case of uniformly-spaced linear or planar arrays with pencil beams the classical synthesis methods can often provide a good starting point. There is no similar way to select \hat{A}_0 in the case of more complex requirements (eg. shaped or contoured patterns) and more complex geometries (eg. conformal arrays). In most cases it is not satisfactory to simply set all excitations equal to unity.

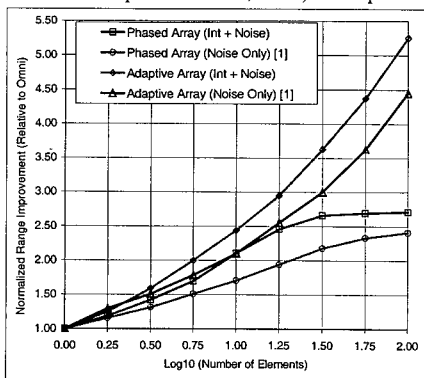
In this paper we discuss three different possibilities for selecting the starting point: (a). Averaging the radiation pattern constraint mask & applying the backward operator, (b). Using a component beam technique, and (c). Using a component beam technique with an adjusted pattern phase function. We will illustrate and compare the use of these approaches on several synthesis problems.

The Range Increase of Adaptive Versus Phased Arrays in Mobile Radio Systems: Interference Included

M. da Silveira*, J. W. Odendaal, J. Joubert
 Department of Electric and Electronic Engineering,
 University of Pretoria, 0002, South Africa

It is well known that a phased array system can receive a signal, with the same BER, over a longer range than an omni antenna system. In a multipath environment, this range increase is proportional to the number of phased array elements up to the point where the beamwidth of the phased array is narrower than the multipath angular spread, in which case the range increase tapers off. An adaptive array on the other hand, does not have this limitation. Through its optimization of the signal to noise ratio, more constructive addition of multipath components results. It was shown ([1] J.H. Winters & M.J. Gans, IEEE Trans. Veh. Tech., Vol. 48, No. 2, Mar. 1999) that even in a wide angular spread environment (60°), an increase in adaptive array elements leads to a range increase.

The presence of interfering signals will alter the range increase capabilities of both phased and adaptive arrays. This was not taken into account in [1] and is the focus of this paper. Monte-Carlo simulations were performed to determine the BER (function of signal to interference plus noise ratio, SINR) of the phased and adaptive array received phase-



shift-keyed signals. The desired and interfering signals are Rayleigh faded (generated with twenty scatterers uniformly distributed in a circle around each source), each with a specified mean incidence angle and maximum angular spread. The omni received mean SINR was adjusted for a BER of $1E-2$. The ranges to the sources (assumed to be equal) were increased until the BER of the array equals $1E-2$, which gives the range increase. The simulated range increase is shown in the figure for a maximum angular spread of 20°

and a single interferer with an incidence angle of 30° . The desired signal is on boresight. The mean signal to noise ratios of the desired and interferer are 18 dB and 0dB respectively. The interferer reduces the omni range, but both the phased and adaptive arrays reduce the effect of the interferer. The net result is that the range increase of phased and adaptive arrays in the presence of the interferer exceeds that without an interferer. Furthermore, when the incidence angle of the interferer approaches the desired signal incidence angle, the performance of the phased array is worse than the adaptive array.

Ultra Broadband Antenna Array for Mobile/Wireless Communications, Square-Kilometer-Array Telescope and Other Applications

T.B. Vu
Electronic Engineering Department
City University of Hong Kong

With mobile/wireless services becoming even more glamorous by the combination of e-commerce, mobile communications and the internet, there is an ever-increasing demand for extra services, and consequently a steady pressure for more spectral bandwidth.

For designers of antenna systems to be used in mobile/wireless communication networks, a steady increase in system bandwidth means that there is an urgent need to develop new design methods in order to achieve very wideband antennas. Clearly, the proliferation of mobile/wireless frequency bands means that service providers must employ several antenna systems to cater for all the different frequency bands. This not only is against the popular trends towards less visible antennas, but also means much higher infrastructure costs. Thus, it makes good sense to develop ultra-wideband antenna arrays, which can operate over many (and possibly all) frequency bands. To be more specific, take the case of conventional sector-antennas for base-stations. Up to now, much research effort has been concentrated on the design of broadband individual antennas for the azimuth coverage. However, one should not forget that the elevation pattern must also be shaped by employing an array of elements in the vertical plane. If the shape of such an elevation pattern is frequency dependent, the sector antenna will not give satisfactory performance over the required mobile/wireless frequency bands. The problem becomes even more challenging in the case of smart antennas, where the depths as well as the locations of the nulls must be maintained over the whole design bandwidth. In fact, if ultra-wideband smart antennas can be designed, it would be highly attractive for service providers to deploy them.

Currently, however, the most urgent requirement for ultra-wideband phased arrays is arguably in the field of radio-astronomy. The Square-Kilometer-Array Telescope, which has received a lot of attention recently, represents a revolutionary concept in radio-telescope design that was conceived in 1997, with research commitment from many countries, including the USA, The Netherlands, India, China, Canada and Australia. Due to its tremendous technical challenge arising from the very wide bandwidth of the signals of interest, as well as the high level of radio pollution, it is likely that DSP-based adaptive array would be one of the ultimate design goals. Here again, the success depends greatly on the development of ultra-wideband adaptive phased arrays.

Wideband antenna arrays are also required in other fields like satellite communications. Apart from array feeds that are widely used to shape the footprint of satellite reflector antennas, direct-radiating antenna arrays have also gained popularity. Due to the very high cost of satellite payloads, it is highly desirable to design an antenna array that can cover many satellite frequency bands.

This paper discusses some of the most promising design techniques for ultra-wideband antenna arrays. The results show that a bandwidth close to eighty per cent is achievable.

Comparison of Beamforming Techniques for W-CDMA Communication System

Hsueh-Jyh Li* and Ta-Yung Liu

Graduate Institute of Communication Engineering
National Taiwan University
Taipei, Taiwan R.O.C.

In the code division multiple access (CDMA) system, multiple users use different code sequences to share the same frequency band at the same time. Due to the imperfect orthogonality among the different code sequences, multiple access interference (MAI) is a major limitation to the channel capacity. Beamforming is a technique that can be used to focus the antenna beam to the desired user so that the SINR (signal to interference plus noise ratio) can be increased. In the W-CDMA system, an antenna array at the basestation can be utilized to form beam patterns for the uplink and downlink.

In this paper different beamforming techniques are employed in the W-CDMA basestation and their uplink and downlink SINR performances are compared. The uplink beamforming techniques to be considered are the complex-conjugate method and the direction of arrival (DOA) method. The downlink beamforming methods to be considered are: 1. The single-beam complex-conjugate method; 2. The multiple-beam complex-conjugate method; 3. The single-beam DOA method; 4. The equal-gain multiple-beam DOA method; and 5. The maximal-ratio multiple-beam DOA method.

It was found that the DOA method and the complex-conjugate method almost have the same uplink SINR performance, but the complex-conjugate method will shift the downlink main beam direction slightly due to the difference between the uplink and downlink carrier frequencies. However, the degradation in the downlink mean SINR performance is less than 1dB compared with that obtained by the DOA method. In the downlink it was found that the single-beam method has a poorer SINR performance in the low SINR region because it is more likely to suffer from deep fading. While in the moderate or high SINR region the single-beam method has a much better SINR performance because it has a higher gain in the main path direction and a smaller angular coverage of the mainlobe, which will result in a stronger signal level and smaller MAI at the mobile receiver.

A Two Dimensional Coupled Oscillator Array with MMIC Frequency Multipliers

Jinjin Shen and L. Wilson Pearson
Holcombe Department of Electrical and Computer Engineering
Clemson University
Clemson, SC 29634-0915
jshen@clemson.edu, pearson@ces.clemson.edu

Coupled oscillator arrays are capable of beam-steering by applying signals at the elements on the perimeter of the array alone. In recent years some one-dimensional coupled oscillator arrays have been presented, and a two-dimensional array was also demonstrated by Porgozelski last year.

Phase lead or lag generated between elements in a coupled oscillator array is limited to a value whose magnitude is less than 90 degrees. This restricts the achievable scan angle. beam To overcome this shortcoming, harmonic mixing can be used to increase the phase difference. In this way, the phase difference is multiplied by the harmonic number. In our circuit, MMIC frequency doublers are used to generate the second harmonic of the fundamental running frequency. Thus, the signal with doubled frequency carries phase difference which is twice of that at the fundamental frequency.

The beam-steering circuit is a 4x4 array with 16 units of oscillator, frequency doubler and microstrip patch antenna. The circuit has a double-layer structure with a common ground plane. The top layer is the radiation side with microstrip patch antennas and MMIC frequency doublers, and the bottom layer is the circuit side with microwave HEMT oscillators. Each oscillator running at 12 GHz has a Filtronic LPD200 HEMT die. The frequency doublers generate 24 GHz signal fed to microstrip patch antennas, and each of them consists of a UMS CHX2090 12-24 GHz MMIC frequency multiplier. The frequency doublers are driven by the oscillators through slot coupling. And the oscillators are mutually coupled through 50-Ohm microstrip lines loaded with 47-Ohm resistors in the way of nearest-neighbor coupling. The free-running frequency of peripheral oscillators are tunable through changing the bias voltages on their varactors.

We demonstrate that beam-steering can be obtained on a two-dimensional surface through changing the biases on the peripheral elements in the coupled oscillator array and a wider beam-steering range is obtained by radiating the second harmonic of the oscillator running frequency, compared with that at the fundamental running frequency. We also show that the circuit design is suitable for a realization of the system with three-dimensional micromachined circuit fabrication technology.

PRECISE ANALYSIS OF COMMERCIAL LOG-PERIODIC DIPOLE ARRAYS
USING WIRE-ANTENNA ALGORITHMS

Antonije Djordjevic

Alenka Zajic

Branko Kolundzija

School of Electrical Engineering, University of Belgrade

P.O. Box 35-54, 11120 Belgrade, Yugoslavia

Tapan Sarkar*

Department of Electrical Engineering and Computer Science

Syracuse University, Syracuse, New York 13244-1240, USA

The log-periodic dipole array (LPDA) has become the most popular commercial antenna for reception of TV signal in VHF and UHF bands in Europe. The antenna consists of two booms of a square cross section to which dipoles are attached (Figure 1). The booms play the role of the feeding two-conductor line. The dimensions of the boom are relatively large compared to the wavelength and the dipole length. Hence, this antenna cannot be accurately analyzed as a wire structure unless special precautions are taken. On the other hand, the wire-antenna computer programs are the fastest and thus the most convenient tool for interactive design. The aim of our paper is to span this gap.

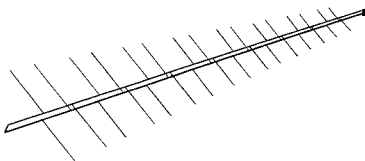


Figure 1. Commercial LPDA.

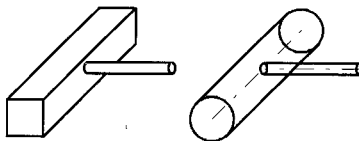


Figure 2. Exact dynamic three-dimensional model and thin-wire model of a boom and attached dipole arm.

The paper presents results that establish equivalence between transmission lines whose conductors have a square viz. a circular cross section. Two approaches to the equivalence are considered. The first is an exact approach, which rigorously takes into account the current and charge distribution over the conductors. Conditions are established for the equivalence between two transmission lines. They take into account both the characteristic impedance and coupling with the electromagnetic environment. This equivalence is considered using two-dimensional quasi-static transmission-line models.

The second approach follows from the standpoint of using the thin-wire kernel in numerical codes. The objective is to provide accurate results for the LPDA from wire-antenna programs. This equivalence is obtained by comparing three sets of results. The first set is computed using the two-dimensional models. The second set follows from a rigorous three-dimensional dynamic analysis of the boom with attached dipoles (Figure 2). The third set is obtained from wire-antenna codes (Figure 2).

In addition to the data for the transmission line, corrections are established for the end effect of dipole arms, as well as junctions between dipoles and booms. All these corrections are included in a wire-antenna model. Experimental and computed results agree remarkably well, both for the input impedance and for the radiation pattern of LPDA.

Ray Analysis of the Radiation from a Large Finite Phased Array of Antennas on a Grounded Material Slab

P. Janpugdee¹, P. Pathak¹, P. Nepa², O. Civi³ and H.-T. Chou⁴

¹ The Ohio State Univ. ElectroScience Lab., Dept. of Electrical Eng., 1320 Kinnear Rd., Columbus, Ohio 43212, USA; pathak.2@osu.edu

² Dept. of Information Engineering, University of Pisa, Via Diotisalvi, 2-5612 Pisa, Italy

³ Dept. of Electrical and Electronics Eng., Middle East Tech. Univ., 06531, Ankara, Turkey

⁴ Dept. of Electrical Engineering, Yuan Ze University, Chung-Li 320, Taiwan

An asymptotic high frequency (HF) ray solution is developed for describing the fields produced by large finite-sized phased arrays consisting of antenna elements on a grounded material slab. This work is of interest in the analysis of many practical planar array configurations such as dielectric covered slot arrays, strip dipole and microstrip patch arrays, etc. Such a HF analysis provides useful physical insights into the array radiation mechanisms, which are generally not directly available from the purely numerical methods of solutions. Furthermore, the HF solution obtained here also leads to a hybrid approach for significantly increasing the speed of ordinary numerical solution methods by utilizing the HF ray based functional behavior of the various radiation mechanisms, and thereby drastically reducing the large number of independent unknowns to be solved numerically otherwise. It is noted that conventional numerical solutions can become highly inefficient or even intractable for large arrays; thus, a hybrid combination of asymptotic ray and numerical methods provides a useful practical approach for obtaining the array current distribution and element input impedances, in a highly efficient manner. Also, once the array current distribution is known from a hybrid solution, when the element excitation for the array is given, one can then utilize a highly efficient Discrete Fourier Transform (DFT) expansion to represent the current distribution in terms of only a few DFT spectral components (the total number of significant DFT coefficients for large high gain arrays is usually less than 25% of the total number of array elements) because each global DFT basis function produces array fields, in closed form, that are associated with just a few rays emanating from specific points on the array in this present HF solution. Useful ray solutions have been developed previously (L. Carin, L.B. Felsen and T-T. Hsu, *IEEE Trans. AP-44*, no. 1, Jan. 1996, pp. 1-11; A. Polemi, A. Toccafondi and S. Maci, 2000 Intl. IEEE AP-S Symp., Salt Lake City, Utah, Jul. 16-21, 2000) for essentially two-dimensional (2-D) array problems involving grounded dielectric substrates. Here, the above work by Carin and Felsen is extended to the fully three-dimensional (3-D) planar array, and it produces more complex surface wave effects as compared to those present in the simpler 2-D case. In particular, surface waves are seen to be excited from the array edges and also corners. As is well known, the surface waves affect the array mutual coupling and can lead to scan blindness in arrays. In addition to the surface and leaky wave contributions, there are the usual array Floquet modes which are now radiated only into a bounded region of space due to the finiteness of the array; the latter finiteness also introduces diffraction of such modes by the array edges and corners which also keep the total array fields continuous. The relationship of the present HF solution to a new hybrid numerical solution for determining the current distribution for large finite arrays of strip dipoles on a grounded dielectric slab will be indicated along with numerical results, which would include the scan blindness case as well. Also, results for the fields of finite arrays with known, realistic current distributions will be shown in terms of the present simple HF solution upon utilizing the compact DFT current representation.

Applications of Forward-Backward Method in the Fast Analysis of Two-Dimensional Array Structures

Hsi-Tseng Chou* and Hsien-Kwei Ho

Department of Electrical Engineering, Yuan Ze University, Chung-Li 320, Taiwan

The fast but accurate analysis of large array problems remains interested and challenging due to the increasing trend to use very large arrays in practical applications. Rigorous numerical techniques such as method of moment (MoM), finite element method (FEM) and finite difference in time domain (FDTD) are usually intractable because of numerical limitation unless some reasonable approximations are assumed at the cost of reducing the accuracy. However, efficient approaches to accelerate the numerical exact methods are very desirable in the studies.

A Forward-Backward Method (FBM), initially developed for the fast analysis of scattering from ocean-like rough surfaces, is an efficient MoM-based approach that has advantage of fast convergence and requires least memory storage. It has potential to treat the analysis of large array problems. In the earlier studies, the FBM has been successfully implemented in the fast analysis of one-dimensional array structure. An $O(N)$ (N is the number of elements) complexity has been obtained in both computation and memory requirement at a fixed frequency as the size of array increase. This paper will describe its implementation to treat two-dimensional array problems. Particular attentions will focus on developing a simple procedure based on the fundamental concepts of forward and backward sweeps to minimize the iteration number and hence obtain a fast convergence. Furthermore, similar to previous studies in the one-dimensional array problems, an acceleration algorithm, which is particularly suitable for the F-B procedure, will be developed. This acceleration algorithm is based on the decomposition of strong and weak interaction regions on the array for a given receiving element. Due to a fact that strong interaction region is a small area and dominates the field contributions, exact computation will be employed for the strong interaction to maintain the accuracy. An approach based on the discrete Fourier transform (DFT) representation of weak region is developed to accelerate the computation of weak interaction. Usually only a few DFT terms are sufficient to represent the weak region contribution, and as a result, the efficiency can be expected. Numerical examples based on the analysis of a rectangular dipole array will be presented to demonstrate the validity of the present F-BM approach.

Scattering

Chairs: R. MacPhie, Canada and D. Werner, USA

	Page
1:00 Scattering of a Plane Wave by Two Perfectly Conducting Coalescing Spheres, <i>R. MacPhie*, T. Lo, University of Waterloo</i>	94
1:20 The Backscattering Characteristics of Wires Actively Loaded with Negative Impedance Elements, <i>B.R. Long*, D.H. Werner, The Pennsylvania State University</i>	95
1:40 Plane Wave Diffraction by a Grounded Semi-Infinite Dielectric Slab, <i>B. Polat*, Technical University of Denmark, L.W. Pearson, Clemson University</i>	96
2:00 Floquet Wave Diffraction Theory for the Truncated Phased Dipole Array Green's Function on an Infinite Grounded Dielectric Slab, <i>S. Maci*, A. Polemi, A. Toccafondi, University of Siena, L. Felsen, Boston University</i>	97
2:20 Theoretical Model for the Backscatter Response of Roadside Pebbles at Millimeter-Wave Frequencies, <i>E. Li*, National Chi Nan University, K. Sarabandi, University of Michigan</i>	98
2:40 Backscatter From Inhomogeneities Illuminated by a Focused Beam, <i>J. Schultz*, E. Hopkins, R. Moore, Georgia Tech Research Institute, M. Kessler, J. Maloney, Photonex Corporation</i>	99
3:00 Near-Field Probe Study of Scattering from Simple Inhomogeneities, <i>J. Schultz*, E. Hopkins, E. Kuster, Georgia Tech Research Institute</i>	100
3:20 A Fast Method to Calculate The Radar Cross Section of Cavities, <i>O. Gutierrez*, F. Saez de Adana, P. Lozano, E. Garcia, L. Lozano, I. Gonzalez, M. Catedra, Universidad de Alcala</i>	101
3:40 Effect of Target Size on the Detection of Buried Objects Using Microwave Radiometry, <i>B. U. Ungan*, J.T. Johnson, The Ohio State University</i>	102
4:00 Investigation of the Scattering Characteristics of Subsurface UXO for Classification, <i>K. H. Lee*, C.C. Chen, R. Lee, The Ohio State University</i>	103
4:20 Use of PCA and Quadratic TFR Techniques in Electromagnetic Target Classification from Scattered Data, <i>G. Turhan-Sayan*, M. Karaduman, Middle East Technical University</i>	104

Scattering of a Plane Wave by Two Perfectly Conducting Coalescing Spheres

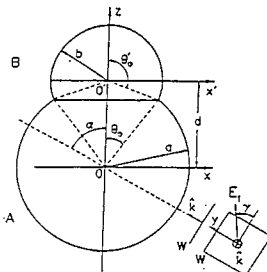
Robert H. MacPhie* and T. Lo

Department of Electrical & Computer Engineering
University of Waterloo, Waterloo, ON N2L 3G1 Canada
Tel: (519) 888-4567 (Ext. 2842) Fax: (519) 746-3077
E-mail: r.macphie@ece.uwaterloo.ca

In a classic paper (*IEEE Trans.* AP-19, pp. 391-400, 1971) Bruning and Lo obtained the formally exact solution to the problem of plane wave EM scattering by two perfectly conducting spheres. The limiting case of two spheres in point contact was considered.

In this paper we treat the case of plane wave scattering by two partially coalescing perfectly conducting spheres A and B, as illustrated in the figure below. The plane wave is incident at the angle α measured with respect to the z axis and has a polarization angle γ measured between the E-field and the projection of $00'$ on the incident wavefront. As did Bruning and Lo, we assume multipole expansions of the fields scattered from spheres A and B given in the coordinates systems centered at O and O' respectively. We enforce the boundary conditions that the tangential E fields vanish on A for $\theta_0 < \theta < \pi$ and on B for $0 < \theta' < \theta'_0$. Using Galerkin's Method, together with the translational addition theorem (Bruning and Lo, AP-19, p. 389, 1971) to express the field scattered from A in terms of the coordinates of B and vice versa, leads to a system of linear equations for the amplitudes of the multipole fields scattered from each sphere. Due to the reduced ranges of θ and θ' the orthogonality of the multipole fields on A and B (Stratton, *Electromagnetic Theory*, pp. 417-418, 1941) no longer exists. Nevertheless, closed form expressions for the matrix elements are obtained. However, unlike an earlier formulation, (MacPhie and Do-Nhat, *Digest of USNC/URSI Radio Science Meeting*, p. 109, 1995) the matrix elements do not involve the Incomplete Beta Function.

Numerical results will be presented for a variety of configurations of the two coalescing conducting spheres.



The Backscattering Characteristics of Wires Actively Loaded with Negative Impedance Elements

B. R. Long* and D. H. Werner
The Pennsylvania State University
Department of Electrical Engineering and
Applied Research Laboratory
University Park, PA 16802
dhw@psu.edu

This paper investigates the use of active loads to control the backscattering properties of PEC wire structures. In particular, a class of active loads known as negative impedance converters in the form of single elements, both real and reactive, as well as simple networks will be considered. The EFIE analysis technique originally developed in (K. M. Chen and V. Liepa, *IEEE Transactions on Antennas and Propagation*, 13, 262-270, 1965) will be adapted for the purpose of this study. Results will be compared with a numerically rigorous solution technique based on the method of moments.

The electromagnetic response of a dipole actively loaded with negative resistance has been documented in (R. F. Harrington, *IRE Transactions on Microwave Theory and Techniques*, 10, 165-174, 1962). Due to the constant gain-bandwidth product of the structure, it was demonstrated that increasing the magnitude of the negative resistance increases the backscattering cross-section at resonance while simultaneously reducing the relative bandwidth.

Here we show that negative capacitance and negative inductance loading applied separately, have complementary effects shifting the resonant frequency and altering the Q but also make no change in the system gain-bandwidth product. However, applied in combination as a series connected negative LC load leaves the resonant frequency and cross-section magnitude largely unaffected but significantly increases bandwidth as illustrated in Figure 1. Stability criteria useful in the design of networks containing active negative impedance converters will be discussed. Experimental confirmation of the stability of these circuits will also be presented.

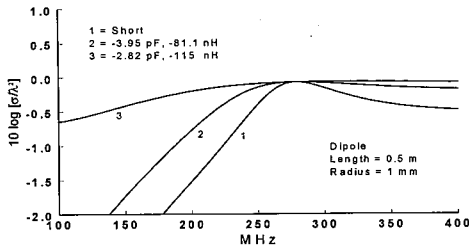


Figure 1. Dipole Backscatter with Series Negative LC Load.

Plane Wave Diffraction by a Grounded Semi-infinite Dielectric Slab

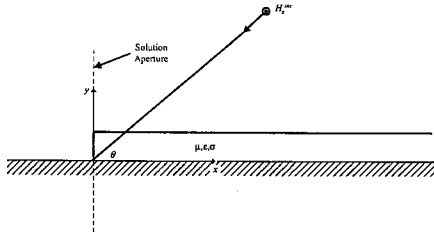
Burak Polat
Oersted-DTU Electromagnetic Systems
Technical University of Denmark
Building 348, Oersteds Plads
DK-2800 Kgs. Lyngby, Denmark
bp@oersted.dtu.dk

L. Wilson Pearson
Holcombe Department of Electrical and Computer Engineering
Clemson University
Clemson, SC 29634-0915
pearson@ces.clemson.edu

Electromagnetic scattering by truncated dielectric slabs is a canonical problem which has been investigated extensively in literature. We can divide such studies roughly into two groups with respect to the electrical thickness of the slab being much smaller than unity, or not. The first group of works base on modeling the slab by approximate boundary conditions and can provide analytical edge-diffraction coefficients, whereas the latter employ a rigorous formulation with a considerable numerical processing and no analytical diffraction coefficient is available.

However, in the presence of any perturbation in the scatterer structure, for instance an arbitrary edge termination, one has to recourse to alternative hybrid methods. A semi-analytical method for treating such problems has been introduced in 1991 (L.W.Pearson and R.A.Whitaker, Radio Sci.,26,169-174,1991) for the special case of vertically truncated dielectric multiple layers of arbitrary thickness, with a numerical verification of the method for the perfectly conducting half-plane problem. This so-called Transverse Aperture-Integral Equation (TAIE) formulation can be regarded essentially as the extension of the standard Aperture Theory to infinite extent planes normal to the scatterer plane. The formulation includes insertion of the asymptotic anticipation of the geometric optics terms into the formulation for the plane wave incidence case and results in a linear system of equation through a pulse-basis/collocation method of moments formulation. In the past 10 years this method has served to the analysis of a number scattering problems in literature, particularly in connection with the analysis of microstrip patch antennas (cf., V.Volski and G. Vandenbosch, IEEE Trans.AP-48, No.2, 240-245,2000).

In this paper a numerical treatment of the TAIE formulation presented in Pearson and Whitaker is presented for the special case of a single semi-infinite dielectric slab residing on a metallic plane under a plane wave illumination (see Fig.1). The numerical solutions have proven successful and effective in identifying the scattered field. The formulation is contrasted to similar work recently presented by Maci and his coworkers.



FLOQUET WAVE DIFFRACTION THEORY FOR THE TRUNCATED PHASED DIPOLE ARRAY GREEN'S FUNCTION ON AN INFINITE GROUNDED DIELECTRIC SLAB

S. Maci⁽¹⁾, A. Polemi⁽¹⁾, A. Toccafondi⁽¹⁾ and L.B.Felsen⁽²⁾

⁽¹⁾*Department of Information Engineering, University of Siena,
Via Roma 56, 53100 Siena Italy.
E-mail: macis@ing.unisi.it*

⁽²⁾*Department of Aerospace and Mechanical Engineering and Department of Electrical and Computer Engineering, Boston University,
110 Cummington Street, Boston, MA 02215, USA.
Also University Professor Emeritus, Polytechnic University,
Brooklyn NY, 11201 USA.*

The electromagnetic modeling of large printed phased array antennas is often based on the use of the infinite array Green's function (AGF) which, through FW expansion, leads to a computationally efficient formulation via the Method of Moments. When geometrical periodicity does not prevail, as is the case for a truncated array on the infinite slab, the FWs do not represent a complete basis in the truncated domain. However, the FW approach may be adapted to truncation by representing the array Green's function through Poisson summation restructuring in terms of a superposition of continuous equivalent FW source distributions extending over the finite array aperture. In this framework, the AGF of a semi-infinite array of electric dipoles on an infinite grounded slab has recently been analyzed using a spectral domain formulation and relevant high-frequency asymptotics [A.Polemi,A.Toccafondi,S.Maci, *IEEE Trans. Ant. Prop.*, accepted for publication]. This provides the three-dimensional (3D) extension of the 2D analysis for a truncated strip array presented in [L.Carin,L.B.Felsen,T.T.Hsu, *IEEE Trans. Ant. Prop.*, 44, I-II, 1996] which can be adapted to an actual phased array of patches. In [A.Polemi,A.Toccafondi,S.Maci, *IEEE Trans. Ant. Prop.*, accepted for publication], the high frequency AGF is expressed as a superposition of spatially truncated FWs, plus FW-induced diffracted wave, surface wave (SW), and leaky wave (LW) contributions excited at the array edge. Both the truncated FW series and the series of corresponding diffracted field contributions exhibit excellent convergence properties, thereby rendering this representation far more efficient than the direct summation over the spatial contributions from each element of the array.

In this paper, to facilitate the interpretation of the different types of wave processes and their interactions, the semi-infinite AGF on the grounded infinite slab is first rephrased in terms of space domain asymptotic integrations. After discussing the relationships between asymptotically dominant critical points in the spatial and spectral domains, a uniform asymptotic approximation is derived and the resulting wave phenomenology is interpreted. All possible combinations of slab-modulated propagating (radiating) and evanescent (non-radiating) FW and diffracted contributions are considered. Paths of propagating diffracted waves are defined according to a generalized Fermat principle, which is also valid by analytic continuation for evanescent diffracted fields. The periodicity-modulated SW and LW phenomenology is discussed by interpreting the wave propagation paths and the behavior of slowly attenuated LWs in terms of rays. The mechanism of interaction between LWs and propagating FWs, as well as between SWs and evanescent FWs, is highlighted also in connection with the scan blindness phenomenon in actual arrays.

Theoretical Model for the Backscatter Response of Roadside Pebbles at Millimeter-wave Frequencies

Eric S. Li*, Department of Electrical Engineering, National Chi Nan University
Puli, Taiwan 545, R.O.C.

Tel: 886-49-2910960, Fax: 886-49-2917810, email: ericli@ncnu.edu.tw

Kamal Sarabandi, Department of Electrical Engineering and Computer Science
The University of Michigan, Ann Arbor, MI 48109-2122

Tel: (734) 936-1575, Fax: (734) 647-2106, email: saraband@eecs.umich.edu

Considering the growing demands on highly reliable radar sensors used for automotive safety applications, the knowledge of radar backscattering behaviors of targets and clutter in highway environment has attained significant prominence. A complete investigation of radar backscatter response from road surfaces can provide essential information for the highway radar clutter. In the past years, the scattering behaviors of various road surfaces under different physical conditions were studied comprehensively by the authors and many scattering models were developed to accurately predict the backscatter response of the road surfaces (K. Sarabandi and E. S. Li, *IEEE Trans. Antennas Propagat.*, vol. 45, no. 11, 1997 and vol. 47, no. 5, 1999). Another common target observed in highway environment is roadside pebbles. The backscattering behavior of the roadside pebbles is of interest because of its potential application in autonomous vehicle control. The backscatter response of a surface covered by pebbles is determined by the dielectric properties of rocks, size distribution, and surface roughness statistics. A simple model based on physical optics (P.O.) approximation is selected to predict the backscatter response of the roadside pebbles. At millimeter-wave frequencies, the sizes of the rocks are large compared to the wavelength and the rock material is considered relatively lossy, thus P.O. model can provide precise results. Each rock particle can be approximated by a round dielectric target and the mean radius is determined by the rock size distribution. For the radar sensors used in the automotive safety applications, the backscatter response of targets and clutter at low grazing incidence angles is of practical importance. Under such circumstance, the shadowing effect needs to be taken into account in this P.O. model. The shadowing effect is caused by the surface roughness and can be described in terms of the rms height of the surface roughness and the surface autocorrelation function. The validity of the theoretical model will be examined by comparing the simulation results with the experimental data from the University of Michigan where the backscatter measurements at W-band were conducted to obtain the backscatter response of one roadside pebble surface at near grazing incidence angles ($70^\circ - 88^\circ$).

BACKSCATTER FROM INHOMOGENEITIES ILLUMINATED BY A FOCUSED BEAM

John W. Schultz*, Ed Hopkins, Rick Moore
Georgia Tech Research Institute, Atlanta, Georgia 30332

Morris Kesler, Jim Maloney
Photonex Corporation, Bedford, Massachusetts 01730

Measurement of microwave scattering from surfaces is often performed in outdoor or compact RCS ranges, where a test-body is illuminated by an approximate plane wave and the monostatic or bistatic reflection is measured. These measurements require extensive ground plane ranges or large indoor chambers. Further, these measurements characterize a test fixture as a whole, making it difficult to separate contributions of individual scattering sources (e.g. surface inhomogeneities) from that of the overall test-body shape.

In the reported research, we apply a free-space focused beam system, originally developed for dielectric material measurements (P. Friederich et al, *Proc. USNC/URSI Mtg.*, June 1994), to measure scattering from embedded and surface inhomogeneities in planar samples. The system consists of a horn antenna and dielectric lens to provide 'quasi' plane-wave illumination of a test-sample placed at the focus. The illuminating field has a Gaussian-like amplitude taper to minimize illumination of the sample edges, so that finite-sized (but larger than the illuminating beam diameter) samples can be measured. The combination of tapered, localized illumination with constant (planar) phase allows scattering contributions from local inhomogeneities to be distinguished from other scattering sources on the target, such as sample edges and shape. Measured backscatter data from linear discontinuities, inhomogeneous surfaces, and inhomogeneous materials are presented as a function of incidence angle and frequency for the frequency band of 4 - 18 GHz. These data include, scattering from grooves and gaps in metal and finite impedance sheets; joints between dissimilar impedance sheets; periodic and perturbed arrays; and inhomogeneous dielectric sheets. Methodologies for quantifying the measured data are presented, which enable calculation of RCS per unit area for inhomogeneous surfaces and echo-width for linear discontinuities. An analysis of the experimental error sources concludes the presentation.

NEAR-FIELD PROBE STUDY OF SCATTERING FROM SIMPLE INHOMOGENEITIES

John W. Schultz*, Ed Hopkins, Eric Kuster

Georgia Tech Research Institute, Atlanta, Georgia 30332

Far-field monostatic or bistatic scattering measurement can provide information on radiated fields from a test fixture, but supply little information on evanescent fields such as surface waves or local cavity modes. However these non-radiating fields can contribute to radiated fields by local perturbations such as geometric discontinuities or variations in impedance or electromagnetic properties. Near field measurements of scattering bodies can provide additional insight into these scattering mechanisms by measuring both radiated and non-radiated fields. In previous work, a system for unobtrusive measurement of near-fields and surface currents was developed to experimentally measure local H-fields from a scattering body at frequencies up to 4 GHz (Harms et al., *IEEE Trans. AP*, December 2000). This system used a balanced loop antenna to sample the fields in a planar scan spaced approximately $\lambda/10$ from a target, and a horn antenna provided external illumination of the body. A methodology for back-propagating the measured fields to surface currents on the body was applied, and good agreement was obtained between measurements and FDTD simulations.

In the research reported here, a probe was constructed to measure at frequencies up to 8 GHz and used to measure scattering from simple discontinuities in planar bodies. Illumination of the test-body was furnished by a focused lens system with a Gaussian-like tapered beam that locally illuminated inhomogeneities on the body. Measured data and model calculations are presented for scattered H-fields that are near canonical discontinuities (e.g. grooves and gaps in conducting planes). Comparison to plane wave illumination in FDTD calculations showed good qualitative agreement and after a normalization to the Gaussian tapered illumination field, measured data and FDTD simulations quantitatively agreed. Calculation of the plane wave spectrum of the measured and modeled data were used to separate specular reflected components from surface modes, and the system was used to detect surface modes due to traveling waves. A focused beam was simulated in FDTD with a weighted sum of plane waves, which showed agreement with the measured near-field data.

A FAST METHOD TO CALCULATE THE RADAR CROSS SECTION OF CAVITIES.

O. Gutiérrez, F. Saez de Adana, P. Lozano, E. García, L. Lozano,
I. González, M.F. Cátedra

*Dept. Teoría de la Señal y Comunicaciones. Escuela Politécnica.
Universidad de Alcalá. 28806 Alcalá de Henares. Madrid. Spain
Fax: -34 91 885 6699. E-mail: felipe.catedra@uah.es*

In this communication a new method to calculate the radar cross section of cavities will be presented. The method uses an iterative fast algorithm based on the physic optics that allows to compute the radar cross section in complex bodies of any material. The cavity is represented by NURBS surfaces.

The steps of the iterative method are the following:

- 1- For every aperture surface the induced currents for the incident plane wave are computed, $J_a^{(0)}$, $M_a^{(0)}$. These surfaces are called actives.
- 2- The surfaces illuminated by the scatter field radiated by the active surfaces are determined, and the illuminated surfaces are called victim surfaces.
- 3- The induced field and the respective current, $J_c^{(1)}$, $M_c^{(1)}$, are calculated in the victim surfaces.
- 4- The victim surfaces are considered active in a new iteration and the process continue as in the step 2. If the victim is an aperture surface, the current value is stored, $J_a^{(i)}$, $M_a^{(i)}$.
- 5- When are not victims or all are aperture surfaces or after a fixed number of iterations, the iterative process stop and the current values on the aperture surfaces is used to computed scattering field and the radar cross section.

The printed field on the victim surface is calculated over discrete points using the physic optic method. To apply this method we need to know the current in any point over the active surface, then we need to interpolate the discrete values computed in the previous iteration. To interpolate the current is used the same method used to interpolate NURBS surfaces.

To determine the victim surfaces an algorithm based on ray tracing acceleration technique called Angular Z-Buffer is used. The directions of radiation are determined for all the active surfaces, and only the surfaces into the region formed by these directions are considered as possible victims. With this technique the CPU-time is considerable reduced.

Results using this method has been compared with Shooting and Bouncing ray method computations obtaining good agreements.

Effect of Target Size on the Detection of Buried Objects Using Microwave Radiometry

B. U. Ungan* and J. T. Johnson

Dept. of Electrical Engineering and ElectroScience Laboratory
The Ohio State University
1320 Kimear Road
Columbus, OH 43212, USA

Phone: (614) 292-7981. Fax: (614) 292-7297
e-mail: unganb@ee.eng.ohio-state.edu

Microwave radiometry is currently under consideration for use in detection of buried objects. A recent study has suggested that multi-frequency measurements can be advantageous, as an oscillatory behavior is observed in brightness temperatures versus frequency in the presence of a sub-surface object. However, previous studies have modeled the subsurface object as a horizontally infinite layer so that a simple two dimensional analytical solution was obtained. Although such models offer useful insight to the problem, the more realistic case of a finite size target deserves consideration in order to test the validity of conclusions reached with the layered object model. In the case of a three dimensional finite size subsurface object, calculation of thermal emission from the object requires a numerical solution of the electromagnetic boundary value problem. If a constant temperature medium is assumed, brightness temperatures can be obtained from Kirchhoff's law by determining the total amount of power scattered into free space by the subsurface object when illuminated by a field incident from free space.

In this presentation, brightness temperatures and their variations with frequency will be presented for differing target sizes, target depths, and soil properties. The soil is modeled as a homogeneous half-space medium characterized by constant electromagnetic permittivity and physical temperature. Thermal emission from the target is numerically calculated using an iterative method of moments (including half-space Sommerfeld Green's functions) accelerated with the discrete dipole approximation. Amplitudes of brightness temperature oscillations in frequency will be shown to vary according to target size, depth, and the fraction of the observing antenna pattern occupied by the subsurface object. Finite size target solutions will also be compared with results from the horizontally infinite layer model to determine the parameter space under which the layered model is applicable.

INVESTIGATION OF THE SCATTERING CHARACTERISTICS OF THE SUBSURFACE UXO FOR CLASSIFICATION APPLICATION

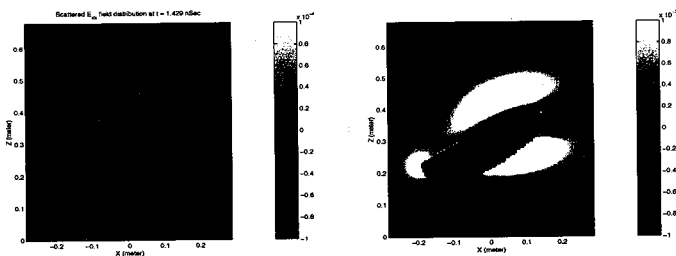
Kwan-Ho Lee, Chih-Chi Chen and Robert Lee

ElectroScience Laboratory at Department of Electrical Engineering
The Ohio State University
1320 Kinnear Rd., Columbus, Ohio 43212
Phone: 614-292-1433, FAX: 614-292-7596
e-mail: lee@ee.eng.ohio-state.edu

Buried Unexploded Ordnances (UXO) detection has long been an important issue in military mission. Classify the subsurface UXO is very difficult so that this area attracts many people to scrutinize in worldwide. Although many previous and on going research focused on this topic, high rate of the false alarm still needs to be reduced to save an amount of money and efforts in this area.

In this research, Finite Difference Time Domain (FDTD) method was employed because of the advantage in obtaining the solutions of Maxwell's differential equations for inhomogeneous or anisotropic lossy medium compared to the frequency domain method. UXO and UXO-like targets are modeled in rectangular FDTD grid with lossy medium implanted. In the lossy medium, higher frequency cannot penetrate deep enough due to soil absorption so that the practical frequency range is restricted to below 1 GHz. Another difficulty of UXO discrimination is its arbitrary orientation and variety of shape. For simulation, UXO, large and small cylinders are modeled with various orientations. Some existing classification algorithms such as linear factor extractions and construction of ellipticities were examined against the simulated data. The limitations of these discrimination methods were also explored. Several new promising approaches will be discussed.

Figures below show the scattered field distributions of the UXO at different time steps with different orientations.



(a) Scattered E_{zz} distribution at $t = 1.420$ nSec.

(b) Scattered E_{zz} distribution at $t = 0.619$ nSec.

Use of PCA and Quadratic TFR Techniques in Electromagnetic Target Classification from Scattered Data

Gönül Turhan-Sayan^{*} and Mehmet Karaduman

Middle East Technical University
Electrical and Electronics Engineering Department
06531 Ankara, Turkey

In this paper, use of Principal Component Analysis (PCA) technique together with various Time-Frequency Representation (TFR) techniques is investigated for the electromagnetic feature extraction and target classification problem.

Performance of a target classification scheme can be remarkably enhanced by the descriptive and distinguishing power of the target-specific features used in the classification process. In the case of electromagnetic target classification problem, in particular, scattered data can not be used directly in classification, as they are highly dependent on aspect and polarization. Instead, such data should be pre-processed to extract some sort of target features whose sensitivities to aspect and/or polarization are minimized as much as possible. The sufficiently late-time scattered field of a target is composed of the target's natural response components oscillating at the target's complex natural resonance frequencies (or poles). The natural response data contain implicit information related to the bulk geometrical features of the target such as its overall shape and size, in addition to the information related to the target's material properties. The target poles, in the meantime, are uniquely determined by all these physical properties of the object and are independent of aspect angle and polarization. Therefore, the set of target poles is a very powerful aspect-independent target feature itself. In cases where the target poles are not available, alternative target features representing the pole information in an indirect manner, such as the late-time natural-response based energy distribution matrices, are found still very useful. Such energy feature matrices can be obtained by using quadratic TFR techniques such as the Wigner and Page distributions. Additional use of the PCA technique is also suggested to obtain a representative late-time energy feature vector for a specific target from the energy feature matrices computed at several different reference aspects for this object. Therefore, the resulting reference feature vector can describe the target in an almost aspect independent manner and can be used for classification purposes.

This novel feature extraction technique combining the PCA, a well-known classical statistical method, with the quadratic TFR techniques is found to be a powerful tool even in the presence of noisy scattered data and is successfully demonstrated for the classification of four different dielectric spheres of varying sizes and refractive indices.

Space Weather: System Effects

Chairs: J. Foster, USA and S. Basu, USA

	Page
1:00 On Effects of Ionospheric Weather on Communication and Navigation System, <i>J. S. Guo*</i> , Chinese Academy of Sciences, <i>J. Wu</i> , Beijing Center of China Institute of Radiowave	106
1:20 Stormtime Ionospheric Perturbations at Sub-Auroral Latitude: GPS Effects, <i>J.C. Foster*</i> , MIT Haystack Observatory, <i>A. Coster</i> , MIT Lincoln Laboratory, <i>F.J. Rich</i> , Air Force Research Laboratory, Hanscom AFB	107
1:40 Effects of Ionospheric Irregularities on GPS-Based Navigation Systems, <i>X. Pi*</i> , Jet Propulsion Laboratory, <i>A. Iijima</i> , <i>A. Mannucci</i> , JPL/California Institute of Technology	108
2:00 Equatorial Ionospheric Scintillations and Their Effect on GPS Signals, <i>P. Kintner*</i> , Cornell University	109
2:20 The Impact of Solar Maximum on GPS Performance in the Equatorial Region, <i>S. Skone*</i> , University of Calgary	110
2:40 Specification and Forecasting of Scintillations in Communication /Navigation Links: Current Status and Future Plans, <i>S. Basu*</i> , <i>K.M. Groves</i> , Air Force Research Laboratory, Hanscom AFB, <i>S. Basu</i> , National Science Foundation, <i>P. Doherty</i> , Boston College	111
3:00 Radar Auroral Clutter Maps: A Mission-Tailored Graphical Product for DoD Warfighters, <i>S. Quigley*</i> , <i>G. Bishop</i> , Air Force Research Laboratory Hanscom AFB, <i>E. Holeman</i> , <i>D. Madden</i> , Boston College, <i>P. Citrone</i> , <i>K. Scro</i> , <i>R. Wilkes</i> , Space & Missile Systems Center	112
3:20 Operational Effects at ALTAIR Due to Ionospheric Disturbances, <i>S. Close*</i> , <i>A. Coster</i> , <i>S. Hunt</i> , MIT Lincoln Laboratory	113
3:40 VLF Remote Sensing of Lower Ionospheric Variability, <i>U.S. Inan*</i> , Stanford University	114
4:00 Recent Validation Results for Selected HF Propagation Prediction Programs Using Space Weather Data, <i>R. Hunsucker*</i> , RP Consultants	115
4:20 OpSEND: Tailored Space Weather Impact Maps for Specific Radio-Based Systems, <i>G. Bishop*</i> , <i>S. Quigley</i> , <i>K. Groves</i> , <i>T. Bullett</i> , Air Force Research Laboratory, Hanscom AFB, <i>P. Doherty</i> , Boston College, <i>P. Citrone</i> , <i>K. Scro</i> , <i>R. Wilkes</i> , Space & Missile Systems Center	116

On effects of ionospheric weather on communication and navigation system

Jian-shan Guo*¹ and Jian Wu²

*1 Space weather Laboratory, Center for Space and Applied Research
Chinese Academy of Sciences, Beijing 100080, P.R. China*

Email: guojs@center.cssar.ac.cn

*2 Beijing Center of China Institute of Radiowave Propagation,
Ministry of Information Industry, Beijing 102206, P.R. China*

In this paper we specifically address our discussion on ionospheric weather and its effects on communication and navigation system.

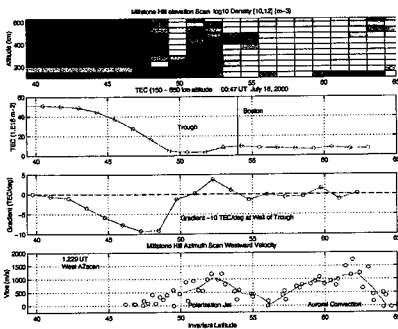
Both quiet and disturbed ionosphere can cause refraction, absorption, scintillation, multiple-path propagation, rotation of polarization, dispersion and Doppler frequency shift for the radio wave propagating through it. These effects give rise to changing wave parameter itself and analog or digital information carried by the wave, and finally lead to variation, degradation or destruction of the communication and navigation system. The ionosphere on the other hand can change environment of satellite and its expose component, and lead to changing the characteristics of the satellite and performance of the components.

One kind of effect is brought about by radio wave propagation. These effects are as follows. large enhancement of electron or ion density changes maximum usable frequency or terminates short wave communication. Irregularity brings the scintillation to bear on the signal of communication system, and causes error rate, even unlocks phase lock loop so that losses signals at all. Group delay and carrier phase advance imposed by quite and disturbed ionosphere degrades the performance of GPS navigation system even for that operated on dull frequencies and P-code model. The phase change imposed on very low frequency by bottom ionospheric variation causes considerable positioning error for ground navigation system. Refraction imposed by ionosphere results in erroneous radar ranging. Another kind of effect is brought about by ionospheric environment. When the satellite antenna is surrounded by strongly variable ionospheric plasma its performance such as radiation pattern and impedance of the antenna and compatibility of the antenna system changes a lot. Some of these effects above are going to be expounded quantitatively in more detail in the paper.

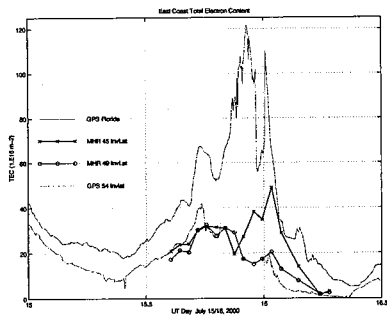
Stormtime Ionospheric Perturbations at Sub-Auroral Latitude: GPS Effects

J. C. Foster, MIT Haystack Observatory, Westford MA
 A. J. Coster, MIT Lincoln Laboratory, Lexington, MA
 F. J. Rich, AFRL/PHG, Hanscom AFB, Bedford MA

During geomagnetic disturbances, the electric fields and particle populations which characterize the auroral region expand equatorward and their effects are felt at previously sub-auroral latitudes. Intense stormtime electric fields of magnetospheric origin extend across mid latitudes and serve to deepen the ionospheric total-density trough and redistribute the ionospheric plasma through advection from one local time region to another. Strong increases and sharp spatial gradients in total electron content (TEC) characterize the sub-auroral latitude ionospheric storm response and these features can significantly impact GPS performance. The Millstone Hill Observatory is located in eastern Massachusetts at 42.6 N latitude, 288.5 E longitude (55 invariant latitude) and is well situated to observe effects related to magnetosphere-ionosphere coupling near the plasma-pause, the inner edge of the magnetospheric ring current, and the ionospheric trough. Millstone Hill incoherent scatter radar observations of the mid-latitude ionosphere between 35° and 65° invariant latitude are combined with DMSP satellite observations of electric fields and particle precipitation to investigate the causes and characteristics of the sub-auroral stormtime ionospheric perturbations which accompany the onset of intense geomagnetic storms. The radar provides latitude-altitude and latitude-longitude maps of the ionospheric perturbations. These are combined with GPS observations of TEC made with good (30-s) time resolution from a grid of observing sites across the continental United States to address the spatial extent and stormtime variability of the ionospheric features. We have constructed a time history of 2-D maps of TEC perturbations from the GPS data set during the major disturbance of July 15/16, 2001. Plasma advection from lower latitudes brings a swath of storm-enhanced density (SED) [Foster, *J. Geophys. Res.*, 98, 1675-1689, 1993] with total electron content (TEC) ~100 TEC units into the region immediately equatorward of the trough. Steep density gradients (> 10 TEC units / deg latitude) and regions of strong mid-latitude scintillations are observed associated with these features. The perturbed ionosphere produced pronounced space weather effects on GPS systems. During the July 2001 event, GPS receivers in the perturbed area suffered loss of lock and seriously degraded performance.



Sharp TEC gradient at ionospheric trough



Storm-enhanced mid-latitude TEC due to SED

Effects of Ionospheric Irregularities on GPS-Based Navigation Systems

Xiaoqing Pi, Byron A. Iijima, Anthony J. Mannucci,
Lawrence Sparks, and Brian D. Wilson
Jet Propulsion Laboratory, California Institute of Technology

Abstract

Irregularly structured ionospheric electron density distributions are often associated with low- and high-latitudes. The irregularities can also be significantly manifested at mid-latitudes during major geomagnetic storms. Such irregularities have been evidenced with existing regional and global GPS receiver networks that provide snapshots of the geographic distribution of ionospheric total electron content (TEC) with high temporal resolution over various spatial scales.

The presence of mid-latitude irregularities, even though infrequent, has a significant impact on the design and implementation of GPS-based navigation systems being developed in the United States and Europe. Such systems, for example the Wide Area Augmentation System (WAAS) in the U.S., use ground-based GPS receivers to measure ionospheric group delays attributed to line-of-sight TEC. The measured delays between all satellites in view and receivers in a region are used for spatial and temporal mapping and interpolation to provide ionospheric delay corrections to single-frequency GPS users in real-time. Ionospheric irregularities are a major threat to such a system, because accurate modeling or mapping of the ionosphere based on limited numbers of measurements is extremely difficult when the ionosphere is severely disturbed and its density distribution becomes irregular. Compounding the problem, the mapping errors must also be estimated particularly when the accuracy of user positioning affects user safety. An example is airplane landing where users require reliable ionospheric corrections and error estimates be provided by the system.

This paper first presents examples of observed mid-latitude irregularities that developed during space weather events. The effects of the irregularities on GPS-based navigation systems are then assessed using the actual WAAS configuration as a representative case. Methods under development to mitigate the impact of irregularities are also discussed.

Equatorial Ionospheric Scintillations and Their Effect on GPS Signals

Paul M. Kintner
School of Electrical and Computer Engineering, Cornell University
Ithaca, NY, 14853 USA
Phone: (607) 255-5304; Fax: (607) 255-6236; paul@ece.cornell.edu

The well-known phenomena of equatorial spread F produces scintillations in trans-ionospheric radio signals up to GHz frequencies, including GPS satellite signals. After local sunset, 100-km scale plasma bubbles erupt in the ionosphere, producing density irregularities with scale lengths from 100 km to the cm level. This includes the Fresnel length for GPS signals at 1.6 GHz of about 400 m. Since the 400-meter irregularities are translating with the ionosphere at a typical speed of about 100 m/s, we expect to observe scintillations with time scales of about 1 second. However, the observed time scales can be much longer. Since the GPS signal protocol is a CDMA system employing correlation receivers, the time scale of amplitude fades is critical to predicting the performance of GPS receivers.

Figure 1 shows two examples of GPS signal amplitude scintillations with very different time scales. These scintillations were produced by equatorial spread F near the equatorial anomaly. The upper two panels exhibit "typical" scintillation time scales of about 1 second. The left-hand panel is just the signal amplitude versus power whereas the right-hand panel is the autocorrelation function of the signal amplitude whose width is a measure of the fade time scale. The lower two panels show a less typical example of scintillation time scales where the time scale is about seven times longer.

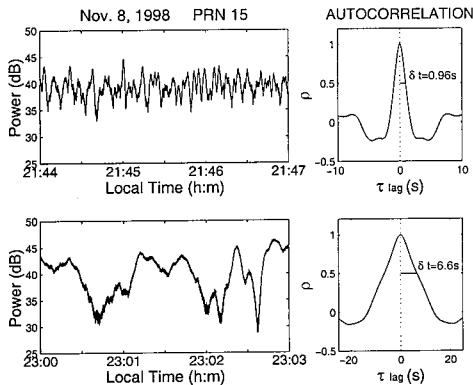


Figure 1. Two examples of GPS signal amplitude scintillations showing different time scales associated with the amplitude scintillations.

360-378, 1982). Since typical aircraft speeds are the order of the equatorial ionospheric drift speed and the order of the scintillation pattern drift speed, this implies that airborne GPS receivers will be more vulnerable to loss of tracking than stationary or slowly moving receivers.

The combination of longer time scales and large amplitude fades the order of 20 dB can cause GPS receivers to stop tracking signals. We show some examples of large time scale and large amplitude fades that cause loss of tracking. Finally, we consider the effect of equatorial scintillations on moving GPS receivers. If the motion of a GPS receiver matches the speed of the scintillation pattern, then fade time scales are expected to lengthen, and this effect has already been demonstrated for signals from geostationary satellites (J. Aarons, *Proceedings of the IEEE*, 70(4),

The Impact of Solar Maximum on GPS Performance in the Equatorial Region

S. Skone
Department of Geomatics Engineering
University of Calgary
2500 University Dr. NW
Calgary, Alberta, Canada T2N 1N4

The Global Positioning System (GPS) is a satellite navigation system, in which 24 satellites currently provide worldwide positioning capabilities. Due to the dispersive nature of the ionosphere, GPS signals experience ranging errors dependent on both the given signal frequency and ionospheric total electron content (TEC). Such range errors translate into a degradation of positioning accuracies. While it is possible to mitigate the impact of ionospheric effects on GPS positioning applications, through differential techniques (DGPS) and/or ionosphere modeling, residual errors may persist in regions where steep gradients or localised irregularities in electron density exist. In addition, loss of GPS signal availability can occur in regions where small-scale irregularities in electron density cause amplitude fading and phase scintillations. Such effects are an issue for the reliable implementation of safety-critical GPS systems.

One area of particular concern is the low latitude region, within 30 degrees of the geomagnetic equator. In this region electrons are lifted away from the geomagnetic equator, under the influence of a strong electric field. Large TEC gradients are present near the resulting equatorial anomaly and scintillations arise from the presence of small-scale irregularities in electron density near the anomaly peaks. Both the magnitude of TEC gradients and the level of scintillation activity are enhanced in this region during periods of solar maximum. In the South American sector, the largest effects are observed during the periods October-November and February-March.

In this paper, GPS positioning accuracies and signal availability are investigated in the equatorial region during the present period of solar maximum. A long-term data set is compiled using GPS data from nine stations in the Brazilian geodetic network, which provides complete spatial coverage of the anomaly region. The impact of solar maximum on GPS is quantified in terms of receiver tracking performance (signal availability) and the magnitude of differential positioning errors. Results indicate a significant impact on GPS applications, with 40 percent of the L2 observations missing and positioning errors degraded by a factor of 5.

SPECIFICATION AND FORECASTING OF SCINTILLATIONS
IN COMMUNICATION/NAVIGATION LINKS: CURRENT
STATUS AND FUTURE PLANS

S. Basu*, K.M Groves

Space Vehicles Directorate, Air Force Research Laboratory, 29
Randolph Road, Hanscom AFB, MA 01731

Su. Basu

Atmospheric Sciences Division, National Science Foundation,
4201 Wilson Boulevard, Arlington, VA 22230

P. Doherty

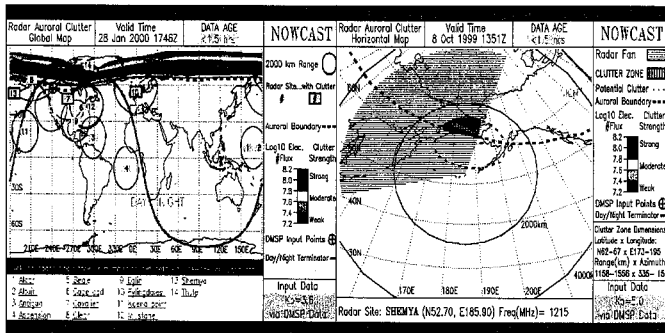
Boston College, Institute for Scientific Research, Chestnut Hill,
MA 02467

The upper atmosphere above 100 km, called the ionosphere, is ionized and often becomes turbulent and develops electron density irregularities. These irregularities scatter radio waves to cause amplitude and phase scintillation and affect satellite communication and navigation systems. The effects are most intense in the equatorial region, moderate at high latitudes and minimum at middle latitudes. Scintillation is maximum during the peak of the solar cycle and minimum during the solar minimum. In the equatorial region, scintillation onset occurs after sunset and may persist through the night. During the solar maximum, the magnitude of equatorial scintillation at L-band frequencies may attain saturation levels at the crests of the equatorial anomaly that are located around 15 degrees north and 15 degrees south magnetic latitudes. Under these conditions, the ground decorrelation distance of VHF satellite signals may become smaller than that of L-band signals. In view of the high incidence of strong equatorial scintillation during magnetically quiet periods, the thermosphere and the ionosphere seem to internally control the generation of irregularities in the equatorial region. However, scintillation and total electron content (TEC) variations in the equatorial region observed during magnetic storms indicate that the forcing of the equatorial ionosphere by solar transients is indeed an additional modulating factor. The ionospheric response to major magnetic storms is indicated by the impulsive onset of scintillation and the development of extremely steep TEC gradients and TEC fluctuations at middle latitudes and longitudinally confined equatorial regions that exhibit scintillation, TEC gradients and TEC fluctuations. The development of a global specification and forecast system for scintillation is needed in view of our increased reliance on space based communication and navigation systems, which are vulnerable to ionospheric scintillation. Such scintillation specification systems are being developed for the equatorial region. An equatorial satellite equipped with an appropriate suite of sensors, capable of detecting ionospheric irregularities and tracking the drivers that control the formation of ionospheric irregularities, has been planned for the purpose of specifying and forecasting equatorial scintillation.

Radar Auroral Clutter Maps: A Mission-Tailored Graphical Product for DoD Warfighters

S. Quigley* and G. Bishop - Space Vehicles Directorate, Air Force Research Laboratory (AFRL/VSBX), 29 Randolph Rd, Hanscom AFB, MA 01731, 781-377-3036, Fax: 781-377-3160, E-mail: Gregory.Bishop@hanscom.af.mil; E. Holeman and D. Madden - Institute for Scientific Research, Boston College, 140 Commonwealth Ave, Chestnut Hill, MA 02467, 781-377-9659, Fax: 781-377-3160, E-mail: Ernest.Holeman@hanscom.af.mil; P. Citrone, K. Sero, and R. Wilkes - Detachment 11, Space & Missile Systems Center (SMC, Det 11/CID), 1050 E. Stewart Ave, Peterson AFB, CO 80914, 719-560-8737, Fax: 719-560-2038, E-mail: Peter.Citrone@cisf.af.mil

The Air Force Research Laboratory and Detachment 11 of the Space & Missile Systems Center have combined efforts to design, develop, test, and implement new graphical products for Air Force space weather operations. As the initial implementation of the Operational Space Environment Network Display (OpSEND) program, these state-of-the-art web page images represent a quantum leap in the Air Force Weather Agency's capability to provide easy-to-visualize nowcasts and short-term forecasts of space weather effects on theater-based military systems operating through the ionosphere. OpSEND's Radar Auroral Clutter Maps provide a current specification of the estimated position and strength of the auroral oval and its potential for causing radar performance degradation caused by auroral clutter. Operating locations and parameters (maximum range, azimuths, and elevation angles) for all applicable radar sites are utilized, along with a near-earth model of the magnetic field. Aside from these, the primary inputs for the Radar Auroral Clutter Maps are in-situ auroral electron flux measurements from Defense Meteorological Satellite Program (DMSP); a current ground-based planetary geomagnetic index (running 3-hour K_p) is used if DMSP data is not available within 3 hours of measurement. The Radar Auroral Clutter Maps are automatically updated every 30 minutes on the US Air Force's Space Weather Operations web page to provide timely, accurate, and mission-tailored displays of potential radar auroral clutter to support early-warning and space surveillance radars. Background theory and product development science issues are presented, along with overall capabilities, limitations, and planned improvements for the product.



Specifications ("nowcasts") of the near-real time radar operations products used to mitigate detrimental auroral clutter are shown. The first product (left side) is a global map, showing all operational radar sites, along with an indication (red border around site number) of those potentially affected by auroral clutter-induced false target returns. The second product (right side) shows a radar site-specific map, with more detailed graphical and numerical information about the auroral clutter zone.

“Operational Effects at ALTAIR due to Ionospheric Disturbances”

S. Close, A. Coster, S. Hunt
MIT Lincoln Laboratory
244 Wood Street
Lexington MA, 02173

The ARPA Long Range Tracking and Instrumentation Radar (ALTAIR) is a dual-frequency (VHF/UHF) radar that supports both missile testing and satellite tracking activities for US Space Command. ALTAIR provides both metric and radar cross section data and is located at the Kwajalein Missile Range (KMR), which lies near the geomagnetic equator at 3°N latitude. The radar operating frequencies, coupled with the complex nature of the ionosphere at this equatorial location, significantly impacts ALTAIR's measurement accuracy and tracking abilities. The techniques applied for ionospheric correction include real-time two-frequency measurement as well as the Ionospheric Error Correction Model (IECM) for single-frequency tracking. The IECM is a data-driven, ionospheric range and elevation correction algorithm that consists of the Parameterized Electron Content Model (PECM) adjusted by Global Positioning System (GPS) based measurements of the Total Electron Count (TEC) as well as ALTAIR's own two-frequency measurements. ALTAIR and GPS data are used as a real-time data acquisition source to continuously scale the IECM to match actual ionospheric conditions surrounding ALTAIR.

This paper presents specific instances of ionospheric effects on the ALTAIR system. The presence of post-sunset Spread-F, gravity waves, and equatorial plumes are routinely observed during ALTAIR operations and have adversely affected both metric and signature data. The corresponding analysis of these data, which include both dual-frequency and single VHF frequency tracking observations, are also discussed. GPS and ALTAIR TEC data are analyzed to identify the source and location of the ionospheric effect, as well as to determine spatial and spectral characteristics.

VLF Remote Sensing of Lower Ionospheric Variability

Umran S. Inan
Space, Telecommunications and Radioscience Laboratory
Stanford University

The nighttime lower ionosphere, at D-region altitudes of <100 km, exhibits a high degree of variability and is generally difficult to measure due to the inaccessibility of this altitude range to *in-situ* measurements and the relatively low (<1000 eI/cc) electron densities which inhibits radar measurements. An effective method for studying this region is via the use of very low frequency (VLF) waves, which propagate to long distances in the earth-ionosphere waveguide. Variations in nighttime electron density at 60 to 85 km altitudes are manifested as amplitude and phase changes of VLF signals that are easily detectable. Examples of such natural variations include relatively solar flares, solar proton events, slow diurnal changes, rapid variations due to lightning-induced ionospheric disturbances, oscillatory changes due to gravity waves, and Space Weather effects such as relatively variations associated with auroral activity as well as relativistic electron enhancements. Quantitative interpretation of observed VLF variations in terms of ionospheric changes requires the use of models of VLF propagation and scattering, and has been generally difficult, especially in cases where the approximate location of disturbances in relation to long-baseline VLF paths is not known. However, recent measurements at closely spaced multiple sites indicate that ionospheric parameters such as electron density and temperature can be determined from VLF data. In this paper, we present examples of the different types of lower ionospheric variability as observed via VLF remote sensing, and review results of recent attempts at quantitative estimation of ionospheric parameters. We also discuss possible use of VLF methods for determination of the long term (many days) variations of energetic electron precipitation in the auroral and South Atlantic Anomaly regions.

G1. Space Weather: systems effects.

RECENT VALIDATION RESULTS FOR SELECTED HF PROPAGATION PREDICTION PROGRAMS USING SPACE WEATHER DATA

R.D.Hunsucker
RP Consultants
7917 Gearhart
Klamath Falls, OR
97601
Rdhrpc1@aol.com

Since the mid 1970's over twenty computer-based HF Propagation Prediction Programs have been developed and employed by users of communication, broadcast and radar system, but there has been a relative lack of validation efforts. Most of the programs are based on monthly and hourly median data and their basic purpose is to aid system planners to design their facilities for frequency, power and directional pattern management for benign ionospheric conditions. All the programs include seasonal and sunspot cycle effects and some recent ones also include other Space Weather data as inputs. In spite of being designed for benign ionospheric conditions and for long-term planning, some users employ the programs for near-real-time predictions.

Signal strength data from the HF "PENEX" experiment in 1993 and from the IARU HF beacon network in 1999 and 2000 were compared with predictions made by several of the HF programs. Using the signal strength data from the PENEX experiment, the near-real-time predictions averaged around 50% correct.

Employing one of the recently developed prediction programs, which contains a near-real-time ionospheric storm algorithm, we compared updated predictions for mostly disturbed conditions on midlatitude paths to F-region MOF's observed on the HF beacon network. Results of this comparison indicate that the algorithm based on the D_{ST} index strongly overestimates ionospheric storm effects. Ionospheric maps derived from an AMIE program were also compared to signals recorded on a high latitude and midlatitude path, with reasonable qualitative results.

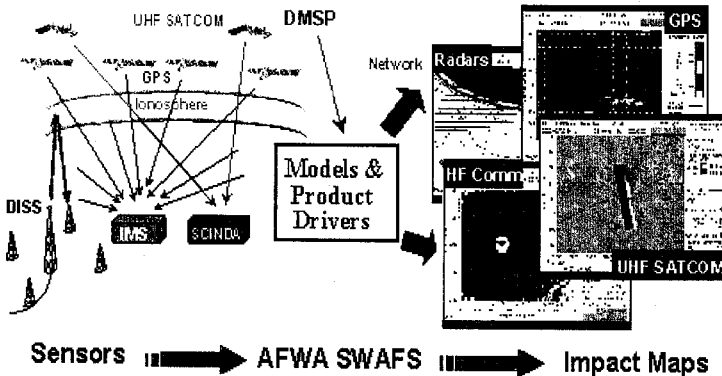
It is suggested that HF propagation data may be of use as a METRIC for evaluating Space Weather predictions.

OpSEND: Tailored Space Weather Impact Maps for Specific Radio-Based Systems

G. Bishop*, S. Quigley, K. Groves and T. Bullett - Space Vehicles Directorate, Air Force Research Laboratory (AFRL/VSBX), 29 Randolph Rd, Hanscom AFB, MA 01731, 781-377-3036, Fax: 781-377-3550, E-mail: Gregory.Bishop@hanscom.af.mil; P. Doherty - Institute for Scientific Research, Boston, College, 140 Commonwealth Ave, Chestnut Hill, MA 02467, 781-377-4283, E-mail: Patricia.Doherty@hanscom.af.mil; P. Citrone, K. Scro, and R. Wilkes - Detachment 11, Space & Missile Systems Center (SMC, Det 11/CID), 1050 E. Stewart Ave, Peterson AFB, CO 80914, 719-560-8737, Fax: 719-560-2038, E-mail: Peter.Citrone@cis.af.mil

Over the past two years, the Air Force Research Laboratory (AFRL/VSB) and Detachment 11, Space & Missile Systems Center (SMC, Det 11/CID) have combined efforts to design, develop, test, and implement brand-new graphical products for 55th Space Weather Squadron (55SWXS) operations. As the initial implementation of the Operational Space Environmental Network Display (OpSEND) program, these state-of-the-art web page images represent a quantum leap in the capability of the Air Force Weather Agency (AFWA) to provide easy-to-visualize nowcasts and short-term forecasts of space weather effects on theater radio-based systems operating through the ionosphere. Advanced computer applications are driven by real-time space environmental measurements to generate user-friendly displays that graphically depict space weather impacts on radio systems in mission-threshold driven color graphics. These sophisticated applications are generated at 55SWXS (whose functions will soon be incorporated in the AFWA Space Weather Analysis and Forecast System [SWAFS]) for network dissemination to specific radio system users.

Operational Space Environment Network Display (OpSEND)



Radar Auroral Clutter Maps provide a current specification (nowcast) of the estimated position and strength of the auroral oval relative to radar coverage regions. UHF SATCOM Scintillation Maps provide a current specification (nowcast) and two-hour forecast of ionospheric scintillation and its potential for causing degradation to UHF SATCOM communication links. HF Illumination Maps provide a current specification (nowcast) and one-hour forecast of the high frequency (HF) communication performance for a fixed ground HF transmitter at a given HF frequency. Estimated GPS Single-Frequency Error Maps provide a current specification (nowcast) and one-hour forecast of estimated positioning errors that result from GPS constellation geometry and inaccurate ionospheric correction for a single-frequency GPS user.

Electromagnetic Theory

Chairs: I. Besieris, USA and I. Lindell, Finland

	Page
1:00 Time-Domain Analysis of the Evanescent Fields Associated with Ultrafast X-Wave Tunneling Through a Planar Slab, A. Shaarawi, The American University in Cairo, <i>I. Besieris*</i> , Virginia Polytechnic Institute and State University, B. Tawfik, Cairo University, Fayoum Campus	118
1:20 Ultra-Fast Transmission of a Transverse-Electric X-Wave Tunneling Through a Multilayered Structure, A. Shaarawi, The American University in Cairo, <i>I. Besieris*</i> , Virginia Polytechnic Institute and State University, B. Tawfik, Cairo University, Fayoum Campus	119
1:40 Analytical and Numerical Evaluation of the Explicit Form of the Electromagnetic Field Propagator, <i>R.D. Nevels*</i> , C. Shin, Texas A&M University	120
2:00 Image Theory for the Prolate Spheroid, I. Lindell, K.I. Nikoskinen, Helsinki University of Technology, <i>G. Dassios*</i> , University of Patras	121
2:20 Spiral as an Electronically Controlled Polarization Transformer, K. Karkkainen*, <i>M.A. Stuchly</i> , University of Victoria	122
2:40 Scattering by Truncated Periodic Arrays of Narrow Strips: A Wiener-Hopf Formulation, <i>F. Capolino*</i> , M. Albani, Università di Seina	123
3:00 Construction and Properties of Scattering Expansions for Magnetic and Electric Cavity Green's Functions, <i>F. Gronwald*</i> , J. Nitsch, S. Tkachenko, Otto-von-Guericke-University Magdeburg	124
3:20 The Homogenization Method and Its Application to Designing Frequency Selective Structures, <i>G. Kiziltas*</i> , H. Syed, Z. Li, J. Volakis, N. Kikuchi, The University of Michigan	125
3:40 Finite-Element-Method Computation of Zero-Sequence Impedance of Three-Phase Underground Pipe-Type Cables, <i>X.B. Xu*</i> , Clemson University, G. Liu, Comtech Communication Inc.	126
4:00 Theoretical Study of a Model Scatter-Probe Optical Microscope, <i>C.I. Valencia*</i> , E.R. Mendez, Centro de Investigacion Cientifica y de Educacion, A.A. Maradudin, T.A. Leskova, University of California-Irvine	127
4:20 Singularities of Space-Time Focusings in Non-Stationary Media, <i>D.N. Chistyakov</i> , A.S. Kryukovsky, D.S. Lukin*, MIPT, Institutskiy per., 9, Dolgoprudny	128

TIME-DOMAIN ANALYSIS OF THE EVANESCENT FIELDS ASSOCIATED WITH ULTRAFAST X-WAVE TUNNELING THROUGH A PLANAR SLAB

Amr M. Shaarawi

Physics Department, The American University in Cairo
P.O. Box 2511, Cairo 11511, Egypt

*Ioannis M. Besieris**

The Bradley Department of Electrical and Computer Engineering,
Virginia Polytechnic Institute and State University, Blacksburg, Virginia 24061, USA

Bassem H. Tawfik

Department of Engineering Physics and Mathematics,
Faculty of Engineering, Cairo University (Fayoum Campus), Fayoum, Egypt

A study is provided of an X-wave undergoing frustrated total internal reflection on the upper surface of a planar slab separating two dielectric media. This is achieved by choosing all the spectral plane wave components of the incident X-wave to fall on the upper interface at angles greater than the critical angle. It is shown that the peak of the field transferred through the slab appears to be transmitted at a superluminal speed (A. M. Shaarawi and I. M. Besieris, *Phys. Rev. E*, **62**, 7415-7421, 2000). The differences between deep- and shallow-barrier penetrations are highlighted. For the former case, it is shown that the peak of the transmitted field can emerge from the backside of the slab before the incident peak reaches the front interface. To understand this *advanced* transmission of the peak of the pulse, a detailed study of the behavior of the evanescent fields in the tunneling region is undertaken. Making use of a closed form time-domain expression for the evanescent fields of an X-wave incident on a semi-infinite half space (A. M. Shaarawi, I. M. Besieris, A. M. Attiya and E. El-Diwany, *J. Acoust. Soc. Am.*, **107**, pp. 70-86, 2000), we can determine several attributes of the X-wave pulsed fields transmitted through the slab. In particular, we can derive a simple expression for the *advanced* position of the peak of the X-wave incident on the front side of the slab at the moment when the peak of the transmitted field emerges from the backside. The same analysis can be used to explain the reason that the transmitted pulse is less localized than the incident one. The results of this work are supported by specific numerical examples showing that our explanation of advanced transmission is fairly accurate and demonstrating that the transport speed of the peak of a tunneling X-wave can be much larger than the speed of light.

ULTRA-FAST TRANSMISSION OF A TRANSVERSE-ELECTRIC X-WAVE TUNNELING THROUGH A MULTILAYERED STRUCTURE

Amr M. Shaarawi

Physics Department, The American University in Cairo
P.O.Box 2511, Cairo 11511, Egypt

*Ioannis M. Besieris**

The Bradley Department of Electrical and Computer Engineering,
Virginia Polytechnic Institute and State University, Blacksburg, Virginia 24061, USA

Bassem H. Tawfik

Department of Engineering Physics and Mathematics,
Faculty of Engineering, Cairo University (Fayoum Campus), Fayoum, Egypt

It has been demonstrated that transverse electric (TE) X-waves undergoing frustrated total internal reflection are partially transmitted through a single slab at ultra-fast speeds that appear to be superluminal. This effect is produced by the reshaping of the low-amplitude, advanced portion of the evanescent field of the pulse tunneling through the barrier region (A. M. Shaarawi and I. M. Besieris, *Phys. Rev. E*, **62**, 7415-7421, 2000). In this work, a study is provided of the transmission of a three-dimensional TE X-wave undergoing frustrated total internal reflection on the upper surface of a multi-layered structure. The stratified structure consists of successive barrier layers separated by free propagation regions. It is shown that the traversal times of the peaks of the incident X-wave are not only independent of the cumulative widths of the barrier regions but are also independent of the lengths of the free propagation regions separating them. This unanticipated result leads to an *advanced* transmission of the pulse; specifically, the peak of the transmitted field emerges at the backside of the stack before the incoming peak reaches the front surface of the stack (A. M. Shaarawi and I. M. Besieris, *J. Phys. A: Math. Gen.*, **33**, 8559-8576, 2000). Under certain conditions, the total traversal time through all the successive evanescent and free propagation sections appears to be less than zero. This behavior leads to swift pulse transmissions that can be much faster than the speed of light. The results obtained in this work are analogous to predictions made in simulations of transmission of pulses through two undersized sections of a waveguide. In such a study, the predicted ultra-fast multiple tunneling requires that the waveguide sections contain weak precursory fields before the arrival of the peak of the pulse. In this work, we investigate the possibility of ultra-fast multiple tunneling for X-waves going through a multilayered structure consisting of successive evanescent and free propagation layers. Using spectral synthesis, a simple analytic solution is obtained for the tunneling of a three-dimensional X-wave through such a stratified structure. Conditions for the materialization of this ultra-fast multiple tunneling of X-waves are highlighted and their consequences and limitations are discussed.

Analytical and Numerical Evaluation of the Explicit Form of the Electromagnetic Field Propagator

R. D. Nevels* and Changseok Shin
Department of Electrical Engineering
Texas A&M University
College Station, Texas 77843-3128

A full wave Feynman Path Integral for the electromagnetic field has recently been derived based on the time domain form of Maxwell's differential equations (R. D. Nevels, J. A. Miller, and R. E. Miller, "A Path Integral Time Domain Method (PITD) for Electromagnetic Scattering", IEEE Trans. Antennas Propagat., April, 2000). The solution is in a form known as a phase space path integral. For the electromagnetic field this means that in order to complete one time step, the initial time electric and magnetic fields are first Fourier transformed into the spectral domain, then multiplied by a state transition matrix and finally this product is inverse Fourier transformed back to the real space-time domain. Each repetition of this set of operations advances the field a single time step. Because Fourier transformation requires utilizing the entire present time field in the numerical space in order to determine the value of the field at any point at the next time step, the PITD approach is an implicit numerical method.

The essential feature of a path integral is the propagator. The propagator for the electromagnetic field can be constructed by interchanging the orders of integration described above so that the Fourier exponentials and the state transition matrix fall under the spectral integral. With this form of the path integral, which is known as the 'standard form', a time step is accomplished by a single integration, which is a convolution of the propagator and the present time field. The authors recently showed that the spectral integrals could be evaluated analytically, thereby producing analytical forms of the propagator in one-, two- and three-dimensions. A remarkable aspect of this result was the fact that the one- and three-dimensional propagators are constructed entirely of delta functions, a property that allows analytical evaluation of the path integral in those dimensions.

In this paper we will present both analytical and numerical calculations using what can be referred to as an explicit propagator method. A simple analytical problem, that of a plane wave propagating in free space, will be used to demonstrate the correctness of the propagator. A numerical method for evaluating this 'standard form' will be presented. Because only nearest neighbor values of the electromagnetic field are required, this can be described as an explicit (rather than implicit) numerical technique. The numerical method will be applied in the 3-D case to find the field scattered from a dielectric slab and to determine the degree of numerical dispersion. We will describe the advantages and limitations of this method as compared to the PITD method.

Image theory for the prolate spheroid

I.V. Lindell, K.I. Nikoskinen, G. Dassios*
Helsinki University of Technology
P.O. Box 3000, Espoo 02015HUT, Finland
Tel: +358-9-451-2266, e-mail: ismo.lindell@hut.fi
*University of Patras, 26110 Patras, Greece

Kelvin's electrostatic image theory from 1845 for the PEC sphere is one of the most elegant methods to treat electromagnetic boundary-value problems. The theory replaces the sphere by the image of the original source which in case of a point source is a point source in the inverse point.

A generalization of the Kelvin theory to a PEC prolate spheroid was more recently suggested by Sten and Lindell (*J. Electro. Waves Appl.* 9(4)599-604, 1995) for a point source at the axis of symmetry. The suggested image consisted of a line source at the axis between the focal points of the spheroid and was given in the form of a series expansion. The image expression was seen to work well when the original source was far enough from the spheroid, while at close distances the image series suffered serious convergence problems. Moreover, by letting the spheroid tend to a sphere, the image would converge to a multipole at the origin and did not directly give the Kelvin image as a simple limit.

In the present paper the theory is improved by extracting an analytic point image out of the series. The point image links the present theory to Kelvin's theory because it reduces to the Kelvin image when the spheroid becomes a sphere while the remaining line image vanishes. On the other hand, at close distances of the source, the remaining line image converges much better and its amplitude appears to be one decade lower than in the original theory. At large distances both theories become the same because the point image is absorbed by the line image.

Spiral as an Electronically Controlled Polarization Transformer

Kimmo Kärkkäinen, Maria Stuchly

Department of Electrical & Computer Engineering, University of Victoria
BOX #3055 Stn.CSC, Victoria, BC, V8W 3P6, Canada

Frequency selective surfaces (FSS) have been extensively used to modify characteristics of reflector antennas (e.g. Hill and Munk, *IEEE Trans. Antennas Propag.*, vol. 44, pp. 368-374, 1996). Modified periodic element have also been used in reflectarrays (Huang and Pogorzelski, *IEEE AP-S/URSI Digest*, vol. 2, pp. 1280-1283, 1997). Many different shapes of FSS elements have been analyzed. Polarization transformers that rotate the polarization of a linearly polarized wave or that convert a linear polarization to circular are important in some antenna applications (McNamara and Baker, *SAIEE Symposium Antennas and Propagation*, pp. R1-9, 1983). In this research, we explore properties of an FSS consisting of spiral elements. Furthermore, one end of the spiral is connected to an electronic switch (e.g. Schotky diode), that can connect it to ground plane.

The finite-difference time-domain (FDTD) method is used for analysis. One period of the studied planar structure consists of thin perfectly conducting (PEC) spiral plate, the ground plane and on/off switchable connection between spiral and ground as shown in Fig.1a. The implementation of periodic boundary conditions is straightforward because we study only the reflection of normal incidence plane waves.

It is found out that spiral patterns offer a flexible way to control the polarization of reflected wave. For a narrow band it is possible to turn polarization 90 degrees. Operating band can be adjusted by varying geometric parameters of the spiral. Furthermore, by using electronic switch we can choose whether to transform polarization or not. Spirals offer also ability to convert linear polarization to circular. Interesting thing is that spiral does not have special direction and hence it treats all incoming polarizations the same way. Fig.1b illustrates how electric field power is transformed to perpendicular polarization in an example structure.

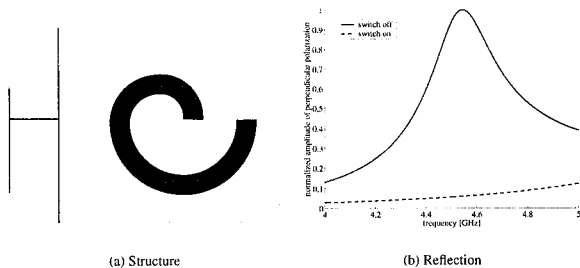


Figure 1: Polarization transforming FSS

Scattering by Truncated Periodic Arrays of Narrow Strips: A Wiener-Hopf Formulation

Filippo Capolino and Matteo Albani

Dipartimento di Ingegneria dell'Informazione, University of Siena,
Via Roma 56, 53100 Siena, Italy.
capolino@ing.unisi.it, albanim@ing.unisi.it

ABSTRACT

Arrays with large dimensions are the subject of an increasing amount of interest in recent years. Assuming the structure as infinite when using a full-wave model, though simple and efficient it may not be satisfactory when truncation effects are relevant. Due to the localization of the truncation-induced diffracted waves for large arrays, many physical insights of the wave processes may be extracted from a canonical problem such as a semi-infinite array (F.Capolino, M.Albani, S.Maci, L.B.Felsen, *IEEE Trans. AP*, 1, 67-85,2000). In this paper, we deal with the exact analysis of a semi-infinite array of narrow strips illuminated by a plane wave. The same structure has been analyzed in (L.Carini, L.B.Felsen, *IEEE Trans. AP*, 4, 412-421,1993) with a hybrid (ray)-(Floquet)-(MoM) efficient formulation, however truncation effects were accounted for using a Kirchhoff approximation. Successively, truncation effects have been numerically refined in (A.Neto, S.Maci, G.Vecchi, M.Sabbadini, *IEEE Trans. AP*, 3, 2000) using a MoM with basis functions shaped as truncation-induced diffracted fields. Here, the problem of a semi-infinite array of narrow strips is solved using a discrete Wiener-Hopf technique which has the advantage of being both exact and analytically explicit. The discrete Wiener-Hopf technique has been applied in (N.L.Hills, S.N.Karp, *Comm. Pure Appl. Math.*, 18, 203-233, 1965) to treat a semi-infinite grating of small cylinders under the hypothesis of electrically-large interelement spacing ($d \gg \lambda$ =wavelength). This restriction is removed in our approach which finds it as a special limit case. In addition, in our formulations many new aspects are introduced: a) Arbitrary basis functions can be chosen to shape the current on the strip elements also permitting to treat both TE and TM polarizations; b) The discrete Wiener-Hopf is implemented using a Z-transform of the sampled distribution of currents. Here, the topology (singular points) of the z-spectral plane is shown explicitly for a general semi-infinite structure by using the infinite Poisson summation formula. The Z-transformed Kernel function has branch points at $z_b = \exp(\pm jkd)$ (with k =wavenumber and d =interelement distance), that (assuming small losses) are located slightly inside and outside the unit circle. c) A complete correspondence between the discrete z-spectral representation and the standard continuous plane wave k_x -spectral representation is established in relation with the Wiener-Hopf solving procedure. d) Solutions for the two limit cases of large ($d \gg \lambda$) and small ($d \ll \lambda$) interelement spacing are automatically obtained from our formulation and will be addressed in details; e) Asymptotic is performed via path deformation and SDP (steepest descent path) evaluation directly in the z-plane (showing the correspondence to the k_x plane); f) Asymptotic results are performed in a totally uniform fashion for both the radiated field and the current on the strips, thus also involving higher order terms.

The diffracted field is then found asymptotically as a sum of Floquet waves with domain of existence bounded by shadow boundary planes plus a cylindrical diffracted field arising from the truncation of the array. A detailed derivation of the solution and some illustrative examples will be presented.

Construction and properties of scattering expansions for magnetic and electric cavity Green's functions

Frank Gronwald*, Jürgen Nitsch, and Sergey Tkachenko
Otto-von-Guericke-University Magdeburg
Institute for Fundamental Electrical Engineering and EMC
P.O. Box 4120, D-39016 Magdeburg, GERMANY
Tel.: +49-391-6711436, FAX: +49-391-6711236
e-mail: Frank.Gronwald@et.uni-magdeburg.de

Background

Electromagnetic boundary problems are often solved by means of the method of Green's functions. This method is particularly essential for practically important investigations of electromagnetic coupling processes within and into metallic cavities.

For canonical cavity geometries (rectangular, cylindrical, spherical, e.g.) it is known how to analytically construct appropriate Green's functions. Usually there exist different equivalent representations for the Green's function of a certain geometry. Such representations typically involve series expressions that are cumbersome to analyze and to evaluate. Therefore it is important to choose the representation which, for a specific problem, is most easily to evaluate or leads to the most physical insight.

Theoretical model

We outline the construction of a general representation for the dyadic magnetic or electric Green's function $\overline{\overline{G}}(\vec{r}, \vec{r}')$ of a cavity which has the physical interpretation of a scattering expansion. This representation follows in a natural way from the perturbative solution of a magnetic field integral equation and its electric analogue which is obtained from duality arguments. It is of the general form

$$\overline{\overline{G}}(\vec{r}, \vec{r}') = \overline{\overline{G}}_0(\vec{r}, \vec{r}') \pm (\mathcal{L}\overline{\overline{k}}_{\sigma 0})(\vec{r}, \vec{r}') + (\mathcal{L}\mathcal{F}\overline{\overline{k}}_{\sigma 0})(\vec{r}, \vec{r}') \pm (\mathcal{L}\mathcal{F}^2\overline{\overline{k}}_{\sigma 0})(\vec{r}, \vec{r}') + \dots \quad (1)$$

with $\overline{\overline{G}}_0(\vec{r}, \vec{r}')$ the dyadic Green's function of free space, $\overline{\overline{k}}_{\sigma 0}$ the induced electric or magnetic surface current, and integral operators \mathcal{L} and \mathcal{F} . The n th term of this expansion takes into account the influence of electromagnetic fields which got scattered $(n - 1)$ times within the cavity. Convergence of the scattering expansion is proven for a cavity of finite quality factor.

Due to its generality, the scattering expansion is *not limited to canonical geometries*. Moreover, if both the source and the observation point are close to the cavity wall it is possible to explicitly evaluate single terms of the scattering expansion by means of differential geometric methods in an analytical way. This presupposes that the characteristic dimensions of the cavity are comparable to or larger than the wavelength considered. In this case it turns out that the integral operator \mathcal{F} is proportional to the principal curvatures of the cavity wall. Therefore it is immediate to obtain for the Green's functions correction terms for cavity walls which *locally deviate* from a flat geometry.

Even though our analysis is based on the frequency domain it can also be applied to investigate the propagation of short electromagnetic pulses within cavities of arbitrary geometric form since it is straightforward to rewrite the series (1) in the time domain. Then the main advantage is that for any finite time moment the iteration expansion contains only a finite number of terms.

Conclusion

The presented scattering expansion for dyadic cavity Green's functions has the advantage of a clear physical interpretation and is applicable in frequency and time domain. Furthermore, it is not limited to canonical geometries. It directly connects electromagnetic quantities to geometric quantities which describe the local geometry of the cavity. If the source and observation point are close to a cavity wall it is possible to explicitly evaluate, in the frequency domain, dominant scattering contributions in an approximate but analytical way.

The Homogenization Method and its Application to Designing Frequency Selective Structures

G. Kiziltas, H. Syed, Z. Li, J. L. Volakis and N. Kikuchi
Dept of Electrical Engineering and Computer Science
University of Michigan
Ann Arbor, MI 48109-2122

Thermo-photovoltaic (TPV) cell panels are increasingly used in production of small lightweight portable generators, hybrid electric vehicles and electric grid independent appliances. A need also exists to protect the TPV panels from broadband radiation by employing high efficiency spectral control filters. However, these filters often lack compactness, good bandpass behavior or the desired efficiency.

The goal of this paper to address the design issues of TPV spectral-control filters with specific operational characteristics. This is accomplished by applying a new design technique, the Homogenization Design Method (HDM). More specifically, the dielectric permittivity is homogenized and used as the design variable in a Sequential Linear Programming (SLP) based optimization algorithm. The main attempt is to optimize the material distribution of the dielectric layers in a Frequency Selective Volume configuration with cascaded planar periodic structures. The HDM methodology is demonstrated in developing a sharp transition TPV filter that becomes reflective at 2.4 μm , which is the onset of inter-band absorption in the TPV device in a working band of 1-10 μm . An additional design requirement is that the filter transmits more than 90% up to 2.4 μm and less than 10% beyond that range.

Finite-Element-Method Computation of Zero-Sequence Impedance of
Three-Phase Underground Pipe-Type Cables

Xiao-Bang Xu* and Guanghao Liu
Holcombe Department of Electrical Comtech Communication Inc.
and Computer Engineering 105 Baylis Road
Clemson University Melville, NY 11747
Clemson, SC 29634-0915

Three-phase underground pipe-type cables are widely used in power transmission systems in urban areas. To protect such systems, utilities engineers need to properly size circuit breakers based on knowledge of fault currents. For an accurate calculation of the fault currents, it is necessary to know the zero-sequence impedance of the underground pipe-type cable. The method currently most widely used in industry for calculating the zero-sequence impedance is based on a paper by J.H. Neher published in 1964 (J.H. Neher, "The phase sequence impedance of pipe-type cables," IEEE Transactions on Power Apparatus and Systems, Vol. PAS-83, pp. 795-804, August 1964). Neher indicates that in the usual case where the pipe is made of steel, the zero-sequence impedance depends upon the permeability of the steel. It is well known that the permeability of steel changes with the magnetic field intensity. Since the magnetic field intensity varies in the steel pipe, the permeability should be different from point to point in the pipe. But, unfortunately, in Neher's computational model, a *constant* "effective permeability" is used for the *whole* steel pipe and the magnetic field intensity used for calculating the "effective permeability" is obtained from an empirical formula. As a result, such calculated zero-sequence impedance has a considerable difference compared with measurement data.

In this paper, we present an improved method for computing the zero-sequence impedance of a three-phase underground pipe-type cable, based on finite-element analysis and iterative solution procedure. The zero-sequence impedance can be computed from knowledge of the source current densities in the conducting regions within the pipe-type cable. To determine the source current densities, integro-differential equations are formulated. They are solved numerically by employing finite-element method, subject to appropriate boundary conditions. In the numerical solution, special attention is paid to the nonlinear B-H characteristic of the steel pipe. An iterative solution procedure is developed for determining the relative permeability in each element of the pipe. Computational results of the zero-sequence impedance at different current levels are presented and analyzed. Also, they are validated by being compared with measurement data.

Theoretical Study of a Model Scatter-Probe Optical Microscope

Claudio I. Valencia and E. R. Méndez

División de Física Aplicada, Centro de Investigación Científica y de Educación Superior de Ensenada, Apartado Postal 2732, Ensenada, Baja California 22800, México

A. A. Maradudin and T. A. Leskova

Department of Physics and Astronomy, and Institute for Surface and Interface Science, University of California, Irvine, California 92697, USA

We study theoretically the scattering of light from a model scatter-probe near-field microscope of two different configurations. The first configuration consists of an infinitely thin half-plane of a perfect conductor defined by $x_1 \geq x_0$, $x_3 = d$ above a rough perfectly conducting surface defined by $x_3 = \zeta(x_1)$ for $-\infty < x_1 < \infty$. In the second configuration the scatter-probe near-field microscope consists of a thin dielectric wire of a dielectric constant ϵ_0 and of a diameter D , $D \ll \lambda$, located at the point (x_0, d) above the rough surface. Both structures are invariant along the x_2 -axis. It is assumed that $\zeta(x_1)_{max} < d < \lambda$, where λ is the wavelength of the incident light. The presence of the half-plane or the dielectric wire within a wavelength of the surface creates a scattered evanescent field that interacts with the rough surface to generate a propagating field that can be detected in the far field. In this way structure on the surface with sub-wavelength dimensions contributes to the scattered intensity in the far field. To extract this information from the far field signal the scattering amplitude is calculated in zero- and first-order in the surface profile function $\zeta(x_1)$ by the analytic solution of an integral equation of scattering theory. The intensity of the scattered light, $|E_2(x_1, x_3|\omega)_{sc}|^2$, in the case of s -polarized incident light, or $|H_2(x_1, x_3|\omega)_{sc}|^2$, in the case of p -polarized incident light, is then calculated at a point of observation (x_1, x_3) in the far field as a function of the position of the half-plane or the dielectric wire x_0 to first order in $\zeta(x_1)$. From this result $\zeta(x_1)$ can be obtained by Fourier analysis from experimental data for the field intensity. For the experimental values of $|E_2(x_1, x_3|\omega)_{sc}|^2$ and $|H_2(x_1, x_3|\omega)_{sc}|^2$ we use the results of an exact numerical solution of the scattering equations based on Green's second integral identity in the plane. From these calculations it is found that $\zeta(x_1)$ can indeed be reconstructed from far-field scattering data with sub-wavelength resolution.

Singularities of Space-Time Focusings in Non-Stationary Media

Dmitry N. Chystyakov (cdn@wave.mipt.ru)
Andrew S. Kryukovsky (kryukov@wave.mipt.ru)
Dmitry S. Lukin* (dmitry@wave.mipt.ru)
Dept. of Phys & Math Problems of Wave Processes
MIPT, Institutsky per., 9, Dolgoprudny
Moscow Region, 141700, Russia
Fax: (095) 408-5144, phone: (095) 408-5066.

In this report the singularities of wave field propagation in non-stationary media are considered. Cold homogeneous dispersive plasma was taken as a model of propagation medium. The problem is to investigate different-order space-time (ST) focusings of wave fields in such media. These focusings are classified as three-dimensional ST catastrophes (one-dimensional focusing is arising due to medium non-stationarity, two-dimensional is occurring due to warpage of the initial wave front).

We assume that time dependence of electron plasma concentration is linear, so that plasma frequency is given by the equation: $\omega_p^2(t) = \omega_1^2(1 - \alpha t)$, where $\omega_p(t)$ – plasma frequency, α – the factor of non-stationarity. In this case the condition of time focusing in non-stationary medium takes a shape: $\frac{\omega_1^2 R \alpha}{2 k^3 c^4 \omega_0} = 1$, where ω_0 – initial

signal frequency, k – wave number, c – light velocity, R – focus distance. The conditions of two-dimensional space focusing are considered earlier (Kryukovsky A.S., Rastyagaev D.V., Vergizaev I.A., *Jour. of Communications Technology and Electronics*, Vol. 44, No. 4, pp. 423-430, 1999).

We investigate the problem of frequency-modulated signal propagation in non-stationary plasma and conditions of compensation both these effects were obtained (that is the conditions under which there is no focusings).

The case of quadratic time dependence of electron plasma concentration is also researched. In order to describe electromagnetic fields in focal regions uniform expansions were obtained using special functions of wave catastrophes. By means of catastrophes theory the classification of three-dimensional ST focusings is developed and dependence of focusing order on the type of catastrophe is analysed.

Propagation Theory

Chairs: F. Bardati, Italy and Z. Zhang, USA

	Page
1:00 Application of the Reciprocity Theorem to Complex Propagation Problem, <i>C. Coleman*, Adelaide University</i>	APS
1:20 Stochastic Modeling of Correlation Radiometer Signals, <i>B. Davis*, University of Arizona, E. Kim, J. Piepmeier, NASA Goddard Space Flight Center</i>	APS
1:40 Scattering From a Land/Sea Transition, <i>M. Casciato*, K. Sarabandi, University of Michigan</i>	APS
2:00 Three Dimensional Simulation of Wave Propagation into a Comet Nucleus in the Frame of the CONSERT Experiment, <i>M. Benna*, Observatoire Midi- Pyrenees, A. Piot, Laboratoire de Planetologie de Grenoble, J. P. Barriot, W. Kofman, Laboratoire de Planetologie de Grenoble</i>	130
2:20 A MFIE-Based Predication for UHF Vertically-Polarized Wave Propagation over Irregular Terrains, <i>F. Moreira*, Federal University of Minas Gerais</i>	APS
2:40 New Computationally Efficient 2.5D and 3D Ray Tracing Algorithms for Modeling Propagation Environments, <i>Z. Zhang*, Z. Yun, M. Iskander, University of Utah</i>	APS
3:00 Development of a New Shooting-and-Bouncing Ray (SBR) Tracing Method That Avoids Ray Double Counting, <i>Z. Yun*, M. Iskander, Z. Zhang, University of Utah</i>	APS
3:20 A Method for Multiple Diffracted Ray Sampling in Forward Ray Tracing, <i>E. Di Giampaolo*, Universita dell'Aquila, F. Bardati, D.I.S.P. Universta di Roma</i>	APS
3:40 Confirmation of Random Matrix Model for the Antenna Array Channel by IndoorMeasurements, <i>R. Muller, H. Hofstetter*, Forschungszentrum Telekommunikation Wien</i>	APS
4:00 Estimation of Propagation Structure by Means of Hopfield Neural Network, <i>T. Maruyama*, Y. Kuwahara., Shizuoka University</i>	APS
4:20 FM Pulses Propagating in Focal Regions of Catastrophe Types, <i>E. Ipatov*, A. Kryukovsky, D. Lukin, D. Rastyagaev, D. Chystyakov, MIPT, Institutsky per., 9, Dolgoprudny</i>	APS

Three Dimensional Simulation of Wave Propagation into a Comet Nucleus in the Frame of the CONSERT Experiment

Mehdi Benna¹, Alexandre Piot², Jean-Pierre Barriot¹, and Wlodek Kofman²

¹ Laboratoire de Dynamique Terrestre et Planétaire, Observatoire Midi-Pyrénées,
14 Avenue Edouard Belin, 31400 Toulouse, France

² Laboratoire de planétologie de Grenoble, Bat. D de physique,
B.P. 53, 38041 Grenoble Cedex 9, France

In this paper we present the latest results of the simulation of the CONSERT (Comet Nucleus Sounding Experiment by Radiowave Transmission). This experiment is part of the scientific package of the ROSETTA space probe to be launched in 2003, and that is planned to reach comet 46P/Wirtanen in 2011. The CONSERT Experiment is based on the analysis of the propagation delays of 90 MHz radiowaves crossing the comet nucleus from ROSETTA orbiter to a lander on the comet surface. The final goal of the CONSERT Experiment is to provide a three dimensional probing of the comet interior.

For this simulation, we define a three dimensional dielectric permittivity model of a comet nucleus. This model includes a plausible shape and inhomogeneities distribution. We simulate the radiowave propagation using a ray tracing technique giving the complete received radio pattern in orbit. Our ray tracing algorithm has the capability to compute complex paths including partial and total reflections and is able to provide a radio pattern map with a high spatial and temporal resolution. The validation of our method is made by comparison with the solution of Maxwell equations in a two dimensional model. We show that the ray tracing method produces accurate values for the case of a smooth comet shape and small inhomogeneities scale. This validation enables us to have confidence in our ray tracing algorithm for a three dimensional shape which is very hard to verify otherwise.

We study several lander/orbiter configuration in order to determine the parameters influencing the repartition and the quality of the measurements.

Microstrip Antenna Analysis

Chair: J. Mosig, Switzerland

	Page
1:00 Effect of Feeding Symmetry on Resonances in Patch and Capacitor Structures, <i>E. Semouchkina*</i> , <i>W. Cao</i> , <i>R. Mittra</i> , <i>M. Lanagan</i> , <i>The Pennsylvania State University</i>	APS
1:20 Investigation on Phase Properties of Circular Microstrip Antenna, <i>M. Daneshmand*</i> , <i>L. Shafai</i> , <i>P. Mousavi</i> , <i>The University of Manitoba</i>	APS
1:40 FDTD Analysis of a Compact, H-Shaped Microstrip Patch Antenna, <i>S.C. Gao*</i> , <i>L.W. Li</i> , <i>M.S. Leongand</i> , <i>T.S. Yeo</i> , <i>The National University of Singapore</i>	APS
2:00 Temperature Effects in Multilayered (An)isotropic Superstrate-Substrates on the Characteristics of Packaged Multiconductor Microstrip Devices, <i>W.Y. Yin*</i> , <i>M. Miao</i> , <i>L.W. Li</i> , <i>B.L. Ooi</i> , <i>P.S. Kooi</i> , <i>M.S. Leong</i> , <i>T.S. Yeo</i> , <i>The National University of Singapore</i>	132
2:20 Analysis of a Square Microstrip Antenna with an Eccentric Slot, <i>M. Hurtado*</i> , <i>H.E. Lorente</i> , <i>C.H. Muravchik</i> , <i>Universidad Nacional de La Plata</i>	APS
2:40 Irregularly Shaped Patch as Perturbation of Regularly Shaped Patch, <i>Y. Sun*</i> , <i>Y. L. Chow</i> , <i>D.G. Fang</i> , <i>City University of Hong Kong</i>	APS

Temperature Effects in Multilayered (An)isotropic Superstrate-Substrates on the Characteristics of Packaged Multiconductor Microstrip Devices

Wen-Yan Yin, M. Miao, Le-Wei Li, B. L. Ooi, Pang-Shyan Kooi, M. S. Leong, and T. S. Yeo
MMIC Laboratory, Department of Electrical and Computer Engineering
National University of Singapore, Singapore 119260
Tel: +65+8746489; Fax: +65+7791103; E-mail: eleyimwy@nus.edu.sg

ABSTRACT

It is known that the dispersion characteristics of open and enclosed single and edge-coupled microstrip lines, finlines, slotlines, and bilateral coplanar waveguides on uniaxial and biaxial substrates have been treated by some people. On the other hand, there have been a number of advances which have taken place in the theoretical analysis of thermal characteristics of various microwave integrated circuits and devices more recently [1, 2]. Actually, microwave and millimeter wave systems integrated by a large number of active and passive microwave circuits and devices must operate in a real environment, and sometimes, these systems have to meet harsh environments characterized by large temperature variations. So it is necessary for us to evaluate possible effects resulted from temperature variation in multilayered superstrate-substrate on the characteristics of microstrip devices. However, there are very few data concerning with the temperature dependence of permittivity or permeability parameters of actual microstrip or antenna substrates.

In this talk, we examine the mode characteristics of packaged multiconductor microstrips and filters by taking account of the temperature variation in multilayered (an)isotropic superstrate-substrate. For anisotropic structure, we use sapphire as the microstrip superstrate-substrate. It has been proven that sapphire, monocrystalline aluminum oxide, has the desire properties of high hardness and strength, abrasion resistance, chemical inertness, stability for corrosive, inexpensive, and is one of the best thermal conductors for building monolithic integration circuits as either superstrate or substrate. While for isotropic structure, the isotropic substrate can be made of ceramic filler laminate composite, and its temperature dependence has just been obtained by Kabacik and Bialkowski's more recently. The Galerkin's method in spectral domain has been applied in our mathematical treatment. Therefore, the characteristics of packaged multiconductor microstrip lines and filters are investigated and the temperature effects of superstrate-substrate on the propagation of dominant mode is taken into account. Our numerical investigations show that, when the permittivity parameter of materials is sensitive to the temperature variation, the dispersion characteristics of packaged multiconductor microstrip lines could be influenced by temperature variation. Fortunately, the combination of materials with different temperature responses can effectively weaken the temperature effects on the propagation of guided modes in multiconductor microstrip lines or filters, for example, by combining sapphire with ceramic filler laminate C in superstrate-substrate here.

Methods for Layered & Stratified Media

Chair: L. Carin, USA

	Page
3:00 Application of the Locally Corrected Nystrom Method to Planar Layered Problems in Packaging, <i>F. Caliskan*</i> , <i>A. Peterson</i> , <i>Georgia Institute of Technology</i>	134
3:20 Lattice Sum Approach to Scattering by Periodic Layered Structures, <i>J. Thomas*</i> , <i>A. Ishimaru</i> , <i>University of Washington</i>	135
3:40 Study of the Scalar Potentials Arising in Stratified Media, <i>T. Grzegorzczuk*</i> , <i>Research Laboratory of Electronics, MIT</i> , <i>J.R. Mosig</i> , <i>Ecole Polytechnique Federale de Lausanne</i>	136
4:00 Multilayered Media MPIE Green's Functions, <i>J. Sarvas*</i> , <i>P. Yla-Ojala</i> , <i>M. Taskinen</i> , <i>University of Helsinki</i>	137
4:20 Efficient Evaluation of the Half-Space Green's Function for Fast-Multipole Scattering Models, <i>Z. Liu*</i> , <i>L. Carin</i> , <i>Duke University</i>	138
4:40 Dielectric Resonator Antenna on a Slotted Ground Plane, <i>C. Y. Huang*</i> , <i>Yung-Ta Institute of Technology</i> , <i>K. L. Wong</i> , <i>T.W. Chiou</i> , <i>National Sun Yat-Sen University</i>	139

Application of the Locally Corrected Nyström Method to Planar Layered Problems in Packaging

Fatma Çalıřkan*, Andrew F. Peterson
Packaging Research Center
School of Electrical & Computer Engineering
Georgia Institute of Technology
Atlanta, GA, 30332

The method of moments (MoM) is very popular for the solution of open field problems, particularly for printed structures in planar layered media. In a previous report, the mixed potential integral equation (MPIE) was solved with the required Green's functions calculated using the generalized pencil of functions (GPOF) algorithm. Rooftop basis and testing functions were used in the MoM formulation to ensure cell-to-cell current continuity.

Recently, an alternate approach called the locally corrected Nyström method (LCN) has been applied to solve integral equations in electromagnetics [L. F. Canino et al., "Numerical solution of the Helmholtz equation in 2D and 3D using a high-order Nyström discretization," *Journal of Computational Physics*, vol. 146, pp. 627-663, 1998]. The LCN uses a numerical quadrature rule as the process for discretization. Recent research suggests that the LCN is well-suited for higher-order implementations and does not require cell-to-cell current continuity in the underlying representation. Thus it may offer advantages over the MoM, especially for problems involving complex 3-D structures. If cell-to-cell continuity is not required, nonconforming meshes may offer simpler geometrical modeling. In addition, the LCN can provide a representation that varies in quadrature order from cell to cell, offering enhanced accuracy in needed regions.

In this presentation, the LCN is adapted to solve the MPIE for layered medium problems arising in microelectronic packaging applications. The formulation will be described and results from the LCN and MoM will be compared in order to evaluate the performance of the LCN. In addition, the effect of not imposing current continuity will be investigated.

LATTICE SUM APPROACH TO SCATTERING BY PERIODIC LAYERED STRUCTURES

John R. Thomas* and Akira Ishimaru

Electrical Engineering Department, University of Washington, Seattle, Washington USA 98195

This paper presents a calculation of scattering from a periodic layer of cylindrical (2-dimensional) structures based on a method suggested by Yasumoto and Kushta (Russian Academy of Sciences, Far Eastern Branch Computing Center, The Far-Eastern School Seminar on Mathematical Modeling and Numerical Analysis, Khabarovsk, 1999). The lattice sum function S_n is a sum of Green's functions over the (infinite) periodic set of scatterers. It separates the Floquet mode problem into two parts, the lattice sum matrix L , where $L_{mn} = S_{m-n}$, which is determined by just the array spacing and angle of incidence, and the scattering matrix T of an individual cylinder in the array. The scattered wave is given compactly in cylindrical harmonic representation by

$$b^n = (I - T \cdot L)^{-1} T a^i$$

where a^i is the column vector amplitude of the incident wave and b^n is the column vector scattering amplitude of the array. Specifically for one example, formulated in terms of a magnetic Hertz potential for the TE scattering case, with only a Z (axial) component of magnetic field

$$\Pi_{inc} = \sum_{n=-\infty}^{\infty} a_n^i J_n(kr) e^{-jn\phi} \quad \text{and} \quad \Pi_s = \sum_{n=-\infty}^{\infty} b_n^s H_n^{(2)}(kr) e^{-jn\phi}$$

Here the free-space wave number $k = \omega/c$, and (r, ϕ) are the cylindrical coordinates. For an incident plane wave of unit E field, $a_n^i = \exp(jn(\phi_o - \pi/2))/(\omega\mu k)$. With an incident wave propagating in the direction of \hat{k} in the X-Y plane, ϕ_o is the angle between \hat{k} and the positive X direction.

Our idea is to calculate the T matrix for a variety of interesting shapes, such as a "C"-shaped dielectric (lossy or not, also block or square C's, helices, winged C's) with a method of moments procedure and combine this with the lattice sum to get scattering amplitudes for models that could represent certain photonic crystals or frequency selective surfaces. With the MoM method, the directly calculated quantity is the scattered electric field E_ϕ as a function of (r, ϕ) , for a given incident field angle ϕ_o . For any incident field angle, if the numerical field evaluations are made at a set of $M = 2N+1$ scattering angles and some fixed large distance r , a Fourier series expansion that gives the angular dependence may be calculated with a discrete Fourier transform algorithm. For objects that are reasonably small compared to a wavelength, only a reasonably small number of angular harmonics will be needed. The conventional scattering amplitudes B_{sn} at angle ϕ_o for scattering from one of these individual shapes is then determined by equating coefficients of $e^{-jn\phi}$ in the cylindrical harmonic expansion of the ϕ component of scattered electric field (e.g., Ishimaru, *Electromagnetic Wave Propagation, Radiation and Scattering*, Chapter 12, Prentice Hall, 1991). With $2N+1$ of these calculations for $2N+1$ different values of ϕ_o^m we obtain a matrix equation for the T matrix (through the N^{th} angular harmonic) in the form $B_s = T \cdot A$, where B_s and A are $M \times M$ matrices with, respectively, the elements $B_{sn}(\phi_o^m)$ and $a_n^i(\phi_o^m)$ in the (n, m^{th}) position.

This over-all approach has the advantage that the lattice sum function need be evaluated only for a wavelength-to-lattice-spacing ratio and angle of incidence. The lattice sum is obtained efficiently by the method of Yasumoto and Yoshitomi (*IEEE Trans. Antennas Propagat.*, 47, 1050-1054, 1999). Then, results of placing a variety of different objects on this lattice require only calculations of the T matrix of the individual objects. An Australian group (including Botten, Nicorovici, McPhedran and others) has published several papers (two in *J. Opt. Soc. Am. A*, 17, 2165-2190, 2000, one in *J. Math. Phys.*, 41, 7808-7816, 2000) that emphasize this usefulness and provide many analytic details.

STUDY OF THE SCALAR POTENTIALS ARISING IN STRATIFIED MEDIA

Tomasz M. Grzegorzcyk* and Juan R. Mosig**

* Research Laboratory of Electronics, MIT.

** Laboratoire d'Electromagnétisme et d'Acoustique (LEMA)

Ecole Polytechnique Fédérale de Lausanne (EPFL)

CH-1015 Lausanne, Switzerland

Tomasz.Grzegorzcyk@epfl.ch, Juan.Mosig@epfl.ch.

The extensive study of laterally infinite stratified media with arbitrarily oriented sources by integral equations methods and Sommerfeld's choice has for long shown the existence of two expressions for the scalar Green's functions G_V . These are generated by point charge sources associated with horizontal and vertical sources and thus, both need to be used in CAD softwares aiming at the analysis of complex 3-D structures embedded in stratified media. The difference between these two expressions is very important (e.g. they do not present the same set of surface wave poles, yielding a very different behavior in that context) and may even appear in contradiction with the electrostatic case where of course, only one expression of G_V exists.

These facts have been recognized a long time ago in the open literature and several schemes have been proposed to integrate these potentials into different formulations of the mixed potential integral equation (MPIE) model. In this presentation, we revisit this topic and carefully study the properties of these potentials with the help of the single layer case, where simple analytical expressions can be obtained in the spectral domain. In particular, the surface wave poles are determined and the continuity properties of the potentials in terms of source and observer position as well as dielectric interface are carefully discussed.

It is also shown that both potentials can be expressed as series expansions of k^{2n} terms (where k is the wavenumber and $n = 0, 1, 2, \dots$). These expansions, although different for $n > 0$, share the same static term ($n = 0$), equal to the well-known electrostatic value. Moreover, some apparent discrepancies in the expressions of these potentials are explained by involving reciprocity and an appropriate choice of integration constants.

In a similar way, it could be shown that the magnetic vector potential \underline{G}_A also reduces in the near field context to the well-known static expression. Ultimately, the full spectral expressions of \underline{G}_A and G_V can be used in an MPIE-MoM formulation to analyze 3-D structures and a proper implementation allows the simultaneous use of both scalar potentials in a simple way. This is demonstrated by analyzing a coaxially fed patch antenna over a thick substrate and obtaining theoretical predictions in good agreement with measurements.

Multilayered Media MPIE Green's Functions

Jukka Sarvas*, Pasi Ylä-Oijala and Matti Taskinen
Rolf Nevanlinna Institute, University of Helsinki,
PO Box 4, FIN-00014 Helsinki, Finland

Electromagnetic field computing in layered media is more complicated than in the free space, because the Green's functions are dyadic and involve highly oscillating and slowly converging Sommerfeld integrals. Furthermore, in using the surface integral equation method, the Green's function's must be given in the mixed potential integral equation (MPIE) form, i.e in terms of scalar and vector potentials.

In this talk, we give a compact representation for the complete set of three dimensional multilayered media MPIE Green's functions for general electric and magnetic current sources. These Green's functions can be, for instance, applied to EM-field computing with objects buried in a multilayered medium, or to the analysis of complicated 3-D microstrip structures.

In deriving the wanted Green's functions, we use the classical Hertzian potential approach rather than the usual way to first decompose the source currents into TE and TM components. In this generality our approach is new, and we feel that it is more straightforward and simpler, and it leads to a unified and numerically very efficient set of formulas. Our approach also directly yields the needed correction term for the general MPIE scalar potentials, and this term coincides with that of the Michalski-Zheng C-formulation.

Using the Hertzian potentials, the multilayered media Green's dyads for electric and magnetic sources, can be presented in the terms of 6 scalar functions. We show that all 32 components of the spectral domain MPIE Green's functions can be given in terms of two of these functions, which, furthermore, can be computed with a single iterative algorithm.

The computing of the spatial domain MPIE Green's functions from the spectral ones, is carried out, as usual, with the Sommerfeld integrals. Utilizing the properties of the Hertzian potentials, we are able to reduce the number of the needed Sommerfeld integrals to ten for the complete set of Green's functions. If only the electric field is computed for electric sources, only 4 Sommerfeld integrals are needed. We also carry out all partial differentiations in the spectral domain, and so no numerical differentiation is needed to obtain the final Green's functions.

We have numerically verified our formulas for Green's functions by comparing the results to those in the literature and observed a good agreement. Also in this talk, numerical examples are presented.

Efficient Evaluation of the Half-Space Green's Function for Fast-Multipole Scattering Models

Zhijun Liu* and Lawrence Carin
Department of Electrical and Computer Engineering
Duke University
Durham, NC 27708-0291
zliu@ee.duke.edu, lcarin@ee.duke.edu

There are many applications for which one is interested in scattering from targets situated in the presence of a lossy half space, e.g. for scattering from vehicles above soil and for unexploded ordnance (UXO) under soil. One of the principal tools for the analysis of such scattering is the method of moments (MoM), with such recently extended via the fast multipole method (FMM) and the multi-level fast multipole algorithm (MLFMA). In such formulations one of the most complicated issues to be addressed is evaluation of the half-space dyadic Green's function. Each component of the dyadic is represented in general via a Sommerfeld integral, the direct numerical evaluation of which makes a MoM analysis prohibitive. Moreover, the FMM and MLFMA models were developed originally in the context of the free-space Green's function, such not directly transferable to the dyadic half-space Green's function. In previous half-space FMM and MLFMA studies the "near" terms are evaluated via the complex-image technique, as in the MoM, and the "far" FMM/MLFMA terms are evaluated via an approximation to the dyadic Green's function, using a single appropriately weighted image in real space. The real-image representation of the Green's function is analogous to a first-order asymptotic steepest-descent-path (SDP) evaluation, this appropriate for expansion and testing function separated by a wavelength or more. This is typically appropriate for the "far" FMM/MLFMA terms, although we have found that the accuracy of this first-order approximation vitiates as the target becomes close to the half-space interface. In this paper we consider a higher-order approximation for efficient evaluation of the half-space Green's function, with the resulting formulation still applicable to the FMM formulation. After presenting the simple formulation, example results are discussed, which address the accuracy of the Green's-function evaluation. We also compare MLFMA-computed scattered fields, using the previous and current method for representation of the Green's function, with focus on scattering from a target near a half-space interface.

Dielectric Resonator Antenna on a Slotted Ground Plane

Chih-Yu Huang¹, Kin-Lu Wong² and Tzung-Wern Chiou²

¹Department of Electronic Engineering,

Yung-Ta Institute of Technology, PingTung, Taiwan 909, R.O.C.

E-mail: huang220@seed.net.tw

²Department of Electrical Engineering,

National Sun Yat-Sen University, Kaohsiung, Taiwan 804, R.O.C.

I. Introduction

Dielectric resonator antennas have received much attention in recent years. Since DR antennas are usually with a relatively large permittivity, small fabrication errors can cause large shifting of the resonant frequency of the constructed DR antennas. This characteristic causes a problem for practical applications of the DR antenna at a desired specific frequency. And due to the inherent hardness of the DR element, it is almost impossible to make slight geometrical modifications to a constructed DR to tune its resonant frequency. Recently, to overcome the problem, the methods of loading a conducting disk on top of a DR antenna fed by a coaxial probe [1, 2] to tune the antenna's resonant frequency or loading a conformal parasitic strip on a conformal-strip-excited semispherical DR antenna [3] to achieve resonant frequency tuning have been reported.

In this paper, we propose a new and easy method for post-manufacturing resonant frequency tuning of the DR antenna. It is found that simply by embedding a pair of narrow slots in the ground plane of the DR antenna, the resonant frequency of the DR antenna can be effectively varied by varying the lengths of the embedded slots. This is probably because the embedded slots in the ground plane can cause the meandering of the excited surface current path in the antenna's ground plane, especially in the portion of the ground plane under the DR element, and thus the resonant frequency of the DR antenna can be varied. The proposed method applied to a coplanar waveguide-fed square-disk DR antenna [4] is demonstrated. Details of the experimental results are presented and analyzed.

II. Antenna design and experimental results

Fig. 1 shows the proposed frequency agile DR antenna. A square-disk DR element having a side length of L and a height of t was used. The DR

element was centered above a grounded square FR4 substrate of thickness h ($= 1.6$ mm) and relative permittivity ϵ_r ($= 4.4$). Two identical narrow slots of length ℓ and width 1 mm ($\ell \gg 1$ mm) were embedded in the ground plane of the FR4 substrate. The distance between the two narrow slots is S , which was fixed to be 5 mm in this study. The two narrow slots are placed symmetrical with respect to the y -axis (see Fig. 1), and have a distance of d_2 to the open-circuited end of the coplanar waveguide (CPW) feed, which excites the DR antenna and has a characteristic impedance of 50Ω with a signal strip (center conductor) of width 6.37 mm and a distance 0.5 mm between the signal strip and the coplanar ground. The distance between the center line (x -axis) of the ground plane and the open-circuited end of the CPW feed is denoted as d_1 . By adjusting the distance d_1 , good impedance matching of a CPW-fed DR antenna can easily be obtained [4].

Several prototypes were constructed. Fig. 2 shows the measured return loss against frequency for the cases with $\ell = 0, 10, 14, 19$ and 25 mm; the case with $\ell = 0$ represents a corresponding regular DR antenna without embedded slots in the ground plane. In this study the square-disk DR was constructed using a low-loss ceramic material with a very high relative permittivity of $\epsilon_{ra} = 79$. The square-disk DR had a side length of 28.2 mm (L) and a height of 4.9 mm (t). The corresponding measured data are also listed in Table 1 for comparison. The prototypes were excited at the fundamental $HEM_{11\delta}$ mode. It is clearly seen that the resonant frequency is decreased with increasing slot length. Fig. 3 shows the measured resonant frequency against slot length. [Note that for the case with $\ell = 25$ mm, good impedance matching was not achieved. This is because in the study the distance d_1 for various slot lengths was all fixed to be 0 mm (i.e., the open-circuited end of the CPW feed was along the center line of the ground plane and the DR element). By adjusting the distance d_1 , better impedance matching for the case with $\ell = 25$ mm is possible.] For the case with $\ell = 19$ mm, the resonant frequency is 240 MHz or about 11% lower than that of a corresponding regular DR antenna (1865 MHz vs. 2105 MHz). This suggests that a resonant frequency tuning range of 240 MHz in this study for the constructed DR antennas is obtained.

Also, the impedance bandwidth for the case with $\ell = 19$ mm was measured to be 2.7%, which is greater than that of a corresponding regular DRA (2.1%). This behavior is largely owing to the embedded slots in the ground plane, which causes the lowering of the quality factor of the DR antenna. Radiation characteristics of the constructed prototypes were also

studied. Radiation patterns of the prototypes are measured. Good broadside radiation characteristics are observed, and the obtained antenna gain was about 6 dBi, which is about the same as obtained in [4] for the regular CPW-fed DR antenna.

III. Conclusions

CPW-fed frequency agile DR antennas have been demonstrated. Experimental results of the constructed prototypes show a resonant frequency tuning range of more than 10% of the antenna's resonant frequency. Also, the proposed antenna allows post-manufacturing resonant frequency tuning to compensate for manufacturing tolerances or possible fabrication errors to meet precise frequency specifications in practical designs.

References

1. Z. Li, C. Wu, and J. Litva, "Adjustable frequency dielectric resonator antenna," *Electron. Lett.*, vol. 32, pp. 606-607, 1996.
2. Z.N. Chen, K.W. Leung, K.M. Luk, and E.K.N. Yung, "Effect of parasitic disk on a coaxial probe-fed dielectric resonator antenna," *Microwave Optical Technol. Lett.*, vol. 15, pp. 166-168, 1997.
3. H.K. Ng, and K.W. Leung, "Conformal-strip-excited dielectric resonator antenna with a parasitic strip," 2000 IEEE Antennas Propagat. Soc. Int. Symp. Dig., pp. 2080-2083
4. J.Y. Wu, C.Y. Huang, and K.L. Wong, "Low-profile, very-high-permittivity dielectric resonator antenna excited by a coplanar waveguide," *Microwave Optical Technol. Lett.*, vol. 22, pp. 96-97, 1999

Tables

Table 1: Performance of the proposed frequency agile DR antenna; $S = 5$ mm. $d_1 = 0$ mm, $d_2 = 4$ mm, $\epsilon_r = 4.4$, $h = 1.6$ mm, $\epsilon_{ra} = 79$. $L = 28.2$ mm. $t = 4.9$ mm, ground-plane size = 75 mm \times 75 mm.

	ℓ mm	f_r MHz	10dB return-loss BW MHz, %
Reference	0	2105	45, 2.1
Antenna 1	10	2065	50, 2.4
Antenna 2	14	1950	53, 2.7
Antenna 3	19	1865	51, 2.7

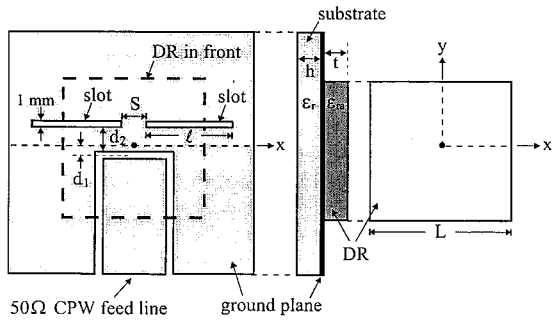


Fig. 1 Geometry of the proposed coplanar waveguide-fed frequency agile dielectric resonator antenna.

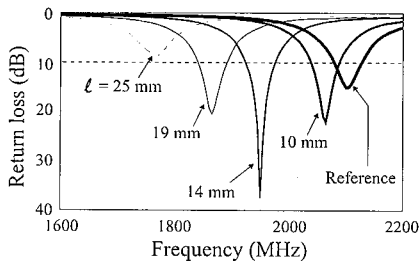


Fig. 2 Measured return loss against frequency for constructed prototypes. Antenna parameters are given in Table 1.

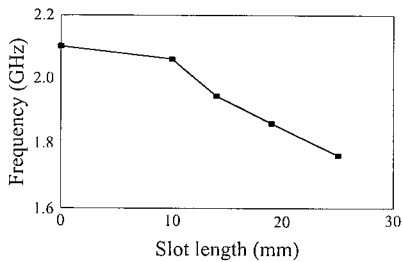


Fig. 3 Measured resonant frequency against slot length l .

Antenna Design Optimization

Chair: L. Desclos, USA

	Page
1:00 Shape Optimization of Microstrip Antennas Using Genetic Algorithm, <i>H. Choo*</i> , <i>A. Hutani</i> , <i>H. Ling</i> , <i>University of Texas at Austin</i>	144
1:20 Patch Antenna Size Reduction by Combining Inductive Loading and Short Points Technique, <i>L. Desclos*</i> , <i>S. Reed</i> , <i>Y. Mahe</i> , <i>G. Poilasne</i> , <i>S. Toutain</i> , <i>Ecole Polytechnique de Nantes-IRCCYN Div. SETRA</i>	145
1:40 Mutual Coupling Between Microstrip Line Fed Printed Antennas on Large Coated Cylinder, <i>V.B. Erturk</i> , <i>Bilkent University</i> , <i>K.W. Lee</i> , <i>R.G. Rojas*</i> , <i>The Ohio State University</i>	146
2:00 Analysis of Microstrip Patch Antenna Elements Using Several Software Packages, <i>C. Peixeiro</i> , <i>C. Fernandes*</i> , <i>Technical University of Lisbon</i>	147
2:20 Improved Electrically Small Planar Microstrip Antenna, <i>C.S. Lee*</i> , <i>A. Mahmood</i> , <i>Southern Methodist University</i>	148

Shape Optimization of Microstrip Antennas Using Genetic Algorithm

Hosung Choo*, Adrian Hutani and Hao Ling

Department of Electrical and Computer Engineering
The University of Texas at Austin
Austin, TX 78712 U.S.A

The use of genetic algorithm (GA) in designing optimized microstrip patch shapes has recently been reported in the literature (J. M. Johnson. and Y. Rahmat-Samii, *IEEE Tran. Antennas Propagat.*, **47**, 1606-1614, 1999; H. Choo et al, *Electron. Lett.*, **36**, 2057-2058, 2000). The attractiveness of GA shape optimization is that performance improvement can be achieved with little increase in patch size or manufacturing cost. In this paper, we investigate the use the GA to obtain optimized performance on standard FR-4 substrate for three applications: (i) broadband, (ii) dual-band, and (iii) circular polarization (CP).

In our GA implementation, two-dimensional (2-D) chromosome is used to encode each patch shape into a binary map. The metallic sub-patches are represented by ones and the no-metal areas are represented by zeros. Since it is more desirable to obtain optimized shapes that are well connected from the manufacturing point of view, a 2-D median filter is applied to the chromosomes at each generation of the GA. We utilize a full-wave EM simulation code to evaluate the performance of each patch shape. The cost function that is specifically defined to achieve each design goal (broadband, dual-band or circular polarization) is then calculated for each patch. Based on the cost function, the next generation is created by a reproduction process that involves crossover, mutation and geometrical filtering.

Optimized shapes for broadband, dual-band and circular polarization are obtained using the above approach. For broadband application, we report a four-fold improvement in bandwidth compared to a standard square patch. For dual-band operation, the GA designs show good operating characteristics for two frequencies. Moreover, arbitrary frequency ratio between the two frequency bands ranging from 1.2 to 2 can be designed. For CP application, we obtain a CP bandwidth of 1.6% based on 3-dB axial ratio by using the GA methodology. Return loss, far field radiation pattern and current distribution on the microstrip patch will be presented. In addition, physical interpretation for the optimized structures will be discussed.

Patch Antenna size reduction by combining inductive loading and short points technique

L. Desclos, S. Reed, Y. Mahe, G. Poilasne, S. Toutain

IRCCYN division SETRA, Laboratoire SEI, IRESTE, Ecole polytechnique de Nantes, Rue Christian Pauc La chantrerie, BP 60601, 44306 Nantes Cedex France

Abstract:

In this communication, we consider the reduction of the global size of a patch antenna by combining two techniques, on one hand, slots are inserted as inductive loading and on the other hand by making some short points in the middle of a patch excited originally in TM₁₀₀ mode. Such combined solutions allow to have a global reduction of 80%. This enables to develop several small applications especially in portable communication systems.

The authors have already proposed a solution to reduce the size of a patch by a factor of two (S. Reed, L. Desclos, C. Terret and S. Toutain, "Size reduction of a patch antenna by means of inductive loads", MOTL March 2001). The principle relies on the loading of the non-radiating edges by slits (Hoefler W.J.R., "Equivalent series inductivity of a narrow transvers slit in microstrip", IEEE Trans on MTT, Vol. 25, N 10 october 1977, pp.822-824). This allowed having still the classical behavior of a patch excited with a TM mode. However, it has to be noticed that the shift in the field along the axis of non-radiating edge is faster than in a classical non-reduced patch and has to be controlled carefully when combining with other kind of technique.

It is well known that as long as the patch is in the TM₁₀₀ mode, the electrical field has constant amplitude along x-axis - fig. 1-, and varies with \cos^2 along the y-axis. It has been proposed (Kuga. N and Arai. H., "Circular patch antennas miniaturized by shorting posts", Elect. And Comm. In Japan, 1996, Part I. Vol. 79, N.6, June, pp.51-58) to reduce the size by having a set of short points forcing the field to reach the ground in the middle of the patch. As long as the decay is $\pi/2$, as it is in this case, it is possible to consider that only one radiating equivalent slot will suffice to radiate. When the condition of reduction is respected then we are able to have an equivalent length of $\lambda_g/4$ (λ_g is the guided wavelength).

Here is an example of an antenna printed on a Duroid substrate with a dielectric constant of 3.38 and 62 mils of thickness. Considering an original antenna designed for a 2.2GHz application, the original antenna had a size of 75mm (corresponding to the half wavelength size) by 35mm. Using only the inductive loading principle we can make an antenna of 37.5mm by 35mm. However, by combining the two principles of reduction we have an antenna of 9mm by 30mm. The matching of such an antenna easily reaches -19 dB and the gain is estimated at around 1.5 dBi in the main axis.

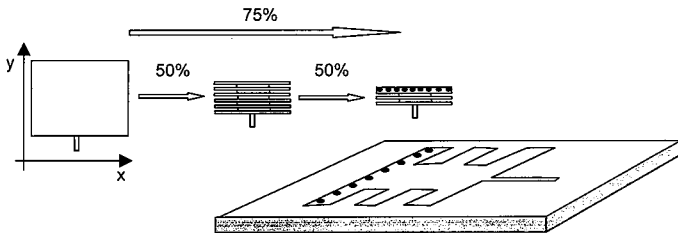


Fig.1: Antenna dimensions reduction.

Mutual Coupling Between Microstrip Line Fed Printed Antennas on Large Coated Cylinder

V.B. Ertürk

Dept. of Electrical & Electronics Eng.
Bilkent University, TR-06533 Bilkent, Ankara Turkey

K.W. Lee and R.G. Rojas*

Dept. Electrical Engineering, ElectroScience Laboratory
The Ohio State University, Columbus, Ohio 43212-1191, USA

Printed antennas fed along their edges by microstrip lines is a simple and common configuration. A variety of methods (i.e. transmission line model, cavity model, moment method and other numerical techniques) have been presented to analyze the antenna performance for planar and curved structures. Hybrid methods that combine the Method of Moments (MoM) and spectral domain Green's function are often used to analyze the characteristics of conformal antennas. However, these methods are only useful for electrically small structures because they become computationally expensive when the distance between the antennas increases. Therefore, it is necessary to develop an efficient and accurate method to calculate the coupling characteristics of printed antennas on large dielectric coated cylinders.

The efficiency and accuracy of the hybrid MoM/Green's function method depends strongly on the computation of the Green's function. In this paper, an efficient hybrid MoM/spatial domain Green's function method to compute the input impedance and mutual coupling between microstrip antennas on a dielectric coated electrically large cylinder is presented. Based on their computational efficiency and regions where they remain highly accurate, three type of representations in the spatial domain are employed in the Green's function calculation. A Steepest Descent Path (SDP) representation is frequently used and valid everywhere except in the paraxial region and when the separation between source and observation points is electrically small. For the paraxial region, an asymptotic-based spatial domain Green's function representation is used, whereas, an efficient integral representation of the planar microstrip dyadic Green's function is employed when the separation is electrically small.

The printed conformal antennas and microstrip lines are modeled with subdomain basis functions where the continuity of the current at the junction between the feed line and the patch is enforced. Note that a Maxwellian current distribution is assumed for the basis functions on the transmission line. The unknown currents are then solved with a standard moment method solution employing the space domain Green's function described above. Details on the analysis method and simulated results for the mutual coupling between microstrip line fed microstrip antennas on an electrically large dielectric coated cylinder will be presented.

ANALYSIS OF MICROSTRIP PATCH ANTENNA ELEMENTS USING SEVERAL SOFTWARE PACKAGES

Custódio Peixeiro and Carlos A. Fernandes*

Instituto de Telecomunicações/Instituto Superior Técnico
Technical University of Lisbon
Av. Rovisco Pais, 1 1049-001 Lisboa Portugal
E-mails: custodio.peixeiro@lx.it.pt , carlos.fernandes@lx.it.pt

As a result of the huge and continuous improvement in personal computer speed and memory, many electromagnetic simulators are nowadays commercially available for the analysis and design of microstrip patch antennas and circuits. Such software tools allow a substantial decrease if not elimination of the previous lengthy and costly cut and try design, fabrication and test procedure. Moreover they provide physical insight into the working mechanisms of the device under development. However there is a great variety of CAD software packages with different capabilities, performances and prices.

In this paper we compare four commercial software packages in the analysis of microstrip patch antenna elements. They are PCAAD 4.0 from Antenna Design Associates, Inc., ENSEMBLE 5.1 from Ansoft Corporation, IE3D 7.0 from Zeland Software, Inc., and WIPL-D (Windows Version) whose demonstration version is sold through Artech House. PCAAD is an antenna CAD package that uses cavity and transmission line models to analyse common microstrip structures. It can not deal with general multilayer structures. ENSEMBLE and IE3D are based on full-wave moment method solutions of integral equation formulations. They can be used to analyse general 2.5D planar antenna and circuit structures. IE3D has also optimization capabilities. WIPL-D is a numerical electromagnetic code based on the method of moments that can model general three-dimensional structures using wires and metal and dielectric plates. Wires can be cylindrical or conical. Plates are represented by bilinear surfaces. Currents over the structure are calculated as solutions of the electrical field integral equation (EFIE).

A set of commonly used microstrip patch antenna elements comprising different patch shapes, feeding methods and number of layers have been selected. These examples were chosen to stress the software package features. Specifically four different microstrip antenna structures are compared in this paper. They are: a common coaxial probe fed rectangular patch printed on a thin substrate; an irregular shape patch also printed on a thin substrate; a double layer aperture coupled microstrip line fed rectangular patch and a rectangular patch printed on a thick substrate. Input return loss and far field radiation patterns will be presented. Comparison with experimental results will be provided.

IMPROVED ELECTRICALLY SMALL PLANAR MICROSTRIP ANTENNA

Choon Sae Lee and Aamer Mahmood
Electrical Engineering Department
Southern Methodist University
Dallas, Texas 75275

The microstrip antenna size is determined mainly by the wavelength within the substrate. As the operating frequency decreases, the antenna size becomes too large to be implemented for practical applications. The patch size can be reduced with a substrate of high dielectric constant or meandering stripline, in which case the antenna efficiency is significantly reduced.

It has been proposed that the antenna size can be greatly reduced by replacing the radiating metallic surface with two abutting microstrip patches of different widths (C. S. Lee, P.-W. Chen and V. Nalbandian, 2000 IEEE AP-S International Symposium Digest, 778-781). The discontinuity in width in the middle of the radiating patch shortens the total patch length required for the impedance transition from the point where the wave impedance vanishes to the patch. The resultant resonant frequency is significantly lower than that of a comparable conventional microstrip antenna. The patch length required for resonance decreases monotonically as the ratio of the width of the wider patch to that of the narrower patch increases, while the frequency bandwidth becomes smaller. When the antenna size becomes smaller, the cross polarization level increases significantly because the radiation from the traditionally non-radiating edges is not negligible any more.

In this presentation, we will introduce how to reduce the cross polarization level while maintaining the size reduction. The scheme is to suppress the radiation to the cross polarization by modifying the traditionally non-radiating edges.

Antenna Measurements and Calibration

Chair: R. Rotman, Israel

	Page
1:00 Calibration of Large Phased Arrays Including Monopulse Ratios, R. Rotman*, Y. Oz, A. Benaish <i>Elta Electronics Industries IAI</i>	APS
1:20 Design of An L-Band Test Range Validation Antenna, L. Foged*, L. Duchesne, P.O. Iversen, SATIMO, J. Lemaczyk, <i>European Space Agency, ESTEC</i>	150
1:40 Minimization of the Truncation Impact on Measured Radiation Pattern in Spherical Near-Field Antenna Test Ranges, L. Foged*, L. Duchesne, Ph. Garreau, P.O. Iversen, SATIMO, J-Ch. Bolomey, <i>SUPELEC</i>	151
2:00 Precision Dipoles for Antenna Test Range Validation, L. Duchesne*, M. Le Goff, P.O. Iversen, <i>SATIMO</i>	152
2:20 Active Measurements of Wireless Devices in a Spherical Near Field Test Range, A. Gandois*, P. Garreau, G. Barone, <i>SATIMO</i>	153
2:40 Microwave Measurements of the Complex Permittivity of the Construction Materials Using Fresnel Reflection Coefficients and Reflection Ellipsometry, F. Sagnard*, C. Vignat, V. Montcourtois, E. Rolland, <i>Universite de Marne-la-Vallee</i>	APS

DESIGN OF AN L-BAND TEST RANGE VALIDATION ANTENNA

L. Foged⁽¹⁾, L. Duchesne⁽¹⁾, P. O. Iversen⁽¹⁾, J. Lemanczyk⁽²⁾

*⁽¹⁾ SATIMO, 22 Avenue de la Baltique, Z.A de Courtaboeuf, 91953 Courtaboeuf, France
Email: lfoged@satimo.fr, lduchesne@satimo.fr, piversen@satimo.fr*

*⁽²⁾ European Space Agency, ESTEC, Keplerlaan 1, P.O. Box 299, AG Noordwijk ZH, The Netherlands
Email: jerry.lemanczyk@estec.esa.nl*

ABSTRACT

Calibrated antennas with repeatable radiation characteristics in a reasonable range of physical environments and good correlation between predicted and measured performances are indispensable tools for the validation of antenna test ranges. An L-band test range validation antenna has been developed by SATIMO under contract with the European Space Agency (ESA). This paper describes the initial considerations and antenna design process.

Particular attention has been paid to the definition of the radiation characteristics of the validation antenna. These characteristics should allow to verify the existence of undesired phenomena in the antenna test range. The selection of an adequate antenna technology is a compromise between desired radiation characteristics, repeatability, physical robustness, temperature and humidity invariance.

MINIMIZATION OF THE TRUNCATION IMPACT ON MEASURED RADIATION PATTERN IN SPHERICAL NEAR-FIELD ANTENNA TEST RANGES

L. Foged⁽¹⁾, L. Duchesne⁽¹⁾, Ph. Garreau⁽¹⁾, P.O. Iversen⁽¹⁾, J-Ch. Bolomey⁽²⁾

⁽¹⁾ SATIMO, 22 Avenue de la Baltique, Z.A de Courtaboeuf 91953 Courtaboeuf, France
Email: lfoged@satimo.fr, lduchesne@satimo.fr, pgarreau@satimo.fr, piversen@satimo.fr

⁽²⁾ SUPELEC, Plateau de Moulon, 3 Rue Joliot-Curie, 91992 Gif-Sur-Yvette, France
Email: bolomey@supelec.fr

ABSTRACT

In spherical near-field test ranges the accuracy of the measured back radiated fields can be strongly influenced by either blockages or truncation errors in the back radiated zone. This issue can be readily investigated by measuring the pattern of a known reference antenna or by measuring the same antenna in different positions.

Different methods to minimize the impact of truncation errors are available in the literature. These methods are generally based on mathematically formulated interpolation of the missing field points. This paper discusses and compares the efficiency of field interpolation techniques derived from electromagnetic considerations.

The efficiency and validation of the proposed interpolation schemes will be illustrated by measurements of known reference antennas in the spherical near-field test range at SATIMO.

PRECISION DIPOLES FOR ANTENNA TEST RANGE VALIDATION

L. Duchesne, M. Le Goff, P. O. Iversen

SATIMO, 22 Avenue de la Baltique, Z.A de Courtaboeuf, 91953 Courtaboeuf, France

Email: lduchesne@satimo.fr, mleoff@satimo.fr, piversen@satimo.fr

ABSTRACT

Today's interest in the accurate radiation measurements of wireless devices, has contributed to the ongoing international effort in developing standards for the validation of antenna measurement ranges. In order to verify if the performance of a test range are compliant with a manufacturers requirements and the applicable international standards, very accurate validation tools are needed. Such validation tools shall allow the accurate measurement of the reflectivity of the range and detection of any potential error sources over specific frequency bands.

SATIMO has developed very accurate vertical dipoles aimed at qualifying antenna test ranges. The dipoles have typically less than 0.3 dB peak to peak gain variations in the horizontal cut, thus allowing to detect scatterers and quiet zone ripples of very small magnitudes. The dipoles have been optimized for the main operating frequency bands (GSM, US Cellular, PCS, GPS, etc...) and are delivered with calibration certificates.

This paper describes the design of the dipoles, their measured electrical performance and the results obtained in the spherical near field test range at SATIMO.

ACTIVE MEASUREMENTS OF WIRELESS DEVICES IN A SPHERICAL NEAR FIELD TEST RANGE

A. Gandois, P. Garreau, G. Barone

*SATIMO, 22 Avenue de la Baltique, Z.A de Courtaboeuf, 91953 Courtaboeuf, France
Email: agandois@satimo.fr, pgarreau@satimo.fr, gbarone@satimo.fr*

ABSTRACT

Active and multimode antenna measurements for the ever-growing number of wireless applications are becoming more and more important. There is a need driven by the mobile phone and Bluetooth industries among others to develop a test set-up capable of measuring active radiating devices under real operating conditions. For example, it is of great interest to measure the radiation characteristics of a mobile phone without the disturbing effects of a RF cable. The implementation of such measurements involves aspects of control, synchronization and receivers dedicated to multi-mode test configurations.

SATIMO has developed a test configuration for active measurements that is integrated in a spherical near field antenna test range. The active measurement system is using the multi-sensors measurement capability of the range, thus benefiting of very rapid measurement possibilities.

This paper describes the active measurement configuration. Measurements performed in the near field test range at SATIMO are presented and illustrate the capabilities of the system.

Grand Challenges in CEM

Chairs: T. Cwik, USA and R. Mittra, USA

	Page
8:00 Opening Remark, <i>K. Hill, Wright Laboratory-Dayton OH</i>	156
8:10 Some Grand Challenges in Computational Electromagnetic, <i>R. Mittra*, The Pennsylvania State University</i>	157
8:20 Future Directions in Electromagnetic Modeling of Antennas and Scattering, <i>D.R. Wilton*, University of Houston, R. Adams, Virginia Tech, R.D. Graglia, Dip. Elettronica C. Duca Abruzzi, A. Peterson, Georgia Institute of Technology</i>	APS
8:40 MacroBasis Functions and MultiLevel Algorithms for Printed Antenna, <i>J.R. Mosig*, Ecole Polytechnique Federale de Lausanne, J. Rius, Universitat Politecnica de Catalunya</i>	158
9:00 Monte Carlo Simulation of Random Rough Surfaces: A Grand-Challenge Class Electromagnetic Scattering Problem, <i>S.Q. Li, City University of Hong Kong, M. Xia, Chinese Academy of Sciences, C.H. Chan*, City University of Hong Kong</i>	159
9:20 Developments and Research Challenges in Frequency Domain Computational Electromagnetic, <i>J. Volakis*, K. Sertel, University of Michigan, T.F. Eibert, T-Nova Deutsche Telekom</i>	160
9:40 Large-Scale Design and Optimization Using Cluster Computer, <i>T. Cwik*, G. Klimeck, F. Villegas, California Institute of Technology / JPL</i>	161
10:00 Fast Time Domain Integral Equation Solvers: Trends and Challenge, <i>E. Michielssen*, K. Ayygun, M. Lu, K. Yegin, University of Illinois at Urbana-Champaign, B. Shanker, Iowa State University, D. Weile, University of Delaware</i>	APS
10:20 Grand Challenges in Analyzing EM Band-Gap Structures: An FDTD/Prony Technique Based on the Split-Field Approach, <i>H. Mosallaei*, Y. Rahmat-Samii, University of California, Los Angeles</i>	162
10:40 FEM-Based Reduced-Order Modeling of Electromagnetic System, <i>A. Cangellaris, Y. Zhu, University of Illinois at Urbana-Champaign</i>	163
11:00 Detection and Classification of Complex Targets in Foliage, <i>L. Carin*, Duke University</i>	

Some Grand Challenges in Computational Electromagnetics

R. Mittra
Electromagnetic Communication Laboratory, 319 EE East
Penn State University, University Park PA 16802
Mittra@engr.psu.edu

The purpose of this opening paper is to identify some of the challenging problems in Computational Electromagnetics encountered in the analysis and design of complex electromagnetic system. The paper begins by describing a number of practical problems that the author has recently encountered in connection with governmental and industrial projects with which he has been involved. These include:

- (i) Design of a millimeter wave and infrared sensor system for the nose-cone of a supersonic vehicle.
- (ii) EMI/EMC issues associated with an Integrated Topside Design of a Navy ship.
- (iii) RCS Computation of Large Complex Targets, including cavity type inlets.
- (iv) Design of Large Conformal Array.
- (v) Interaction of a Large Phased array with a truncated FSS radome located in close proximity of the array.
- (vi) Design of an end fire array mounted on a missile-like structure.
- (vii) Biological interaction of EM fields radiated by PCS systems, base station antennas and radar systems.
- (viii) Scattering by rough surfaces, such as the ocean.

It is hoped that the identification of the computational aspects of the above problems would serve as a springboard for discussions in the presentations that would follow in the rest of the session.

FUTURE DIRECTIONS IN ELECTROMAGNETIC MODELING
OF ANTENNAS AND SCATTERERS

D. R. Wilton*	R. J. Adams	R. D. Graglia	A. F. Peterson
Dept. Electrical and Computer Engr. Univ. Houston Houston, TX 77204-4793 USA wilton@uh.edu	Dept. Electrical and Computer Engr. Virginia Tech Blacksburg, VA 24061-0111 USA riadams@vt.edu	Dip. Elettronica C. Duca Abruzzi, 24 Politecnico Torino 10129 ITALY raglia@polito.it	Sch. Electrical and Computer Engr. Georgia Inst. Tech. Atlanta, GA, 30332-0250 USA peterson@ee.gatech.edu

The numerical modeling of electromagnetic scatterers and antennas generally consists of most or all of the following steps:

- Choose a formulation resulting in a linear system of equations to be enforced. The modeler may have a choice between integral, differential, or hybrid formulations, and between enforcement of various boundary conditions, including absorbing conditions. Different formulations may require different Green's functions and excitations, have different solution uniqueness properties, and employ different regularization schemes.
- Select a representation for unknown fields or currents. Appropriate basis functions, for example, may be curl-, divergence-, or non-conforming; higher order or singular; or may effect an approximate Helmholtz decomposition.
- Decide how equations are to be enforced. This generally involves selection of a set of testing functions used for weighted integrations, and resulting in a so-called weak formulation. Testing function choices generally involve considerations similar to choosing basis functions.
- Assemble the equations. Considerations here include the efficient handling of singular integrals, rapid computation of Green's functions, and the efficient assembling of matrix contributions using so-called fast methods such as FMM or AIM.
- Solve the resulting equations. Symmetry may often be used to reduce the size of the system matrix to be solved. While direct solution methods often prove adequate for electrically small problems, large problems generally require the use of iterative methods. The evaluation of multiple matrix-vector products required by iterative methods may be accelerated using Fast methods; good regularization schemes or preconditioners reduce the total number of iterations required.
- Extract the desired parameters. For efficiency's sake, it may be desirable to compute only a few sample parameters and to fit them to an appropriate model.
- Repeat the last three steps until a satisfactory design is obtained. Standard optimization approaches, genetic algorithms, and neural networks can all be used to guide and accelerate the design process.

This paper examines these steps with an eye towards significant new developments that appear to promise improved accuracy and efficiency in solving complex electromagnetic scattering and antenna problems.

Monte Carlo Simulation of Random Rough Surfaces: A Grand-Challenge Class Electromagnetic Scattering Problem

¹S.-Q. Li, ²M.-Y. Xia and ¹C. H. Chan*

¹Wireless Communications Research Center, City University of Hong Kong, China

²Institute of Electronics, Chinese Academy of Sciences, Beijing 100080, China

Monte Carlo simulation of random rough surface has been a topic of continued study for many years because of its broad applications. For example, through numerical simulations of microwave emissions of ocean surfaces, we can retrieve wind field information from satellite data. The spectrum of the ocean surface depends on both the wind speed and wind direction. The anisotropy of the ocean surface created by the wind will generate nonzero third and fourth Stokes parameters. Computation of the emissivities of all four Stokes parameters at various wind speeds, incidence angles, frequencies, and wind directions will certainly help us in unfolding the scattering physics of ocean surfaces and will eventually lead to the successful mapping of the wind field.

As ocean surfaces have a large permittivity, we need to use a large number of sampling points per linear wavelength. The problem is compounded by the need of a fine surface resolution when the surface has a large roughness. In the integral-equation formulation of the random rough surface, a tapered incident wave is employed to minimize the effects of edge diffraction of the finite numerical surface. Therefore, the surface size must be sufficiently large for the simulation results to be meaningful. As the surface size is inversely proportional to the cosine of the incident angle measured away from the vertical axis of the incident plane, the surface size becomes prohibitively large for near-grazing applications. All these factors make the Monte Carlo simulation of random rough surfaces a "grand challenge" problem.

In addressing the grand challenge of Monte Carlo simulation of random rough surfaces, we have to tackle the problem on three different fronts. First we formulate the problem so that each surface sample point involves the least number of unknowns. We then need to improve existing fast algorithms for solving the large system of equations. Finally, these algorithms should be suitable for implementation on cost-effective parallel computing platforms. In this paper, we will present different formulations of the integral equation method resulting in different numbers of unknowns per surface sample point. These equations will be solved iteratively by sparse-matrix/canonical grid approaches. In these approaches, the matrix-vector multiplications are computed efficiently using the fast Fourier transforms (FFT's). For slightly rough surfaces, two-dimensional FFT's are sufficient. In contrast, three-dimensional FFT's are used instead for rougher surfaces. This difference is due to different choices of the canonical grid. These algorithms have been implemented on a cost-effective parallel computing platform running Message Passing Interface (MPI). We will report our simulation results, CPU time, and maximum size of solvable problem using the 164 Motorola Power PC 604 cluster housed in the Chinese Academy of Sciences.

Developments and Research Challenges in Frequency Domain Computational Electromagnetics

J.L. Volakis*, K.Sertel* and T.F. Eibert^{††}

*Radiation Laboratory
Electrical Engineering and Computer Science Dept.
University of Michigan
1301 Beal Ave
Ann Arbor, MI 48109-2122

^{††} T-Nova Deutsche Telekom
Technologiezentrum Darmstadt
Am Kavalleriesand 3
64295 Darmstadt
Germany

Research over the past five years has led to the development of electromagnetic algorithms and codes which now provide for $O(N \log N)$ or $O(N)$ algorithmic speed ups and memory requirements. Algorithms such as the multilevel fast multipole, adaptive integral and fast spectral domain methods have allowed for solution of full scale aircraft, large finite arrays in minutes and hours as compared to hours and several days in the past. Volumetric fast formulations have also been developed for material treatments along with hybrid finite element method for scattering and radiation applications. A 200,000 unknown matrix solution can now be carried out in 2-3 minutes (per iteration) on a desktop, and millions of unknowns can be solved on processors that can be purchased for a few thousand dollars. In conjunction with these dramatic speed-ups, much work has also been carried out on basis functions, adaptive error control, solvers and preconditioners of the underlying iterative algorithms. With such capability, one begs some possible questions: (1) what is the next step in computational electromagnetics? what are some upcoming challenges? (2) what new practical applications and new problems can now be solved and should be pursued?

With respect to upcoming challenges, it is clear that speed-up alone is not sufficient for robust solution of scattering and radiation problems. Robust solvers, solution convergence, error control, usage rules of thumb, etc., are all key issues that will occupy the community the next few years. In concurrence with this, the capability to model material junctions, and reliably deal with domains involving small and large details, thin material layers etc. are critical issues that must be overcome in providing the community with computational tools which can be used by entry level engineers in analysis and design of practical problems.

However, it is likely that some of the above developments will indeed take place as new practical applications of computational electromagnetics are being pursued. Some of these may involve (1) antenna and material design, where for the first time rigorous tools can be integrated with optimization and topology algorithms, (2) mixed-signal modeling, where dense passive circuits are used in integrated analog and digital devices, (3) electromagnetic compatibility, where calculations involving extremely complex structures and large dynamic ranges are involved, (4) propagation models for urban environments, particularly in the immediate region of the antenna or the mobile source and receiver. Some of the challenges in pursuing these applications will be discussed at the conference.

Large-Scale Design and Optimization Using Cluster Computers

Tom Cwik*, Gerhard Klimeck and Frank Villegas

Jet Propulsion Laboratory, California Institute of Technology,
4800 Oak Grove Dr., Pasadena, CA 91109

The NASA/JPL goal to reduce payload in future space missions while increasing mission capability demands miniaturization and integration of active and passive sensors, analytical instruments and communication systems among others. Currently, typical system requirements include the detection of particular spectral lines, associated data processing, and communication of the acquired data to other systems. At high frequencies, advances in lithography and deposition methods result in more advanced components for space application, with sub-micron resolution opening a vast design space. Even relatively low frequency systems demand confined volume, low mass and component integration. Though an experimental exploration of this widening design space—searching for optimized performance by repeated fabrication efforts—is unfeasible, it does motivate the development of reliable software design tools. These tools necessitate models based on the fundamental physics and mathematics of the component for an accurate model. The software tools must lead to convenient turn-around times and include interfaces that promote efficient use. The first issue is addressed by the application of high-performance computers and the second by the development of graphical user interfaces driven by properly developed data structures. These tools can then be integrated into an optimization environment, and with the available memory capacity and computational speed of high performance parallel platforms, simulation of optimized components can proceed.

In this paper we outline the use of a genetic algorithm running on cluster computers to synthesize optimized designs for infrared filters and a synthetic aperture radar antenna. A standard genetic algorithm package, integrated with design software specific to the filter or antenna, and executing on cluster computers is described. This framework is being developed for a wide range of applications. It is also currently being used in nanotechnology modeling efforts.

Fast Time Domain Integral Equation Solvers: Trends and Challenges

Eric Michielssen[†], Kemal Aygun[†], Mingyu Lu[†], Korkut Yegin[†],
Balasubramaniam Shanker^{††}, and Daniel S. Weile^{†††}

[†]CCEM, Dept. of Electrical and Computer Engineering,
University of Illinois at Urbana-Champaign

^{††}Electrical and Computer Engineering Dept., Iowa State University

^{†††}Dept. of Electrical and Computer Engineering, University of Delaware

Recent developments have rendered time domain integral equation (TDIE) solvers viable and desirable candidates for analyzing a wide variety of transient electromagnetic phenomena. Plane Wave Time Domain (PWTD) algorithms [1] constitute a key component of modern TDIE solvers. PWTD schemes permit the numerically rigorous reconstruction of transient near-fields from their far-field expansions and can be considered the time domain analogue of the frequency domain fast multipole method. The computational cost of analyzing transient surface scattering phenomena using PWTD-enhanced TDIE solvers scales as $O(N_r N_s \log^2 N_s)$ as opposed to $O(N_r N_s^2)$ for classical TDIE solvers (Here, N_r and N_s denote the number of spatial unknowns and time steps in the analysis, respectively.)

Without a doubt, PWTD-based TDIE techniques promise to solve many long-standing scientific and engineering problems. This presentation will highlight some of their successes to date within the realm of scattering and antenna analysis. In addition, present research trends and open-ended challenges will be reviewed. Indeed, current PWTD implementations are still too slow and their underlying assumptions too restrictive to tackle many real-life problems; hence, further research is required for PWTD-enhanced TDIE solvers to reach their full potential. Present PWTD kernels only apply to surface scatterers that are devoid of small geometric details and embedded in homogeneous, lossless, and unstructured backgrounds. Invariably, these kernels are tuned for serial execution. The TDIE solvers associated with present PWTD kernels have a low order of convergence and assume linear material characteristics. Current research efforts aim at alleviating these restrictions. To advance the state of the art in PWTD-enhanced TDIE solvers and to bring their performance up to par with that of fast frequency domain integral equation solvers, current research efforts focus on the development of:

- memory-efficient PWTD kernels that permit the fast evaluation of electromagnetic fields produced by bandlimited sources embedded in lossless, lossy, dispersive, diffusive, nonlinear, layered, and quasi-planar media that apply uniformly to clustered and uniform source distributions.
- higher-order, error-controllable, and grid-robust TDIE solvers that permit the analysis of electromagnetic wave interactions with objects composed of dispersive and nonlinear media.

In addition to these goals, the development of parallel implementation strategies that scale will be key to the success of future PWTD enhanced TDIE solvers. Their construction, however, remains an open-ended challenge.

Reference:

- [1] A. A. Ergin, B. Shanker, and E. Michielssen, "Fast evaluation of transient wave fields using diagonal translation operators," *J. Comp. Phys.*, vol. 146, pp. 157-180, 1998.

FEM-Based Reduced-Order Modeling of Electromagnetic Systems

Andreas C. Cangellaris and Yu Zhu

ECE Department, University of Illinois at Urbana-Champaign
1406 W. Green Street, Urbana, IL 61801, U.S.A.

Tel: 217-333-6037; Fax: 217-333-5962; E-mail: (cangella, yuzhu)@uiuc.edu

The demand for first-pass design and rapid prototyping of the electromagnetic devices and components used in state-of-the-art computing, communication, and sensing hardware cannot be met without the use of computer-aided electromagnetic analysis tools. As a result, electromagnetic computer-aided design (CAD) has experienced a tremendous growth over the past five years, both in terms of advances in the sophistication of modeling methodologies and the robustness of the associated computer implementations and in terms of its pervasive application in the design and prototyping of state-of-the-art electronic components and systems. Among the various electromagnetic modeling methodologies, finite element methods (FEM) are the methods of choice when detailed electromagnetic analysis of structures of high geometric and material complexity is required. In addition to outstanding modeling versatility and accuracy, simulation efficiency is another attribute that is critically needed for rapid prototyping and short design cycles. As a result, significant progress has been made over the past few years in the advancement of methods for accelerating FEM electromagnetic analysis both at the component and system level. Among them, model order reduction methods have had a significant impact on advancing both the modeling versatility and the simulation efficiency of FEM-based electromagnetic analysis.

This presentation reviews the fundamentals of model order reduction methodologies for FEM approximations of electromagnetic boundary value problems, and provides a comprehensive list of examples from their applications. The advantages and shortcomings of the various approaches used currently for model order reduction are highlighted through the presentation of various examples. This review helps us illustrate the current status of capabilities of FEM-based model order reduction, identify areas in which further advances are needed, and stipulate on the challenges involved. Particular emphasis is placed on one of the most striking attributes of reduced-order modeling, namely, the direct generation of compact macro-models for electromagnetic devices and components in terms of frequency-dependent transfer function matrices that are compatible with general-purpose, network analysis-oriented simulators. In addition to facilitating electromagnetic analysis at the system level, such a capability enables *abstraction of electromagnetic complexity*, which is of utmost importance for making electromagnetic modeling as pervasive as SPICE-based circuit simulation.

Detection and Classification of Complex Targets in Foliage

Lawrence Carin
Department of Electrical and Computer Engineering
Duke University
Durham, NC 27708-0291

One of the outstanding problems in electromagnetics involves detection and classification of a man-made target embedded in foliage. A properly designed foliage-penetrating (FOPEN) radar system emits electromagnetic waves that propagate through leaves and small branches well (VHF and low UHF frequencies), with the principal clutter sources coming from tree-trunk and large-branch scattering. In practice both the target identity and orientation (pose) is unknown. Statistical signal processing algorithms require as much *a priori* knowledge as possible, concerning the connection between target shape and the associated radar scattered waveform. Moreover, this connection is also required for the tree scattering (clutter) and for targets in the presence of multiple trees. In this talk we discuss the FOPEN radar problem from both an electromagnetic-modeling and a signal processing perspective. Concerning the former, we develop the multi-level fast multipole algorithm (MLFMA), and demonstrate how it can be applied to the problem of modeling realistic targets in the presence of soil and foliage. Outstanding issues for further modeling work are also discussed. The connection between multi-aspect target scattering and signal processing is discussed in the context of a hidden Markov model (HMM). It is demonstrated that the HMM is a statistical algorithm that accounts for target-pose uncertainty, as well as complex wave scattering. The outstanding signal-processing issues will be discussed, as well as possible solution methodologies for the future. Several example results are presented, using both measured and computed FOPEN data.

Array Design Including Mutual Coupling

Chairs: R. Pogorzelski, USA and P. Niemand, South Africa

	Page
8:00 DOA Estimation for Nonuniformly Spaced Arrays Incorporating Mutual Coupling, <i>K. Kim*</i> , <i>T. Sarkar</i> , <i>Syracuse University</i>	166
8:20 Analysis and Design of a Open Ended Waveguide Array Considering the External Mutual Coupling, <i>E. Arnold</i> , <i>M. Boeck</i> , <i>F. Holtzhausen</i> , <i>P. Ruetzel*</i> , <i>EADS Deutschland GmbH</i>	167
8:40 Mutual Coupling in Dual-Polarized Microstrip Patch Arrays for 2D Synthetic Aperture Microwave Radiometry at L-Band, <i>K. Carver*</i> , <i>S. Kadambala</i> , <i>H. Zhu</i> , <i>J. Bertram</i> , <i>University of Massachusetts Amherst</i>	168
9:00 Mutual Coupling Effects and Compensation for Cylindrical Null-Steering Microstrip Patch Arrays, <i>P. Niemand*</i> , <i>J.W. Odendaal</i> , <i>J. Joubert</i> , <i>University of Pretoria</i>	169
9:20 Analysis of a Phased Array of Rectangular Waveguides Feeding a Parallel Plate Waveguide, <i>S. Rengarajan*</i> , <i>California State University</i>	170
9:40 Post-Wall Waveguide Slot Array with a 4-Way Planar Butler Matrix for Base Station Antennas in Wireless Communications, <i>J. Hirokawa*</i> , <i>S. Yamamoto</i> , <i>M. Ando</i> , <i>Toyko Institute of Technology</i>	171
10:00 Full Scan Coverage Spherical Conformal Spiral Antenna Array, <i>A. Vallecchi*</i> , <i>University of Salerno</i> , <i>A. Mazzei</i> , <i>G. Gentili</i> , <i>University of Florence</i>	172
10:20 A Five by Five Element S-Band Coupled Oscillator Array with Diagnostic System, <i>R. Pogorzelski*</i> , <i>California institute of Technology / JPL</i>	173
10:40 Novel Techniques for Analysis of Array Antennas, <i>K. Takamizawa*</i> , <i>W. Davis</i> , <i>W. Stutzman</i> , <i>Virginia Polytechnic Institute and State University</i>	174
11:00 Spectral Containment Using Integer Wavelength Time Delays in Phased Arrays, <i>J.D. Kramer*</i> , <i>E. Ostroff</i> , <i>S. Parisi</i> , <i>MITRE Corporation</i>	175
11:20 Field Analysis Of A Ultra Broadband Wide Scan Dual Polarized Array Of Ridge Elements, <i>K. K. Chan*</i> , <i>Chan Technologies Inc</i> , <i>B.T. Toland</i> , <i>TRW Inc.</i>	APS

DOA Estimation for Nonuniformly Spaced Arrays Incorporating Mutual Coupling

Kyungjung Kim and Tapan. K. Sarkar

Department of Electrical Engineering & Computer Science

Syracuse University

Syracuse, NY 13244-1240

Email: kkim08@mailbox.syr.edu

tk Sarkar@mailbox.syr.edu

ABSTRACT

This paper investigates an interpolation technique for dealing with non-uniformly spaced arrays in the presence of mutual coupling between array elements by utilizing a uniform linear virtual array (ULVA). The least squares method is used to develop a preprocessing transformation matrix in a super-resolution direct data domain signal processing algorithm called the Matrix Pencil Method to correct for the non-uniformity effects and the mutual coupling between the elements including presence of near field obstacles of the non-uniformly spaced array. Presence of near field scatters can also be taken into account in this analysis. This transformation matrix obtained using the least square method is then used to eliminate the effects of non-uniformity and mutual coupling associated with the array, including presence to near field scatters, simultaneously.

Hence, our problem can be stated as follows: Given the array manifold matrix $A(\theta)$ of a non-uniformly spaced array in the presence of mutual coupling between array elements and near field coupling effects between the platform and other electromagnetic obstacles, we obtain numerically an ideal uniform linear manifold matrix of a virtual array using the interpolation technique. The elements of this virtual array are omnidirectional point radiators radiating in free space. Thus, we compensate for the lack of non-uniformity and presence of mutual coupling between the elements in the real array in addition to near field coupling effects. Then, we apply, the Matrix Pencil Algorithm to these virtual interpolated array voltages directly to obtain simultaneously the DOA and their strengths. Therefore, in this methodology a single snapshot of the voltages measures across the loads of the antenna elements at a particular instance of time t are used to find the DOA's. The various signals impinging on the array can be coherent.

Analysis and design of an open ended waveguide array considering the external mutual coupling

Eugen Arnold, Markus Boeck, Falk Holtzhausen, Peter Ruetzel*
EADS Deutschland GmbH, VAE51, 89077 Ulm, Germany

1. Abstract

The authors developed a method for the design of an open ended waveguide array considering the external and internal mutual coupling. This type of antenna can be used for arrays which are electronically scanned in one dimension.

2. Design of the open ended waveguide array

For the design the antenna is split into several independent functional blocks (power divider, waveguide bends, ...), linked together by the use of scattering matrix description. The external mutual coupling is calculated with a model using electrical boundaries in one dimension (infinite array) and modeling the complete finite array in the other dimension. The model also contains the radom.

In a first iterative process the incident wave into the open ended waveguides (aperture plane) is determined so that the desired distribution is attained (including the effect of external mutual coupling). The second step is the design of the waveguide power divider. The impedance of each branch was determined in the first step. Due to reflections and internal coupling the desired ratio of the power divider is disturbed. In an iterative process the ratio of the power divider is changed so that the desired ratio is attained. Now the incident wave into the input ports of the power divider is calculated. With this incident wave we design the next layer of power dividers, until the model of the whole waveguide array is completed.

The final analysis of the array is done by linking the scattering matrices together. The external mutual coupling is calculated in a finite array.

3. Results

Figure 1 (left side) shows a comparison of the farfield pattern of the open ended waveguide array between simulation and measurement (NearField-Measurement). An excellent agreement between simulation and measurement is achieved. On the right side a hardware model of the array without the covering metal plate is shown.

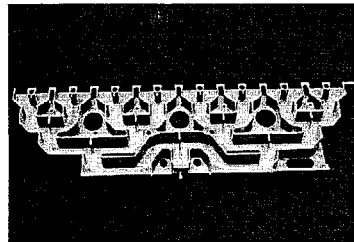
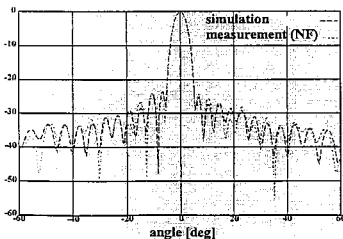


Fig. 1: Farfield pattern and picture of the hardware.

Mutual Coupling in Dual-Polarized Microstrip Patch Arrays For 2D Synthetic Aperture Microwave Radiometry at L-band

K. R. Carver, S. Kadambala, H. Zhu, and J. Bertram
University of Massachusetts at Amherst, Amherst, MA 01003, and
D. M. Le Vine, NASA Goddard Space Flight Center, Greenbelt, MD 20771

Aperture synthesis for passive microwave remote sensing has been successfully demonstrated with thinning in one dimension using an L-band airborne instrument called, ESTAR (Le Vine, D. M., A. J. Griffis, C. T. Swift and T. J. Jackson, 1994, *Proc. IEEE*, 82 (12), 1787-1801). ESTAR obtains resolution in the along-track dimension using the real antenna aperture (linear dipole array). Resolution across-track is obtained using aperture synthesis and permits thinning in this dimension. If all the antenna patterns in the across-track dimension are identical, then reconstructing the image is essentially a Fourier transform. However, there is significant mutual coupling in the actual ESTAR array and because of the irregular spacing due to thinning, the *in-situ* patterns in the across-track dimension are not identical (Weissman, D. E. and D. M. Le Vine, *Radio Science*, 33 (3), 767-779). This means that a simple Fourier inversion technique cannot be used, complicating the construction of images of brightness temperature.

Mutual coupling plays a similar role in the design of microwave radiometers that employ aperture synthesis in two-dimensions. A technique has been developed for the prediction of mutual coupling effects in antennas for L-band radiometers that employ synthesis in 2 dimensions where the antenna consists of dual-polarized planar arrays of square microstrip patch elements. This technique has been applied to two separate L-band test bed planar arrays of dual-polarized patch elements, the first an 8 x 8 -element array with inter-element spacing of 0.5λ (at 1413 MHz), and the second a 6 x 6 -element array with inter-element spacing of 0.62λ . Both of these arrays are large enough to experimentally verify the sensitivity of *in-situ* patterns to mutual coupling for elements located in the array interior, as well as those located near the array edge. An extensive set of amplitude and phase patterns was measured for both arrays.

Mutual coupling among dual-polarized square patch elements is dominated by contributions from the nearest neighboring elements in the E-plane, H-plane and diagonal-plane(s). Network analyzer measurements of E-plane and H-plane scattering parameters S_{ij} in these planes provide a straightforward method of characterizing the parasitic currents induced on the patches by mutual coupling. This permits the calculation of *in-situ* patch voltage patterns, including mutual coupling effects. The voltage amplitude patterns exhibit smooth "bumps" or perturbations, typically not exceeding 3 dB, about the pattern of an isolated patch. The computed patterns agree well with measured amplitude and phase patterns.

It is shown that this predictive technique leads to a more accurate characterization of the spatial transfer function for the 2-D dual-pol aperture synthesis radiometer. This knowledge improves the accuracy of the reconstructed images of brightness temperature.

**Mutual coupling effects and compensation for cylindrical null-steering
microstrip patch arrays**

P. Niemand*, J.W. Odendaal and J. Joubert
Centre for Electromagnetism
Department of Electrical, Electronic and Computer Engineering
University of Pretoria
Pretoria, 0002, South Africa
Phone: +27 12 420 3604
Fax: +27 12 362 5000
E-mail: pnienmand@eng.up.ac.za

In some mobile communication systems, an antenna array that provides omni-directional coverage as well as one or more steerable nulls can be advantageous. Previously, cylindrical arrays of equally spaced omni-directional elements were used to provide omni-directional radiation patterns with steerable nulls (J. Abele, J. Joubert and J.W. Odendaal, *Signal Proces.*, **80**, 141-149, 2000). Since microstrip patch antennas can be made conformal to non-planar surfaces such as cylinders to form cylindrical arrays, the null synthesis method was modified to include the radiation pattern of a cylindrical microstrip patch. The technique was extended to implement a constraint least square optimisation algorithm. Constraints were placed on the widths and depths of the nulls as well as on the gain ripple. The resulting element excitations formed a constrained optimum radiation electric field with the desired amplitude pattern characteristics.

The mutual coupling between the antenna elements in the cylindrical patch array must be considered to prevent distortion of the radiation pattern when null-steering is implemented. The effects of mutual coupling on the characteristics of the nulls and the gain ripple in the amplitude pattern are shown for different array configurations. These mutual coupling effects can be overcome by modifying the physical dimensions of the microstrip patches in the array. The lengths and feed positions of the patches are adjusted to match the driving impedances of all the antenna elements given the required set of excitations. The compensation technique is applied to both linear and cylindrical arrays. Measured and simulated results will be shown.

Analysis of a Phased Array of Rectangular Waveguides Feeding a Parallel Plate Waveguide

Sembiam R. Rengarajan

Department of Electrical and Computer Engineering
California State University
Northridge, CA 91330-8346
srengarajan@csun.edu

Introduction and motivation:

Linear array feeds are used to illuminate parabolic cylinder reflectors. In radar applications with a requirement of electronic scanning in one plane, a linear array of sectoral horns illuminating a parabolic cylinder is a potential antenna. The sectoral horns may be designed to feed the parabolic aperture with the required illumination taper. From a manufacturing point of view it is convenient to have two flared plates (parallel plate waveguide version of a rectangular waveguide horn) fed by a number of rectangular waveguides. The waveguides may be phased to provide electronic scanning in the plane of the array. If the angle of flare is small, the reflection coefficient at the input of each rectangular waveguide is obtained by considering the simpler problem of the junction of rectangular waveguides and a parallel plate waveguide. To the best of our knowledge there is no solution to this problem available in the literature.

Analysis:

In this work we consider the problem of exciting a parallel plate waveguide by an array of rectangular waveguides. A single junction of a rectangular waveguide and the parallel plate waveguide is considered first. Subsequently the problem is extended to include an array of waveguide feeds. The parallel plate waveguide is considered to be infinitely wide and semi-infinitely long. At the junction of the rectangular waveguide and the parallel plate waveguide we have an aperture. The remaining part of the transverse plane of the parallel plate waveguide is assumed to be shorted unless there are other waveguides. Integral equation is formulated in terms of the aperture electric field by enforcing the continuity of the tangential components of the aperture magnetic fields. Method of moments technique is employed to obtain the numerical results for the aperture electric field and the input reflection coefficient. Global sinusoidal expansion and testing functions corresponding to the waveguide modal fields are employed. Numerical results obtained for the TE_{10} and TE_{10} modes of excitation are found to be similar to results for waveguide planar arrays for H-plane and E-plane scanning (Amitay et al., Theory and Analysis of Phased Array Antennas, Wiley Interscience, New York, 1972). The central elements of large arrays exhibit characteristics similar to infinite arrays modeled by the finite element techniques.

In the symposium we will discuss the results of the reflection coefficient, and mutual coupling of finite and infinite arrays and their applications.

Post-Wall Waveguide Slot Array with a 4-Way Planar Butler Matrix for Base Station Antennas in Wireless Communications

Jiro Hirokawa*, Shin-ichi Yamamoto and Makoto Ando
Dept. of Electrical & Electronic Eng., Tokyo Institute of Technology

The authors propose a post-wall waveguide slot array integrating a 4-way power planar Butler matrix on a single layer of dielectric substrate with metals on the surfaces as shown in Fig.1. Four beams can be switched for the corresponding input ports in Butler matrix. The antenna is easily fabricated at low cost for mass production only by via-holing and metal plating for the post-wall waveguides and etching for the slot array.

The slot array has a cosecant radiation pattern with null filling in a plane parallel to the waveguide axis in order to obtain uniform illumination in a coverage area. Slots are paired as a radiation element to achieve traveling wave excitation because the phase as well as the amplitude has to be controlled for null filling in a cosecant pattern. In a slot pair, the amplitude is controlled by the length of one slot and the reflection is cancelled by the spacing between the two slots and the length of the other slot. The excitation phase among the elements is changed by the distance between adjacent elements. A 16-element array on a single waveguide has 17.1dBi gain with 3dB ripples in the cosecant pattern in experiments at 26GHz band.

The 4-way Butler matrix is realized by a single layer using short slot couplers in the cross junctions (or 0dB couplers) and the 3dB hybrids. Each coupler has two additional posts for matching. The phase shifters are obtained by controlling the width of the post-wall waveguides.

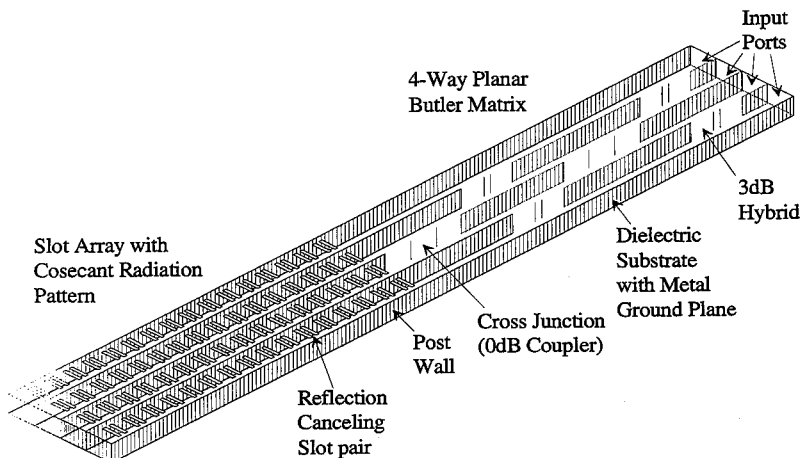


Figure 1: Post-Wall Waveguide Slot Array with a 4-Way Planar Butler Matrix

Full scan coverage spherical conformal spiral antenna array

A. Vallecchi ^{†*}, A. Mazzei [‡], G. Biffi Gentili [‡]

[†] *Dept. of Information Engineering and Electrical Engineering, University of Salerno, Via Ponte Don Melillo, I-84084 Fisciano (Salerno), Italy*

[‡] *Dept. of Electronics and Telecommunications, University of Florence, Via C. Lombroso 6/17, I-50134 Florence, Italy*

Spherical volumetric or conformal arrays can potentially provide full scan coverage in both elevation and azimuth planes and, as the projected aperture of a spherical array is direction independent, the beamwidth of the antenna remains constant for all scan angles. Because of their ability to scan the main beam in any direction, a wide range of applications exists in mobile and modern telecommunication systems. In particular, these kinds of antennas appear very promising for LEO (Low Earth Orbit) ground terminals, base-station tracking in mobile communications, WWLAN (Wireless Wideband Local Area Network) front-ends, as well as multifunction monostatic and bistatic radar systems.

It is more convenient to randomly locate the radiating elements of a spherical array, rather than positioning them on a periodic lattice. This non-periodic arrangement eliminates grating lobes and results in an average sidelobe level that is inversely proportional to the number of elements. Several theoretical studies have been devoted to the analysis of spherical random array fundamental characteristics in the past two decades (T. A. Dzekov *et al.*, *Electron. Lett.*, vol. 14, no. 16, pp. 495-496, 1978). Recently, experimental results for a volumetric array comprised of 64 log-periodic dipoles have been presented (A. Tennant *et al.*, *Electron. Lett.*, vol. 33, no. 24, pp. 2001-2002, 1997). This antenna operates over a broad bandwidth (8÷12 GHz) but provides only hemispherical scan coverage and linearly polarized radiation, the performances of the array being strongly influenced by the element characteristics.

In this contribution, a random spherical conformal array of Archimedian spiral antennas is proposed for obtaining full scan coverage and dual polarization, which is especially important in radar applications and defense electronics. Spiral antennas are known for their ability to produce very wide-band, almost perfect circularly-polarized radiation (W. L. Curtis, *IRE Trans. Antennas Propagat.*, vol. 8, pp. 298-306, 1960). This latter feature gives the array the advantage of polarization diversity. To achieve an effective spherical scan coverage each spiral antenna lies in the plane orthogonal to the vector from the center of the spherical surface describing the array envelope to its feed point. Since mutual coupling between the antenna elements is significant in determining the ultimate performance, the radiation characteristics of the array are evaluated by using the method of moments (MoM). The radiation patterns calculated by means of the MoM are compared with those calculated by the pattern multiplication principle and the mutual coupling among spiral elements is investigated.

A FIVE BY FIVE ELEMENT S-BAND COUPLED OSCILLATOR ARRAY WITH DIAGNOSTIC SYSTEM

R. J. Pogorzelski
Mail Stop 138-307
Jet Propulsion Laboratory
Calif. Institute of Technology
4800 Oak Grove Drive
Pasadena, CA 91109

It has been suggested and demonstrated both theoretically and experimentally that an array of electronic oscillators coupled to nearest neighbors will provide a set of signals with linear phase progression across the array. [R. A. York, *IEEE Trans.*, MTT-41, pp.1799-1809][P. Liao and R. A. York, *IEEE Trans.*, MTT-41, pp. 1810-1815] [R. J. Pogorzelski, to appear in MWGWL, December 2000.] The rate of phase progression is controllable by adjusting the tuning (free running frequency) of the oscillators on the perimeter of the array. Such a set of signals is suitable for excitation of an array of equally spaced radiating elements thus producing a steerable radiated beam.

In this paper a two-dimensional array based on this principle is described. It consists of 25 S-band voltage controlled oscillators in a 5 by 5 square configuration coupled to nearest neighbors by microstrip transmission lines. The coupling strength is controlled by series chip resistors at the ends of the lines and the Q of the coupling network is decreased by means of parallel terminating chip resistors across the lines at each end.

The phase progression across the array is measured by a unique diagnostic system. The system is based on a set of mixers and quadrature hybrids used as phase detectors to indicated the phase differences between oscillators. The signals are coupled from the oscillator board by means of an array of microstrip couplers in which the output line of each oscillator is coupled to a transmission line on a separate circuit board sandwiched against the oscillator board. The mixer outputs are digitized and fed to a computer running a virtual instrument in Labview. The inferred phase differences are integrated to produce phase relative to the center element and then displayed as a three dimensional surface plot. The radiating aperture consists of a five by five array of microstrip patches on yet another circuit board. The patches are excited by pins extending through the oscillator circuit board and then through the aperture board to each patch. Thus, the diagnostic system can be attached or removed as a unit leaving the oscillator board and the radiating aperture intact.

Novel Techniques for Analysis of Array Antennas

K. Takamizawa*, W. A. Davis and W. L. Stutzman
Virginia Tech Antenna Group
Bradley Department of Electrical and Computer Engineering
Virginia Polytechnic Institute and State University
Blacksburg, VA 24061-0111
www.antenna.ece.vt.edu

The performance of large array antenna systems is limited by the mutual coupling between the elements. Mutual coupling effects vary with frequency and scan direction. Design of wideband phased array is especially difficult if mutual coupling is appreciable. Full electromagnetic analysis of a large array for the prediction of fully excited array are usually not possible due to the limitations in computational power and memory capacity. Thus, the characteristics of a large array must be predicted using a combination several techniques such as infinite array antenna analysis techniques, active element pattern analysis and network analysis.

This paper will present two novel techniques to analyze large array antennas. The first technique is eigen value analysis of the coupling matrix. In this technique, antenna characteristics of infinite array are predicted from the coupling matrix of a subsection of the infinite array using eigen value analysis. The second technique is a generalized active element pattern technique. The active element pattern method is extended to include the effects of source or load mismatch. It allows direct connection between array network parameters and array radiation pattern.

Comparisons are made between the new techniques and the traditional large array analysis techniques. Both numerical and experimental application of coupling matrix eigen value analysis method and generalized active element pattern method will be presented.

Title: Spectral Containment Using Integer Wavelength Time Delays in Phased Arrays

Authors: J. David R. Kramer, Edward D. Ostroff, and Samuel J. Parisi of The MITRE Corporation

A simple modification of UHF Phased Arrays provides sequential turn-on of each subarray with a corresponding increase in the rise time of the transmitted RF waveform. This technique has been analyzed for an array face consisting of 64 subarrays each containing 32 T/R modules. The PAVE PAWS array face employs 56 subarrays. The Class C amplifier transmit modules have a rise time that is typically less than 10 ns. An integer wavelength at UHF corresponds to a delay of 2.3 ns. With a 64 element subarray model, the rise time of the ensemble becomes 147 ns. This arrangement is equivalent to a tapped delay line band-pass filter. In these days of competition for spectrum use, this application appears attractive. Thus we can achieve the advantage of a linear filter with a high efficiency Class C amplifier.

The phase setting of the subarray drive transmit modules will need to be reset as the RF frequency changes. It may be possible to combine this technique with true-delay compensation for the RF frequency change during a linear FM chirp waveform. Instead of a linear ramp, rise-time shaping can be performed by varying the number of subarray elements that are turned on at each integer wavelength. Computer simulations will demonstrate the improvement in spectral containment that can be achieved with this approach.

This approach to spectral containment is analogous to MITRE's Pulse Waveform Generator (U.S. Patent Number 5,781,066) in which the turn-on time of sequential power amplifiers is controlled digitally.

Calibration Techniques & Package Structures

Chair: W. Davis, USA

	Page
8:00 Calibration of the C-Probe for NDE of Concrete Structures, <i>A. Al-Derbas, Kuwait University, Y. Khalaf, S. Riad*, Virginia Polytechnic Institute and State University</i>	178
8:20 Antenna Gain Measurement Using TRL Calibration Method, <i>H. C. Lu*, T. H. Chu, National Taiwan University</i>	179
8:40 Cluster Computing in Printed Circuit Board Simulation, <i>F. Liu*, J.E. Schutt-Aine, University of Illinois at Urbana-Champaign, J. Chen, Motorola, Inc.</i>	180
9:00 Analysis of Electromagnetic Emissions from IC Package Lead-Frames in Automotive Applications, <i>U. Navsariwala*, N. Buris, J. Meyerhoff, Motorola Inc.</i>	181
9:20 Design of Narrow-Band Filters Based on Photonic Waveguides, <i>A. Boag*, B. Steinberg, R. Licitsin, Tel Aviv University</i>	182
9:40 Electromagnetic Coupling to a Wire Residing Inside a Rectangular Cavity with Apertures Due to External Radiating Sources, <i>M. Deshpande*, NASA Langley Research Center</i>	183

CALIBRATION OF THE C-PROBE FOR NDE OF CONCRETE STRUCTURES

Aref J. Al-Derbas,
Department of Civil Engineering
Kuwait University, Kuwait

*Yaser A. Khalaf and Sedki Riad**
The Bradley Department of Electrical Engineering
Virginia Polytechnic Institute and State University
Blacksburg, Virginia 24061-0111
Phone: 540-231-4463 Fax: 540-231-3362
Email: sriad@vt.edu

A capacitance probe (C-Probe) design has been proposed for nondestructive evaluation of concrete structures. The C-Probe is a planer structure that can be used to attractively access the material-under-test from one side only. It is used to measure the dielectric constant of the concrete material from which some properties pertaining to the concrete (e.g. internal flaws) can be detected. A calibration method has also been developed for the C-Probe to measure accurate dielectric constant of concrete material over frequency range (1 – 10 MHz) in the field. The dielectric constant is obtained from the measured reflection coefficient using the Network Analyzer (HP4195A).

The measured reflection coefficient of the C-Probe has been derived in terms of the dielectric constant of the material to end up with three error terms. In order to estimate the three error terms over the frequency range of interest, we need three standards with well-known dielectric constants over the same frequency range. Many calibration standards were tested for the C-Probe calibration method and it was found that "open", short, and a Teflon slab terminations have been proven to provide the best calibration standards for measuring the dielectric constant of the concrete using the C-Probe. The open and short standards were chosen because they are easily achievable. On the other hand, the Teflon slab termination was chosen because of its homogeneous and isotropic properties, also because of the flatness of its dielectric constant over a wide frequency range.

Measurements using the C-Probe have been verified versus the Impedance Analyzer measurements to reveal good agreement. The C-Probe fixture has been shown to have a significant capability for detecting concrete flaws such as delamination that occurs underneath the surface.

Antenna gain measurement using TRL calibration method

Hsin-Chia Lu* and Tah-Hsiung Chu
 Department of Electrical Engineering,
 National Taiwan University, Taipei, Taiwan, R.O.C.
 E-mail: leonardo@ew.ee.ntu.edu.tw, thc@ew.ee.ntu.edu.tw

The thru-reflection-line (TRL) calibration method has been widely used in the vector network analyzer calibration. It uses two transmission lines with different length and a reflection termination to deembed the two error boxes at the input and output ports of the test device. In this paper, we apply this calibration method for antenna gain measurement without using standard gain horn antenna as that in conventional method.

As two antennas are placed in a forward measurement arrangement as shown in Fig. 1(a), it becomes a two-port network as shown in Fig. 1(b). Therefore, the "thru" connection can be considered as two antennas are separated by a distance. Similarly, the "line" connection is that these two antennas are moved apart by another distance. The "reflection" connection is then achieved by having a scattering object located in front of each antenna.

After the TRL calibration process, the transmission matrices of two error boxes can be derived except for a constant. One can show that even this constant is unknown, the scattering parameters such as $S^{(1)}_{11f}$, $S^{(1)}_{22f}$ and $(S^{(1)}_{12f})^2$ can be calculated. As shown in Fig. 1(b), these parameters contain the propagation term T to account for the distance between reflector and antennas. One can then solve the antenna scattering matrix and calculate the antenna gain accordingly.

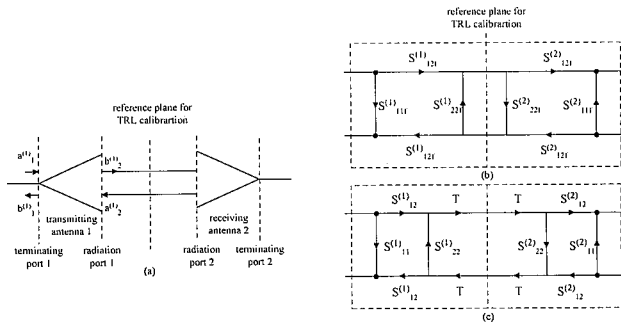


Fig.1 (a) Schematic diagram of two antennas in a forward measurement arrangement and its scattering parameter representation (b) with and (c) without the propagation term T included.

Cluster Computing in Printed Circuit Board Simulation

F. Liu*, J.E.Schutt-Ainé
Department Of ECE
University of Illinois
Urbana, IL 61801
mail: fliu,jose@decwa.ece.uiuc.edu

J. Chen
PCS Research Labs
Motorola, Inc.
Harvard, IL 60033
chenji@srl.css.mot.com

Due to smaller feature sizes and increased operating frequency, the importance of interconnects in printed circuit board (PCB) design is growing. Feature size reduction leads to complex interconnect routing and decreased spacing among them. Consequently, the electromagnetic field coupling between closely spaced interconnects and the signal integrity of critical paths become major concerns on board level system design. Also the complexity of the design makes the modeling of the whole board error-prone and tedious work. In this study, an integrated automatic simulation tools is developed and implemented on a 32-node cluster to analyze the cellular phone PCBS. The finite difference time domain(FD-TD) and finite difference(FD) methods have been adopted as the numerical techniques for the electromagnetic field simulation. Recent advances in cluster computing make the FDTD/FD a practical method in board simulation. The FDTD/FD method itself leads to easy parallelization since the field value at each node of the discretized mesh can be related to those of its nearest neighbors only. This locality also leads to high computation-communication ratio. To explore the computational power, all the algorithms are developed in parallel forms. The software tools consist of a translator, a code generator and an electromagnetic simulator. The parallel algorithms of translator are developed to parse the design information. The design files are analyzed and the information related to the electromagnetic simulation are extracted. These information will be projected into a grid mesh. The parallel FDTD/FD codes are generated automatically and the simulation is deployed on the clusters. This work integrates the board design and electromagnetic modeling. Numerical results will show the efficiency and validation of this technique.

Analysis of electromagnetic emissions from IC package lead-frames in automotive applications.

Umesh Navsariwala*, Nick Buris and Jerry Meyerhoff
Motorola, Inc.

The density of electronic sensors in automobiles has been increasing steadily. As a result, the proper design of sensors to meet Electromagnetic Compliance (EMC) and avoid Electromagnetic Interference (EMI) has become very important. The present paper discusses the design and performance of the lead frame of a pressure sensor IC for automobile applications. To this end, electromagnetic simulations were performed on the IC package and lead-frame using the Finite Element Method (FEM) to model the measurement setup used in EMC testing. The IC silicon die has several outputs that are connected by wire-bonds to the leads of the lead-frame. This assembly is over-molded with a plastic and the leads of this package are connected to an Engine Control Unit (ECU) by several cables 2m in length. Damping capacitors are placed between the leads of the package to reduce the currents on the cables and contain the fields. The sensor ASIC's A/D, D/A converters and DSP engine are clocked at 2.88 MHz. Therefore, its harmonics could interfere with the FM radio service at 88 MHz to 108 MHz and a police band at 150 MHz to 174 MHz.

This sensor modeling is a challenging application for FEM based solvers, as the geometrical dimensions in the problem vary from 0.1 mm to 2 m, which leads to a very large mesh with high aspect ratios. This problem was analyzed using a FEM solver with multi-point Asymptotic Waveform Expansion (AWE). A few alternative lead-frame layouts were analyzed to compare the EMI from different designs. Several studies were carried out to determine the sensitive design parameters. This technique was found to be very effective in predicting and reducing the EMI from the IC package.

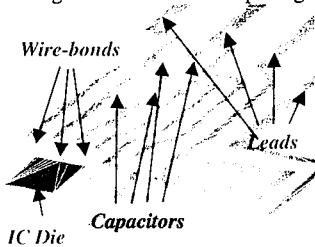


Figure 1: Sample lead-frame layout.

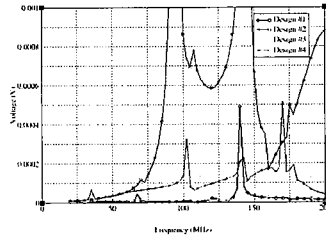


Figure 2: Voltage measured by a 10 mm probe at a distance of 1 m.

Design of Narrow-Band Filters Based on Photonic Waveguides

Amir Boag*, Ben Z. Steinberg, and Ronen Licitsin
Faculty of Engineering, Tel Aviv University, Tel Aviv 69978, Israel

Photonic band gap materials attracted much attention in the context of designing optical and microwave devices. Recently, numerical experiments have shown that line defects in photonic crystals can be used not only to guide but also to multiplex and demultiplex optical signals (E. Centeno, B. Guizal, and D. Felbacq, *J. Opt. A.: Pure Appl. Opt.* **1**, L10-L13, 1999). Most researchers studying the wave guiding by line defects employ photonic waveguides obtained by removal of consecutive posts in the periodic structure. The strong coupling between the adjacent defects produces relatively wideband waveguides.

In this paper, we address the issue of designing photonic-crystal waveguides with a prescribed center frequency and narrow bandwidth. Specifically, we concentrate on a problem of a waveguide formed by widely spaced periodic defects in the photonic crystal. Each defect site with a resonant frequency in the band gap serves as a microcavity. Tunneling of radiation between the defect sites allows wave propagation along the line of defects. Sections of such waveguides can be employed as ultra narrow band filters in optical routing devices. Here, we propose a design procedure based on the weakly coupled cavity model. This approach resembles the tight binding perturbation theory of the solid state physics. It is shown that the center frequency of the waveguide is determined mainly by the resonant frequency of the single defect. Thus, the eigenmode of a single defect embedded in an infinite photonic crystal is analyzed first. Continuous tuning of the resonant frequency is achieved by perturbing the local parameters of the microcavity. The frequency tuning can be analyzed using the conventional cavity perturbation theory. Weak coupling between the periodic defects causes a discrete spectral line to turn into a narrow band of guided frequencies only slightly shifted from the original frequency of a single defect. The perturbation theory facilitates an approximate calculation of both the frequency shift and the band structure of the periodic microcavity waveguide. Furthermore, these parameters are linked by an analytic relationship to the distance between the defect sites. Consequently, the latter distance can be directly adjusted to achieve the desirable properties of the waveguide.

The above design procedure based on the perturbation theories is verified by studying specific examples and comparing the results with those of numerically rigorous computations. In this work, we concentrate on photonic crystals formed by two dimensional periodic arrays of dielectric posts. The defects are formed by increasing the radii of the posts selected as defect sites. The resonant frequency of the defects is tuned by slightly varying the radii of the selected posts. Within certain limits, the frequency depends linearly on the defect cylinder radii as predicted by the cavity perturbation theory. The frequency shift due to intercavity coupling was found to be negligible in all the cases considered. On the other hand, the bandwidth decreases exponentially with increasing the distance between the microcavities. Thus, the intercavity spacing serves as a robust means of bandwidth control.

ELECTROMAGNETIC COUPLING TO A WIRE RESIDING INSIDE A RECTANGULAR CAVITY WITH APERTURES DUE TO EXTERNAL RADIATING SOURCES

M. D. Deshpande

NASA Langley Research Center, Hampton VA

SUMMARY

In a military or civilian aircraft various electric wirings run from the cockpit to the aircraft subsystems through its fuselage. An electric voltage/current induced on these wires due to incident electromagnetic (EM) waves may be carried to various subsystems causing its malfunction. For the safe operation of these subsystems through a hostile EM environment, it is therefore important that the EM energy coupled to these wires must be below standard established levels. It is also important to be able to estimate the maximum EM energy coupled to these wire due to given incident electromagnetic waves as a function of their lengths and locations.

In this paper, a numerical method is presented to estimate electromagnetic energy delivered to these wires running through fuselage cavity of an aircraft. The EM field penetration into the aircraft cavity enclosure and coupling to a wire residing inside the cavity can be estimated using Finite Element Method (FEM) or Finite Difference Time Domain (FDTD) method. However, for large size fuselage ($> 3\lambda$) at frequencies of interest large number of unknowns prohibit use of these methods to estimate EM energy delivered to the aircraft wiring. In this paper, by approximating a fuselage by a rectangular cavity with rectangular apertures on its side representing passenger windows, the moment method solution is developed to estimate EM energy from an external RF source coupled to a wire residing inside the cavity. Figure 1 shows electric field shielding factor of a rectangular box with four rectangular apertures and illuminated by a linearly polarized incident EM plane wave. Other numerical results on EM energy coupled to a wire as a function of wire length, its location inside the cavity will be presented.

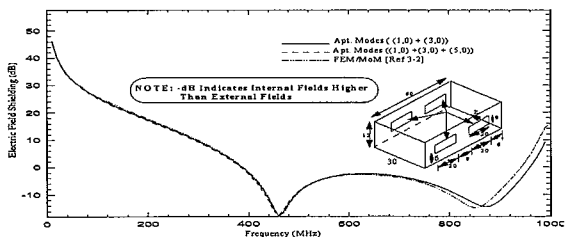


Figure 1: Electric field shielding of rectangular cavity with four rectangular apertures. Observation point (30, 6, 15) cm

Transient & Ultra-Wideband Measurements

Chair: S. Riad, USA

	Page
10:00 Time-Domain Measurements for Path-Loss Prediction on a Scaled Model of an Urban Environment, <i>D. Erricolo*, P.L.E. Uslenghi, University of Illinois at Chicago</i>	186
10:20 Impulsive Field Computation and Measurement, <i>M. Morgan*, Naval Post Graduate School</i>	187
10:40 Progress of Ultra-Wideband Fully-Polarimetric GPR Classification of Subsurface Unexploded Ordnance, <i>M. Higgins*, C.C. Chen, Ohio State University, K. O'Neill, US Army Corps of Engineers Research & Development Center</i>	188
11:00 A New Subnano-Second Pulsed Oscillator for Ultra-Wideband Applications, <i>J. S. Lee*, C. Nguyen, T. Scullion, Texas A&M University</i>	189
11:20 E-Pulse Diagnostics for Layered Materials, <i>G.J. Stenholm, E.J. Rothwell*, D.P. Nyquist, L.C. Kempel, K.M. Chen, Michigan State University</i>	190

TIME-DOMAIN MEASUREMENTS FOR PATH-LOSS PREDICTION
ON A SCALED MODEL OF AN URBAN ENVIRONMENT

D. Erricolo(*) and P. L. E. Uslenghi
Department of Electrical and Computer Engineering
University of Illinois at Chicago
851 South Morgan Street, Chicago, Illinois 60607-7053, USA
Phone: 312 996 6059; Fax: 312 996 8664; Email: uslenghi@uic.edu

The authors consider a scaled model of a simple two-dimensional urban environment to investigate propagation along a vertical plane. Specifically, measurements of path-loss are taken for different positions of the transmitting and receiving antennas. The measurement results are then compared with the theoretical predictions computed using the two-dimensional ray-tracing simulator developed by the authors. The two-dimensional simulator computes path-loss and time-delay associated with each trajectory.

The scaled model is located inside the anechoic chamber at the Andrew Electromagnetic Laboratory of the University of Illinois at Chicago. The use of a scaled model allows for the verification of the theoretical model within a controlled environment, where all the parameters of the problem are known. This is an advantage in comparison with operating in an actual three-dimensional environment, where too many factors are unknown. In fact, in the latter case, it is not possible to relate the measurements to the assumptions and/or simplifications adopted in developing the theoretical model.

The time-domain analysis allows the measurement of the multipath components of a single transmitted pulse. The different times of arrival of the components at the receiver are used to relate each component to a specific ray trajectory. The measurements inside the controlled environment of the anechoic chamber verify the simulator predictions as to which trajectories provide the stronger contributions. Furthermore, the effect of different electrical boundary conditions (i.e., of different values of the relative surface impedance) at the walls and roofs of the buildings on the strengths of the field components at the receiver can be easily controlled by changing the experimental setup.

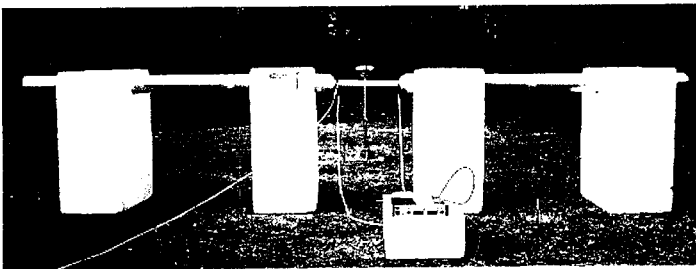
The results obtained in this study complement the numerical and experimental frequency-domain results previously obtained by the authors (D. Erricolo and P. L. E. Uslenghi, "Two-dimensional simulator for propagation in urban environments", *IEEE Trans. VT*, accepted; U. Crovella, G. D. Elia, D. Erricolo and P. L. E. Uslenghi, *Digest of National Radio Science Meeting*, Boulder, Colorado, January 2001).

IMPULSIVE FIELD COMPUTATION AND MEASUREMENT

Michael A. Morgan
ECE Department, Naval Postgraduate School
833 Dyer Road, Monterey, CA 93943-5121

Transient near-fields of UWB impulse-driven antennas located over ground are computed using NEC-4 frequency-domain calculations and compared to measurements (see below). Stepped-frequency data is extracted from the NEC-4 output file and post-processed using inverse FFT based algorithms programmed in MatLab. Impulsive excitation is introduced using either circuit modeling of the pulse generator or by way of measured terminal voltages or currents. The procedure includes the frequency-dependent effects of impedance mismatch, lossy earth and penetration of impulsive fields into structures.

Comparisons of computations and experimental data will be shown for measurements of near-fields produced by impulsively driven asymmetric horizontal dipoles over ground. Animations of computed fields in the region near to the dipoles will be displayed and discussed.



Progress of Ultra-Wideband Fully-polarimetric GPR Classification of Subsurface Unexploded Ordnance

Matthew B. Higgins¹ and Chi-Chih Chen
The Ohio State University ElectroScience Laboratory

Kevin O'Neill
US Army Corps of Engineers Research and Development Center (ERDC)
Cold Region Research and Engineering Laboratory (CRREL)

Subsurface unexploded ordnances (UXOs) classification has been an important problem since there are still many subsurface UXOs left over from previous wars and decommissioned proving grounds. The clearance of subsurface unexploded ordnance (UXO) has been a dangerous, slow and high-cost process. Although recent technology advances in autonomous survey and active magnetic sensing using the electromagnetic induction approach have greatly increased the detection sensitivity as well as speed, they still face a massive amount of false alarms resulted from underground shrapnel and other metal debris.

Ground Penetrating Radars (GPR) has been applied to the classification of subsurface ordnance for years with a reasonable promising success. Recently, several innovative GPR antennas and systems have been developed at OSU/ESL. A UXO discrimination radar system using a dielectric-loaded horn-fed bow-tie (HFB) antenna was developed to provide broad-bandwidth, full-polarimetric features such as UXO's linear geometry, resonant length, depth, orientation, etc under the support of DoD Environmental Security Testing and Certification Program. The antenna consists of two orthogonal, linearly polarized HFB elements. The four antenna arms are terminated with tapered resistive films to reduce the antenna ringing. Each element can be configured to be transmitting or receiving. If the radar responses is transmitted and received from the same element, a "co-polarization" data is obtained. If the response is transmitted from one element and received from the other, perpendicular elements, the "cross-polarization" data is obtained. Recording both co-polarization and cross-polarization data provides complete, two-dimensional radar information about the target's scattering properties.

Baseline performance of UXO classification of the said system was obtained from a UXO test site located at the Tyndall AFB, Florida in January 2000. A thorough study of the data revealed various sources that caused incorrect classifications. There were three major sources for causing a non-UXO item to be classified as a UXO: (1) Non-linear objects that were shallow and offset from the center of the antenna's scanning direction; (2) Vertical thin plates; (3) Linear objects with a length to diameter ratio similar to that of a UXO. It was also found that many UXOs with large inclination angles were incorrectly classified due to the resonance excitation and the lack of linear feature when observed directly above.

Based on the previous important findings, several improvements have been made since then. The first major improvement was achieved by adding multiple-position data are now collected to produce the spatial distributions of the extracted features. This could avoid making incorrect classification based on a single position data in the case of position offset. The improvement of classification capability in rejecting non-UXO objects was also verified by measurement results.

A NEW SUBNANO-SECOND PULSED OSCILLATOR FOR ULTRA-WIDEBAND APPLICATIONS

Jeong-Soo Lee*¹, Cam Nguyen¹, and Tom Scullion²

¹Department of Electrical Engineering

²Texas Transportation Institute

Texas A&M University

College Station, TX 77843-3128

ABSTRACT

Ultra-wideband systems, such as pulsed radar, are important in many scientific and engineering disciplines. One of the most important applications of these systems is perhaps subsurface sensing, which has attracted a widespread interest in various engineering fields. Pulsed oscillator is an essential component for these systems. In general, a monocycle pulsed oscillator is preferred than an impulse oscillator because it has a much narrower bandwidth. This eases considerably the design of other system components.

This paper presents the development of a new pulsed oscillator operating in the subnano-second regime. This circuit employs Schottky diodes, step recovery diodes, and simple charging and discharging circuitry, and is completely fabricated using coplanar waveguides. The pulsed oscillator produces a monocycle pulse having 333-ps pulse width and more than 2 Volts from an input square wave of 10-MHz repetition rate. The generated monocycle pulses have very symmetrical positive and negative portions and low ringing level. Analysis, design, and performance of this circuit will be presented.

E-Pulse Diagnostics for Layered Materials

G.J. Stenholm, E.J. Rothwell*, D.P. Nyquist, L.C. Kempel, and K.M. Chen
Department of Electrical and Computer Engineering
Michigan State University
East Lansing, MI 48824

The characteristics of a layered material may be described by the thickness and material properties (complex permittivity, complex permeability) of each layer. Under certain practical circumstances the existing parameters may be inappropriate for the intended application, or may have changed over time due to environmental effects. It is thus important to have a measurement technique capable of determining if the layer properties of an actual material match those that are expected.

Illumination of a layered medium using a wideband pulse provides an efficient means for characterizing the parameters of the various layers. The transient scattered field may be used as a useful (albeit non-unique) signature for comparison against known material responses. In a straightforward implementation, a library of common layer parameter combinations is stored in computer memory, and the expected response is created using a theoretical formula for the scattered field. Comparison with a measured response then either identifies the parameter combination, or provides an indication that the combination has changed or is not what is expected.

Since the frequency-domain transfer function of a layered material may be represented as a pole series, there is an alternative means for implementing a parameter comparison. An E-pulse waveform (E. Rothwell, et. al., IEEE Trans. AP, **AP-35**, 426-434, 1987) may be constructed for each parameter combination with the property that when convolved with the transient scattered field response of the corresponding layered material, a null late-time signal is produced. If the E-pulse is convolved with the measured response of a medium with parameters other than those used to construct the E-pulse, the resulting signal is nonzero.

This paper examines the practical implementation of an E-pulse system for layered material diagnosis, using both theoretical and measured transient scattered-field signals.

Applications of Numerical Methods

Chairs: C. Furse, USA and D. Sullivan, USA

	Page
8:00 Broadband Dispersion Compensation Scheme for FDTD in Anisotropic, Layered Media, <i>C. Moss*</i> , MIT, <i>F.L. Teixeira</i> , The Ohio State University, <i>A. Kong</i> , MIT	192
8:20 FDTD Analysis of Microstrip Antennas Immersed in Anisotropic Space Plasma, <i>J. Ward*</i> , <i>C. Furse</i> , <i>C. Swenson</i> , Utah State University	193
8:40 Thin Wire Hybrid FETD/FDTD Broadband Antenna Prediction, <i>N. Montgomery*</i> , <i>R. Hutchins</i> , TRW S&ITG, <i>D.J. Riley</i> , Sandia National Laboratories	194
9:00 Analysis of Scattering from a Large Arbitrary-Shaped Conducting Cylinder by Iterative FEM with Fast Multipole Updates, <i>J. Park*</i> , <i>J. Lee</i> , <i>H. Chae</i> , <i>S. Nam</i> , Seoul National University	195
9:20 Pulsed Radiation by Periodic Structures via a Combined (Time Domain-Floquet Wave) - (FDTD) Algorithm), <i>F. Capolino*</i> , Universita di Seina, <i>G. Marrocco</i> , D.I.S.P. Universta di Roma	196
9:40 ALPEN - A Versatile FDTD Tool for Analyzing Microstrip PCB Circuits, <i>F. Rivas*</i> , Universidad de Jaen, <i>I. Gonzalez</i> , Universidad de Alcala, <i>W. Yu</i> , <i>N. Farahat</i> , <i>R. Mittra</i> , Pennsylvania State University, <i>F.Saez de Adana</i> , <i>O. Gutierrez</i> , Universidad de Alcala, <i>J.P. Roa</i> , Universidad de Jaen, <i>M.F. Categra</i> , Universidad de Alcala	197
10:00 Numerical Modeling of Electromagnetic Wave Scattering by Multi Parametrical Structures, <i>A. Perov*</i> , Institute of Radiophysics & Electronics, <i>M. Monod</i> , <i>R. Rouveure</i> , <i>M. Chanet</i> , CEMAGREF	198
10:20 Highly Efficient Numerical Analysis of an Open Hemispherical Resonator, <i>M. Rewiński*</i> , MIT, <i>M. Mrozowski</i> , Technical University of Gdansk	199
10:40 Low Complexity Model Order Reduction for FDTD/FIT Systems, <i>T. Wittig*</i> , <i>I. Munteanu</i> , <i>R. Schuhmann</i> , <i>T. Weiland</i> , Darmstadt University of Technology	200
11:00 FDTD Simulation of Subsurface Water Conductivity Mapping, <i>D. Sullivan*</i> , <i>M. Kerschbaum</i> , University of Idaho, <i>J. Morrison</i> , Bechtel BBWI	201
11:20 Macromodeling of Transmission Line Networks in the FDTD Technique Using the Equivalent Source Method, <i>I. Rumsey*</i> , <i>M. Picket-May</i> , University of Colorado at Boulder	202

Broadband Dispersion Compensation Scheme for FDTD in Anisotropic, Layered Media

C. D. Moss¹, F. L. Teixeira², and J. A. Kong¹

¹Department of Electrical Engineering and Computer Science.
Massachusetts Institute of Technology, Cambridge, MA 02139

²ElectroScience Laboratory and Department of Electrical Engineering
The Ohio State University, Columbus, OH 43235

We describe a broadband dispersion compensation scheme for numerical grid dispersion in a FDTD grid (Yee's lattice) for anisotropic and layered host media.

First, we derive the grid dispersion relations for a plane wave propagating on a discrete lattice where the host medium is anisotropic. We obtain discrete wavenumbers which depend both on the frequency and lattices spacing, as well as on the particular anisotropy considered.

We then derive the exact formulas for the reflection and transmission Fresnel coefficients (TM and TE) for the dielectric interfaces on a lattice. These resulting coefficients in the discrete case reduce to the usual Fresnel coefficients (continuum case) only as the lattice spacing goes to zero.

These results are combined in a recursive scheme to obtain the generalized reflection and transmission coefficients for a n -layered medium, where each layer is anisotropic, on the lattice. This allows us to obtain the exact expressions for the discrete fields after they have propagated over a finite region of such a medium on the lattice.

We describe applications in FDTD simulations of subsurface problems, where the host medium (soil) is modeled as a layered, uniaxial medium. The dispersion compensation is used to obtain the correct form of the scattered fields by the host medium and permits a more accurate extraction of the scattered fields over a Huygens' surface in the total/scattered field formulation. For typical discretization and problem sizes, this produces an increase of more than 20 dB in the dynamic range of the FDTD results, and allows the FDTD simulation of the scattering from buried objects in complex media with much lower contrast than before.

FDTD ANALYSIS OF MICROSTRIP ANTENNAS IMMERSSED IN ANISOTROPIC SPACE PLASMA

Jeff Ward, Cynthia Furse, Charles Swenson

Department of Electrical and Computer Engineering
Utah State University
Logan, Utah 84322-4120
Phone: (435) 797-2870
FAX: (435) 797-3054
Furse@ece.usu.edu

Abstract

The Plasma Frequency Probe (PFP) makes use of a short dipole antenna (approx. 1 meter long) to probe ionospheric plasmas. This measurement technique has been flown on sounding rockets by the Space Dynamics Laboratory and Utah State University for over three decades. These probes are used to measure the electron density, temperature, and collision frequency of the ionosphere based on the change of the electrical impedance of the antenna in contact with the space plasma. The data analysis for these probes has traditionally been based on analytical theory and several simplifying assumptions including cold plasma, antenna fully aligned with the earth's magnetic field, and an approximate prescribed current density on the antenna.

This paper extends our previous FDTD analysis based on the fluid model of space plasma to a realistic, warm anisotropic ionospheric plasma. The permittivity and permeability tensors are applied as matrix operators in the FDTD method. The response of an antenna to isotropic and anisotropic media is compared.

In addition, we would like to replace the conventional dipole-type plasma frequency probe with an antenna that is smaller, lower profile, and more rugged, in particular something that does not need to be deployed in space. This would enable measurements of the ionosphere to be taken during the ascent and descent of sounding rockets, which could yield very interesting information useful for determining long term weather patterns. In order to do this, we have analyzed microstrip antennas in ionospheric plasma to determine their sensitivity to critical plasma parameters, in both isotropic and anisotropic plasmas.

Thin Wire Hybrid FETD/FDTD Broadband Antenna Prediction

*Norma Montgomery¹, Robert Hutchins¹, Douglas J. Riley²

¹TRW S&ITG, Albuquerque, NM 87110

²Sandia National Laboratories, Albuquerque, NM 87185

Broadband antennas are often complex structures including the following:

- 1) thin wire spiral or conical helix geometries,
- 2) conductors etched on 3D dielectrics,
- 3) arbitrarily shaped cavities,
- 4) arbitrarily shaped absorbers inside those cavities,
- 5) coax feeds.

A hybrid FETD/FDTD code, *Volumetric Maxwell Equation Solver (VOLMAX)*, recently developed at Sandia National Laboratories, has been shown to accurately predict electromagnetic characteristics for a wide variety of structures. VOLMAX includes a state-of-the-art thin wire and thin slot capability for unstructured FETD grids. The thin wire capability of this code will be used to model an inverted conical helix having continuous curvature along its arm. This continuous curvature is modeled with VOLMAX's FETD formulation, which is able to follow the curvature of that wire easily. An FDTD grid, having relatively large grid size, is used in the surrounding free space, minimizing run time. By coupling thin wires to FETD, arbitrary material inhomogeneities can be easily accommodated. For instance, the effect of dielectric support structures for the wire could be investigated. The thin-wire algorithm is conditionally stable local to the wire, while the surrounding edge-based FETD formulation is unconditionally stable. Thus, in a case where the mesh size tapers into small elements away from the wire, the wire's segment length is the factor dictating the time step. This minimizes run time when fine FETD meshes are included in the model. The antenna may be excited by either incident fields or by voltage sources having arbitrary time variation.

This presentation focuses on broadband antenna predictions using VOLMAX. Predictions are made over several octaves by exciting the antenna with a time domain signal. The ratio of the Fourier transform of the antenna response, divided by the Fourier transform of the antenna excitation, provides the antenna behavior as predicted by traditional continuous wave frequency domain methods. With this standard approach, designers of broadband antennas are given the ability to observe the antenna's response over a nearly continuous spectrum of frequencies using a single time-domain run. Being able to easily examine this wide spectrum is especially useful when designing structures having regions where the antenna characteristic of interest changes, perhaps unexpectedly, in very narrow frequency bands. As a well-known example, designers of log periodic antennas must be aware of periodic narrow band anomalies in gain, in order to eliminate them from their final designs.

Antennas that may be analyzed by VOLMAX include, but are not excluded to, the following:

- 1) archimedean and logarithmic spirals,
- 2) multiple-arm log periodic antennas,
- 3) conical wire helices,
- 4) multiple-arm printed sinuous antennas,
- 5) broadband antennas etched on conical dielectric shells.

**Analysis of scattering from a large arbitrary-shaped conducting cylinder by
iterative FEM with fast multipole updates**

Jongkuk Park*, Jungwon Lee, Heeduck Chae and Sangwook Nam

School of Electrical Engineering, Seoul National University

A FEM-based hybrid method or an iterative FEM for scattering by a large body is proposed and applied to a 2D conducting cylinder. For the first time, an iterative FEM is introduced by T. Roy, T.K. Sarkar and so on (T. Roy, T. K. Sarkar, A. R. Djordjevic and M. Salaza, *IEEE Trans. Microwave Theory Tech.*, 1996, **44**, (12), pp. 2145-2151), and complemented by S. Alfonzetti, G. Borzi, and N. Salerno (S. Alfonzetti, G. Borzi, and N. Salerno, *Int. J. Numer. Meth. Engng.*, 1998, **42**, pp. 601-629). In the above paper, a mixed boundary condition has been incorporated with FEM to eliminate an internal resonance instead of the Dirichlet condition used previously. As good features to be exploited in the iterative FEM, a system matrix generated by the iterative FEM preserves a sparsity, which is a good property in FEM, and it does not change during iterations. Besides, a matrix for updating a field quantity on the artificial boundary is also invariant during iterations, so that it is computed only once at the beginning of the procedure. These properties make the iterative FEM competitive with other methods concerning computation time and memory requirements. However, this method has failed when it is applied to solve a scattering problem from a large body. A matrix for updating the residual field is calculated by an integral equation with Green's function, so that it is a full matrix. Hence, according to the increase of unknowns, the storage of this matrix and the multiplication between this matrix and a working variable vector become serious problems. Therefore, in this paper, the typical fast multipole method is modified and adapted to the updating procedure of the iterative FEM so that the increasing rate of field updating time and memory requirements may decrease. Since the mesh termination can be placed very close to a scatterer in iterative FEM, the excessive increase of unknowns does not occur as the size of a scatterer. Also, a highly sparse system matrix requires the computational load linearly proportional to the increase of total unknowns, so that the FEM solution is obtained efficiently. And with the help of fast multipole updates, the computational load and memory requirements for updating can be reduced to $O(N^{3/2})$, where N is the number of nodes on the conductor surface. Therefore, this method is competitive with other fast methods such as typical FMM or FE-FMM in respect to computation time and memory requirements. To verify the proposed method, scattering by a large conducting circular cylinder is analyzed as a simple example. The result is compared with that given by a standard MoM and an exact FMM, and shows an efficiency and a good agreement with other methods.

Pulsed Radiation by Periodic Structures Via a Combined (time domain-Floquet wave)-(FDTD) algorithm

Filippo Capolino
Dept. of Information Eng.
University of Siena - Italy
capolino@dii.unisi.it

Gaetano Marrocco
Dept. of Information, Systems. and Prod.
University of "Tor Vergata", Roma - Italy
marrocco@disp.uniroma2.it

ABSTRACT

Recently, an accurate investigation of the wave phenomenology associated to pulse radiation by an infinite line array [L.B. Pelsen and F. Capolino, *IEEE Trans. Ant. Prop.*, **48**, 921-931, 2000] or by an infinite planar array of sequentially excited pulsed dipoles [F. Capolino and L.B. Pelsen, *IEEE AP-S Symp.*, **1**, 90-93, 2000] has been carried out in terms of time domain (TD) Floquet waves (FW). Though various other geometries of infinite or truncated periodic structures have been studied in the frequency domain, only a few prototypes have been analyzed in the TD. In the present investigation, some of the concepts developed in the cited papers are generalized for periodic planar arrays of geometrically and electrically complex objects when a numerical fullwave method, such as the Finite-Difference Time-Domain (FDTD) is used to model the periodic cell. In a recent paper [G. Marrocco, *IEEE AP-S Symp.*, **4**, 1974-1977, 2000] it was shown how the FDTD can be efficiently applied to model wide-band antenna radiation inside a truncated waveguide in terms of TD waveguide modes. By following a similar approach, we show that, by a suitable definition of time-domain TEM, TE and TM modes inside the periodic cell, field radiated away from the array by each TD-FW modes can be represented via equivalent transmission lines excited by localized current or voltage modal generators computed on a cross-section of the periodic cell by the FDTD. PML absorbing conditions are used to truncate the computational domain in the boundaries parallel to the array plane, while periodic boundary conditions are enforced to take into account of the periodicity. Finally, electric (magnetic) TD fields at any point are expressed as superposition of the TD-FW modal voltages (currents) in that point computed as the convolution between the TD Green function of each equivalent transmission line (known in both exact closed form and asymptotic representation) and the corresponding modal generator. Both the cases of a pulsed (wide band) excitation within the cells (radiation) and of an impinging pulsed plane wave (scattering) are analyzed.

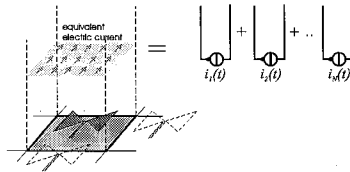


Figura 1: left) periodic cell; right) equivalent transmission line scheme

The combination of FDTD with both exact and asymptotic TD-FW results are analyzed and compared. The asymptotic TD-FW is dominated by an instantaneous frequency times the frequency spectrum of the modal voltage generator obtained via the FDTD algorithm. It is shown that the asymptotic algorithm is very accurate also close to the wavefront, due to the finiteness of the excitation bandwidth. Numerical examples will be shown and compared.

ALPEN—A VERSATILE FDTD TOOL FOR ANALYZING MICROSTRIP PCB CIRCUITS

*F. Rivas **, *I. González ***, *Wenhua Yu ****, *Nader Farahat ****, *Raj Mittra ****,
*F. Saez de Adana ***, *O Gutiérrez ***, *J. P. Roa **, *M.F. Cátedra ***

* *Dept de Electrónica. EUP de Linares. Universidad de Jaén. Linares. Jaén. Spain*

** *Dept. Teoría de la Señal y Comunicaciones Escuela Politécnica. Universidad de Alcalá
28806. Alcalá de Henares. Madrid. Spain*

*** *EM Communication Laboratory. 319 EE East, Pennsylvania State University
University Park, PA 16802 USA*

The paper will describe the computer code ALPEN, which is a Finite Difference Time Domain (FDTD) software package designed to analyze microstrip printed circuit board (PCB) circuits. Recently, a Conformal FDTD Software Package has been described by Wenhua Yu, Raj Mittra. (*Antennas and Propagation Magazine*, Vol 42, pp 28-39 October 2000). The ALPEN code can be viewed as an enhanced version of the above software. Both codes share the same "kernel," and utilize the Conformal Finite Difference Time Domain (FDTD) scheme.

The ALPEN code enhances the original CFDTD code by adding a versatile geometrical tool for inputting the geometry of the object. The format for the geometrical input data is DXF, and can be generated by most commonly used CADG tools, *e.g.*, DXF files from AutoCAD, Microsistem, CADDs and others. In particular, using Autocad to draw the tracks of the circuit that are located in the x-y plane, a "polyline" entity is used. "Polyline" entity allows one to represent curve and straight segments of an etch, so that an arbitrary track can be easily modeled. Moreover, in the current version it is possible to combine a polyline and a spline curve in order to define a more general entity, and to analyze arbitrary track layouts. Note that this option is not available in version 14 of AutoCAD 2000.

As for the tracks of the PCB circuit, it is assumed that the metalization has zero thickness that and it is perfectly conducting. The FDTD mesh is not restricted to be uniform, and the user can generate a non-uniform grid to model the geometry.

The code has a user-friendly graphical interface, which makes it quick and easy to handle. It enables the user to see the geometry being modeled and to visualize the results of the FDTD analysis with different output options.

Numerical Modeling of Electromagnetic Wave Scattering by Multi Parametrical Structures.

Andrey Perov^{*(1)}, Marie-Odile Monod⁽²⁾, Raphael Rouveure⁽²⁾, Mariam Chanet⁽²⁾.

- (1) Institute of Radiophysics and Electronics of National Academy of Sciences of Ukraine, 12, Ak. Proskury St., Kharkov, 61085, Ukraine
tel: 38 0572 448557, fax 38 0572 441105, e-mail: sirenko@ire.kharkov.ua
(2) CEMAGREF, 24 Ave des Landais, 63172, Clermont-Ferrand, France
fax: 04 73 44 06 97, e-mail: marie-odile.monod@cemagref.fr

The earth surface remote sensing find nowadays wide range of applications. In their major part that are the global monitoring systems, installed on satellites providing the information over considerably large areas. The alternative tendency of earth surface monitoring is connected with application of ground-based radar (M.O Monod, P.Faure, J.Dusi. Colloque RADAR'97, 14-17, October 1997, Edinburgh). The utilization of the monitoring systems of such a kind is rather promising as by means of ground-based system it is possible to obtain more detailed information about the state of soil over considerably small areas in any required by local needs moment of time. The applications of ground based systems has certain special requirements to the data retrieving algorithms and, consequently mathematical models, describing the object under investigating that is the fertile layer of soil. For the unambiguous treatment of the remote sensing data the development of mathematical models of electromagnetic wave scattering by soil, accounting soil's structure peculiarities in wide frequency range becomes rather urgent. In SHF frequency range, when the characteristic dimensions of surface roughness and inhomogeneities in soil structure may be of comparable values with wave length, such treatment requires the consideration and accurate estimation of contribution of rather large number of parameters within the mathematical model.

The objective of present study is the development of mathematical model, that describe the soil in adequate way and is mathematically correct. The mathematical model suggested herein is based on the application of FDTD-method with explicit radiation conditions (A.O. Perov, Yu. K. Sirenko, N. P. Yashina. Journal of Electromagnetic Waves and Applications" 1999, vol 13, No.10).

Within the frames of 2D the soil is considered as randomly inhomogeneous media with rough surface. The Monte-Carlo method is applied for modeling of random distribution of inhomogeneities. For model tests the numerical experiments had been performed. The results of computations based on the known models of soil and developed herein with experimental soil study had been carried out.

Incorporation of explicit conditions for the limiting of computational domain essentially increases the efficiency of FDTD algorithm. The boundaries of the computational domain can be chosen just in the vicinity from scattering surface. The direct difference schema in TD enables us to avoid such "inconveniences" as ill conditioned matrixes describing scattered field, that is conventional problem in direct numerical techniques in FD.

The code implementation of the algorithm is most efficient in the range of parameters when wave length is compared with characteristic dimensions of inhomogeneities of scattering surface.

Highly Efficient Numerical Analysis of an Open Hemispherical Resonator

Michał Rewieński*, Michał Mrozowski**

* was with Faculty of Electronics, Telecommunications and Informatics,
Technical University of Gdańsk,
currently with Department of Electrical Engineering and Computer Science
Massachusetts Institute of Technology, 02139 Cambridge, MA, USA

**Faculty of Electronics, Telecommunications and Informatics,
Technical University of Gdańsk, 80-952 Gdańsk, Poland

An open hemispherical resonator is often employed in measurements of properties of high temperature superconductors. Because side walls are not present the conductor losses are low. Moreover, this arrangement offers thermal isolations so the sample can be measured at low temperature while the measurement gear is operated at room temperature. To reduce the radiation and diffraction loss a high order quasi-TEM mode is used. This makes the numerical modeling of the structure an extremely challenging problem. There are two major difficulties: a) the computational domain is electromagnetically large, has complex shape and contains different media, b) the mode to be computed is far from the spectrum ends and hence has to be calculated using non-standard numerical techniques.

In order to overcome these difficulties we propose the following approach. Due to rotational symmetry of the structure the 3D domain defined in a cylindrical coordinate system was first reduced to a 2D domain using two (D_r, D_z) electric flux components. The resulting wave equation was converted to a highly sparse standard nonsymmetric matrix eigenvalue problem by means of the FDFD method based on regular Yee's mesh. To reduce the numerical dispersion error (which is significant in this case due to large size of the domain) the finite difference formulas were modified so that they produce the minimum phase error at the estimated resonance frequency. Subsequently, the parallel implementation of the implicitly restarted Arnoldi method was applied to solve the matrix eigenproblem generated by the FDFD algorithm. The direct mode was used since the LU decomposition required in the shift-and-invert mode was impossible given the size of the matrix problem. In order to enable the computation of the mode of interest the problem was preconditioned using the FIR bandpass digital filter. The filter was implemented using Chebyshev polynomials and Horner's rule. Moreover, the matrix was regularized in order to obtain load balancing and scalability in parallel computations. The numerical tests show that the solver based on the above mentioned techniques is highly scalable and yields very accurate results.

Low Complexity Model Order Reduction for FDTD/FIT Systems

T. Wittig^{1*}, I. Munteanu^{1,2}, R. Schuhmann¹, T. Weiland¹

¹ Darmstadt University of Technology, Computational Electromagnetics Laboratory (TEMF), Schlossgartenstr. 8, 64289 Darmstadt, wittig@temf.tu-darmstadt.de

² „Politehnica“ University of Bucharest, Romania, Electrical Engineering Department

With the continuously increasing complexity of electromagnetic devices and the growing need of coupled electric circuit-electromagnetic field simulations, the development of reduced-order models has become an important area of research over the last few years. Krylov-subspace-based methods, especially the Padé Via Lanczos (PVL) algorithm have been shown to reliably generate reduced models of large linear electric circuits (P.Feldmann, R.W. Freund, *IEEE Trans. CAD of Int. Circ. Syst.*, 14, 639-649, 1995) as well as of the discretized Maxwell's equations in conjunction with FDTD and the Finite Integration Technique (FIT). However, though the models obtained by PVL are known to have very low order, the computational complexity is quite large, since it requires the inversion or factorization of the system matrix, which can be of the order of hundreds of thousands.

In this abstract a method is described to avoid the expensive inversion of the initial system by application of a projection technique - also based on the Lanczos algorithm. In a first step the Lanczos algorithm is applied directly to the system of spatially discretized Maxwell's equations (I. Munteanu, T. Wittig, et al., *IEEE Trans. Magn.*, 36, 1421-1425, 2000). This way a first reduced approximation is obtained, which - however - does not represent a Padé approximation of the system's transfer function. To reliably ensure the approximation of the lowest poles, which are typically the dominant ones in electromagnetic problems, a much larger number of Lanczos iterations is necessary compared to PVL. But since each Lanczos iteration only requires a matrix-vector multiplication, the numerical cost is much lower than the inversion of the system. The order of the reduced model is typically below a tenth of the initial one. Although this is too large to be a "low-order" one, PVL can easily be applied in a second step, since the dimension of the matrix is now much smaller and its inversion/factorization does not require a large computational effort anymore.

The proposed algorithm was applied to a filter structure (Figure 1). The structure discretization yielded an initial system of order of about 3300. The impedance matrix Z was used to compute the S-Parameters of the structure. Figure 2 shows indistinguishably the absolute value of the transmission factor (S_{12}) of the initial system, the PVL-reduced system (order 12) and the two-step algorithm (order 250/12); obviously, only 200 Lanczos iterations did not yield a satisfying approximation. With the new two-step Lanczos algorithm the computation time was reduced by a factor of ten.

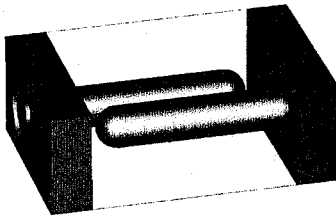


Fig. 1. Filter Structure

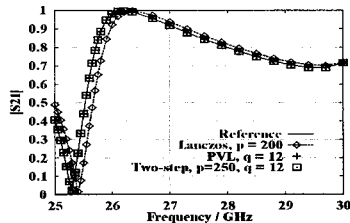


Fig. 2. Scattering parameter S_{12}

FDTD Simulation of Subsurface Water
Conductivity Mapping

Dennis Sullivan*, Ph. D.,
dennis@ee.uidaho.edu
Matt Kerschbaum

Department of Electrical and Computer Engineering
University of Idaho
Moscow, ID 83844-1023

John Morrison, Ph. D.
Bechtel BBWI
1625 Fremont
Idaho Falls, ID 83415

A method is being developed for the accurate mapping of contaminated subsurface water movement. An approach has been formulated using the integration of two separate mapping techniques. The first technique utilizes two arrays of probes submerged vertically in two separate wells. Data is acquired from different combinations of one probe from one array passing low frequency current to a probe in the other array while pairs of other probes measure the voltage drop between them. The data acquired from this sequence can be processed with a conventional algorithm to obtain a conductivity map of the region. The second technique will use the same probes two at a time to inject current at frequencies around 400 Hz, and a GPS located flux-gate magnetometer to map the resulting magnetic fields on the surface. The data obtained from the surface mapped 400 Hz magnetic fields, when corrected to remove signal cable magnetic field components, are used to estimate the current flow paths beneath the surface. A new method will fuse the data from both measurement techniques with an advanced algorithm, which has greatly improved resolution, to map the subsurface conductivity and thus the contaminated water movement.

Computer simulation is used in the development of the signal cable correction algorithm for the above-mentioned magnetic method to determine optimal signal frequency for both methods, and to optimize the electrode arrays for both methods. It is further used in the integration of the two methods with the development of the advanced data fusion algorithm. The fundamental simulation method is the finite-difference time-domain (FDTD) method. The basic simulation techniques will be described along with their verification with measured data. The resulting design will be described, including the integration of the two techniques. Finally, we describe preliminary results in the detection of underground water movement.

Macromodeling of Transmission Line Networks in the FDTD Technique using the Equivalent Source Method

Rumsey, I.*, Picket-May, M.
University of Colorado at Boulder
Department of Electrical and Computer Engineering
Campus Box 425
Boulder, CO 80309
rumsey@colorado.edu

Frequently in finite difference time domain simulation of high speed digital and microwave circuits, there are devices and transmission line building blocks which can be represented by their port characteristics without considering the full-wave electromagnetic behavior of the physical structure. Separating these circuit-like features from the important electromagnetic features of a problem can lead to a significant reduction in model complexity, as well as computational savings. A method for linking a behavioral description of these circuit subsystems with the time domain electromagnetic solver is needed to determine the overall performance of complex signal propagation paths. In the approach presented here, a modified set of update equations at the FDTD/macromodel interface are used to emulate the behavior of the network represented by the macromodel.

A macromodeling methodology for representing arbitrary frequency dependent multiport networks in finite difference time domain (FDTD) simulation involving transmission lines will be presented. This method (I. Rumsey, IEEE Trans. Ant. and Prop., submitted Oct. 1999) applies Z-transform theory (D. Sullivan, IEEE Trans. Microwave Theory and Tech., vol. 44, no.1, pp.28-34) to the equivalent source method (J. Mix, 1998 USNC/URSI National Meeting, p. 75) to implement a reduced-order model of an arbitrary network by operating on the reflection and transmission coefficients at a transmission line interconnect. The reflection and transmission behavior of each port is approximated as a rational function in the Z domain and implemented as a time domain recursive convolution. Issues concerning implementation of this method in microstrip transmission line will be discussed, as well as validating examples and applications.

Reflector and Feed Designs

Chairs: A. Zaghloul, USA and S. Duffy, USA

		Page
8:00	Reflector Antenna Solutions for Multisatellite DBS Reception, <i>A. G. Pino*, E.T.S.I. Telecomunicacion. Campus Universitario, F. Ares, Universidade de Santiago de Compostela</i>	APS
8:20	Comparison of Two Flat Reflector-Type Designs for Dual-Polarization, Dual-Band Operation, <i>S. Duffy*, S. Targonski, MIT Lincoln Laboratory</i>	APS
8:40	Design of Terrestrial Sector-Beam antennas Using Advanced Spacecraft Contoured Beam Synthesis Software, <i>H.H. Viskum*, TICRA</i>	APS
9:00	A Dual-Band Feed System for the Parkes Radio Telescope, <i>C. Granet, H.Z. Zhang, K.J. Greene, G.L. James. A.R. Forsyth, T.S. Bird*, Telecommunications & Industrial Physics, R.N. Manchester, M.W. Sinclair, P. Sykes, Australia Telescope National Facility</i>	APS
9:20	Multibeam Earth Station Antenna for a European Teleport Application, <i>S.G. Hay, S.J. Barker, C. Granet, A.R. Forsyth, T.S. Bird*, M.A. Sprey, K.J. Greene, CSIRO Telecommunications and Industrial Physics</i>	APS
9:40	Design and Experimental Validations of a New FSS Conformal Subreflector Structure for Cassegrain Systems, <i>M.G. Floreani, R. Zich*, Politecnico di Milano, G. Aulisio, Telesystem, P. Besso, CSELT, A. Somma, COMELIT</i>	APS
10:00	Simple Design Method of Feed Cluster for Array-Fed Reflector Type Multi-Spot Beam Antennas, <i>I. Naito*, S. Makino, N. Miyahara, Mitsubishi Electric Corporation</i>	APS
10:20	Multi-Moded Horns in Reflector Antenna Systems Exemplified by the Planck Telescope, <i>T. Bondo*, S. Sorensen, P. Nielsen, K. Pontoppidan, TICRA</i>	APS
10:40	Ultra-Wide Band Corrugated Gaussian Profiled Horn Antenna Design, <i>J. Teniente-Vallinas*, R. Gonzalo-Garcia, C. del-Rio-Bocio, Public University of Navarre</i>	APS
11:00	A Compact Low-Cross-Polarization Horn Antenna with Serpentine-Shaped Taper, <i>H. Deguchi*, M. Tsuji, H. Shigesawa, Doshisha University, S. Matsumoto, Mitsubishi Electric Corporation</i>	APS
11:20	85 - 115 GHz Corrugated Conical Horn Antenna for the Radio Telescope System, <i>T. Son*, Soonchunghyang University, S.T. Han, Korea Astronomy Observatory, B. Lee, Soonchunghyang University</i>	APS
11:40	Genetic Algorithm Synthesis of a Shaped Dual-Reflector Antenna, <i>A. Armogida, G. Manarra, A. Monorchio, PL. Nepa, G. Rossi, University Of Pisa, E. Pagana, Antenna Consultant</i>	204

Genetic Algorithm Synthesis of a Shaped Dual-Reflector Antenna

A. Armogida, G. Manara, A. Monorchio, P. Nepa, G. Rossi

Dept. of Information Engineering, University of Pisa, Via Diotisalvi 2, I-56126 Pisa, Italy

E. Pagana

Antenna Consultant, Via G.D. Cassini 95, I-10129 Turin, Italy

The use of new antennas operating in the microwave and millimeter-wave regions is growing up rapidly also in terrestrial mobile radio channel, due to the need of exploiting the spectrum capability. Reflector antennas have been, and still are, largely adopted to operate at the above frequency ranges, as they provide high efficiency and high gain. Nevertheless, due to strict radiation requirements in modern applications there is actually a need for effective synthesis techniques to design high performance reflector antennas. In particular, point-to-multipoint radio links often adopt the sector cover approach as an alternative to the use of omnidirectional antennas, with some advantages, namely a greater flexibility in the choice of the antenna location and more efficient frequency reuse capability in the cellular network. Hence, such systems require a central station (CS) antenna with a uniform azimuthal pattern and a shaped vertical coverage, in order to keep the signal to noise ratio as constant as possible independently on the distance between the CS and the user. A flat plate array in microstrip technology to operate as a point-to-multipoint CS sector antenna at 25 GHz has been proposed (A. Armogida et al., 2000 *IEEE AP-S Int. Symp.*, pp. 1038-1041) as a possible solution, which is light, compact, low profile and low cost, and can represent a valid alternative to the traditional reflector antenna solution. In the above paper a genetic algorithm (GA) was adopted to perform optimization in the array synthesis. The GA synthesis of an offset shaped dual-reflector antenna for point-to multipoint application in the Q band is presented here. The antenna operates in the frequency range of $40.5 \div 43.5$ GHz with linear polarization and a radiation solid characterized by an azimuthal sector of 90 degrees and a cosecant squared like vertical profile. To reduce the cross-polarization level on the azimuthal plane, a gregorian configuration has been chosen, with a suitable offset horn feeder. Moreover, both vertical and horizontal polarizations can be used adopting an orthomode device, thus rendering simultaneous receiving and transmitting operations possible. In order to obtain the required radiation patterns on the principal planes, both reflectors have been simultaneously synthesized through a GA optimizer combined with a physical optics analysis. In particular, distortions are imposed on canonical surfaces, namely a bifocal paraboloid for the main reflector and an ellipsoid for the subreflector. Distortions are mathematically described by rectangular polynomials (P.G. Mantica, E. Pagana, *Italian Nat. Conf. on Electromagnetics*, 1988) containing a set of unknown coefficients, which represent the genes constituting the chromosome of our GA. The use of real-coded chromosomes instead of binary-coded ones has proved to be more efficient in fastening the convergence of the algorithm. The fitness function minimizes the error between the trial and the desired patterns on both principal planes and its definition requires a particular care. Advanced GA techniques have been widely investigated and experimented in order to implement a successful and efficient GA for this specific application. The results of the synthesis will be presented at the conference.

Tribute to Professor R.W.P. King

Chairs: S. Long, USA and G. Smith, USA

	Page
1:00 Sixty Years at Harvard: The Career of Professor Ronold W.P. King, <i>S. Long*</i> , <i>University of Houston</i>	APS
1:20 Scattering of a Plane Wave by a Conducting Grounded Half-Cylinder and by a Periodic Surface, <i>C.T. Tai*</i> , <i>University of Michigan</i>	206
1:40 A Review of Genetic Antennas, <i>E. Altshuler*</i> , <i>Air Force Research Laboratory</i>	207
2:00 Some Thoughts on Teaching Antenna Analysis at the Introductory Level, <i>G. Smith*</i> , <i>Georgia Institute of Technology</i>	208
2:20 Inductance of a Practical Shielded Coil, <i>C. Butler*</i> , <i>Clemson University</i>	209
2:40 Break	
3:00 A Novel Microwave Beacon For Coastal Navigation, <i>R. King*</i> , <i>Harvard University</i>	210
3:20 Comment on Professor King's Microwave Beacon for Coastal Navigation, <i>T.T. Wu*</i> , <i>Harvard University</i>	211
3:40 Wideband Subarray Systems: Evolution of a Research Area, <i>R. Mailloux*</i> , <i>Air Force Research Laboratory, Hanscom AFB</i>	APS
4:00 Simulation of Electromagnetic Well Logging Tools, <i>L. Shen*</i> , <i>University of Houston</i>	212
4:20 Submarine Towed Communication Antennas: Past, Present and Future, <i>D. Rivera</i> , <i>Naval Undersea Warfare Center</i> , <i>R. Bansal*</i> , <i>University of Connecticut</i>	APS

**Scattering of a Plane Wave
by a Conducting Grounded Half-Cylinder
and by a Periodic Surface**

C.T. Tai
The Radiation Laboratory
Department of Electrical and Computer Science
The University of Michigan
Ann Arbor, MI 48109-2122

Abstract

The scattering of a plane wave by a conducting grounded half-cylinder is investigated with the aid of the image theory. The problem is then equivalent to the scattering of a direct wave and an image wave by a whole cylinder. Two cases are considered, corresponding to $2\pi a/\lambda = 1$ and 3 where a denotes the radius of the cylinder and λ , the wavelength. The angle of incidence varies from near grazing incidence to normal incidence, and two distinct polarizations are considered. The results are displayed in several graphs.

For small half-cylinders it appears that the back-scattered field is, in general, greater than the forward scattered field when the incident electric field is perpendicular to the axis of the cylinder. The trend is reversed when the incident electric field is paralleled to the axis of the cylinder.

Scattering of a plane wave by a periodic conducting surface has also been investigated. The reflected waves from the surface, then, consists of an infinite set of plane waves, of which all modes higher than a certain order are evanescent when the ratio of λ_w , the mechanical wavelength of the surface, to λ_0 , the electromagnetic wavelength of the incident wave, is smaller than the reciprocal of $1 + \sin \theta_0$, where θ_0 is the angle of incidence. As a result when the angle of incidence is increased from that of a normal incidence to that of glance incidence, the forward waves of the reflected rays are always susceptible to become evanescent before the backward waves. This criterion bears a direct relation to that of simple grating theory. Amplitudes of a few of the low-order modes have been calculated to illustrate the formulation.

A REVIEW OF GENETIC ANTENNAS

Edward E. Altshuler
Air Force Research Laboratory
Sensors Directorate
Hanscom AFB, MA 01731-2909

Tel: 781 377 4662, Fax: 781 377 1074, e-mail:edward.altshuler@hanscom.af.mil

There is a large class of electromagnetic radiators designated as wire antennas. As a rule, an inductive process is used to design these antennas. Either an integral equation is formulated or a simulator is used that gives the current distributions on the wires of the antenna, from which the electromagnetic properties of the antenna can be determined. Once the antenna properties are known, the parameters are optimized. However, using an electromagnetics simulator in conjunction with a Genetic Algorithm (GA), it is possible to design an antenna using a completely deductive approach; the desired electromagnetic properties of the antenna are specified and the wire configuration that most closely approaches the desired results is then synthesized by the algorithm.

In this paper we describe two types of genetic antennas. In the first type an existing antenna design is further optimized using a GA. We illustrate this approach using a Yagi antenna. We allowed the length and spacing of the elements to float and specified a configuration that produced maximum gain. It was shown that a genetic Yagi having the same boom length as a conventional Yagi had a higher gain.

In the second type of genetic antenna we do not specify a starting configuration; we simply place the wires in a volume and we instruct the GA to connect these wires to form an antenna that has the desired electromagnetic properties. We illustrate this approach by describing two types of antennas, a circularly polarized antenna that has near hemispherical coverage and a very small resonant antenna. The circularly polarized antenna was designed to be used as a vehicular antenna for both GPS and Iridium. It consisted of 5 wires connected in series and operated over the band from 1225-1625 MHz. The electrically small genetic antennas consisted of 5 to 10 wires, the smaller the antenna the more wires. For this application a volume is specified and the GA is instructed to connect the wires so that a resonant antenna is formed. Resonant antennas that fit inside a cube having sides of $1/30^{\text{th}} \lambda$ and over a ground plane have been simulated, built and tested.

It will be obvious that these antennas, with their unusual shapes, could not have been designed using an inductive approach. We believe that this new process may revolutionize the design of wire antennas.

Some Thoughts on Teaching Antenna Analysis at the Introductory Level

Glenn S. Smith

School of Electrical Computer Engineering
Georgia Institute of Technology
Atlanta, GA 30345-0250, USA

Tel: 404-894-2922, e-mail: glenn.smith@ece.gatech.edu

Introductory courses on electromagnetics usually include treatments of both transmission lines and simple wire antennas. For transmission lines, a time-domain analysis involving pulse propagation is often presented initially, so that physical phenomena such as propagation times and end reflections can be clearly illustrated. The time-harmonic case is treated later, and additional concepts such as standing waves and the VSWR are introduced. On the other hand, for wire antennas, harmonic time dependence is almost always used, and the time-domain analysis is almost never mentioned. The purpose of this paper is to offer a systematic treatment for wire antennas that more closely resembles the conventional one for transmission lines: the time-domain analysis (pulse excitation) is presented first followed by the time-harmonic case. The approximations (thin-wire, assumed current distribution) and level of difficulty for the time-domain analysis are comparable to those for the conventional time-harmonic approach; however, the former provides a better understanding of the physical concepts associated with radiation than the latter.

A systematic approach is developed whereby wire antennas of different shape (linear, loop, vee, etc.) are easily analyzed in the time domain. First, the complete electromagnetic field (near field as well as far field) of a pulse-excited, straight filament (basic traveling-wave element) is determined, and then the given antenna is decomposed into a group of these elements. The electromagnetic field of the antenna is the superposition of the fields from these elements. This procedure is easily implemented with a simple, fairly general computer program. Graphical results show that the field consists of a series of pulses, each of which can be associated with radiation from a particular point on the antenna: drive point, open end, bend, etc. A strong analogy can be developed between the radiation from the pulse of current/charge on the wire antenna and the radiation from a classical, moving point charge. This analogy can be used in as an intuitive tool for predicting the radiation from wire antennas of more general shape.

References

- [1] G.S. Smith, *An Introduction to Classical Electromagnetic Radiation*, Cambridge Univ. Press, Cambridge, UK, 1997.
- [2] G.S. Smith, "Teaching Antenna Radiation from a Time-Domain Perspective," *American Journal of Physics*, to be published, 2001.

INDUCTANCE OF A PRACTICAL SHIELDED COIL

Chalmers M. Butler
Holcombe Department of Electrical and Computer Engineering
Clemson University
Clemson, SC 29634-0915

Inductors play an important role in loading of antennas in many applications yet little attention has been given to the determination of the inductance of a practical helical coil. A coil must be physically supported and, usually, is shielded. In most practical cases, the presence of a structure which serves these purposes significantly affects the properties of the coil. In this paper, we determine the inductance of a thin-wire, helical coil wound on a supporting form and located inside a conducting cylindrical shield. Inductance is a stationary current notion whose valuation depends upon the computation of time-invariant magnetic flux in the coil caused by the coil current I . Even though determined from time-independent current and the flux created thereby, inductance finds its utility in circuit analyses involving time-varying quantities. In principle, the time-independent magnetic flux due to the stationary current employed in the definition of the self inductance L of the coil does not interact with the support form or surrounding shield, yet the presence of the material form and shield does influence the current in the coil in any application of L in a circuit. Clearly, this is true because, in any circuit in which L plays a role, the current in the coil depends upon time, provided, of course, the circuit itself is stationary in space.

We determine the inductance of a practical coil wound on a cylindrical core, which is made of either a conductor or of material characterized by (μ_c, ϵ_c) , and shielded by a conducting cylindrical shell. Full account is taken of the presence of the form and shield. The magnetic field due to the coil current I is not conservative in any region containing the current, yet it can be represented as the gradient of a magnetic scalar potential Ψ satisfying Laplace's equation in contiguous regions not containing the filamentary current. To account for I , the two branches of Ψ must exhibit derivative continuity and discontinuity conditions at the cylindrical surface in which the filament resides. The presence of the core and shield is incorporated in the analysis by defining L in terms of the zero-order term of a Rayleigh series expansion of the time-harmonic flux linkage, with the needed conditions at core and shield interfaces provided by first-order terms in the expansion. With these needed conditions in hand, one can obtain a Fourier integral representation of L for the shielded coil wound on a material core.

Data are presented for the inductance of the practical coil in which one observes a significant reduction in L as the shield diameter approaches that of the coil.

A NOVEL MICROWAVE BEACON FOR COASTAL NAVIGATION

Ronold W. P. King

Gordon McKay Laboratory, Harvard University, Cambridge, MA 02138-2901

A typical section of the rugged coast of Maine is along East Penobscot Bay including the harbors of Rockport and Camden. The entrance to each of these is partly blocked by an island on which is a discontinued lighthouse. These have been replaced by flashing red lights. The light at the end of a long reef at the entrance to Rockport harbor flashes 10 times per minute, that at the entrance to Camden harbor 15 times per minute. On a rock in the middle of the channel from Rockport to Camden is a light that flashes 12 times per minute. To further help the lobsterman or sailor find his way on a dark foggy night, wave-activated bells are located in the channel outside each harbor. However, on a calm night in a dense fog a boat may not be close enough to hear a bell or near enough to see a flashing light. The boat's radar can locate rocks that extend above the surface of the sea, but not submerged reefs. This raises the question: Can a fog-penetrating microwave beacon be provided to supplement the red lights by sending out the same number of flashes at 3 GHz as does a particular red light? The answer is yes, with the use of a recently invented circular array of coplanar vertical dipoles.

The new array (G. Fikioris, R. W. P. King and T. T. Wu, *J. Appl. Phys.*, **68**, 431–439, 1990) consists of 90 identical dipoles with half-length $h = 0.18\lambda$, radius $a = 0.028\lambda$, equally spaced by the distance $d = 0.437432095\lambda$ and operated at $f = 3$ GHz with $\lambda = 0.1$ m = 10 cm. Hence, $h = 1.8$ cm, $a = 0.28$ cm, $d = 4.37432095$ cm. Only element #1 is driven, the others are parasitic. Element #1 sends a wave in each direction around the array that generate large resonant currents in all of the elements. These differ in phase by 180° from element to element so that at a given instant all odd-numbered elements have a maximum current upward, all even-numbered elements a maximum current downward. The driving-point admittance of the driven element #1 is a pure conductance with the value $G_{1,1} = 0.109$ S.

In the equatorial plane, the electric field consists of 90 sharp nulls between 90 sharp peaks which alternate + and – from peak to adjacent peak. In the vertical plane, the field pattern is flat like a pancake. At a distance of 1 km from the center of the array, the magnitude of the electric field in each spike is 0.444 V/m. This is the electric field per volt applied to the driven element that would be received by a boat 1 km from the beacon when directly illuminated by one of the peaks. The boat would have to have its receiver tuned to 3 GHz. The transmitted signal could be modulated so that an audible signal could be heard with a cellular telephone. By slowly rotating the array, any desired number of flashes can be received including 10, 15, and 12 per minute.

The discussion so far assumes the 90 dipoles to be perfectly conducting. As shown by G. Fikioris (*IEE Proc. Microw. Ant. Propag.* **145**, 92–98, 1998), the efficiency with copper conductors is only about 40% so that the electric field is about 0.4 that for the assumed perfect conductors. For the same radiated field the driving voltage of element #1 would have to be 2.5 times that given for perfect conductors. However, the resonant frequencies remain the same.

A practical beacon consists of 90 antennas mounted in holes in a thin plexiglass sheet. The conductors that supply power to element #1 are fastened to this sheet and extend radially inward as a two-wire transmission line. At the inner end they become a shielded-pair line that extends downward in the central metal tube to the generator. The entire structure is protected from the elements by styrofoam cones.

COMMENT ON PROFESSOR KING'S MICROWAVE BEACON
FOR COASTAL NAVIGATION

Tai Tsun Wu

Gordon McKay Laboratory, Harvard University, Cambridge, MA 02138-2901

In the preceding paper, Professor King has proposed a novel and important application of the resonant circular array to produce a microwave beacon for coastal navigation. In particular, this array is rotated mechanically to duplicate the rate of flashing red lights. It is natural to inquire whether this mechanical rotation can be replaced by an electronically rotating beacon.

For this purpose, since driving only one of the elements of the resonant circular array can produce only a stationary beacon, it is necessary to drive two of the elements. It turns out that, for the array used in the preceding paper with 90 elements and 90 sharp nulls in the field pattern, such a rotating beacon without mechanical parts is not possible by driving any number of the dipole antennas in the array.

Attention is therefore turned to an alternative resonant circular array consisting of 72 identical dipole antennas and 54 sharp nulls (G. Fikioris, R. W. P. King and T. T. Wu, *Progress in Electromagnetic Research*, 8, J. A. Kong, Ed., EMW Publishing, Cambridge, MA, 1994). By driving this array with two suitably chosen modulated microwave voltages on two neighboring dipoles, a rotating field pattern can be achieved without any mechanical rotation.

The fundamental property that distinguishes this alternative array qualitatively from the original one is that the number of dipole antennas is not equal to the number of sharp nulls. When this inequality is satisfied, it is possible to perform the rotation either mechanically or electronically.

The amount of information available about this array of 72 dipoles is much less than that for the 90-dipole array that Professor King used. For this reason, an asymptotic theory for such resonant circular arrays with a large number of dipoles has been developed recently.

Rotating the microwave beacon electronically has an additional significant advantage. The use of mechanical rotation is intrinsically limited to a circular array, because the entire field pattern must necessarily rotate. In contrast, the proposed method of driving two of the dipoles is equally useful whether the resonant array is circular or not. This freedom is helpful in various ways, such as making more efficient use of the resonant array, for example by concentrating the radiation pattern in the desired directions.

The rotation discussed so far pertains to that in the plane of the dipole array. If rotation of the field pattern is desired in some other direction, then there is no way to accomplish this electronically. Therefore, when it is desirable to cover a larger solid angle, it is useful to combine the electronic rotation in the plane of the array with a mechanical rotation in some other direction.

Simulation of Electromagnetic Well Logging Tools

Liang C. Shen
Department of Electrical and Computer Engineering
University of Houston

Abstract

Using electric method to probe subsurface mineral deposits was first conducted by Schlumberger brothers in 1912. Since then many instruments have been invented for logging in boreholes. In the past decade various computer codes have been developed to simulate electromagnetic well-logging tools. The objectives are to interpret the measured data more accurately, and to understand the capabilities and limitations of those tools. A useful simulation code must satisfy three basic criteria. First, it ought to be reasonably accurate in simulating the responses of the instrument in various geological environments. Second, it must be fast in computation speed because timeliness of the log interpretation is an essential requirement in the exploration process. Third, the simulation code must be user friendly. In this paper a review is given to outline the methods that are currently used to satisfy these criteria.

To accurately simulate the tool response in various environments, one must develop a mathematical model for the tool and the earth formation. Then the boundary-value problem is solved in accordance with the Maxwell's equations. Unfortunately, closed-form analytic solutions do not exist except for some trivial cases. For some simple cases like horizontally layered formation or concentric cylindrically layered formations, analytic solutions may be obtained but the results are expressed in terms of indefinite integrals or infinite series. In the complex situations such as the case where the tool is located in an invaded dipping bed formation, pure numerical methods such as the finite element or finite difference method must be employed. Fast algorithms have been developed to speed up numerical evaluation. Furthermore, due to the advance in programming languages, graphical interface can be designed to make the simulation codes easy to use.

Wireless Antennas & Base Station Design

Chairs: J. Bernhard, USA and C. Furse, USA

	Page
1:00 Switched-Beam Antennas Performance Evaluation in UMTS Vehicular Environments, <i>R. Martinez, D. Martinez, L. de Haro*, M. Calvo, Universidad Politecnica de Madrid</i>	214
1:20 Characterization of Conductor-Backed CPW-Fed Slot Antenna with Two-Layered Dielectric Substrate, <i>J.P. Jacobs*, J. Joubert, J.W. Odendaal, University of Pretoria</i>	215
1:40 Multiple Spot Beam Spherical Antenna for High Capacity Fixed Wireless Local Loop, <i>S. Guerouni*, Radiophysics Measurement Institute, A. Cardiasmenos, L-3 Communications ESSCO</i>	216
2:00 A Biocompatible Antenna for Communication with Implantable Medical Devices, <i>C. Furse*, R. Mohan, A. Jakayar S. Kharidehal, B. McCleod, S. Going, Utah State University</i>	217
2:20 Methods for Optimizing the Location of a Base Station for Indoor Wireless Communications, <i>Z. Ji*, T. Sarkar, Syracuse University, B.H. Li, Shanghai Jiao Tong University</i>	218
2:40 Effects of the Human Head and Handset on Antenna Radiation Patterns: A Simplified Model and Fast Algorithm, <i>Y. Huang*, R. Narayanan, University of Nebraska, G. Kadambi, Centurion Wireless Technologies, Inc.</i>	219
3:00 Application of Characteristic Modes to Antenna Placement on Portable Wireless Devices, <i>D. Strohscchein*, K. Sivaprasad, University of New Hampshire, J. Bernhard, University of Illinois at Urbana-Champaign</i>	220
3:20 Analysis and Measurements of Compact-Size DRA with CPW-Feed, <i>M.S. Al Salameh*, Hashemite University, Y.M.M. Antar, Royal Military College of Canada, G. Seguin, Canadian Space Agency, A. Petosa, Communication Research Center</i>	221
3:40 NRD Guide Compatible Pyramidal Horn Antenna for Multiple Access Wireless LAN at 60GHz, <i>F. Kuroki*, A. Takada, M. Eguchi, Kure National College of Technology, T. Yoneyama, Tohoku Institute of Technology</i>	222
4:00 A GSM Fully-Adaptive Antenna System Test-Bed: Unlink Trials, <i>G.F. Cazzatello*, M. Crozzoli, D. Disco, L. Ferrero, CSELT</i>	223
4:20 Smart Antennas at Wireless Mobile Computer Terminals and Mobile Stations, <i>J. Lu*, T. Ohira, ATR Adaptive Communications Research</i>	224

SWITCHED-BEAM ANTENNAS PERFORMANCE EVALUATION IN UMTS VEHICULAR ENVIRONMENTS

Ramón Martínez, David Martínez, Leandro de Haro*, Miguel Calvo
Grupo de Radiación. Dpt. Señales, Sistemas y Radiocomunicaciones.
Universidad Politécnica de Madrid.
Mail address: E.T.S. de Ing. de Telecomunicación. Ciudad Universitaria.
E-28040 Madrid (SPAIN)
Phone: +34 91 549 57 00 ext. 397 Fax: +34 91 543 20 02
e-mail: ramon@gr.ssr.upm.es

Third Generation Universal Mobile Telecommunications System (UMTS) is demanding new technologies in order to provide high data rate Internet service to a higher number of users. Two methods to allocate the exceeded demand would be the assignment of more frequency bands and the reduction of cell size. But these techniques will not be sufficient in the long term. In order to improve the capacity offered by WCDMA systems, some methods have been proposed to exploit the different spatial locations of mobile users using smart antennas in the base stations. Smart antennas technology ranges from phased arrays to fully adaptive antennas, including switched beam antennas, whose performance is addressed in this paper. The key benefits that smart antennas bring to WCDMA wireless communications systems are enhanced coverage, interference reduction and link quality improvement.

We present the performance improvement obtained with four switched-beam antennas in UMTS compared to typical 120° sectored antennas for different propagation conditions. The vehicular macrocellular scenario proposed in the ETSI-UMTS standard has been simulated. The improvement obtained is shown in terms of intracell, out-of-cell and total C/I for both antenna systems (see figure 1). As can be seen, switched-beam antennas contribute a many-fold increase in the number of active users for the same value of C/I, thanks to its beam directivity and interference reduction capability. It can be concluded that the number of users in the system has been increased four times with the use of four switched-beam antennas with respect to 120° sectored ones.

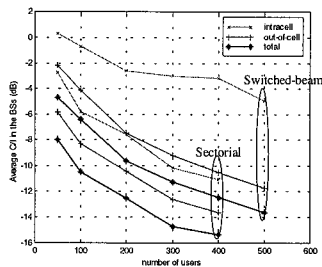


Figure 1. Average reverse link C/I under Rayleigh fading conditions.

Characterization of Conductor-Backed CPW-Fed Slot Antenna with Two-Layered Dielectric Substrate

J. P. Jacobs, J. Joubert and J. W. Odendaal*

Centre for Electromagnetism

Department of Electrical, Electronic and Computer Engineering

University of Pretoria, Pretoria, 0002, South Africa

Tel.: +27-12-420-2167, Fax: +27-12-362-5000

E-mail: jjjacobs@postino.up.ac.za

Slot antennas fed by coplanar waveguide (CPW) in its original form (i.e., without conductor backing) have recently received increased attention due to their wider bandwidth and advantageous impedance matching properties in comparison with microstrip patch antennas. On the other hand, very few studies are available on the properties of slots fed by conductor-backed coplanar waveguide (CBCPW). This deficiency is important since for many potential applications a conducting backplane is integral to the structure of the antenna.

A significant drawback of CBCPW-fed antennas is the possible excitation of parasitic parallel-plate modes at the discontinuity posed by the radiating slot. Even for antennas on a two-layer dielectric substrate, within which the TEM parallel-plate mode cannot exist, power leakage into higher-order parallel plate modes may degrade radiation efficiency to the extent that practical use of the antenna is not feasible.

The slot dipole is perhaps the most rudimentary form of a CBCPW-fed slot antenna with two-layered dielectric substrate. Yet the number of case studies of this antenna available from prior reports is quite small. Furthermore, rigorous characterization of these antennas apparently has not been attempted; rather, only rough outlines for tuning have been provided. In this paper, we present a systematic investigation of the effect of antenna dimensions and parameters on properties such as radiation efficiency, cross-polarization, resonant frequency and impedance bandwidth. Pertinent quantities of which the effects are explored include length and width of the slot dipole, CPW-feedline dimensions, substrate layer heights and dielectric permittivities. Theoretical findings will be discussed in conjunction with measured data.

MULTIPLE SPOT BEAM SPHERICAL ANTENNA FOR HIGH CAPACITY FIXED WIRELESS LOCAL LOOP

Souren P. Guerouni^{*1} and Apostle G. Cardiasmenos²

(1) Radiophysics Measurement Institute, 49/4 Komitas Av. Yerevan 375051, Armenia
email: iri@sci.am

(2) L-3 Communications ESSCO, Old Powder Mill Road, Concord, MA 01742
email: apostle.cardiasmenos@essco.L-3com.com

A Multiple Spot Beam Spherical Antenna ("MSBSA") has been developed which provides a large number of spot beams and allows a significantly increased number of simultaneous users in a given base station coverage zone when compared to traditional base station sector radiators such as are used in most existing LMDS base stations. The MSBSA is constructed of three spherical primary reflectors typically 1 x 2 meter in cross-section which are arrayed together such that each reflector provides azimuthal sector scan coverage of slightly greater than 120°. The reflectors share a common central mount to provide complete 360° azimuthal scan coverage over an elevation scan coverage zone of approximately $\pm 15^\circ$ for a typical base station application.

As part of an ongoing ISTC study entitled "Antenna Terminal for Microwave Telecellular Communication", a MSBSA prototype of one azimuthal sector was constructed and tested. In the configuration demonstrated during the study, the beams were separated by between 2° to 3° and each spot beam had a -3dB beamwidth of about 1° at ~ 40 GHz. Spot beam gains of about +43dB were realized for overall antenna efficiencies of ~ 50% when the feed locations were optimized to reduce the feed blockage and further adjusted to keep the efficiency loss due to spherical aberration to an acceptably low level.

The MSBSA was implemented with multiple conical feeds having aperture diameters of 15 mm designed for operations at near 40 GHz. More than thirty beams per azimuthal sector are possible with feed array blockage of between 5% - 15% depending upon the specific spot beam locations. Each MSBSA feed illuminates a region on the spherical primary of about 500 mm diameter and these regions may be superimposed on each other without interference.

A key advantage of the MSBSA is the high achievable spot beam gain which allows the use of very low power transmitters for both the base station and the customer premises terminal in each spot beam -- *of the order of 10 milliwatts* -- to achieve broadband communications over distances in excess of 20 km. Significant gain margin exists in each spot beam to compensate for gain loss due to MSBSA feed array blockage and efficiency, and for weather related link fade in most fixed wireless applications at millimeter wavelengths.

Although multiple base station transponder electronics are required to interface to each feed of the MSBSA, these transmitters and LNA's are relatively cost effective low power devices. The system designer can also use beam to beam switching matrices or can combine multiple beams using frequency and/or time domain combining networks at the base station to achieve a variety of versatile high capacity fixed wireless network designs.

The MSBSA is a compact structure that can be mass produced at relatively low cost and is well suited for installation on a monopole support structure. In most applications, the MSBSA will be enclosed in an aesthetically pleasing tuned hydrophobic radome having typical transmission losses of 0.3 dB or less near 40 GHz.

A Biocompatible Antenna for Communication with Implantable Medical Devices

Cynthia Furse*, Ruby Mohan*, Arvind Jakayar*, Sriram Kharidehal*, Brad McCleod**, Shawn Going**

*Department of Electrical and Computer Engineering
**Department of Mechanical and Aerospace Engineering
Utah State University
Logan, Utah 84322-4120
Phone: (435) 797-2870
FAX: (435) 797-3054
Furse@ece.usu.edu

Abstract

Numerous medical devices are implanted in the body such as pacemakers and defibrillators, hormone and drug delivery pumps, and nerve stimulators. With the advancement and miniaturization of bio-electronics it is likely that the array of implantable medical devices will continue to expand in the years to come. Medical implants are intended to stay in the body for many years or decades, and it is often necessary to communicate with the device to download data about the health of the device or its batteries or the health of the patient, or to upload changes in settings or new procedures specified by the doctor. It is even conceivable that the patient could control the setting of his or her medical implant with the touch of a button from a wireless device or that medical data from the patient could be automatically transferred to the hospital over a wired or wireless telephone link.

The design of antennas that can communicate with implantable devices is an interesting and challenging problem. The antenna must be small, low profile and long-term biocompatible, preferably able to be mounted on existing implant hardware or to utilize part of the hardware itself. In previous work, we demonstrated the usefulness of a spiral microstrip antenna that can be mounted flush on the battery pack of a medical device. This paper describes improvements to this design and the use of biocompatible materials for the antenna for long-term implantation in the body. The antennas will be mounted in the chest or hip cavity on the titanium battery pack of the medical implant, which is approximately 1.25x1.25x0.375" in size. This box acts as the ground plane for the microstrip antenna and is in direct contact with the body. Several commercial plastics and silicones are compared for use in the antenna design, as well as an analysis of adhesives for longterm use and the use of titaniums for antenna designs. The antennas are simulated using FDTD software for a realistically implanted case. The input impedance, radiation pattern, gain, and SAR distribution are analyzed, and the antenna design is optimized using genetic algorithms. Prototyping and testing of these designs in homogeneous phantom material is presently underway.

Preliminary designs of the overall communication system are also given. The new medical implant frequency band of 402-405 MHz is used, and commercially available transceiver modules are evaluated for their usefulness in this design. Two types of systems are considered, one that directly transmits data from internal to the body to a receiver 10 meters away, and another that transmits data from the interior to the surface of the body, with an additional transmitter sending data to the receiver 10 meters away. The second type of system is shown to be effective with present technology, and technological advances required to make the first system functional are discussed.

Methods for Optimizing the Location of A Base Station For Indoor Wireless Communications

Zhong Ji*, Tapan K. Sarkar¹ and Bin-Hong Li**

* 121 Link Hall, Department of EECS,
Syracuse University, Syracuse, NY, 13244-1240

E-mail: zji@mailbox.syr.edu, tksarkar@mailbox.syr.edu

** Department of Electronic Engineering

Shanghai Jiao Tong University

1954 HuaShan Road, Shanghai, China 200030

E-mail: bhli@mail1.sjtu.edu.cn

ABSTRACT

When designing wireless communication systems, it is very important to know the best location for the base stations. In this paper, a model has been developed to set up an optimization problem, the solution of which provides the information for the best location of the base station antenna particularly for an indoor environment. Several methods for the optimization of the objective function are presented and the final results compared with each other. Simulation results have been presented to illustrate the application of these methods which can be used in the design and planning of mobile wireless communication systems.

The optimum indoor location of a base station or a transmitter can be posed as a nonlinear programming problem. In this paper, we consider the spatial coordinates of the location of a base station as the variables to be optimized. By making use of a propagation model which involves the parameters for the path loss, an objective function showing the coverage of the system of interest can be thus defined. There are many methods that can be used to solve the nonlinear programming problem. Some of these minimization methods require the information for the derivatives of the objective function, while others do not. The various methods that have been applied in our optimization methodology are Steepest Descent method, BFGS method(Quasi-Newton method), Simplex method, Suplex method, Hooke and Jeeves' method, Rosenbrock's method, Simulated Annealing method and Genetic algorithm. From the simulation results, we compared all these methods. It can be seen that different computation time is required for the optimization process which is a function of the initial guess for the best spatial location. Suitable choice of parameters for some methods such as simulated annealing and the genetic algorithm can reduce the number of evaluations of the objective function. It is seen that methods that make use of the information for the derivatives are not suitable because the objective function is not analytical.

Effects of the Human Head and Handset on Antenna Radiation Patterns: A Simplified Model and Fast Algorithm

Yeqin Huang¹, Ram M. Narayanan¹, and Govind R. Kadambi²

¹ Department of Electrical Engineering, University of Nebraska, Lincoln, NE 68588, USA

² Centurion Wireless Technologies, Inc., Lincoln, NE 68504, USA

Handheld antenna radiation patterns are significantly altered by the presence of the human head, since the handset is generally placed close to a human head. The interaction between the antenna and the head is therefore of great interest for handsets. By modeling head and handset as dielectric bodies of different dielectric constants, a fast algorithm is proposed for pattern computation in the presence of the human head and the handset of various shapes.

Two types of models have been proposed in previous work. One is the canonical model of the human head, such as a homogeneous sphere or a box, while the other is the anatomical model based on CT and MRI images of the human head. For the canonical model, the geometry of the human head is highly simplified and deviates significantly from the actual shape of the head. The anatomical model details the structure of the human head, but it resorts to numerical techniques such as MoM and FDTD. This model is time-consuming in computation and has limited flexibility in accounting for variations in geometry. Most of the efforts are focused on the numerical modeling and computation. Once the model is chosen, the physical geometry of the model cannot be changed.

In this work, we address the combined effects of the presence of the human head and the handset on the antenna radiation patterns. Considering that the typical size of the human head is comparable with the wavelength of the GSM system operating at 900 MHz, the optical thickness of the skull and the penetration depth of the wave are much smaller than the wavelength; hence the far field pattern would be sensitive to the contour of the head but insensitive to the layered structure. The human head and the handset are modeled as homogeneous dielectric bodies of different dielectric constants.

An algorithm is proposed for the computation of radiation patterns of such a system consisting of a handset and the human head. The field representation includes the geometry of the head as an input function; once the geometry is given, the field is derived.

Application of Characteristic Modes to Antenna Placement on Portable Wireless Devices

David A. Stroschein* and Kondagunta Sivaprasad
Department of Electrical and Computer Engineering
University of New Hampshire
Durham, NH 03824

J. T. Bernhard
Electromagnetics Laboratory
Department of Electrical and Computer Engineering
University of Illinois at Urbana-Champaign
Urbana, IL 61801

This work examines the use of characteristic modes as part of an embedded antenna system synthesis paradigm for portable wireless devices operating in the near-resonant range. Systems composed of an antenna mounted in close proximity to a comparably-sized conductive structure cannot be accurately modeled as an antenna in free-space or an antenna against an infinitely large conducting plane. Instead, the antenna and the device are more appropriately treated as two elements of an "antenna system." Characteristic mode information obtained for this system can be used to predict total surface current and ultimately, the far-field radiation pattern. The goal of this work is to develop an improved quantitative understanding of the relationship between antenna position and the effect on the dominant characteristic modes of the antenna system.

The use of characteristic modes to determine far-field radiation has previously been applied to two cases. In one case, the structure of the radiating system is fixed and the feed point is determined to obtain the desired radiation pattern. In the other case, the antenna is so electrically small that its presence does not significantly affect the characteristic modes of the structure upon which the antenna is mounted. The work presented here examines the case where the geometry of the system changes as the antenna moves and the characteristic modes associated with the system distort in response to antenna location. This knowledge will be incorporated into an antenna synthesis approach to determine the antenna position that will result in the approximation of the desired system radiation pattern.

The system under study is composed of an antenna positioned above a rectangular plate. The antenna is a half-wave wavelength dipole and the plate ranges in size from 1×1 wavelength to 2×2 wavelengths. The plate's shape varies from square to rectangular with a maximum length to width ratio of ten. The system operates at 2.45 GHz. The antenna is positioned 0.1" above the plate at numerous locations within the same quadrant of each of the various plates. Characteristic modes of the isolated plate and the antenna are computed and compared with those of the plate and antenna when positioned closed to each other. The characteristic modes are compared for both the isolated components and the combined system. Based on the observed changes to the characteristic modes, a functional relationship between antenna position, characteristic mode shape and plate shape is generated. This relationship is based on the correlation of the system's characteristic mode response and the characteristic modes of the isolated plate and antenna. Results obtained from these test positions are extrapolated so that characteristic mode shape prediction can be applied to a similarly shaped plate and embedded antenna operating in the near-resonant region. This relationship forms the basis for the antenna placement paradigm. Additionally, this work examines the range of validity for such a synthesis paradigm.

Results suggest guidelines for this technique and the useful application range with respect to shape and size of the plate. The paradigm's utility is examined by assessing its application to the synthesis of an antenna system with a prescribed radiation pattern. Results of the designed system simulations and measurements will be presented.

Analysis and Measurements of Compact-Size *DRA* with *CPW*-Feed

M. S. Al Salameh*, Y. M. M. Antar*, G. Seguin*, and A. Petosa*

*On leave from Hashemite University, Zarqa, Jordan

*ECE Dept., Royal Military College of Canada, Kingston, Ont., Canada

*Canadian Space Agency, Saint-Hubert, Quebec, Canada

*Communication Research Center, Ottawa, Ont., Canada

The development of small and cost-effective antennas for mobile communications is essential due to the large number of base-stations and portable sets. Recently, there has been increased interest in dielectric resonator antennas in view of the advantage they offer such as high efficiency, wider band width, and flexibility in terms of fabrication and mode configuration. In this paper, a novel simple and efficient design of a reduced-size dielectric resonator antenna (*DRA*) is presented. This is achieved through the use of half-volume resonator whose plane of symmetry is short-circuited. The proposed design provides a new configuration of planar antenna fed by coplanar waveguide (*CPW*) and a slot configuration.

Use of *CPW* configuration provides advantages such as ease of integration with active devices and flexibility in terms of design parameters for the feed network. The slot width and length are parameters that were optimized for optimum coupling to the required mode.

In this compact antenna, the resonator size is reduced to half its original size for the same operating frequency. Alternatively, the operating frequency is reduced to two-thirds of its original value without increasing the size of the resonator. For example, in one design the operating frequency of the resonator utilized was 4.52 GHz, while the operating frequency of the same resonator when it was short circuited at its plane of symmetry decreased to 3.03 GHz.

The antenna shows good performance in terms of low cross-polarization, matching to the feeding structure, and high front-to-back radiation ratio. The antenna was fabricated and measurements match well with the predicted results.

Key words: Dielectric Resonator Antenna, *CPW*, Compact Antennas

NRD Guide Compatible Pyramidal Horn Antenna for Multiple Access Wireless LAN at 60GHz

Futoshi KUROKI, Atsutoshi TAKADA, and Masanori EGUCHI
 Department of Electrical Engineering, Kure National College of Technology.
 2-2-11 Aga-Minami Kure 737-8506, Japan

Tsukasa YONEYAMA
 Department of Communication Engineering, Tohoku Institute of Technology.
 35-1 Yagiyama-Kasumichou, Taihaku-Ku, Sendai 982-8577, Japan.

Abstract As is well known, it is preferable that radiation patterns of antennas for wireless point to multi-point LAN use are broad in the base station and narrow in the terminal station, respectively. In this paper, a simple technique to control the radiation pattern of the pyramidal horn antenna fed by the NRD guide [1] has been developed at 60GHz. Figure 1(a) shows the structure of the horn antenna with 16mm × 22mm aperture, where the dielectric strip made from teflon, having the height of 2.25mm and the width of 2.5mm, is tapered at truncated end and is inserted into the horn antenna as shown in Fig.(b). In this structure, the phase distribution on the aperture is influenced by the tapered dielectric strip because the dielectric strip acts as a slow wave element similar to dielectric lens. Thus the radiation pattern can be controlled by changing the length L of the dielectric strip inserted into the horn. Figure 2 and 3 show the measured radiation patterns and gains versus the length L. As is obvious, when the length L is set to be 2mm, the narrow pattern with the half-power beam-width of 11° can be obtained because of the good phase distribution on the aperture. On the other hand, when the length L is changed to 8mm, the half-power beam-width is expanded to 40° due to making the dent in equiphase surface on the aperture. We plan to apply the antennas for the terminal and base stations in our multiple access wireless LAN system.

Reference [1] I. Uchida, F. Kuroki, and T. Yoneyama, "Miniaturization of the NRD Guide Transmitter and Receiver at 35GHz". IEICE, C-I, Vol. J76-C-I, No. 7 (1993)

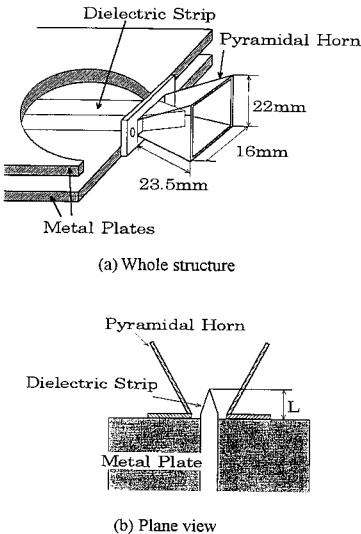


Fig. 1 Pyramidal horn antenna fed by NRD guide

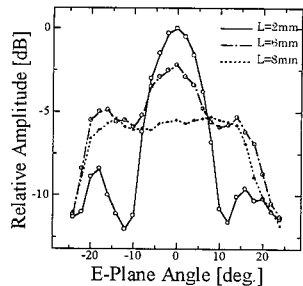


Fig. 2 Measured radiation pattern versus length of dielectric strip inserted into the horn

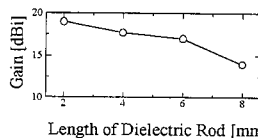


Fig. 3 Measured antenna gain versus length of dielectric strip inserted into the horn

A GSM fully-adaptive antenna system test-bed: uplink trials

G. F. Cazzatello M. Crozzoli D. Disco L. Ferrero
CSELT - Via G. Reiss Romoli, 274 - 10148 Torino, Italy

E-mail: maurizio.crozzoli@cse.lt.it

In recent years, space-time processing is being considered one of the most promising solution to spectral crowding. Adaptive antenna systems, performing such a processing, are expected to help mobile communication companies to face the ever increasing number of wireless subscribers.

First prototypes were multi-beam systems. As a natural evolution, in recent years world-wide reasearch activity is moving towards fully-adaptive systems, made possible by nowadays digital signal processing hardware improvements. In our activity the fully-adaptive concept has been applied to the GSM system, a GSM base station (BTS) was realised and a test-bed has been setup for making trials on it.

The BTS design was devided into three main steps.

- Adaptivity is based on the ability of shaping the beam radiated by an array antenna by controlling its element weights. In order to take advantage of its low-profile and low-cost characteristics, a **microstrip array** was designed (A. P. Ansbro, M. Crozzoli, L. Destro, D. Forigo, R. Vinassa, *A dual-linear polarised microstrip array for fully-adaptive GSM antenna systems*, IEEE AP-S, vol.2, pp. 932-935, Salt Lake City, USA, July 2000).
- A digital wide-band receiver can make many GSM channels available at intermediate frequency at the same time. Working with this kind of equipment, a PCI-bus-based multi-board **hardware architecture** was designed and manufactured for performing digital signal processing: digital down conversion, adaptivity, MLSE equalization. Assembler codes for letting all the devices in the architecture (DDC's and DSP's) work together were developped.
- In order to evaluate the performance of adaptive algorithms applied to the GSM system, a C code was developped implementing a vectorial channel. By exploiting its intrinsic stability and easiness, a **LMS adaptive algorithm** was chosen so as to make real-time processing feasible without using giga-flop processors. An assembler code matched to our hardware architecture was carried out.

A suitable test-bed has been setup for measuring the system performance. Up-link trials are being carried out whose results will be presented.

Smart Antennas at Wireless Mobile Computer Terminals and Mobile Stations

Junwei Lu* and Takashi Ohira

ATR Adaptive Communication Research Laboratories

2-2-2 Hikaridai, Seikacho, Sorakugun, Kyoto, 619-0288 Japan

* Tel. +61 7-3875 5118, e-mail: J.Lu@me.gu.edu.au, Fax: +61 7-3875 5384

Wireless communications have become a significant area of growth within the last decade. The importance of using the smart antenna (or adaptive antenna) in wireless communication systems has been recognized in recent years. However, the application of smart antennas at wireless mobile computing terminals and mobile stations has received little attention, in spite of the significant advances made in this area for military, satellite land mobile communications. Only very few papers mentioned the importance of using smart antenna at mobile computing terminals or mobile stations and discussed the problems, such as the antenna size and weight, integration into an arbitrary mobile computer terminals or mobile stations. In fact, the smart antenna technology for mobile wireless computing terminals or mobile stations is still under developing stage due to several trade-offs and antenna structure constrains associated with the antenna technology. This paper will introduce two newly developed antennas; electronically reactively terminated parasitic elements, ESPAR antenna and electronically switched to parasitic and active elements, ESMB antenna for wireless computer terminals and mobile stations, and the possibility of using these smart antennas at mobile computing terminals and mobile stations. The implementation of smart antenna using ESPAR antenna as a beam-forming antenna, and ESMB antenna as a switched-beam antenna as shown in Fig 1 and Fig. 2, will be discussed in the paper.

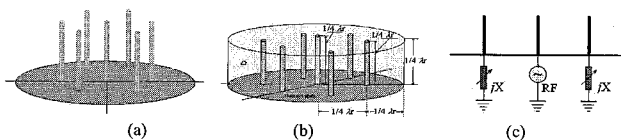


Fig. 1 ESPAR antenna configurations, (a) free space monopole, (b) dielectric embedded monopole for size reduction, (c) beam control circuit of electronically reactively terminated parasitic elements

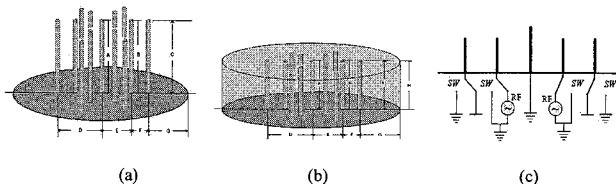


Fig. 2 ESMB antenna configurations, (a) free space monopole, (b) dielectric embedded monopole for size reduction, (c) beam control circuit of electronically switched to parasitic and active elements

Propagation Effects in Satellite & Urban Environments

Chairs: C. Spillard, UK and M. Jensen, USA

	Page
1:00 On the Spectral Properties of Rain Attenuation Dynamics, <i>A.D. Panagopoulos*, G. Fikioris J.D. Kanellopoulos, National Technical University of Athens</i>	226
1:20 A Comparison of Empirical and Physical Models for Attenuation and Depolarization Due to Rain, <i>N. Terri*, F. Hastings, ITT Industries</i>	227
1:40 Calculation of Interface Levels Due to Rain Scatter on a High-Altitude Platform Link, <i>C. Spillard*, J. Thornton, D. Grace, T. Tozer, The University of York</i>	228
2:00 Propagation Effects in a Low Altitude Radio Link for Interactive Services at 2.4GHZ, <i>M. Ozdemir*, F. Retnasothie, C. Lumberas, Philips Broadband Networks, E. Arvas, Syracuse University</i>	229
2:20 Spatio-Temporal Fade Characteristics on a Millimetre-Wave Terrestrial Path, <i>M. Evans*, Radio Science & Propagation Group</i>	230
2:40 Infrared Satellite Communication Comparisons, <i>P. Christopher*, PFC Associates</i>	231
3:00 Direction-of-Arrival Statistics of Urban Propagation Channel at 1.9 GHz Based on Measurement and Ray Tracing, <i>T. Su*, H. Ling, The University of Texas at Austin, H. Foltz, The University of Texas At Pan American</i>	232
3:20 Loss Characteristics in Urban Environment with Different Buildings' Overlay Profiles, <i>N. Blaunstein*, D. Censor, D. Katz, University of the Negev</i>	233
3:40 Design of Microcells for Mobile Communications Using Genetic Algorithms, <i>I. Gonzalez*, J.A. de Prado, F. Saez de Adana, O. Gutierrez, M.F. Catedra, Universidad de Alcala</i>	234
4:00 Performance of the V-BLAST Space-Time Coding Algorithm Using Measured Wireless Channel Characteristics, <i>M. Morris, J. Wallace, M. Jensen*, Brigham Young University</i>	235

On the Spectral Properties of Rain Attenuation Dynamics

A. D. Panagopoulos*, G. Fikioris, and J.D. Kanellopoulos

Division of Electromagnetics, Electrooptics and Electronic Materials
Department of Electrical and Computer Engineering
National Technical University of Athens
9 Iroon Polytechniou Street
GR-15773, Athens-Greece
email: (thpanag, gfiki, ikanell)@cc.ece.ntua.gr

Abstract

The statistics of rain attenuation are important for the design of both terrestrial and earth-satellite radio links using frequencies above 10 GHz. Empirical models for the dynamic characteristics of rain attenuation can be found in the literature (A. Safaai-Jazi, H. Ajaz and W. L. Stutzman, IEEE Trans. on Ant. and Prop., 43, 12, 1995). These are based on propagation experiments yielding rain-attenuation duration data for different frequencies, path lengths and geographical locations. The only stochastic dynamic model of rain attenuation has been proposed by T. Masseng and P. Bakken (IEEE Trans. on Comm., 29, 5, 660-669, 1981). It is based on the lognormal distribution of rain attenuation for long-term statistics and utilizes a memoryless nonlinear device to transform it into a one-dimensional Gaussian stationary Markov process. Maseng and Bakken introduce the dynamic properties of rain attenuation with only one parameter and consider it global for any location and link. In the ACTS Rain Attenuation Prediction Model (R. M. Manning, Int. Jour. of Sat. Commun., 8, 11-30, 1990), the model by Maseng and Bakken is applied for the specific rain attenuation or point rainfall rate. In order to evaluate the rain attenuation dynamics for the whole path, Manning introduced a smoothing procedure after the output of a memoryless nonlinear device, and proposed a two-dimensional Markov model with two parameters for the rain attenuation dynamics. In the present paper, a review of the above models is presented using a systems-oriented approach. Analytical expressions for the power spectrum of the rain attenuation for both cases (as a signal driven by a process with or without aftereffect) are given. Asymptotic expressions for both small and large frequencies are also derived. These are useful for the design of rain-fade compensation algorithms, as they enable one to separate the rain-induced fades from scintillation fades. In addition, some spectral parameters for rain attenuation time series are defined for both models. Their relation to fade duration statistics is finally investigated.

A Comparison of Empirical and Physical Models for Attenuation and Depolarization Due to Rain

Nathan Terril* (nathan.terril@itt.com) and Frank Hastings (fdhastings@uswest.net),
ITT Industries
45145 Research Place
Ashburn, VA 20147

Above about 10 GHz, the effects of rain on earth-space telecommunication systems become important, and these effects become more severe as the frequency increases. Two important effects of rain on a communication signal are attenuation and depolarization. Currently, empirical models are typically used to predict these effects. In particular, the International Telecommunication Union (ITU) provides widely used models for long term predictions of attenuation and depolarization that have been validated with experimental data up to 55 GHz and 35 GHz, respectively. For systems planned outside this frequency regime, the accuracy of these models is uncertain because the models are based on the frequency-localized behavior of the underlying experimental data. The transmission matrix model is based on scattering and absorption by raindrops, and this physical basis provides better accuracy for frequency scaling. However, the overall accuracy of this model depends on the knowledge of the physical characteristics of the rainstorm, such as rain rate, drop size distribution, drop canting angles, and rain rate profiles. Various models have been recommended for the average behavior of these physical quantities, but it is unclear as to how these models translate into overall performance of the transmission matrix.

In this paper, selected formulations of the transmission matrix model will be compared with the current ITU models for a range of frequencies. The measurement parameters will include co-polar attenuation and cross-polarization discrimination computed for a particular set of geographic regions, system availabilities, and elevation angles. The comparison will be made over a frequency range from 10-100 GHz, thereby showing the relative agreement between the two types of models both inside and outside the frequency range where the ITU models have been validated. The selected transmission matrix formulations will consist of combinations of different models for the rainstorm characteristics. Particular attention will be given to the effects of choosing different rain rate profiles and drop size distributions. Where possible, comparison with experimental data will be used to show the relative error associated with each type of model.

This comparison study has several purposes. It examines the dependence of the transmission matrix model's performance on its underlying physical models. It provides a case study that shows a limited sampling of the performance of the transmission matrix model relative to the widely used empirical models. It compares the frequency scaling behavior of the empirical and physical models over a wide range of frequencies.

Calculation of Interference Levels due to Rain Scatter on a High-Altitude Platform Link

Candida Spillard* John Thornton David Grace
 Tim Tozer
The University of York, Heslington, York YO10 5DD, U.K.
email: cls9@ohm.york.ac.uk, fax +44 1904 433224

The trend towards services requiring higher bandwidth, and reaching an increasing number of users, is resulting in operators having to consider the use of higher frequencies. The consequent transition from microwave to millimetre-wave operation affects the choice of link geometry, in that line-of-sight conditions are necessary, and rain attenuation and scattering have to be considered.

Recent advances in the technologies of solar panels, fuel cells and lightweight materials have generated a lot of interest in the potential use of High-Altitude Platforms (HAPs) in fields such as telecommunications. HAPs have the advantage over satellites of being cheaper to build and operate as well as having more favourable link budgets, and the advantage over terrestrial masts of guaranteeing line-of-sight propagation and being easier and more flexible to deploy.

HeliNet is a project supported by the European Union, involving 10 industrial and academic partners from 6 European countries in research into all aspects of HAP technology, from a feasibility study into the use of HAPs in southern Europe in telecommunications, traffic monitoring and remote sensing to the construction of a prototype. The University of York is responsible for assessing the potential of HAPs to support broadband services, and for propagation studies.

The presentation will explore the effect of bistatic scatter due to rain on co-channel interference within an array of spot-beams forming a cellular configuration on the ground.

For reasons discussed elsewhere by the authors (Spillard et al, International Conference on Antennas and Propagation ICAP01, Manchester, April 2001), the bistatic Radar Equation can be applied, with the scattering cross-section per unit volume of rain given by the product of the number of drops with radii between r and $r + dr$, and the differential scattering cross-section of one such drop, summed over all r . Circular polarisation is modelled as the sum of 2 orthogonal linear polarisations.

The smallest raindrops radiate like small dipoles and have the Rayleigh scattering cross-section. Rayleigh cross-sections for large ($r = 0.35\text{mm}$) drops were compared with those obtained by Morrisson and Cross (The Bell System Technical Journal, July 1974) using extensive calculations based on the method of Oguchi, and found to be accurate to within 20%. The choice of raindrop size distribution (DSD) was found to have a dramatic effect on the predicted scattered power. The DSD developed by Levin (C. Cerro et al. J. Appl. Meteorol. vol. 36, 1997) for Mediterranean conditions gave some three times the scattered power than the Marshall and Palmer DSD (J.S. Marshall and W.McK. Palmer, J. Meteorology, August 1948). The effects on system design will now be considered.

The quality of service requirements for the type of service being offered from a HAP specify a Bit Error Rate (BER) of 10^{-9} . This corresponds to a required CINR of at least 30.8dB to support a 64QAM channel, whereas a lower data-rate, but more robust, 50% coded Reed Solomon QPSK channel requires a CINR of only 10.8dB. Assuming that interference and noise give roughly equal contributions, the required CIR due to interference alone should be double the above figures, ie 33.8dB and 13.8dB respectively.

Results from simulations of rain events of the kind found in Southern Europe on 48GHz links with antenna beamwidths of 5° and cell diameter 7 km show that a 42mm/hr rain event, such as might be exceeded for 0.01% of the time in the Mediterranean region, can reduce the CIR to 25dB. This figure is further reduced by clear air interference caused by the sidelobes of the HAP antennas. Further simulations have shown that below a critical ground antenna beamwidth, sidelobe levels are the main design factor affecting interference due to rain scatter. Above that beamwidth, rain scatters energy into the ground station main beam and rain events of as little as 10mm/hr, such as are exceeded for 0.1% of the time, can cause a critical reduction in CIR.

Thus, moderately heavy rainfall may affect less robust modulation schemes and require the system to switch to a lower data-rate, but more robust, scheme.

PROPAGATION EFFECTS IN A LOW ALTITUDE RADIO LINK FOR INTERACTIVE SERVICES AT 2.4GHZ

Mehmet Kemal Ozdemir[†], Francis Retnasothie, Christina Lumbreras, and Ercument Arvas[‡]
 Philips Broadband Networks, 100 Fairground Dr. Manlius, NY 13104, Tlf:(315) 682915
[†]Syracuse University, 121 Link Hall, Syracuse, NY 13244, Tlf:(315) 4431319, Fax:(315) 4434441
 email : kemal.ozdemir@philips.com, francis.retnasothie@philips.com,
christina.lumbreras@philips.com, earvas@svr.edu

Abstract: Resurgence of radio wave propagation is widely experienced in the infocomm industry for its inherent advantages (low infrastructure costs and mobility) over wired media. Every possible segment of the unused radio spectrum is being exploited. Recently the use of the unlicensed 2.4 GHz band has been very popular. This project proposes a cost-effective alternative for internet and other interactive services over a low altitude radio link. An omnidirectional transmit antenna is placed at the edge of an infocomm network, normally a fiber optic node at a fixed height of 30 ft above the ground. Highly directional receive antennas, placed from 10 to 200 ft above the ground, permit reception to single and multiple dwellings. Effects of buildings, trees of various types and foliage, and other obtrusive objects are investigated through extensive lab and field experiments. Empirical data are analyzed. In one such experiment, the transmit antenna with a gain of 8.6 dBi is placed on the edge of the roof of a 40-foot building. The transmitted power level is 22.7 dBm*. The receive antenna with a gain of 24 dBi is placed at a predefined location to establish the baseline measurement (LOS). The receive antenna is then moved to various locations to study the effects of trees. A similar experiment with the highly directive antenna being the transmitter and the omnidirectional antenna being the receiver is also performed to establish the base for interactive services. Additional experiments were performed for different environmental conditions including rain, snow, and for trees with no foliage. Table below represents a partial listing of measured data obtained on a sunny, dry fall day with trees having full foliage. The expected power level for the 8th, 9th, and 10th row is calculated assuming no obtrusive objects since the attenuation for foliage is not described well enough. Based on these results, it is concluded that the proposed system can provide wireless interactive services to a cell of 1-mile radius, with a receiver sensitivity of -84 dBm, with a margin of 10.3 dBm.

	Distance (mile)	Obtrusive objects	Received Power Level (dBm)	Expected Power Level (dBm)
1	0.100	None (LOS)	-34.0	-31.0
2	0.160	1 tree	-43.0	-45.0
3	0.160	1 small tree	-39.0	-45.0
4	0.120	2 trees	-44.0	-53.0
5	0.120	4 trees, not completely	-45.0	-73.0
6	0.170	1 pine tree completely	-56.0	-46.0
7	0.200	a 4-story building	-50.0	-47.0
8	0.375	Foliage	-59.0	-43.6
9	0.300	A house and foliage	-67.0	-41.4
10	1.000	Foliage	-81.0	-52.2
11	1.000	None (LOS)	-62.0	-52.2

* Maximum transmit power allowed is 30dBm according to FCC regulations.

SPATIO-TEMPORAL FADE CHARACTERISTICS ON A MILLIMETRE-WAVE TERRESTRIAL PATH

M Evans

Radio Science and Propagation Group,
D701, DERA Malvern, St. Andrews Road,
Malvern, Worcestershire WR14 3PS, UK
Tel. 01684 896487, Fax 01684 895241
E-mail: markevans@dera.gov.uk

Abstract:

Introduction: As interest in terrestrial broadband systems for applications such as interactive digital television and multimedia services continues to grow, the millimetre-wave (30-300 GHz) part of the electromagnetic spectrum is actively being considered as an alternative to the congested microwave region of the spectrum. To date, research into millimetre wave propagation has mainly concentrated on earth-space links. As a result, much less is known about the spatio-temporal characteristics of the terrestrial propagation channel at such frequencies, especially for medium to long links e.g. greater than 15km.

Experiment: A measurement campaign was conducted in Worcestershire, UK, over a period of 22 days during May and June 2000. The experiment was performed at 36 GHz (CW) over a 17.3km path. The transmitter (3° beam-width, 34dBi gain) was located at an elevation of 211m. A 3-element receive array (same antenna specification as for the transmitter) was located at an elevation of 90m. Meteorological instrumentation was based at the link mid-point and at the receiver.

Results: The data collected identified ground-based layers (fog) as significant propagation impairments. Long-term signal fading (periods of hours), multipath fading (>18dB) and scintillation events of 9dB lasting periods of a few minutes were observed. Fade statistics comprising of the cumulative distributions of fade duration, interval and slope were calculated. Figure 1 shows an example of a sub-set (4 days) of fade duration data at 5 fade depths (the key in Figure 1 corresponds to the top-

down order of fade depth curve e.g. -21dB is the top curve etc) below an average received level. Generally it can be seen that as the fade depth increases the percentage of time the fade is likely to last increases.

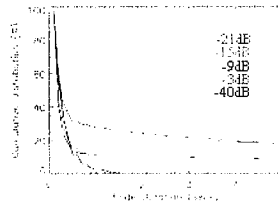


Figure 1: Fade duration distributions

Spatial analysis of the scintillation events observed at antenna separation distances of 3m, 5m and 8m were compared with the theoretical curve of Tatarski (Figure 2).

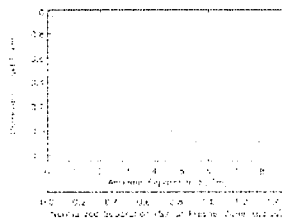


Figure 2: Scintillation decorrelation

It can be seen that the measured values show good agreement with the theory (except at small separation distances), and that small-scale spatial diversity could prove a useful technique in mitigating the effects of scintillation.

This paper will present the results from the experiment discussed and outline the design of the measuring instrument used.

Infrared Satellite Communication Comparisons

Paul Christopher
PFC Associates
Leesburg, VA 20175
703-777-3239
pfchristop@aol.com

The Foundation Ugo Bordone has shown valuable worldwide zenith attenuation maps for severe but non-rainy conditions (Barbaliscia *et al*, Ka conference, Sorrento Italy, 1998). They referred to a number of their most useful maps as '99% non rainy' conditions. Recent 22.2 and 49 GHz millimeter wave attenuation maps from the Foundation Ugo Bordone are shown. They have been useful for deriving general attenuation maps for a wide range of frequencies from 10 to 100 GHz (Christopher, Ka Conference, Taormina Sicily, 1999). Attenuation versus frequency is shown for interesting locations, and optimum frequency maps are shown for wide areas of the earth. The temperate zones emphasize the 40 to 47 GHz and 90 to 95 GHz regions.

Cloud cover maps are then derived from Barbaliscia's millimeter wave attenuation maps. They are applied to infrared satellite to ground links, with the aid of Chu and Hogg's classic results, to estimate link attenuation. The severe 99% cloud cover is seen to cause very severe 10 micron attenuation over most interesting communication areas. However, Barbaliscia also indicated probability density functions for attenuation in Europe: When applied worldwide, the 80 to 90% non-rainy attenuation maps indicate only 20 dB zenith attenuation over key communication areas to the north of 44° N. Infrared links are compared with millimeter wave attenuation and shown to offer clearly higher attenuation in many areas of the earth. However, when the gain at constant aperture size is included, 10 micron infrared links appear to be competitive with millimeter wave links in large areas of the Northern Temperate zone. Large areas of the Rocky Mountain States are suggested to be attractive for 10 micron links if site diversity is available. The state of Maine is also indicated to be attractive. The 10 micron infrared links are shown to offer much larger service areas than one micron links, while retaining the advantages of optical links over millimeter wave links.

Infrared links would need special care in the choice of satellite orbits. Inclined elliptic orbits are shown to keep elevation angles high and path loss relatively low for infrared links. A constellation of 5 satellites would be especially attractive for key parts of the Northern Hemisphere.

Direction-of-Arrival Statistics of Urban Propagation Channel at 1.9 GHz Based on Measurement and Ray Tracing

Tao Su* and Hao Ling
Department of Electrical and Computer Engineering
The University of Texas at Austin
Austin, TX 78712, USA

Heinrich Foltz
Department of Electrical and Computer Engineering
The University of Texas at Pan American
Edinburg, TX 78539, USA

In the evaluation of diversity antenna performance for mobile handsets in a multipath environment, it is desirable to know how the energy distribution of the incoming signal is clustered in angle. In this work, we present the direction-of-arrival (DOA) statistics in a typical urban environment extracted from both measurement data and ray tracing simulation.

The measurement data came from a 1997 data collection in Austin, Texas. During the collection, the transmitter was mounted on an 18-m tower in the center of the city. A single mobile receiver was moved along the streets in a car and the received signal strength was recorded as a function of time. We employ a synthetic aperture technique to extract the DOA information. The collected data in time is first re-sampled uniformly in space based on the recorded vehicle speed. The superresolution algorithm ESPRIT is then used to estimate the incident angles from the collected data within a short distance. Since the synthetic array is a linear array, there is a 180° ambiguity in the DOA estimation. For the simulation, we use the ray tracing code Cpatch to simulate the propagation channel based on a CAD model of the Austin downtown. At each receiver position, the DOA and strength of each ray are computed directly from the ray-tracing code.

The statistics of the DOA characteristics are generated from both sets of data. At every location in the city, the DOA angles are first averaged within a window of 20 wavelengths. The following four quantities are then extracted: the number of incoming DOA, the normalized amplitude of each incoming signal, the mean direction of the incoming signals, and the standard deviation in angle of the incoming signals. The statistics of the above four quantities are then tabulated over the entire city. Since the measurement data contains the 180° ambiguity, we first enforce the same ambiguity on the simulation data in order to compare the two results. The DOA statistics from the measurement and the simulation data are found to correlate well. Results for the simulation data without the angular ambiguity are then generated and will be presented. The impact of the clustering of DOA on diversity antenna performance will also be discussed.

LOSS CHARACTERISTICS IN URBAN ENVIRONMENT WITH DIFFERENT BUILDINGS' OVERLAY PROFILES

N. Blaunstein, D. Katz, and D. Censor

Department of Electrical and Computer Engineering, Ben-Gurion
University of the Negev, P. O. Box 653, Beer Sheva 84105, Israel

ABSTRACT

The prediction of propagation characteristics has become an essential part of radio wireless networks planning. To successfully predict the design of these local networks, detailed experiments and theoretical investigations have been carried out to examine wide band radio channel characteristics and their dependence on the various real urban environment parameters. In reality many towns and cities sprawl over irregular terrain and one needs to simultaneously account for the presence of rough terrain and obstructing buildings in the propagating model. In such a situation it cannot be proposed some general theoretical model to predict loss characteristics in the urban scene. Each concrete model describes a special situation in urban propagation channel [1, 2]. In this work we continue the analysis of a probabilistic approach and the corresponding stochastic multiparametric model of wave propagation in built-up areas with randomly distributed buildings [2-5]. We improve existing multiparametric model by taking into account the real buildings' overlay profile concentrating on its influence on signal decay within the UHF/X-band urban propagation channels. Using different buildings' overlay profiles, the field intensity attenuation is examined taking into account single scattering and multiple scattering phenomena, and diffraction from buildings' corners and rooftops, for various positions of receiver and transmitter antenna with respect to surrounding obstacles. We present a comparison between the theoretical prediction and the results of experiments carried out in urban areas with non-regularly distributed buildings.

REFERENCES

- [1] H. L. Bertoni, *Radio Propagation in Modern Wireless Systems*, Prentice Hall PTR, NJ, 2000.
- [2] N. Blaunstein, *Radio Propagation in Cellular Networks*, Artech House Books, Boston-London, 1999.
- [3] N. G. A. Ponomarev, A. N. Kulikov, and E. D. Telpukhovskiy, *Propagation of Ultra-Short waves in Urban Environments*, Rasko, Tomsk, USSR, 1991.
- [4] N. Blaunstein, "Prediction of cellular characteristics for various urban environments", *IEEE Antennas Propagat. Magazine*, vol. 41, pp. 135-145, Dec. 1999.
- [5] N. Blaunstein and M. Levin, "Parametric model of UHF/L-wave propagation in city with randomly distributed buildings", *Proc. of IEEE Antennas and Propagat. Society/URSI Int. Symp.*, Atlanta, Georgia, June 21-26, 1998, vol.3, pp. 1684-1687.

DESIGN OF MICROCELLS FOR MOBILE COMMUNICATIONS USING GENETIC ALGORITHMS

I. González, J. A. de Prado, F. Saez de Adana, O. Gutiérrez, M.F. Cátedra

*Dept. Teoría de la Señal y Comunicaciones
Escuela Politécnica, Universidad de Alcalá
28806 Alcalá de Henares. Madrid. Spain
Fax: +34 91 885 6699. E-mail: felipe.catedra@uah.es*

This communication presents a method based on Genetic Algorithms (GA) to design microcells for mobile communications. To resolve the electromagnetic analysis, FASPRO code has been used. FASPRO is a full 3D GTD-based code that calculates the propagation in urban environments, considering the possible first and second order reflections and diffractions on every building of the urban environment and on the ground. FASPRO has been probed in several urban environments achieving very good results.

For every microcell there will be two zones: inner zone where the coverage will be maximized and the outer zone, where the coverage will be minimized to reduce the interference between the adjacent cells. At the moment, the parameters to be optimized of every microcell are relative to the antenna: acimut, elevation and position. Associated to the antenna, there will be a valid area (3D cube) where the antenna will be placed.

The Genetic Algorithms (GA) will be used to find these optimum parameters. The two zones will be discretized obtaining observation points where the electromagnetic field will be calculated using FASPRO code. The best solution will be chosen at the end of the process having into account the level of the received power in every observation point of the two zones: observation points inside the inner zone with a power level greater than the threshold power fixed will contribute positively to this election, but observation points inside the outer zone with a power greater than the threshold will contribute negatively.

This method has been tested in a microcell of Madrid obtaining good results.

Performance of the V-BLAST Space-Time Coding Algorithm using Measured Wireless Channel Characteristics

Matthew L. Morris, Jon W. Wallace, and Michael A. Jensen*
Department of Electrical and Computer Engineering
Brigham Young University
Provo, UT 84602

Recent years have witnessed an unprecedented growth in the area of wireless communications, with applications ranging from cellular phone technology to wireless networking. The resulting demand for increased communications bandwidth has motivated a search for new techniques that more efficiently exploit the available bandwidth. Recent research has demonstrated that the multiple-input-multiple-output (MIMO) channel exhibits a substantial increase in capacity over the single-input-single-output (SISO) channel when multipath propagation occurs. A variety of space-time coding schemes have emerged to exploit this increased capacity, the most widely known of which is perhaps the Bell Laboratories V-BLAST algorithm (G. Golden et al, *Electronic Letters*, 35, 14-15, 1999). However, most coding development and performance assessment is based upon simplified analytical channel models coupled with independent signal statistics for each antenna. Since the spatial characteristics of the indoor and outdoor wireless channel is not well understood, the performance of such algorithms in realistic channels remains uncertain.

In this paper, we summarize the performance of the V-BLAST algorithm using a realistic description of the wireless MIMO channel. To accomplish this investigation, we have constructed a measurement platform capable of capturing the channel transfer matrix (\mathbf{H}) for MIMO wireless channels with up to 16 transmit and receive antennas. Data has been taken in a variety of indoor environments and using a number of different antenna array geometries at a center frequency of 2.45 GHz. The resulting measured \mathbf{H} matrices are applied to simulations of the V-BLAST scheme to assess bit error rate (BER) versus SNR for different modulation formats and different symbol rates. The results from this study are compared with those obtained from Monte Carlo simulations using two different types of \mathbf{H} matrices: 1) matrices whose elements are independent identically distributed complex Gaussian random variables, and 2) matrices whose elements are jointly distributed complex Gaussian random variables with a spatial correlation matrix as computed from Jake's classic model.

The presentation will highlight the measurement platform used to obtain the data as well as the simulation procedure for estimating the V-BLAST performance. A wide variety of results will be presented to provide a comprehensive illustration of the behavior of such this and other similar algorithms in true indoor propagation environments.

Rough Surfaces and Random Media

Chairs: A. Ishimaru, USA and G. Whitman, USA

	Page
1:00 Applications of the Unified Full Wave Approach to Backscatter Cross Sections of Two-Scale Pierson-Moskowitz Type Random Rough Surfaces, <i>P. Crittenden*, E. Bahar, University of Nebraska</i>	238
1:20 An Improved Small-Contrast Perturbation Theory for the Coherent and Incoherent Scattering of X-Rays from a Randomly Rough Metal Surface, <i>T.A. Leskova*, A.A. Maradudin, University of California - Irvine</i>	239
1:40 2nd Order Statistical EFIE ("S"-EFIE) for Object in the Presence of a "Smooth" Rough Surface, <i>A. Ishimaru*, Y. Kuga, S-W Lee, J.D. Rockway, University of Washington</i>	240
2:00 Small-Slope Approximation and a Two-Scale Model, <i>A. Voronovich*, NOAA/Environmental Technology Laboratory</i>	241
2:20 Fast and Accurate Prediction of Scattering from Randomly Rough Ocean-Like Dielectric Surfaces via the Multi-Grid Method, <i>H. Ku*, R. Awadallah, The Johns Hopkins University</i>	242
2:40 Validity of Asymptotic Models to Simulate L-Band Scattering Over Sea Surface, <i>N. Floury, G. Crone, G. Toso* European Space Agency-ESA ESTEC</i>	243
3:00 An Improved Method for Determination of Rough Surface Immittance at Very Low Grazing Angles at Microwave Frequencies, <i>R.M. Jha*, R. Janaswamy, Naval Postgraduate School</i>	244
3:20 Beam-Wave Propagation and Scattering in a Random Medium Half-Space for an Incident Diverging Beam-Wave Using Radiative Transfer Theory, <i>G. Whitman*, New Jersey Institute of Technology, F. Schwering, US Army/CECOM, M. Wu, New Jersey Institute of Technology</i>	245
3:40 MLFMA Analysis of Scattering from a Three-Dimensional Rough Dielectric Surface Embedded in an Infinite Dielectric Half Space, <i>Z. Liu*, L. Carin, Duke University</i>	246
4:00 Reference-Wave Solutions for the High-Frequency Fields in Random Media, <i>R. Mazar* A. Bronshtein, Ben-Gurion, University of Negev</i>	247
4:20 A Time Domain Signature Investigation for the GPR Detection of Plastic Land Mines Buried in Soils, <i>A. J. Dumanian*, C. M. Rappaport, A. Morgenthaler, Northeastern University</i>	248

Applications of the unified full wave approach to backscatter cross sections of two-scale Pierson-Moskowitz type random rough surfaces

Paul E. Crittenden

Department of Mathematics, University of Nebraska
Lincoln, NE 68588-0323

Ezekiel Bahar

Electrical Engineering Dept., University of Nebraska
Lincoln, NE 68588-0511

The unified full wave solution is applied to one-dimensional random rough surfaces characterized by surface height spectral density functions, W_T , that are superpositions of two Pierson-Moskowitz type spectra.

$$\begin{aligned} W_T(k) &= \frac{B_1|k|^5}{\pi(k^2 + \kappa_1^2)^4} + \frac{B_2|k|^5}{\pi(k^2 + \kappa_2^2)^4} \\ &\equiv W_1(k) + W_2(k) \end{aligned} \quad (1)$$

where $\kappa_2 > \kappa_1$ and B_1 and B_2 are physical parameters related to the mean square height. Pierson-Moskowitz spectra are frequently used to model the sea surface. To evaluate the backscatter cross sections, the decomposition of the rough sea surface into smaller and larger scale rough surfaces, W_s and W_ℓ , is not restricted by the small perturbation limitations ($\beta = 4k_0^2 < h_s^2 > \ll 1$) when the unified full wave approach is used. Thus the mean square height of the smaller scale surface, $< h_s^2 >$, is not restricted to very small values. Using the unified full wave approach, the radar cross sections are obtained by regarding the rough surfaces as ensembles of arbitrarily oriented patches of smaller scale surfaces that ride upon the larger scale surface. Thus the rough surface radar cross sections are expressed as weighted sums of two cross sections. The smaller scale surface contribution to the radar cross section is given by the original full wave solution modulated by the slopes of the larger scale surface. The larger scale surface contribution to the radar cross section is the weighted (down) physical optics solution. Consistent with energy conservation, the larger scale surface contribution is multiplied by the magnitude squared of the characteristic function of the smaller scale surface. In the small slope limit, the total surface is regarded as the small scale surface, thus $W_s = W_T$. In the high frequency limit, the total rough surface is regarded as a large scale surface, thus $W_\ell = W_T$. For the intermediate case it is assumed that $W_s(k) = \frac{(B_1+B_2)|k|^5}{\pi(k^2+\kappa_1^2)^4}$ where $W_s \leq W_T$ for all k . It is shown that the full wave solutions are stationary over a wide range of small scale mean square heights associated with κ_s .

An Improved Small-Contrast Perturbation Theory for the Coherent and Incoherent Scattering of X-Rays from a Randomly Rough Metal Surface

T. A. Leskova and A.A. Maradudin

Department of Physics and Astronomy, and Institute for Surface and Interface Science, University of California, Irvine, California 92697, USA

The coherent and incoherent scattering of x-rays from a two-dimensional, randomly rough, metal surface are calculated on the basis of an improved version of small-contrast perturbation theory (Waves in Random Media, **7**, 395-434 (1997); **9**, 461-462 (1999)). In this approach the reflectivity of x-rays of frequency ω and polarization $\alpha (= p, s)$ is calculated on the basis of self-energy perturbation theory as a function of the angle of incidence θ_0 from

$$R_\alpha(\theta_0) = \left| \frac{\kappa_\alpha(\omega) \cos \theta_0 - [\epsilon(\omega) - \sin^2 \theta_0]^{1/2} + i(c/\omega)\kappa_\alpha(\omega)M_\alpha(\theta_0, \omega)}{\kappa_\alpha(\omega) \cos \theta_0 + [\epsilon(\omega) - \sin^2 \theta_0]^{1/2} - i(c/\omega)\kappa_\alpha(\omega)M_\alpha(\theta_0, \omega)} \right|^2,$$

where $\epsilon(\omega)$ is the dielectric function of the metal, $\kappa_p(\omega) = \epsilon(\omega)$, $\kappa_s(\omega) = 1$, and $M_\alpha(\theta_0, \omega)$ is a proper self-energy. In the present treatment the self-energy for each polarization of the x-rays is expanded not in powers of the surface profile function of the random surface, but in powers of the dielectric contrast $\eta(\omega) = 1 - \epsilon(\omega)$, which lies in the range $10^{-6} - 10^{-3}$. The first two terms in the expansion of the self-energy in powers of η , of zeroth and second order in $\eta(\omega)$, are obtained. The coefficient of each power of $\eta(\omega)$ contains terms of all orders in the surface profile function. The reducible vertex function that enters the expression for the contribution to the mean differential reflection coefficient from the x-rays scattered incoherently is calculated as an expansion in powers of $\eta(\omega)$ through terms of fourth order. Again, the coefficient of each power of $\eta(\omega)$ contains terms of all orders in the surface profile function. In the numerical calculations based on these results the surface profile function is assumed to be a zero-mean, stationary, isotropic Gaussian random process with a Gaussian surface height autocorrelation function. From the results of these calculations the roughness induced shift of the critical angle for total internal reflection and the Yoneda peaks are obtained and studied as functions of the parameters characterizing the surface roughness.

2nd order Statistical EFIE (“S”-EFIE) for object in the presence of a “smooth” rough surface.

A. Ishimaru*, Y. Kuga, S-W Lee and J.D. Rockway

*Department of Electrical Engineering
University of Washington, Box 352500
Tel (206) 543-0478, Fax(206) 543-6185
Seattle, Washington 98195-2500
Email: ishimaru@ee.washington.edu*

In electromagnetics, the Green's function provides the propagation mechanism by which objects interact and scatter. Recently we have investigated several properties of a rough surface Green's function that is applicable to rough surfaces with small rms heights. We now focus on the response of a radiating object within the presence of the rough surface. The description of the scattering process will be provided by the stochastic Green's function. Several approximations are made to develop an electric field integral equation (EFIE) to calculate the coherent and incoherent fields. The stochastic EFIE is described in terms of a 1st order EFIE for the coherent current produced on the object and the 2nd order EFIE for the incoherent or fluctuating current distribution. In a previous conference paper, given at AP-S (Salt Lake City, Utah '00), a solution to the 1st order EFIE was determined and presented. In this conference paper we focus on the 2nd order EFIE to obtain a description of the fluctuating current distribution. The fluctuating current distribution will be used to produce an error/tolerant analysis of the object's current distribution near the rough surface. To examine this problem in detail, we consider the current distributions produced on a square cylinder located above a conducting rough surface with small rms heights excited by a plane wave for TM case. Various rms heights will be examined to determine the response of the current's fluctuation to rough surface height.

Small-slope approximation and a two-scale model

Alexander G. Voronovich

NOAA/Environmental Technology Laboratory
325 Broadway, Boulder, CO 80305-3328
Phone: 303-497-6464; E-mail alexander.voronovich@noaa.gov

Two-scale model is widely used for theoretical interpretation of experimental data. It is based on separation of surface roughness spectrum into small- and large scale components according to a scale-dividing parameter k_d . This parameter is not defined uniquely, and different authors' choice varies from $k_d = K / 1.5$ to $k_d = K / 30$ where $K = \omega / c$. This ambiguity adds up to the uncertainty in theoretical estimates. Calculations show also that for scattering from rough sea-surface in the dependencies of backscattering cross-sections on incidence angle there exist a "gap" in the range of 20-30 deg where two-scale model is not applicable at all. Another drawback of a two-scale model is that not being a systematic expansion it does not allow to calculate corrections to it. Hence, the accuracy of calculations can not be estimated.

On the other hand, the results provided by two-scale model are intuitively appealing and have clear physical meaning. Rough surface is represented as a set of locally-plane tilted facets. Backscattering is due to Bragg scattering mechanism at each facet, and contributions from different facets are summed up incoherently. Tilt of each facet is determined by a long-wave component of roughness (undulating surface) and it varies from facet to facet. Tilt modulation affects backscattering cross-section in different ways. *First*, the value of appropriate Bragg wavenumber changes. *Second*, backscattering coefficient changes due to variations of local incidence angle at different facets. *Third*, in the case of vector fields such as electromagnetic waves, polarization states of both incident and scattered field for different facets is also different. Calculations according to two-scale model take into account all these effects.

On the other hand, small-slope approximation (SSA) represents systematic expansion in terms of roughness slope. Hence, in a "perfect" two-scale situation SSA has to account for all tilt-modulation effects. It was already demonstrated that the effect of modulation of local Bragg number is taken into account by SSA of the lowest order, however two other mentioned above effects are not. It will be demonstrated that the second-order of SSA correctly takes into account all three tilt-modulation effects.

Fast and Accurate Prediction of Scattering from Randomly Rough Ocean-Like Dielectric Surfaces via the Multi-grid Method

Hwar C. Ku* and Ra'id S. Awadallah
The Johns Hopkins University
Applied Physics Laboratory
11100 Johns Hopkins Road
Laurel, MD 20723

A multi-grid method is presented for direct numerical simulation of radar scattering from 1-D randomly rough dielectric surfaces. A pair of coupled integral equations governing the surface electric and magnetic currents induced by a tapered incident field is set up and converted to a matrix system via the method of moments (MoM). Since the ocean surface consists of various wave scales ranging from long gravity waves to short capillary waves, the faithful representation of such a surface as a set of discrete points mandates a sampling interval equal to half of the shortest ocean wavelength according to the Nyquist criterion. This results in a large number of surface-current unknowns, which grows as the radar footprint gets larger, i.e. for near-grazing incidence. A problem size of $O(10^4)$ is typical for X band frequencies. The multi-grid method iteratively solves the resulting matrix system while smoothing the various spatial frequencies of the iteration error on separate grids resulting in accelerated convergence. The CPU time used by the multi-grid method increases significantly as the problem size increases.

To enhance the computational efficiency of the multi-grid method, an innovative approach, combining the desired features of parallel (multiple processor) computing and the Johnson-Chou spectral acceleration algorithm ("A Novel Acceleration Algorithm for the Computation of Scattering from Rough Surfaces with the Forward-Backward Method," *Radio Science*, 33, 1998), is proposed. Numerical simulations showed that this approach marks down the CPU time by a factor $O(10^2)$. Parallel computing is used for the most CPU time consuming operations of the scattering code, while the spectral acceleration algorithm is used to expedite the most time consuming operation of the iterative procedure, namely the matrix-vector product operation. The number of operations required by the accelerated matrix-vector product is $O(N)$ compared to the $O(N^2)$ operations required by the original multi-grid method. Rough surface scattering results at X and Ka bands for various angles of incidence will be presented to demonstrate the versatility of the proposed approach.

**Validity of asymptotic models to simulate
L-band scattering over sea surface**

N. Flourey[#], G. Crone[§], G. Toso^{§*}

Electromagnetic Division, Wave Interaction & Propagation Section TOS-EEP
European Space Agency, ESA ESTEC
Postbus 299-2200 AG Noordwijk, The Netherlands
Tel: +31-71-5653581; Fax: +31-71-5654999; Email: Nicolas.Flourey@esa.int

§ Electromagnetic Division, Antenna Section TOS-EEA
European Space Agency, ESA ESTEC
Postbus 299-2200 AG Noordwijk, The Netherlands
Tel: +31-71-5654478; Fax: +31-71-5654999; Email: Giovanni.Toso@esa.int

The development of microwave altimetry and of wind-speed measurement from space has generated a strong need for modelling the interaction of microwaves with the sea surface. These studies were most of the time dedicated to frequencies above C-band; the choice of electromagnetic models and sea surface descriptions being somehow subsequently biased.

New potential applications of microwaves over oceans involve lower frequencies such as L-band, both for active (use of reflected GNSS signals for scatterometry and altimetry) and passive (extraction of ocean salinity from radiometric products) measurements. These applications require a thorough understanding of the interaction mechanisms between the electromagnetic wave and the sea surface. However, it is still unknown how well classical models can be applied to these lower frequencies.

As measurements at L-band are still scarce, a first step is to compare the predictions of asymptotic interaction models, such as PO or two-scale models (A. Ishimaru, *Wave propagation and scattering in random media*, Academic Press, 1978), to the results of a full-wave approach, such as the moment method (M. Saillard and G. Toso, *Radio Sci.*, 4, 1347-1359, 1997). This enables 1) an assessment of the validity range of the asymptotic models at L-band, 2) the derivation of a new parameterisation of these models for optimal use and 3) the study of the interaction mechanisms and the derivation of the main contributors to the measured signal.

The scattering predictions of the classical two-scale approach (SPM + Kirchhoff) are compared to those predicted by the full-wave moment method for the same sea state description (i.e. sea spectrum) (Elfouhaily, T., B. Chapron, K. Kastaros and D. Vandemark, *Journal of Geophysical Res.*, C7, 781-796, July 1997) and for different wind conditions. Conclusions are derived on the validity of the simplified approach at L-band and on its parameterisation (e.g. through the cut-off frequency between its two scales). Results obtained in the case of scattering are subsequently extended to radiometric measurements.

AN IMPROVED METHOD FOR DETERMINATION OF ROUGH SURFACE IMMITTANCE AT VERY LOW GRAZING ANGLES AT MICROWAVE FREQUENCIES

R.M. Jha*,
Email: rmjha@nps.navy.mil

R. Janaswamy
Email: janaswam@ece.nps.navy.mil

Code EC/
Department of Electrical & Computer Engineering
Naval Postgraduate School, Monterey, CA 93943
Fax: 1 (831) 656 2760

Code EC/Js

It is well known that the surface roughness can significantly alter the immittance of a ground plane. For most practical situations over the ocean, rough surface immittance values for the microwave frequencies are vastly different than those for the smooth surface. A rather simplistic approach to the ground immittance is provided by Miller, Brown and Vegh (MBV) in terms of a roughness correction factor thereby implicitly assuming that it is adequate to modify the smooth surface immittance (AR Miller *et.al.*, *IEE Proc.*, **131** (2), Pt. H, 114-116, 1984). However, the *Monte Carlo simulations* of rough surfaces employing the exact modal theory have shown the MBV formulation to be wanting at 500 MHz (D.E. Barrick, *IEEE Trans.*, **AP-46**, 73-83, 1998), thus rendering its application to the microwave frequencies, suspect.

We have observed that for a given set of transmitting and receiving antenna heights, the Monte Carlo simulations in the microwave region, *yield immittance values only for a limited range of angles*. The clipping of the angular range follows from the fact the valid immittance on any vertical profile must exceed the highest peak of rough surface height of all the Monte Carlo realizations. Furthermore, the extrapolation becomes difficult since the range of interest to be covered is much larger than the limited range of grazing angles where Monte Carlo simulations yield the immittance values.

In this presentation, we propose a novel scheme to circumvent this problem of the limited angular range, by smoothening the actual surface roughness profile at the two (transmitting and receiving) ends. The validity of this approach follows from the equivalence of the power density spectrum of the modified roughness profile (by smoothening at the two ends) to that of the original roughness profile. This method may be considered essentially as spatial filtering similar to the Hanning window in the Fourier transform applications. Thus this method, not only yields the immittance values at very low grazing angles, but is also expected to be robust due to its inherent anti-aliasing nature.

Beam-Wave Propagation and Scattering in a Random Medium Half-Space for an Incident Diverging Beam-Wave using Radiative Transfer Theory

Gerald Whitman*, New Jersey Institute of Technology
Felix Schwering, US Army, CECOM
Michael Wu, New Jersey Institute of Technology

For line-of sight communication, cellular communication in particular, interest centers on radio-link performance, and how it is affected by wave attenuation, fading and co-channel interference. If vegetation, such as a forest, lies along the path of the link, the radio performance will be affected and hence needs to be understood. Since vegetation, a random medium of discrete scatterers with a wide variety of sizes and shapes, is a very complex propagation medium, multiscattering plays a dominant role affecting the radio signal. A theoretical approach to study multiscattering effects is transport theory. Here, the scalar equation of radiative transfer is used to develop a theory of beam-wave propagation and scattering in a forest. The forest is modeled as a half-space filled with many random discrete scatterers that scatter energy strongly in the forward scattering direction. A diverging (spherical) beam-wave is taken to be normally incident from free space onto the forest interface. Such a beam-wave is characteristic of the radiation produced by microwave or mm-wave antennas. After splitting the specific intensity into the reduced incident and the diffuse intensities, the solution of the transport equation expressed in cylindrical coordinates is obtained by expanding the angular dependence of both the scatter (phase) function and the diffuse intensity in Associate Legendre polynomials, by using the Fourier/Bessel transform to obtain the equation of transfer for each spatial frequency, and by employing the method of weighted residuals to satisfy the boundary condition that the forward traveling diffuse intensity be zero at the interface. Numerical results for the received power will be presented that will yield information concerning the range dependence and the angular spread (beam broadening).

**MLFMA Analysis of Scattering from a Three-Dimensional
Rough Dielectric Surface Embedded in an Infinite Dielectric Half Space**

Zhijun Liu* and Lawrence Carin
Department of Electrical and Computer Engineering
Duke University
Durham, NC 27708-0291
zliu@ee.duke.edu, lcarin@ee.duke.edu

In rough-surface scattering one typically must address the problem of terminating the extent of the surface. In narrow-band calculations this is often performed by utilizing Gaussian-beam excitation, with the beam width chosen to avoid the edges of the truncated rough surface. While this is a widely employed technique, it is known that surface waves can be generated on a rough interface, with these not limited to the extent of the Gaussian-beam excitation. Moreover, in the context of wideband scattering, it is difficult to utilize a beam width wide enough at low frequencies of interest (the required beam width is frequency dependent). Therefore, an alternative solution to this problem is to embed the rough surface in the presence of an infinite half space, utilizing a smooth transition (taper) between the half space and rough surface. Surface waves excited on the rough surface will propagate relatively unperturbed into the half-space region. In the context of an integral equation solution, the problem complexity is enhanced significantly, however, by the need to handle the Sommerfeld integrals characteristic of the half-space Green's function. In the work presented here we consider a three-dimensional dielectric rough surface embedded in an infinite dielectric half space (with identical electrical properties for the half space and the dielectric rough surface). Plane-wave excitation is considered. For consideration of electrically large rough surfaces, the integral equations are solved via the multi-level fast multipole algorithm (MLFMA). Special considerations are addressed such that the MLFMA is applicable to scattering from a dielectric target (the rough surface) that is in direct contact with the half-space interface.

Reference-Wave Solutions for the High-Frequency Fields in Random Media

Reuven Mazar and Alexander Bronshtein
Department of Electrical and Computer Engineering,
Ben-Gurion University of the Negev,

Wave propagation taking place either in the natural environments or in the artificial structures is usually accompanied by random phenomena caused by the fluctuations of the medium's parameters. An increase in the propagation ranges and the need to operate with fields having greater spatial and angular extents require that the complexity of the propagating environments and the resulting multipath effects induced by the scattering of the field by boundaries and scattering centers to be accounted for. Prescriptions how to incorporate all these effects into stochastic propagation are given in a Stochastic Geometrical Theory of Diffraction (SGTD) that has been especially formulated to deal with such types of phenomena. The SGTD is based on the localization concept according to which the high-frequency fields are concentrated along the ray trajectories specified by the deterministic GTD. As in the deterministic GTD, the field at the observer can comprise a number of field species arriving along different ray trajectories resulting from the reflection, refraction, and (or) diffraction of the local plane-wave fields by boundaries, inhomogeneities, and (or) scattering centers. The statistical properties of the observed field patterns can be derived from the analysis of their statistical moments. For the construction of these moments, it would be useful to possess a field solution that accounts for the information accumulated by the propagating field along its propagation path. To derive such a solution a new reference wave method was developed. The methodology is based on defining a paired field product consisting of an unknown field propagating in a disturbed medium and its complex conjugate component propagating in a medium without random fluctuations. Defining paired field product and extensions to higher dimensional spaces allows to deal simultaneously with location in a configuration space together with defining the ray slope and the spectral properties of the radiation. In addition, performing a proper scaling gives the ability to emphasize "slow" and "fast" variables and to define expansion parameters with the subsequent application of asymptotic techniques. Once a solution of the equation for the paired field measure is obtained, the solution of the unknown field can be easily extracted from the paired solution in an explicit form if one knows the solution of the deterministic component. Several applications of the reference-wave solution are presented.

A Time Domain Signature Investigation for the GPR Detection of Plastic Land Mines Buried in Soils

Audrey J. Dumanian^{1,2}, Carey M. Rappaport¹, and Ann Morgenthaler¹

¹**Northeastern University, 235 Forsyth Street, Boston, MA 02115**
Tel: (617) 373-2043, Fax: (617) 373-8627, email: rappaport@neu.edu

²**MIT Lincoln Laboratory, 244 Wood Street, Lexington, MA 02420**

Abstract

The problem of detecting small buried dielectric targets, such as nonmetallic antipersonnel land mines, in lossy dispersive rough soil with a ground penetrating radar (GPR) is extremely challenging and critical to the humanitarian demining effort.

For this investigation, a two-dimensional finite difference frequency domain (FDFD) simulation code was used to generate the near zone scattered electric fields resulting from a normally incident TM plane wave on a random rough dielectric half-space containing a buried dielectric mine-like target. Data was generated over a densely sampled wide frequency bandwidth (.5 to 5 GHz).

Several realistic land mine scenarios were modeled. The parameters varied in the simulation datasets were the shape of the land mine (circular, elliptical, and rectangular), the soil type (dry sand and "Bosnian" soil), and the burial depths of the mine in the soil (2.5, 5, and 10 centimeters).

In this analysis, the power spectral density of the reflected signal yields a time domain signature dependent on the soil characteristics as well as the burial depth and radius of the mine. Specifically, two or more characteristic time peaks indicative of the burial depth are observed suggesting that the ultra-wideband spectral radar response may yield particular advantages not exploited by currently-employed detection systems. In addition, a radar transmitter and/or receiver is often held within a few wavelengths of the mine and/or ground surface. Therefore, several receiver heights at/or above the soil are also examined in the time domain. This study determines the feasibility of detecting mine-like targets based on stepped-frequency GPR time signatures.

FDTD and Multi-Resolution Methods

Chairs: A. Cangellaris, USA and L. Carin, USA

	Page
8:00 Construction of Fast 3D FDTD Boundary Kernals Using 1D Spectral Schemes, <i>K. Yegin*</i> , <i>University of Illinois at Urbana-Champaign</i> B. Shanker, <i>Iowa State University</i> , E. Michielssen, <i>University of Illinois at Urbana-Champaign</i>	250
8:20 Numerical Boundary Conditions at Material Interfaces for High-Order FDTD Schemes, <i>K.P. Hwang*</i> , A. Cangellaris, <i>University of Illinois at Urbana-Champaign</i>	251
8:40 Design of Perfectly Matched Absorbers for Low Frequency Scattering Problems, <i>M. Kuzuoglu*</i> , <i>Middle East Technical University</i> , R. Mittra, <i>Pennsylvania State University</i>	252
9:00 Definition and Conservation of Energy in FDTD Schemes, <i>R. Schuhmann*</i> , T. Weiland, <i>Darmstadt University of Technology</i>	253
9:20 Comparison with the Algorithms for Near Zone to Far Zone Transformation in FDTD Computation, <i>Y. He*</i> , <i>Osaka Electro-Communication University</i>	254
9:40 Algorithm Study of ADI-FDTD, <i>S. Staker*</i> , M. Piket-May, <i>University of Colorado at Boulder</i> , C. Holloway, <i>Nat'l Institute of Science & Technology-US Dept. of Commerce</i>	255
10:00 Experience with ADI-FDTD Techniques on the Cray MTA Supercomputer, <i>M. ElHelbawy*</i> , S. Staker, M. Piket-May, S. Bokhari, H. Jordan, J. Sauer, <i>University of Colorado at Boulder</i>	256
10:20 Advances Towards Next Generation FDTD Modeling Capabilities, <i>N. Chavannes*</i> , H. Gerber, A. Christ, J. Frohlich, H. Songoro, N. Kuster, <i>Swiss Federal Institute of Technology</i>	257
10:40 The Finite Difference Multi-Resolution Time Domain (MRTD) in View of the Multi-Resolution Homogenization Theory (MRH), <i>V. Lomakin*</i> , B. Steinberg, E. Heyman, <i>Tel Aviv University</i>	258
11:00 Multiresolution Time-Domain Modeling Using CDF Biothogonal Wavelet Expansion, <i>T. Dogaru</i> , L. Carin*, <i>Duke University</i>	259
11:20 Three-Dimensional MRTD Modeling of Time-Domain Radar Systems, <i>X. Zhu*</i> , L. Carin, <i>Duke University</i>	260
11:40 A Well Posed PML Absorbing Boundary Condition for Lossy Media, <i>G. Fan*</i> , Q. Liu, <i>Duke University</i>	APS

Construction of Fast 3D FDTD Boundary Kernels Using 1D Spectral Schemes

Korkut Yegin[†], Balasubramaniam Shanker^{††}, and Eric Michielssen[†]

[†]Center for Computational
Electromagnetics
Electrical and Computer Engineering
Department
University of Illinois at Urbana-
Champaign, Urbana, IL 61801

^{††}Electrical and Computer Engineering
Department
2215 Coover Hall
Iowa State University
Ames, Iowa, IA 50011

The recently introduced plane wave time-domain (PWTD) algorithm (A. A. Ergin, B. Shanker, and E. Michielssen, *J. Comp. Phys.*, **146**, 157-180, 1998) permits the efficient evaluation of so-called exact boundary kernels for truncating 3D FDTD grids. Assuming that an FDTD boundary is occupied by N_s equivalent sources that are active for N_t time steps, the classical evaluation of the fields they generate in a lossless medium at N_s observers requires $O(N_t N_s^2)$ operations; this cost rises to $O(N_t^2 N_s^2)$ if the medium is dissipative. PWTD algorithms accomplish the same in only $O(N_t N_s \log^2 N_s)$ operations.

PWTD schemes for dissipative media (K. Yegin, A. A. Ergin, B. Shanker, and E. Michielssen, "Fast FDTD Boundary Kernels for Dissipative Media," 2001 URSI EMT Symposium, accepted) constitute a generalization of PWTD schemes for lossless media and likewise express three-dimensional wave fields as superpositions of plane waves. The evolution of these plane waves is governed by one-dimensional wave equations with dissipative term, and accomplished using a spectral scheme. The domain over which these plane waves evolve must however be truncated. To date, two fast schemes for accomplishing this truncation have been developed. Both schemes permit the fast convolution of 1D boundary kernels with bandlimited source densities to arbitrary (spectral) accuracy. The first scheme evaluates the boundary integral by breaking up these source densities into time-limited subsignals and by computing the fields they generate for future observation using a (hierarchical) FFT. The second scheme relinquishes the convolutional nature of the boundary integral and instead exploits rank deficiencies of the boundary operator to achieve a fast evaluation of the boundary fields.

This presentation (i) will provide a detailed description of these new fast and spectrally accurate 1D boundary kernels for dissipative media, (ii) expose their respective merits and disadvantages in terms of computational and memory complexity, and (iii) discuss their incorporation into 3D PWTD kernels.

Numerical Boundary Conditions at Material Interfaces for High-Order FDTD Schemes

Kyu-Pyung Hwang* and Andreas C. Cangellaris
Department of Electrical and Computer Engineering
University of Illinois at Urbana-Champaign
1406 W. Green Street, Urbana, Illinois 61801-2991
Tel:(217)244-8277 Fax:(217)333-5962
E-mail:{khwang1,cangella}@uiuc.edu

Yee's finite-difference time-domain (FDTD) scheme has been widely used over the past twenty years for the computer simulation of electromagnetic interactions in structures and media of very high complexity, mainly due to its simplicity and flexibility. However, several challenges still remain in the generation of accurate FDTD solutions to electromagnetic interactions in electrically large structures. More specifically, the numerical dispersion introduced by the discrete approximation of the wave operator is responsible for the accumulation of significant phase error in the modeling of electromagnetic wave interactions in structures spanning several tens or hundreds of wavelengths. To overcome this obstacle, higher-order finite difference schemes have been and continue to be explored by various research groups. The implementation of a high-order explicit finite-difference scheme often involves an extended stencil. This becomes problematic in the vicinity of material interfaces where the fields and their derivatives exhibit discontinuities. The success of a high-order scheme is strongly dependent on the way the stencil is modified in the vicinity of material boundaries to accommodate the field discontinuities without impacting the order of the scheme.

In this paper, a new set of equations is proposed for updating the electromagnetic fields in the vicinity of metallic boundaries and dielectric interfaces in the context of Fang's (4,4) scheme (J. Fang, *Time Domain Finite Difference Computation for Maxwell's Equations*, Ph.D. Dissertation. Berkeley, CA: Univ. California at Berkeley, 1989). For the case of a perfect electric conductor (PEC) boundary, a one-sided finite difference approximation of the third derivatives in the (4,4) scheme is used. For the case of a dielectric interface, semi-implicit update equations are derived through the discretization of the integral forms of Maxwell's equations over finite volumes containing the interface. Numerical experiments involving several test geometries are used to demonstrate that the generated difference equations at the material boundaries preserve the fourth-order accuracy of Fang's (4,4) scheme both in space and time.

Design of Perfectly Matched Absorbers for Low Frequency Scattering Problems

Mustafa Kuzuoglu (*)
Department of Electrical Engineering
Middle East Technical University
06531, Ankara TURKEY

Raj Mittra
EM Communication Laboratory
319 EE East, Pennsylvania State University
University Park, PA 16802 USA

Perfectly matched absorbers have been extensively used in the Finite Difference Time Domain (FDTD) and Finite Element (FE) formulations for mesh truncation. In this work, we propose a formulation that employs perfectly matched absorbers in the solution of low frequency electromagnetic scattering problems via the Finite Element Method. For this purpose, the anisotropic PML has been modified to handle the difficulties encountered in mesh truncation in low frequency applications.

One of the major difficulties in low frequency electromagnetic scattering (or radiation) problems is the truncation of the unbounded spatial domain. If local absorbing boundary conditions (ABCs) are employed, the truncation boundary must be far away from the surface of the antenna or scatterer, so that the evanescent waves are negligible at the outer boundary. This causes an undesired increase in the number of variables in the finite element solution. A similar problem arises also in PML mesh truncation. Here, the magnitude of the PML parameter increases as the frequency is decreased, and this introduces undesired reflections from the boundary of the PML.

In the anisotropic PML, the parameter a is in the form

$$a = 1 + \frac{\alpha}{jk}$$

where k is the wave number and the parameter α starts from zero at the PML-free space interface and increases in the direction normal to the boundary. It is evident from this expression that the magnitude of the parameter a will increase as k decreases. To circumvent this difficulty, a is modified as

$$a = 1 + \frac{\alpha}{\beta + jk}$$

by introducing an additional parameter β . By adjusting these two parameters properly, it is possible to obtain an effective mesh truncation even at low frequencies. The paper will present the application of the modified PML to some representative two- and three-dimensional scattering problems to demonstrate its usefulness.

Definition and Conservation of Energy in FDTD Schemes

Rolf Schuhmann*, Thomas Weiland

Darmstadt University of Technology
Faculty of Electrical Engineering and Information Technology (FB18)
Computational Electromagnetics Laboratory (TEMF)
Schlossgartenstr. 8, 64289 Darmstadt, Germany
schuhmann@temf.tu-darmstadt.de

The application of the leapfrog scheme within the FDTD method is widely accepted to be responsible for an energy conserving time integration, i.e. for the absence of parasitic dissipation or even instabilities during the iteration.

For an exact algebraic proof of this property, however, also the spatial discretization of the method has to be investigated. This includes on the one hand a rigorous eigenvalue analysis of the discrete spatial operators and the complete system matrix. Such an analysis can be easily performed using the notation of the Finite Integration Technique (FIT, cf. Weiland, *Int. J. Num. Mod.* 9, 259-319, 1996). For the standard FDTD scheme (without extensions like subgridding or advanced boundary operators) we find that the spatial operators build a symmetric system with real and non-negative eigenvalues.

On the other hand, we need to establish a relation between the algebraic reasoning (with norms of matrices and component vectors) and the physical interpretation of field components and energy definitions. For this step we again utilize the basic theory of the FIT: We propose the definition of a local discrete energy quantity as the product of the two state variables of the FIT: the electric grid voltages and the electric grid fluxes which are defined as integrals of the physical quantities \vec{E} and \vec{D} over the edges of the primary grid or the facets of the dual grid, respectively. It can be shown that the approximations involved in this energy definition are of the same type and order as the approximations in the discrete material relations which are part of the FIT (and FDTD) scheme. Similar results can be found for the magnetic energy.

As consequences of this energy definition we present some consistency laws of the Finite Integration Technique, including the equality of the stored electric and magnetic energy in lossfree structures and a discrete formulation of Poynting's law. Finally some important rules can be derived for the implementation of extensions of the standard FDTD scheme (like dispersive material relations, the usage of generalized grids, or the coupling of FDTD to other methods in hybrid approaches). From the theoretical results it becomes evident, that a violation of these rules will most probably lead to energy dissipation and instabilities.

Comparison with the Algorithms for Near Zone to Far Zone Transformation in FDTD Computation

Yiwei He

Osaka Electro-Communication University
Hatu-cho 18-8, Neyagawa, 572-0833 Japan
heyiwei@emt.osakac.ac.jp

FDTD method has been widely used in the numerical analysis of antenna and radar cross-section (RSC). Many algorithms have been developed to transform the near zone results of the FDTD calculation to the far zone radiation fields by integrating the equivalent electric and magnetic currents on a surface enclosing the antenna or/and the objects. In generally, these methods can be classified into two types. One of them implements the integration at every time step in the FDTD repetition (R.Luebbers *et al.*, *IEEE Trans. Antennas Propagat.* 39, 429-433, Apr. 1991). Thus the transient radiation fields are available and the frequency characteristics in a wide range can be obtained by Fourier transforming the result. Another type only calculates the equivalent electric and magnetic current at required frequencies during the FDTD repetition. The near zone to far zone transformation is performed after the FDTD calculation.

The former algorithm is suited for the problems where the transient radiation field or the frequency characteristics in a wide range are interested. However, the computation load is quite heavy because the integration of the equivalent electric and magnetic currents on the enclosing surface must be performed for every required direction at every time step. Consequently, the computation load is in proportion to the number of directions. If the algorithm is utilized in an antenna analysis, the computation time of the radiation pattern may become several times of that of the normal FDTD computation. It is also noted that the algorithm is performed inefficiently in a super-computer. The latter algorithm is suited for the problems where the far zone field is only interested at one or a few frequencies because the memory requirement and the computation load are in proportion to the number of the interested frequencies. Because the near zone to far zone transformation is performed after the FDTD calculation, influence of the number of the directions to the computation time can be ignored.

The computation time and the memory requirement of two algorithms are compared numerically. The code of the former algorithm was created according to the above mentioned paper of Prof. Luebbers. The code of the latter one calculates the equivalent electric and magnetic current at the required frequencies during the FDTD repetition by performing the discrete Fourier Transform. The near zone to far zone transformation is carried out after the FDTD calculation. Suppose that the enclosed surface is ranged N_x cells in x -direction, N_y cells in y -direction and N_z cells in z -direction, the required total times of the addition and the multiplication of the former and the latter algorithms in one time step is about $86(N_x N_y + N_y N_z + N_z N_x) N_d$ and $32(N_x N_y + N_y N_z + N_z N_x) N_f$, respectively, where, N_d is the number of directions of the far zone field and N_f is the number of the frequencies that are interested.

ALGORITHM STUDY OF ADI-FDTD

Shawn W. Staker *, Melinda Piket-May
ECEE Dept. University of Colorado, Boulder, CO 80309 USA
staker@ll.mit.edu, mip@colorado.edu
(781)981-3675

Chris L. Holloway
National Institute of Science and Technology
U.S. Dept. of Commerce, Boulder, CO 80309, USA
holloway@its.bldrdoc.gov

The Finite-Difference Time-Domain (FDTD) scheme is a well established technique for simulating electromagnetic systems. The alternating direction implicit method for FDTD (ADI-FDTD) has been reported as a means to decrease run time (Zheng, Chen and Zheng, *IEEE Microwave and Guided Wave Letters*, November 1999). ADI-FDTD is unconditionally stable, allowing delta t to be increased and the resulting run time decreased.

ADI-FDTD has previously been reported as a means to increase delta t at a cost to accuracy. A class of problems which have the ability to increase delta t while maintaining the acceptable level of error are reported. These problems are referred to as ADI class problems and are over resolved in space. For ADI class problems, ADI-FDTD greatly reduces run time while maintaining the acceptable level of error. ADI-FDTD is a more computationally intensive as compared to the traditional FDTD. The real time for a single delta t update in ADI-FDTD is significantly longer as compared to a single delta t update in FDTD. Because of this an increase in delta t does not necessarily result in a reduction in run time. An empirical formula for estimating the true time savings of ADI-FDTD is given.

Higher order ADI-FDTD schemes are explored and the results are presented. Higher order spatial schemes are shown to provide no benefit to ADI class problems, while higher order temporal schemes are shown to possess potential improvement. Necessary criteria for any higher order temporal scheme is given.

The ability to incorporate material dispersion into ADI-FDTD is presented. Update equations and validations are presented for one and three dimensional cases. ADI-FDTD with material dispersion is shown to be unconditionally stable and possess a level of accuracy allowing it to be applicable to ADI class problems. Finally techniques for implementing other features such as absorbing boundary conditions are discussed.

Experience with ADI-FDTD Techniques on the Cray MTA Supercomputer

M. ElHelbawy*, S. Staker, M. Picket-May, S. Bokhari, H. Jordan, and J. Sauer
Department of the Electrical and Computer Engineering
University of Colorado at Boulder

In the FDTD (Finite Difference Time Domain) algorithm for Maxwell's curl equations established by Yee, the Courant-Friedrich-Levy (CFL) stability condition must be satisfied, thus limiting the time step for high spatial resolution. Recently, an application of the alternating direction implicit (ADI) method to FDTD has been investigated. The advantage of the ADI-FDTD technique over the conventional FDTD algorithm is that it is unconditionally stable, which means there exists no CFL bound on the time step. The ADI-FDTD technique's ability to allow larger time steps is especially important for the 3-D problems with fine spatial resolution that require supercomputer level computational performance.

In this paper, we discuss our experience porting an ADI-FDTD FORTRAN code to the Cray MTA supercomputer. The MTA is well suited for this new technique because an ADI algorithm solves coupled equations over each of the cardinal directions one at a time, updating the fields after each sweep. This can be very inefficient on cache-based or distributed memory systems. The Cray MTA - a revolutionary commercial computer based on a multithreaded architecture - has no data caches; instead, all memory references processed through a 3-D toroidal network connecting processors and memory modules. The Cray MTA is supported by a state-of-the-art compiler, which generates efficient multithreaded programs from serial code. Only minor modifications of the serial code were required to achieve high performance.

Results of our work have shown that the parallelized version of the modified code runs nearly three times faster on one processor of the Cray MTA when compared to the original serial code on a 500 MHz Alpha machine. The performance on the Cray MTA scaled almost linearly from one to eight processors, achieving a measured 2.06 Gflops when all eight processors were used. Additionally, the ADI-FDTD code has been tuned to run well on the Cray T90 supercomputer. A comparison between the performance of the ADI technique on the MTA and the Cray T90 will be presented.

The FDTD method is often one of the few approaches available for solving Maxwell's equations in complex 3-D geometries. These complex problems are extremely demanding computationally and often require the power of a supercomputer to solve fast enough for a reasonable design/simulate iteration cycle. The ADI-FDTD algorithm is quite promising for this type of problem but has features that limit the type of parallel computer architecture that can be effectively used to execute it. This investigation is an initial step in exploiting the potential of ADI-FDTD.

Advances Towards Next Generation FDTD Modeling Capabilities

N. Chavannes*, H.-U. Gerber, A. Christ, J. Fröhlich, H. Songoro and N. Kuster
Swiss Federal Institute of Technology (ETH)
8092 Zurich, Switzerland

Phone:+41-1-632 2755, Fax:+41-1-632 1057, e.mail: chavanne@itis.ethz.ch

Introduction

In recent years, numerical modeling and simulation in electromagnetics (EM) has gained increasing interest as an efficient design tool and complement to experimental methods. Motivated by the rapid growth of computational power, the Finite-Difference Time-Domain (FDTD) method in particular has proven to be well suited for the simulation of antennas embedded within highly complex environments. However, major drawbacks with respect to graphic user interface (GUI) and FDTD modeling capabilities complicate an efficient progress within today's simulation platforms. Moreover, the common FDTD scheme implies fundamental restrictions due to the rectilinear mesh arrangement and limited grid resolution. Within this study, novel and robust local mesh refinement algorithms were developed and combined with a powerful TCAD and automeshing environment.

Objectives

The objective of this study was the provision of a greatly advanced, reliable and user friendly EM modeling and simulation platform targeted for the analysis of EM transmitters operating within highly complex non-homogeneous environments.

Methods

A novel subgrid algorithm proposes a highly efficient way of improving local grid resolution. It makes use of 3-D cubic smoothing splines for the information transfer from the coarse to the fine grid and vice versa. A specific method of interpolation is applied for PEC material passing through this interface region. In addition, temporal interpolation has been significantly improved by taking EM field information from current, past and future time steps into account. An improved treatment of FDTD grid non-conformally oriented PEC structures has been achieved by implementing a novel 3-D contour path (CP) algorithm and its combination with the subgridding. Integrated within an ACIS based solid modeling environment featured by an automated generation of graded mesh, the methods have been applied to simulate various configurations of transmitter structures interacting with homogeneous and non-homogeneous human head models. The simulations were validated by experimental data using the near-field scanning system DASY3.

Results and Discussion

The method of field interpolation and temporal updating used in the subgridding scheme causes very low reflections of about 120 dB (at $\lambda_{min}/10$) in the mesh interface region, even for materials traversing the boundary. Furthermore, it shows high stability for a large number of time-steps ($>50'000$, main grid) by only slightly reducing the timestep to 0.95 CFL. A combination of graded mesh and a 1:4 subgrid transition allows a tremendous reduction of computational resources. For the simulation of a human head exposed to a mobile phone, the memory and runtime requirements were reduced from 1.2 GB to 100 MB and from 1 week to 6 hours, respectively, while preserving the same level of accuracy. Particularly for the numerical assessment of absorption data, the necessity of refinement methods is obvious, since averaged and peak SAR values show strong variation with respect to grid resolution and modeling detail.

By embedding FDTD local mesh refinement techniques into advanced TCAD and automeshing environments, the performance of EM simulations of real-world structures can be substantially improved. Especially the simulation of complex non-homogeneous structures, as can be found in mobile communications applications, reveal the essential need for such next generation modeling capabilities.

The Finite Difference Multi-Resolution Time Domain (MRTD) in view of the Multi-Resolution Homogenization Theory (MRH)

Vitaliy Lomakin, Ben Zion Steinberg and Ehud Heyman

Faculty of Engineering, Tel Aviv University
Tel Aviv 69978, Israel, fax: +972-3-6423508,
e-mail: heyman@eng.tau.ac.il, steinber@eng.tau.ac.il

The multi-resolution time domain (MRTD) is an efficient numerical solver for electromagnetic modeling of complex configurations involving both micro and macro scales, such as microwave circuits and antennas, dielectric resonators and cavities, and rough interfaces. The multi-resolution homogenization (MRH) theory has been introduced recently as an effective tool for studying the macro-scale structure of the field solutions (field *observables*) in complex media, and for exploring the relations between the field observables and the medium details.

In the present work a unified view point of the MRTD and MRH is suggested. This study is performed on the canonical EM problems of excitation and propagation in complex laminates characterized by multiscale heterogeneities. The proposed merge of MRTD and homogenization theory can find applications in diverse areas such as composite material analysis, fault interrogation, geophysical exploration and circuits design.

Specifically, in this paper we apply multi-resolution homogenization of *differential operators* to analyze propagation in complex multi-scale laminates, in order to study the smoothing properties of the MRTD formulation. For complex laminates considered the original Maxwell's equations are reduced to transmission line type equations with are then set in a hierarchy of multi-resolution spaces. The MRH provides a systematic framework for deriving the *effective medium* (the homogenized medium, including the micro-scale effects), clarifies its properties, and provides analytic error bounds for the field in the observable space (the space of the smooth components of the field).

These bounds are functions of the medium properties and of the excitation temporal spectrum, as well as of the homogenization scale (the resolution scale used for the medium) and the observable scale (the spatial resolution scale used for the field). We establish an asymptotic equivalence of the two approach in a certain resolution space, and evaluate the observable-space bounds on the computational errors in the MRTD. These bounds and the additional insight gained by the MRH are used to tune the parameters associated with the MRTD algorithm, such as lattice sizes and wavelet bases.

Multiresolution Time-Domain Modeling Using CDF Biorthogonal Wavelet Expansion

Traian Dogaru and Lawrence Carin*
Department of Electrical and Computer Engineering
Duke University
Durham, NC 27708-0291
tdogaru@ee.duke.edu, lcarin@ee.duke.edu

The multi-resolution time-domain (MRTD) method has been applied recently to a number of electromagnetic field problems, such as microwave cavities and structures, as well as scattering by various targets. It was demonstrated that the method produces significant savings in computational resources *vis-à-vis* the conventional finite-difference time-domain (FDTD) scheme, for a given accuracy in the solution. The essence of the MRTD algorithm is constituted by an expansion of the fields in a wavelet basis, followed by a Galerkin-type discretization of Maxwell's equations. Previous work on this method has concentrated on Haar, Battle-Lemarie or orthonormal Daubechies wavelet families. More recently, we introduced an expansion in terms of the Cohen-Daubechies-Feauveau (CDF) biorthogonal wavelets, trying to balance good numerical dispersion properties and algorithmic simplicity. The MRTD technique allows the treatment of large electromagnetic problems with reduced computer resources by addressing two basic issues present in the context of FDTD: the numerical dispersion is decreased by achieving higher-order approximation of the derivatives, and the multi-resolution approach allows for denser discretization only in selected regions of the computational domain, while keeping low sampling rates in the regions of slow field variation. In addition, the MRTD algorithm incorporates a sub-cell model for treating a non-conformal boundary between dielectric media, resulting in increased accuracy as compared to a staircase model of the same boundary. In this paper we apply the algorithm to several two-dimensional scattering problems and compare the results with the traditional FDTD scheme. We emphasize the advantages of the CDF-MRTD scheme in terms of computational resources involved.

Three-Dimensional MRTD Modeling of Time-Domain Radar Systems

Xianyang Zhu* and Lawrence Carin
Department of Electrical and Computer Engineering
Duke University
Durham, NC 27708-0291
xyzhu@ee.duke.edu, lcarin@ee.duke.edu

Subsurface sensing is of interest for many applications, including detection of buried pipes, unexploded ordnance (UXO) and land mines. There has consequently been significant interest in the development of modeling tools for the analysis of electromagnetic-based subsurface sensing, with application to radar and electromagnetic induction. In particular, authors have considered both frequency- and time-domain models, the former including the method of moments (MoM), the extended-Born method, and fast-multipole methods. With regard to time-domain methods, the finite-difference time-domain (FDTD) has been applied widely. The FDTD can be viewed in terms of a pulse expansion of the electromagnetic fields, in both space and time. With this understanding, one can generalize the FDTD by considering an alternative expansion. For example, there has recently been interest in expanding the fields in terms of a wavelet basis, this realizing what has been termed a multi-resolution time-domain (MRTD) analysis. The multi-resolution property is a consequence of the wavelet expansion, with the lowest resolution manifested in terms of the scaling functions, with higher resolution (refinement) added by wavelets. Wavelets of successively higher resolution can be added to the scaling-function expansion, to realize a field representation of a desired resolution. There are an infinite number of possible orthogonal or biorthogonal wavelet classes, but one typically imposes requirements (e.g., differentiability and/or vanishing low-order moments) that restrict the wavelet form. In the work presented here we consider three-dimensional modeling of a complete radar system for sensing of buried land mines, with inclusion of the transmitting and receiving antennas. The system includes a resistively tapered horn antenna, and it is demonstrated how this is well modeled via MRTD. The MRTD results are compared with those of FDTD, and to measured data.

Fast Numerical Techniques for Integral Equations

Chairs: R. Mittra, USA and K.K. Mei, Hong Kong

	Page
8:00 Analyzing the Waveguide Problems with a Relaxed Iterative Domain Decomposition Method, <i>H.Q. Zhu*</i> , <i>Y. Long</i> , <i>Z.D. Wu</i> , <i>University of Electronic Science and Technology</i>	APS
8:20 Multi-Frontal Preconditioners for Iterative Solvers, <i>V.V.S. Prakash*</i> , <i>R. Mittra</i> , <i>Pennsylvania State University</i>	APS
8:40 New Iterative OSMEI Technique to Decompose MoM Matrix of 3D Acoustic Scattering Problem, <i>J. Ma*</i> , <i>Xidian University</i> , <i>W. Che</i> , <i>K.K. Mei</i> , <i>Y.W. Liu</i> , <i>City University of Hong Kong</i>	APS
9:00 A Fast Evanescent Wave Algorithm, <i>W. Chew</i> , <i>L.J. Jiang*</i> , <i>S. Velamparambil</i> , <i>University of Illinois at Urbana-Champaign</i>	APS
9:20 Fast Capacitance Computation Using Three-Dimensional Second-Kind Integral Equation and AIM, <i>C.F. Wang*</i> , <i>L.W. Li</i> , <i>B.L. Ooi</i> , <i>P.S. Kooi</i> , <i>M.S. Leong</i> , <i>National University of Singapore</i>	APS
9:40 A Precorrected-EFT Approach for Capacitance Extraction of General Three-Dimensional Structures, <i>X. Nie*</i> , <i>L. Li</i> , <i>N. Yuan</i> , <i>National University of Singapore</i>	APS
10:00 Coverage Analysis Over Terrain Profiles Using an Adaption of the Spectral Accelerated Forward-Backward Method, <i>J.A.L. Fernandez*</i> , <i>M.R. Pino</i> , <i>F. Obelleiro</i> , <i>J.L. Rodriguez</i> , <i>Univeridade de Vigo</i>	APS
10:20 Crosstalks Between Lossy Conducting Structures, <i>J. Zhao*</i> , <i>W.C. Chew</i> , <i>University of Illinois at Urbana-Champaign</i>	APS
10:40 A Generalized Forward-Backward Method for the Efficient Analysis of Large Array Problems, <i>H.T. Chou*</i> , <i>H.K. Ho</i> , <i>Yuan-Ze University</i>	APS
11:00 Investigation of Electromagnetic Field Coupling to Wire Structures in Cavities, <i>S. Tkachenko*</i> , <i>J. Nitsch</i> , <i>F. Gronwald</i> , <i>H.G. Krauthauser</i> , <i>T. Steinmetz</i> , <i>University of Magdeburg</i>	262
11:20 On the Development of a Physical Integral Equation, <i>R. Adam*</i> , <i>Virginia Tech</i>	263

Investigation of Electromagnetic Field Coupling to Wire Structures in Cavities

S.Tkachenko*, J.Nitsch, F.Gronwald, H.G.Krauthäuser, and T.Steinmetz
University of Magdeburg
P.O.Box 4120, D-39016 Magdeburg, GERMANY
Tel. +49-391-6711088, Fax. +49-391-67-11236,
e-mail: Sergey.Tkachenko@et.uni-magdeburg.de

The problem of electromagnetic field coupling to different scatterers and antenna-like objects located inside cavities is of great interest in regard to many EMC applications. Examples for such applications are: 1) the estimation of the currents and voltages induced in the wiring of electronic equipment located in enclosures by an external electromagnetic field penetrating through slots and apertures; 2) the evaluation of the mutual coupling between such wiring elements to achieve internal electromagnetic compatibility of facilities; 3) theoretical investigations of reverberation chambers.

In this paper some results of analytical, experimental, and numerical investigations of simple wire structures in cavities are presented. As a basic theoretical model we consider an electrically small wire antenna (a dipole or a monopole) located inside a rectangular cavity (S.Tkachenko et al., Proceedings of EMC Zurich'99, p.379). Although the antenna under consideration is small it may have its own resonances. This approximation gives the possibility to describe different electrically small scatterers (antennas, loops, printed circuit boards, microchips, etc.), which themselves may have a complex internal structure and natural resonances, and to understand the basic physical features of electromagnetic field interactions with such scatterers. This analytic approach is an electromagnetic analogue of the zero-range potential method in quantum mechanics (S.Albeverio et al. *Solvable models in quantum mechanics*, Springer, 1988) and it allows to take into account the wire self-interaction due to reflections of the signal from the cavity walls. It is shown that the current in an electrically small antenna within a resonator, which is excited by an electromagnetic field, is equal to the current of the same antenna in free space, excited by the same field, but with a special kind of a primarily reactive resonance load which accounts for the resonator. This load parameters depend on both the resonator parameters and the antenna parameters.

The excitation field in the cavity may be produced by several different mechanisms and, therefore, the analysis may be applied in various disciplines for the estimation of currents and voltages induced on internal conductors by the field penetrating into packages; the calculation of an input impedance of an active wire antenna located in a cavity or the calculation of the mutual coupling of antennas located in a cavity.

Analytical formulae for the input impedance of the active antenna in the cavity and for the current transfer ratio of two wire antennas located in a cavity, taking into account the reverse influence of the reception antenna on the radiated antenna, have been obtained. A comparison of the calculated results with measurements in the Magdeburg Mode Stirred Chamber (MSC) and with results of the numerical simulation by the CONCEPT code has shown a good agreement between the theory, experiments, and numerical calculations.

On the Development of a Physical Integral Equation

R.J. Adams

ElectroMagnetic Interactions Laboratory

Bradley Department of Electrical and Computer Engineering

Virginia Tech, Blacksburg, VA 24061-0111

An important factor which impacts the total computational cost of an iterative solver is the number of iterations required to achieve a specified residual error level. For boundary integral methods, the iteration count is in turn a function of the condition number of the matrix obtained by discretizing the original boundary integral equation (BIE). Thus, one method of reducing the computational complexity of a numerical simulation is to use well-conditioned BIEs. Unfortunately, the standard BIEs of electromagnetic theory do not provide the desired, well-conditioned problem formulations. The standard BIEs are often ill-conditioned with respect to a scatterer's size and shape and typically have condition numbers which increase as the mesh used to numerically discretize the equation is refined.

An improvement in this situation has recently been obtained through the introduction of modified forms of the combined-field and combined-source integral equations (MCFIE and MCSIE, respectively). These formulations provide stable, well-conditioned formulations of smooth, convex geometries. They do not, however, provide well-conditioned formulations of more general configurations due to their reliance on a Green function which incorporates strong nonphysical field interactions.

This presentation considers the feasibility of obtaining a boundary integral equation formulation exclusively in terms of physically-correspondent field interactions. It is shown for a specific class of non-convex canonical geometries that the nonphysical field interactions included by the MCFIE and MCSIE can be re-summed in an efficient manner in order to achieve a boundary integral formulation free of nonphysical interactions. The various computationally desirable properties of the resultant formulation will be illustrated relative to the original MCFIE and MCSIE formulations, and issues that must be addressed in order to extend the resulting concepts to more general scattering configurations will be outlined.

Guiding Structures and Circuits I

Chairs: A. Mathis, USA and A. Neto, USA

	Page
8:00 The Nature of the Current Excited by a Source on Microstrip Line, <i>F. Mesa*</i> , <i>University of Seville</i> , <i>D.R. Jackson, University of Houston</i>	266
8:20 Hertz Potential Green's Function Representing a Volume Current Source in A Generalized Stripline Structure, <i>D. Infante*</i> , <i>The Aerospace Corporation</i> , <i>D. Nyquist, Michigan State University</i>	267
8:40 Difficulties of the Quasi-TEM Extraction Model and Definition of a General Representation of Longitudinal and Transversal Couplings, <i>S. Wane*</i> , <i>ENSEEIH, D. Bajan, SUPAERO, H. Baudrand, ENSEEIH, P. Gamand, Philips Semiconductors</i>	268
9:00 The Electromagnetic Theory of Wave Propagation in Microstrip Structures, <i>T.A. Leskova*</i> , <i>D.L. Mills, University of California, Irvine</i>	269
9:20 Extrapolation Methods for a Class of Inverse Fourier Integrals, <i>A. Mathis*</i> , <i>Ansoft Corporation</i>	270
9:40 Field Distribution in Metal-Insulator-Semiconductor (MIS) Transmission Lines, <i>N. Wongkasem*</i> , <i>T.C.K. Rao, University of Massachusetts Lowell</i>	271
10:00 Mode Coupling and Cutoff Behavior in Planar Anisotropic Dielectric Waveguides, <i>A. Yakovlev*</i> , <i>University of Mississippi</i> , <i>G. Hanson, University of Wisconsin-Milwaukee</i>	272
10:20 Steepest Descents Evaluation of Asymmetric Planar Dielectric Waveguide Field, <i>J. Lee*</i> , <i>D. Nyquist, Michigan State University</i>	273
10:40 Ultra Low Loss Ceramic Ribbon Waveguides for Millimeter/Submillimeter Wave, <i>C. Yeh*</i> , <i>F. Shimabukuro, P. Stanton, V. Jamnejad, W. Imbriale, F. Manshadi, California Institute of Technology/JPL</i>	274
11:00 Characteristic Impedance Calculation of Microstrip Line on Ferrite-Dielectric Substrate Using the Method of Lines, <i>I. Barseem*</i> , <i>E. Abdallah, Electronics Research Institute</i> , <i>E. Hashish, M. EL-Said, Cairo University</i> , <i>H. Taher, Electronics Research Institute</i>	275
11:20 An Analytic Approach for the Linvill Method, <i>W.N. Amaral Pereira*</i> , <i>M. Silveira, INATEL</i>	276

THE NATURE OF THE CURRENT EXCITED BY A SOURCE ON MICROSTRIP LINE

F. Mesa* and D. R. Jackson**

*Microwave Group, Department of Applied Physics 1
University of Seville, 41012 Seville, Spain

**Department of Electrical and Computer Engineering
University of Houston, Houston, TX 77204-4793

At low frequencies, the propagation on microstrip lines is described adequately by transmission line theory. A practical source placed on the line, such as a 1-volt delta-gap voltage source, will excite a quasi-TEM transmission line mode that propagates away from the source. This quasi-TEM mode is a bound mode, meaning that the modal fields decay exponentially away from the structure. Conventional transmission line theory describes the excitation amplitude of the bound mode accurately at low frequencies. For an infinite line, the current amplitude is simply $1/(2Z_0)$, where Z_0 is the characteristic impedance of the bound mode.

As the frequency increases, the phenomenology of wave excitation from a source becomes much more complicated. The bound mode is no longer quasi-TEM. In addition, one or more leaky modes may be excited by the source. The leaky modes decay exponentially along the line due to radiation loss, with radiation occurring into space and/or into the surface waves of the grounded substrate. Although there is exponential decay, the leaky modes may be sufficiently strong at high frequencies to cause significant spurious effects.

By studying the complete spectrum of current excited by the source, it is found that there are three additional types of current waves that the source produces, which are denoted as "residual waves". One type of residual-wave current, called the surface-wave type, propagates with a wavenumber equal to that of a surface wave on the grounded substrate, but decays along the line as $z^{3/2}$ (where z is the distance from the source). A second type of residual-wave current, called the leaky-wave type, behaves similarly, except that the wavenumber corresponds to the (complex) wavenumber of a physical (fast-wave) leaky mode on the grounded substrate. The third type of residual-wave current is called the space-wave type. This current wave propagates with a wavenumber of free-space, but decays along the line away as z^{-2} .

In this presentation the nature of the current excited by a practical delta-gap source on microstrip line will be examined, and the above conclusions will be verified, both analytically and numerically. Examples will also be presented to show how both the leaky modes and the residual waves can be responsible for spurious effects on microstrip line at high frequencies.

Hertz Potential Green's Function Representing a Volume Current Source in a Generalized Stripline Structure

David J. Infante*
The Aerospace Corporation
Reconnaissance Systems Division
Chantilly, VA 20151

Dennis P. Nyquist
Department of Electrical and Computer Engineering
Michigan State University
East Lansing, MI 48824

Stripline waveguide structures are widely used for many applications. Here, a Hertz potential Green's function is established for a three-dimensional volume current source suspended in the space between two parallel, infinitely-wide, perfectly-conducting plates, one of which is coated with a non-magnetic dielectric material. Previously, the authors have exploited a similar, more specific Green's function to develop a full-wave theory for stripline structures having a homogeneous (air-filled) cross-section. An electric field integral equation (EFIE) for currents on the stripline was developed by enforcing boundary conditions for tangential fields at the perfectly conducting surface of the center conductor. The result of the more general case presented here, in which a dielectric layer is present within the waveguide, may be used to examine a variety of additional structures, such as covered microstrip, using a similar technique.

Analysis begins by expressing the electric and magnetic fields present within the structure in terms of the electric Hertz potential maintained by a volume current source. Using these representations, a Helmholtz equation is established. Boundary conditions on the Hertz potential at the surface of the perfect conductors, and at the free space/dielectric interface are determined by examining the boundary conditions on the electric and magnetic fields. The uniformity of the generalized stripline cross-sectional geometry prompts the use of Fourier transforms to solve the Helmholtz equation. Solution is further facilitated by decomposing the resulting transform domain expression into scattered and principal components. Final results are expressed in terms of Sommerfeld integral Green's function representations. Pole and branch point singularities associated with this Green's function will be identified and examined. Parallel-plate and surface-wave modes will also be identified.

Difficulties of the Quasi-TEM extraction model and Definition of a general representation of Longitudinal and Transversal Couplings.

S. Wane*, D. Bajon**, H. Baudrand* and P. Gamand***

*ENSEEIHT 2 rue Camichel Toulouse France -Tel : 05 61 58 82 47 wane@len7.enseeiht.fr

**SUPAERO 10 av. Edouard Belin, 31055 Toulouse France-Tel : 05 62 17 80 81 bajon@supaero.fr

***Philips Semiconductors 2 rue de la girafe 14079 CAEN France

SUMMARY

To represent by an equivalent circuit the behaviour of coupling phenomena is a practical way to obtain an electrical model from a full-wave analysis. For CAD purposes equivalent circuit enables an evaluation of couplings between conductors in a circuit simulator where a full-wave analysis tool would require important CPU time or memory storage. Although usual quasi-TEM extraction model supplies, for the representation of two coupled microstrip lines, a mutual inductance M and an inter-capacitance C_c , it does not distinguish the longitudinal coupling from the transversal one. In multilayer structures including buried diffusions layers inducing depleted layers, it would be of great interest to examine separately the longitudinal and transversal couplings in order to decide how the substrate, the resistive layers and the metallic losses have to be distributed between the serial parameter R (defining the resistance per unit length) and the parallel one G (representing the conductance per unit length).

In this paper a full-wave analysis of couplings in multilayer Silicon IC's with buried diffusions taking into account as well metallic as substrate losses is presented. A general equivalent circuit involving eight parameters (Fig.1-b) is introduced to circumvent the quasi-TEM model extraction difficulties. Such representation allows to avoid the usually used simplifying hypothesis assuming, in the case of symmetric structures the even and odd mode serial parameters (R_{even} and R_{odd}) to be equal, with a possible extension to structures having floating ground plane. New parameters D_L and D_T related to (Z_L, Z'_L) and (Y_T, Y'_T) in Fig.1-b define respectively the longitudinal and transversal couplings parameters and are less dependent to the definition of the characteristic impedance unlike the mutual and coupling capacitance M and C_c parameters. Fig.2-a gives their evolutions against the substrate resistivity while the effect of a localised buried diffusion on the transmission parameter S_{12} is analysed in Fig.2-b in the slow-wave region ($\rho = 0.1 \Omega\text{-cm}$) and in the lossy dielectric domain ($\rho = 10^8 \Omega\text{-cm}$) at 2 GHz.

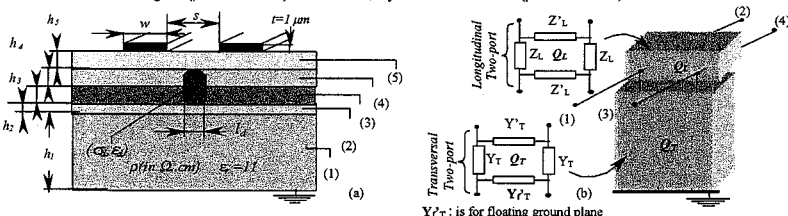


Fig.1 Schematic of microstrip coupled lines on multilayer Si substrate with diffusion layers (a) general equivalent circuit (b) $h_1 = 400 \mu\text{m} - h_2 = 1.5 \mu\text{m} - h_3 = 0.8 \mu\text{m} - h_4 = 1.8 \mu\text{m} - w = 10 \mu\text{m} - s = 20 \mu\text{m} - t = 1 \mu\text{m} - \sigma = 3.310^7 \text{ S/m} - \epsilon = 10 \mu\text{m}$ (1): P* Si substrate, (2): Depleted layers, (3): BP-layer, (4): Epi layer, (5): Oxide layer.

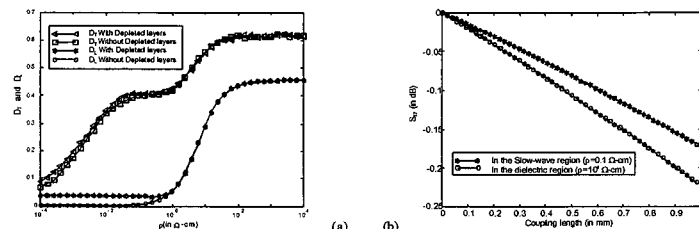


Fig.2 Evolution of D_L and D_T against the substrate resistivity at the frequency 6 GHz with and without Depleted layers (a). Effect of the localised buried diffusion on the transmission parameter S_{12} in the slow-wave and the lossy dielectric regions (b)

The Electromagnetic Theory of Wave Propagation in Microstrip Structures

T. A. Leskova and D. L. Mills

Department of Physics and Astronomy University of California
Irvine, California 92697 U. S. A.

In this paper, we present the theory of electromagnetic wave propagation in microstrip structures, based on the application of the full Maxwell equations. We do not introduce a postulated current distribution within the microstrip, but instead its current is driven by the electromagnetic fields in the normal modes of the structure, via the electrical conductivity of the material used to form it. A consequence is that our theory incorporates the electromagnetic response characteristics of the material from which the microstrip is fabricated, a feature essential to calculations in the high frequency domain, where the skin depth is comparable to the thickness of the microstrip. By invoking an assumption that the microstrip is thin, and its skin depth is small in a sense described in the text, we obtain effective boundary conditions applicable to the structure. These combined with Maxwell equations lead us to integral equations of the Wiener Hopf form, which admit analytic solution. We present a series of numerical calculations of the frequency variation of the impedance of the microstrip, the dispersion relation of waves in the structure, and we compare the current distributions which emerge from our treatment with forms introduced in an ad hoc manner by earlier authors.

Extrapolation Methods For A Class Of Inverse Fourier Integrals

Andrew W. Mathis
Ansoft Corporation
3800 Arapahoe Ave., Suite 250
Boulder, CO, 80303
email: mathis@ansoft.com
TEL: (303) 541-9525, x24

The use of extrapolation methods for the integration of infinite tails which comprise an oscillating term and a monotonic term is explored. Integrands of this type are frequently encountered when using the Spectral Domain method to analyze the electrical properties of transmission lines in layered media. These integrands occur when calculating the impedance (or admittance) matrix elements if the basis and testing functions overlap and when calculating the power transmitted.

Typically, the inverse Fourier integration is done either by assuming sidewalls and converting the integration into a summation or by applying extrapolation methods. Extrapolation methods convert the integration of the infinite tail into a summation of integrals over subintervals. Series acceleration techniques are then used to quickly sum the series. Unfortunately common extrapolation methods, e.g. method of averages and Shank's transformation, are not directly applicable if the integrand tail comprises a monotonically decreasing term and an oscillating term. The standard way to handle these cases is to subtract the large argument approximation of the monotonic terms and integrate the remaining oscillating term using the method of averages.

However, it is a simple matter to remove the oscillatory component of the tail by properly choosing the limits of integration of the subintervals. This results in a summation of a monotonically decreasing series, and there exist extrapolation methods to handle this case. Two techniques applicable to the acceleration of monotonic series are the θ -algorithm and the ρ -algorithm. A comparison of these two algorithms and their efficacy is presented. The extension of this method to the summation associated with assumed sidewalls is also presented.

FIELD DISTRIBUTION IN METAL-INSULATOR-SEMICONDUCTOR (MIS) TRANSMISSION LINES

N. Wongkasem* and T. C. K. Rao

Department of Electrical and Computer Engineering
University of Massachusetts Lowell, Lowell, Massachusetts 01854

One-dimensional analysis of a metal-insulator-semiconductor (MIS) transmission line is useful in obtaining the equivalent circuit representation of wide microstrip lines fabricated on silicon substrates backed by thick metallic films of high conductivity. Such lines are used for modeling high-speed very large-scale integration (VLSI) interconnects, tunable filters and phase shifting networks. Several investigations have been reported on it including quasi-TEM analysis (Y. R. Kwon *et al*, IEEE Trans. MTT, 35, p.545, June 1987), mode-matching methods (R. Sorrentino *et al*, IEEE Trans. MTT, 32, p.410, Apr. 1984), spectral-domain method and finite-element methods. Most of the previous investigations deal with the determination of the transmission-line parameters and calculations of the quantities like the characteristic impedance and the losses (H. Hasegawa *et al*, IEEE Trans. MTT, 19, p.869, Nov. 1971 and D. F. Williams, IEEE Trans. MTT, 47, p.176, Feb. 1999). While these circuit models are useful and have helped us to enhance understanding of more complicated MIS lines, the electric field distribution inside the insulating layer or the semiconductor layer is not known for any of the propagating transverse magnetic modes. The primary emphasis of this paper is on the variation of the field distribution. The electric field is determined by finding the usually complex transverse propagation constants in the structure, which is done by solving the transcendental equation for the axial propagation constant. The regions of existence of different modes and the variation of the attenuation characteristics with frequency for these modes will be studied. In addition, the effect of the variation of the insulator thickness, substrate thickness and resistivity on the field distribution will also be studied.

Mode Coupling and Cutoff Behavior in Planar Anisotropic Dielectric Waveguides

Alexander B. Yakovlev

Department of Electrical Engineering, The University of Mississippi
University, Mississippi 38677-1848

George W. Hanson

Department of Electrical Engineering and Computer Science
University of Wisconsin-Milwaukee, Milwaukee, Wisconsin 53201-0784

The characterization of modal coupling and cutoff in dielectric waveguides is important for the design and analysis of passive waveguiding structures. Often, waveguides are constructed using anisotropic dielectrics, either unintentionally, e.g., processing-induced anisotropy in PTFE circuit boards, or intentionally, e.g., ferrites and solid-state plasmas. In any event, the material anisotropy can have a substantial affect on modal coupling and cutoff properties, and must be accounted for in electromagnetic simulations for design and analysis purposes. In particular, the presence of anisotropy can induce mode coupling in a waveguiding structure which would not admit such coupling when constructed using isotropic media.

In this paper we discuss modal coupling and cutoff properties using the concept of critical points which occur in dispersion space. These critical points lead to the presence of complex frequency-plane branch points which completely explain observable modal behavior related to coupling and cutoff. The case of an isotropic waveguiding medium has been previously investigated, leading to various classes of frequency-plane branch points. In the anisotropic case, similar points occur, and new branch-points are identified which depend on the presence of anisotropy.

In particular, mode coupling in the presence of anisotropy is associated with the occurrence of a non-degenerate Morse critical point in the mode-coupling region. In addition, it is observed that there are two complex frequency-plane branch points which always accompany the Morse critical point in the region of mode coupling. These branch points, migrating across the real frequency axis as the material anisotropy varies, separate qualitatively different mode interaction regimes. Moreover, cutoff characteristics of proper and improper (leaky) modes are associated with the presence of real and complex-valued fold points in dispersion space, corresponding again to complex frequency-plane branch points. The occurrence of all complex-plane branch points, each of which directly relates to a physical coupling or cutoff process, will be discussed for several important cases.

STEEPEST DESCENTS EVALUATION OF ASYMMETRIC PLANAR DIELECTRIC WAVEGUIDE FIELD

Jeong Lee and Dennis P. Nyquist
Department of Electrical Engineering
Michigan State University
East Lansing, Michigan 48824
U.S.A.

Phone:(517)432-4146, FAX:(517)353-1980, E-mail:jeonglee@egr.msu.edu

Integrated waveguide structures consist of conducting or dielectric guiding regions immersed in a planar-layered background environment. Integral representations for the complete electromagnetic field maintained by excitatory electric currents are obtained by subsequent inverse transformation of the spectral-domain fields. Evaluation of the integral representations requires that singularities of the spectral-domain currents/fields be identified. Those singularities consist of simple poles associated with the integrated guiding structure and branch points contributed by the layered background environment. The latter branch points arise from both the wavenumber parameters and the discrete surface/leaky-wave poles of the layered background. Numerical evaluation of the near fields proceeds through the integration along a steepest-descent path of the axial transform plane and a saddle-point approximation of the axial inverse-transform integral representation is employed for the asymptotic radiation field. A simple canonical waveguiding structure which shares the presence of multiple non-removable branch points is investigated to obtain insight into the more practical integrated structures.

The asymmetric planar dielectric-slab waveguide is perhaps the simplest canonical waveguiding structure for which multiple non-removable branch points are present in its spectral-domain field. This structure consists of a dielectric guiding layer of finite thickness located between semi-infinite substrate and cover layers. Line-source excitation of TE waves on the asymmetric slab is considered. Wavenumber parameters for each of the three planar layers lead to branch point singularities of the spectral field; although the branch point associated with the guiding layer is removable, those associated with the substrate and cover layers are not. Appropriate choice of branch cuts consequently leads to a four-sheeted Riemann surface in the axial transform plane. Steepest-descent numerical evaluation for the near (to the line source) total fields as well as asymptotic steepest-descent approximations to the distant ones are studied. For the cover field, the steepest-descent path in the axial transform plane replaces the cover branch cut while that of the substrate is retained. Similarly, in the substrate region, the substrate branch cut is replaced while that of the cover is retained.

The steepest descents evaluation of both the near and the distant field for the asymmetric planar waveguide is complicated by the presence of multiple non-removable branch cuts in the spectral-domain fields, which leads to the inclusion of an additional new contribution in the field representation. If the observation aspect angle exceeds a minimal threshold value then the SDC crosses one of the branch cuts odd times such that its initial end lies on the top sheet while its terminal end resides on a lower sheet. To implement connection of the SDC into the ends of the real-axis contour on the top sheet, the terminal end of the SDC must cross the cut even times and then be deformed about it to make the connection on the top sheet. This results in the inclusion of a new continuous-spectrum branch cut contribution in the field representation.

The steepest-descent integration path must be deformed about the remaining branch cut to end on the top Riemann sheet. The substrate branch cut contribution to the cover layer field is annulled in the far zone due to wavenumber parameter for the cover layer, but the cover branch cut contribution to the substrate field remains significant. In the near zone, both the branch cut contributions exist. The lateral wave arising from deformation of the integration contour about the cover layer branch cut is negligible near the threshold aspect angle, the field discontinuity due to the branch cut contribution is resolved. The field discontinuity due to deformation of the integration contour about the substrate branch cut is considerable near the threshold aspect angle but the field phase compensates for the discontinuity so that the total radiation field is still continuous over that region.

Ultra Low Loss Ceramic Ribbon Waveguides for Millimeter/Submillimeter Wave

C. Yeh*, F. Shimabukuro,
P. Stanton, V. Jamnejad, W. Imbriale, and F. Manshadi
Jet Propulsion Laboratory
California Institute of Technology
4800 Oak Grove Dr., Pasadena, CA 91109

Ever since the discovery by Kao and Hockman that ultra-low-loss optical fiber can be made from pure silica through the elimination of impurities, the ability to guide signals in the optical spectrum with very low attenuation loss is assured. There remains a spectrum from 30 GHz to 3000 GHz (called the millimeter/submillimeter (mm/submm) wave band), where low loss waveguides are still unknown. Because of the presence of inherent vibrational absorption bands in solids, the elimination of impurities is no longer the solution for finding low loss solids in this spectrum. High skin-depth loss in this spectrum also eliminates the use of highly conducting material. It appears that since the material loss factor and the dielectric constant of a solid are fixed, the only way to reduce the attenuation constant of a pure dielectric waveguide is to find the proper cross-sectional geometry of that waveguide. Here we shall report the new way to design a waveguide structure which is capable of providing an attenuation coefficient of less than 0.01 dB/m for the guided dominant mode. This structure is a ceramic (Coors' 998 Alumina) ribbon with an aspect ratio of 10:1. At operating frequency band around 100 GHz, this attenuation figure is more than one hundred times smaller than that for a typical ceramic or other dielectric circular rod waveguide, that for the traditional metallic rectangular waveguide, and that for the microstripline. Both theoretical and experimentally measured results will be shown. A new way to measure ultra-low attenuation constant for the guided wave will be described. Practical considerations, such as, low interference supports for the ceramic ribbon structure, highly efficient launching device, low-loss ceramic ribbon connections, non-radiating cornering device, etc., will also be discussed and demonstrated.

**Characteristic Impedance Calculations of Microstrip Line
on Ferrite-Dielectric Substrate Using
The Method of Lines**

I. Barseem¹, E. Abdallah¹, E. Hashish², M. EL-Said², H. Taher¹
¹ Electronics Research Institute, El-Tahrir street, Dokki, Cairo, Egypt
² Faculty of Engineering, Cairo University, Giza, Egypt

Abstract:

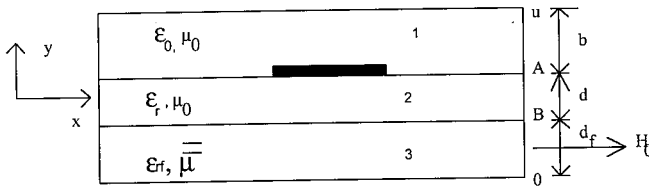


Fig 1 Cross-section of shielded microstrip on ferrite-dielectric substrate

In this paper, the characteristic impedance of shielded microstrip line on a magnetized ferrite/dielectric substrate is derived using the method of lines. The characteristic impedance is an important factor, e.g. for low-reflection phase shifter design. The calculation of characteristic impedance is based on the power flow in the three regions of the structure and the total current on the strip. With the method of lines, the wave-equation is discretized in one direction and the resulting differential-difference equation is solved analytically for each homogeneous region to obtain the transverse field components at interfaces 'A' and 'B' as shown in Fig.1. First, we obtain expressions for the transverse electric and magnetic field components $\vec{E}_{x,y}, \vec{H}_{x,y}$ at each region as a function of transverse field components at the interfaces, then we compute the average power at each region by integrating the Poynting vector. The total power is given by adding the power at the three regions. The total current on the strip is given by the summation of the current components in the direction of propagation. FORTRAN-77 programs were developed to compute the dispersion curves of the characteristic impedance of shielded microstrip line on a magnetized ferrite/dielectric substrate. In order to check the correctness of the analysis and programs, single microstrip line on dielectric substrate structure has been computed numerically and the results were found to be in good agreement with the available published data. The effect of the geometric dimensions and physical properties of the structure are studied and dispersion design curves are obtained. The method of lines has been proved to be very efficient for calculating the characteristic properties of planar microwave structures, e.g. microstrip, it can give high accuracy with little numerical effort, no spurious solutions occurred, it avoids the choice of basis functions, also it does not have the problem of relative convergence.

AN ANALYTIC APPROACH FOR THE LINVILL METHOD

W. N. Amaral Pereira and M. Silveira
INATEL - National Institute of Telecommunication, Brazil (www.inatel.br)

MEMS devices need electronic circuits able to processing high speed data signals. Sometimes they work up to RF or VHF band and design amplifiers and others active circuits means to deal with high frequency technology. The earliest work that presents a consistent theoretical approach to design small signal RF amplifiers had been introduced by Linvill and Gibbons (*Transistor and active circuits*, McGraw-Hill, 1961). Working in the Stanford Electronic Laboratories they have improved a power flow analysis applied to the active two ports performed in Y parameters. The target is to establish if the active element has unconditional stability or if there exist some loads which lead the amplifier to oscillate (potential instability). The optimal RF design needs to take into account the load which optimize the power gain for a convenient sensitivity (δ). In this sense Linvill (G.Johnson, *Solid State Comms*, McGraw-Hill, 1966) derived a graphical procedure in the Smith Chart to calculate an optimal Y_L (load admittance) in the operating and in the cutoff frequencies (lower and upper). However, many actual designs the real part of the optimal normalized load admittance g_L presents normalized values greater than 50. This order of magnitude do not permit to obtain a good resolution in the Smith Chart. Nowadays, the modern semiconductor active devices lead to g_L values over 100. The main purpose of this paper is to present a complementary numerical way to calculate the output parameters done by Linvill method. Applying some geometrical relations concerned with that graphical approach, one can derive the following expressions:

$$g_L = \frac{G_L}{g_0} = g = \frac{4g_2(1-C \cos \theta)}{[1+g_2(1-C \cos \theta)]^2 - C^2}$$

$$\text{where: } g_2 = \frac{|Y|}{g_0}, \quad Y = \frac{|y_{12} y_{21}|}{|y_{11}| \delta}, \quad g_0 = \text{Re}[y_{22}], \quad C = 2 \frac{|y_{12}|^2}{4g_{1i}g_{22} - 2 \text{Re}[y_{12}y_{21}]} \frac{|y_{12}|}{|y_{21}|},$$

$$\theta = 180^\circ - \angle y_{12} - \angle y_{21}$$

Thus, the optimal load Y_L and the susceptance changing in the desired bandwidth ΔB can be calculated by: $Y_L = G_L + jB_L$, and $\Delta B = g_0/b_1 - b_2$, where:

$$B = b_0 g_0 - \text{Im}[y_{22}], \quad b_j = \frac{2v_j}{(v_j)^2 + (1-u_j)^2}, \quad j=0,1,2, \quad u_0 = 1 - \frac{1 + \cos \varphi}{1 + g_2}, \quad v_0 = \frac{\text{sen } \varphi}{1 + g_2}$$

$$v_i = \frac{F - H + (G - D)u_i}{E}, \quad i=1,2, \quad \text{where } u_i \text{ are solutions of the equation: } Ru^2 + Su + T = 0;$$

$$R = E^2 + (G - D)^2, \quad S = G.E^2 + 2(F - H)(G - D), \quad T = (F - H)^2 - H.E^2;$$

$$D = -(g.C/2) \cos \theta, \quad E = -(g.C/2) \text{sen } \theta, \quad F = 1 - (g/2), \quad G = \frac{2g_2}{1+g_2}, \quad H = \frac{(1-g_2)}{1+g_2}; \text{ and}$$

$$\varphi = \text{Arcsen} \left\{ \frac{(g.C/2) \text{sen } \theta}{[1/g_2 + 1] + [(1-g + (g.C/2)^2)^{1/2}]} \right\}$$

For illustration purpose, using the transistor *MRF-904* in 100 MHz and taking $\delta = 0.3$, one can obtain $g = 405.13$; $C = 2.2$; $\varphi = -34.02^\circ$; $\Delta B = 83.71$ (mS) and $Y_L = 37.93 - j.12.61$ (mS).

Rough Surface Scattering I

Chairs: J. Johnson, USA and M. El-Shenawee, USA

	Page
10:00 Diffuse Intensities of Electromagnetic Waves in a Layer of Randomly Inhomogeneous Medium Bounded by Randomly Rough Surfaces, <i>S. Mudalier*, Arcon Corp.</i>	278
10:20 Non Local Small Slope Approximation Technique TE and TM Solutions Including The Grazing Angles, <i>G. Berginc*, Thales Optronique, Y. Beniguel, IEEA, France</i>	279
10:40 Backscattering Enhancement Study with the Non Local Small Slope Approximation Method for Scattering of Vector Waves from Randomly Rough, <i>A. Soubret*, G. Berginc, Thomson-CSF Optronique, C. Bourrely, Centre de Physique, CNRS-Luminy</i>	280
11:00 Scattering by Two-Dimensional Rough Surfaces: Comparison Between Moment Method and Small Slope Approximation, <i>G. Soriano*, C-A. Guerin, M. Saillard, Institut Fresnel</i>	281
11:20 Iterative PE Techniques for Rough Surface Scattering, <i>M.F. Levy*, Rutherford Appleton Laboratory, UK</i>	282
11:40 An Improved FB/NSA Algorithm for the Computation of Scattering from Two-Dimensional Extremely Large-Scale Perfectly Conducting Rough Surfaces, <i>D. Torrungrueng*, J.T. Johnson, Ohio State University</i>	283

DIFFUSE INTENSITIES OF ELECTROMAGNETIC WAVES IN A LAYER OF RANDOMLY INHOMOGENEOUS MEDIUM BOUNDED BY RANDOMLY ROUGH SURFACES

S Mudaliar
ARCON Corporation
260 Bear Hill Road
Waltham MA 02154 USA

Although enormous work has been reported on scattering from random media and randomly rough surfaces the problem, which involves both random media and rough boundaries, poses many questions and difficulties. One approach, a numerical one based on direct simulations of the underlying wave equations, can be potentially accurate and hence useful in our understanding of the problem; but it is computationally intensive and is feasible only in some special situations. An alternate approach is based on radiative transfer theory (RTT). Here the medium scattering is described by the volumetric transport equations, whereas boundary scattering is described by the surface transport equations. These equations are usually formulated phenomenologically and independently. Within the radiative transfer regime these equations adequately describe multiple scattering within the medium and from the boundaries but do not appear to capture the basic multiple scattering interactions. Furthermore if the basic statistical elements are correlated then the problem is beyond the scope of RTT. This is the motivation for our work.

The geometry of the problem consists of a random medium layer bounded by rough boundaries which are parallel planes on the average. The permittivity of the random medium has a deterministic part and a randomly fluctuating part. All basic statistical fluctuations are small and smooth; they are stationary Gaussian independent of each other. The bottom surface is assumed to be perfectly conducting.

We use transferred boundary conditions and unperturbed Green's functions to represent the problem as an integral equation in which all the fluctuations of the problem are represented by a zero mean random operator. Equations for the first two moments of the electric fields are obtained from this integral equation. The paper is devoted to the analysis of the equation for the second moment known as the Bethe-Salpeter equation (under ladder approximation). We use spectral representation for the diffuse fields and assume that the waves travelling in different directions are uncorrelated. We also use spectral representation for the correlation functions and the coherent Green's functions and derive an equation for the diffuse intensities in phase-space. This is a vector valued integral equation describing the various scattering processes of the problem. We then derive transport equations and compare them with those in the literature. On examining several special cases we found that our system is in agreement with RTT when the problem contains a single basic statistical parameter, but in problems where more than one parameter is involved our system differs from RTT. This is because of multiple scattering interactions which are not properly accounted for by RTT.

Non Local Small Slope Approximation Technique TE and TM solutions including the grazing angles

G. Berginc, Thalès Optronique, rue Guynemer, 78283 Guyancourt, France
Gerard.berginc@tco.thomson-csf.com

Y. Béniguel, IEEA, 13 Promenade Paul Doumer, 92400 Courbevoie, France
Beniguel@club-internet.fr

The field scattered by a rough surface is calculated by the Non Local Small Slope Approximation (NLSSA) technique (A.G. Voronovitch, Waves in random media, April 1996). As compared to the SSA technique (A. G. Voronovitch, Waves in random media, July 1994), it allows to consider multiple interactions on the surface. One point of special interest is the case of double interactions which creates the backscattering enhancement. This contribution mainly occurs for large slopes and high values of the RMS height on the surface.

Such a calculation, involving double interactions on a surface, is difficult to perform with other techniques which usually allows to consider multiple interactions only for a 1D profile. In this paper we will present the technique developed in both cases of TE and TM polarisations for dielectric and perfectly conducting surfaces. The 1D and 2D algorithms have been developed. Comparisons have been made with respect to 1D results obtained both by second order Kirchhoff technique and Monte Carlo simulations using an integral equations approach (A. Ishimaru, J. Chen, JOSA, 1990) for cases exhibiting backscattering enhancement.

The NLSSA solution leads to expressions containing singularities for both cases of TE and TM polarisations, the TM case singularity being one order higher than the one corresponding to the TE case. This singularity can easily be removed for the TE case. For the TM case, far from grazing angles a similar solution may be derived. For grazing angles the solution must be modified introducing statistical properties of the slope of the irregularities in order to deal with the singularity. The solutions obtained will be presented :

- Far from grazing angles : the TE and TM cases
- At grazing angles : the modified solution for the TM case.

Backscattering Enhancement study with the Non Local Small Slope Approximation Method for Scattering of Vector Waves from Randomly Rough Surfaces.

A. Soubret*, G. Berginc
Thomson-CSF Optronique, rue Guynemer,
BP 55, 78233 Guyancourt Cedex, France

C. Bourrely
Centre de Physique Théorique, CNRS-Luminy,
13288 Marseille Cedex 09, France

Analytical theory of vector waves scattering by rough surfaces was mainly studied with the Small Perturbation method (SPM) or the Kirchoff approach (KA). However the domain of validity of these two methods are too restrictive in order to apply it in most cases. The Small Slope Approximation (SSA) developed by Voronovich (Sov.-Phys.-JETP **62** 65-70, 1985) is one of the method which makes a synthesis between the (SPM) and the (KA). The (SSA) is valid provided the slope of roughness is smaller than the angles of incidence and scattering. The slope which is treated as a small parameter has the advantage to be wave-length independent contrary to (SPM) and (KA). A further improvement of the (SSA) has to be considered when multiple scattering effects become important, namely the Non Local Small Slope (NLSSA) developed also by Voronovich (Waves in Random Media **6**, 151-167, 1996).

In this work, we consider an electromagnetic plane wave of arbitrary polarization incident upon a two-dimensional conducting rough surface or upon a 3D dielectric slab with an upper rough surface deposited on a conducting plane. We assume that the rough surface is a Gaussian random process and the autocorrelation function is chosen to be Gaussian too. We propose to calculate the incident cross section with the (NLSSA) using a new approximation which selects enhanced backscattering contributions in such a way that the number of integrations required for the cross-section computation is reduced. Illustrative examples are presented with different incident angles and polarizations. Possible extensions of (NLSSA) to the case of a slab with two rough surfaces or with one rough surface and a volume disorder will be discussed.

This analysis is relevant to problems of laser cross-section, remote sensing of irregular layered structures, remote detection of chemical coatings and for interpretation of ellipsometric data from irregular layered media.

**Scattering by two-dimensional rough surfaces:
comparison between moment method and small slope approximation**

G. Soriano*, C.-A. Guérin and M. Saillard

Institut Fresnel (UMR 6133), case 162, D.U. St Jerome
13397 Marseille Cedex 20, France
gabriel.soriano@fresnel.fr

Abstract: We aim at comparing the results of the Moment Method and the Small Slope Approximation for the scattering of electromagnetic waves from two-dimensional perfectly conducting surfaces with gaussian and ocean roughness spectra.

Since the first simulation of the scattering of electromagnetic waves from two-dimensional rough surfaces in 1994, several fast numerical approaches have been developed. Significant improvements have been made to overcome the limitations of the conventional Moment Method. We have developed a method strongly inspired by the Sparse Matrix Flat Surface Iterative Approach. It involves two nested iterative methods, the Generalized Minimum Residual algorithm and the BiConjugate Gradient Stabilized method. Moreover, the multilevel expansion of the canonical grid method is used in order to speed up the computation. This technique consists, for interactions between remote points, in expanding the Green's function around a 3-D regularly spaced grid. At this point, the incident beam width is still limited by the numerical resources. This limitation can be overcome by using the Beam Decomposition method generalized to two-dimensional surfaces. And finally we have been able to consider in a single diffraction problem a surface realization including the full ocean roughness spectrum.

However, such a method still requires a large amount of memory and is time-consuming. Therefore, a need for fast and accurate methods remains for operational applications such as Earth observation by satellites. In the field of the scattering by the ocean surface, the Small Slope Approximation of Voronovich is one of the most popular methods. We have considered the first- and the second-order Small Slope Approximation.

We have started our comparative study on two-dimensional perfectly electric conducting gaussian surfaces. We then have employed the ocean unified directional spectrum (T. Elfouhaily *et al.*, *J. Geophys. Res.*, 102, 15781-15796, 1997) at frequency bands commonly used by satellites and for various wind speeds and directions.

Iterative PE techniques for rough surface scattering

M. F. Levy, Rutherford Appleton Laboratory, UK
m.levy@rl.ac.uk

Computation of scattering from the sea surface at low grazing angles is already an extremely difficult problem if one neglects atmospheric refraction effects, although much progress has been made recently with forward-backward methods. Difficulties get far worse still if ducting effects are taken into account. Techniques merging high fidelity forward parabolic wave equation models with empirical clutter models have been proposed (J.P. Reilly and G.D. Dockery, *IEE Proc. F*, **137**, 80-88, 1990). More recently, the method of ordered multiple interactions (R.S. Awadallah and G.S. Brown, *IEEE Trans. AP*, to appear) was used to model clutter in an infinite linear duct: this method makes no approximations but is difficult to generalize to more complex refractivity environments.

Here we use a form of the rotated parabolic equation method (M.F. Levy and A.A. Zaporozhets, *JASA*, **103**, 735-741, 1998) to solve the clutter problem in anomalous propagation environments, by splitting boundary conditions on the scattering surface between forward and backward propagating fields (M.F. Levy, *RTO-MP*, **60**, 18.1-18.7, 2000). At each forward step, two computations are made: the first pass assumes that the sea surface is not present at the next range and is used to define the incident field at the surface for the backscattering calculation, while the second pass includes the sea surface. The backward computation of the scattered field enforces a non-homogeneous boundary condition at the surface, given in terms of the previously calculated incident field. The iterative PE method deals accurately with multiple scatter and shadowing in ducting environments, and is computationally cheap. Comparisons with boundary integral equation results are given for the homogeneous case, and the method is applied to realistic ducting environments.

An Improved FB/NSA Algorithm for the Computation of Scattering from
Two-Dimensional Extremely Large-Scale Perfectly Conducting Rough
Surfaces

D. Torrungrueng* and J. T. Johnson
Ohio State University
Dept. of Electrical Engineering
ElectroScience Lab.
1320 Kinnear Rd.
Columbus OH 43212
Tel: (614)292-7981
Fax: (614)292-7297
torrund@ee.eng.ohio-state.edu
johnson@ee.eng.ohio-state.edu

The forward-backward method with a novel spectral acceleration algorithm (FB/NSA) has been shown to be a very efficient $\mathcal{O}(N_{tot})$ iterative method of moments, where N_{tot} is the total number of unknowns to be solved, for the computation of electromagnetic wave scattering from two-dimensional (2-D) rough surfaces (3-D scattering problems). The algorithm is based on the spectral domain representation of the Green's function in the x -direction, and it is specifically designed for 2-D finite rectangular surfaces. However, it is found that as the size of the strong region increases its efficiency decreases due to the increase of the direct computation of the mutual coupling in the strong region.

In this paper, an additional NSA formulation based on the spectral domain representation of the Green's function in the y -direction is incorporated into the original NSA algorithm to improve its computational efficiency. In addition, for the case of *extremely* large-scale rough surfaces, a "multilevel" algorithm (i.e. decomposing 2-D extremely large-scale surfaces into more than one weak region and appropriately choosing the NSA parameters for each weak region) is incorporated into the original FB/NSA algorithm to improve its accuracy. It is found that only a few weak regions are sufficient to obtain accurate results for most practical 2-D extremely large-scale surface problems. However, the improved FB/NSA algorithm remains $\mathcal{O}(N_{tot})$. Numerical results show that the efficiency and accuracy of the original FB/NSA algorithm for the computation of scattering from 2-D extremely large-scale surfaces with *relatively large* surface cross-range sizes are indeed improved by incorporating the y -expansion and the "multilevel" algorithm at the cost of increasing algorithmic complexity and memory requirements.

Inverse Scattering

Chairs: H. Ling, USA and M. Morgan, USA

	Page
8:00 Comparison of Colton-Kirsch Linear Sampling with Linearized Tomographic Inverse Scattering, <i>M. Brandfass*</i> , <i>Aero-Sensing Radar Systeme GmbH</i> , <i>K. Warnick</i> , <i>Brigham Young University</i>	286
8:20 Shape Reconstruction of Metallic Objects with Strong Multiple Scattering Using Genetic Algorithm, <i>Y. Zhou*</i> , <i>H. Ling</i> , <i>The University of Texas at Austin</i>	287
8:40 Localization and Determination of an Optimal Sphere for 3D Objects, <i>H. Tortel*</i> , <i>M. Saillard</i> , <i>Institut Fresnel</i>	288
9:00 3-D Radar Image Formation from Undersampled Aspect Data Using Adaptive Feature Extraction, <i>J. Li*</i> , <i>H. Ling</i> , <i>The University of Texas at Austin</i>	289
9:20 Null Spaces for Near Field Imaging, <i>M. Morgan*</i> , <i>D. Steenman</i> , <i>Naval Postgraduate School</i>	290
9:40 Reconstruction of 3D Lossy Media by using Microwave Measurements, <i>Z. Q. Zhang*</i> , <i>Q. H. Liu</i> , <i>Duke University</i>	291
10:00 Geophysical Analysis of Cross-Borehole Propagation and Reflection Using Triaxial Sources, <i>C. Pendley*</i> , <i>C. Furse</i> , <i>A. Tripp</i> , <i>V. Rayala</i> , <i>Utah State University</i>	292
10:20 A Foliage Penetration Imaging Radar System, <i>C. Beaudoin*</i> , <i>A. Gatesman</i> , <i>M. Testorf</i> , <i>M. Fiddy</i> , <i>R. Giles</i> , <i>J. Waldman</i> , <i>University of Massachusetts Lowell</i>	293
10:40 An Electromagnetic Inversion Algorithm to Detect Neural Activity Using MEG, <i>F. Borelli*</i> , <i>O.P. Gandhi</i> , <i>University of Utah</i> , <i>G. D'Inzeo</i> , <i>University of Rome</i>	294
11:00 Microwave Imaging on an Arbitrary Tilted Plane by a Scalar Inverse Scattering, <i>T. Hasegawa*</i> , <i>T. Iwasaki</i> , <i>The University of Electro-Communications</i>	295
11:20 FDTD Analysis of Spinal Cord Response to Plane Wave Incidence, <i>S. Balaguru*</i> , <i>M. Hashemkhani</i> , <i>B.P. Kumar</i> , <i>California State University-Sacramento</i> , <i>G.R. Branner</i> , <i>University of California, Davis</i>	APS
11:40 The Use of Superresolution Methods for Inverse Scattering - Implications for Imaging Strongly Scattering Targets, <i>M. Testorf</i> , <i>A. Morales-Porras</i> , <i>M. Fiddy</i> , <i>University of Massachusetts Lowell</i> , <i>R. McGahan*</i> , <i>Air Force Research Laboratory</i> , <i>Hanscom AFB</i>	296

Comparison of Colton-Kirsch Linear Sampling with Linearized Tomographic Inverse Scattering

Michael Brandfass

Aero-Sensing Radarsysteme GmbH
Muenchner Strasse 20, D-82234 Wessling, Germany

Aaron Lanterman

Coordinated Science Laboratory
University of Illinois at Urbana-Champaign
1308 W. Main, Urbana, IL 61801, USA

Nathaniel B. Shelton and Karl F. Warnick*

Department of Electrical and Computer Engineering
Brigham Young University
459 Clyde Building, Provo, UT 84602

Inverse scattering algorithms have generally fallen into two broad categories: fast, approximate linear algorithms or slow, accurate nonlinear algorithms. The linear algorithms often amount to simply inverting a Fourier transform. By contrast, nonlinear algorithms, such as the distorted Born iterative method, usually require an expensive Newton-like search. Historically, there have been few options available between these two extremes. Recently, the so-called "regularized linear sampling" method was developed by D. Colton and A. Kirsch. On one hand, it does not employ any linearizing approximations, but on the other hand, it also does not have to use expensive search techniques to iteratively approach a solution. This new method represents an alternative to the usual extremes in inverse scattering. We present numerical comparisons of the linear sampling method with linearized tomographic inverse scattering algorithms based on either holographic filtered backpropagation principles or a matrix inversion scheme. Both methods, unlike linear sampling, make use of linearizing approximations, so that multiple scattering effects are neglected. The most striking feature of the comparison between reconstructions is that linear sampling is not noticeably better than linearized methods, for the cases we tried, even though it takes multiple scattering into account.

In general, reconstructions for TM polarization are superior to the TE polarization. We give some possible explanations for this observation. The theory on which linear sampling is based assumes full aperture data, so we compare methods for the case of limited aperture data as well.

We also study the behavior of linear sampling near internal resonance of closed scatterers. The theorem on which the method is based fails at these frequencies. For the case of the cylinder, the main qualitative feature of linear sampling near resonances is that the scatterer reconstruction becomes an outline rather than a solid image. As electrically large scatterers have many closely spaced internal resonances, resonance effects may be unavoidable at high frequencies.

Shape Reconstruction of Metallic Objects with Strong Multiple Scattering Using Genetic Algorithm

Yong Zhou* and Hao Ling

Dept. of Electrical and Computer Engineering
The University of Texas at Austin
Austin, TX 78712-1084 USA

Inverse synthetic aperture radar (ISAR) imaging is a linearized form of electromagnetic inverse scattering. While the algorithm is fast and robust in obtaining the shape of an object, it suffers from resolution limitation and image artifacts due to multiple scattering phenomena. Rigorously solving the electromagnetic inverse scattering problem, on the other hand, remains much more challenging. Recently, some researchers have explored the use of genetic algorithm (GA) together with computational electromagnetic solvers to attack the inverse scattering problem. In this paper, we investigate the solution of inverse scattering of metallic objects using genetic algorithm. In particular, we address the resolution issue and attempt objects with strong multiple scattering effects such as cavity structures.

In our GA procedure, we encode the object shape into an $N \times N$ binary array with ones representing the metal and zeros representing free space. A geometrical median filter is utilized on each member of the population to avoid unrealistic shapes. A method of moment solution is applied to obtain the rigorous scattered field to each shape. To evaluate the performance of each shape, a cost function is defined as the difference between the scattered field from the GA member and the real object. The inverse problem is then cast into a minimization problem and GA is applied to minimize the cost function. The selection, crossover, mutation and geometrical filtering operators are applied in order on each member to produce the next generation. This process is iterated until the cost function reaches a sufficiently small threshold.

Several test objects are studied based on the GA scheme and simulated field data. For multiple cylinders, good shape reconstruction to the real object is obtained, even when the spacing between the cylinders is on the order of half a wavelength. In the cavity problem, the cavity shape can be reconstructed correctly without any artifacts. In addition, we study the effects of different sensor scenarios including monostatic versus bistatic collection, single frequency versus multi-frequency data, and amplitude-and-phase versus amplitude-only data. High-frequency ray tracing is also attempted in place of the moment method solver to study electrically large objects.

Localization and determination of an optimal sphere for 3D objects

H. Tortel*, M. Saillard
Institut Fresnel, UMR CNRS 6133
Faculte St-Jerome, case 162
13397 Marseille Cedex 20, France

We address the problem of the reconstruction of the shape of 3D perfectly conducting objects, embedded in a lossy homogeneous medium and illuminated by electric dipoles located in two parallel boreholes. This work is a generalization to 3D objects of a method developed in our laboratory for cylinders. In this case, the inverse scattering problem is classically transformed into the minimization of a cost function, achieved through an iterative process with the help of a conjugate gradient method. At each step, a rigorous boundary integral formalism is used to solve the direct problem. (Inverse Problems, **14**, 1998, 521-534).

Previous studies have shown that the method may present local minima and requires an accurate initial guess for convergence to be ensured. As a regularization, the shape of the object has been expanded onto a Fourier basis, and, step by step, a growing number of Fourier coefficients is optimized. The process is thus as follows: first, a backpropagation allows detection and localization of the scatterer, and a low frequency approximation provides a circular cylinder as initial guess. Then the coordinates of the center and the radius of the circle are optimized, leading to an "optimal circle". Finally, higher Fourier coefficients are introduced to fit the real shape.

From the reconstruction of both synthetic and real data, it clearly appeared that once the "optimal circle" is accurately localized and once its cross section area is of same order of magnitude as that of the scatterer, the reconstruction process succeeds. Of course, the accuracy of the solution depends on the frequency, on the noise and on the number of measurements, but the true minimum of the cost function is reached.

Therefore, with the aim of applying the same strategy to 3D problems, we focus here on the determination of an optimal sphere. First, this requires the detection and the localization of the object. Unfortunately, our backpropagation method does not give any estimation of the coordinate in the direction perpendicular to the plane of the two boreholes, and also requires very deep boreholes to be accurate. In the present case, it only permits one to detect scatterers and to determine their depth. To circumvent this problem, we have developed a new method, based on the polarization properties of the backscattered field in the low frequency range. When the incident electric dipolar moment \mathbf{P}^{inc} is parallel to the direction joining the emitter to the scatterer, the backscattered electric field \mathbf{E}^{b} is also directed along this direction. Therefore, maximizing the (normalized) scalar product $|\mathbf{P}^{\text{inc}} \cdot \mathbf{E}^{\text{b}}|$ tells one in which direction the scatterer is located. Using the two boreholes allows one to locate the scatterer at the intersection point of the two lines.

As in two dimensions, the refinement of the initial guess leading to the "optimal sphere" is performed by minimizing the cost function with respect to the four real parameters characterizing a sphere, through a conjugate gradient method. The gradient of the cost function is analytically calculated in the frame of Mie's theory. Numerical results will be presented for various scatterers, like spheres, oblate and prolate spheroids.

3-D Radar Image Formation from Undersampled Aspect Data Using Adaptive Feature Extraction

Junfei Li and Hao Ling

Department of Electrical and Computer Engineering
The University of Texas at Austin
Austin, TX 78712-1084

The formation of three-dimensional (3-D) radar images of a target requires the collection of range-compressed radar data over a two-dimensional (2-D) angular aperture. If a Fourier-based imaging algorithm is to be used, the data sampling must satisfy the Nyquist criterion over the 2-D aperture. However, for real-world data collection scenarios such as SAR (synthetic aperture radar) and ISAR (inverse SAR), the collection of densely sampled data in a 2-D angular aperture can rarely be accomplished. In this paper, we investigate the use of the adaptive feature extraction (AFE) algorithm for the formation of 3-D radar images from undersampled radar data over a 2-D angular aperture.

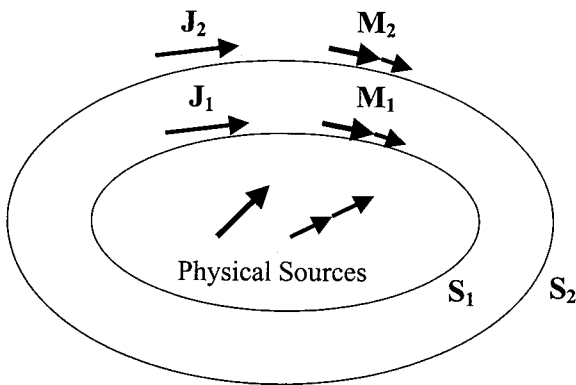
The AFE algorithm used here is a generalization of our previous work on 2-D radar image construction from undersampled data along one angular dimension (Y. Wang and H. Ling, *IEEE Trans. Antennas Propagat.*, **48**, 329-331, 2000). First, a 3-D point scatterer model is used as the basis function in the AFE procedure. The algorithm begins by exhaustively projecting the radar data onto the basis set and selecting the point scatterer with the maximum projection value. The response of the selected point scatterer is then subtracted from the radar data and the process is repeated for subsequent, weaker point scatterers. The iteration is terminated when the residual signal energy reaches a preset threshold. Since the point features are selected and removed one at a time starting from the strongest, the sidelobe interference from the strong point scatterers on the weaker ones is greatly reduced. This is accomplished at the expense of computational burden.

The algorithm is applied to simulated radar data under various sensor collection scenarios such as ISAR collection of air targets with multiple fly-bys or ISAR collection of ships on a rough sea. The resulting images are compared to those from Fourier-based algorithms. It is found that focused target images can be achieved with the AFE algorithm while Fourier-based methods fail to produce meaningful results. The effects of data noise and inaccuracy in aspect information are investigated to determine the limitation of the algorithm. Work on using genetic algorithm to accelerate the AFE search is also discussed.

Null Spaces for Near Field Imaging

Michael A. Morgan* and Daryl G. Steenman
Electrical and Computer Engineering Department
Naval Postgraduate School
833 Dyer Road, Room 437, Monterey, CA 93943

The Equivalence Theorem is used to demonstrate null space properties for equivalent current based field generation. Referring to the figure below, fields on S_2 due to sources enclosed within S_1 can be computed by integration of the physical currents or by integration of equivalent currents J_1 and M_1 generated from tangential fields on S_1 . The resultant Green's function integration from inner surface J_1 and M_1 to obtain the outer surface J_2 and M_2 forms an exact surface-to-surface transfer function. This transfer function can be approximated as an $N \times M$ array operator by using basis expansions for the equivalent currents. Inversion of this operator was investigated as a means to back-propagate measured near-fields between surfaces to obtain high-resolution images of physical source distributions. Attempted inversions indicated strong ill-conditioning of the inverse operator, irrespective of surface separations. A resultant theoretical investigation led to the discovery of null spaces of equivalent currents on S_1 that generate no fields exterior to the surface.



Reconstruction of 3D Lossy Media by Using Microwave Measurements

ZHONG QING ZHANG* AND QING HUO LIU
DEPARTMENT OF ELECTRICAL AND COMPUTER ENGINEERING
DUKE UNIVERSITY
DURHAM, NC 27708-0291

In this work we investigate the inverse problem of three-dimensional lossy media by using microwaves. In the past two decades tremendous efforts have been made in two- and three-dimensional scalar inverse methods to reconstruct the complex permittivity. These developments represent significant progress from the previous capability. However, for accurate microwave imaging, further improvements are needed in order to remove the artifacts due to the two-dimensional assumptions and due to the 3-D scalar approximation. For examples, using the 2-D inversion, the depth of the object perpendicular to the 2-D plane cannot be accurately determined; using the 3-D scalar approximation, the cross polarization of vector electromagnetic fields is not accounted for.

The main contribution of this work is to apply the contrast-source inversion (CSI) method to the full three-dimensional inversion of complex permittivity. Instead of scalar approximation, we use vector field directly to invert the three-dimensional permittivity. The cost functional is composed of two parts in the reconstruction procedure: One is from the state equation which describes the vector scattering field; the other is from measured data which defines the measured scattering field. By using Polak-Ribiere conjugate-gradient procedure, we can minimize the total cost functional to an acceptable value to invert for the three-dimensional complex permittivity. These procedures are essentially the same as our previous 2-D implementation. This inverse algorithm requires $O(N)$ memory, and $O(N \log N)$ CPU time, where N is the number of pixels to be reconstructed. This represents a substantial reduction in computational costs compared to other inverse scattering algorithms.

We apply this CSI algorithm to simulate a prototype microwave imaging system in our laboratory. In our numerical results, the measured data is obtained from synthetic simulation using our fast forward solution method based on a weak-form biconjugate gradient FFT method. This BCG-FFT method solves the full three-dimensional vector electromagnetic fields. In the inversion, the initial solution is obtained through the back propagation. Since this inverse problem is highly ill-posed, we adopt a recently proposed minimal total variation constraint to enhance the resolution of the three-dimensional complex permittivity.

This work was supported by U.S. EPA through a PECASE grant CR-825-225-010, and by the NSF through a CAREER grant ECS-9702195.

Geophysical Analysis of Cross-Borehole Propagation and Reflection Using Triaxial Sources

Chad Pendley, Cynthia Furse, Alan Tripp, Vinod Rayala

Department of Electrical and Computer Engineering
Utah State University
Logan, Utah 84322-4120
Phone: (435) 797-2870
FAX: (435) 797-3054
Furse@ece.usu.edu

Abstract

Induction logging is a technique that is used to evaluate the production potential of the preponderance of petroleum and gas wells drilled in the world. In this technique, an oscillating magnetic source (a wire loop) is lowered into a borehole to induce an electric current in the geological material surrounding the well. The magnitude and geometry of the electric current is dependent on the electrical conductivity distribution in the geological material. In particular, since geological formations saturated with hydrocarbons are electrically resistive and those saturated with water tend to be conductive, the two have different electric current distributions. These differing electric current distributions lead to differing magnetic fields, which are measurable using induction coils in the same borehole or a different borehole nearby. A great deal of work has been done to quantify the relationship between the amount and distribution of hydrocarbons in the formation and the measured magnetic field in vertical wells that intersect electrically isotropic geological beds.

There are compelling reasons, however, to deviate boreholes away from the vertical direction. First, since hydrocarbon bearing formations tend to be stratified, production from the formation is enhanced if the borehole, and hence the recovery surface, can be aligned along the formation. Another reason for using deviated wells is that multiple wells can be drilled from a single well drilling platform. This reason is very significant if the platform is very expensive, such as for ocean drilling platforms. When wells deviate from vertical, the effect of electrical anisotropy must be considered. Electrical anisotropy occurs when the resistivity is different in different directions. Even vertical wells in Utah's overthrust belt are anisotropic formations, because the rock bedding layers have been tilted by tectonic movement.

The results of our simulations indicate that for z-directed sources (sources propagating in the vertical direction), magnetic fields were strongest in the x-direction, followed by y- and z-directed fields, respectively. As the source's propagation direction changed, the magnetic fields parallel to the source remained consistently weaker. Another detail that we observed was that though electrical anisotropy can strongly affect field magnitudes (in our results, on the order of 1,000), some fields seem to be more sensitive than others to the changes in dielectric properties. The fields that showed greatest sensitivity related to the direction of the source and the dominant direction of the anisotropic irregularities. Findings indicate that there may be significant benefits for employment of triaxial sources as well as receivers in the geophysical realm.

A Foliage Penetration Imaging Radar System

Chris Beaudoin¹, Andrew Gatesman², Markus Testorf¹, Michael Fiddy¹, Robert Giles², and J. Waldman²

¹Department of Electrical and Computer Engineering

²Submillimeter-Wave Technology Laboratory

600 Suffolk Street, Lowell, MA 01854, USA

Phone: 978) 458-3807, Fax: 978) 452-3333, Email: Andrew_Gatesman@uml.edu

Synthetic aperture radar (SAR) imaging of ground vehicles through foliage is still an unsolved problem. The difficulty in finding a satisfying solution is partly due to the reduced image resolution which results from the low radar frequencies required for penetrating typical tree canopies. Additional problems arise when one wants to distinguish between man-made objects and natural features in the target area, which both can cause backscattered signals of similar strength.

We describe a measurement system for collecting inverse SAR (ISAR) data for FOPEN frequencies (230 – 350 MHz) by measuring the X-band (8.2 – 12.4 GHz) radar signature of $1/35^{\text{th}}$ scaled vehicles and terrain scenes. A compact radar range has been constructed to acquire data from scaled ground vehicles as well as ground terrain, trees, and a vegetation canopy. While the entire geometry is scaled by a factor of $1/35$, the electromagnetic properties of the target and terrain are tailored to be equal to the full-scale scene as required by scale modeling laws. Due to the small size of the target as compared to the wavelength it is necessary to use additional target information to obtain an ISAR image of acceptable quality.

In our contribution we discuss the radar system we have used for our experiment. This includes details about the scattering geometry and beam profile as well as the evaluation of the radar beam quality. As a further point we will discuss the method used to fabricate high quality $1/35^{\text{th}}$ scale models as well as the techniques used to scale a material's complex dielectric constant dielectrically.

To image the target we used a linear spectral estimation technique, which can incorporate a wide variety of available prior information. This method has previously proved successful for imaging targets in a homogeneous background, but this is the first time it has been applied to objects embedded in a potentially cluttered background. We will show reconstructions based on the collected real data including an assessment of the merits of the method.

AN ELECTROMAGNETIC INVERSION ALGORITHM TO DETECT NEURAL ACTIVITY USING MEG

F. Borelli, O. P. Gandhi, and G. D'Inzeo¹

Department of Electrical Engineering, University of Utah, Salt Lake City, UT 84112, USA

¹Department of Electronics, University of Rome, "La Sapienza", Rome 00184, Italy

Non-invasive techniques using the measured MEG data have been used to determine the location, orientation, and magnitude of two to three equivalent current dipoles that are excited in the cerebral cortex in response to various stimuli e.g. visual, auditory, and neuromuscular stimuli. However, a homogeneous sphere model of the head is often used for such inversion algorithms [1]. An important aspect of inversion problems is to have good forward models such as those that have previously been developed for dosimetry of EM fields. For the present paper, we have used a shaped model of the head represented by 6 mm voxels in the first instance, and the quasi-static impedance method [2] to calculate the forward magnetic fields at 74 locations of the MEG sensors. To obviate the need for anatomic details, we show that the external magnetic field distributions are affected little by using a shaped but homogeneous model rather than the detailed heterogeneous model. It is recognized that the measured MEG signals may be corrupted by white noise. Noise levels with standard deviation up to 25% for the signal intensity are, therefore, included with the signals for each of the 74 sensors. Adding up to 50 independent recordings for the evoked MEG signals helps to improve the signal-to-noise ratio. To locate two possible current dipoles in two subvolumes in the auditory cortex of the brain, each one represented by 58 voxels, we need to find the solution of the matrix equation $Ax = b$, where b is the MEG data vector (signal + noise), A is the lead field matrix, and x is the vector representing the current distribution in the subvolumes. To solve the system, we have used Tikhonov method

$$\left(x_{\lambda} = \arg \min \left\{ \|Ax - b\|_2 + \lambda \|L(x - x^*)\|_2 \right\} \right)$$

as the regularization method but we implement an iterative procedure that modifies the A matrix using the estimate of the solution obtained at the previous step, to lower the effect of spurious solution and obtain a more focused solution. Up to seven iterations are generally needed to pinpoint the location, orientation, and magnitude of the source dipoles for each of the time steps of the measured MEG signals.

The authors have greatly benefited from many helpful discussions with Professors Mathews and Nagarajan of the University of Utah.

- [1] J. C. Mosher, R. M. Leahy, and P. S. Lewis, "EEG and MEG: Forward Solutions for Inverse Methods," *IEEE Trans. Biomed. Eng.*, Vol. 46(3), 245-259, 1999.
- [2] N. Orcutt and O. P. Gandhi, "A 3-D Impedance Method to Calculate Power Deposition in Biological Bodies Subjected to Time-Varying Magnetic Fields," *IEEE Trans. BME*, Vol. 35, 577-583, 1988.

Microwave Imaging on an Arbitrary Tilted Plane

by a Scalar Inverse Scattering

Tomonori Hasegawa* and Takashi Iwasaki

The University of Electro-Communications, Chofu, Tokyo, 182-8585 Japan
Tel: +81-424-43-5189, Fax: +81-424-43-5210, E-mail: don@snow.ee.uec.ac.jp

Background:

Microwave imaging is useful for detecting invisible enclosed objects and for evaluating electromagnetic absorbers. In such applications, imaging on an arbitrary tilted plane is desired to reduce computational cost and to improve the reconstructed images.

Reconstruction method:

A scalar inverse scattering has been formulated in an integral form. Using this equation and a multi-frequency processing, we can reconstruct a three-dimensional image from measured scattering fields. However, the full three-dimensional imaging requires a lot of computation time.

In order to reconstruct a two-dimensional object tilted against the measurement plane, we present the following technique. First, two-dimensional images are reconstructed on several planes parallel to the measurement plane. Then, a part of the object will appear in each reconstructed image. Next, the tilt angle is estimated from these images, and the final image is reconstructed in the observation plane on the object. The formulated scalar inverse scattering makes this reconstruction possible because of its integral form. This method has an advantage of computational cost over the three-dimensional imaging.

Experiment:

An experiment was made to validate the proposed imaging method. The frequency range is from 8 GHz to 13 GHz at an interval of 0.1 GHz. Archimedean spiral antennas were scanned for emitting and detecting. The total area of scanning plane is 1.0 m x 1.0 m with the scanning resolution of 0.02 m. A "T" shaped metal object (10cm x 10cm) was placed on 0.485 m distance from scanning plane as shown in Fig.1. The images of Fig. 2 show that the proposed method is useful for reconstructing a tilted object two-dimensionally.

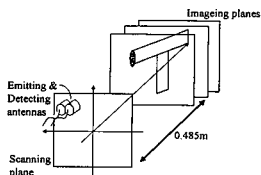


Fig.1: Schematic diagram of reconstruction method



Fig.2: reconstructed image at 0.465m (left), 0.485m (center) and 0.485m tilted 20deg.(right).

The Use of Superresolution Methods for Inverse Scattering - Implications for Imaging Strongly Scattering Targets

Markus Testorf, Andres Morales-Porras, Michael Fiddy, Robert McGahan*

University of Massachusetts-Lowell, Dept. Elec. & Comp. Eng.

One University Ave., Lowell, MA 01854, USA

Phone: (978) 934 3395, Fax: (978) 934 3027, Email: testorf@galileo.eng.uml.edu

*Air Force Research Laboratory, 31 Grenier St., Hanscom AFB, MA 01731-3010

The standard configuration to image permittivity distributions from scattered electromagnetic field data assumes sources and detectors are located in the far zone of the target. One consequence of this arrangement is the fact the only non-evanescent wave modes are detected and from scattering experiments only spatial frequencies with a modulus smaller or equal to twice the wave number can be determined. The Rayleigh limit then predicts a target resolution of not better than half the wavelength. Particularly for subsurface and foliage penetration radar imaging, however, the Rayleigh limit is a serious limitation, if subwavelength features are required to identify the target. To resolve this problem numerous schemes have been proposed to overcome Rayleigh limit. This can be achieved by including prior information about the target.

The concept of analyticity applied to scalar diffraction seems to support the idea that superresolution can be achieved for all objects of compact support, at least in principle and depending on the noise background. However, there are at least two examples, which seem to contradict this assumption. Firstly, the design of subwavelength diffractive optical elements represents an example where the response of subwavelength features is intentionally made equivalent to that of an element with macroscopic features. Since the information about microscopic features is not present in the diffracted field there should be no way to employ superresolution methods to resolve the ambiguity.

A second example is the interpretation of images obtained from strongly scattering targets by using an inverse Fourier transform algorithm applied to far field data. Considerable intensity can be found outside the target area due to multiple reflections between different parts of the target. The scattering integral interprets these images as the result of multiplying the target permittivity with the total field and a subsequent low pass filter step. Due to the Fourier relation between the far field and the product of field and permittivity the intensity hot spots outside the target should disappear for the case of perfect spectral extrapolation. However, an interpretation of these intensity hot spots as the result of multiple scattering indicates that all superresolution methods are able to do is enhance these undesired features.

From examples we show that superresolution methods are limited to particular classes of objects. This has particular implications to methods, which have been proposed to address the problem strong scattering. In particular, we demonstrate the non-uniqueness can be partially removed by including appropriate prior information, or by increasing the number of scattering experiments.

Fractal Antennas

Chairs: D. Werner, USA and J. Romeu, Spain

		Page
1:00	Fracton Vibration Modes in the Sierpinski Microstrip Patch Antenna, <i>C. Borja, J. Romeu*, Universitat Politecnica de Catalunya (UPC)</i>	APS
1:20	Analysis of a Sierpinski for Fractal Patch Antenna Using the Concept of Macro Basis Functions, <i>J. Parron*, J.M. Rius, J. Romeu, Universitat Politecnica de Catalunya (UPC)</i>	APS
1:40	An Efficient Recursive Procedure for Calculating the Driving Point Impedance of Linear and Planar Fractal Arrays, <i>D. Baldacci*, D.H. Werner, The Pennsylvania State University</i>	APS
2:00	The Electrically Small Limit of Fractal Element Antennas, <i>R. Hohlfeld*, Boston University, N. Cohen, Fractal Antenna Systems, Inc.</i>	APS
2:20	Genetically Engineered Dual-Band Fractal Antennas, <i>D.H. Werner*, P.L. Werner, The Pennsylvania State University, K.H. Church, CMS Technetronics Inc., J.W. Culver, S.D. Eason, Raytheon Systems Company</i>	APS
2:40	A Novel Design Approach for Small Dual-Band Sierpinski Gasket Monopole Antennas, <i>D.H. Werner*, J. Yeo, The Pennsylvania State University</i>	APS
3:00	UHF Fractal Antennas, <i>S.D. Eason*, R. Libonati, J.W. Culver, Raytheon Systems Company, D.H. Werner, P.L. Werner, S. Mummareddy, The Pennsylvania State University</i>	APS
3:20	Fractal Patch Antennas: Miniaturizing Resonant Patches, <i>J. Gianvittorio*, Y. Rahmat-Samii, University of California, Los Angeles</i>	298
3:40	Fractal FSS: Various Self-Similar Geometries Used for Dual-Band and Dual-Polarized FSS, <i>J. Gianvittorio*, Y. Rahmat-Samii, University of California, Los Angeles, J. Romeu, Universitat Politecnica de Catalunya (UPC)</i>	APS
4:00	Observation of the Localized Modes in the Koch Waveguide, <i>J. Romeu, A. Aguasca, S. Blanch*, Universitat Politecnica de Catalunya (UPC)</i>	APS
4:20	Resonant Frequency of Hilbert Curve Fractal Antennas, <i>K.J. Vinoy*, K.A. Jose, V.K. Varadan, V.V. Varadan, The Pennsylvania State University</i>	APS

Fractal Patch Antennas: Miniaturizing Resonant Patches

John Gianvittorio and Yahya Rahmat-Samii

Department of Electrical Engineering
University of California, Los Angeles
Los Angeles, California 90095-1594
rahmat@ee.ucla.edu

Fractals are space filling geometries that can efficiently incorporate large electrical lengths. The dimension of the geometry can be interpreted as a quantification of the space filling ability of the geometry. While Euclidean geometries have integer dimensions, 1 for a line and 2 for a plane, fractals have fractional dimensions. By exploring the correlation between the dimension of the geometry and its radiating characteristics, efficient radiating geometries may be discovered beyond the simple linear dipoles and rectangular patches that are common today.

Simple fractals are structures that are generated using an iterative technique. The starting structure, called the initiator, defines the general shape of the structure. For the 2nd order example shown inset in Fig.1 the initiator is a square. Slots are added at each iteration decreasing in size each time. The fractal dimension of the structure can be modified by adjusting the size of the slots.

It has been shown previously that fractals can be used to miniaturize wire antennas. Patch antennas are investigated here as a logical extension of a study of fractal dimension on radiating structures. The fractal described above has been simulated as a patch antenna on a 0.7874 mm thick substrate with $\epsilon_r=2.2$. The calculated input match, plotted in Fig. 1, shows the 2nd iteration is resonant at a frequency which is 56% of the resonant frequency of the square patch with the same width.

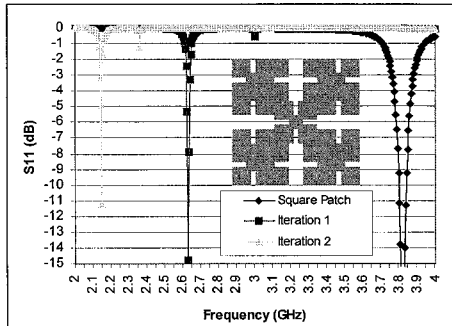


Figure 1: Computed input match for a square patch and the first two fractal iterations with the same width. The 2nd iteration fractal patch shows a miniaturization of 44%.

This patch and other fractal geometries will be investigated to derive further conclusions about the correlation between radiators and fractal dimension.

RF MEMS for Antenna Applications

Chairs: R. Reid, USA and M. Zaghoul, USA

	Page
1:00 MEMS-Switched Reconfigurable Antennas, <i>W. Weedon*, W. Payne, Applied Radar, Inc., G. Rebeiz, University of Michigan</i>	APS
1:20 A Wideband Beam Switching Antenna Using RF MEMS Switches, <i>J. Schaffner*, D. Sievenpiper, R. Loo, HRL Laboratories, J. Lee, S. Livingston, Raytheon</i>	APS
1:40 MEMS True-Time Delay Circuit for Broadband Antennas, <i>M. Kim, Korea University, J.B. Hacker, R.E. Mihalovich*, J.F. DeNatale, Rockwell Science Center</i>	APS
2:00 Micromachined Waveguides and Horns for Submillimeter-Wave Components, <i>T. Crowe*, University of Virginia</i>	300
2:20 A Hybrid-Statistical Approach for Accurate Characterization of MEMS on Complex Platforms, <i>T. Ozdemir*, K.F. Sabet, E. Yasan, M.C. Bega, EMAG Technologies, Inc., J. Ebel, AFRL/SNDD-Wright Patterson AFB, G. Creech, C. Lesniak, AFRL/SNDM-Wright Patterson AFB, L. Katehi, K. Sarabandi, University of Michigan</i>	APS
2:40 Low Voltage Tunable Capacitors for RF MEM Filters and Antenna Applications, <i>K.A. Jose*, H. Yoon, K.J. Vinoy, P. Sharma, V.K. Varadan, V.V. Varadan, Pennsylvania State University</i>	APS
3:00 Reconfigurable Array Antenna Using Microelectromechanical Systems (MEMSS) Actuators, <i>R. Simons*, Dynacs Engineering Company, Inc, D. Chun, L. Katehi, University of Michigan</i>	APS
3:20 MEMS Microswitches for Reconfigurable Microwave Circuitry, <i>S. Duffy, C. Bozler, S. Rabe, J. Knecht, L. Travis, P. Wyatt, M. Gouker, C. Keast*, MIT Lincoln Laboratory</i>	301
3:40 RF MEMS Components Using CMOS Technology, <i>M. Ozgur, M. Zaghoul*, The George Washington University</i>	APS
4:00 Development of Very Low Loss 2-Bit and 4-Bit Monolithic X-Band MEMS Phase Shifter, <i>G.L. Tan*, G.M. Rabiez, University of Michigan, J.B. Hacker, R.E. Mihalovich, J.F. DeNatale, Rockwell Science Center, N. Karabudak, W. Taft, T. Karras, Lockheed Martin Space Systems, W. Kornrumpf, GE Corporate R&D</i>	302

Invited paper: Special session on "MEMS for antenna applications," Session number SS-3

Micromachined Waveguides and Horns for Submillimeter-Wave Components

Thomas W. Crowe

Department of Electrical Engineering
University of Virginia
351 McCormick Road
PO Box 400743
Charlottesville, VA 22904-4743

Corresponding Author: Thomas W. Crowe (twc8u@virginia.edu)

Abstract

Micromachining technology makes possible the cost-efficient production of large numbers of identical components with extremely fine control of critical features. This paper discusses the fabrication of micromachined waveguide components based on the use of standard semiconductor processing technologies. A micromachined horn antenna with easy to control flare angle and good Gaussian coupling efficiency has been integrated with precisely defined rectangular waveguides and microstrip channels. A 585 GHz fundamentally pumped Schottky mixer with record performance demonstrates this technology. It consists of an etched silicon horn, a diced waveguide and a lithographically formed microstrip channel for the diode circuit. The block dimensions are precisely controlled and extremely sharp. The measured mixer noise temperature is 1,200 K (DSB), which is equivalent to the best result obtained with standard metal machining. A similar assembly scaled to 1.6 THz has also been successfully fabricated.

Index Terms - Micromachining, Submillimeter-wave Circuits.

MEMS Microswitches for Reconfigurable Microwave Circuitry¹

Sean Duffy, Carl Bozler, Steven Rabe, Jeffrey Knecht, Lauren Travis,
Peter Wyatt, Mark Gouker and Craig Keast

MIT Lincoln Laboratory
244 Wood St.
Lexington, MA 02420-9108

Abstract

The performance is reported for a new micro-electro-mechanical-structure (MEMS) cantilever microswitch. We report on both DC- and capacitively-contacted microswitches. The DC-contacted microswitches have contact resistance of less than 1Ω , and the RF loss of the switch up to 40 GHz in the closed position is 0.1 – 0.2 dB. Capacitively-contacted switches have an impedance ratio of 141:1 from the open to closed state and in the closed position have a series capacitance of 1.2 pF. The capacitively-contacted switches have been measured up to 40 GHz with S_{21} less than -0.7 dB across the 5 – 40 GHz band and under hot and cold switching conditions with 2 watts of RF power. In addition, preliminary reliability data on both DC and capacitive switch designs will be presented.

A reconfigurable microstrip antenna containing 2080 gang-addressable DC-contacted switches has been designed, fabricated and characterized at 14 and 21 GHz. In addition, a tunable notch filter containing 8 capacitively-contacted switches has been characterized. The measured results of the fabricated two-state filter closely match the simulation predictions with ~40 dB deep troughs at 8.2 and 10.4 GHz.

¹ This work was sponsored by the Defense Advanced Research Projects Agency under Air Force Contract #F19628-00-C-0002. Opinions, interpretations, recommendations, and conclusions are those of the authors and are not necessarily endorsed by the United States Government.

Development of Very Low Loss 2-Bit and 4-Bit Monolithic X-Band MEMS Phase Shifters

*Guan-Leng Tan and Gabriel M. Rebeiz
University of Michigan, Ann Arbor, MI*

*J. B. Hacker, R. E. Mihailovich, J.F. DeNatale
Rockwell Science Center, Thousand Oaks, CA*

*N. Karabudak, W. Taft, T. Karras
Lockheed Martin Space Systems, Newtown, PA*

*W. Kornrumpf
GE Corporate R&D, Schenectady, NY*

The talk will present the design, fabrication and measurement of very low-loss phase shifters for X-band applications. The design is based on the unique low capacitance characteristics of the Rockwell Science Center MEMS series switch, and result in DC-18 GHz performance. The phase shifters exhibit an average insertion loss of 0.7 dB for the 2-bit design and 1.0 dB for the 4-bit design (modeled). The modeled reflection coefficient is less than -20 dB up to 16 GHz in all 4-states (or 16 states). The MEMS phase shifters are monolithically integrated on a 200 um-thick GaAs substrate, and result in a much lower cost than the hybrid-type X-band phase shifters of Raytheon and Hughes Research Labs. Furthermore, the new designs are quite small, with a size of 11mm² for the 2-bit design and 14mm² for the 4-bit design. Since the Rockwell Science Center MEMS switch is compatible with GaAs post-processing, the phase shifters can be integrated with low-noise GaAs amplifiers (or medium power amplifiers) to form a complete X-band front-end module. The talk will also discuss a novel packaging technique, developed at GE Corporate R&D, which allows wafer-scale packaging of MEMS switches and phase shifters.

This work is done under the DARPA/MEM-Tenna Program. Program Manager: J.K. Smith

New Results in Space Based Sounding

Chair: G. Sales, USA

	Page
1:00 New Tools for Analysis of Space-Borne Sounding Data, <i>I. Galkin*</i> , <i>G. Khmyrov</i> , <i>A. Kozlov</i> , <i>B. Reinisch</i> , <i>X. Huang</i> , <i>G. Sales</i> , <i>University of Massachusetts Lowell</i>	304
1:20 Radio Sounding of the Plasmopause, <i>M. Salvati*</i> , <i>D. Carpenter</i> , <i>U. Inan</i> , <i>T. Bell</i> , <i>Stanford University</i> , <i>B. Reinisch</i> , <i>University of Massachusetts Lowell</i>	305
1:40 Observations of Ducts in the Plasmasphere by RPI, <i>G. Sales*</i> , <i>X. Huang</i> , <i>B. Reinisch</i> , <i>P. Song</i> , <i>University of Massachusetts Lowell</i> , <i>D. Carpenter</i> , <i>Stanford University</i> , <i>S. Fung</i> , <i>R. Benson</i> , <i>J. Green</i> , <i>NASA Goddard Space Flight Center</i>	306
2:00 Electron Density Distributions Along Magnetic Field Lines in the Magnetosphere Deduced from RPI Plasmagrams, <i>X. Huang*</i> , <i>B. Reinisch</i> , <i>P. Song</i> , <i>University of Massachusetts Lowell</i> , <i>R. Benson</i> , <i>J. Green</i> , <i>S. Fung</i> , <i>NASA Goddard Space Flight Center</i> , <i>D. Carpenter</i> , <i>Stanford University</i>	308
2:20 Ionospheric Occultation Measurement with Single Frequency GPS Onboard Receiver, <i>J-S. Guo*</i> , <i>S-P Shang</i> , <i>M-L. Zhang</i> , <i>H. Zheng</i> , <i>X-G. Luo</i> , <i>J. Shi</i> , <i>Q-Y. Zhang</i> , <i>Chinese Academy of Sciences</i>	309

NEW TOOLS FOR ANALYSIS OF SPACE-BORNE SOUNDING DATA

Ivan Galkin, Grigori Khmyrov, Alexander Kozlov, Bodo Reinisch,
Xueqin Huang, Gary Sales
*Center for Atmospheric Research
University of Massachusetts Lowell*

In an effort to maximize the efficiency of the space exploration, research agencies are beginning to open public access to the complete, high-resolution datasets from their missions. This paper discusses a new generation of software tools designed to support the full range of data manipulation services for the high-resolution dataset from the Radio Plasma Imager (RPI) aboard NASA's IMAGE spacecraft.

The software tools, known collectively as the "RPI BinBrowser", target a wide user community ranging from college students to the domain experts, and from the casual visitors to the RPI science team members. The BinBrowser therefore admits a wide variety of computing platforms and data access scenarios. To accommodate for the platform inhomogeneity, the core of BinBrowser is written in Java, and its installation can be done seamlessly over the Web (refer to <http://ulcar.uml.edu> for more details). The BinBrowser workstations can communicate over the Internet with the central database at UML where RPI telemetry, derived, orbital and predicted geophysical data are archived. Where connection bandwidth permits, the UML database provides the complete raster of data products to the BinBrowser user. Binary telemetry data files can be acquired independently on CD-ROMs, DVD-ROMs, or over Internet from NSSDC and other RPI data dissemination institutions, so that the traffic between BinBrowser workstations and the UML database can be significantly reduced to the data catalog queries and requests of auxiliary data. An important part of the auxiliary data stored in the UML database is the expert ratings. The expert ratings allow a novice user to subset the whole archive to the measurements considered worthy of attention by the experts registered with UML and to set the suggested BinBrowser visualization options to create the optimal data presentation.

The BinBrowser visualization and analysis tools are specific to the RPI instrument. As a radio sounder, RPI takes images of the surrounding plasma in the range-frequency domain, "plasmagrams". Echoes from the plasma features within the radar range form traces on the plasmagrams. The BinBrowser provides means for interactive highlighting of the traces and calculation of the electron density along the echo paths. The echo arrival angles can be calculated as well, so that the trace data are presented as an "echomap" indicating locations of the plasma features responsible for the trace formation. Further technical details of the BinBrowser implementation are briefly discussed.

The RPI BinBrowser tool brings a new potential for analysis of high-resolution datasets by combining powerful platform-independent software solutions with the ease of data access, search and referencing to the expert knowledge.

Radio Sounding of the Plasmapause

M. Salvati, D.L. Carpenter, U.S. Inan, T.F Bell
Space, Telecommunications and Radioscience Laboratory
Stanford University

B.W. Reinisch
Center for Atmospheric Research
University of Massachusetts, Lowell

The Radio Plasma Imager (RPI) on the IMAGE mission is a low-power radar which operates in the radio frequency bands which contain the plasma resonance frequencies characteristic of the Earth's magnetosphere (3 kHz to 3 MHz). RPI can locate regions of various plasma densities by observing radar echoes from the plasma that are reflected where the radio frequency is equal to the plasma frequency. For sounding densities in the region of the plasmapause, the appropriate frequency range is approximately 10-300 kHz. The original expectations of the RPI team were that echoes from the plasmapause region would be discrete, consisting of a single return echo received at each frequency. However, the typical echo patterns received as IMAGE approaches the plasmasphere at low magnetic latitudes include diffuse echoes, involving returning signals which reflected at ranges of up to two Earth radii, and highly efficient field aligned ducting within or adjacent to the region of steep plasmapause gradients. These initial results suggest that irregular structure is regularly present in the plasmapause boundary region. Such structure has been identified in in-situ radio data from a number of satellites. We will present examples of diffuse plasmapause echoes and interpret them in terms of overall characteristics of plasmapause structure. We will also present results of initial attempts to quantitatively model the reflections from the irregular plasmapause density structures in terms of normal incidence of ordinary and extraordinary electromagnetic plasma waves on a horizontally stratified multi-layered interface.

Observations of Ducts in the Plasmasphere by RPI

G.S. Sales, X. Huang, B.W. Reinisch, P. Song
*Center for Atmospheric Research
University of Massachusetts Lowell*

D. L. Carpenter
Stanford University

S. Fung, R. Benson, J. Green
NASA Goddard Space Flight Center

The IMAGE satellite is in an eccentric orbit that allows the satellite to move from the magnetospheric cavity into the plasmasphere on each orbit. RPI radio sounding observations made from the IMAGE satellite, as it approaches and recedes from the plasmasphere, suggests that the predominant echoes correspond to signals ducted along magnetic field-aligned electron-density structures. These echoes are frequently observed on successive plasmagrams covering a period of 8 to 10 minutes while the spacecraft moves a few thousand kilometers across the geomagnetic field lines. Multiple ducted mode echoes are often observed with time delays corresponding to guided paths in both directions along the magnetic field near $L = 4$. They appear to be a somewhat consistent feature of the plasmasphere/plasmapause region. The RPI three orthogonal-axis antenna system makes it possible to determine the arrival angles of reflected signals. These arrival angle calculations are made at each frequency for each echo within a plasmagram using the received signal amplitude and phase on the three orthogonal antennas. The measured angle-of-arrival is compared with the geomagnetic field direction at the satellite using a model of the earth's field. The result of this comparison indicates that the echoes arrive from a direction that is close to the model magnetic field direction at the satellite and are thus consistent with the ducting interpretation. From the available RPI data for approximately 200 orbits acquired over a four-month period, statistics on the frequency of occurrence, duration, the physical location of these ducts and spatial dimensions are presented.

Electron Density Distributions along Magnetic Field Lines in the Magnetosphere Deduced from RPI Plasmagrams

Xueqin Huang, Bodo W. Reinisch, and Paul Song
*Environmental, Earth, and Atmospheric Sciences Department
Center for Atmospheric Research, University of Massachusetts Lowell*

Robert F. Benson, James L. Green, and Shing F. Fung
NASA Goddard Space Flight Center

Don L. Carpenter
Stanford University

The Radio Plasma Imager (RPI) on the IMAGE satellite (launched on March 25, 2000) transmits short pulses into all directions and signals are reflected back to the satellite from the locations where the electron plasma frequency is equal to the radio frequency (for the ordinary mode). RPI data are displayed in the form of plasmagrams showing echo amplitude as a function of range and frequency. The echo arrival direction can be calculated from measurements of the three orthogonal dipole antennas. An algorithm has been developed that inverts the observed echo traces into electron density profiles. Using a model magnetic field, the inversion algorithm takes into account the variations of the magnitude and direction of the field along the ray path. In a first iteration the inversion program assumes straight-line propagation from the spacecraft to the reflecting plasma contour in the direction given by the arrival angle measurement. This procedure produces plausible N_e profiles if the echoes propagate in a straight line from the polar cap or plasmapause. If, however, there are field-aligned ducts in the magnetosphere linking the hemispheres, echoes can be trapped inside a duct and propagate along the magnetic field, resulting in the so-called ducted echoes. In this case the measured delay times must be expressed as an integral along the magnetic field line. Inversion of ducted echo traces along model magnetic field lines has recently been developed. It provides the density profile along the magnetic field. By analyzing a series of plasmagrams the spatial and temporal plasma distributions can be determined. This paper will show RPI observations of ducted waves and describe the inversion procedures for obtaining field-aligned density profiles.

Ionospheric occultation measurement with single frequency GPS onboard receiver

Jian-shan Guo* She-ping Shang Man-lian Zhang Hong Zheng
Xi-gui Luo Jiankui Shi and Qing-yi Zhang

*Laboratory of Space Weather Study, Center for Space Science and Applied Research,
Chinese Academy of Sciences, guo's Email: guojs@center.cssar.ac.cn*

The possibility of ionospheric profile sounding by making use of single frequency GPS occultation measurement is discussed in this paper. The GPS program is a part of Multiple Small Satellite Mission (MSSM) project conducted by the Center for Space Science and Applied Research (CSSAR), so the design of GPS experiment is subject to a finalized spacecraft and the availability of GPS receiver by CSSAR. The GPS occultation measurement system consists of three subsystems: onboard GPS receiver, ground fiducial network and data processing center. The GPS receiver payload planned to be put on the MSSM satellite orbiting at about 500km height with 97.4° inclination, therefore the electron density profile below 500km is anticipated to be obtained. The specifications of the GPS receiver that required by the single frequency measurement were discussed together with the method of electron density profile retrieval. The errors for the measurement imposed by wave propagation and the GPS system itself were analyzed quantitatively. The data procession technique that could effectively avoid SA interference was suggested, and coordinated measurement and analysis with ground based digital ionospheric sounder and other probes carried on the MSSM spacecraft was considered.

Waves in the Ionosphere: Simulation and Modeling Techniques

Chair: L. Dyrud, USA

		Page
2:40	Plasma Simulations and Analysis of Meteor Trails, <i>L.P. Dyrud*</i> , <i>M.M. Oppenheim, A.F. vom Endt, Boston University</i>	310
3:00	Dynamic Processes of Ionospher-Magnetosphere Coupling: A Three Fluid Treatment, <i>P. Song*</i> , <i>B. Reinisch, University of Massachusetts Lowell</i>	311
3:20	Direct Measurements of the Ionospheric Current, <i>B. Reinisch*</i> , <i>P. Song, V. Paznukhov, University of Massachusetts Lowell</i>	312

"On the Average Properties of Doppler Spectra at Moderate to Grazing Incidence Angles"

Bruce L. Gotwols*
Mary Ruth Keller
Rick Chapman

all at: The John Hopkins University/Applied Physics Laboratory
11100 Johns Hopkins Road, Laurel, Maryland 20723

The average properties of X-band HH and VV polarization Doppler spectra obtained under a variety of environmental conditions on the open ocean are presented. Spectra conditioned on the mean Doppler frequency show strong correlation between the strength of the backscatter and Doppler frequency excursions. A technique was devised, which we name wave-following processing, which removes the effects of variations in mean Doppler frequency due to wave orbital motion. When this processing is combined with conditional averaging it is found that the resulting Doppler spectra looking into the wind are all remarkably similar in shape and do not vary as a function of long wave phase.

The shape of the wave-following spectrum is nearly triangular, resembling a Greek upper case Lambda. This shape is neither Gaussian nor Voigtian and will be the subject of further investigation since it has a direct bearing on the rms velocity and lifetime of the scatterers in the footprint. Thus, these properties have a direct influence on SAR imaging of the moving ocean surface.

At a given incidence angle, the Doppler center frequencies and bandwidths increase with increasing wind speed. On average for a given wind speed, the Doppler center frequency and bandwidth increase with increasing incidence angle at HH polarization, and decrease with increasing incidence for VV polarization. However, between incidence angles of 50 and 60 degrees, the VV polarization bandwidth increase to a maximum, then decline with a further increase of incidence angle. Since this behavior has not been observed in other spectral studies, this result requires further verification and examination.

For the wave-following spectra, the Doppler center frequency and Doppler bandwidth also both increase with increasing incidence angle. The VV polarization center frequency reaches a maximum between 50 and 60 degrees incidence, then drops back to a lower value before increasing again. The Doppler bandwidth for VV polarization in this same incidence angle range is actually wider than the HH polarization bandwidth, a surprising result that must be examined in greater depth.

Sea Spikes and Doppler Spectra at Moderate to Grazing Incidence Angles

Mary Ruth Keller*
Bruce L. Gotwols
Rick Chapman

all at: The John Hopkins University/Applied Physics Laboratory
11100 Johns Hopkins Road, Laurel, Maryland 20723

Sea spikes, distinguishable as high cross section, short time-duration excursions from mean cross section levels, are ubiquitous in radar backscattered returns from the ocean surface. In the early 1990's, these spikes were shown, at moderate incidence angles, to be related to visibly-breaking dominant wind-waves and swell as evidenced by white-capping. At vertical polarization, sea spikes resulting from breaking waves were found to exhibit the expected high cross section excursions, but also wide bandwidths in close temporal proximity that lagged the cross section peak from between 0.25 sec to 0.5 sec.

Extensive field campaigns have been undertaken since that time to examine ocean microwave properties at a range of incidence angles from near-specular to near-grazing (30 degrees to 85 degrees) across a wide range of microwave frequencies (L-band, or 1 GHz, to Ka-band, or 35 GHz) for HH (horizontal transmit-horizontal receive) and VV (vertical transmit-vertical receive) polarizations. The ocean conditions available spanned the shallow littoral (MISE in the summer of 1996, off the Outer Banks of North Carolina in 8 meters of water) to deep ocean shelf (COPE in the fall of 1995, off the coast of Oregon in 130 meters of water) over a broad range of fetches. Intermediate water depths and fetches underlay the experimental results from the SAXON-FPN experiment, conducted in the fall of 1990 from the North Sea Platform in 30 meters of water.

An in-depth examination of the average Doppler spectrum properties yielded unexpected new results. These included an underlying universal shape for the Doppler spectrum once the effects of long-waves were removed, as well as bandwidth reversals over the incidence angle range of 50 degrees to 60 degrees. Since the average properties of the Doppler spectrum were surprising, these same data are being used to extract sea spike characteristics as a function of geophysical parameters like wind speed, wind direction, and wave height, as well as the microwave parameters outlined above. Initial results indicate the properties of sea spikes are not as straightforward as those determined by the early 1990's investigators, especially at HH polarization. Further, the statistics of spiking show some indication of being dependent on fetch and water depth. This conclusion, while not unexpected, was not readily apparent in data from sensors with spatially-limited beamspots under conditions of developing wind-wave seas.

Modeling of Multipath Scattering from Breaking Water Waves with Rough Faces

Zhiqin Zhao* and James C. West

Electrical & Computer Engr., Oklahoma State University, Stillwater, OK 74078
Voice:405/744-6096, Fax:405/744-9198, email:jwest@okstate.edu

“Sea spikes” are short events of strong radar backscatter from the ocean surface at low-grazing-angle (LGA) illumination. Sea spikes can last up to a second, and are often characterized by horizontally polarized (HH) backscatter that exceeds that at vertical polarization (VV) by as much as 10 dB. One of the more popular theories to explain sea spikes is the multipath scattering model introduced by Trizna (*IEEE Trans. Geosci. Remote Sensing*, **35**, 1232-1244). In this, direct backscatter from the crests of breaking water waves interferes with multipath scattering that scatters off the crest and then reflects from the front face of the wave. Due to Brewster angle effects at VV, the HH interference is much stronger than at VV. Constructive interference of the HH signal leads to large HH/VV ratios. Recently, a ray tracing treatment of the multipath scattering from an idealized breaking wave was compared with “exact” moment-method based calculations (West, *IEEE Trans. Geosci. Remote Sensing*, **37**, 2725-2727), and demonstrated the validity of the Trizna model under special conditions. However, the front face of the modeled wave was smooth, limiting the validity of the test.

Here the multipath scattering model is tested when random roughness is added to the front face of the breaking wave. The roughness was generated from the Pierson-Moskowitz wind-wave spectrum, and RMS roughnesses of up to 1 electromagnetic wavelength were used. The large-scale roughness introduces reflection shadow boundaries that prevent simple ray tracing from predicting the multipath scattering even when no small-scale roughness is included. However, physical optics is much more successful. The incident field scattered from the crest region was first found using a moment method approach. Physical optics was then applied to the crest-scattered field on the front face, and that current reradiated to give the multipath field. Direct backscatter from the small-scale roughness on the wave face was then found using a deterministic implementation of the two-scale model. The total backscatter found shows very good agreement with the reference scattering calculated using the moment method even for individual realizations of the random roughness. Monte-Carlo averaging of the backscattering from multiple surface realizations shows that at VV the crest is comparable to the mean direct backscatter from the small-scale roughness on the front face. The backscatter from the small scale roughness and the crest give a random interference pattern in the VV backscattering when a single realization is considered. Multipath propagation is damped by the Brewster angle effect and is not important. At HH the small-scale roughness is much less important, and the multipath interference pattern predicted by Trizna that may yield sea spikes is maintained despite the added roughness.

An Analytical Two-Scale Model for the Microwave Emissivity of the Ocean Surface

David Lyzenga¹, John Vesecky², and Nai-Yu Wang¹

¹University of Michigan, Ann Arbor

²University of California at Santa Cruz

The microwave emissivity of the ocean surface is influenced by both the small-scale and the large-scale surface roughness. Many features of the emissivity are accounted for by the geometric optics (GO) model, which takes account of only the large-scale roughness (*i.e.* length scales longer than the wavelength of the microwave radiation). However, several aspects of the emissivity, especially at smaller incidence angles, require the inclusion of the small-scale roughness through the small perturbation method (SPM). Accounting for both length scales in the most straightforward manner is computationally intensive, however. This is because the larger scales are accounted for by integrating the local or small-scale emissivity over all surface slopes, weighted by the large-scale slope probability density function. The local emissivity is computed using the SPM, which requires a two-dimensional integration for each local surface slope. Thus, a four-dimensional integral must be evaluated in order to calculate the emissivity at each angle of observation, surface temperature, wind speed, etc. Inversion algorithms for estimating the wind speed and direction, for example, typically require repeated model evaluations, and computation time is therefore an issue of concern for the application of such algorithms.

We have investigated a method of approximating the two-scale emissivity by computing the Taylor expansion of the local emissivity as a function of the local slope. Having computed this Taylor expansion, the slope integration can then be evaluated analytically using either a Gaussian slope pdf or the Cox and Munk (Gram-Charlier) slope distribution. The contribution of the first-order and higher-order Taylor expansion terms (as compared to the zeroth order term) is small, and the difference between the GO and SPM emissivity is also quite small. Therefore, to make the Taylor expansion tractable, we use the SPM to compute the zeroth order term and the GO approximation to compute the derivatives of the local emissivity with respect to the local slopes. Hydrodynamic modulation effects are also included in the SPM calculation, to first order in the surface slope. The effects of various terms on the azimuthal dependence of the Stokes parameters, including the upwind-downwind difference, are discussed in the paper. The results of this procedure are also compared with those of a full (numerical) two-scale model, and with measurements of the Stokes parameters.

FDFD Modeling of Plane Wave Interactions with Buried Objects Under Rough Surfaces

Carey M. Rappaport and Ann Morgenthaler
235 Forsyth Building, Northeastern University, Boston, MA 02115
email: RAPPAPORT@NEU.EDU

Misha Kilmer
113 Bromfield Pearson Bldg. Tufts University, Medford MA 02155

In finite difference modeling of plane wave interactions with objects, the usual approach is to calculate the scattered fields directly, using the incident field over the support of the scatterer as the source excitation. This approach avoids special considerations for specifying the incident wave at the edges of the computational boundary. However, if the scattering object is embedded in a half-space with a realistic random rough interface, this approach must be modified, as the transmitted field in the half-space cannot be determined analytically.

The necessary modification is to consider the rough interface as a series of perturbations to a nominal flat boundary, with depressions treated as "air pocket" scatterers in the soil, and protrusions treated as finite regions of soil scatterers in the air. The incident, reflected, and transmitted fields used to determine the scattered field excitation are those of plane wave scattering from the nominal planar boundary.

For example, for a plane wave normally incident from air (with wavenumber k_0) onto a lossy half space with free space permeability (such as soil, with wavenumber k_s), first the unperturbed normally incident plane wave H_{unp} is determined analytically, using standard reflection/transmission theory, with transmission coefficient given by: $T = 2/(1 + \sqrt{\epsilon' - j\sigma/\omega\epsilon_0})$. The fields above and below the nominal ground surface at $y = y_0$ is:

$$H_{\text{unp}} = \begin{cases} E_0 \left(e^{-jk_0(y-y_0)} + R e^{+jk_0(y-y_0)} \right), & y > y_0 \\ T E_0 \sqrt{\frac{\epsilon_s}{\mu_0}} e^{-jk_s(y-y_0)}, & y < y_0 \end{cases}$$

with incident E-field E_0 at the surface, and $R = T - 1$. The total field, $H_t = H_s + H_{\text{unp}}$ satisfies the Helmholtz equation: $[\nabla^2 + k^2(x, y)]H_t = 0$ for space-dependent wavenumber $k(x, y)$. Since the unperturbed magnetic field in the half-space satisfies the Helmholtz equation with the constant scatterer-free wavenumber k_s , this equation can be separated into an inhomogeneous Helmholtz equation for the unknown scattered H-field as:

$$[\nabla^2 + k^2(x, y)] H_s = -k_s^2 O(x, y) H_{\text{unp}}$$

where the right hand side is non-zero over the support of the buried target object (with wavenumber k_t), the depressions below the surface and the protrusions above the surface. The object function $O(x, y)$ is given by:

$$O(x, y) = \begin{cases} k_t^2/k_s^2 - 1, & \text{over the buried objects} \\ k_s^2/k_s^2 - 1, & \text{over the depressions} \\ 1 - k_0^2/k_s^2, & \text{over the protrusions} \end{cases}$$

In addition, the since all scatterers should be sufficiently far from the absorbing grid boundaries in finite difference calculations, it is important that the roughness perturbations at the ends of the interface smoothly approach zero.

Results for plane wave illumination of rough ground with buried mines using the Finite Difference Frequency Domain method compare well with other numerical methods, and indicate that this is a valuable tool for realistic subsurface sensing of inhomogeneous environments.

EM SCATTERING FROM A 3D TARGET ON A ROUGH SEA SURFACE USING FORWARD-BACKWARD IPO

Robert J. Burkholder

The Ohio State University Department of Electrical Engineering
ElectroScience Laboratory, 1320 Kinnear Road, Columbus, Ohio 43212
E-mail: burkhold@ee.eng.ohio-state.edu Phone: (614) 292-4597

The forward-backward iterative physical optics (FBIPO) method (R. J. Burkholder, *Digest of the 1999 USNC/URSI Meeting*, 224, 1999) is applied to the problem of electromagnetic (EM) scattering from a 3D target on a rough sea surface. The FBIPO method is extremely rapidly convergent in terms of the number of iterations for this class of problem. It is also more efficient than rigorous surface integral equation approaches because the numerical sampling density is lower; FBIPO requires approximately 32 unknowns per square wavelength, whereas typical method of moments (MoM) approaches require 128. Numerical results are presented to demonstrate the accuracy of FBIPO compared with MoM. The higher efficiency of FBIPO is needed so that relatively large rough surfaces can be analyzed.

The geometry of interest is an arbitrary 3D target, such as a ship or periscope, located on a randomly generated rough sea surface. The infinite sea surface is modeled with a finite section of the surface in the vicinity of the target, and is illuminated by an incident EM plane wave. The scattering due to the presence of the target is extracted by subtracting the scattering from the surface with the target absent. This effectively removes the first-order scattering from the edges of the finite surface, and approximates the scattering from the target on an infinite surface. The accuracy of this approach is checked for the case of a target on a finite flat surface compared with the same target on an infinite flat surface (found via image theory). Good accuracy is obtained for elevation angles down to about 3° for the cases shown.

The rough surface is modeled as a zero-mean Gaussian random process with a power law spectrum. The high-frequency cut-off of the spectrum is held fixed while the low-frequency cut-off is varied to simulate an ocean surface with a given RMS roughness. The sea water is modeled as an impedance surface and the target is a perfect electrical conductor. A block target and a low observable trapezoidal target are considered. A small scale Monte Carlo simulation is performed by computing the radar cross section (RCS) of the target as a function of elevation angle for several randomly generated surfaces with the same RMS roughness. The coherent and incoherent components of the RCS are extracted and plotted. It is observed that the RCS becomes more coherent for low elevation angles. This is because the incident field, composed of the incident plane wave and its reflection from the rough sea surface, becomes more coherent for low elevation angles.

Electromagnetic Wave Scattering from Two Nearby Objects Buried Under Random Rough Surface Using the SDFMM: Subsurface Sensing Applications

*Magda El-Shenawee¹ and Carey Rappaport²

¹Department of Electrical Engineering
3217 Bell Engineering Center
University of Arkansas
Fayetteville, Arkansas 72701
Tel: (501)-575-6582, Fax: (501)-575-7967
magda@uark.edu

²Center for Subsurface Sensing and Imaging Systems
Department of Electrical and Computer Engineering
Northeastern University, 235 Forsyth BLD
Boston, MA 02115
Tel: (617)-373-2043, Fax: (617)-373-8627
rappaport@ece.neu.edu

In anti-personnel mine detection applications, explosive objects buried under ground with rough soil surface could be surrounded by different clutter objects such as rocks, roots, sticks, metallic nails, vegetation, etc. Target discrimination between the AP mine and any sort of object clutter is necessary to minimize false alarms.

In this work, we present the analysis of the electromagnetic wave scattered from two objects buried under a 2-D random rough surface. These two buried objects could both be perfect electric conductors (PEC), one plastic object and one PEC, or two plastic objects. The random height variation of the rough ground is assumed to have Gaussian probability density function and the surface autocorrelation function is assumed Gaussian as well. A carefully tapered Gaussian beam is assumed for incident waves.

The integral equation-based fast algorithm, the Steepest Descent Fast Multipole Method (SDFMM), will be implemented in this work to calculate the electric and magnetic surface currents on the soil/ground interface and the multiple objects. The great advantage of the SDFMM lies in its $O(N)$ computational complexity versus the $O(N^2)$ for the Method of Moment (MOM) to solve N linear system of equations using an iterative solver. The SDFMM was originally developed at UIUC.

In our previous work, we used the SDFMM to analyze the near electric field scattered from single plastic object buried under the rough ground. The rough ground surface was the only source of clutter in the surrounding environment. Here, we are adding another source of clutter that is the proximity of an un-explosive object to the AP mine. The effect of the proximity and orientation of clutter object on target signature will be investigated here. Our objective is to understand the physics behind the mechanism of scattering from these two buried objects and hence to be able to discriminate between the explosive target and the clutter object.

**Numerical Computation of Scattering from
a Penetrable Target Above a Slightly Rough Surface**

Joel T. Johnson
Dept. of Electrical Engineering and ElectroScience Laboratory
The Ohio State University
205 Dreese Laboratories, 2015 Neil Ave
Columbus, OH 43210
Phone: (614)292-1593, FAX (614)292-7297
johnson@ee.eng.ohio-state.edu

Understanding scattering from dielectric targets located above a rough air-ground interface is important for improving radar performance and signal processing algorithms. The presence of a rough surface profile causes both an additional "clutter" backscattered signal which interferes with the desired target return and a modification of the field incident on the target so that target responses become distorted. Although approximate analytical methods can be developed for the target above a rough surface problem, numerical solutions are advantageous due to their inclusion of all possible scattering effects. However, the computational cost of numerical methods can often be prohibitive, particularly when both 3-D target and surface geometries must be discretized, and when dielectric media are considered.

In this presentation, an efficient numerical approach for predicting scattering from penetrable targets above a rough interface will be described. The method is based on an approach previously applied in studies of sub-surface target scattering: an iterative method of moments for both the surface and target regions in which matrix multiplies are accelerated through use of the canonical grid expansion for surface to surface coupling and the discrete dipole approximation for target to target coupling. The algorithm modifications necessary to consider targets above the interface will be discussed, and issues associated with proper definitions of radar cross sections for the problem reviewed. Tests of the method will also be presented for verification of both accuracy and efficiency. The influence of a slight surface roughness on target backscattering will then be demonstrated for canonical penetrable targets, and implications of these results for radar systems summarized.

Dual Frequency Microwave-Enhanced Infrared Thermography

By

Tianchen Shi, Gerhard O. Sauermaun, Carey M. Rappaport, Charles A. DiMarzio

CENSSIS, the Center for Subsurface Sensing and Imaging Systems
235 Forsyth, Northeastern University, Boston, MA 02115

Voice #: (617) 373-8570

Abstract

Humanitarian landmine detection and clearance is one of the most challenging, difficult and time-consuming tasks to be completed with existing technologies. Infrared (IR) Imagery images differences in heat transfer on the surface of the soil due to a buried object. Based on sunlight heating, it is only useful at certain times. Microwave heating has been proposed to enhance the thermal signature, but it is limited by surface roughness.

We have proposed a method called *Dual Frequency Microwave Enhanced Infrared Thermography*. Heating with microwaves instead of natural sunlight leads to a number of advantages, such as more efficient heating, more feature parameters like frequency, modulation and incident angle. Moreover, two different frequencies are used consecutively, and the heating image subtracted to minimize background noise introduced by the rough, irregular surface of the ground itself, and vegetation covering the ground. The dependence of scattered fields on frequency makes this possible.

A 2-D computational model of this method has been developed to simulate real-world landmine detection. The model includes two main parts: a microwave model to get an image of absorbed power density and a 2-D thermal diffusion model to get temperature distribution on the surface of the ground. Finally, to evaluate the performance of a system using this method, ROC (Receiver Operational Characteristic) curves are used.

High-Order High-Frequency Solvers for Rough Surface Scattering Problems

Oscar P. Bruno

Applied and Computational Mathematics, Caltech, Pasadena, CA 91125

We present a new algorithm for the computation of electromagnetic scattering from rough surfaces, with emphasis on ocean scattering applications. Our new methods couple a high-order boundary variation technique with an approach based on high-order, high-frequency asymptotic expansions of singular integrals. We demonstrate the high accuracy of our methods for a wide variety of configurations.

To solve a general rough surface scattering problem this approach separates the low and high frequency components of the scattering surface, and it views the high frequency components as perturbations from the low order ones. The boundary variations method, used extensively in previous studies (Bruno O. and Reitich F., *J. Opt. Soc. A.*, **10**, 1168-1175, 2307-2316, 2551-2562, 1993; Sei et al., *Radio Science*, **34**, 385-411, 1999) is then used to evaluate the scattered field from such rough surfaces by means of analytic continuation of an associated perturbation series of *high order* (Bruno O. and Reitich F., *Proc. R. Soc. Edinburgh. A*, **122**, 317-340, 1992).

The evaluation of each one of the coefficients in this perturbation expansion requires the solution of a scattering problem on a relatively smooth surface with highly oscillatory boundary conditions. The solution of this notoriously difficult problem is computed efficiently and accurately by means of a new, high-order, high-frequency asymptotic expansion for the surface currents. Our high-frequency solver, which is designed to apply in the small wavelength regime in which geometrical optics and the Kirchhoff approximation are frequently used, is applicable to a wide range of scattering problems and it exhibits fast, high order *convergence* to the solution of the problem. Unlike the geometrical optics type expansions, for which amplitudes can become unbounded (at caustics), our high frequency algorithm is entirely rigorous and highly accurate.

This presentation will describe our approach to the general rough surface problem with a detailed discussion on the boundary-variation and high-frequency components. Numerical results in a variety of cases will be presented, demonstrating the accuracy and computational efficiency of our methods.

Joint work with M. Caponi and A. Sei

Multigrid and Fast Multipole Applications

Chair: W. Chew, USA

	Page
3:00 Multigrid Analysis of Scattering by Large Planar Structures, O. Livne*, A. Brandt, Weizmann Institute of Science, A. Boag, Tel Aviv University	326
3:20 Parallel Implementation of the MLFMA for Dielectric Targets, J. Pormann*, J. Board, J. He, E. Jones, L. Carin, Duke University	327
3:40 High Frequency Asymptotic Representation of the Fast Multipole Method Translation Operator, K. Warnick*, Brigham Young University W. C. Chew, University of Illinois at Urbana-Champaign	328
4:00 Comparison of Interpolation Methods in the Multilevel Fast Multipole Algorithm, N. Ozdemir*, Ohio State University, K. Sencer, Middle East Technical University	329
4:20 MLFMA Analysis of Multiple Conducting and Dielectric Targets in the Presence of a Half Space, J. He*, L. Carin, Duke University	330
4:40 MLFMA Analysis of Wideband Scattering from Single and Multiple Trees, J. He*, L. Carin, Duke University	331

Multigrid Analysis of Scattering by Large Planar Structures

Oren Livne*, Achi Brandt,
Department of Applied Mathematics
The Weizmann Institute of Science
Rehovot 76100, Israel

Amir Boag
Department of Physical Electronics
Tel Aviv University
Tel Aviv 69978, Israel

Wave scattering by periodic structures has been extensively treated by many researchers since the pioneering work of Lord Rayleigh. On the other hand, scattering by finite periodic and quasi-periodic geometries received relatively meager attention, especially, in terms of numerically rigorous analysis. Examples of such structures comprise Fresnel lenses and planar reflector antennas as well as realistic finite Frequency Selective Surfaces (FSS) and patch antenna arrays. Scattering by planar structures can be formulated in the integral equation form, which is conventionally discretized using the Method of Moments (MoM). The direct solution of the MoM matrix equations for electrically large bodies is impractical due to $O(N^3)$ complexity of direct solvers. Recently, a number of fast direct and iterative algorithms for the solution of the problem have been proposed (see E. Michielssen, A. Boag, W. C. Chew, *IEE Proc.-Microw. Antennas Propag.* **143**, 277-283, 1996).

In this paper, we propose an alternative iterative solution based on the general multilevel approach for fast evaluation of integral transforms with oscillatory kernels presented in (A. Brandt, *Comp. Phys. Comm.*, **65**, 24-38, 1991). This approach avoids the fixed discretization inherent to the MoM and allows for local refinements of the solutions leading to higher order accuracy. We consider a two dimensional scattering by a large but finite array perfectly conducting strips. The problem is that of solving the one dimensional electric field integral equation. In the one dimensional case, the oscillatory kernel is represented as a linear combination of two "directional" kernels. Each such directional kernel is not oscillatory, but asymptotically smooth: it is singular at short distances, but gets increasingly smoother for larger distances. As a result, it can be further decomposed into a local part (whose contribution to the total field is local and inexpensively computed), and a smooth part, which can be efficiently recovered from its values on a coarser grid. The task of evaluating the original field over N nodes is thus replaced by the evaluation of the contribution of the smooth part of the kernel, on a coarser resolution of about $N/2$ nodes, which may still be too large to compute directly. Consequently, further coarsening is applied recursively until a grid is reached on which the evaluation task can be computed directly in $O(N)$ operations. This implies that the original field evaluation can be carried out in only $O(N)$ computer operations. The multilevel integral evaluation can be adapted to the efficient solution of the integral equation for the current, again in linear complexity.

Parallel implementation of the MLFMA for dielectric targets

John B. Pormann John A. Board, Jr. Jiangqi He Eric A. Jones
Lawrence Carin

Department of Electrical and Computer Engineering
Duke University, Durham, NC, USA

January 12, 2001

1 Abstract

We present a computer program for calculating the surface currents on dielectric targets using a multi-level fast multipole algorithm (MLFMA). This algorithm greatly reduces the computational resources needed for a solution, both in terms of run-time and memory, relative to equivalent method of moments calculations. For a target with N edges, the MLFMA algorithm, using hierarchical cluster-to-cluster interactions, can reduce the order of complexity to $O(N)$ compared to $O(N^2)$ for the method of moments, edge-to-edge based, approach.

The MLFMA algorithm presented here has been enhanced to allow dielectric targets as well as perfect electric conductors. The inclusion of such complexity allows us to begin investigating new targets such as plastic explosives and land mines, as well as new scenarios such as the "tank under tree" (TUT) and foliage-penetrating radar (FOPEN) problems.

To investigate these large-scale, multiple scatterer, problems, we have implemented the MLFMA algorithm on a distributed memory parallel computer thus enabling us to combine the processing power and memory space of many, otherwise separate, machines. The program has been developed on top of the industry standard Message Passing Interface (MPI) library and thus is highly portable, from clusters of ethernet-connected workstations to tightly coupled supercomputers, such as the IBM SP and Cray T3E. Note that while the code uses a distributed memory paradigm, it can also be run on shared memory multiprocessors such as the SGI Origin and the Sun Enterprise 10000.

High Frequency Asymptotic Representation of the Fast Multipole Method Translation Operator

Karl F. Warnick*

Department of Electrical and Computer Engineering
Brigham Young University
459 Clyde Building, Provo, UT 84602

Weng Cho Chew

Center for Computational Electromagnetics
University of Illinois, 1406 West Green St., Urbana, IL 61801-2991

Much of the work in computational electromagnetics (CEM) over the past few decades has sought to improve the efficiency of low frequency methods or to increase the accuracy of asymptotic methods. The multilevel fast multipole algorithm (MLFMA) has greatly extended the frequency range of the method of moments. Because the number of multipole terms grows with the electrical size of source groups, the computational cost is still larger at high frequencies than asymptotic methods such as ray tracing. A numerical method is needed which spans this gap by allowing a continuous tradeoff between the accuracy of the method of moments and the computational efficiency of an asymptotic method. With the goal of obtaining such a method, we propose the use of an expansion of the FMM translation operator in inverse powers of frequency to reduce the number of terms required at high frequencies.

The translation operator $T(\hat{k})$ is a distribution which satisfies

$$\iint d\mathbf{r} d\mathbf{r}' g(\mathbf{r}, \mathbf{r}') u(\mathbf{r}) v(\mathbf{r}') = \int d\hat{k} T(\hat{k}) U(\hat{k}) V(\hat{k})$$

where $g(\mathbf{r}, \mathbf{r}')$ is the free space Green's function and u and v are source and receiver functions, with far field patterns $U(\hat{k})$ and $V(\hat{k})$. By making use of the Fourier representation of the Green's function, it can be shown that

$$T(\hat{k}) = \frac{e^{ik_0 r}}{4\pi r} \sum_{l=0}^{\infty} \left(\frac{i}{k_0 r} \right)^l \delta^{(l)}(\cos \theta - 1)$$

where r is the separation between group centers and θ is the angle of \hat{k} away from the line joining the centers. The superscript on the Dirac delta function denotes the distribution obtained by differentiating the delta function l times. The usual multipole representation can be obtained from this result by expanding the $\cos \theta$ dependence as a Legendre series. For point sources in non-overlapping groups, this series is absolutely convergent. The derivatives of the delta function imply that numerical implementation requires computation of the derivatives of the far field patterns of source and receiver groups.

COMPARISON OF INTERPOLATION METHODS IN THE MULTILEVEL FAST MULTIPOLE ALGORITHM

Ozdemir, Nilufer A.^{(1)(*)}, Koc Sencer⁽²⁾

^{(1)(*)} : The Ohio State Univ., Department of Electrical Engineering, ElectroScience Laboratory, 1320 Kinnear Road Columbus OHIO 43212-1191, USA

⁽²⁾ : Middle East Technical Univ., Department of Electrical and Electronics Engineering, 06531, Ankara, Turkey

Electromagnetic scattering represents an important class of problems in physics and engineering. The need to compute scattered field in an efficient way has stimulated the development of fast algorithms among which the Multilevel Fast Multipole Algorithm (MLFMA) takes an important part with numerical complexity of $O(N)$ in three dimensions, where N is the number of scatterers. Numerical efficiency of the MLFMA is due to the nested grouping scheme which divides the computational domain into subgroups repeatedly resulting in a multilevel structure, where each level consists of cells at the same level of division. The MLFMA is considered in two steps: downward pass and upward pass. In the upward pass, outgoing multipole expansion at the center of a cell at any level is expressed in terms of the outgoing multipole expansions at the centers of lower level cells which constitute it through interpolation and translation. In the downward pass, numerical quadrature in a cell at any level is transformed into numerical quadrature at a lower level through interpolation of the kernel of the integral, then exchanging the order of numerical quadrature and interpolation (S. Koc, and W.C. Chew, *J. Acoust. Soc. Am.*, vol. 103, no. 2, Feb. 1998, pp. 721-34).

The focus of this study is the interpolation problem in the upward pass of the MLFMA. When outgoing multipole expansions at any level are interpolated at the Gauss-Legendre points for accurate quadrature in the downward pass, the sample points in θ , where θ is the elevation angle in spherical coordinates, for different levels are quite different and nonuniform. One method is to apply local Lagrangian approximation in θ variables, which leads to $O(pN_\theta(q))$ numerical complexity at level q , where p is the number of local points used in interpolation and $N_\theta(q)$ is the number of sample points at level q . In this study, the Adaptive Conjugate Toeplitz (ACT) algorithm by Feichtinger, Grochenig, and Strohmer (*Numerische Mathematik*, vol. 69, 1995, pp. 423-40) is proposed for the nonuniform interpolation in θ and improved by the nonuniform FFT and inverse FFT algorithms due to Dutt and Rokhlin (*SIAM J. Sci. Comput.*, vol. 14, no. 6, Nov. 1993, pp. 1368-93). The numerical complexity of the improved ACT algorithm is $O(mN_\theta(q)\log_2(N_\theta(q)) + N_\theta(q)q')$, where m and q' are parameters to control efficiency and accuracy in the nonuniform FFT algorithm, respectively. By the proper choice of these parameters, the error due to the ACT algorithm is shown to be several orders of magnitude smaller than the error due to the local Lagrangian approximation while the numerical complexity tends to remain almost $O(N_\theta(q)\log_2(N_\theta(q)))$ which is sufficiently close to $O(N_\theta(q))$.

MLFMA Analysis of Multiple Conducting and Dielectric Targets in the Presence of a Half Space

Jiangqi He* and Lawrence Carin
Department of Electrical and Computer Engineering
Duke University
Durham, NC 27708-0291
jhe@ee.duke.edu, lcarin@ee.duke.edu

The need to detect targets concealed in foliage has been and continues to be a critical and technically challenging military problem. A foliage-penetrating (FOPEN) radar system operating at VHF and UHF frequencies constitutes one of the most promising means by which this task can be accomplished. It is difficult to measure the SAR signature of all targets of interest, at all target-sensor orientations, thereby necessitating an accurate electromagnetic model. Knowledge of the target-signature variability with pose is essential for development of precise detection and classification algorithms. In this paper we develop an iterative scheme for extending the MLFMA to multiple conducting and dielectric targets, in the presence of a half space. For example, a vehicle embedded in foliage. Consider N targets in the presence of a half space, with target n being either a vehicle or tree. An iterative and scalable (parallel) algorithm is developed, as follows. The fields incident on each of the N targets are initially set equal to the radar excitation, in the absence of all other targets (isolated targets). The N individual MLFMA scattering problems are solved in parallel, for the individual-target scattered fields. The incident fields on the n^{th} target are subsequently updated as the isolated radar excitation, plus the scattered fields from the $N-1$ other targets (computed in previous step). This process is repeated iteratively until the currents induced on all N targets converge. In addition to developing the algorithm itself, several example results are presented for targets of interest.

MLFMA Analysis of Wideband Scattering from Single and Multiple Trees

Jiangqi He* and Lawrence Carin
Department of Electrical and Computer Engineering
Duke University
Durham, NC 27708-0291
jhc@ee.duke.edu, lcarin@ee.duke.edu

Four electromagnetic models are employed for the investigation of wideband VHF and UHF scattering from tree trunks situated over flat and sloped terrain. Three of the models are numerical, each employing a frequency-domain integral-equation formulation solved via the method of moments (MoM). A body-of-revolution (BoR) MoM formulation is applied for a tree trunk on a flat terrain, implying that the BoR axis is perpendicular to the layers of an arbitrary layered-earth model. For the case of sloped terrain, the BoR model is inapplicable, and therefore the MoM solution is performed via general triangular-patch basis functions. Both MoM models are very accurate, but computationally expensive. Consequently, we also consider a multi-level fast multipole algorithm (MLFMA) for general dielectric targets in the presence of lossy dispersive soil. The MLFMA model allows consideration of electrically large problems, including the branch structure of the tree. The MLFMA also allows consideration of interaction with multiple arbitrarily spaced trees. In addition, we consider a fourth model, it employing approximations based on the closed-form solution for scattering from an infinite dielectric cylinder in free space. The fourth model is highly efficient computationally and, despite the significant approximations, often yields accurate results, relative to data computed via the reference MoM and MLFMA solutions. Data from the four models are considered, and several examples are addressed, of application to wireless propagation and remote sensing. In particular, we consider an iterative procedure to address multiple scattering effects due to a cluster of trees, addressing attenuation and depolarization issues.

Novel Time-Domain Methods & Related Issues

Chair: E. Michielssen, USA

	Page
1:00 An Application of the T-Matrix Method to Time-Domain Scattering, <i>S.S. Koc*, O. Aydin Civi, O.M. Buyukdura, Middle East Technical University</i>	334
1:20 Multidomain Pseudospectral Time-Domain Method for 2.5-D Problems, <i>G. Zhao, Q.H. Liu, Duke University</i>	335
1:40 Some Preliminary Observations from a Simple Time-Domain Magnetic Field Integral Equation Implementation, <i>R. Burkholder*, J.F. Lee, P. Pathak, Ohio State University</i>	336
2:00 D.O.R.T. Method as Applied to Wide-Band Signals for Detection of Buried Objects, <i>G. Micolau*, M. Saillard, Institut Fresnel, P. Borderies, ONERA</i>	337
2:20 An FFT-Accelerated MOT Scheme for the Analysis of Scattering in Lossy Media, <i>A. Yilmaz*, J.M Jin, E. Michielssen, University of Illinois at Urbana-Champaign</i>	338

AN APPLICATION OF THE T-MATRIX METHOD TO TIME-DOMAIN SCATTERING

S. S KOC, O. AYDIN CIVI and O. M. BUYUKDURA
Dept. of Electrical and Electronics Engineering
Middle East Technical University, 06531 Ankara, Turkey

This paper is concerned with the application of the T-Matrix method to the problem of time-domain scattering of scalar waves by an object in free space. The T-Matrix method is well known to be a powerful method in the frequency domain provided that the scattering object is small as compared to the wavelength at the frequency of interest and that its shape satisfies the Rayleigh condition. The same is found to be true of the application of the method in the time domain. In this case the "smallness" of the scatterer is measured by comparing its size to the wavelength at the highest significant frequency component of the incident waveform.

For the T-Matrix formulation, one needs a free space Green's function in the form of an expansion in terms of wave functions which are orthogonal over spherical surfaces centered at the coordinate origin. For the problem at hand we need such a Green's function which is valid in the time domain. Precisely this is provided in (O.M. Buyukdura and S.S. Koc, J. Acoust. Soc. Am. **101**, 87-91, 1997). Once this is available, the formulation is very similar to that in the frequency domain: The total field in the vicinity of the scatterer surface is expanded in terms of regular wave functions with unknown coefficients. To solve for these coefficients, the null-field condition is imposed on a spherical surface which is entirely enclosed by the scatterer surface and the orthogonality of the wave functions is exploited to obtain a matrix equation the solution of which yields the unknown coefficients.

As a numerical example to validate the formulation, the scattering from an acoustically soft (Dirichlet boundary condition) sphere is considered. The center of the sphere is displaced from the coordinate origin such that it simulates a non-spherical surface for which the T-Matrix is not diagonal and the surface integrals necessary to find the matrix entries are evaluated numerically. The results obtained are compared to the exact result for the centered sphere which is also given in the above cited paper. An excellent agreement is observed.

Multidomain Pseudospectral Time-Domain Method for 2.5-D Problems¹

Gang Zhao* and Qing Huo Liu
Department of Electrical and Computer Engineering
Duke University
130 Hudson Hall, Box 90291
Durham, NC 27708-0291

In many applications, electromagnetic problems can be treated as 2.5-dimensional. This is a special 3-D problem where the medium is inhomogeneous in only two dimensions, but electromagnetic fields vary in three dimensions. For examples, in ground penetrating radar application for the detection of buried pipes or other long objects, the medium can be treated as invariant along the direction parallel to the pipe and the ground surface; for wave propagation in dielectric or perfect conductor waveguides, the medium along the waveguide direction is invariant, but the fields inside the waveguide vary in all three directions.

For this class of 2.5-D problems, the solution of Maxwell's equations can be simplified by using the Fourier transform. In this work, we present an efficient method based on the recently developed multidomain pseudospectral time-domain (PSTD) method. Assuming that the medium is invariant in z direction, we first Fourier transform Maxwell's equations in z so that the fields only depend on two spatial variables (x, y) and one spectral variable k_z . Then, for each value of k_z , we solve the six coupled equations for the electric field \mathbf{E} and magnetic field \mathbf{H} .

In this work, we extend the multi-domain Chebyshev PSTD (pseudospectral time-domain) algorithm to 2.5-D problems with lossy media. We utilize a new well-posed PML (perfectly matched layer) for lossy media in 2.5D to truncate the computational domain, which consists of several subdomains with piecewise homogeneous media. In our multidomain PSTD method, for each given value of k_z , spatial derivatives are represented by Chebyshev polynomials. At the interface between two adjacent subdomains, the characteristic conditions are used as the patching conditions if these subdomains have the same material; the physical boundary conditions are used as the patching conditions if these subdomains have different materials. The time derivatives are approximated by the fourth-order Runge-Kutta method. We show that this scheme has an exponential convergence property. With the solution available for electromagnetic fields corresponding to all values of k_z , the spatial-domain fields are then obtained by inverse Fourier transform in k_z .

Applications of this 2.5-D multidomain PSTD method will be shown for (1) inhomogeneous waveguides with perfect conductor walls, (2) inhomogeneous dielectric waveguides, and (3) ground penetrating radar detection of buried objects. Our results show that this PSTD algorithm allows a small sampling rate of only π points per wavelength.

¹This work is supported in parts by the U.S. EPA under a PECASE grant CR-825-225-010, by the NSF under a CAREER grant ECS-9702195.

Some Preliminary Observations from a Simple Time-Domain Magnetic Field Integral Equation Implementation

R. J. Burkholder*, J.-F. Lee, and P.H. Pathak

The Ohio State University Department of Electrical Engineering
ElectroScience Laboratory, 1320 Kinnear Road, Columbus, Ohio 43212
E-mail: burkhold@ee.eng.ohio-state.edu Phone: (614) 292-4597

A relatively simple time-domain magnetic field integral equation (TD-MFIE) formulation is investigated for computing the electromagnetic scattering from arbitrary 3D objects. The approach roughly follows the procedure of Rao and Sarkar (*Microwave Opt. Tech. Let.*, **17**(5), 321-325, 1998), but with some subtle differences. The surface currents are expanded using RWG basis functions to represent the spatial variation as

$$\bar{J}(\bar{r}, t) = \sum_n I_n(t) \bar{f}_n(\bar{r})$$

where $I_n(t)$ are the unknown expansion coefficients which are a function of time. The expansion is substituted into the TD-MFIE and tested at the centroid of each triangle in the RWG basis set. It is assumed that the time function is slowly varying over each triangle and is factored out of the surface integral, as done in the Rao and Sarkar paper. However, unlike that paper and some other TDIE papers, the time-derivative in the TD-MFIE is not *a priori* approximated by a finite difference formula. Instead, each $I_n(t)$ is represented by a continuous piece-wise linear function interpolated between discrete time steps of size Δt . The time function and its derivative are defined at any point in time from two discrete values before and after that point.

The TD-MFIE is solved implicitly at $t = t_0, t_1, t_2, \dots$ (for a causal incident field) to find the expansion coefficients $I_n(t_j)$, where $t_j = j\Delta t$. As in the Rao and Sarkar paper, it is observed that the solution is stable for arbitrarily large time steps. (Although, of course, the solution becomes inaccurate if the time step is too large for the piece-wise linear function to adequately reproduce the incident field.) This is contrary to some other TDIE papers which have set an upper bound on the time step based on the smallest triangle in the spatial expansion to insure a stable solution. This is undesirable for arbitrary 3D geometries, because CAD generated meshes may be non-uniform and contain some very small triangles relative to the spatial variation of the incident field. The small time step then requires the TD-MFIE to be solved at more points in time, which greatly degrades the efficiency. The simple approach presented here does not appear to have this limitation, although it is observed that there is a lower bound for the time step. The solution becomes unstable if $c\Delta t$ is less than about half the size of the largest triangle in the RWG expansion. It is noted that the same observations may not extend to the TD electric field integral equation.

D.O.R.T. method as applied to wide-band signals for detection of buried objects

G. Micolau[#], M. Saillard[#] and P. Borderies^{*}

[#] Institut Fresnel, UMR CNRS 6133
Faculte St-Jerome, case 162
13397 Marseille Cedex 20, France

^{*}ONERA
2, av. Edouard Belin, B.P. 4025
31055 Toulouse Cedex 4, France

The D.O.R.T. method (French acronym for "Decomposition of the Time Reversal Operator", see C. Prada and M. Fink, *Wave Motion*, **20**, 1994, 151-163.) provides an interpretation of experiments achieved in the time domain with ultrasonic pulses, where it is shown that the back emitted time-reversed scattered wave focuses on the bright point responsible for the echo. The set of transducers is called "time reversal mirror", since it extends to transient waves the phase conjugation mirrors known in Optics. In principle, the D.O.R.T. method permits one to derive how many scatterers lie in the probed area and it gives the means of generating a wave focusing on each one, provided the spatial resolution is high enough to separate them.

Our aim is to study the capabilities of this method for detecting buried objects with the help of electromagnetic waves. In a first step, we have focused on the theoretical assumptions leading to the basic results. Clearly, the invariance of the wave equation with respect to time reversal is not satisfied in most practical applications. Except in dry sand, losses cannot be neglected in the subsoil. Therefore, to give a reliable interpretation of the results after propagation in lossy media, a simple post-processing has been suggested. Another key point concerns the assumption of independent point-like scatterers surrounded by transducers. Since the low frequency range leads to low echoes and poor resolution, it is not suited for accurately characterizing a scatterer. In addition, an interface often prevents from illuminating the scatterers from every direction. We have thus investigated the consequences of, the finite size of the scatterers on one hand, the restriction of available measurements to a piece of line on the other hand. Our study has shown that, even though only a few antennas along a short piece of line are used, the use of D.O.R.T. method remain very simple, whatever the polarization and for objects with size comparable to the wavelength. This last property is very important for characterizing the object, either by finding its resonant frequencies or by solving the inverse scattering problem.

But these optimistic conclusions assume the ability of isolating the contribution of the scatterer from that of the interface. With this goal, numerical simulations based on a FDTD method have been conducted, with short incident pulses. Once the echo is filtered, a Fourier transform is performed, and the D.O.R.T. method is applied for a set of frequencies covering the whole range, with special attention devoted to the resonant frequencies. This technique is also suited to remove the noisy contribution from other inhomogeneities. In addition, using short pulses allows one to recover a good resolution in depth.

An FFT-accelerated MOT Scheme for the Analysis of Scattering in Lossy Media

Ali E. Yilmaz*, Jian-Ming Jin, and Eric Michielssen

Center for Computational Electromagnetics
Department of Electrical and Computer Engineering
University of Illinois at Urbana-Champaign, Urbana, IL 61801

Recently, various FFT-based algorithms for accelerating marching-on-in-time (MOT) methods have been reported. Their performance, however, has not kept up with that of the frequency-domain FFT-based algorithms. For example, the FFT-MOT solver, which computes spatial convolutions in the spectral domain similar to the CG-FFT method, requires $O(N_t N_s^{1.5})$ operations to analyze plate-like scatterers that reside in free space, for N_s spatial unknowns and N_t time steps. For this class of scatterers, the hierarchical FFT (HIL-FFT) algorithm requires $O(N_t N_s \log^2 N_s)$ operations. In lossy media, where the impulse response has an infinite temporal tail, the following MOT system is obtained upon discretizing a time-domain integral equation (with $\tilde{\mathbf{V}}_n$ initialized to 0 for $n = 1, 2, \dots, N_t$):

$$\begin{aligned} & \text{for } j = 1, 2, \dots, N_t: \\ & \quad \mathbf{Z}_0 \mathbf{I}_j = \mathbf{V}_j + \tilde{\mathbf{V}}_j, \quad (\text{solve}) \\ & \quad \tilde{\mathbf{V}}_n = \tilde{\mathbf{V}}_n - \mathbf{Z}_{n-j} \mathbf{I}_j, \quad (\text{update}) \quad \text{for } n = j + 1, j + 2, \dots, N_t. \end{aligned}$$

The bottleneck of MOT solvers is the computation of the space-time convolutions in the update step, for which the FFT-MOT and HIL-FFT-MOT solvers require $O(N_t^2 N_s^{1.5})$ and $O(N_t^2 N_s \log^2 N_s)$ operations, respectively.

The three-dimensional integral equation in question is an example of the non-linear Volterra integral equations, whose fast numerical solutions have also been pursued by the applied mathematics community. Unfortunately, the literature on FFT-based solutions of Volterra integral equations has mostly been limited to the one-dimensional case (E. Hairer et. al., *SIAM J. Sci. Stat. Comput.*, **6**, 532-541, 1985). Nonetheless, because space and time dimensions are independent and because the MOT scheme forms a convolution structure in time, the methodology can be extended to the temporal convolutions in the FFT-MOT solution of the three-dimensional integral equation. These convolutions are accelerated similar to the one-dimensional case, specifically, $\tilde{\mathbf{V}}_{j+1}$ is updated once every two time steps by using spatial FFTs, $\tilde{\mathbf{V}}_{j+1}, \tilde{\mathbf{V}}_{j+2}$ is updated once every four time steps by using space-time FFTs of size three in the temporal dimension, and so on.

We have applied this acceleration to the MOT analysis of transient scattering from plate-like scatterers in lossy media, with the resulting scheme requiring only $O(N_t N_s \log(N_t N_s) \log N_t)$ operations. Although HIL-FFT acceleration, which also employs space-time FFTs while making use of the sparsity of \mathbf{Z}_n matrices, is faster by a constant and requires 1/10th to 1/20th of the memory for finite-tail scattering scenarios, it cannot compete with this scheme for infinite-tail scenarios.

In the presentation we will elucidate the above FFT-based scheme for the analysis of scattering in lossy media, provide numerical results that demonstrate its efficiency, and compare it to the HIL-FFT algorithm. We will further explore the hybridization of these two competing schemes.

Distributed & Filter Structures

Chair: A. Neto, USA

	Page
3:00 Microstrip Excited Double Slot Antennas as Elements for 2.5 THz Imaging Array Camera: Equivalent, <i>A. Neto*, P. Siegel, California Institute of Technology/JPL</i>	340
3:20 A Ka-Band Planar Type Dielectric Resonator Filter With Balanced Outputs, <i>C. Yuan*, Z. Chen, Dalhousie University</i>	341
3:40 Distributed-Source-Excitation of Coplanar Waveguides: An Antenna Loaded Traveling-Wave Photomixer, <i>D. Pasqualini*, University of Siena, A. Neto, R. Wyss, California Institute of Technology/JPL</i>	342
4:00 Low-Loss and Wide-Band NRD Guide Band-Pass Filter with Ceramic Resonators at 60GHz, <i>F. Kuroki*, S. Shinke, Kure National College of Technology, T. Yoneyama, Tohoku Institute of Technology</i>	343
4:20 A Compact Design of Photonic Bandgap Structure for Microstrip Lines, <i>S.F. Yeh, C.L. Tai, H.H. Chen*, Huafan University</i>	344
4:40 Parametric Analysis of Electrode Geometry for LiNbO3 Electro-Optic Modulators, <i>P. Savi*, Politecnico di Torino, I.L. Gheorma, Columbia University</i>	345

Microstrip-Excited Double-Slot Antennas as Elements for a 2.5 THz Imaging Array Camera: Equivalent Network Model and Design

Andrea Neto and Peter H. Siegel

California Institute of Technology Jet Propulsion Laboratory, 4800 Oak Grove Dr, Pasadena CA 91109

An ultimate goal of any sensor technology must be the ability to produce diffraction limited imaging at a specified wavelength. In the optical, UV, infrared, radio and now even at sonic wavelengths, imaging is commonplace. At millimeter and submillimeter-wavelengths (frequencies from 100 GHz – 3 THz) this goal is still a technologist's dream. In this presentation the authors discuss and numerically analyze a front-end antenna design which allows diffraction limited imaging, true heterodyne operation, and monolithic fabrication, with the goal of realizing a room temperature high sensitivity 2.5 THz camera.

Key properties of the proposed planar array antenna design are diffraction limited element spacing, minimal mutual coupling, linear polarization, symmetric radiation patterns, and a high overall RF coupling efficiency over a 5-10% frequency bandwidth. Heterodyne behavior, for greatly improved pixel sensitivity, is enabled by the integration of monolithic THz GaAs Schottky diodes and intermediate frequency (IF) removal lines and filters, with each of the antenna elements. Since the impedance properties of these diodes is not measurable at THz frequencies, nor can the devices be characterized by any existing physical models, matching the antennas to the diodes cannot be accomplished with a high degree of accuracy a priori. Thus the design has the additional constraint that it has to be tunable, i.e. it has to be possible to perform slight variations at the wafer level to alter, and ultimately tune out, the reactive field contributions arising from the parasitics of the diode and feed structure.

The proposed 2.5 THz heterodyne camera front-end is composed of a 10x10 array of double slot antennas printed on a 3 micron thick GaAs membrane which is suspended above a close spaced metallic reflector. The slots are excited from the underside of the membrane via coupled lines which terminate at the submicron Schottky diode. Capacitive filters printed along the lines block RF from traveling out while allowing the down-converted IF (near 1 GHz) to pass unobstructed. From the point of view of the electromagnetic design, significant difficulties must be overcome. In the first place, as in all practical arrays, the characterization of the mutual coupling between the close spaced elements is of great importance. Secondly there is a great need to model the very fine details of the antenna feed structure at these high frequencies, including the transition between the feed lines and the diode as well as the geometry of the diode itself. Both of these aspects make it difficult if not impossible to analyze the design based on brute force method of moments or finite difference tools. We have therefore subdivided the problem and developed independent characterizations of some key elements present in the array geometry. 1) The active impedance of each slot antenna pair is characterized, including the mutual coupling with neighbor elements. 2) The reactive energy stored in the slot itself due to its transmission line excitation is explicitly accounted for. 3) The connection of the feed line to the Schottky diode is characterized. The ensemble of the solution of these three problems constitutes the full equivalent network of the array front-end which can then be evaluated using a simple circuit CAD tool.

After developing the full equivalent network for the array, the detailed dimensions of the antenna and feed structures have been optimized with the aim of maximizing the power coupled into the diodes. It turns out that polarization purity, coupling efficiency over 70%, and rotationally symmetric beam patterns are achieved over a 6% relative bandwidth around 2.5 THz. These and other results will be shown during the presentation.

A Ka-Band Planar Type Dielectric Resonator Filter With Balanced Outputs

Chenghao Yuan and Zhizhang Chen
Department of Electrical & Computer Engineering
Dalhousie University
Halifax, Nova Scotia
Canada B3J 2X4
E-mail: cyuan@is2.dal.ca, z.chen@dal.ca

With the rapid development of wireless data communication systems, highly integrated RF front-end circuits are needed without deteriorating electrical performance. One way to reduce the size of the circuit is to integrate together the components that are normally cascaded with each other in a conventional microwave circuit. Such integration is normally not easy to accomplish due to mutual couplings and varieties in functions and characteristics of each RF/microwave component.

In a conventional RF front-end module, a filter is usually placed before a mixer (normally a balanced mixer) to remove unwanted RF components. A balun is then required in between the filter and the mixer to realize the transformation of the signals from unbalanced to balanced. Conventionally, the filter and the balun are constructed separately and then cascaded together. However, if the balun can be integrated into the filter, the RF circuit can be made more compact with lower cost. In this paper, we present out recent results on such integration where a multilayer planar structure is designed.

In our design, planar dielectric resonators are employed as filtering resonators since they can provide high Q , low loss and easy frequency scaling. The two balanced output signals are obtained by placing two co-planar line segments underneath the resonators in the opposite direction. A center resonant frequency of 27.32GHz with a 3-dB transmission bandwidth of 2.85GHz and return loss of -24dB was obtained. The phase difference between the two balanced outputs is 180 ± 3.5 degree, and the magnitude difference is not visible in the figure obtained. However, the out-of-band rejection is not very high, about -6.6dB.

In conclusions, an attempt has been made to design a filter that is integrated with a balun. The initial results show that the integration is feasible although out-of-band filtering rejection needs to be further improved by enhancing the quality factor of the resonators. In addition, since the design was made on planar structures, it can be easily implemented in the semiconductor IC environment.

DISTRIBUTED-SOURCE-EXCITATION OF COPLANAR WAVEGUIDES: AN ANTENNA LOADED TRAVELING-WAVE PHOTOMIXER

D. Pasqualini[†], A. Neto and R.A. Wyss

Jet Propulsion Laboratory, California Institute of Technology, Pasadena, CA 91109

Abstract

An electromagnetic model is presented for the characterization of a distributed source excitation in coplanar waveguides (CPW). The solution to this problem is directly applicable to the understanding and optimization of membrane traveling-wave photomixers (S. Matsuura *et. al, Appl. Phys. Lett.* 74, 2872 (1999)). This local oscillator technology is capable of generating radiation above 1 THz and may make the implementation of future wide-band electronically tunable heterodyne receivers possible. The methodology we present allows the determination of the intrinsic dynamic propagation constant along the CPW, the optimal lengths of the active area needed to generate the maximum RF power, and an evaluation of the amount of radiated power when matching to a slot antenna.

The analysis is performed in two steps: First, the magnetic current distribution is evaluated in the two gaps of an infinitely extended CPW excited by a distributed impressed electric current. We achieve this by assuming that the dependence of the magnetic currents are separable in the transverse and longitudinal dimensions. The transverse dependence is well represented by one-edge-singular basis functions. These basis functions have opposite signs in the two slots to represent the propagating asymmetric mode. The longitudinal magnetic current distribution is obtained by superposing the solutions of plane wave scattering problems. Each of these plane waves arises from the longitudinal expansion of the impressed magnetic field, which is distributed over a finite area. In the second step, a slot antenna that is matched to the CPW line is introduced, to launch the maximum possible power into free-space. We validated the procedure described in step one and the behavior of the entire structure, CPW and slot antenna, with a custom-developed Galerkin Method-of-Moments code.

[†]Present address: Department of Information Engineering, University of Siena, Italy.

Low-Loss and Wide-Band NRD Guide Band-Pass Filter with Ceramic Resonators at 60GHz

Futoshi KUROKI and Satoru SHINKE

Department of Electrical Engineering, Kure National College of Technology,
2-2-11 Aga-Minami Kure 737-8506, Japan

Tsukasa YONEYAMA

Department of Communication Engineering, Tohoku Institute of Technology,
35-1 Yagiyama-Kasumichou, Taihaku-Ku, Sendai 982-8577, Japan.

Abstract Although TE_{0n5} mode ceramic resonators are usually used at centimeter frequencies[1], they have a difficulty in making wide-band band-pass filters in the millimeter-wave region. EH_{nm5} modes are more attractive than the TE_{0n5} modes because the coupling factors between resonators and input/output waveguides are larger than those of the TE_{0n5} modes. With this in mind, we have built the EH_{115} mode resonators into the NRD guide band-pass filters as shown in Fig. 1. The comparison between the relative bandwidths of EH_{115} mode and TE_{025} mode band-pass filters, designed as a 3-pole 1dB chebyshev ripple type, is shown in Fig. 2. The band-widths are calculated by their coupling coefficients and loaded Q factors, measured as a parameter of the coupling spacing at 60.5GHz. It is obvious that the wide-band band-pass filter can be obtained by using the EH_{115} mode resonator. Figure 3 shows the calculated insertion loss versus the relative band-width, where the unloaded Q factors of the EH_{115} and TE_{025} modes are set to be 2300 and 4000, respectively. Even if the unloaded Q of the EH_{115} mode is lower than that of the TE_{025} mode, the low loss nature can be kept in the region of the wide band-width because the insertion loss is in inverse proportion to the relative band-width. Based on the results of Fig. 2 and 3, we have fabricated the EH_{115} mode band-pass filter with the band-width of 1GHz at the center frequency of 60.5 GHz. The performance is shown in Fig. 4 as a dotted curve. Since the band-width is measured to be 1.1GHz, agreement between the theory and measurement is quite satisfactory. The performance of the 5-pole, 1dB chebyshev ripple band-pass filter, designed for applications of the multi-TV signal distribution system and the multiple access wireless LAN, is also shown in this figure as a solid curve. The filter has great advantages such as the wide band-width of 2.5GHz and low insertion loss of 0.3dB.

Reference [1] A. W. Glisson, D. Kajfez, and J. James, IEEE, MTT-31, No12 (1983)

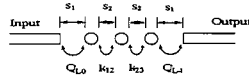


Fig.1 Plane view of NRD guide 3-pole band-pass filter

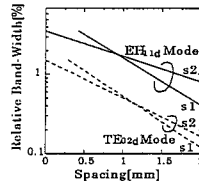


Fig.2 Relative band-width of 3-pole, 1dB chebyshev ripple band-pass filter versus coupling spacing

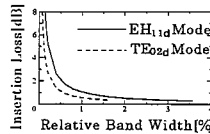


Fig.3 Insertion loss of 3-pole, 1dB chebyshev ripple band-pass filter versus relative band-width

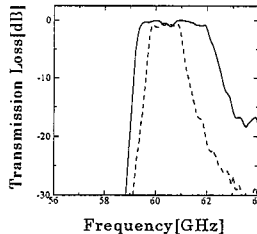


Fig.4 Measured performances of 1dB chebyshev ripple band-pass filter (Dotted curve: 3-pole. Solid curve: 5-pole)

A Compact Design of Photonic Bandgap Structure for Microstrip Lines

Sheng-Feng Yeh, Chia-Liang Tai, and Hao-Hui Chen*
Department of Electronic Engineering
Huafan University, Taipei, Taiwan, R.O.C.

Recently, there has been an increasing interest in microwave and millimeter-wave applications of photonic bandgap (PBG) structures. A PBG structure is generally an infinite periodic structure which prevents wave propagation in certain frequency bands (bandgap effect). It also provides the slow-wave characteristics. For microstrip-circuit applications, the PBG structures can be achieved by using dielectric PBG, that is, drilling a periodic pattern of holes in the substrates. A more effective approach is to etch a periodic pattern of circles or metal pads on the ground plane. In practical applications, only finite number of periods would be used. However, to effectively exploit the bandgap effect (which is created by the periodicity), the number of periods should be large enough to obtain a significant insertion loss in the forbidden frequency range. It would be then difficult to accommodate the physical size of the PBG structure. In this work, we propose a compact design of PBG structure for the microstrip lines. The PBG structure is formed using a 2-D square lattice with circle etched on the microstrip ground plane. A microstrip meander line is then fabricated on the PBG structure. Each leg of the meander line is designed to pass through N PBG lattices. A microstrip incorporating a PBG structure of $M \times N$ lattices would be then realized compactly using a M -legs meander line. To investigate the PBG properties of the proposed design, a 3-legs meander line fabricated on the substrate with 3×3 lattices etched on the ground plane (as shown in Fig.1) is simulated using the FDTD method in this paper. Fig.2 compares the transmission characteristics of this circuit design (solid line) with those of a straight microstrip line passing through 9 PBG lattices (broken line). It can be observed that the bandgap effect of this compact design is significant and comparable to that of a straight line. More results will be shown and discussed at the conference.

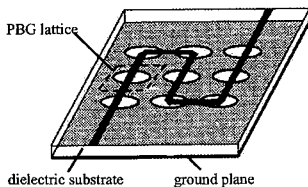


Fig.1. A 3-legs meander line fabricated on the substrate with 3×3 PBG lattices

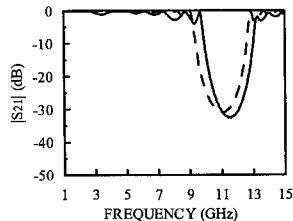


Fig.2. Transmission characteristics of a meander line and a straight microstrip line on PBG structure.

Parametric Analysis of Electrode Geometry for LiNbO₃ Electro-optic Modulators

P.Savi*, I-L. Gheorma[†]

*Politecnico di Torino, Dipartimento di Elettronica
Corso Duca degli Abruzzi 24, 10129 Torino, Italia
Tel: +39-011-5644074, Fax: +39-011-5644015, e-mail: savi@polito.it
+ Microelectronic Sciences Laboratory
Columbia University, New York, NY, email: isg12@columbia.edu

Recently a Finite Element Method based on high order interpolatory forms of curl-conforming vector basis (R.D. Graglia et al., IEEE Trans. AP, 45, 329-342, 1997) has been proposed for the analysis of electro-optic modulators on LiNbO₃ substrates with planar electrodes configurations. (P.Savi et al., APS/URSI Symposium, Salt Lake City, 2000). The formulation adopted avoids spurious solutions and yields directly the propagation constant of the structure at a given frequency. Moreover, it is able to analyze lossy anisotropic substrate and treats the finite conductivity of the electrodes by including them in the discretized domain.

Reduction of the microwave effective refractive index and attenuation are essential to achieve the synchronous coupling of an optical signal with the RF signal and a very large modulation bandwidth.

The microwave effective refractive index is lowered by inserting low-epsilon buffer layers underneath the electrodes, by using etched grooves and ridges and by increasing the metallization thickness through electroplating up to 30µm.

In the case of thick and lossy electrodes, it will be shown that a good convergence of the attenuation computations can be obtained by using edge elements of order $p=3$ even with a poor discretization of the metallic region.

In order to improve the performances of electro-optic modulators, different configurations have been investigated. A detailed analysis of different geometries will be presented to find out the effects of electrode width to gap ratio ($W/G=0.25,0.5,1,2$), electrode thickness ($t = 5, 15, 30 \mu\text{m}$), and electrode shape (rectangular or trapezoidal – ie the effect of the slope of the electrode lateral wall) on the microwave effective index and attenuation frequency dispersion. Comparison of our simulations with experimental data will also be shown.

Adaptive Arrays in Communications

Chairs: P. Wahid, USA and K. Cho, Japan

		Page
8:00	A Study of Transfer Function Estimation Error and A Practical Multi-Beam Antenna System with Pre-Coding Interference Cancellation, <i>K. Tsunekawa*</i> , NTT DoCoMo Inc.	APS
8:20	Optimum Element Arrangement of Adaptive Arrays for SDMA Considering Angular Spread and Doppler Effect, <i>K. Cho*</i> , <i>Y. Takatori</i> , <i>K. Nishimori</i> , <i>T. Hori</i> , Nippon Telegraph and Telephone Corp.	APS
8:40	A Novel Multitarget Adaptive Array Algorithm for Wireless CDMA Systems, <i>A. R. de Matos*</i> , <i>L.M. de Mendonca</i> , <i>A.G. D'Assuncao</i> , Universidade Federal do Rio Grande do Norte	APS
9:00	Single-Port Electronically Steerable Passive Array Radiator Antenna Based Space-Time Adaptive Filtering, <i>K. Yang*</i> , <i>T. Ohiro</i> , ATR Adaptive Communications Research	APS
9:20	Improvement of Elevation Directivity for ESPAR Antennas with Finite Ground Plane, <i>Y. Ojiro*</i> , <i>H. Kawakami</i> , Antenna Giken Co., Ltd., <i>K. Gyoda</i> , <i>T. Ohira</i> , ATR Adaptive Communications Research Laboratories	APS
9:40	Smart Antenna System for Wideband CDMA Signals, <i>M. Hefnawi*</i> , Royal Military College of Canada, <i>G. Delisle</i> , Laval University	APS
10:00	Smart Antennas for Wireless Communications, <i>S. Bellofiore*</i> , <i>J. Foutz</i> , <i>C.A. Balanis</i> , <i>A. Spanias</i> , Arizona State University	APS
10:20	Computational Complexity Reduced MMSE Adaptive Array Antenna with Space-Temporal Joint Equalization, <i>Y. Ichikawa*</i> , <i>K. Tomitsuka</i> , <i>S. Obote</i> , <i>K. Kagoshima</i> , Ibaraki University	APS
10:40	Minimization of a Rectangular Patch using Genetic Algorithms, <i>N. Herscovici*</i> , Spike Broadband Systems, <i>M. Osorio</i> , University of Valencia, <i>C. Peixeiro</i> , Technical University of Lisbon	APS
11:00	Mutual Coupling Analyses for Small GPS Adaptive Arrays, <i>E. C. Ngai*</i> , <i>D.J. Blejer</i> , MIT Lincoln Laboratory	APS
11:20	Analysis of an Adaptive Planar Yagi Array for WLAN Applications, <i>M.A. Ali*</i> , <i>P. Wahid</i> , University of Central Florida	348

Analysis of an Adaptive Planar Yagi Array for WLAN Applications

Maha Abdelmoneim Ali and Parveen Wahid
School of Electrical Engineering and Computer Science
University of Central Florida
Orlando, Florida 32816
email: wahid@mail.ucf.edu

In this paper, the design of an adaptive planar array configuration for omni-directional coverage at 5.8 GHz for wireless LAN applications is presented. The microstrip Yagi antenna consists of six identical elements along with the radiating element and the director. The antenna has a 3 db beamwidth of 44° and a gain of 10.9 db. Planar arrays consisting of four and six identical Yagi antennas are considered. A deterministic least square adaptive algorithm is implemented to cancel interference and clutter noise due to multipath signals. This deterministic least square approach, (T.K. Sarkar, J. Koh et-al, *IEEE AP Magazine*, V 42, No.2, April 2000, pp. 39-55), has the advantage over conventional adaptive algorithms in that it can handle non-stationary environments where the noise statistics change very rapidly. The forward-backward method introduced in the above reference, which reduces the drawback of fewer degrees of freedom associated with the deterministic approach will be used. This new approach will be implemented on and tested for a novel configuration of an array of Yagi elements. Numerical examples of the use of the adaptive algorithm for the two array configurations will be presented.

History of Phased Array Development and Applications in the New Millennium

Chairs: L. Poles, USA and L. Hubbard, USA

	Page
8:00 Some Historical Phased Array Antennas, <i>H. Schrank*, Consultant</i>	350
8:20 A History of Scanned Impedance and Blind Angles, <i>R.C. Hansen, Consultant</i>	351
8:40 Radar Prehistory, Soviet Side: Three-Coordinated-Band Pulse Radar Developed in Ukraine in the Late 30s, <i>A. A. Kostenko*, A.I. Nosich, I. A. Tishchenko, The A. Usikov Institute of Radio-Physics and Electronics</i>	APS
9:00 The Development of Smart Antennas, <i>R. Haupt*, Utah State University</i>	APS
9:20 Multi-Function Interleaved Phased Arrays, <i>L. Poles*, J. Turtle, E. Martin, R. Wang, Air Force Research Laboratory, Hanscom AFB</i>	352
9:40 Sketching the Evolution of Array Antenna Pattern Synthesis, <i>H. Steyskal*, Air Force Research Laboratory, Hanscom AFB, L. Josefsson, Ericsson Microwave Systems AB</i>	353
10:00 Phased Arrays for New Millenium, <i>E. Brookner*, Raytheon Systems Company</i>	354

Some Historical Phased Array Antennas

Helmut E. Schrank
Consultant, Hunt Valley, MD

This paper reviews some of the earliest array and phased array antennas developed in the 20th Century. It is not a complete history of the subject, but it is a sampling of the antennas known to the author from his personal experience (mainly at Bell Labs and Westinghouse).

While most phased array antenna applications are for military radar systems, it is interesting to note that the earliest array antennas were developed for communication applications. One of the earliest array antennas is the well-known Yagi-Uda antenna, an endfire array of three or more dipole elements developed in Japan in the 1920's. It is the fore-runner of more complex endfire arrays, such as the log-periodic and similar broader band antennas widely used for radio/TV reception. These are arrays, but not phased arrays, in that they do not involve electronic beam steering by means of phase shifter devices.

The earliest phased array known to the author is the MUSA (Multiple Unit Steerable Array) antenna developed in the mid 1930's by Bell Labs for trans-Atlantic short wave telephone communication. A 16 element array used motor-driven phase shifters to reduce signal fading.

Military radar requirements motivated and produced many of the phased array antenna developments during the 1940's. Frequency-scanned phased arrays were developed by Hughes for the U.S. Navy to provide horizon search during rough sea-states. Many shipborne radar antennas used parabolic cylinder reflectors fed by linear dipole arrays. A true phased array antenna using poly rod elements was developed by Bell Labs. It provided continuous azimuth beam scanning by means of motor-driven phase shifters. The first ground-based radar antenna installed at Pearl Harbor used a planar array of dipoles, developed by Westinghouse for the U.S. Army.

Electronically Scanned Arrays (ESA) became more and more necessary for surveillance and tracking radars as aircraft speeds and numbers increased. This was true for ground, shipborne, and airborne systems. The airborne surveillance radar known as AWACS required an ultra-low sidelobe antenna. This was provided by a slotted-waveguide phased array developed by Westinghouse for the U.S. Air Force in the mid-1970's.

Many antenna R & D programs were frustrated by the unacceptable high cost of phase shifters and associated components required. An example of a successful cost reduction effort was the EAR (Electronically Agile Radar) antenna design. It not only provided reasonably low-cost components, but also demonstrated a multi-function phased array with navigation, search, fire control, and other capabilities, including low RCS (stealth) features.

Future applications of the above (and other) array antenna developments are unbounded. One example is the technique of combining array technology with reflector designs for earth and space applications. The ARSR-4 antenna provides multi-beam, low-sidelobe dual polarization performance by illuminating a large reflector with a non-planar phased array feed system. The opportunities for antenna designers in the New Millennium to build upon past accomplishments are wide open, In this new century we can expect many more dazzling success stories.

A HISTORY OF SCAN-IMPEDANCE AND BLIND ANGLES

R. C. Hansen
Consulting Engineer
Tarzana, CA 91357
818-345-0770

This brief history is based on published papers, with the intent of showing the discovery and development of Scan Impedance and blind angles. The mutual impedance series approach is probably very old, but an early paper in 1960 is by Carter Jr., probably building on the classic 1932 dipole mutual impedance work by Carter. Also in 1960, Edelberg and Oliner invented the Floquet mode, unit cell approach, also called K-space, for calculation of conductance. This led to a formulation of Scan Impedance and Scan Element Pattern for dipole and slot arrays by Oliner and Malech, in 1966. Hannan developed the ideal element pattern ($\cos \theta$ in power) in 1964. Also that year Rhodes, and Wheeler in 1965, conceived the element impedance crater, with impedance in U,V coordinates. Decay of mutual coupling in an array environment was shown by Hannan in 1965 and later by Galindo and Wu for circular waveguide arrays. A most useful concept was the current sheet by Wheeler in 1965; this gedanken shows simply how Scan Resistance behaves with scan. The mutual impedance double series was recast using impedance craters; the result was the grating lobe series of Wheeler, in 1966. An example of synchronicity was the development of waveguide simulators for Scan Impedance in 1963, by Brown and Carberry, and by Hannan, Meier and Balfour. Scan Impedance is difficult to measure directly; the WG simulator proved to be a most valuable tool. The late sixties had an outpouring of Scan Impedance work. Plane wave expansions (Floquet unit cell) were utilized by Stark; Van Koughnet and Yen; Borgiotti, Chang, Diamond, Wu, and Galindo. Additions included the relation of element efficiency to Scan Element Pattern, Wasylkisky and Kahn 1968; inclusion of higher waveguide modes, Tang and Wong, Farrell and Kuhn. Waveguide arrays allowed scan compensation through use of dielectric plugs, sheets, and iri: Amitay, Galindo, Wu, Lee, Tang, Wong, Jones, DuFort, Tsandoulas, Knittel; all circa 1970. A different twist on exciting the necessary TE and TM modes for scan compensation was the slot with monopoles of Clavin, 1974. Another was the use of external transformer layers of Munk and colleagues, 1989. Inevitably the unit cell approach was applied to patch arrays by Liu, Shmoys, and Ressel, 1982. Finally a Gibbsian model for finite array Scan Impedance edge effects was presented by Hansen, 1995.

Turning now to blind angles, where the reflection coefficient magnitude is unity, Bates, 1965 showed blind angles due to a dielectric sheet cover. These phenomena were believed to be due to surface waves, Allen 1965, and a surface wave appeared in a waveguide simulator, Hannan and Balfour, 1965. Lechtreck, 1968, showed that blind angles could occur when the steering phase matched the mutual coupling phase. Work by Hessel, Knittel, and Oliner reduced blind angles to two types: a leaky wave over the array surface with the coupling and scan phases matched, and a forced surface wave supported by dielectrics, corrugations, etc. A definitive review was given by Oliner in 1969.

This review has attempted to mention the key developments that have produced our mature understanding of phased arrays.

APS 2001 Symposium, Boston July 9-13

Special Session: History of Phased Arrays

Title: Multi-function Interleaved Phased Arrays

Authors: Livio Poles, John Turtle, Edward Martin, Richard Wing

POC: Livio Poles AFRL/SNHA (781) 377-4087 - livio.poles@hanscom.af.mil

Trends toward reducing sensors platform size coupled with multifunction antenna performance requirements has driven to antenna designs that employ multiple antenna elements interleaved within a given aperture. Examples of recent and past development efforts of phased array antenna architectures that employ interleaved antenna elements have successfully demonstrated operation at several bands of frequencies.

In this presentation the performance and design complexity of a full duplex satellite communications hybrid phased arrays antenna with interleaved elements for 20 GHz and 44 GHz will be discussed. Measurement data including antenna patterns recorded over each band, with and without the radome, and with and without polarizer will be presented. Linearly polarized patterns, as well as circularly polarized patterns, along with gain measured over the scan range and compared to predicted values will also be presented.

Results from a study of a dual band phased array suitable for future tactical application capable of meeting the search, track and identification for benign and jamming requirements will be discussed. In this antenna the radiating structure which can operate over two frequency bands utilizes various techniques including interleaved multiple radiating elements, shared radiating element aperture and wideband element/diplexing design. Along with measurement results other examples of past and present multi-function phased arrays antenna concepts will be presented.

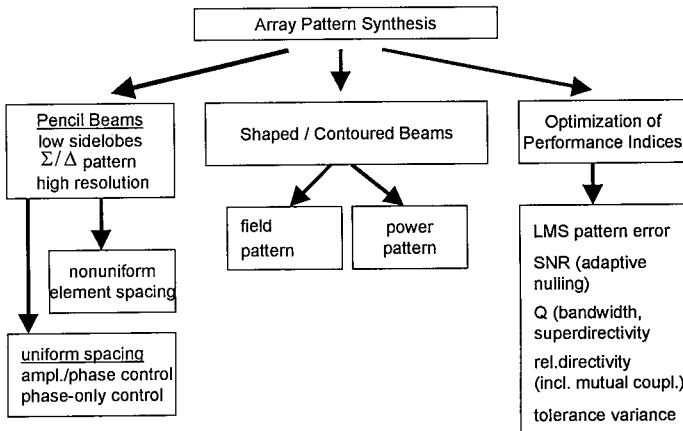
Sketching the Evolution of Array Antenna Pattern Synthesis

Hans Steyskal, AF Research Laboratory, Hanscom AFB, MA 01731, USA
Lars Josefsson, Ericsson Microwave Systems AB, Molndal, Sweden

Array antennas come in many different shapes – linear, planar, conformal – often leading to different, specific pattern synthesis methods. Furthermore, although pattern synthesis in the strict sense of the word implies synthesis of a shaped beam, it is customary to also include pencil beams, and patterns obtained by optimization of various performance indices. Because of this diversity, pattern synthesis over time has evolved along different tracks, as depicted below. However, several of these tracks are well covered by the more recent, general numeric techniques.

This is a vast subject and therefore the presentation is necessarily sketchy. We attempt only to highlight some of the most significant steps in the evolution of array pattern synthesis, starting from the early elegant analytic approaches to the present powerful numeric techniques. We limit ourselves mainly to linear arrays, commenting along the way when a technique is applicable also to other array shapes, or when importing results from continuous line source synthesis.

We conclude by evaluating where pattern synthesis is presently and what some future directions might be.



Phased Arrays for the New Millennium

Dr. Eli Brookner

Raytheon Systems Company
M/S 3-1-162
528 Boston Post Road
Sudbury, MA 01776
Telephone: 978-440-4007
Fax: 978-440-4040
E-Mail: Eli_Brookner@notes.res.ray.com

Abstract: This is a survey paper summarizing the recent developments and future trends in passive, active bipolar and Monolithic Microwave Integrated Circuitry (MMIC) phased arrays for ground, ship, air and space applications. Covered would be the THAAD (formerly GBR), European COBRA and Israeli BMD radar antennas; Dutch shipboard APAR; airborne USF-22, European AMSAR, Swedish AESA, Japanese FSX and Israeli Phalcon; Iridium (66 satellites in orbit for a total of 198 antennas) and Globalstar MMIC spaceborne antenna systems; Thompson-CSF wafer integration 94 GHz seeker antenna; digital beamforming ferroelectric row-column scanning; optical electronic scanning for communications and radar; the MMIC C-band to Ku-band Advanced Shared Aperture Program (ASAP) antenna for communications, radar electronics countermeasures (ECM) and ESM; and continuous transverse (CTS) voltage-variable dielectric (VVD) antenna.

Phased arrays have come a long way in the last three decades. This paper will cover phased array development over the last two and a half decades followed by a discussion of future trends. Covered will be the dramatic entrance into the new era of active MMIC phase-phase steered arrays for ground, air, and space; digital beamforming and its advantages; potential use of arrays for radar, communications, ESM, ECM and ECCM; how arrays can cope with jammers and ARM missiles through the use of ultra-low sidelobes and adaptive nulling and the potential simultaneous use of an array for radar, communications, ESM and jamming. Presented will be example fielded phased arrays (COBRADANE, PAVEPAWS, THAAD, and IRIDIUM®) and arrays about to be fielded (F-22, APARS, AMSAR, SAMPSON). Also covered will be the research work geared to reducing the cost and through the novel electronically steerable plasma mirror antenna. Finally, the work toward the development of a 95 GHz reflectarray using 4 inch MMIC wafers will be covered!

Efficient and Higher Order Methods

Chairs: W. Chew, USA and D. Wilton, USA

	Page
8:00 A Multilevel Direct Solver for the Method of Moments, <i>D. Gope, V. Jandhyala*, University of Washington</i>	356
8:20 New Boundary Integral Equations for Computer-Aided Design of 3-Dimensional Optical Waveguide, <i>M. Tanaka*, K. Tanaka, Gifu University</i>	357
8:40 Combined-Source Formulations for Electromagnetic Scattering from Convex Geometrics, <i>R. Adams*, Virginia Tech</i>	358
9:00 Iterative Preconditioned Solvers In Electromagnetic Computations, <i>V. Cable*, California Institute of Technology/JPL</i>	359
9:20 Experimental Results for Implementing a Combination of AP and RWG Basis Functions Using MoM to Solve the EFIE, <i>J. Gulick*, Michigan State University, M. Kowolski, University of Illinois, L. Kempel, Michigan State University, J. Jin, University of Illinois</i>	360
9:40 Higher Order Loop-Star Basis Functions for Method of Moment Computations, <i>J.F. Lee*, R.J. Burkholder, P.H. Pathak, R. Lee, The Ohio State University</i>	361
10:00 A Grid-Robust, Higher-Order Multilevel Fast Multipole Algorithm for 3-D Electromagnetic Scattering Analysis, <i>K.C. Donepudi*, J.M. Jin, W.C. Chew, University of Illinois</i>	362
10:20 Full-Wave Time-Domain Analysis of Conducting Surface Including the Singular Edge Behavior, <i>Y. Yu*, University of Illinois at Urbana-Champaign, D.S. Weile, University of Delaware, M. Lu, E. Michielssen, University of Illinois at Urbana-Champaign</i>	363
10:40 Topics in 3D Higher Order Modeling in the BEM/FEM Hybrid Formulation, <i>P. Fink*, NASA-JSC, D.R. Wilton, University of Houston, N. Champagne, R. Sharpe, D. White, LLNL</i>	364
11:00 Accurate Large-Scale CEM Modeling Using Hybrid FEM/MOM Technique, <i>S.S. Navale, Y.C. Ma., M. Sancer, Northrop Grumman Corporation, K.C. Hill*, Air Force Research Laboratory, Wright Patterson AFB</i>	365
11:20 Dissimilar Mesh Formulation for the Finite Element-Boundary Integral Method, <i>J. Meese*, L. Kempel, Michigan State University</i>	366

A Multilevel Direct Solver for the Method of Moments

Dipanjan Gope and Vikram Jandhyala*

Dept of Electrical Engineering, University of Washington
Box 352500 Seattle WA 98195, Tel: 206-543-2186 Fax: 206-543-3842
Email : jandhyala@ee.washington.edu

Quasi-static parasitic extraction is an important problem in digital circuits and in mixed-signal IC analysis. While several fast integral equation-based techniques have been proposed and developed to address this problem, all these methods (e.g. the fast multipole method, QR-based methods, FFT-based techniques) rely on fast algorithms to accelerate the iterative solution of the method of moments (MoM) system. These methods accelerate matrix-vector products (from $O(N^2)$ time and memory to $(N \log N)$ or $O(N)$), and continue to rely on appropriate preconditioners and iterative methods in order to achieve solution convergence in a short time. Moreover, notwithstanding continuing efforts to use multiple-right-hand side iterative methods, these approaches primarily solve one right-hand-side (RHS) at a time, and therefore become considerably slower when a problem involves a large number of RHS vectors, such as substrate coupling, or parasitic extraction in the presence of a large number of nets. The run time of these methods is proportional to $(N \log N)pR$, where N is the number of unknowns, p is the average number of iterations per RHS, and R is the number of right hand sides. Even with a multiple RHS solver, the number of iterations p is a strong function of the iterative solver used, the effectiveness of the preconditioning strategy, as well as the inherent conditioning of the physical problem.

In this work, an iteration-free scheme is proposed that produces a representation of the inverse of the MoM matrix with reduced computational complexity and memory. This representation can then be applied to each RHS vector in $O(N \log N)$ cost, making the dominant solution time for large R proportional to $(N \log N)R$. This approach thus bypasses the need for an iterative solver, associated preconditioning, and the uncertainty and time of convergence in an iterative scheme. While the approach is general enough in nature to be relevant to both quasi-static and full-wave analyses, and to free-space and multi-layered media, here we restrict our implementation to the quasi-static free-space and multi-layered cases. The compression scheme is based on the separation of an MoM matrix into a dominant (near-field) and a low-rank (far-field) portion (as is done in iterative fast schemes). This is followed by a recursive application of the Woodbury inversion formula (F.X. Canning and K. Rogovin, IEEE Antennas and Propagation Magazine, pp. 15-26, vol.40, no. 3, June 1998), so that only a small portion ($O(N)$ time) of the MoM matrix needs to be inverted explicitly. The remainder of the matrix is effectively inverted through recursive low-rank decompositions. These decompositions can be obtained from multipole approximations, FFT schemes, or QR methods. Here, we use the QR method to obtain low-rank approximations for the far-field portion of the matrix in the quasi-static limit.

Results presented at the conference will include memory and time analyses of the algorithm, and applications to large-scale IC capacitance extraction and mixed-signal substrate coupling, both of which inherently have a large number of RHS vectors, through a large number of nets, and through a large number of excitation points, respectively. The stability of the recursive Woodbury scheme for MoM matrices at low frequencies will be discussed, and extensions to more general MoM matrices will be proposed.

New boundary integral equations for computer-aided design of 3-dimensional optical waveguide

Masahiro Tanaka and Kazuo Tanaka

Department of Information Science, Gifu University, JAPAN

An optical waveguide will be more used in optical communication and optical circuit. Development of Computer-Aided Design (CAD) for an optical waveguide is very important subject in electromagnetics. In this presentation, we propose basis theory of CAD for a 3-dimensional optical waveguide.

We have proposed new type of boundary integral equations for a 2-dimensional optical waveguide, which is namely a slab waveguide structure. In this presentation, we propose new type of boundary integral equations for a 3-dimensional optical waveguide. The cross section of the waveguide is circular, and the waveguide satisfies the single mode condition.

Defining new unknown function which is subtracted guided-modes from total field, we can obtain the new boundary integral equations. The new integral equations are based on combined field integral equations.

The new boundary integral equations are similar formulas with the conventional boundary integral equations for 3-dimensional scattering problem. Therefore, it is possible to apply the method which has been developed in order to solve the conventional integral equations with high accuracy and high speed.

In this presentation, we solve the new boundary integral equations by the conventional moment method which is simple method and widely used in order to solve boundary integral equations. The RWG triangle patch is used as the basis function and the testing function, and the matrix equation is solved by Gauss eliminate method. However, we expect that iterative methods, high order basis function and another methods which have been developed to solve the conventional integral equations with high accuracy and high speed can be applied to the new boundary integral equations.

Combined-Source Formulations for Electromagnetic Scattering from Convex Geometries

R.J. Adams

ElectroMagnetic Interactions Laboratory

Bradley Department of Electrical and Computer Engineering

Virginia Tech, Blacksburg, VA 24061-0111

Boundary integral equation (BIE) methods constitute an important set of techniques for the numerical simulation of electromagnetic radiation and scattering phenomena. The scope of problems in which BIEs find useful application is often limited by the numerical costs associated with the method. An important factor that determines the feasibility of simulating a given class of scattering and/or radiation problems using BIE methods is the numerical stability (or conditioning) of the discretized BIE. This is in turn determined by the conditioning of the original integral equation. Unfortunately, the standard forms of the boundary integral equations of electromagnetic theory are generally unstable with respect to the size and shape of convex geometries. Furthermore, the forms of these equations typically used to perform numerical simulations are also unstable with respect to the mesh used to discretize the integral equation.

An improvement in this situation has recently been obtained through the introduction of a modified form of the combined-field integral equation (MCFIE) for perfect electrically conducting objects. The MCFIE provides a stable, well-conditioned formulation of scattering from smooth, convex geometries. As is well known, however, there are important (e.g., radiation) problems for which a combined-source formulation is more useful than the corresponding combined-field formulation. This presentation provides a discussion of a modified combined source integral equation (MCSIE) that is analogous to the MCFIE. It is shown that the resultant MCSIE shares many of the desirable numerical properties of the corresponding MCFIE. A detailed consideration of the properties of the MCSIE illustrates that, whereas the improved conditioning provided by the MCFIE is in large part due to its incorporation of a highly directional operator, the improved conditioning of the MCSIE results from the incorporation of directional sources. The feasibility of combining these aspects of the MCFIE and MCSIE to obtain a formulation with further improved numerical properties is also considered.

Iterative Preconditioned Solvers In Electromagnetic Computations

Vaughn P. Cable
Jet Propulsion Laboratory
California Institute of Technology
Pasadena, CA 91109-8099

The application of fast methods for calculating electromagnetic behavior of large structures promises to yield significant speed-ups and memory savings [e.g., FASTSCAT by Wandzura, et al., FISC by Chew, et al., AIM by Bleszynski, et al.]. While iterative methods are the basis of all fast methods, a priori knowledge of the best iterative solver to use or the best preconditioner to use is normally not available. Such information is difficult to come by for the average user and specific algorithms with preconditioners that work well are usually closely held by their developers. Also, adding someone else's "black box" preconditioners to existing iterative code is often not practical due to the inability of any one preconditioner to handle all geometries and wide dynamic ranges in calculations. Finally, there has been little discussion on the practicalities of adding fast solvers to existing MOM codes. Although, it can be done with almost any existing MOM code, the amount work involved is difficult to estimate since most fast codes to date have evolved from research codes.

This paper discusses choices of iterative method and guidelines for selecting or developing preconditioners for the MOM/FMM. Results from numerical experiments are presented on convergence for changes in geometry as well as preconditioning. These results also show the sensitivity of these factors to wide dynamic range calculations.

The paper opens with a discussion of the common thread in all fast methods, i.e., the iterative solution of sparse, complex systems of simultaneous equations. The approach is straight forward and it seems ideally suited for a quick jump to fast methods. However, experiments have indicated that the performance and accuracy of a given method and preconditioner often fall short when geometry and dynamic range requirements change. Convergence and preconditioning issues are described for scattering analysis of simple PEC tip shapes (cone) and more complex structures (duct). This investigation is limited to EFIE in order to remain compatible with existing model descriptions using open (thin) surfaces.

Experimental Results for Implementing a Combination of AP and RWG Basis Functions using MoM to Solve the EFIE

John R. Gulick*[†], Marc Kowolski[‡], Leo C. Kempel[†], and Jian-Ming Jin[‡]
Electromagnetics Lab, Michigan State University, East Lansing, MI
Center for Computational Electromagnetics, University of Illinois, Urbana, IL

In solving the electrical field integral equation (EFIE) to find the currents on a PEC surface using the method of moments, one encounters a large number of unknowns due to the need to capture the rapid current variation across the surface. Rao-Wilton-Glisson (RWG) vector basis functions have been successfully used in solving the EFIE for the past twenty years (Rao, Wilton, and Glisson, IEEE T-AP, 1982). Unfortunately, the required number of unknowns is on the order of 100 per square wavelength making electrically large problems impractical. The use of asymptotic phase (AP) basis functions (Aberegg, 1995) can drastically reduce the number of unknowns (Kowolski et al, PIERS, p. 136, 2000) for the case of RCS calculations for large, smooth metallic bodies. This is due to the fact that the rapid spatial variation in the current is due to phase variations rather than magnitude variations. The AP basis function incorporates the anticipated phase and hence represents a more efficient basis function for a large class of problems.

However, use of RWG basis functions for monostatic calculations is more efficient since the matrix entries need not be recomputed for each new incidence angle as is the case for an AP expansion. One can combine the methods selecting RWG or AP basis functions for a given geometry based on an element's location within the geometry. This allows the relaxation of mesh density in smooth flat regions not near the discontinuities resulting in a significant reduction of unknowns.

Recently, the motivation and theoretical implications for combining Rao-Wilton-Glisson (RWG) and asymptotic phase (AP) basis functions on the same perfect electrical conductor (PEC) for Method of Moments (MoM) numerical solution was presented (Gulick and Kempel, USNC/URSI Meeting, 2001). In this subsequent talk, results are presented for several objects along with MoM convergence and mesh reduction analysis.

Several PEC objects are considered along with rate of convergence data comparing basis function techniques. Additionally, we present a mesh reduction analysis concerning the effectiveness of the mixed basis function technique in reducing the unknowns for a given object. Experimental results verify the theory explaining advantages and disadvantages to implementing mixed vector basis functions with MoM to solve the EFIE for three-dimensional scattering objects.

Higher Order Loop-Star Basis Functions for Method of Moment Computations

J.-F. Lee*, R. J. Burkholder, P. H. Pathak, and R. Lee
The Ohio State University Department of Electrical Engineering
ElectroScience Laboratory, 1320 Kinnear Road, Columbus, Ohio 43212
E-mail: jinlee@ee.eng.ohio-state.edu Phone: (614)292-7270

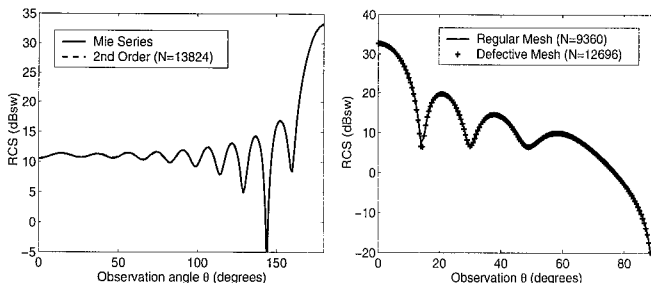
It is well documented that the use of the conventional RWG basis functions in the MOM computations becomes ill conditioned at lower frequencies. This could also manifest into problems such as slow convergence in iterative matrix solution techniques when small elements are used in the simulation. To circumvent this difficulty, many authors (Wilton and Glisson, *IEEE AP-S Symposium*, 124-133, 1981; Uckun, Sarkar, Rao, and Salazar-Palma, *IEEE MTT*, 45(4), 486-491, 1997) have proposed in the past solutions that lead to the development of the loop-star splitting (Vecchi, *IEEE AP*, 47 (2), 339-346, 1999) of the RWG basis functions. Fundamentally, the loop-star splitting is an in-exact Helmholtz decomposition, where the loop basis functions are divergence-free, and corresponds to magnetic dipole moments, and the star basis functions are loosely curl-free, and behave like finite length electric dipoles.

The main focus of this presentation is to extend the loop-star splitting to higher order ones. We are helped greatly by the realization that the $H(\text{div})$ conforming basis functions on three-dimensional surfaces are closely related to the rotation of $H(\text{curl})$ conforming basis functions that are commonly used in the finite element community. This link has been previously established by Graglia, Wilton and Peterson (*IEEE AP*, 45 (3), 329-342, 1997) and will form the foundation of our current work. In particular, we developed a set of hierarchical loop-star higher order basis functions that will enable the employment of hp-type method of moment computations: smaller elements and low order basis functions for sharp corner regions (h regions) and larger elements and high order for smooth regions (p regions). Details of our implementations will be discussed in the presentation.

A Grid-Robust, Higher-Order Multilevel Fast Multipole Algorithm for 3-D Electromagnetic Scattering Analysis

K. C. Donepudi*, J. M. Jin, and W. C. Chew
Center for Computational Electromagnetics
Department of Electrical and Computer Engineering
University of Illinois
Urbana, Illinois 61801-2991

Traditional Galerkin-based method of moments (MoM) for solving integral equations of 3-D scattering employs basis functions that guarantee the normal continuity of the expanded unknown current density. Consequently, the method can be applied only to well-connected meshes. This is too restrictive for practical applications since the generation of high-quality meshes is often very time-consuming and technically challenging. Recently, a set of novel, grid-robust, higher-order vector basis functions was proposed for the MoM solution of integral equations for 3-D scattering (G. Kang, *et al.*, *IEEE AP-S Digest*, vol. 1, pp. 468-471, 2000). These basis functions are defined over curvilinear triangular patches and represent the unknown electric current density within each patch using the Lagrange interpolation polynomials. The Lagrange interpolation points are chosen to be the same as the nodes of the higher-order Gaussian quadratures. As a result, the evaluation of the integrals in the MoM is greatly simplified. More important, these basis functions do not require the side of a triangular patch to be entirely shared by another triangular patch; hence, the resultant MoM is applicable even to defective meshes. In this work, we implement the multilevel fast multipole algorithm (MLFMA) (J. M. Song and W. C. Chew, *Microwave Opt. Tech. Lett.*, vol. 10, pp. 14-19, 1995) using these new basis functions. This implementation results in a grid-robust, higher-order MLFMA that has a computational complexity of $O(N \log N)$, where N denotes the total number of unknowns. The implementation is carried out for the electric-field integral equation (EFIE), the magnetic-field integral equation (MFIE), and the combined-field integral equation (CFIE). Shown below are two preliminary examples. The one on the left is the bistatic scattering by a metallic sphere having a radius of 2.0λ and the one on the right is the bistatic scattering by a $4\lambda \times 4\lambda$ plate. Both computations are done using the second-order, four-level MLFMA, with the second made on a defective mesh.



Full-Wave Time-Domain Analysis of Conducting Surface Including the Singular Edge Behavior

Yongxue Yu^{†*}, Daniel S. Weile[‡], Mingyu Lu[†], and Eric Michielssen[†]

[†]Center for Computational Electromagnetics
Dept. of Electrical and Computer Engineering
University of Illinois at Urbana-Champaign
1406 W. Green St., Urbana, IL 61801.
e-mail: yxyu@decwa.ece.uiuc.edu

[‡]Dept. of Electrical and Computer
Engineering
University of Delaware
217B Evans Hall
Newark, DE 19716

In recent years, time-domain integral equation (TDIE) solvers for analyzing electromagnetic scattering phenomena have steadily gained popularity. Classical marching-on-in-time (MOT) schemes for solving TDIEs can now be enhanced by fast multipole-like and fast Fourier transform-based accelerators, e.g., the plane-wave time-domain and hierarchical Fast Fourier transform algorithms. In addition, implicit time-stepping schemes have emerged that render MOT based TDIE solvers unconditionally stable. Despite these advancements, however, accuracy enhancements for TDIE-based methods remain largely unstudied, especially within the context of the analysis of structures with sharp edges and corners where fields exhibit singular behavior.

This paper reports on the development of an MOT-based TDIE solver that uses singular basis functions near corners and edges. It will be shown that this modification improves the accuracy and efficiency of the present scheme relative to MOT methods that expand edge currents with nonsingular basis functions. The benefits associated with usage of singular basis functions in frequency domain method of moment codes have been extensively documented (Jeannick Sercu, Niels Fache, Frank Libbrecht, and D. De Zutter, *IEEE Trans. on MIT*, 1581-1588, 1993). In this study, we analyze transient scattering from plate-like structures using modified rooftop basis functions that accurately model the singular behavior of electric currents near edges and interior/exterior corners. Depending on the location of a basis function relative to a boundary corner or edge, one of four types of modified rooftop basis functions is employed to ensure that the singularity is modeled correctly. The components of the current parallel and perpendicular to the edge of these modified rooftops are proportional to $1/\sqrt{d}$ and \sqrt{d} , respectively, where d measures distance to an edge (J. Meixner, New York Univ., Rep. EM-72, 1954).

Numerical results will be presented that demonstrate improved accuracy resulting from the use of this set of modified rooftops. Higher order basis functions defined on curvilinear surfaces that incorporate edge and corner singularities are currently being studied. Preliminary results obtained using this higher-order / singular MOT solver will be discussed.

Topics in 3D Higher Order Modeling in the BEM/FEM Hybrid Formulation

P. W. Fink
NASA-JSC
Houston, TX 77058

D. R. Wilton
University of Houston
Houston, TX 77204-4793

N. Champagne
R. Sharpe
D. White
LLNL
7000 East Ave., L-154
Livermore, CA 94550

This paper addresses several issues associated with higher order modeling in the BEM/FEM hybrid formulation. First, the efficiency of higher order modeling in the hybrid BEM/FEM formulation is examined for various situations. In the absence of geometrical singularities, and with careful attention to integration accuracy, high convergence rates can be achieved. However, in problems involving, for example, metallic edges, benefits of higher order modeling may not be as significant.

Accurate integration of singularities and near-singularities of potentials on the boundary is crucial in effectively realizing the benefits of higher order modeling. This paper presents and evaluates options in the treatment of these near-singularities. The authors recently developed schemes in which the element containing the source is adaptively meshed according to the location of the observation point. Although this approach permits near arbitrary accuracy, it is somewhat inefficient. Alternate techniques involving extensions of the Duffy method to observation points outside of the source triangle are presented.

The CFIE is commonly employed to avoid resonances associated with the EFIE and MFIE. In this paper, we discuss issues associated with the testing functions for the electric- and magnetic-field components of the CFIE in the hybrid formulation. An approximate transformation between divergence- and curl-conforming bases, previously used in a BEM solution of the Leontovitch problem (A. Bendali, et. al., *IEEE AP*, **47**, pp. 1597-1605, 1999) is shown to be useful in the hybrid formulation with the CFIE.

Finally, several methods of solving the resulting system of equations are presented. The system matrix in the hybrid BEM/FEM formulation has a dense block associated with BEM formulation and a sparse block associated with the FEM formulation. Without preconditioning, the system is often too poorly conditioned to converge quickly using iterative solvers. Convergence results are presented for several iterative solvers with and without the application of simple preconditioners.

ACCURATE LARGE-SCALE CEM MODELING USING HYBRID FEM/MOM TECHNIQUE

Sunil S. Navale, Yan-Chow Ma & Maurice Sancer
Northrop Grumman Corporation
El Segundo, CA 90245

Kueichien C. Hill*
Air Force Research Laboratory
Wright Patterson Air Force Base, OH 45433

The advent of parallel computers and fast solver technology in the 90's has drastically increased the problem size that can be solved using first principle based computational electromagnetic (CEM) techniques. As parallel computers and fast solver technology continue to mature, we continue to push the state-of-the-art of the CEM techniques by solving problems at even higher frequencies. In addition, the use of CAD packages allows the modeling of geometry with greater complexity and fidelity. As a result, the number of unknowns for a problem can easily reach a few millions at frequencies of application interest. The question arises whether one can blindly apply the current CEM techniques, especially those based on the partial differential equation form of the Maxwell's equations, to a problem with a few millions unknowns. What kind of accuracy can one expect? Will the accumulated dispersive and dissipative errors render the solution useless? In this paper we attempt to answer these questions and provide alternative approaches that address the accuracy issue.

We chose the hybrid finite element method/method of moments (FEM/MoM) for this study. In the past, the hybrid FEM/MoM technique has been applied to antenna problems by many researchers mainly because of its material and geometry modeling flexibility inside the antenna cavity and its incorporation of the exact radiation boundary condition outside the antenna cavity. The solutions are reasonably accurate due to the relatively small antenna physical dimensions. In this study, we apply the FEM/MoM technique to a large engine duct-like cavity instead of the usual antenna size problem. We noticed that the hybrid FEM/MoM technique loses its accuracy when the sparse unknown count inside the cavity reaches half a million. By refining the grids, increasing the order of the FEM basis functions, and employing a novel domain decomposition technique, we can improve the accuracy of the hybrid FEM/MoM technique for large problems. The conclusion we draw is that bigger computers and faster solvers should not be the only solutions to our continuing quest for accurate large-scale modeling. Developing novel CEM techniques and algorithms that reduce the operation count by incorporating a priori knowledge of the physics of the problem needs to be the focus as well.

Dissimilar Mesh Formulation for the Finite Element-Boundary Integral Method

Jeff Meese* and Leo Kempel
Electromagnetics Laboratory
Michigan State University
East Lansing, MI 48824

Abstract

A method is presented to use dissimilar mesh elements to model complex three-dimensional antennas and scatterers. Different elements with separate basis functions are used for the surface and the volume resulting in a coupled Finite Element-Boundary Integral (FE-BI) equation to describe the system. The coupling terms are required for dissimilar elements in order to enforce the essential boundary condition of tangential electric field. This coupling does not, however, increase the memory requirements since the use of simpler elements on the surface allows a boundary integral matrix with much smaller memory requirements. This formulation reduces the computational complexity of a large class of problems while maintaining the ability to model complex three-dimensional geometries using the FE-BI method. Such an approach has been used in the past for finite element representations combined with a surface-of-revolution (T. Cwik, *IEEE Trans. Antennas Propagat.*, 40, pp. 1496-1504, Dec. 1992.) In this paper, a method suitable for conformal antenna analysis and design is presented.

The FE-BI system is stored as a system matrix. The finite element portion of the matrix represents the volume interactions and is sparsely populated due to local coupling as a result of the partial differential equation formulation. The boundary integral portion of the matrix is fully populated due to coupling across the aperture. Since the majority of memory and computer time is dedicated to the boundary integral solution, this paper presents a method to decrease both the memory and computer time requirements for the boundary integral portion of the matrix. Using rectangular elements on the surface and either prism or tetrahedral elements in the volume allows the use of an FFT-based method solution to the boundary integral portion of the system while still maintaining a high fidelity geometrical model for the volumetric region. A surface mesh depicting this scheme is shown in Figure 1.

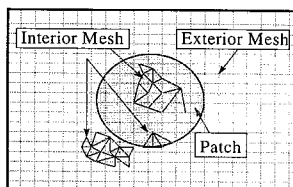


Figure 1. Dissimilar mesh scheme for a rectangular exterior mesh and a triangular interior mesh.

A partial differential equation formulation is presented that is used to describe the FE-BI system. An algorithm is then presented that is used to determine the coupling terms that arise from using dissimilar mesh elements. A patch antenna backed by a conducting cavity is then modeled to test and validate the formulation.

Guiding Structures and Circuits II

Chair: K. Webb, USA

	Page
8:00 Synthesis and Performance of Irregular Field Transformation Elements, <i>K. Webb*, M-C. Yang, J-H. Li, Purdue University</i>	368
8:20 Full-Vectorial Finite Element Modal Analysis of Dielectric Waveguides Considering Corner Field Singularities, <i>D.U. Li, H. Chang*, National Taiwan University</i>	369
8:40 Robust Complex Images Analysis of Multislot Transmission Lines, <i>J. Bernal*, F. Medina, R. Boix, Universidad de Sevilla</i>	370
9:00 Practical Characteristic Analysis of a Parallel-Plate EMP Simulator via the Interpretation of UTD Field Decompositions, <i>H.T. Chou*, Yuan Ze University, J.J. Ju, Chung-Shan Institute of Science and Technology, H.Y. Chen, Yuan Ze University</i>	371
9:20 Application of Chalcogenide-Based Materials For Use in Programmable Circuitry for a Microstrip Antenna, <i>D. Vreeland*, C.G. Christodoulou, University of New Mexico, J.C. Lyke, Air Force Research Laboratory/VSSE</i>	372

Synthesis and Performance of Irregular Field Transformation Elements

Kevin J. Webb*, Ming-Chuan Yang, and Jia-Han Li
School of Electrical and Computer Engineering
Purdue University, West Lafayette, IN 47907

While the performance features of periodic scatterers in a waveguide or in free space is well understood through a harmonic field expansion, the character of general irregular elements is yet to be quantified. For instance, a waveguide mode converter can be realized using a periodic array of perturbations in the waveguide with a period of $\delta = 2\pi/|\beta_i - \beta_o|$, where β_i and β_o are the input and output mode phase constants, respectively, and the structure can be designed using coupled mode theory. Another example is the frequency selective surface, where numerical solutions are employed over a unit cell or the complete structure for a finite, locally periodic system. Yet another example is the photonic bandgap structure family. We have proposed rough, irregular conducting wall waveguide mode converters (T. Haq, K. J. Webb, and N. C. Gallagher, *IEEE Trans. Microwave Theory and Techniques*, **43**, 559-565, Mar. 1995; T. Haq, K. J. Webb, and N. C. Gallagher *J. Opt. Soc. of Am. A*, **13**, 1501-1505, July 1996; T. Haq, K. J. Webb, and N. C. Gallagher, *IEEE Trans. Microwave Theory Tech.*, **46**, 1856-1867, Nov. 1998). These structures were designed using nonlinear optimization and have features which introduce strong evanescent mode content and result in a family of designs that are more compact and offer bandwidth variability which depends on the shape of the local optimization surface. Of particular significance is that it is possible to transform multiple modes and to incorporate waveguide transitions. There are also unguided scatterer implementations of these structures.

We present results for two classes of irregular diffractive structures, a parallel plate geometry that has steps or fins as the scattering element, and an unbounded media example comprising conducting strips. The frequency-dependent field transformation properties of these structures will be addressed and the synthesis strategy described. The goal of this work is to develop an understanding of achievable transformation properties using iterative nonlinear optimization coupled to a numerical forward field solver, and ultimately to fabricate and test these structures.

**FULL-VECTORIAL FINITE ELEMENT MODAL ANALYSIS OF
DIELECTRIC WAVEGUIDES CONSIDERING CORNER
FIELD SINGULARITIES**

Day-Wei Li and Hung-chun Chang*

Department of Electrical Engineering, National Taiwan University
Taipei, Taiwan 106-17, Republic of China

*also with the Graduate Institute of Electro-Optical Engineering and the
Graduate Institute of Communication Engineering, National Taiwan University

- (1) Commission and session topic: **B3**. Guiding structures and circuits.
(2) Statement of what new knowledge is contributed by this paper:

Singular field behavior at the corner in the cross section of the rectangular dielectric waveguide is numerically calculated by our recently proposed finite element method mode solver. The relationship between the accurate modeling of such singular field and the accurate prediction of the modal effective index is studied in detail.

- (3) The relationship of this work to previous work:

This work is an application and generalization of our recently published work (D.-U. Li and H.-C. Chang, *IEEE J. Quantum Electron.*, **36**, 1251-1261, 2000).

Robust complex images analysis of multislot transmission lines

Joaquín Bernal[†], Francisco Medina^{††} and Rafael R. Boix^{††}

[†]Dept. Física Aplicada III, E.S. Ingenieros Industriales. Universidad de Sevilla, 41092 Sevilla (SPAIN). email: jbmendez@cica.es

^{††}Dept. Electrónica y Electromagnetismo. Facultad de Física. Universidad de Sevilla. Avda. Reina Mercedes s/n 41012-Sevilla (SPAIN)
Fax.- +34 5 4239434; email: medina@cica.es

Planar structures can be efficiently analyzed by means of integral equations formulated either in the spectral or the spatial domains. Spatial domain formulations have become popular since efficient methods to implement inverse Fourier transform of closed form spectral domain Green's functions are available. In particular, the powerful discrete complex image technique (DCIT) (D.G. Fang et al., *IEE Proc. pt. H*, **135**, 297-303, 1988) has become almost the standard method to generate the spatial domain Green's function for planar structures. Thus, various versions of DCIT have been extensively employed in the analysis of 3D planar circuits, antennas or scatterers involving layered media. Moreover, DCIT has been also applied to a typical 2D problem: the analysis of the wave propagation along multiconductor transmission lines embedded in layered substrates. The advantages derived from using DCIT in this type of problems are even more obvious than in the 3D case. In a first stage the quasi-TEM model was used but, recently, DCIT has been successfully adapted, thanks to the use of a 2D version of the Sommerfeld's identity, to deal with the full-wave analysis of multiconductor strip-like structures embedded in stratified substrates (J. Bernal et al., *IEEE Trans. Mic. Theory Tech.*, **48**, 445-452, 2000). An essentially identical approach was almost simultaneously reported by Soliman et al. (E.A. Soliman et al., *IEEE Trans. Mic. Theory Tech.*, **47**, 1782-1787, 1999) for slot-like structures. The purpose of this contribution is to incorporate in the DCIT analysis of slot-like structures a number of refinements that make the computed code faster, more accurate and more reliable. Indeed, some potential drawbacks and limitations of straightforward application of DCIT are addressed and solutions are provided. The role of an adequate choice of the expansion variable and the elimination of surface wave poles is studied in depth. It is demonstrated that the use of the two-steps sampling procedure used in the above mentioned work without pole extraction and proper branch point consideration may lead to numerical problems when the frequency increases. The complex images expansion becomes unstable when surface wave poles appear on the real axis of the complex plane of the expansion variable. Thanks to the use of reliable methods to identify those poles (even for arbitrarily layered geometries) they can be removed and stability is then recuperated. Nevertheless, the two-steps procedure is shown to be essential to account for thin layer geometries such as the ones involved in MCM technologies.

Practical Characteristic Analysis of a Parallel-Plate EMP Simulator via the Interpretation of UTD Field Decompositions

Hsi-Tseng Chou^{1*}, Jiann-Jong Ju² and Hsing-Yi Chen¹

¹ Department of Electrical Engineering, Yuan Ze University, Chung-Li 320, Taiwan

² Chung-Shan Institute of Science and Technology, Taiwan

With the increasing threat from the electromagnetic pulses (EMP) produced from the lighting or nuclear explosion, developing technologies that can be employed to protect the electronic equipment is very important. An EMP simulator, which produces a field distribution similar to the realistic EMP field response, is one of the essential technologies since a realistic experimental test should be performed before the protection technologies can be employed in the practical applications.

The fundamental consideration of EMP simulator is to have a uniform field distribution in the test volume at low frequencies in the frequency domain. Simulator in terms of parallel plates is a potential candidate since the fundamental low frequency characteristics of parallel plates as transmission lines are capable of producing relatively uniform field distribution.

In the realistic design, characteristic analysis is important since the finitely sized plates of the EMP simulator potentially cause a non-uniform field behavior. Previous studies focus on the conventional characteristics of finite transmission line or employ numerical electromagnetic codes, in which most of them based on the method of moment (MoM), to predict the field behavior. Even though those numerical results sufficiently present the field pattern variation and can indicate the uniformity of the field distribution, it does not, however, provide any physical interpretation on the field mechanism that allows one to improve the design of the simulator effectively. An effective and meaningful interpretation on the other hand provides meaningful parameters that optimize the field behavior in the test volume.

This paper studies the field mechanism of the parallel-plate EMP simulator. In particular, physical interpretation in terms of field decompositions by the Uniform Geometrical Theory of Diffraction (UTD) is employed. Even though currently available UTD solutions can only be applied in the range of higher frequencies, but they remain valid in terms of physical interpretation since the fundamental mechanism in the wave propagation remains the same. The UTD decomposes the total electromagnetic field in terms of four fundamental components: incident field that is radiated directly from the feed source, reflected field, edge diffracted field and corner diffracted field due to the presence of simulator structures. The advantage of this decomposition is that each component can be considered independently in the design, and provides useful parameters for the improvement on the design. Numerical experiments based on the MoM as well as an improved design will be employed to validate the proposed physical interpretation via UTD field decompositions.

Application of Chalcogenide-Based Materials For Use in Programmable Circuitry for a Microstrip Antenna

David Vreeland*, C. G. Christodoulou,
Electrical and Computer Engineering Department
University of New Mexico,
Albuquerque, NM. 87131

and

James C. Lyke
(Microsystems Engineer)
Air Force Research Laboratory/VSSSE
Albuquerque, NM

Recent research investigating the feasibility of using $\text{Ge}_2\text{Te}_2\text{Sb}_5$ thin film chalcogenide as both a digital and analog memory is suggestive of potential use as an element in a variety of applications requiring adaptive circuits. It has been demonstrated that a thick film chalcogenide memory device can be used as an analog memory element. Chalcogenide materials exhibit a phase-shifting nature that can vary between amorphous to FCC crystalline structure. The resistance of the chalcogenide device varies in a manner proportional to the phase state of the material and covers a range that can vary on the order of two magnitudes. The phase state can be set into the chalcogenide material by sending programming pulses which heat the chalcogenide above its melting point within a specific domain of the material. The phase state is determined by the cooling profile of the material. This paper presents an application of chalcogenide-based materials as an adaptive element in a microstrip antenna. The chalcogenide material can be used a weighted device that can be used to alter the resistance anywhere along a microstrip and hence to be able to vary the phase of signals reaching an antenna. The behavior of chalcogenide material is characterized up to a frequency of 1 GHz, and the potential effects on the antenna modeled.

Propagation Modeling

Chair: R. Janaswamy, USA

	Page
8:00 A 3D Parabolic Equation Method for Imperfectly Reflecting Vertical Obstacles on Flat Ground, <i>R. Janaswamy*</i> , <i>Naval Postgraduate School</i>	374
8:20 Microwave Propagation Over Sea Surfaces at Low Grazing Levels, <i>R.M. Jha*</i> , <i>R. Janaswamy, Naval Postgraduate School</i>	375
8:40 Parabolic Equation Modeling of 3-D Tropospheric Electromagnetic Wave Propagation, <i>R. Awadallah*</i> , <i>J. Kuttler, The Johns Hopkins University</i>	376
9:00 An Accelerated Boundary Integral Equation Propagation Scheme, <i>M. Lamar*</i> , <i>R. Awadallah, J. Kuttler, The Johns Hopkins University</i>	377
9:20 Comparisons Between Various Propagation Models and Softwares - Application to Detection Systems, <i>J. Claverie*</i> , <i>M. Le Palud, G. Le Poulard, Ecoles Militaires de Coetquidan</i>	378
9:40 Extremely Low Frequency (ELF) Mixed-Path Propagation Model, <i>E. Wolkoff*</i> , <i>Science Applications International Corp, J. Casey, Naval Undersea Warfare Center</i>	379

A 3D Parabolic Equation Method for Imperfectly Reflecting Vertical Obstacles on Flat Ground

R. Janaswamy

Code EC/Js, Department of Electrical & Computer Engineering

Naval Postgraduate School, Monterey, CA 93943

Email: janaswam@ece.nps.navy.mil

Path loss models are very important for determining the coverage area in a wireless network. Accurate prediction of path loss is particularly important in urban areas, characterized by high-rise buildings, where the attenuation tends to be rather high. Recently we presented a 3D wide-angle parabolic equation based technique for predicting path loss in an urban type of environment with perfectly reflecting obstacles (R. Janaswamy, *URSI Meeting*, paper C3-2, Boulder, CO, January 8, 2001). Because the technique is based on plane wave decomposition of fields on aperture planes it is also suitable for the prediction of angular spread of waves that becomes important in the study of antenna arrays.

In this paper we investigate the performance of the split-step parabolic equation technique for the case of imperfectly reflecting vertical obstacles on flat ground. The method accounts for reflections by ground, diffractions by rooftops, and lateral reflections and diffractions by buildings. Imperfect reflections are accounted for via an impedance type boundary condition. These, together with diffractions, cause depolarization of the wave that couples vertical polarization to horizontal polarization and vice versa. Test obstacles will be considered and comparisons will be shown with ray methods or with measurements where appropriate. The method is appropriate for the prediction of path loss and angular spread for both outdoor urban and indoor environments.

MICROWAVE PROPAGATION OVER SEA SURFACES AT LOW GRAZING ANGLES

R.M. Jha*,
Email: rmjha@nps.navy.mil

R. Janaswamy
Email: janaswam@ece.nps.navy.mil

Code EC/
Department of Electrical & Computer Engineering
Naval Postgraduate School, Monterey, CA 93943
Fax: 1 (831) 656 2760

Code EC/Js

Radiowave propagation over long range is characterized by the fact that it encounters varied ground conditions; these arise from the intrinsic EM properties of the constituent materials, the surface profiles, and the surface roughness. The *rough surface reflection coefficients* required in the wave propagation formulations such as the *parabolic equation (PE) method*, have often followed from the classical derivation for a Gaussian rough surface as the starting point (P. Beckmann and A. Spizzichino, *The Scattering of Electromagnetic Waves from Rough Surfaces*, 1963). The closed form expression essentially led to the identification of a *rough surface reduction factor*. Researchers in the past have focused on the analysis of this reduction factor; amongst these, the one derived heuristically by Miller Brown and Vegh (MBV) is often used (A.R. Miller *et al.*, *IEE Proc.*, **131** (2), Pt. H, 114-116, 1984).

However, the exact modal analyses below 500 MHz have now shown the MBV factor to diverge from the exact modal solutions at low grazing angles (D.E. Barrick, *IEEE Trans.*, **AP-46**, 73-83, 1998); unfortunately, the radiowave propagation over long range falls in this domain.

In contrast, this paper employs the rough surface reflection coefficient for specular waves, determined directly as a function of the grazing angle by the Monte Carlo simulations of the rough surface problems (R. Janaswamy, *URSI Meeting*, Colorado, **F3 Fr-AM**, 217, Jan. 2000). A novel PE formulation applicable to non-constant impedance plane (R. Janaswamy, *IEEE APS/URSI B Meeting*, Salt Lake City, 60, July 2000) is then employed which eliminates the need for the determination of grazing angle at each range step.

Computational results shall be obtained in the microwave region (3, 10 and 17 GHz) for the propagation factor, both as a function of range and the receiver antenna height. Furthermore, both the surface and the evaporation ducts will be considered. In the case of the radiowave propagation over the ocean, the *wind-induced sea surface roughness* of up to 1m-rms (*i.e.*, wind speed of 13.69 m/sec) will be considered which corresponds to the *sea state five*. These computational predictions shall be compared with those obtained by the MBV roughness model as well as with some available measurements.

Parabolic Equation Modeling of 3-D Tropospheric Electromagnetic Wave Propagation

Ra'id S. Awadallah* and James R. Kuttler
Johns Hopkins University Applied Physics Laboratory
11100 Johns Hopkins Rd.
Laurel, MD 20723

In order to facilitate practical long-distance over-terrain electromagnetic propagation calculations many assumptions and approximations have been employed over the previous several decades. The starting point is usually the spherical coordinate system with the source being modeled as a vertical or horizontal dipole located on the z -axis. The next step is to assume that the propagation is confined to the vicinity of the plane of the great circle containing the source and destination point. Based on that, the effect of lateral ground waves is ignored and the problem is recast into an azimuthally symmetric one where the Maxwell equations are reduced into a scalar wave equation governing the azimuthal electric field component (horizontal polarization) or the azimuthal magnetic field component (vertical polarization). A proper conformal map transforms the problem into a 2-D Cartesian coordinate system, where the transformed 2-D scalar wave equation is approximated by a parabolic wave equation (PWE) under the assumption of predominant forward propagation. This equation is then solved by marching the field over range increments. In the APL propagation code *TEMPER*, the marching solution is carried out via the Fourier split-step method. The finite-difference method is a viable alternative.

In an attempt to Benchmark the above model, a 3-D, fully-polarized, PWE-based, vector propagation model, which avoids the above assumptions and properly accounts for out-of-plane scattering, shadowing and depolarization due to lateral terrain variations, was developed. In this model, the PWE governing each one of the three Cartesian components of the electric field (or magnetic field), along with the terrain boundary condition, which couples these field components, is discretized using the finite-difference method. Close to the terrain, the coupled system of equations is solved using an efficient sparse-matrix bi-conjugate gradient method. Away from the terrain, the field components are independent and the solution is carried out via the alternating direction implicit method (ADI). Perfectly matched layers were used to prevent reflection artifacts from numerical boundaries. The model was tested for simple urban structures and benchmarked using analytical results of scattering from simple geometries such as spheres and cylinders. Some of these calculations are presented in this paper.

The APL 2-D propagation code *TEMPER* (designed to handle 1-D terrain only) calculates propagation over a 2-D terrain by slicing the terrain into N slices and independently calculating the propagating field for each slice. By putting the results for the N slices together, an approximate 2-D terrain result is obtained. This approach, which does not properly account for shadowing and totally ignores out-of-plane scattering, is benchmarked against our 3-D vector propagation model for simple 2-D terrain configurations.

An Accelerated Boundary Integral Equation Propagation Scheme

Michael T. Lamar*, Ra'id S. Awadallah and James R. Kuttler
Johns Hopkins University Applied Physics Laboratory
11100 Johns Hopkins Rd.
Laurel, MD 20723

Rigorous and efficient modeling of long distance electromagnetic (EM) propagation over the ocean surface, with application to radar imaging and communication technology, has been attracting the attention of engineers and applied physicists for the past several decades. The difficulty of such modeling stems from the fact that the ocean surface possesses roughness scales that range from sub-centimeter to several meters. To preserve the fidelity of the numerically calculated EM fields, these roughness scales should be appropriately taken into account by the numerical simulations that represent the ocean surface as a set of discrete points. This is accomplished by using a surface discretization interval that conforms to the small-scale surface roughness.

Among the existing numerical simulation techniques are the popular parabolic wave equation (PWE) and the boundary integral equation (BIE) techniques. The PWE method handles the ocean surface by introducing a coordinate transformation that transforms the ocean surface into a flat surface at the expense of complicating the governing PWE, which is, in turn, solved by Fourier transform techniques. This approach requires the maximum surface slope to be less than $15^\circ - 20^\circ$. The wind-driven ocean surface is very likely to have steeper slopes, in which case the BIE method, which rigorously handles large surface slopes resulting from small-scale roughness, provides the alternative. The BIE method remained virtually outside the propagation-modeling arena until fast and accurate iterative techniques such as the method of multiple ordered interactions (MOMI) were developed. An efficient MOMI-based propagation scheme was proposed by Rino and Ngo ("Forward Propagation in a Half-Space with an Irregular Boundary," *IEEE Trans. Antennas Propagat.*, 45, 1997). However, this scheme is still much less efficient than the PWE method since the number of operations required to calculate the current induced on the ocean surface via MOMI is $O(N^2)$, where N is the number of surface samples. Rino and Ngo reduced the number of operations to $O(MN_x^2)$ by dividing the surface into M pieces each with N_x points and updating the propagated field at the beginning of each piece.

In this paper, an accelerated Rino-Ngo propagation algorithm, which reduces the total number of iterations to, $O(MN_x)$ is proposed. The acceleration is based on the Johnson-Chou algorithm ("A Novel Acceleration Algorithm for the Computation of Scattering from Rough Surfaces with the Forward-Backward Method," *Radio Science*, 33, 1998). The presented results are for the perfectly electric conducting surfaces. The general impedance surfaces are left for future work. Comparisons with PWE-based results for both TE and TM polarizations are presented for a sinusoidal surface as well as ocean-like surface. CPU time comparisons are also provided.

COMPARISONS BETWEEN VARIOUS PROPAGATION MODELS AND SOFTWARES – APPLICATION TO DETECTION SYSTEMS

Jacques CLAVERIE¹, Marc LE PALUD, Grégory LE POULARD
Ecoles Militaires de Coëtquidan – CREC St-Cyr - 56381 GUER CEDEX - FRANCE
Email : jacques_claverie@mailhost.esm-stcyr.terre.defense.gouv.fr

INTRODUCTION

The development of future detection systems needs more and more accurate prediction models in order to reach optimized performances. For this purpose, various propagation phenomena (atmospheric refraction, ducting, diffraction along the propagation path, etc..) have to be precisely taken into account.

PROPAGATION MODELS AND SOFTWARES

Nowadays, the radar engineers can make use of several propagation softwares based upon different scientific approaches in the way of solving the propagation equations. So, we found quite natural but extremely useful to compare the results provided by some of these available tools. As the Parabolic Equation Method (PEM) is actually widely employed, we focused our study on 3 softwares using a pure PEM or an hybrid one : AREPS and TPEM (A. E. Barrios, *IEEE AP*, Vol 42, n° 1, 90-98, 194) developed by the SPAWARSYSCEN, USA, and TERPEM (M.F. Levy and K.H. Craig, *BAC Conf. Proc.*, 497-505, 1996) developed in the UK. We also included in our comparisons the French software CARDIF (J.P. Torchut et al, 1st *SEE Propagation Conf. Proc.*, 1991) based upon a knife-edge method for terrain diffraction, and "reference" solutions when available.

COMPARISONS AND DISCUSSION

We have performed several comparisons assuming the following configurations, for H or V polarization and different frequency waves:

- Propagation over a medium dry plane ground in the case of a standard atmosphere
- Propagation over a calm sea in presence of an evaporation duct.
- Propagation over an irregular medium dry ground consisting of a single broad wedge or of a double broad wedge in the case of a standard atmosphere.

The figure 1 below illustrates the case of a single broad wedge assuming a transmitter's height of 10 m and a frequency of 300 MHz. The plot concerns the variations of the propagation path loss versus the receiver's height at a distance of 5 km from the transmitter. Here, our "reference" solution is given by the Geometrical Theory of Diffraction (GTD).

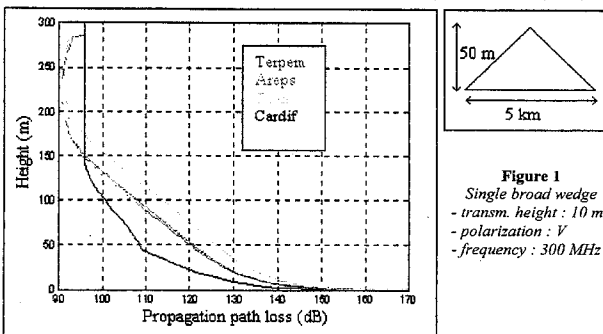


Figure 1
Single broad wedge
- transm. height : 10 m.
- polarization : V
- frequency : 300 MHz

For most of the studied cases, the values that we have obtained indicate significant variations between the results provided by the different softwares. Moreover, these variations are observed for softwares based upon the same scientific method (PEM). This shows, for practical applications, that the implementation of a method may lead to similar effects than the choice of the method itself.

EXTREMELY LOW FREQUENCY (ELF) MIXED-PATH PROPAGATION MODEL

Edwin A. Wolkoff*
Science Applications International Corporation
New London, CT 06320

John P. Casey
Submarine Electromagnetic Systems Department, Code 3413
Naval Undersea Warfare Center
Newport, RI 02841

The United States Navy transmits messages to submarines from a transmit array of four horizontal wire antennas operating in the ELF band. At the lower end of the ELF band (below 100 Hz), electromagnetic waves penetrate sea water with sufficiently low attenuation to enable communication to submarines operating at secure depths. A pair of crossed transmit antennas is located in Northern Wisconsin and a similar pair is located in the Upper Peninsula of Michigan. The power radiated by the transmit array is sufficient to provide global coverage. Because the length of each transmit antenna is less than 2% of a free-space wavelength, the antennas are electrically short and are modeled as horizontal electric dipoles (HEDs).

An earlier ELF fixed-path propagation model was developed to predict the electromagnetic field of an HED. In the fixed-path model, the propagation parameters were considered to be constant along the propagation path, and only the forward (shorter) great-circle path contribution to the field from each antenna was considered. The fixed-path model provides good field strength estimates for ranges less than 10 Mm from the transmit array center.

In order to extend the prediction range from 10 Mm to the region of the transmitter antipode, a new ELF mixed-path propagation model is required. This model will need to consider the variation of the propagation parameters along each propagation path, and the contribution to the electromagnetic field of both the forward and the reverse (longer) great-circle paths.

This paper describes an ELF mixed-path propagation model for predicting the field strength at any location on the surface of the earth. The mixed-path model accounts for:

- (a) the anisotropic surface impedance of the earth along each transmit antenna;
- (b) the magnitude and phase of the four transmit antenna currents;
- (c) the contributions to the field of signals arriving by the forward and reverse great-circle paths;
- (d) the variation of the propagation parameters along each propagation path as functions of solar elevation;
- (e) the performance characteristics of the ELF submarine receivers.

The model has been validated by comparing predicted to measured field strengths for three receive sites established by the Navy to monitor ELF message traffic. The receiver locations are in Virginia, Georgia, and Hawaii.



Complex Media

Chairs: R. Ziolkowski, USA and N. Engheta, USA

	Page
1:00 Negative Permittivity and Permeability Meta-Materials and Their Applications, <i>R. Ziolkowski*, The University of Arizona</i>	382
1:20 A Combined Numerical and Analytic Approach for Generalized Models of Complex Bi-Anisotropic Meta-Materials, <i>V. Jandhyala*, A. Ishimaru, S-W Lee, Y. Kuga, University of Washington</i>	383
1:40 High Permittivity Dielectric Composite Materials, <i>S-W Lee*, Y. Kuga, University of Washington, E. Savrun, Sienna Technology</i>	384
2:00 Computation of Static Effective Permittivity for 2-D Anisotropic Composite Materials, <i>F. Wu*, K. Whites, University of Kentucky</i>	385
2:20 Semi-leaky Waves in Dielectric Pseudo-chiral Slabs, <i>A. Topa*, C. Paiva, A. Barbosa, DEEC-IT - Technical University of Lisbon</i>	386
2:40 Dipole Radiation Near a Wire-Medium Sheet Above a Ground Plane, <i>N. Engheta*, University of Pennsylvania</i>	387
3:00 Active High Impedance Ground Planes, <i>G. Poilasne*, L. Desclos, Photonic RF Corp.</i>	388
3:20 Lattices of Cubes as Phenomenological Maxwell/Maxwell Garnett Materials Containing Large Particle Interaction, <i>K. Whites*, F. Wu, University of Kentucky</i>	APS
3:40 The Method of Auxiliary Sources (MAS) and Some EM Properties of Complex Material Objects, <i>R. Zaridze*, F. Bogdanov, d. Karkashadze, K. Tavzarashvili, A. Bijamov, Tbilisi State University</i>	389
4:00 Optimized Electromagnetic Inverse Scattering Theory for the Reconstruction of Electron Density Profiles, <i>A.K. Jordan*, Naval Research Laboratory, Y. Zhang, Massachusetts Institute of Technology</i>	390

NEGATIVE PERMITTIVITY AND PERMEABILITY META-MATERIALS AND THEIR APPLICATIONS

Richard W. Ziolkowski

Department of Electrical and Computer Engineering
The University of Arizona
1230 E. Speedway
Tucson, AZ 85721-0104 USA

Tel: (520) 621-6173

Fax: (520) 621-8076

E-mail: ziolkowski@ece.arizona.edu

In the past few years, there has been a renewed interest in using structures to develop materials that mimic known material responses or that qualitatively have new response functions that do not occur in nature. Artificial dielectrics were explored, for example, in the 1950's and 1960's for light-weight microwave antenna lenses. Artificial chiral materials were investigated in the 1980's and 1990's for microwave radar absorber applications. Recent examples of these artificial material activities include photonic band gap structured materials, artificial electric and magnetic molecules, and artificial electric and magnetic materials which, like many of the chiral materials, can exhibit positive or negative permittivity or permeability properties. Very recent experiments involving artificial materials with simultaneous negative permittivity and permeability have captured the public's attention.

The qualitatively new response functions of these "meta-materials" are often generated by artificially fabricated, extrinsic, low dimensional inhomogeneities. For instance, the artificial molecules are based upon the introduction of arrays of electrically small, loaded antennas into a host substrate. Design rules for obtaining the molecule meta-materials that exhibit the common Debye and Lorentz material model responses and their generalizations have been given for both electric and magnetic properties. More recently, a number of electromagnetic structures that exhibit effective permittivity and permeability properties have been designed and experiments have been performed.

A basic review of these meta-materials and their ability to achieve negative permittivity and permeability values will be reviewed. Several applications of meta-materials with simultaneous negative epsilon and mu values will be discussed and demonstrated with both FEM and FDTD simulations. It will be shown that electromagnetic band gap structures constructed with negative permittivity or permeability values lead to interesting filter designs having very narrow bandwidths. It will also be shown that a particular choice of meta-materials with unusual fast-wave properties can lead to a faster-than-light propagation of information having no conflict with causality.

A Combined Numerical and Analytic Approach for Generalized Models of Complex Bi-Anisotropic Meta-Materials

Vikram Jandhyala*, Akira Ishimaru, Seung-Woo Lee, and Yasuo Kuga
 Department of Electrical Engineering
 University of Washington, Box 352500, Seattle, WA 98195-2500

The complex permittivities and permeabilities of composite materials have been studied in the past using effective media models. One of the deficiencies of current effective media models is their inability to integrate scattering characteristics of arbitrarily shaped particles such as small rings and coils. In addition, many models do not consider the combination of effective permittivity and permeability. In this paper, we will describe the derivation of generalized models for complex bi-anisotropic meta-materials. In particular, we will analyze the material properties of "meta-materials" comprising of a host material with embedded rings and split-rings. It has been shown that meta-materials with split ring resonators demonstrate negative permeability in the microwave range.

In the past, extensive research has been conducted on EM propagation and scattering through periodic structures of metal and dielectric materials, including stacked gratings, photonic band-gap materials, and frequency-selective surfaces. Numerical solutions have been obtained using Floquet modes and lattice-sum techniques with transition matrices (Botten et. al 2000; Yasumoto and Yoshitomi, 2000). This approach gives exact numerical solutions for periodic structures, but requires extensive computer time and memory. A more efficient, but approximate approach is based on quasi-static formulations which are relatively simple and flexible enough to deal with a variety of meta-materials including chiral meta-materials (Lindell et al., 1994). The method proposed here uses an analytic form in conjunction with the analysis of electrically small inclusions.

In the presented approach, the generalized tensor flux-field linkage parameters are obtained for general meta-materials in terms of the electrical and magnetic properties of the inclusions. The equivalent electromagnetic moments of the inclusions are computed using a full-wave and low-frequency (for small electrical sizes) method of moments code, and these moments are used in a generalized Lorentz formula of the form

$$\begin{bmatrix} D \\ B \end{bmatrix} = \begin{bmatrix} \epsilon & \xi \\ \zeta & \mu \end{bmatrix} \begin{bmatrix} E \\ H \end{bmatrix} \quad \begin{bmatrix} \epsilon & \xi \\ \zeta & \mu \end{bmatrix} = \begin{bmatrix} \epsilon_0 U & 0 \\ 0 & \mu_0 U \end{bmatrix} + N[a] \quad \left[\begin{bmatrix} U & 0 \\ 0 & U \end{bmatrix} - \frac{N}{3} \begin{bmatrix} U & 0 \\ 0 & U \end{bmatrix} \begin{bmatrix} \epsilon_0 & 0 \\ 0 & \mu_0 \end{bmatrix} \right]^{-1} [a]$$

where N is the density of inclusions. In this manner equivalent material parameters for the composite material are obtained, and no periodic assumptions are required for the inclusions.

High Permittivity Dielectric Composite Materials

Seung-Woo Lee* and Yasuo Kuga
Department of Electrical Engineering
University of Washington, Box 352500, Seattle, WA 98195-2500
Tel: (206)543-0478, Fax: (206)543-6185, E-mail: lsw@ee.washington.edu

Ender Savrun
Sienna Technology
Woodinville, WA 98072

Materials with very high refractive index are useful as substrates of miniature-sized antennas and dielectric resonators because the effective wavelength inside the materials is much smaller than that of free-space, and it helps to reduce the physical dimension of the devices. Some of the high- ϵ_r materials are barium-tetratinanate ($\epsilon_r \approx 37$) and titanate ($\epsilon_r \approx 100$) which are widely used as antenna substrates. However, it is difficult to achieve ϵ_r much higher than 100 with natural materials, and new man-made materials must be developed. It is known that when dielectric materials are loaded with conducting particles, both the real and imaginary parts of permittivity will increase as the fractional volume of the inclusion increases. The rates of increase of both ϵ' and ϵ'' are related not only to the particle concentration but also to the particle size, shape and orientation. Since the acceptable range of a loss tangent for microwave substrates is less than 0.01, it is important to find the optimum configuration of the particles in order to obtain high ϵ' while keeping ϵ'' small enough.

We will discuss the development of very high- ϵ_r dielectric materials using the conductor loading technique at microwave frequency. In order to increase ϵ' while keeping ϵ'' low, special caution should be exercised when selecting the size, shape, orientation and concentration of the conducting particles. A traditional approach of modeling composite materials is the effective medium theory. However, because it is difficult to include the arbitrary particle-shapes and periodic or semi-periodic particle-distributions in the effective medium theory, we will use the numerical technique. In our work, the FDTD method combined with the transmission/reflection method was adopted for the analysis and inversion process. In the transmission/reflection method, the test samples are usually put inside a waveguide, coaxial line and microstrip. Here the waveguide and microstrip are used for our work because the orientation of the particles can be uniformly aligned to the direction of the electrical fields.

Computation of Static Effective Permittivity for 2-D Anisotropic Composite Materials

Feng Wu* and Keith W. Whites
Department of Electrical Engineering
University of Kentucky
453 Anderson Hall
Lexington, KY 40506-0046

The calculation of electric permittivity/permeability/conductivity for composite materials has been conducted extensively for more than a century. However, this fundamental problem keeps challenging scientists as the complexity of the materials increases. Many types of mixing formulas can give accurate predictions on the effective parameters for composite materials that are dilute, low in contrast, or have only inclusions with simple shapes (A. Sihvola, *Electromagnetic Mixing Formulae and Applications*. IEE Press, 2000). As the packing ratio increases and the shapes of inclusions become complicated, these analytical approximations are not expected to work satisfactorily because of increasing mutual interactions among the inclusions.

Possible alternatives to such analytical techniques involve numerical methods. So far, a few numerical techniques have been proposed to address this issue (B. Sareni, et al., *IEEE Trans. Magnetics*, 33(2), 1580-1583, 1997). Additionally, we have recently completed numerical calculations for lattices of complex shaped inclusions. Experimental results for conducting cubic inclusions have also been conducted therein.

Our research is ongoing in this area. In this work, we will present a moment method technique to evaluate the static effective permittivity of a two-dimensional periodic material composed of anisotropic inclusions. We assume that the composite material is illuminated by a uniform electric field. Then we use the equivalence theorem and periodicity of the geometry to obtain the equivalent problems, and hence set up the integral equations in terms of the fictitious sources on the particle surfaces and the unit cell interfaces. Once these sources are solved, the electric dipole moments of the particles can be easily determined. The effective permittivity that accounts for all mutual interactions among the inclusions is then obtained by properly equating a macroscopic model to the original problem. This technique is actually an improvement to our previous method (F. Wu and K. W. Whites, to appear, *IEEE Trans. Antennas Propagat.*, Aug. 2001) wherein effective isotropy of the materials is required. Nevertheless, the new method allows us to handle materials composed of anisotropic inclusions, which is more practical in nature.

Semileaky Waves in Dielectric Pseudochiral Slabs

António L. Topa*, Carlos R. Paiva, and Afonso M. Barbosa
*Departamento de Engenharia Electrotécnica e de Computadores
and Instituto de Telecomunicações,*

Instituto Superior Técnico, Technical University of Lisbon, PORTUGAL

In this paper, we investigate the occurrence of *semileaky* waves in dielectric pseudochiral slabs. It is shown that a thin-film dielectric pseudochiral slab waveguide, in which both the film and the substrate are pseudochiral but with isotropic substrate, can support *semileaky* waves provided that the constitutive parameters are properly chosen. These waves, which radiate energy into the substrate, are well known for their role in several devices such as beam couplers that convert the energy of a beam to the guided modes of a thin-film dielectric slab waveguide. They cannot be found in common isotropic waveguides, where only leaky unguided modes may occur. The radiation into the substrate is caused by one of the two characteristic waves, which ceases to be totally internal reflected at the film-substrate interface. These hybrid waves are termed *semileaky* waves, since one characteristic wave still remains completely guided by the film layer.

The *pseudochiral* or *omega* medium is an artificial complex medium, which is obtained by doping a host isotropic medium with Ω -shaped conducting microstructures. External electric and magnetic fields induce both electric and magnetic polarizations, which are perpendicular to each other. The electromagnetic properties of these media suggest promising applications in the design of devices and components for the microwave and millimeter wave regimes.

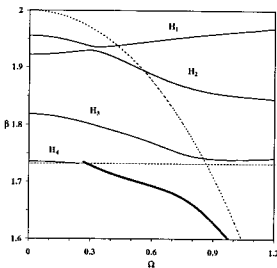


Fig.1

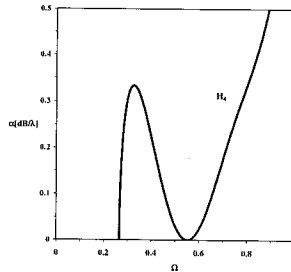


Fig.2

In this configuration, the modes propagating on the structure are hybrid. At some transition values for the pseudochiral parameter Ω , the longitudinal wavenumber becomes complex (thick line in Fig. 1 represents the real part), and guided modes turn into *semileaky* modes (attenuation constant on Fig. 2).

Dipole Radiation near a Wire-Medium Sheet above a Ground Plane

Nader Engheta
University of Pennsylvania
Moore School of Electrical Engineering
Philadelphia, Pennsylvania 19104, U.S.A.
Tel: +1 (215) 898-9777, Fax: +1 (215) 573-2068
E-mail: engheta@ee.upenn.edu
Web: <http://www.ee.upenn.edu/~engheta/>

The idea of wire media, which can be envisioned as a class of composite media composed of thin wire inclusions that need not be necessarily electrically short (i.e., the wire inclusions can be from a fraction of a wavelength in length to multiple wavelengths in length), was explored and studied by us in recent years [C. A. Moses and N. Engheta, "Electromagnetic Wave Propagation in the Wire Medium: A Complex Medium with Long Thin Inclusions," to appear in the Special Issue of *Wave Motion* in 2001; and C. A. Moses and N. Engheta, "An Idea for Electromagnetic 'Feedforward-Feedbackward' Media," in *IEEE Transactions on Antennas and Propagation*, Vol. 47, No. 5, pp. 918-928, May 1999] In principle, these wire inclusions can have different forms and geometries. In our previous work, the electromagnetic properties of media that could be synthesized by embedding many identical, finite-length (with some arbitrary identical length), parallel, thin wire inclusions within an otherwise isotropic host medium were studied in detail.

In this talk, we consider the radiation of an infinitesimal electric dipole in the vicinity of a complex surface made of such a wire medium (i.e., a sheet made of these identical, finite-length, parallel thin wires) above a ground plane. In particular, we explore how the presence of such a wire-medium complex surface affects the radiation pattern of this electric dipole antenna, and how the dipole's pattern is changed as the operating frequency varies. Since the surface is made of wire inclusions that are permitted not to be small compared with the operating wavelength, the surface possesses an interesting frequency response. This, along with the presence of a ground plane placed at a short distance under this surface, would provide the entire structure with surface impedance that will depend on frequency as well as on the angle of incidence. With proper choice of wire length, wire density and the ground plane distance, one can achieve high surface impedance for this structure for certain frequency band and angular region, which significantly affects the radiation properties of dipole antenna in its vicinity.

These issues will be discussed and presented in this talk, and potential applications of this study in the antenna design will be mentioned.

ACTIVE HIGH IMPEDANCE GROUND PLANES.

G. Poilasne, L. Desclos*

Electrical Engineering department, UCLA, Los Angeles, CA, 90095, USA

*NEC, CCRL, Princeton New Jersey, USA

Both now at Photonic RF Corp, Los Angeles, CA, 90024

High Impedance ground planes are periodic structures based on the behavior of Photonic Band-Gap materials (IEEE MTT, Vol.47, n.11, Nov. 1999, pp.2059-2074). They exhibit surface waves band-gap within a given frequency range. Figure 1 presents one of these structures. High impedance ground planes can be considered as a parallel LC circuit where the inductance is due to the loop and the capacitance is either due to the fringing capacitance or the facing capacitance as the structure can be two or three layers.

The first interest in such structures is that the period is much smaller than the wavelength. It is around one tenth of the wavelength for two-layer structure and one thirtieth of the wavelength in the case of three-layer structure. They also exhibit two interesting electromagnetic behaviors. The first one comes from the fact that they have a high impedance. This means that the phase of the reflection coefficient at the resonant frequency is equal to 0deg rather than 180deg in the case of a classical metallic reflector. The second interesting behavior is the suppression of the surface waves around the resonant frequency.

The two electromagnetic behaviors are very interesting for modern antenna applications. As the ground plane is high impedance, the antenna can be directly placed on its top rather than being a quarter wavelength away. Moreover, the suppression of the surface waves avoids the ripples on the front part of the radiation pattern and strongly reduces the interaction with the backward environment. They also allow the reduction of the coupling between electromagnetic sources which can be important to solve EMC problems. Unfortunately, these structures have some physical limitations. One of these important limitation is their band-width and the variation of their characteristics versus frequency.

By introducing active elements on such structures, it is possible to reconfigure dynamically the electromagnetic characteristics of such ground planes. The authors have already introduced successfully active elements on photonic band-gap materials in order to obtain different kinds of diversity effective (G. Poilasne et al, IEEE Trans on AP, Jan. 2000). By using field effect transistors, it is possible to modify the equivalent inductance or capacitance and therefore to control the resonant frequency. In this case, two different configurations can be considered. Either the active element is introduced along the loop, or it is introduced near the capacitance. The polarization of such active components is always a problem when they are placed inside an electromagnetic structure. The solution used by the authors will be presented as well as numerical and experimental results.

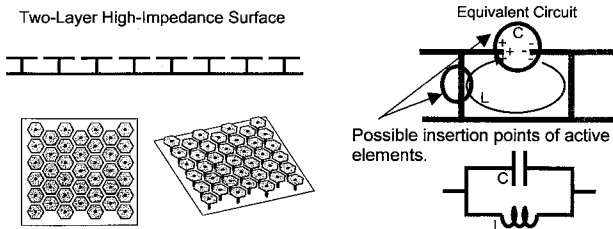


Fig.1: High Impedance Ground Planes, structures and equivalent model.

THE METHOD OF AUXILIARY SOURCES (MAS) AND SOME EM PROPERTIES OF COMPLEX MATERIAL OBJECTS

R. Zaridze*, F. Bogdanov, D. Karkashadze, K. Tavzarashvili, A. Bijamov
Tbilisi State University, 3 Chavchavadze Ave, 380028 Tbilisi, Georgia
Tel.: +995 32 290821, fax: +995 32 290845, e-mail: rzaridze@resonan.ge

It is known that materials with complex electromagnetic properties (like anisotropic, biisotropic, chiral, etc.) are already used to minimize the radar cross section of various scatterers. Together with common dielectric parameters the new ones like two magnetoelectric admittances give more flexibility to achieve the particular properties of the designed devices. That is why recently more attention is paid to utilize the new distinctive electrodynamic properties of complex materials in applied problems, i.e. to explore the characteristics resulting from complex constitutive relations. To study in full these new properties, the efficient methods for solving the scattering problems upon the realistic, complicated 3D objects are required. In this contribution, the MAS is suggested to solve 3D scattering problems upon the complicated objects of optically active materials. The MAS is the method of solution of the boundary problems by representing the unknown scattered field in terms of fundamental or other singular solutions, Auxiliary Sources (AS), of appropriate differential equation. The basis for such a representation is completeness and linear independence of AS on the surface of the boundary. Once the AS are derived, the problem is to determine the amplitudes of these AS to construct the unknown scattered field. The proper choice of location and type of AS significantly reduces the total number of unknowns in the problem, improves also accuracy and convergence of the solution and therefore leads to a highly efficient and fast solving algorithm

In this contribution, the physical properties of 3D objects made of various complex materials (chiral, Tellegen, biisotropic) with complicated shape are studied. The influence of material type on the radiation, scattering, absorption and polarization properties of voluminous bodies is determined. Investigations of light and microwave scattering upon complex material objects have shown the possibility to separate the fields with different (right-hand and left-hand) polarization, as well as to radiate them in different directions. The comparative analysis of the objects made of different complex materials is conducted. New numerical results for such objects are considered, and the program package for calculating characteristics and visualizing the properties of these objects is demonstrated. This software, which is capable of studying radiation, scattering, absorption and polarization characteristics of complicated 3D objects, is demonstrated.

IEEE Antennas & Propagation Society Annual Meeting
8-13 July, 2001; Boston, MA

Optimized Electromagnetic Inverse Scattering Theory
for the Reconstruction of Electron Density Profiles

A. K. Jordan, Naval Research Laboratory, Washington, DC 20375
Y. Zhang, Massachusetts Institute of Technology, Cambridge, 02139

Analytic solutions of the inverse scattering problem for electromagnetic waves reflected from layers of ionospheric electron plasmas have been demonstrated by Jordan and Reilly [1]. The reflection coefficients $r(k)$ were approximated by rational functions of the wavenumber k and analytic solutions of the electron density profiles $N(x)$ were obtained by using the inverse scattering theory of Kay [2]. In order to obtain realistic profiles of naturally occurring electron plasmas, adaptable rational approximations of the reflection coefficient. The nonlinear least-squares approximation of Levenber & Marquardt [3] provides a method to obtain the electron density profiles corresponding to the optimum rational function approximation of $r(k)$ profiles which can be compared with standard profiles [4].

1. Jordan, A., and Reilly, M., *Trans. IEEE Ant. & Prop.* AP-29, 245 (1981).
2. Kay, I., *Comm. Pure & Applied Math.* 13, 371 (1961).
3. Marquardt, J. *Ind. & Appl. Math.*, 11, 431 (1963).
4. Epstein, P. S., "Reflection of waves in an inhomogeneous absorbing medium", *Proc. Nat., Acad. Sci.*, 16, p. 627 (1930).

Numerical Methods

Chairs: W. Chew, USA and B. Barrowes, USA

		Page
1:00	Simulation of 3D EM Fields by a Weak-Form Biconjugate Gradient FFT Method, <i>Z. Q. Zhang*</i> , <i>Q.H. Liu, Duke University</i>	APS
1:20	Fast Algorithm for Matrix-Vector Multiply of Asymmetric Multilevel Block-Toeplitz Matrices, <i>B.E. Barrowes*</i> , <i>Massachusetts Institute of Technology</i> , <i>F.L. Teixeira, The Ohio State University</i> , <i>J.A. Kong, Massachusetts Institute of Technology</i>	APS
1:40	Electromagnetics Optimization Using an Evolutionary Algorithm with a Mixed-Parameter Self-Adaptive Mutation Operator, <i>A. Hoorfar*</i> , <i>S. Nelaturi, J. Zhu, Villanova University</i>	APS
2:00	A Sparse Data Fast Fourier Transform (SDFFT) - Algorithm and Implementation, <i>A. Aydiner*</i> , <i>W.C. Chew, J. Song, University of Illinois at Urbana-Champaign</i>	APS
2:20	Application of Domain Decomposition and Finite Element Method to Electromagnetic Compatible Analysis, <i>Z. Qian*</i> , <i>PLA University of Science and Technology</i> <i>L. Yin, Ultima Interconnect Technology Inc.</i> , <i>W. Hong, Southeast University</i>	APS
2:40	Higham-Cheng Algorithm for Solving the Generalized Eigenproblem Applied to the Computation of the Characteristic Modes, <i>G. Angiulli*</i> , <i>Universita di Reggio Calabria</i> , <i>G. Amendola, G. Di Massa, Universita della Calabria</i>	APS
3:00	Application of Intervallic Wavelets to the Problem of EM Scattering on Multiple Bodies, <i>G. Pan*</i> , <i>M. Touppikov, Arizona State University</i> , <i>B. Gilbert, Mayo Foundation</i>	APS
3:20	Computation of 2.5-Dimensional Static Fields in Uniaxial Anisotropic Media, <i>R. Remis*</i> , <i>P. van den Berg, A. de Hoop, Delft University of Technology</i>	APS
3:40	An Improved Method for the Mesh Termination in the Finite-Difference Solution of Scattering Problems, <i>Z. Lou, Y. S. Xu*</i> , <i>D. Fan, University of Science and Technology of China</i>	APS
4:00	Spectral Domain Analysis of 2-D Cylindrical Transmission Lines Composed of Iso/Anisotropic Substrates, <i>A. Omar*</i> , <i>Hashemite University</i>	APS
4:20	Parallel Implementation of the Finite Difference Time Domain Method Using the ZPL Language, <i>A. Semichaevsky*</i> , <i>D. Rey, J. Stubblefield, C. Chan-Aidebol, M. Testorf, J. Canning, M. Fiddy, University of Massachusetts Lowell</i>	392

Parallel Implementation of the Finite Difference Time Domain Method Using the ZPL language

Andrey Semichaevsky¹, Demetrio Rey², Joss Stubblefield², Carl Chan-Aldebol², Markus Testorf¹, Jim Canning², Michael Fiddy¹

¹Dept. Elec. & Comp. Eng., ²Computer Science Dept.
One University Ave., Lowell, MA 01854, USA

Phone: (978) 934 3306, Fax: (978) 934 3027, Email: semichae@wesun.uml.edu

For many applications the finite-difference time-domain method has become a standard method to solve Maxwell's equations. One of the most important advantages of a finite-difference formulation is the flexibility in simulating any target geometry with a wide range of electromagnetic properties. This and the simplicity of the finite difference equations outweighs the difficulties arising from numerical issues, such as the truncation of the simulation area, the excitation of the incident field and inaccuracies caused by numerical dispersion. A further advantage of the finite-difference time-domain method is the numerical complexity depending on the shape of the target. For instance, for highly elongated simulation domains the increase in computation time is almost linear with the number of data points, since a larger simulation area does not increase the time a wave front requires to pass region of interest.

A subject of current efforts is the efficient implementation of fully 3-D simulation code. Since the computational load is significantly increased, if a third dimension is added implementations on parallel computers are one possibility to reduce the execution time of the simulation. However, the necessity to use low level instructions to access the libraries of parallel computers often turns out to be a major stumbling block, since this requires sufficient knowledge about programming of parallel computers as well as numerical electromagnetics to ensure success. While not being a principle issue, it is of great practical relevance for promoting the finite-difference time-domain method.

In our contribution, we present an implementation of the standard finite-difference time-domain scheme, as well as variants we have been using to obtain synthetic data for layered media and subsurface objects. We describe the implementation of the simulation code using the ZPL language, which permits execution on a parallel computer.

The finite-difference time-domain method is evaluated by comparing simulation results with analytic solutions. We discuss the results of this comparison pointing out the most likely candidates of simulation errors. We provide a brief introduction of the ZPL language, which is particularly useful for coding finite-difference schemes, and we discuss important features of the ZPL language.

Our investigation includes numerical experiments, which indicate that the ZPL language provides an efficient parallel implementation of the simulation problem, although the distribution of the computational load onto a set of processors is almost completely shielded from the programmer.

Calibration and Remote Sensing of the Atmosphere and Objects

Chair: J. Hancock, USA

	Page
1:00 Numerical Simulations of Effects of Ionospheric Irregularities on SAR Imaging, <i>J. Liu*, Y. Kuga, A. Ishimaru, University of Washington, X. Pi, T. Freeman, Jet Propulsion Laboratory</i>	394
1:20 Diagnostics of Subauroral Ionosphere with HF Radar, <i>D.V. Blagoveshchensky*, S.V. Nozdrachev, University of Aerospace Instrumentation</i>	395
1:40 Retrieval of Water Vapor Profiles Using the 54-, 118-, and 183-GHz Bands, <i>J. Hancock, W. Blackwell, R. Leslie, P. Rosenkranz, D. Staelin, Massachusetts Institute of Technology, J. Wang, NASA/Goddard Space Flight Center</i>	396
2:00 Island Wake Impact on Evaporation Duct Height and Sea Clutter in the Lee of Kauai, <i>S. Burk*, Naval Research Laboratory, L.J. Wagner, Space and Naval Warfare Systems Center, T. Haack, Naval Research Laboratory, L. T. Rogers, Space and Naval Warfare Systems Center, P. Whittman, Fleet Numerical Meteorology and Oceanography Center</i>	397
2:20 Temperature Profile Retrievals with an Airborne Passive Microwave Radiometer NAST-M, <i>R. Leslie*, W. Blackwell, J. Barrett, P. Rosenkranz, Massachusetts Institute of Technology</i>	398
2:40 Precipitation Signatures Observed Near 54 and 118 GHz, <i>F. Chen*, J. Barrett, W. Blackwell, R. Leslie, P. Rosenkranz, D. Staelin, Massachusetts Institute of Technology</i>	399
3:00 Millimeter Cloud Radar System Upgrades and Calibration During the ARM Cloud IOP 2000/ARESE II Experiment, <i>L. Li*, S. Sekelsky, M. Bergada, University of Massachusetts Amherst</i>	400
3:20 Corrosion Detection and Thickness Evaluation Using Microwave Nondestructive Testing Techniques, <i>W. Saleh*, N. Qaddoumi, American University of Sharjah</i>	401

Numerical Simulations of Effects of Ionospheric Irregularities on SAR Imaging

Jun Liu, Yasuo Kuga and Akira Ishimaru
Department of Electrical Engineering
University of Washington, Seattle, WA 98195-2500

Xiaoqing Pi and Tony Freeman
Jet Propulsion Laboratory, Pasadena, CA

Synthetic aperture radar (SAR) provides high-resolution images by coherently processing the signals returned from the ground. Perturbations of the propagation channels such as the ionosphere and the troposphere lead to phase change within the effective aperture of the system. This phase perturbation caused by the irregularities of the refractive index structure of the ionosphere will distort the SAR image. In Ishimaru et al., 1999, a homogeneous layer of constant electron density for the ionosphere is assumed. The average electron density is specified, and the irregularity of the ionosphere is given by the two-parameter spectrum. The SAR image resolutions were then obtained using this model. The simulation results indicate substantial change in azimuthal resolution for a UHF-band SAR system, while the change of range resolution is negligible. The actual ionosphere, however, is quite inhomogeneous, and if the SAR is flying over the boundary of a high-to-low electron density concentration region, it will experience a substantial amount of change over the effective aperture.

To include the inhomogeneous nature of the ionosphere and also to develop realistic simulation tools to conduct the SAR calibration, numerical simulation models are developed in this paper. Our model simulates the degradation of SAR image due to large-scale changes of the electron density. Two cases are investigated. In the first case, a linear slope for the average electron density over the effective aperture is assumed. In the second case, a fluctuation given by a Gaussian correlation function is imposed on an average value. A point-spread function is obtained for given SAR and ionospheric parameters such as effective aperture size and electron density variations. From a -3 dB point of the point-spread function, the expected SAR resolution is estimated as a function of effective aperture size and TEC (Total Electron Content) change. A significant degradation of the SAR resolution is observed in the simulation.

The Faraday rotation effect has been proved to be substantial at 500 MHz [Ishimaru et al., 1999]. For a uniformly distributed ionosphere, since the refraction index for each data collecting path is constant and the path length difference from each SAR sampling point to the same ground point is small, the Faraday rotation angle for each path is predictable, and the SAR image resolution will not be seriously affected by this effect. However, the electron density of the ionosphere is nowhere near constant even within a small scale such as a SAR aperture. Analysis and simulations in this paper show that small perturbation of the TEC within a SAR aperture can cause serious degradation of the SAR image.

Diagnostics of Subauroral Ionosphere With HF Radar

D.V. Blagoveshchensky* and S.V. Nozdrachev
University of Aerospace Instrumentation, 67, Bolshaya Morskaya,
St. Petersburg, 190000, Russia
Tel.: +007 812 538 1475, fax: +007 812 315 7778, e-mail: dvb@aanet.ru

The possibilities of the BIZON facility as diagnostic means by the oblique backscatter method for analysis of processes in the ionospheric plasma during its drastic variations caused by geomagnetic disturbances are described. The studied object is the subauroral ionosphere located above northern regions of Finland, Sweden, Norway and Russia. Here the main ionospheric trough is a major feature. The poleward edge of the trough is the projection of the plasmopause on the ionosphere and for a steady state it conforms to the boundary of diffusive auroral precipitation (BDP) of plasma layer particles. Several important geophysical phenomena on a ionospheric level are connected with a position of the BDP: convection boundary, longitudinal current boundary, sharp typical changes of ionospheric parameters in the F-region, electron concentration irregularities, radio waves and whistlers propagation changes and so on.

The purpose of this paper is to show some possibilities of the oblique backscatter method in studying the subauroral ionosphere particularly during magnetic disturbed conditions when there is a complex and changeable picture of plasma distribution in the ionosphere.

The BIZON is a two-channel version of the digital ionosonde of vertical/oblique incidence ionospheric sounders. This implement operates as a radar and enables to determine simultaneously the following characteristics: frequency of signal reflected from the ionosphere, height (range) of reflecting layer of the ionosphere, amplitude and phase of received signal, Doppler shift and spectrum, wave polarization. The frequency range is 1 - 30 MHz, the transmitter power is 10 kW. The BIZON facility is installed at Gorkovskaya observatory near St. Petersburg. Receiving and transmitting antennas are oriented northward.

It is shown that the oblique backscatter method provides some useful information about the ionosphere simultaneously from areas of great sizes. Observations by the BIZON facility allow to study properly a complex picture of signals scattered from irregularities of E- and F-regions of the ionosphere. Different types of oblique backscatter traces - discrete, diffusive, flat, with group delay, rapid arising and disappearing - reflect the essence of happened geophysical phenomena.

Retrieval of Water Vapor Profiles using the 54-, 118-, and 183-GHz Bands

Jay B. Hancock, William J. Blackwell, Robert V. Leslie, Philip W. Rosenkranz,
David H. Staelin, and James R. Wang*

*Research Laboratory of Electronics, Massachusetts Institute of Technology,
Cambridge, Massachusetts 02139*

**NASA/Goddard Space Flight Center, Greenbelt, Maryland*

Clear air atmospheric relative humidity profiles have been retrieved using data from NAST-M (NPOESS Aircraft Sounder Testbed Microwave radiometer) and MIR (Millimeter-wave Imaging Radiometer) in combination. The 54-, 118-, and 183-GHz bands incorporate 8, 8, and 3 channels, respectively. In addition, 89-, 150-, and 220-GHz window channels are included. The instruments were flown on the ER-2 aircraft at approximately 20-km altitude during CAMEX-3 (Convection and Moisture Experiment), which was conducted over the southeastern United States during August and September of 1998.

Retrievals were performed using a Multilayer Feedforward Neural Network (MFNN). The MFNN architecture utilizes 22 input channels, and 2 hidden layers consisting of 30 and 15 nodes, respectively. It produces relative humidity estimates for 20 pressure levels. The training data was simulated using a radiative transfer forward calculation on data from the SATIGR radiosonde database, which comprises 1761 radiosondes spanning all climates, locations, and seasons. The surface emissivity was modeled for these simulations using uniformly random numbers between 0.4 and 1 for each channel. The emissivities across channels were correlated according to measured surface correlations with an added margin (excess decorrelation) to be conservative.

Prediction errors on the validation set for the trained MFNN range from 5 to 14 percent rms at pressure levels ranging from 131 to 1013 mbar. NAST-M/MIR retrievals were validated with coincident retrievals from NAST-I (NPOESS Aircraft Sounder Testbed interferometer) in the 3.5- to 15-micron infrared band, and also with nearly coincident radiosondes. The main atmospheric features of the NAST-M/MIR retrievals agree with NAST-I retrievals and with the radiosondes, except that some features are centered at altitudes slightly offset from the NAST-I and radiosonde predictions, and the values vary somewhat.

Island wake impact on evaporation duct height and sea clutter in the lee of Kauai

S.D. Burk¹, L.J. Wagner², T. Haack¹, L. Ted Rogers², and P. Wittman³

¹Naval Research Laboratory
Monterey, CA 93943-5502

²Space and Naval Warfare Systems Center, Code D858
San Diego, CA 92152-7385

³Fleet Numerical Meteorology and Oceanography Center
Monterey, CA 93943-5502

Perturbed flow over and around an island can produce leeside vortices, as well as a long wake region of reduced wind speed and altered thermodynamic structure. The island wake thereby alters the evaporation duct height field and directional wave spectra, both of which impact radar sea clutter returns. During a 1999 at-sea demonstration using Lockheed-Martin's TEP (Tactical Environmental Processor), data from a SPY-1 phased array tactical radar were collected aboard the destroyer USS O'Kane stationed leeward (west) of Kauai, HI. TEP extracts NEXRAD-like weather information from the SPY-1 radar. Substantial range and azimuthal variability in radar sea clutter was observed and postulated to result from the presence of an island wake. To test this hypothesis, the Naval Research Laboratory's Coupled Ocean/Atmosphere Mesoscale Prediction System (COAMPS) was run with 3km x 3km horizontal resolution to: (a) examine COAMPS ability to forecast an island wake and its impact upon the wind, thermodynamic, and evaporation duct fields, and (b) to investigate the feasibility of assimilating COAMPS forecast fields and radar observations to optimally infer structural refractivity features.

Both idealized simulations of tradewind flow past Kauai and real-data mesoscale forecasts during the period of the TEP experiment (Dec 1999) reveal: (i) development of atmospheric vortices that shed from the island, (ii) strong cornering winds on the island's flanks, and (iii) a long, low-wind-speed wake trailing leeward of the island in a sinuous, oscillatory manner. Evaporation duct height, δ , is found to be elevated in the high wind regions flanking the island and in the shear zones laterally bounding the wake, while δ in the wake itself is reduced from its upstream value. Thus, COAMPS forecasts pronounced inhomogeneity in the δ field leeward of the island. As a further step, COAMPS has been used to drive a wave model (Wavewatch III) to calculate the directional sea spectra $F(\theta, \omega)$ around Kauai, particularly in the island wake vicinity (here θ is wave direction and ω is the wave frequency). The fields of δ and $F(\theta, \omega)$ are used in conjunction with a parabolic equation (PE) propagation model and the Georgia Institute of Technology (GIT) clutter model to calculate relative levels of clutter power as a function range and bearing from the O'Kane. This novel linkage of a hierarchy of sophisticated specialized models (i.e., atmospheric mesoscale model ==> ocean wave model ==> PE propagation model ==> radar clutter model) produces results that compare favorably with the observed clutter distribution. With sufficient computational power, such forecasts of the highly inhomogeneous radar clutter distribution present in the island wake (as well as other settings) could be performed operationally. Further, data assimilation techniques such as being developed for the NRL Nowcast project should be able to fuse radar and meteorological observations with model forecast fields to provide improved *a posteriori* estimates of δ and $F(\theta, \omega)$.

Temperature Profile Retrievals with an Airborne Passive Microwave Radiometer NAST-M

R. Vincent Leslie, William J. Blackwell, Jack W. Barrett, Philip W. Rosenkranz,
David H. Staelin

Research Laboratory of Electronics
Massachusetts Institute of Technology, Cambridge, Massachusetts

The National Polar-orbiting Operational Environmental Satellite System (NPOESS) Aircraft Sounder Testbed (NAST) is used for evaluating potential remote sensing instrument concepts for future NPOESS satellites. The microwave imager/sounder (NAST-M) has two coregistered total-power spectrometers with a scanning reflector. This paper presents the first airborne temperature profile retrievals obtained using the NAST-M instrument.

The 54-GHz spectrometer has eight channels between 50.2 and 56.2 GHz (BW from 180 to 400 MHz) and the 118-GHz spectrometer has six operational channels between 118.75 ± 0.8 GHz and 118.75 ± 3.5 GHz (BW from 400 to 1000 MHz). The receiver noise temperature for the 54-GHz radiometer is ~ 500 K, and for the 118-GHz radiometer it is 1200 K. Channel sensitivities (rms) range between 0.2 K-0.25 K for the 54-GHz system and 0.2 K-0.4 K for the 118-GHz system. The measured brightness temperature was calibrated within 1.5 Kelvin with a three-point periodic absolute calibration. For this paper, NAST's platform is the NASA ER-2 high-altitude aircraft. From a 20-km altitude, the swathwidth is 100 km ($\pm 64.8^\circ$) and the spatial resolution is 2.6 km at nadir.

A non-linear statistical temperature profile retrieval was implemented with a multilayer feedforward neural network (MFNN) trained on a seasonal ~ 400 subset of the TIGR radiosonde ensemble. The NAST-M brightness temperature and the aircraft's altitude are preconditioned (decorrelated, normalized, and mean removed) and entered into the MFNN to estimate the coefficients of the orthogonal expansion of the temperature profiles. For training, Liebe's Millimeter-wave Propagation Model is used to transform the TIGR profiles into simulated NAST-M brightness temperatures. The rms simulated retrieval errors based on the training and validation sets were less than two Kelvin in the mid-troposphere and closer to 2.5 Kelvin at the surface. The scanning reflector allows two-dimensional image of the temperature profiles at 25 discrete atmospheric pressures along with skin surface temperature.

The first case study includes temperature profile retrievals within the eye of hurricane Bonnie on August 26, 1998 during the Convection And Moisture EXperiment (CAMEX-III). The warm core perturbation aloft is clearly visible in the retrieval. The second case study is during the WINTER EXperiment (WINTeX) on March 29, 1999 and showed a 4-K wedge-shaped cold region over Lake Michigan.

Precipitation signatures observed near 54 and 118 GHz

Frederick W. Chen*, John W. Barrett, William J. Blackwell, R. Vincent Leslie,
Philip W. Rosenkranz, David H. Staelin
Research Laboratory of Electronics, Massachusetts Institute of Technology,
Cambridge, MA

Methods for estimating precipitation rate from passive millimeter-wave spectral data are being developed and tested. The data studied were collected using the NPOESS Aircraft Sounding Testbed – Microwave temperature sounder (NAST-M) aboard the NASA ER-2 high-altitude aircraft. Eight channels in each of the 54- and 118-GHz oxygen bands were used. Hurricanes and other precipitation events were observed.

Microwave precipitation-rate retrievals that utilize opaque and nearly-opaque spectral bands capitalize on information contained in the altitude profiles of temperature, humidity, and hydrometeor properties, including abundance, size, and phase. These are related in turn to the vertical wind velocity and the relative humidity profile, and therefore to the precipitation rate.

Each channel of the NAST-M is most sensitive to a specific layer of the atmosphere, and observations with multiple channels therefore enable estimates of cell-top altitude. Cell-top altitude is correlated with vertical wind velocity and therefore with the rate at which the saturated air is being dehumidified. In addition, hydrometeor size also is correlated with vertical wind velocity because only high vertical velocities can keep large particles aloft. The data show that the 54-GHz channels are more sensitive to the larger particles characterizing heavy precipitation than are those near 118-GHz, while the 118-GHz channels are more sensitive to small particles. Particle sizes at an altitude of interest can be inferred by evaluating the ratio of the perturbation on the 54-GHz channel which peaks near that altitude with the perturbation on the corresponding 118-GHz channel. Larger hydrometeors generally produce larger values of this ratio than do smaller particles because many large hydrometeors are in the Rayleigh scattering regime near 54 GHz but not near 118 GHz (thereby suppressing the 118-GHz relative scattering cross-section), whereas smaller hydrometeors Rayleigh scatter in both bands (thereby suppressing the 54-GHz relative scattering cross-section). Moreover, total hydrometeor population is also correlated with precipitation rate and is independently registered in the microwave albedo of cell tops.

In summary, three signatures are available for correlation with precipitation rate: cell-top altitude, average cell albedo, and characteristic particle size. The relationships between these three signatures can be observed without reference to ground truth.

Millimeter Cloud Radar System Upgrades and Calibration during the ARM Cloud
IOP 2000/ARESE II Experiment

Lihua Li *, Steve Sekelsky, Marc Bergada

Knowles Bldg., Rm 201
Department of Electrical and Computer Engineering
University of Massachusetts, Amherst, MA 01003
Tel:413-545-4567, Fax:413-545-4652
email:lihua@mirsl.ecs.umass.edu

During the spring 2000, two millimeter cloud radar systems were deployed by the University of Massachusetts in support of the DOE Atmospheric Radiation Measurement (ARM) Cloud Intensive Observation Program (IOP) and the ARM Enhanced Shortwave Experiment (ARESE II). The ground-based Cloud Profiling Radar System (CPRS) is a portable dual-wavelength (33 GHz and 95 GHz) polarimetric Doppler radar. The Airborne Cloud Radar (ACR), jointly developed by the University of Massachusetts and NASA's JPL, is a W-band polarimetric Doppler radar. ACR was designed as a research facility in support of the development of the 94 GHz Cloud Profiling Radar (CPR), which is the central instrument for NASA's CloudSat mission.

Recently, a series of hardware upgrades were performed for ACR. It was then installed on board a new airborne platform, the DOE's Twin Otter aircraft for ARM UAV missions. In order to simulate satellite geometry for its radiometers, the Twin Otter flew at 6.7 km above the sea level during Cloud IOP 2000/ARESE II experiment. However, at this altitude, critical equipment designed to operate at low altitude will fail in an unpressurized environment. Therefore, such equipment used by ACR was replaced or modified, and the entire radar system was tested in an environmental chamber before the field experiment.

This paper first describes ACR hardware upgrades and system installation on the DOE's Twin Otter aircraft, then presents preliminary results of instrument calibrations and intercomparison conducted during the Cloud IOP 2000/ARESE II experiment. The ground-based CPRS was calibrated using two different kinds of calibration targets: corner reflectors and metal spheres. The corner reflector was mounted atop a 10 m tower which was placed at two different distances from the radar antenna. When metal spheres were used, the precision machined steel balls were launched into the air above the tower using an air-gun. A series of calibrations were performed using corner reflectors and metal spheres in different sizes. Since ACR was mounted on the Twin Otter for either zenith or nadir pointing observation, it could not be calibrated with corner reflectors or spheres. However, simultaneous cloud measurements using CPRS 95 GHz and ACR allowed CPRS calibration to be transferred to ACR.

Corrosion Detection and Thickness Evaluation Using Microwave Nondestructive Testing Techniques

Wael Saleh and Nasser Qaddoumi
Electrical, Electronics and Computer Engineering Department
American University of Sharjah
Sharjah, P.O. Box 26666
United Arab Emirates

The use of near field microwave and millimeter wave nondestructive testing methods, utilizing open-ended rectangular waveguide sensors, has shown great potential for detecting minute thickness variations in laminate structures, in particular those backed by a conducting plate. Slight variations in the dielectric properties of materials may also be detected using a set of optimal detection parameters including the standoff distance and the frequency of operation. A recent investigation showed that rust could be detected using microwave nondestructive testing techniques. In addition, the dielectric properties of several rust samples from different environments were measured. In this investigation, our goal is to improve the detection sensitivity of the presence of rust and to estimate its thickness. Consequently, an electromagnetic model that simulates the interaction of fields radiated by an open-ended rectangular waveguide aperture with layered structures is utilized to come up with an optimal set of parameters for rust detection. To enhance the detection sensitivity, the standoff distance was replaced by an optimized dielectric layer with known properties. Results show drastic improvement in the measured parameters (phase and magnitude of the reflection coefficient at the aperture of the waveguide) indicating enhanced detection of the presence of rust. To estimate the thickness of rust, an empirical mixing model describing the effective dielectric properties of the media in front of the waveguide was obtained. This mixing model is found using the dielectric properties and thickness of the paint and rust layers as well as the measured reflection coefficient. The dielectric properties of rust and paint are fixed and only the thickness of rust can change. Thus, using the mixing model with knowledge of the effective dielectric properties, the thickness of rust can be obtained. If the thickness of both rust and paint were of interest, the use of two measurements at two different frequencies can resolve the problem. The results of an experimental investigation on detecting the presence and evaluating the thickness of very thin rust layers (0.01 mm - 0.08 mm) using an open-ended rectangular waveguide probes will also be presented.



Frequency and Polarization Diversity

Chairs: D. McNamara, Canada and G. Kadambi, USA

	Page
1:00 The Effect of Slot Contour on the Polarization Characteristics of A Single Feed Dual Band PIFA, <i>G. Kadambi*</i> , <i>K. Simmons</i> , <i>S. Yarasi</i> , <i>J. Sullivan</i> , <i>T. Hebron</i> , <i>Centurion Wireless Technologies</i>	404
1:20 Comparison of Helmet and Vest Mounting Configurations for Switched Diversity Antennas, <i>H. Foltz*</i> , <i>S. Silva</i> , <i>S. Ledezma</i> , <i>E. Guzman</i> , <i>E. Hobbs</i> , <i>M. Garces</i> , <i>J. de D. Ramirez</i> , <i>G. Arellano</i> , <i>G. Montiel</i> , <i>University of Texas-Pan American</i> , <i>J. McLean</i> , <i>EMC Automation, Inc.</i>	405
1:40 Multi-Frequency Printed Dipole with Built-In Filter, <i>R.B. Hermida*</i> , <i>Santander University</i> , <i>L. Desclose</i> , <i>Y. Mahe</i> , <i>S. Toutain</i> , <i>Ecole polytechnique universite de Nantes</i>	406
2:00 Diversity PIFAs With Common and Compact Ground Plane, <i>G. Kadambi*</i> , <i>K. Simmons</i> , <i>T. Hebron</i> , <i>S. Yarasi</i> , <i>J. Sullivan</i> , <i>Centurion Wireless Technologies, Inc.</i>	407
2:20 Multi-band, Multi-Mode Antenna Using Meanderline Structures, <i>F. Caimi*</i> , <i>J. Kralovec</i> , <i>SkyCross, Inc.</i>	408
2:40 The Application of Numerical Optimisation to the Design of Meanderline Polarisers, <i>D. McNamara*</i> , <i>University of Ottawa</i>	409
3:00 Size Reduction of Circularly-Polarized Microstrip Antennas, <i>J. Powell*</i> , <i>R. Jedlicka</i> , <i>B. Blevins</i> , <i>New Mexico State University</i>	410
3:20 A Comparative Analysis of Different Microstrip Antenna Structures Designed to Function as Single Frequency Technology, <i>S. Khan*</i> , <i>Kansas State University</i>	411
3:40 Discretized-Phase-Space Slant-Stack Transform for Time-Dependent Radiation from Aperture Sources, <i>A. Shlivinski*</i> , <i>E. Heyman</i> , <i>A. Boag</i> , <i>Tel Aviv University</i> , <i>A. Fluerasu</i> , <i>C. Letrou</i> , <i>I.N.T.</i>	412
4:00 Dual Frequency Circular Polarization Printed Antennas, <i>L. Desclos*</i> , <i>Y. Mahe</i> , <i>G. Poilasne</i> , <i>S. Toutain</i> , <i>Ecole polytechnique de Nantes</i>	413
4:20 Dual-Polarized Operations of A Compact Microstrip Antenna, <i>J.S. Row*</i> , <i>W.S. Chen</i> , <i>Chien Kuo Institute of Technology</i> , <i>S.H. Yeh</i> , <i>National Sun Yat-Sen University</i>	414

THE EFFECT OF SLOT CONTOUR ON THE POLARIZATION CHARACTERISTICS OF A SINGLE FEED DUAL BAND PIFA

Govind R. Kadambi*, Kenneth D. Simmons, Sripathi Yarasi, Jon L. Sullivan and Ted Hebron

Centurion Wireless Technologies, Inc.
3425 N. 44th Street, Lincoln, NE 68504, U.S.A.

There is an enhanced emphasis on internal antennas for cellular handsets instead of a conventional external wire antenna. Internal antennas have several advantageous features such as being less prone for external damage, a reduction in overall size of the handset with optimization, easy portability, and potential for low SAR Characteristics. The concept of internal antenna stems from the avoidance of protruding external radiating element by the integration of the antenna into the handset. Among the various choices for cellular internal antennas, Planar Inverted F antenna (PIFA) appears to have great promise. Many distinguishing features characterize the PIFA: it has omni directional radiation pattern in orthogonal principal planes for vertical polarization and multiple approaches for the size reduction. The capacitive loading and the slot loading techniques are the most commonly invoked methods to realize the miniaturization of the size of the PIFA. The PIFA also finds useful applications in Diversity Schemes. The sensitivity of the PIFA to both the vertical and horizontal polarization is an additional advantage for cellular communication in which the orientation of the antenna is not fixed. Therefore the polarization performance of the PIFA is an important design attribute for its overall performance evaluation. Although the single feed dual band PIFA has been a topic of specific emphasis and special relevance to cellular communication, an in depth study of the polarization characteristics of the PIFA seems to have not been dealt in the open literature.

This paper presents the polarization performance of a single feed dual band PIFA. In particular, this paper deals with the effect of slot on the polarization characteristics of the PIFA. The presented study deals with the free space radiation characteristics of the PIFA not only in its principal planes but also in User Position, which is analogous to the diagonal plane of conventional antenna measurement. The design principle of the single feed dual band PIFA of this paper is based on an earlier paper by the authors [G.Kadambi et.al, URSI Symposium, 2000, Salt Lake City, pp. 221]. The above cited paper deals with a simplified and novel design of single feed dual band PIFA devoid of the physical partitioning and the concept of slot loading to reduce the resonant frequency of the PIFA. To supplement the resonance characteristics of the earlier design, this paper emphasizes the importance of polarization property of the single feed dual band PIFA. In this paper, a straight slot and orientations of the inclined slots in relation to the position of the shorting pin have been considered to study the polarization properties of the dual band PIFA. In addition, the possible effect of the aspect ratio (length/width) of the PIFA on the polarization of the dual band PIFA is also illustrated. This paper also presents the gain and the return loss characteristics of dual band (AMPS-PCS) PIFAs with straight and inclined slots. To facilitate a viable comparison, the size of the ground plane, the location of the PIFA on the ground plane, the height of the PIFA as well as the perimeter of the PIFA contour are retained identical in all the case studies considered. The practical importance of the relative merits and demerits of each of the case studies in the overall design of a single feed dual band PIFA is also highlighted in this paper. It is inferred that the experimental studies reported in this paper in conjunction with the earlier preliminary single feed Dual band PIFA design would find useful applications in Mobile communication.

COMPARISON OF HELMET AND VEST MOUNTING CONFIGURATIONS FOR SWITCHED DIVERSITY ANTENNAS

H. Foltz¹, S. Silva¹, S. Ledezma¹, E. Guzman¹, E. Hobbs¹,
M. Garces¹, J. de D. Ramirez¹, G. Arellano¹, G. Montiel¹, J. McLean²

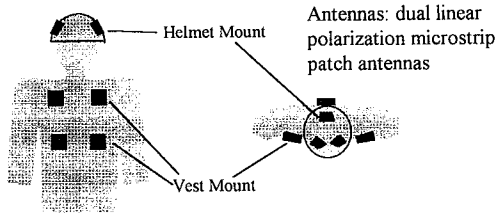
¹University of Texas - Pan American, Edinburg, TX

²EMC Automation, Inc., Austin, TX

Personnel mounted communications systems, designed for mobile usage in hostile environments where cellular/PCS infrastructure is unavailable, operate at a disadvantage due to power constraints, low elevation at both ends of the link, and frequent absence of a line of sight path. Mitigation of multipath fading is of particular interest in these situations. While spread spectrum techniques are useful for reducing multipath, indoors and in close proximity to other structures nulls can persist over tens of MHz bandwidth. In this work we are investigating the combined usage of polarization, spatial, and pattern diversity; in particular, the use of switched diversity in combination with a number of dual polarization patch antennas mounted at various locations on the upper body.

Previously presented work has shown that three dual-polarization patches mounted on a helmet can yield diversity gains of 10-12 dB (1% fade probability) over a whip antenna. The slope of the fading curve was equivalent to that for 2.5 ideal uncorrelated channels. For a variety of safety and convenience considerations, mounting the patches at locations other than the head may be desirable. We have conducted a study comparing helmet mounting with upper torso and mid torso mounting on a vest with attached patched elements. Field measurements have been conducted in light urban and open areas, with and without a line of sight present, using a rapidly multiplexed scalar receiver at 2.45 GHz. The receiver was mounted in a backpack tethered to a mobile instrumentation cart.

Preliminary results shown an average 1.5 dB penalty (relative to a helmet) in signal strength for mounting at the upper torso, and a 3 dB penalty for mounting at the mid torso. These signal reduction appear to be primarily due to reduced height. The slope of the fading curve is also slightly less favorable when the patches are vest mounted. This is most likely due to a decrease in pattern diversity.



Multi-frequency printed dipole with built-in filter

Rosa Belen Hermida*, Laurent Desclos, Yann Mahé, S. Toutain

IRCCyN-SETRA, Ecole polytechnique université de Nantes, BP 50609, 44306 Nantes cedex 3

* Santander University de Santander, Spain

Abstract:

Mobility and multi-services are becoming more and more the appealing point of new telecommunication systems. In order to fulfill the requirements of such projects, the need of antenna with multi frequency characteristics is a must. Moreover it is interesting to develop a concrete a repeatable way of treating this problem. One of the aims is there to deal with a quite well know antenna: the printed dipole.

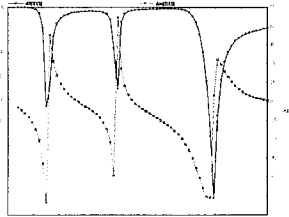
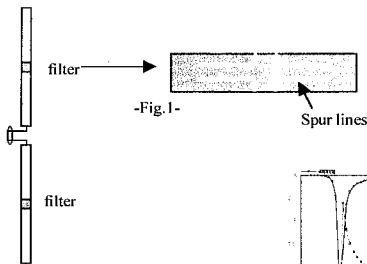
This antenna is well known and few derivations have been made in order to help it becoming multi-frequency. It consisted most of the time in adding a kind of parasitic element. This approach creates many difficulties in the sense that it is relying on the mastering of coupling effects between the elements and do not offer a maximum efficiency for both frequency (loss by coupling).

It was then interesting to develop an approach in which the dipole itself will be considered as a line and divided by portions that could be connected through the response of interconnecting filters. If we imagine a design for a couple of frequency f_1 and f_2 , f_1 being larger than f_2 , then considering a printed line that will serve as a core radiator for the antenna -fig1- it is possible to determine a filter that will let pass the frequency f_2 while stopping the f_1 . This is made simple as we use a classical transmission line theory.

Then as the filter will be acting as a low pass then the full length L_2 of the dipole will be used for radiation when a signal of frequency f_2 will be present and the L_1 length will be the radiator for a signal with frequency f_1 as no signal will flow on the higher portion of the dipole. The filter is made out of spur lines that could be of different forms, several investigations have been performed in order to be able to integrate totally the filter within the line as in fig.1 (left).

Several cases have been treated successfully for dual frequency and we see in fig.2 a result for a dual frequency at 360 MHz and 2 GHz. The matching is better than 10 dB as the gain is comparable to a single frequency dipole.

More experiments have been performed and show that a triple and quadruple frequency approach is possible and interesting to continue. The approach will be shown along with the different examples as well as some interesting facts about the spurious frequency appearing between two bands.



-Fig. 2-

DIVERSITY PIFAs WITH COMMON AND COMPACT GROUND PLANE

Govind R. Kadambi*, Kenneth D. Simmons, Sripathi Yarasi, Jon L. Sullivan
and Ted Hebron

Centurion Wireless Technologies, Inc.
3425 N. 44th Street, Lincoln, NE 68504, U.S.A.

In its simplest term, the diversity technique is a means of achieving reliable and enhanced overall system performance with the utilization of an additional antenna. To meet the requirement of sustained and effective fast rate of data transfer, of late specific emphasis is placed on Diversity Antennas in RF data communication. Theoretically, the spatial diversity technique warrants a physical separation of a wavelength between the two antennas. In many practical applications, it may not be feasible to realize the required separation between the two antennas of a spatial diversity scheme. In view of the above constraint, the emphasis is being shifted to arrive at a compactness of the overall spatial diversity scheme to meet the acceptable performance. As an internal antenna, the PIFA has been a topic of special relevance to both the Mobile Voice and RF Data communications. Easy portability, being less prone for external damage and the absence of protruding radiating element are some of the advantageous features of the internal antenna. The sensitivity of the PIFA to both the vertical and horizontal polarization makes it a good choice for Diversity applications. In this paper several new schemes of designing a Compact Diversity Layout comprising PIFAs with small and common ground plane are proposed. This paper also demonstrates that it is possible to retain the pattern performance of individual antennas of a spatial diversity scheme even when the separation between the antennas is only a fraction of a wavelength.

In the first scheme, the two PIFAs are placed back to back on a small rectangular ground plane (18 mm x 42 mm). The two PIFAs are placed such that the shorted ends of the two PIFAs face each other. Such an arrangement ensures better isolation between the two PIFAs despite being placed in a close proximity. In the second scheme, the ground plane is bent at its opposite ends to form vertical sections. The two PIFAs are placed (outward) on the vertical sections at the opposite ends of the ground plane. The second scheme allows the placement of some system components between the two vertical sections of the bent ground plane. The distortion of the radiation patterns of the PIFAs is minimized despite the presence of some components between the two PIFAs. This is mainly due to the blockage effect offered by the vertical sections of the ground plane. Much contrary to the first two schemes, in the third scheme there is no physical separation between the two PIFAs placed on a common rectangular ground plane. Only a single shorting pin or post partitions the two PIFAs resulting in an extremely simple and compact diversity layout. In the fourth scheme, which is a modification of the third scheme, the two PIFAs, which are not physically separated, are placed on a common ground plane of L shape. The partitioning of the two antennas is again realized through a common shorting post. Unlike the third scheme, in the fourth scheme the two PIFAs are oriented orthogonal to each other. The basic concepts proposed in all the schemes have been proved through the design of Diversity PIFAs for ISM Band applications. In all of the above schemes of Diversity Layout using the PIFAs, good VSWR performance is achieved. The individual PIFAs of the above schemes show satisfactory gain performance. Without loss of generality, the concept proposed in this paper can be extended to other frequency bands of interest.

Multi-band, Multi-mode Antenna using Meanderline Structures

Frank Caimi and Jay Kralovec
SkyCross, Inc.
300A North Drive
Melbourne, FL 32934

The prospect of designing efficient multi-band antennas to meet the demands of cellular phone and wireless equipment manufacturers is a challenge for antenna engineers. High radiation efficiency and small size are paramount goals for obtaining communications system performance while meeting packaging constraints. A goal for a given service is to reach the performance specified by the Chu-Harrington limit that says for a given bandwidth, there exists a minimum theoretical radius for the enclosing sphere containing the antenna. Dipole, PIFA, and Goubau antennas approach this limit successively.

This paper describes a highly efficient three-dimensional antenna structure that approaches the Chu-Harrington limit. One form of the antenna is roughly a cubic structure of approximately 0.15 - 0.2 wavelengths per side. The antenna is capable of operating in a multi-mode fashion producing both monopole and endfire patterns in two separate frequency regimes. Depending on the configuration, linear horizontal and vertical polarization can be obtained simultaneously or circular polarization can be obtained. These features allow the antenna to be used for simultaneous satellite reception and terrestrial communications. Antenna prototypes have been designed and tested for use in satellite antenna applications, as well as for GPS and cellular modalities.

The basic structure and operating characteristics of the antenna will be discussed as well as its measured performance in the PCS and PHS bands. For the small size, the antenna gain achieved is highly competitive with that of a current cell phone handset antenna. The antenna employs a patented design using slow wave meanderline structures for tuning.

The Application of Numerical Optimisation to the Design of Meanderline Polarisers

Derek A. McNamara

School of Information Technology & Engineering, University of Ottawa, Ottawa,
Ontario K1N 6N5, Canada

Meanderline circular polarisers (eg. L.Young, L.A.Robinson & C.A.Hacking, *IEEE Trans.*, AP-23, 376-378,1973) continue to be used with antennas intended for many disparate applications. Most published material consists of data for a few specific designs (eg. McNamara, *IEEE AP-S Symp. Digest*, 16-19,1981), or methods for an electromagnetic analysis of such polarisers. However, the outcome of a comprehensive application of numerical optimization methods to the design of these polarisers does not appear to have been previously published.

The particular meanderline polariser configuration most suited to a specific application will depend on the requirements of that application. Apart from the obvious RF performance requirements, in some applications a trade-off has to be done of many factors, such as the material/assembly costs of additional polariser sheets and spacers versus the tightness of dimensional and positional tolerances needed during part fabrication and polariser assembly. The achievement of a design with multiple requirements is most conveniently done using design tools that employ optimization algorithms. This paper integrates an existing approximate yet reliable electromagnetic analysis model (R.Chu & K.Lee, *IEEE Trans.*, AP-35,652-661,1987; Correction in AP-36, 1041, 1988), plus existing numerical optimization algorithms, into a meanderline polariser design tool. We will discuss the application of this tool to several polariser configurations.

In order to apply numerical optimisation it is of course necessary to translate a set of practical requirements into mathematical expressions which define the objective functions to be minimized. This is an important step, since no matter how reliably and rapidly we are able to achieve this minimisation, it will be of little use if it results in a polariser whose performance is not what we are really trying to achieve. These functions must also have properties that encourage rapid convergence. We will discuss and illustrate how the optimal solutions for the polariser design change with alterations to the objective functions selected.

Use of the approximate analysis mentioned above allows very rapid computation of the objective functions and hence efficient optimization. Full-wave numerical electromagnetic models (eg. K.K.Chan, S.R.Gauthier & G.Dinham, *Proc. 3rd Int. Conf. Electromagn. Aerospace Appl.*, 171-174, 1993) are more accurate, but not always feasible for direct use with automated optimization. If it is indeed necessary to use such fine models they can be related to the coarser model used here via some surrogate optimization approach (eg. M.Bakr, J.Bandler, R.Biernacki, S.Chen & K.Madsen, *IEEE Trans.*, MTT-46, 2412-2425, 1998).

Size Reduction of Circularly-polarized Microstrip Antennas

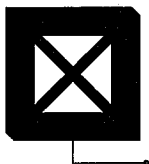
Johnna D. Powell*, Russell P. Jedlicka*, Bruce A. Blevins**

*Klipsch School of Electrical & Computer Engineering, New Mexico State University

**Physical Science Laboratory, New Mexico State University

Substantial work has been done to reactively load microstrip antennas to reduce their size for a specified frequency of operation. Most often the primary concern is the center frequency and impedance bandwidth of the loaded configuration. This study investigates different loading techniques with the emphasis on obtaining not only good impedance characteristics but also maintaining good pattern characteristics; that is, minimize the decrease in efficiency while maintain pattern shape and polarization characteristics.

The two microstrip configurations considered for loading in this study are the nearly-square and chamfered-corners patch. One of the most promising configurations is depicted below. The simulations and measurements are done using standard Teflon fiberglass substrate, $\epsilon = 2.45$, $\tan\delta = 0.002$ and a thickness of $h = 0.120''$.



For a patch of nominal dimensions $2.52''$ square the calculated resonant frequency is 1.438 GHz without the cutouts. When loaded as shown above, the frequency reduced by 197 MHz to 1.241 GHz, a 13.7% shift. Measurements demonstrated a shift of about 203 MHz or about 14.2%. The simulations and measurements are repeated for microstrip antennas with integrated radomes; that is, a $0.060''$ superstrate using the same Teflon fiberglass material. There is only a slight reduction in frequency shift due to the reactive loading for this case, 12.6% (this shift does not include that due to the dielectric superstrate). The predicted resonant frequency is 1234 MHz while the measured value is 1227 MHz. These results are compared to those for an unloaded patch operating at the same. The unloaded patch would have been a nominal $2.988''$ square, an increase in size of 18.6%.

Further size reduction using the same technique as well as other loading schemes are investigated and will be presented.

"A Comparative Analysis of different Microstrip Antenna Structures
Designed to function as Single Frequency Ice Sensors"

Dr. Saeed M. Khan
Department of Engineering Technology
Kansas State University
2310 Centennial Road
Salina, KS 67401

ABSTRACT:

A multi-frequency ice gauge approach targeted for aerospace applications uses a RMPA (Rectangular Microstrip Patch Antenna) to meter ice thickness by searching out shifting resonances. The scheme relies on the fact that a change in ice thickness will result in a change in antenna impedance and, the antenna will become resonant at a different frequency. The system requires a variable frequency generator, an impedance bridge and a frequency controller. In an attempt to reduce the cost, complexity and size of the system the author has suggested the possibility of using a single frequency system where the level of the reflected signal can be used to detect ice. The author has conducted simulations using a patch (with radome) covered by ice of different depths. Results of the S11 under different conditions seem to indicate that while it is relatively easy to detect the presence or absence of ice (2 mm thick and greater, at 1.5 GHz), the problem of finding the correct thickness remains a more difficult one. This paper explores four different antenna structures and their sensitivities to ice thickness through simulations. The constructions include a rectangular patch, a rectangular patch with parasitics, a circularly polarized microstrip patch and, a circularly polarized microstrip patch with parasitics. The three new selections have been made in an effort to use antennas, which are more strongly coupled to the ice layers and possess more radiating edges than a regular RMPA. The results from the simulations, run on each of the four structures for varying depths of ice loads, will be presented. The paper will do a comparative study of these structures and comment on their suitability as effective and reliable ice sensors.

Discretized-Phase-Space Slant-Stack Transform for Time-Dependent Radiation from Aperture Sources

Amir Shlivinski⁽¹⁾, Ehud Heyman⁽¹⁾, Amir Boag⁽¹⁾, Anca Fluerașu⁽²⁾,
Christine Letrou⁽²⁾

⁽¹⁾Department of Physical Electronics, Tel Aviv University
Tel Aviv 69978, Israel, fax: +972-3-6423508, e-mail: heyman@eng.tau.ac.il

⁽²⁾I.N.T., 9 rue Charles Fourier, F-91011 EVRY Cedex, FRANCE
fax: 33 1 60 76 42 84 e-mail: Christine.Letrou@int-evry.fr

The wideband discretized-phase-space beam summation representation introduced in the first part of this two-part sequence [REF] has several attractive features that make it amenable for an extension into the time domain (TD): (a) The same beam lattice is used for all frequencies; (b) The iso-diffracting Gaussian basis provides the "snuggest" frame representation for all frequencies; (c) The propagation parameters of the resulting Gaussian beams (e.g., their complex radii of curvature) are frequency-independent and thus need to be calculated only once.

In this paper we utilize these properties to derive a new TD representation for radiation from extended apertures. In this representation the field is expanded in a discrete lattice of shifted and tilted pulsed beam fields (PB). The excitation coefficients of these PB propagators are extracted from the TD data (the aperture source distribution) via a new transformation termed the "discretized local slant stack transform". These propagators may then be tracked from the aperture plane through the ambient environment.

The paper closes a circle of analogy between frequency domain (FD) and TD spectral representations. In the FD the plane wave, the beam wave and the discretized beam wave transform are, the Fourier, the local Fourier and the Gabor transforms, respectively. In the TD, those are the slant transform (SST) the local slant transform and the new discretized local SST, respectively. Note the new transform is discretized in space and direction but continuous in time.

The new transform presented expresses a function in $\mathbb{R}^2 \times \mathbb{R}$ in terms of its local projections at a discrete grid of points along a discrete set of orientations. It may therefore be relevant in other disciplines, such as image processing in CT and PET. In general, it may utilize arbitrary window functions, yet for the application to the time-dependent radiation problem, we utilize it in conjunction with the iso-diffracting Gaussian basis functions. These functions not only provide the snuggest representation for all frequencies [REF], but in the TD they also yield analytically tractable iso-diffracting PB fields, leading to a new frame-phase space formulation for short-pulse fields directly in the TD.

[REF] A. Shlivinski, E. Heyman, A. Boag, D. Lugaara and C. Letrou, "Gabor-frame phase space beam summation formulation for wideband radiation from extended apertures," *This conference*.

Dual frequency circular polarization printed antennas

L. Desclos, Y. Mahe, G. Poilasne, S. Toutain

IRCCYN division SETRA, Laboratoire SEI, IRESTE, Ecole polytechnique de Nantes, Rue Christian Pauc La chantrerie, BP 60601, 44306 Nantes Cedex France

Abstract:

Communication systems tend to have more and more dual frequency front ends and multi-mode is becoming a common feature on the antenna side. Moreover, the circular polarization exhibits a better robustness to distortion along the transmission path. Therefore dual band circular polarization antennas present a real interest for many applications.

Here, we propose two solutions in order to obtain such behaviors. The two solutions are complementary as they allow to have either two frequency bands near each other or farther from each other, for example 1.9GHz and 2.1GHz or 2.4GHz and 5GHz.

In both cases, the circular polarization is obtained by using almost square patches. Therefore, the excitation point is placed at about one third of the diagonal of the patch. In order to obtain a second resonance, a ring patch in placed around the first one in such a way that the excitation is at one third of the diagonal, as well - fig. 1 left -. In that case, it is possible to obtain two distant resonant frequencies. Realizations have been made on Rogers 4003, 62mil thick. The matching for each resonances is better than -10dB . Results will be shown for a patch working at 2.4GHz and 5GHz as well as a discussion on the parameter optimization. When two near frequencies are targeted, it is possible to add inductive loads on the patch by creating some slits (L. Desclos et al, Atlanta APS 98). This allows a reduction of the resonant frequency keeping the circular polarization. Then, by adding small metallic patches inside the slots it is possible to have a second resonance. This second resonance has similar characteristics compared to the first one, i.e. circular polarization. Realizations have been made too at 1.9GHz and 2.1GHz on duroid 2.2 to show the validity of the approach.

Numerical and experimental results of return loss and radiation pattern will be presented at the conference.

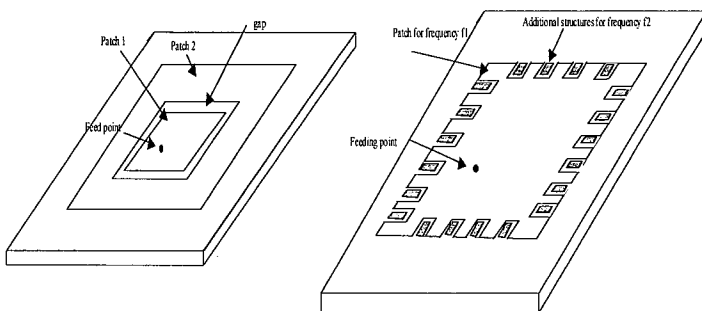


Fig.1: Two solution for dual band circular polarization patches.

Dual-Polarized Operations of A Compact Microstrip Antenna

Jeen-Sheen Row^{1*}, Wen-Shan Chen¹, and Shih-Huang Yeh²

¹Department of Electronic Engineering

²Department of Electrical Engineering

Chien Kuo Institute of Technology

National Sun Yat-Sen University

Chang-Hua 500, Taiwan

Kaohsiung 804, Taiwan

Email: ljs@cc.ckit.edu.tw

Abstract

To meet the requirement of miniaturization of recent wireless communications systems, a variety of slot-loaded microstrip antennas have been implemented for achieving compact dual-frequency operation and compact circularly polarized radiation. Related designs of slot-loaded microstrip antennas for compact dual-polarized radiation, however, are not reported. With the capability of dual-polarized radiation, the antenna can combat with multipath effects of wireless communications and optimize system performances. In addition, the dual-polarized antenna is able to transmit twice as much information as using the same bandwidth, i.e. frequency reuse. To achieve these performances, highly decoupled input ports and low cross-polarization radiation of the two polarizations are required for the design of dual-polarized antennas.

In this article, we demonstrate that a slot-loaded microstrip antenna with a group of four symmetrical bent slots can perform excellent dual-polarized radiation, while the antenna size is significantly reduced for operating at a fixed frequency. The four symmetrical bent slots are aligned in parallel with the patch's central lines for obtaining 0° and 90° polarizations or the patch's diagonals for $\pm 45^\circ$ slanted polarizations, and the two polarizations are excited by using two probe feeds. Due to the perturbation of the bent slots, the excited patch surface current paths are meandered, which results in same lowering of the operating frequencies for the two polarizations. That is, dual-polarized radiation can be obtained with a reduced antenna size at a fixed operating frequency. Many prototypes of the proposed compact dual-polarized microstrip antenna have been successfully implemented. Experimental results show that for such a compact dual-polarized microstrip antenna with an inexpensive FR4 substrate, isolation between the two feeding ports better than 35 dB can easily be obtained, which is also better than that of a corresponding unslotted dual-polarized square microstrip antenna. In addition, the cross-polarization level in the E - and H -plane patterns for the compact dual-polarized microstrip antenna studied is about as good as that of a unslotted square microstrip antenna.

Biology and Medicine

Chair: X. Li, USA

	Page
1:00 3-D Microwave Imaging for Biomedical Applications: Numerical Simulations, <i>Qi.H. Liu*, Z.Q. Zhang, Duke University</i>	416
1:20 Efficient Hybrid Integral Equation and Finite Difference Method for Low-Frequency Electric Induction in Humans, <i>T.W. Dawson*, University of Victoria, S. Velamparambil, University of Illinois</i>	417
1:40 Comparison of Experimental and Numerical Methods for SAR Assessment in Human Head Phantoms, <i>A. Christ*, K. Pokovic, H. Gerber, N. Chavannes, N. Kuster, Swiss Federal Institute of Technology</i>	418
2:00 Fields in Adult and Child bodies from 60 Hz Electric Fields and Contact Currents, <i>M. Stuchly*, T.W. Dawson, K. Caputa, A. Hirata, University of Victoria</i>	419
2:20 Phased-Array Radar for Breast Cancer Detection, <i>O. Ramahi*, R. Thakker, University of Maryland, S. Trabelsi, Richard B. Russell Agricultural Research Center</i>	420
2:40 Microwave Breast Cancer Detection Using Ultrawideband Space-Time Focusing Techniques, <i>X. Li*, E.J. Bond, D. Hagl, B. Van Veen, S. Hagness, J.H. Booske, University of Wisconsin</i>	421
3:00 Localized Heating by Using a Coaxial-Slot Antenna with Two Slots for Microwave Coagulation Therapy, <i>K. Saito*, S.Y. Okabe, T. Taniguchi, H. Yoshimura, K. Ito, Chiba University</i>	422

3-D Microwave Imaging for Biomedical Applications: Numerical Simulations¹

Qing Huo Liu* and Zhong Qing Zhang
Department of Electrical and Computer Engineering
Duke University
130 Hudson Hall, Box 90291
Durham, NC 27708-0291

Over the last few years, microwave techniques have emerged as an important method for biomedical characterization of diseases. In particular, experimental and clinical prototype microwave imaging systems have been developed for breast cancer detection. Preliminary results have shown that microwave breast imaging is a promising technique to complement the existing X-ray mammography.

However, previous microwave imaging (MWI) systems for breast cancer detection are based on two-dimensional data acquisition and processing. As a result, significant artifacts exist in the MWI images due to the 2-D assumptions. The reason for using these 2-D assumptions are mainly due to the difficulties in constructing a 3-D array of microwave transmitters and receivers, and due to the high computational demand in 3-D data processing. It is the aim of this work to significantly reduce the computational burden in 3-D data processing and simulations. This 3-D simulation capability is essential both for the system calibration and for the inverse solution to form images.

We tackle this 3-D forward simulation problem in microwave imaging by using a recently developed weak-form biconjugate-gradient fast Fourier transform (BCG-FFT) method. It solves a hypersingular volume integral equation in three dimensions. Previously, our program was developed for radar cross section computation where the incident field is a plane wave. For microwave imaging, since the measurements are in the near-field zone, we must accurately model effects of a finite microwave source. We first model finite dipole antennas radiating in the vicinity of an inhomogeneous object. The results are compared with analytical solutions for the special case where the object is a multilayer sphere. We then model the actual experimental setup in our laboratory in a multistatic mode. These simulations will be compared with our laboratory measurements.

One major issue we will study with these simulations is the effect of the backing of a tank holding fluid and phantom. In our experimental setup, the tank is surrounded by absorbing materials so that the reflections from the walls of the tank are minimum. The performance of this absorbing backing will greatly affect the quality of the images.

We will also use this forward solver to generate synthetic data for an inverse scattering algorithm to form microwave images. Once our forward solution produces accurate results compared with measurements, we will use these synthetic data to characterize our inverse algorithm in terms of its accuracy, sensitivity and resolution.

¹This work is supported in parts by the U.S. EPA under a PECASE grant CR-825-225-010, by the NSF under a CAREER grant ECS-9702195.

Efficient Hybrid Integral Equation and Finite Difference Method for Low-Frequency Electric Induction in Humans

T. W. Dawson
 Dept. of Electrical and Computer Engineering
 University of Victoria, PO Box 3055 STN CSC
 Victoria BC V8W 3P6 Canada
 tdawson@ece.uvic.ca

S. Velamparambil
 Dept. of Electrical & Computer Engineering,
 University of Illinois, 1406, W. Green St., Urbana, IL-61801
 Sanjay@sunchew.ece.uiuc.edu

Stevenson's method [J. Van Bladel, Electromagnetic Fields, Hemisphere, D.C. 1985] provides a framework for solving problems of low-frequency electromagnetic induction in compact conductors. For an isolated human exposed to 50/60 Hz electric fields, the total external electric field is essentially static, with the body surface being at constant potential. With an $e^{i\omega t}$ factor suppressed, the problem can be formulated as the constrained integral equation

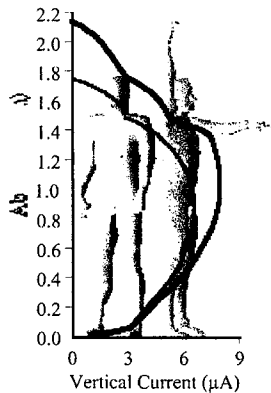
$$\phi_s(y) + \frac{1}{4\pi\epsilon_0} \iint_B \frac{\eta(x)}{|x-y|} da = \phi_0, (y \in B), \quad (1) \quad \iint_B \eta(x) da = 0. \quad (2)$$

Here B is the body surface, $\eta(x)$ the local surface charge density at surface point x , $\phi_s(y)$ the external source potential at surface point y , ϕ_0 is the (constant) potential of the body. The electric field within the body may be expressed as $E(x) = -\nabla\psi(x)$, where the potential satisfies the differential equation $\nabla \cdot [\sigma(x)\nabla\psi(x)] = 0$, ($x \in V$) in the body interior V , subject to the boundary condition $\sigma(x)n(x) \cdot \nabla\psi(x) = j\omega\eta(x)$, ($x \in B$). The charge density is obtained from solution of (1) and (2). The net result is a two-stage hybrid method for computing the induced internal fields.

The body models are anatomically derived and comprise 3.6-mm cubic voxels. A precorrected FFT algorithm [Joel Reuben Phillips, "Rapid Solution of Potential Integral Equations in Complicated 3-Dimensional Geometries", PhD Thesis, MIT, 1997] was implemented to solve the integral equation directly on the surface of the voxel model. The examples pertain to isolated bodies in 60-Hz, 1kV/m vertical electric fields. We show that the hybrid data agree well with values computed by quasistatic FDTD on the arms-down model. The FDTD solution required 1.9 GB of memory and over 18 hours using 6 processors on an IBM SP2 SMP machine. The arms-raised model occupies nearly three times the volume, and memory and time requirements would scale similarly. A complete hybrid PCFFT-SPFD solution for the 3.6-mm model takes under 3 hours for the arms-down model and less than 4 hours for the arms-up model on a 4-processor SGI Origin 2000 machine. Detailed validation, dosimetry and comparisons between the two postures will be presented.

Tissue	Arm	Min	Avg	RMS	Max
brain	u	0.02	0.20	0.21	0.89
	d	0.03	0.34	0.37	1.47
heart	u	0.20	0.57	0.60	1.45
	d	0.14	0.45	0.47	1.14

Table 1. Sample dosimetry for the two postures (mV/m).



Comparison of Experimental and Numerical Methods for SAR Assessment in Human Head Phantoms

Andreas Christ, Katja Poković, Hans-Ulrich Gerber, Nicolas Chavannes, and Niels Kuster
Swiss Federal Institute of Technology (ETH)
8092 Zürich, Switzerland

Phone:+41-1 632 2736, Fax:+41-1 632 1057, e-mail: christ@itis.ethz.ch

Introduction

In the recent years, various different models of human heads have been suggested for the compliance testing of mobile phones. However, the mobile phone industry as well as several governmental regulatory bodies have been stressing on the need for a standardized testing procedure. The cornerstone of such a testing procedure is a well defined human head model which meets the highest requirements with respect to accuracy and repeatability. In order to fulfill these demands, a novel head phantom has recently been proposed by IEEE/CENELEC. This phantom, the specific anthropomorphic mannequin (SAM), is based on a large scale anatomometric survey of US-army personnel. In this study, the new phantom is compared to a high-resolution anatomical head model and the generic head phantom, which is part of the DASY3 dosimetric assessment system and has been serving as a quasi-standard in compliance testing.

Objectives

The goal of this paper was the comparison of the two homogeneous phantoms and the anatomical one with respect to SAR assessment at mobile phone frequencies.

Method

The SAR of the two homogeneous phantoms and the anatomical head model was assessed using a generic mobile phone model equipped with either a monopole or a helix antenna operating at 900 and 1800 MHz. The phone was placed both in "touch" and "tilted" positions as defined in CENELEC ES5905. The SAR measurements were taken with the DASY3 near field scanner. The integrated simulation platform SEMCAD was used to calculate the SAR in the homogeneous and in the anatomical phantom. The CAD environment of SEMCAD enables the accurate positioning of mobile phone and head in the previously mentioned positions. The numerical simulations were performed using the FDTD method with inhomogeneously spaced meshes.

Results

For the SAM phantom, considerably higher SAR values were found for "touch" position when compared to the generic phantom. This is due to the different shapes of the cheeks of the two phantoms and of the higher conductivity of the tissue simulating liquid used in SAM. In the "tilted" position, the SAR of the generic phantom was higher as result of the thinner spacer representing the ear pinna of this phantom. Comparatively low overestimations were found with respect to the anatomical phantom considering that the losses in the ear pinna were evaluated. The comparison of the simulation results to the measured data show very good agreement well within the accuracy of the methods applied.

Conclusion

The findings show the high dependency of the SAR in the human head depending on tissue parameters and geometrical details. Nevertheless, the assessed results compare well and confirm that the proposed procedures represent a conservative approach.

Fields in Adult and Child Bodies from 60 Hz Electric Fields and Contact Currents

M. A. Stuchly*, T. W. Dawson, K. Caputa and A. Hirata
Department of Electrical & Computer Engineering, University of Victoria
Box # 3055, Stn. CSC, Victoria, BC, V8W 3P6, Canada
Email: mstuchly@ecce.uvic.ca

In the last decade extensive computation have been performed of induced electric field and current density in models of adult human body exposed to 60 or 60 Hz electric and magnetic fields (Stuchly and Dawson, Proc. IEEE, 88: 643 – 664, 2000). In this work, for the first time, similar dosimetry computations are reported for an anatomically realistic model of a 5-year old child. Also, not previously available dosimetry data are given for contact current due to touching ungrounded objects in low frequency fields.

The adult model has a resolution of 3.6 mm and child model of 3.2 mm with over 50 organs and tissues identified and assigned corresponding conductivity values. For exposures to 60 Hz vertical electric field, a previously developed (Dawson et al, J. Comp. Physics, 136: 640-653, 1997) hybrid method (the finite difference time domain, FDTD, hybridized with the scalar potential finite difference, SPFD) is used. Three scenarios of contact current are simulated. They include contact by one hand, the other hand and both feet grounded, contact hand to hand, and contact by one hand, both feet grounded. Computations of contact currents are performed with a modified SPFD code.

For the electric field exposure, results obtained are important in view of the difficulty in direct scaling of the induced quantities. In children, the volume of the head and brain is proportionally greater to the total body volume than in adults. This results in lower average electric field (and voxel current density) in the child head. Most average and maximum induced fields are comparable for adult and child, and only the values in the brain and other tissues in the head are lower. Figure 1 gives a comparison. Figure 2 illustrates the current flow for three contact current scenarios. The electric fields in the child model are generally higher than in the adult model, typically by a factor of three.

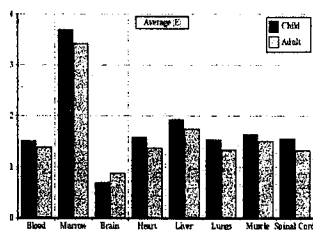


Fig. 1 Average in induced electric field in adult and child in 1 kV/m 60 Hz field

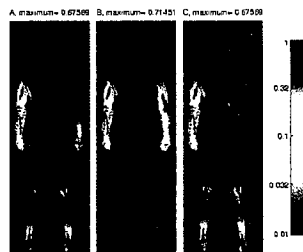


Fig.2 Electric field for contact currents

Phased-Array Radar for Breast Cancer Detection

Omar M. Ramahi and Rikin Thakker 2181 Glenn Martin Hall James Clark School of Engineering University of Maryland College Park, MD 20742	Magda El-Shenawey Electrical Engineering Department 3217 Bell Engineering Center University of Arkansas Fayetteville, Arkansas 72701	Samir Trabelsi Agricultural Research Service, USDA Richard B. Russell Agricultural Research Center P. O. Box 5677 Athens, GA 30604, USA
---	--	---

The idea of using electromagnetic (EM) waves for detection of hidden or remote objects is perhaps as old as the discovery of Maxwell's equations. EM fields have been used successfully in remote sensing. Recently, a strong activity has emerged in mine detection where similar ideas to those used in remote sensing have been implemented. This evolution in the application of the detection or sensing potential of EM waves has recently become more relevant in medical applications; most noticeably in the detection of physiological abnormalities, especially malignant breast tumors.

Present technology used in breast cancer detection includes x-ray mammography, ultrasound, and magnetic resonance imaging (MRI). All of these techniques have contributed significantly to a higher detection rate of malignant breast cancer tumors. However, the number of false negatives as well as false positives remains appreciable.

Microwave imaging of internal biological abnormalities has been of interest for a number of years. The basic underlying principle for detection is the sharp contrast in dielectric properties between tumors and normal tissue. This contrast arises from the higher water content of tumors in comparison to healthy breast tissue. More recently, the idea of microwave con-focal system has been used for breast tumor detection (J. E. Bridges, Microwave Method and System to Detect and Locate Cancer in Heterogeneous Tissues, US Patent No. 5829437, Nov. 3, 1998).

In this work, we propose a phased-array radar system where the target area is mapped in space and time. The frequency choice is a highly critical aspect of this work. There are two fundamental concerns when choosing the frequency of the system. The primary concern is the EM response of healthy and diseased tissue in the frequency domain. Usually, EM radiation at microwave frequencies is used for sensing the physical properties of biological materials containing water. The dipolar character of the water molecules and the dielectric relaxations observed at these frequencies are at the core of this choice. Therefore, by examining the dielectric spectra of tumors and normal tissue, it would be possible to select a frequency for which the EM responses of these tissues are totally different and thus distinguishable. The second concern in the frequency selection relates to adequate time-space resolution of the target area and to aspects related to the practical construction of the system.

In this presentation, we will highlight the different components of the proposed detection system. We present preliminary simulation results showing the feasibility of the phased-array scanning system including dynamic range requirements.

Microwave Breast Cancer Detection using Ultrawideband Space-Time Focusing Techniques

X. Li*, E. J. Bond, D. Hagl, B. Van Veen, S. C. Hagness, and J. H. Booske

Department of Electrical and Computer Engineering
University of Wisconsin, Madison, WI 53706-1691
hagness@engr.wisc.edu

In this paper we present preliminary investigations of ultrawideband space-time microwave imaging (STMI) for detecting early-stage breast cancer. Our ongoing work in this area is motivated by the clinical need for complementary or alternative modalities to screening X-ray mammography, which suffers from relatively high false-negative and false-positive rates. The penetrable nature of normal breast tissue at microwave frequencies up to several gigahertz and the significant contrast in the dielectric properties of normal and malignant breast tissue at microwave frequencies, as suggested by published data (Surowiec et al, *IEEE Trans. Biomed. Eng.*, 35:257-263, 1988; Joines et al., *Med. Phys.*, 21:547-550, 1994; Chaudhary et al., *Ind. J. Biochem. Biophys.*, 21:76-79, 1984) and our own preliminary measurements on freshly excised breast tissue, provides a compelling rationale for the development of microwave detection techniques.

STMI falls under the class of ultrawideband microwave backscatter imaging techniques recently proposed for breast cancer detection (Hagness et al., *IEEE Trans. Biomedical Engineering*, 45:1470-1479, 1998; Hagness et al, *IEEE Trans. Antennas and Propagation*, 47:783-791, 1999; Li and Hagness, *IEEE Microwave and Guided Wave Letters*, in press). In contrast to microwave tomographic approaches that require the solution of a nonlinear inverse-scattering problem, STMI relies on the use of relatively simple, robust space-time beamforming (focusing) techniques developed in the context of radar technology for frequency-dependent processing of wideband signals. This significant departure from the complicated image reconstruction techniques inherent in conventional tomography is a consequence of seeking only to identifying the presence and location of strong scatterers, such as malignant tumors, in the breast, rather than attempting to recover the dielectric-properties profile.

To investigate the performance of STMI, we have applied our space-time beamformer designs to simulated backscatter data obtained from anatomically realistic FDTD models of the breast. Our FDTD models have been created using high-resolution sagittal and coronal MRI data sets from routine MRI scans performed at the University of Wisconsin Hospital and Clinics. The FDTD models include the dispersive dielectric properties of both malignant and adjacent normal breast tissue. FDTD simulations are used to generate a variety of "patient" scans, including the radiographically dense breast scenario. The parameters assigned to normal breast tissue are determined from a family of Debye curves ranging from less dense fatty tissue to more dense glandular tissue. Our Debye curves have been constructed from empirical fits to our most recently measured dielectric properties data from breast biopsy and breast reduction specimens. Realistic simulations demonstrate that the use of space-time beamforming provides spatial selectivity that minimizes the effect of clutter beyond that which can be achieved with simple coherent addition (time-shifting and summing). As a result, high signal-to-clutter ratios are achieved for detecting small malignant tumors embedded in heterogeneous breast tissue comprised of skin, fat, veins, and fibroglandular mammary tissue, ducts, and lobes.

Localized Heating by Using a Coaxial-Slot Antenna with Two Slots
for Microwave Coagulation Therapy

Kazuyuki SAITO¹*, Shin-ya OKABE¹, Takeshi TANIGUCHI¹,
Hiroyuki YOSHIMURA², and Koichi ITO²

¹ Graduate School of Science and Technology, Chiba University

² Faculty of Engineering, Chiba University

1-33 Yayoi-cho, Inage-ku, Chiba 263-8522, JAPAN

In recent years, various types of applications of electromagnetic techniques to microwave thermal therapy have been developed. The authors have been studying thin coaxial antennas for the microwave coagulation therapy (MCT). The MCT has been used mainly for the treatment of hepatocellular carcinoma. In the treatment, the thin microwave antenna is inserted into the tumor and the microwave energy heats up the tumor (at least 60 °C) to produce the coagulated region including the cancer cells.

At present, there is a problem that length of the coagulated region becomes longer into the antenna insertion direction. In order to overcome this problem, we introduced the coaxial-dipole antenna and confirmed the localized heating only around the tip of the antenna. Figure 1(a) shows the longitudinal cross section of tip of the coaxial-dipole antenna.

However, an outer diameter of the coaxial-dipole antenna is not small enough. Therefore, the authors introduced the coaxial-slot antenna with two slots. Figure 1(b) shows the longitudinal cross section of tip of the coaxial-slot antenna with two slots. In this antenna, we confirmed the possibility of generating the localized heating pattern, whose shape is similar to that of the coaxial-dipole antenna, under $L_{ts}=20$ mm and $L_{rs}=10$ mm, by the FDTD calculations. As a further study we should optimize the position of the two slots.

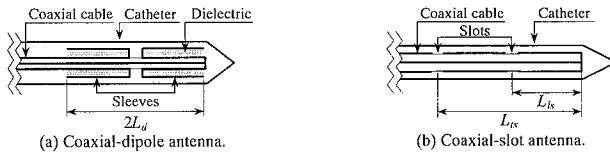


Fig. 1 Longitudinal cross section of the thin coaxial antennas.

Author Index

Abdallah, E.	275	Bishop, G.	112, 116
Abe, Y.	28	Blackwell, W.	396, 398, 399
Adam, R.	263	Blagoveshchensky, D.V.	395
Adams, R.	358	Blaunstein, N.	233
Alatan, L.	43	Blevins, B.	410
Albani, M.	123	Boag, A.	23, 78, 182, 326, 412
Al-Derbas, A.	178	Board, J.	327
Ali, M.A.	348	Boeck, M.	167
Altintas, A.	48	Bogdanov, F.	389
Altshuler, E.	207	Boix, R.	370
Ando, M.	171	Bokhari, S.	256
Ang, T. W.	17	Bolli, P.	16, 35
Antar, Y.M.M.	221	Bolomey, J-Ch.	151
Arellano, G.	405	Bond, E.J.	421
Armogida, A.	204	Booske, J.H.	421
Arnold, E.	167	Borderies, P.	337
Arvas, E.	229	Borelli, F.	294
Awadallah, R.	242, 376, 377	Boriskin, A.	24, 48
Bahar, E.	238	Botha, E.	85
Bajon, D.	268	Bourrely, C.	280
Balzano, Q.	73	Bourry, M.	26
Barbosa, A.	386	Bozler, C.	301
Bardi, I.	67	Brandfass, M.	286
Barone, G.	153	Brandt, A.	326
Barrett, J.	398, 399	Bronshtein, A.	247
Barriot, J. P.	130	Brookner, E.	354
Barseem, I.	275	Bruno, O.	323
Basu, S.	111	Bullett, T.	116
Baudrand, H.	268	Buris, N.	181
Beaudoin, C.	293	Burk, S.	397
Bell, T.	305	Burkholder, R.	17, 319, 336
Beniguel, Y.	279	Burkholder, R.J.	361
Benna, M.	130	Burnside, W.D.	71
Benson, R.	306, 307	Butler, C.	209
Bergada, M.	400	Buyukdura, O.M.	334
Berginc, G.	279, 280	Cable, V.	359
Bernal, J.	370	Caimi, F.	408
Bernhard, J.	220	Caliskan, F.	134
Bertoncini, F.	22	Calvo, M.	214
Bertram, J.	168	Cangellaris, A.	10, 163, 251
Besieris, I.	118, 119	Canning, J.	392
Bijamov, A.	389	Capolino, F.	45, 123, 196

Caponi, M.	323	Collins, P.J.	75
Caputa, K.	419	Costa da Silva, L.	47
Cardiasmenos, A.	216	Coster, A.	107
Carin, L. 138, 246, 259, 260, 327, 330, 331		Coster, A.	113
Carpenter, D.	305, 306, 307	Crittenden, P.	238
Carver, K.	168	Crowe, T.	300
Casey, J.	379	Crozzoli, M.	223
Catedra, M.	101	Cwik, T.	161
Catedra, M.F.	18, 234, 197	da Silveira, M.	86
Cazzatello, G.F.	223	Dandekar, K.	84
Cendes, Z.	8, 9, 67	Das Gupta, C.	50, 51
Censor, D.	233	Dassios, G.	121
Chae, H.	195	Davis, W.	174
Champagne, N.	364	Dawson, T.W.	417, 419
Chan, C.H.	159	de Adana, F. Saez 18, 101, 197, 234	
Chan-Aldebol, C.	392	de Haaij, D.M.	80
Chanet, M.	198	de Haro, L.	214
Chang, H.	369	de Prado, J.A.	234
Chao, H. Y.	68	DeNatale, J.F.	302
Chapman, R.	314, 315	Desclos, L.	145, 388, 413
Chavannes, N.	257, 418	Desclose, L.	406
Chen, C.C.	71, 103, 188	Deshpande, M.	183
Chen, F.	399	Dietrich, C.	74
Chen, H.H.	344	Diez, P.	71
Chen, H.Y.	371	DiMarzio, C.	322
Chen, J.	180	D'Inzeo, G.	294
Chen, K.M.	190	Disco, D.	223
Chen, W.S.	414	Djordjevic, A.	90
Chen, Z.	341	Dogaru, T.	259
Chew, W. C.	68, 328, 362	Doherty, P.	111, 116
Chia, T. T.	17	Donepudi, K.C.	362
Chiou, T.W.	139	Drissi, M.	26
Choo, H.	144	Duchesne, L.	150, 151, 152
Chou, H. T.	91, 92, 371	Duffy, S.	301
Christ, A.	257, 418	Dumanian, A. J.	248
Christodoulou, C.G.	372	Dyrud, L.P.	310
Christopher, P.	231	Eguchi, M.	222
Chu, T. H.	179	Eibert, T.F.	160
Chung, Y. C.	70	ElHelbawy, M.	256
Chystyakov, D.N.	128	El-Said, M.	275
Citrone, P.	112, 116	El-Shenawee, M.	320
Civi, O. A.	43, 91, 334	Engheta, N.	387
Claverie, J.	378	Eroglu, A.	42
Close, S.	113	Erricolo, D.	186
Coleman, C.M.	83	Erturk, V.B.	146

Evans, M.	230
Farahat, N.	197
Faraone, A.	73
Feick, R.	46
Felsen, L.	97
Fernandes, C.	147
Ferrero, L.	223
Fiddy, M.	293, 296, 392
Fikioris, G.	226, 60
Fink, P.	364
Fluerasu, A.	412
Foged, L.	150, 151
Foltz, H.	74, 232, 405
Foster, J.C.	107
Freeman, T.	394
Frohlich, J.	257
Fukao, S.	63
Fung, S.	306, 307
Furse, C.	29, 34, 193, 217, 292
Galkin, I.	304
Gamand, P.	268
Gandhi, O.P.	54, 294
Gandois, A.	153
Garces, M.	405
Garcia, E.	18, 101
Garreau, P.	153
Garreau, Ph.	151
Gatesman, A.	293
Gennarelli, C.	21
Gentili, G.	172
Gerber, H.	257, 418
Gheorma, I.L.	345
Gianvittorio, J.	298
Gilbert, B.	11
Giles, R.	293
Goff, M. Le.	152
Going, S.	217
Golla, K.J.	75
Gonzalez, I.	18, 101, 197, 234
Gope, D.	356
Gotwols, B.	314
Gotwols, B.	315
Gouker, M.	301
Grace, D.	228
Green, J.	306, 307

Greenwood, A.	58
Gronwald, F.	124, 262
Groves, K.	116
Groves, K.M.	111
Grzegorzczuk, T.	136
Guerin, C-A.	281
Guerouni, S.	216
Gulick, J.	360
Guo, J. S.	106, 308
Gutierrez, O.	18, 101, 197, 234
Guzman, E.	405
Haack, T.	397
Hacker, J.B.	302
Hagl, D.	421
Hagness, S.	6, 421
Hanazawa, M.	28
Hancock, J.	396
Hansen, R.C.	351
Hanson, G.	272
Hasegawa, T.	295
Hashiguchi, H.	63
Hashimoto, O.	28
Hashish, E.	275
Hastings, F.	227
Havrilla, M.	38
He, J.	327, 330, 331
He, Y.	254
Hebron, T.	404, 407
Hermida, R.B.	406
Heyman, E.	78, 82, 258, 412
Higgins, M.	188
Hill, K.	156
Hill, K.C.	365
Hirata, A.	419
Hirokawa, J.	171
Ho, H.K.	92
Hobbs, E.	405
Holeman, E.	112
Holloway, C.	255
Holtzhausen, F.	167
Hopkins, E.	99, 100
Hristov, H.	46
Huang* B.	307
Huang, C. Y.	139
Huang, X.	304, 306

Huang, Y.	219	Kanellopoulos, J.D.	226
Hunsucker, R.	115	Kantz, J.	31
Hunt, S.	113	Karabudak, N.	302
Hussar, P.	15	Karaduman, M.	104
Hutani, A.	144	Karkashadze, D.	389
Hutchins, R.	194	Karkkainen, K.	122
Hwang, K.P.	251	Karras, T.	302
Iijima, A.	108	Katz, D.	233
Imbriale, W.	274	Keast, C.	301
Inan, U.	305	Keller, M.	314, 315
Inan, U.S.	114	Kempel, L.	360, 366
Infante, D.	267	Kempel, L.C.	190
Ishimaru, A.	135, 240, 383, 394	Kenneally, W.	3
Iskander, M.F.	30	Kerschbaum, M.	201
Ito, K.	422	Kessler, M.	99
Ittipiboon, A.	39	Khalaf, Y.	178
Iversen, P.O.	150, 151, 152	Khan, S.	411
Iwasaki, T.	295	Kharidehal, S.	217
Jackson, D.R.	266	Khmyrov, G.	304
Jacobs, J.P.	215	Kikuchi, N.	125
Jakayar, A.	217	Kilmer, M.	318
Jamnejad, V.	274	Kim, K.	166
Janaswamy, R.	244, 374, 375	King, R.	210
Jandhyala, V.	356, 383	Kintner, P.	109
Janpugdee, P.	91	Kiziltas, G.	125
Jedlicka, R.	410	Klimeck, G.	161
Jensen, M.	235	Knecht, J.	301
Jha, R.M.	244, 375	Koc, S.S.	334
Ji, Z.	218	Kofman, W.	130
Jin, J.	360	Kolundzija, B.	90
Jin, J.M.	338, 362	Kong, A.	192
Johnson, J.	321	Kooi, P.S.	132
Johnson, J.T.	102, 283	Kornrumpf, W.	302
Johnson, W.A.	62	Kotulski, J.	62
Joly, P.	65	Kouyoumjian, R.G.	22
Jones, E.	327	Kowolski, M.	360
Jordan, A.K.	390	Kozlov, A.	304
Jordan, H.	256	Kralovec, J.	408
Jorgenson, R.E.	62	Kramer, J.D.	175
Josefsson, L.	353	Krauthauser, H.G.	262
Joubert, J.	80, 86, 169, 215	Kryukovsky, A.S.	128
Ju, J.J.	371	Ku, H.	242
Kadamb, G.	404	Kuga, Y.	240, 383, 384, 394
Kadambala, S.	168	Kuroki, F.	222
Kadambi, G.	219, 407	Kuroki, F.	343

Kuster, E.	100	Liu, Z.	138, 246
Kuster, N.	257, 418	Livne, O.	326
Kuttler, J.	376, 377	Lo, T.	94
Kuzuoglu, M.	252	Lomakin, V.	258
Lamar, M.	377	Long, B.R.	95
Landstorfer, F.	31	Louvigne, J.C.	79
Ledezma, S.	405	Lozano, L.	101
Lee, C.S.	148	Lozano, P.	101
Lee, J.	195	Lu, H. C.	179
Lee, J.	273	Lu, J.	224
Lee, J.F.	9, 12, 59, 336, 361	Lu, M.	363
Lee, J.K.	42	Lugara, D.	78
Lee, J.S.	72, 189	Lukin, D.S.	128
Lee, K. H.	103	Lumbreras, C.	229
Lee, K.W.	146	Luo, X-G.	308
Lee, R.	12, 41, 59, 76, 103, 361	Lyke, J.C.	372
Lee, S-W	240, 383, 384	Lyzenga, D.	317
Lee, T. W.	6	Ma., Y.C.	365
Lemanczyk, J.	150	Maci, S.	40, 45, 97
Leong, M.S.	132	MacPhie, R.	94
Leskova, T.A.	127, 239, 269	Madan, N.	29
Leslie, R.	396, 398, 399	Madden, D.	112
Letrou, C.	78, 412	Mahailovich, R.E.	302
Leviatan, Y.	66	Mahe, Y.	145, 406, 413
Levy, M.F.	282	Mahmood, A.	148
Li, B.H.	218	Maloney, J.	99
Li, D.U.	369	Manara, G.	22
Li, E.	98	Manarra, G.	204
Li, H. J.	88	Mannucci, A.	108
Li, J.	289	Manshadi, F.	274
Li, J-H.	368	Maradudin, A.A.	127, 239
Li, L.	33, 400	Marhefka, R.	19
Li, L.W.	132	Marrocco, G.	196
Li, S.Q.	159	Martin, E.	352
Li, X.	421	Martinez, D.	214
Li, Z.	125	Martinez, R.	214
Licitsin, R.	182	Martini, E.	16
Lindell, I.	2, 121	Mathis, A.	270
Ling, H.	84, 144, 232, 287, 289	Mawst, L.	6
Liu, F.	180	Mazar, R.	247
Liu, G.	126	Mazzei, A.	172
Liu, J.	394	McCleod, B.	217
Liu, Q.H.	61, 291, 335	McGahan, R.	296
Liu, Qi.H.	416	McLean, J.	405
Liu, T. Y.	88	McNamara, D.	85, 409

Media, Layered	192	Nozdrachev, S.V.	395
Medina, F.	64, 370	Nyquist, D.	38, 267, 273
Meese, J.	366	Nyquist, D.P.	190
Mendez, E.R.	127	Odendaal, J. W.	80, 86, 169, 215
Mesa, F.	64, 266	Ogucu, G.	43
Meyerhoff, J.	181	Ohira, T.	224
Miao, M.	132	Oijala, P. Yla-	137
Michielssen, E.	23, 250, 338, 363	Okabe, S.Y.	422
Micolau, G.	337	O'Neill, K.	189
Mills, D.L.	269	Ooi, B.L.	132
Mittra, R.	157, 197, 252	Oppenheim, M.M.	310
Mohan, R.	217	Ostroff, E.	175
Monod, M.	198	Ozdemir, M.	229
Monorchio, A.	204	Ozdemir, N.	329
Montgomery, N.	194	Pagana, E.	204
Montiel, G.	405	Paiva, C.	386
Moore, R.	99	Palud, M. Le	378
Morales-Porras, A.	296	Pan, G.	11
Morgan, M.	187, 290	Panagopoulos, A.D.	226
Morgenthaler, A.	248, 318	Parfitt, A.	44
Morris, M.	235	Parisi, S.	175
Morrison, J.	201	Park, J.	195
Mosallaei, H.	162	Park, J.S.	72
Mosig, J.R.	136, 158	Pasqualini, D.	45
Moss, C.	192	Pasqualini, D.	342
Mrozowski, M.	199	Pathak, P.	19, 91, 336
Mudalier, S.	278	Pathak, P.H.	361
Munteanu, I.	200	Paznukhov, V.	312
Muralidhar, Y.	30	Pearson, L.W.	89, 96
Nam, S.	195	Peixeiro, C.	147
Narayanan, R.	219	Pelacchi, P.	35
Navale, S.S.	365	Pelosi, G.	16, 21, 35
Navsariwala, U.	181	Pendley, C.	292
Nealy, R.	74	Pereira, W.N. Amaral	276
Nepa, P.	22, 91	Perov, A.	198
Nepa, P.L.	204	Perry, D.	67
Neto, A.	40, 340, 342	Peterson, A.	134
Nevels, R.D.	120	Petosa, A.	39, 221
Nguyen, C.	72, 189	Pi, X.	108, 394
Niemand, P.	169	Piket-May, M.	202, 255, 256
Nieves, S.	18	Piot, A.	130
Nikolic, N.	44	Plaza, G.	64
Nikoskinen, K.I.	121	Pochini, C.	21
Nitsch, J.	124, 262	Pogorzelski, R.	173
Nosich, A.I.	24, 48	Poilasne, G.	145, 389, 413

Pokovic, K.	418	Ruetzel, P.	167
Polat, B.	96	Rumsey, I.	202
Polemi, A.	20, 97	Saillard, M.	281, 288, 337
Poles, L.	352	Saito, K.	422
Pormann, J.	327	Salameh, M.S. Al	221
Poulard, G. Le	378	Saleh, W.	401
Powell, J.	410	Sales, G.	304, 306
Qaddoumi, N.	401	Salvati, M.	305
Quigley, S.	112, 116	Sampaio, L.	47
Rabe, S.	301	Sancer, M.	365
Rabiez, G.M.	302	Sarabandi, K.	98
Raemer, H.	77	Sarkar, T.	90, 166, 218
Rahmat-Samii, Y.	162, 298	Sarret, M.	26
Ramahi, O.	33, 420	Sarvas, J.	137
Ramirez, J. de D.	405	Sauer, J.	256
Rao, Q.	63	Sauermann, G.	322
Rao, T.C.K.	271	Savi, P.	345
Rappaport, C.	77, 318, 320, 322	Saville, P.	27
Rappaport, C. M.	248	Savrun, E.	384
Rayala, V.	292	Schneider, S.	75
Reed, S.	145	Schrank, H.	350
Reinisch, B.	304, 305, 306, 311, 312	Schuhmann, R.	200, 253
Reinisch, X.	304	Schultz, J.	99, 100
Remski, R.	67	Schutt-Aine, J.E.	180
Rengarajan, S.	170	Schwering, F.	245
Retnasothie, F.	229	Scro, K.	112
Rewienski, M.	199	Scro, K.	116
Rey, D.	392	Scullion, T.	189
Riad, S.	178	Seguin, G.	221
Riccio, G.	21	Sei, A.	323
Rich, F.J.	107	Sekelsky, S.	400
Riley, D.J.	62, 194	Selleri, S.	16, 35
Rius, J.	158	Semichaeovsky, A.	392
Rivas, F.	197	Sencer, K.	329
Roa, J.P.	197	Sertel, K.	160
Rockway, J.D.	240	Shaarawi, A.	118
Rogers, L. T.	397	Shaarawi, A.	119
Rojas, R.G.	146	Shang, S-P	308
Rosenkranz, P.	396, 398, 399	Shanker, B.	250
Ross, J.E.	83	Sharaiha, A.	79
Rossi, G.	204	Sharpe, R.	364
Rothwell, E.J.	83, 190	Shen, J.	89
Rousseau, P.	32	Shen, L.	212
Rouveure, R.	198	Shi, J.	308
Row, J.S.	414	Shi, S.	322

Shifman, Y.	66	Tan, G.L.	302
Shimabukuro, F.	274	Tanaka, K.	357
Shin, C.	120	Tanaka, M.	357
Shinke, S.	343	Taniguchi, T.	422
Shlivinski, A.	78, 82, 412	Tarbell, A.	3
Siegel, P.	340	Taskinen, M.	137
Silva, S.	74, 405	Tavzarashvili, K.	389
Silveira, M.	276	Tawfik, B.	118, 119
Simmons, K.	404, 407	Techentin, B.	11
Siushansian, R.	39	Terril, N.	227
Sivaprasad, K.	220	Terzuoli, A.J.	75
Skone, S.	110	Testorf, M.	293, 296, 392
Slone, R. D.	59	Texeira, F.L.	192
Smith, G.	208	Thakker, R.	420
Smith-Rowland, E.	15	Thomas, J.	135
Song, P.	306, 307, 311, 312	Thornton, J.	228
Songoro, H.	257	Thouroude, D.	79
Soriano, G.	281	Tiberio, R.	20
Soubret, A.	280	Tkachenko, S.	124, 262
Spillard, C.	228	Toccafondi, A.	20, 45, 97
Staelin, D.	396, 399	Tokgoz, C.	19
Staker, S.	255, 256	Topa, A.	386
Stanton, P.	274	Torrungrueng, D.	283
Steenman, D.	290	Tortel, H.	289
Steinberg, B.	182, 258	Toso, G.	243
Steinmetz, T.	262	Toutain, S.	145, 406, 413
Stenholm, G.J.	190	Tozer, T.	228
Steyskal, H.	353	Trabelsi, S.	420
Strohschein, D.	220	Travis, L.	301
Stubblefield, J.	392	Tripp, A.	292
Stuchly, M.	419	Tropp, J.	55
Stuchly, M.A.	27, 122	Turhan-Sayan, G.	104
Stutzman, W.	174	Turtle, J.	352
Su, T.	84, 232	Ungan, B. U.	102
Sullivan, D.	201	Uslenghi, P.L.E.	14, 186
Sullivan, J.	404, 407	Vacus, O.	65
Sun, D. K.	9	Valencia, C.I.	127
Swenson, C.	193	Vallecchi, A.	172
Syed, H.	125	Van Veen, B.	421
Taft, W.	302	Velamparambil, S.	417
Taher, H.	275	Vesecky, J.	317
Tai, C.L.	344	Villegas, F.	161
Tai, C.T.	206	Volakis, J.	125, 160
Takada, A.	222	vom Endt, A.F.	310
Takamizawa, K.	174	Voronovich, A.	241

Vreeland, D.	372	Yarasi, S.	405, 407
Vu, T.B.	87	Yasuoka, Y.	28
Wada, K.	28	Yegin, K.	250
Waddoups, B.	34	Yeh, C.	274
Wagner, L.J.	397	Yeh, S.F.	344
Wahid, P.	348	Yeh, S.H.	414
Waldman, J.	293	Yeo, T.S.	132
Waldmann, J.	31	Yilmaz, A.	338
Wallace, J.	235	Yin, W.Y.	132
Wane, S.	268	Yoneyama, T.	222, 343
Wang, J.	396	Yoshimura, H.	422
Wang, K.	11	Yu, W.	197
Wang, N-Y.	317	Yu, Y.	363
Wang, R.	352	Yuan, C.	341
Ward, J.	193	Yun, Z.	30
Warne, L.K.	62	Zajic, A.	90
Warnick, K.	286, 328	Zaman, A.	41, 76
Webb, K.	368	Zaridze, R.	389
Weiland, T.	200, 253	Zhang, M-L.	308
Weile, D.S.	363	Zhang, Q-Y.	308
Werner, D.H.	95	Zhang, Y.	390
West, J.	316	Zhang, Z.	11, 30
White, D.	364	Zhang, Z. Q.	61, 291, 416
Whites, K.	386	Zhao, G.	61, 335
Whitman, G.	245	Zhao, Z.	316
Whittman, P.	397	Zheng, H.	308
Wilkes, R.	112, 116	Zhou, D.	6
Williams, T.	27	Zhou, Y.	287
Wilton, D.R.	364	Zhu, H.	168
Wittig, T.	200	Zhu, X.	258
Wolkoff, E.	379	Zhu, Y.	10, 163
Wong, K. L.	139	Ziolkowski, R.	382
Wongkasem, N.	271		
Wu, F.	385		
Wu, J.	106		
Wu, M.	245		
Wu, T.T.	211		
Wyatt, P.	301		
Wyss, R.	342		
Xia, M.	159		
Xu, X.	61		
Xu, X.B.	124		
Yakovlev, A.	272		
Yamamoto, S.	171		
Yang, M-C.	368		



